Title
Influence of radiation damage on He diffusivity in apatite: implications and applications to low-temperature thermochronology

Author
Willett, Chelsea Diane

Publication Date
2019

Peer reviewed|Thesis/dissertation

Influence of radiation damage on He diffusivity in apatite: implications and applications to low-temperature thermochronology

by

Chelsea D. Willett

A dissertation submitted in partial satisfaction of the

requirements for the degree of

Doctor of Philosophy

in

Earth and Planetary Science

in the

Graduate Division

of the

University of California, Berkeley

Committee in charge:

Professor David L. Shuster, Chair
Professor Kurt M. Cuffey
Assistant Professor Laura Nielsen Lammers

Fall 2019

Influence of radiation damage on He diffusivity in apatite: implications and applications to low-temperature thermochronology

Abstract

Influence of radiation damage on He diffusivity in apatite: implications and applications to low-temperature thermochronology

by

Chelsea D. Willett

Doctor of Philosophy in Earth and Planetary Science

University of California, Berkeley

Professor David L. Shuster, Chair

The radiogenic production and subsequent temperature-dependent diffusion of ^{4}He in natural apatites provides means of constraining the thermal history of samples in the upper few kilometers of Earth's crust. This technique, known as apatite (U–Th)/He thermochronology, has come into wide use in the past twenty years to quantify both rates and patterns of erosion in terrestrial settings. Critically important to the interpretation of these data, however, is the understanding of the diffusion of He and the effects of radiation damage over geologic time. Chapter 1 of this dissertation provides the background and basic concepts underlying the apatite (U–Th)/He thermochronology technique and describes the fundamental challenge of accounting for radiation damage when applying this technique. Chapter 2 describes one application of apatite (U–Th)/He thermochronology to a novel detrital study of glacially-transported cobbles in central Patagonia. This chapter provides evidence of a transient fast pulse of glacial incision with the onset of periodic glaciation in the region after ∼6 million years ago. As with all geochemical techniques used to study Earth science, the necessary assumptions made when interpreting data can have a consequential effect on the conclusions. Chapter 3 of this dissertation revisits a critical assumption—one regarding the role of radiation damage—that is made in the most often-used data interpretation models and then develops and proposes an alternate model (the alpha damage annealing model, or ADAM). In certain cases, but not all, the comparison between the ADAM and other radiation damage models shows that the radiation damage assumption can greatly affect the conclusions drawn from a data set. Additional experimental work aimed at improving the ADAM is described in Chapter 4, which finds that sample-dependent diffusion kinetics may be the key to interpreting challenging apatite (U–Th)/He thermochronologic data sets.

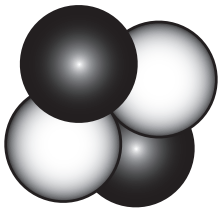

For my parents.

Contents

List of Figures

List of Tables

Acknowledgments

Thank you to my PhD advisor and dissertation chair, David L. Shuster, whose interest in both large-scale Earth surface processes and small-scale laboratory experiments have provided me a wide range of research experiences. In addition, he has continued to be an encouraging and patient mentor as I navigate the scientific research, writing, and publication processes. I am also grateful to the members of my dissertation committee: Kurt M. Cuffey and Laura Nielsen Lammers, and to Bill Dietrich for joining the aforementioned on my qualifying exam committee. Thank you to Michael Manga, whose quick thinking and willingness to help out last-minute made my Exit Seminar a wonderful and memorable occasion. Many members of the faculty enriched my experience by including me as part of their teaching teams: Professors Don DePaolo, David Shuster, Daniel Stolper, Roland Bürgmann, Bruce Buffett, Rudy Wenk, and fellow Central High School alum Nicholas Swanson-Hysell.

Many thanks to my fellow EPS graduate students and postdocs for brightening my time at Cal and helping me through numerous challenging situations. I have been amazed by the scientific work and service you have collectively contributed to date and am certain that this awe will continue throughout your dazzling careers. Thanks are due, in particular, to now-Professor Marissa Tremblay, who set the proverbial bar unimaginably high but supported my journey through graduate school and continues to support me today.

Thanks to the staff at both the Berkeley Geochronology Center and the Department of Earth and Planetary Science: without your hard work, the science could not get done and your contributions should never be overlooked. I would also like to thank the Thriving in Science program at UC Berkeley for the friends I have made and skills I have gained through my involvement.

Finishing graduate school would have been much more difficult without my non-geology hobbies and the friends I made doing them: running, climbing, frisbee, yoga, hiking, knitting, cooking, reading, eating, *etc.* Thank you to all my friends, particularly those in the East Bay whom I have gotten to know the past five years. You have provided helpful perspective on what a big and exciting world lies beyond the campus halls.

Finally—and most importantly—thank you to my amazing family: Diane, Steve, Kyle, and Keirnan, as well as Susannah, Carrie, and Amelia Claire. Your continued interest in my personal and professional pursuits, in tandem with your unending support, is irreplaceable and I am grateful every day.

Chapter 1

Introduction

1.1 (U–Th)/He thermochronometry in apatite

Though individual crystals may be only 100 µm across, the minerals present in rocks found in Earth's upper crust provide valuable information about large-scale processes occurring over geologic timescales. Combinations of radioactive systems and host minerals comprise a suite of thermochronometers: quantities of retained isotopes, produced by radioactive decay and subsequently subject to temperature-dependent diffusion, allow Earth scientists to measure ("-meter") the time elapsed ("-chrono-") since a given sample existed at a known temperature ("thermo-"). These thermochronometric systems, commonly called simply "thermochronometers," number in the double-digits and can record temperatures as high as 1100 °C [1], with more combinations possible in the future. Of these many thermochronometers, a subset is sensitive to a particularly low range of temperatures, common to the upper few kilometers of Earth's crust. These systems are collectively known as "low-temperature thermochronometers." This dissertation is focused on the low-temperature thermochronometer (U–Th)/He in apatite (AHe), both in application and method development. Apatite is an accessory mineral commonly found in intrusive igneous rocks and it has the general chemical formula $Ca_5(PO_4)_3(OH, Cl, F)$.

The AHe thermochronometer uses the production of ^{4}He via α-decay of heavy parent nuclides ^{238}U, ^{235}U, ^{232}Th, and ^{147}Sm to constrain the amount of time elapsed. Each these heavy, radioactive parent nuclides has its own measured half-life:

^{238}U $t_{1/2}$ = 4.47 Ga (giga-anum, or billion years)

^{235}U $t_{1/2}$ = 0.70 Ga

^{232}Th $t_{1/2}$ = 14.0 Ga

^{147}Sm $t_{1/2}$ = 117 Ga

and these half-lives are related to the isotope-specific decay constant by:

$$\lambda = \frac{ln(2)}{t_{1/2}}. \tag{1.1}$$

With the exception of ^{147}Sm, which undergoes one α-decay to produce ^{143}Nd, the heavy, radioactive parent nuclides will undergo a cascade of multiple radioactive decays, both α- and β-decays, until producing a stable isotope of Pb. The number of α-decays associated with each cascade, and therefore the number of ^{4}He atoms produced (as the α-particle simply acquires two electrons), is as follows:

$^{238}\text{U} \longrightarrow {}^{206}\text{Pb} + 8\ {}^{4}\text{He}$

$^{235}\text{U} \longrightarrow {}^{207}\text{Pb} + 7\ {}^{4}\text{He}$

$^{232}\text{Th} \longrightarrow {}^{208}\text{Pb} + 6\ {}^{4}\text{He}$

$^{147}\text{Sm} \longrightarrow {}^{143}\text{Nd} + 1\ {}^{4}\text{He}.$

In AHe thermochronometry, we measure the modern abundance of the heavy, radioactive parent nuclides and the radiogenic ^{4}He and determine the time elapsed using the following age equation:

$$^{4}He = 8[^{238}U(e^{\lambda_{238}t} - 1)] + 7[^{235}U(e^{\lambda_{235}t} - 1)] + 6[^{232}Th(e^{\lambda_{232}t} - 1)] + {}^{147}Sm(e^{\lambda_{147}t} - 1). \tag{1.2}$$

If all of the ^{4}He produced since the formation of the crystal is retained, then t in the above expression would represent the time since crystal formation. However, ^{4}He is subject to thermally-dependent diffusion in apatite. This diffusivity, D/a^2, as a function of temperature, T, follows an Arrhenius relationship:

$$\frac{D}{a^2} = \frac{D_0}{a^2} * \exp\left(\frac{-E_a}{RT}\right) \tag{1.3}$$

where D_0/a^2 is the diffusivity an infinite temperature (called the "frequency factor") in units of s^{-1}, a represents a characteristic diffusion length scale, E_a is the activation energy in units of kJ/mol, and R is the universal gas constant. When the natural logarithm of the measured diffusivity is plotted against $1/T$, the resulting relationship is linear: the slope is proportional to $-E_a/R$ and in y-intercept is $ln(D_0/a^2)$. This slope and intercept are collectively known as the diffusion kinetics parameters and are material-specific, as has been demonstrated by experimental work in multiple fields over many decades. To convert these kinetics parameters into something more intuitive for the Earth sciences, thermochronologists calculate an equivalent "closure temperature" (T_c; ref. [2]), which follows:

$$\frac{E_a}{R * T_c} = ln\left(\frac{A * R * T_c^2 * \frac{D_0}{a^2}}{E_a * \frac{dT}{dt}}\right) \tag{1.4}$$

where A is a geometric constant and dT/dt is an assumed orogenic cooling rate, commonly ∼10 °C/Ma. Combining the production and diffusion of radiogenic ^{4}He in apatite provides a reasonable measure of how much time has elapsed since a sample cooled below the AHe closure temperature.

1.2 Application of AHe thermochronometry to rates of landscape evolution

The ability to constrain the amount of time elapsed since a sample cooled below the AHe closure temperature is particularly useful when considering the geothermal gradient in the Earth's crust. The closure temperature of ∼68 °C corresponds to crustal depths of ∼2–3 km, assuming a typical continental geothermal gradient of ∼25 °C/km. This means that one can quantify how much time passed as a sample was exhumed a fixed vertical distance (i.e., from a known depth to the bedrock surface), shown in Fig. 1.1.

The vertical distance per time yields the average exhumation rate over the measured interval. By sampling strategically at the Earth's surface, the AHe technique provides the means by which trace element chemistry of small mineral crystals can be used to quantify the rates of large-scale (i.e., kilometer-scale) landscape evolution over million-year (Ma), geologic timescales.

Chapter 2 of this dissertation presents a novel application of AHe thermochronometry to glacial detrital samples from the Patagonian Andes. This study presents average rates of erosion over the past ∼10 Ma in one portion of the Andes as the erosive regime transitioned from primarily fluvial to periodically glaciated. We conclude that the addition of flowing ice on the landscape leads to a transient fast pulse of glacial incision, followed by a decreased in erosion rate towards a balance with regional rock uplift rates.

1.3 Issues in AHe thermochronometry data interpretation

While AHe thermochronometry can be used to answer questions in Earth science, certain assumptions about crystal properties have been made in the interpretation of AHe data. Experimental work in the last two decades has demonstrated that the diffusion of ^{4}He in some ways depends on the amount of radiation damage present in an apatite crystal. Each time a ^{238}U, ^{235}U, ^{232}Th, or ^{147}Sm undergoes an α-decay, tens of keV are released and the direct effect is shown in Fig. 1.2. When ^{238}U undergoes spontaneous fission, another form of radioactive decay that happens ∼2 million times less frequently than α-decay, hundreds of MeV are released and the resulting damage zone is of sufficient size (roughly 20 µm) that it forms the basis for the apatite fission track thermochronometer. The damage associated

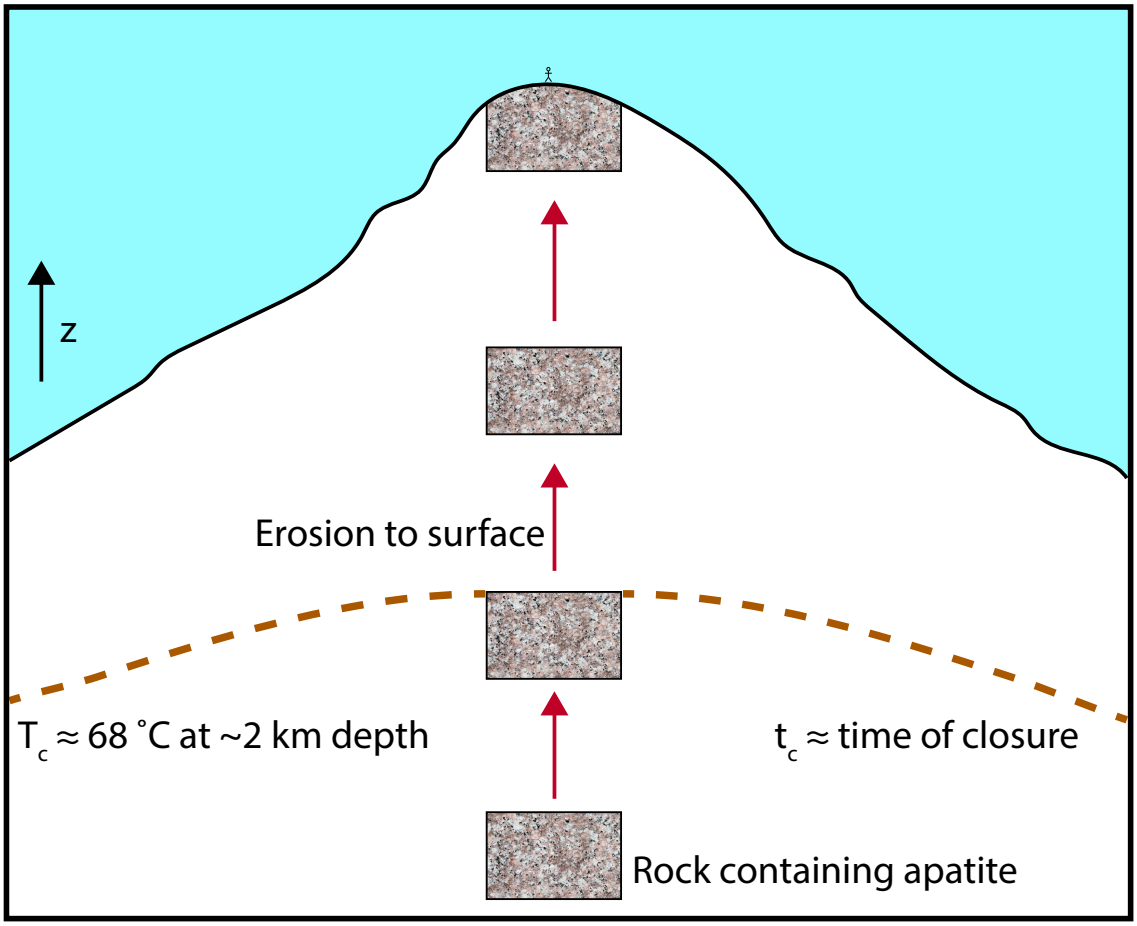

Figure 1.1: This image, redrawn and modified from ref. [3], shows a simplified cross-section of a mountain with an apatite-bearing rock being exhumed towards the surface. Surface topography can lead to vertical deflections of the closure isotherm, as shown (see ref. [4]).

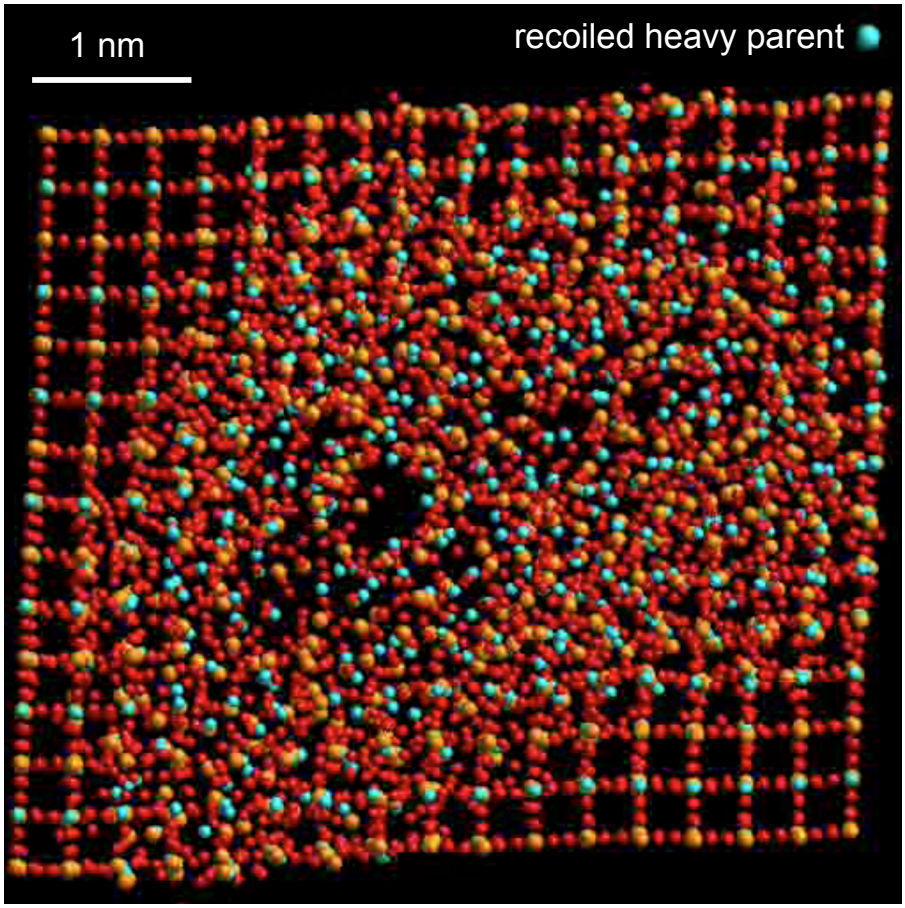

Figure 1.2: This image, modified after a snapshot of a simulation published in ref. [5], shows the modeled effects of α-decay on a crystal lattice, in this case the mineral zircon and the decay of ^{238}U. The displacement of hundreds of atoms over tens of nanometers will, in sum, influence the bulk diffusivity of He through the crystal. A similar phenomenon is thought to occur in the mineral apatite.

with the energy release from these radioactive decays are collectively known as "radiation damage."

In Chapter 3 of this dissertation, I challenge the radiation damage assumptions made in commonly-used AHe models (e.g., refs. [6, 7]). This chapter describes the development of a new model—the alpha damage annealing model (ADAM)—and concludes that, in specific cases like western Grand Canyon, the assumptions made about radiation damage can have a large impact on the interpreted age and timing of topography development. This chapter also demonstrates that simple cooling histories like the ones presented in Chapter 2 of this dissertation should not be substantially affected by this radiation damage assumption. In most cases, particularly those of rapid or steady monotonic cooling, the results from the

ADAM and previous models (e.g., the RDAAM [6]) are comparable.

While Chapter 3 demonstrates the important role of radiation damage annealing in the interpretation of AHe data, the ADAM is based on experimental work conducted on Durango apatite only (published in ref. [8]). Ensuring the applicability of these models to apatites sampled throughout the world will require additional suites of experimental work.

Chapter 4 presents one such attempt at this experimental work, aimed at quantifying the relationship between annealing time, annealing temperature, and resulting He diffusion kinetics in various samples of apatite. By re-measuring Durango apatite and testing apatite from the Sierra Nevada Batholith, this chapter shows that an individual sample's response to thermal annealing conditions likely does depend on the sample and is not universal to all apatites. This may be due to differences in chemistry (particularly anion chemistry, as has been demonstrated in the apatite fission track system; see discussion in ref. [9]), sample age, pre-existing crystal damage, or another parameter not listed here. Due to certain issues pertaining to sample volume and heating schedule design, the data presented in Chapter 4 are not sufficiently precise to calibrate a new radiation damage model, as done in Chapter 3, but they demonstrate nonetheless the importance of considering sample-specific diffusion kinetics and annealing behavior of apatites in future studies. Chapter 4 concludes with a summary of the types of measurements that will help ensure the viability and usability of the AHe thermochronometer for future studies in Earth science.

Chapter 2

Transient glacial incision in the Patagonian Andes from ∼6 to present

As of the publication date of this dissertation, the following chapter is **in press** as Willett, C.D., Ma, K.F., Brandon, M.T., Hourigan, J.K., Christeleit, E.C., and Shuster, D.L., *Science Advances*.

2.1 Abstract

We report a long-term, mountain-scale record of erosion rates in the central Patagonian Andes from >10 Ma to the present, which covers the transition from a fluvial to alpine glaciated landscape. Apatite (U–Th)/He ages of 72 granitic cobbles from alpine glacial deposits show slow erosion prior to ∼6 Ma, followed by a two- to three-fold increase in the spatially-averaged erosion rate of the source region after the onset of alpine glaciations, and a 15-fold increase in the top 25% of the distribution. This transition is followed by a pronounced decrease in erosion rates over the last ∼3 Ma. We ascribe the pulse of fast erosion to local deepening and widening of valleys, which are characteristic features of alpine glaciated landscapes. The subsequent decline in local erosion rates may represent a return towards a balance between rock uplift and erosion.

2.2 Introduction

Late Cenozoic cooling is marked by the onset of widespread periodic glaciations, starting in polar regions 25–10 Ma, and expanding to mid-latitude mountains and continental regions ∼6–2.5 Ma. There has been a long debate focused on the onset of the late Cenozoic "icehouse" climate and how it may have changed the size and shape of mountain ranges around the world, and affected the delivery of continental-derived sediment to the oceans (e.g., refs. [10–13]). This debate has been strongly influenced by studies of modern erosion, which show that, at local scales and short time intervals, temperate glaciers are usually more erosive

than rivers [10]. However, erosion faster than rock uplift would decrease the height of the glacial catchment relative to the equilibrium line altitude (ELA) and subsequently reduce the amount of ice discharge [14, 15]. This negative feedback operates at the scale of the glacial network and will therefore have a response time that is longer than that for the erosion processes operating along the bed of the glacier. This relationship suggests that the onset of mountain glaciations might include an initial phase of fast erosion, followed by a return to rates that are balanced with the local rates of rock uplift. The history of alpine glaciation in Fiordland, New Zealand over the last 2 Ma provides a possible example of this transient response, where the headward carving of deep valley troughs is accompanied by a flattening of the upland landscape [16], which would have reduced the amount of ice discharge.

Low-temperature thermochronology provides a way to study erosion at a regional scale and on a time scale of millions of years (e.g., refs. [13, 16–20]). The "cooling age" measures the transit time of a sample from a closure depth to the Earth's surface. Low-temperature thermochronometers are well suited for this kind of study because the closure depth is fairly close to the Earth's surface. For example, the (U–Th)/He apatite (AHe) system has an approximate closure temperature of 68 °C [19, 21], and an approximate closure depth of 2.5 km, assuming a surface temperature of 0 °C (as expected in a mountain setting) and an average continental thermal gradient of ∼25 °C/km.

Past studies of this kind have focused on bedrock cooling ages, which use bedrock samples collected from the modern landscape surface. Herein, we report detrital cooling ages, which supply samples from older bedrock surfaces, and thus provide a longer record of transit times. The transit time is estimated by the lag time [22], which is the difference between the cooling age of the detrital sample and the age of the deposit containing the sample. This approach carries the assumption that transport from bedrock source to the site of deposition is short relative to the transit time from the closure depth to the Earth's surface. Mountain landscapes generally lack settings with significant residence time, as judged by the age of upland deposits (see discussion in ref. [23]). Exceptions to this, such as the intermontane basins of the Central Andes, are easy to recognize and avoid. The lag-time concept is best applied in settings adjacent to the piedmont transition, where the erosive flux of the bedrock landscape is captured by aggradation in the piedmont region, a conclusion that holds for both fluvial and glacial transport processes.

Our study focuses on distinctive granitic cobbles, which are a widespread component of glacial deposits along the eastern flank of the Patagonian Andes and are known to have been sourced from the Patagonian Batholith, exposed in the core of the range (Fig. 2.1). These cobbles are used to estimate lag times, as defined by their AHe ages and the ages of the glacial deposits in which they are found. We report lag times from 72 cobbles, collected from four glacial deposits with deposition ages from ∼6 Ma to 18.5 ka, and compile 51 published AHe ages from the modern bedrock landscape. These data are used to construct a record of regional-scale erosion rates, extending back to 10 Ma and earlier. This record provides direct evidence about the transition of this mid-latitude mountain range from a fluvial landscape to a largely glacial one.

Conventional studies of bedrock cooling ages are limited to samples currently exposed

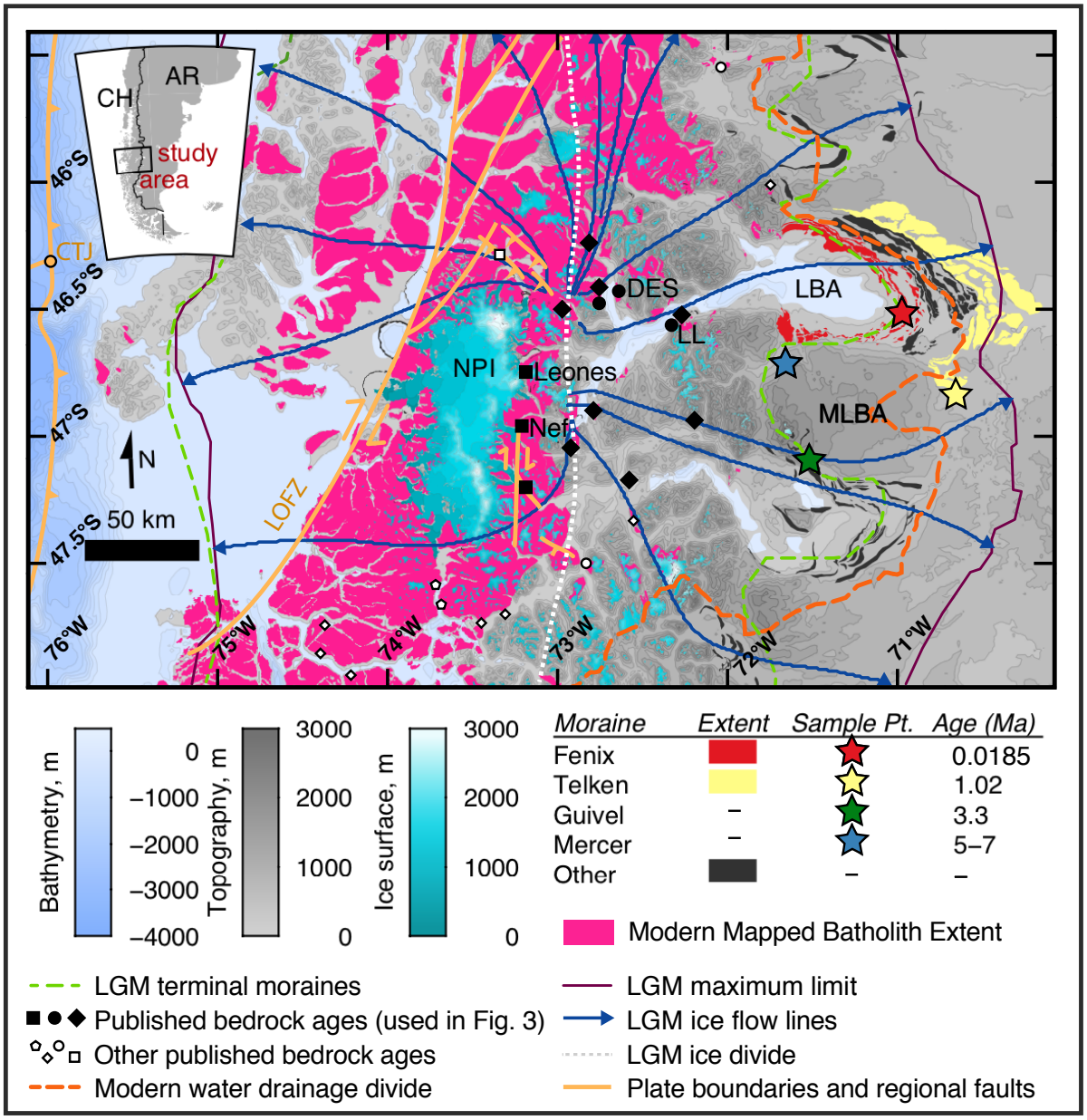

Figure 2.1: (Caption next page.)

Figure 2.1: **(Previous page.)** Study area with the modern exposure of the Patagonian Batholith, faults, and sample locations. LBA = Lago Buenos Aires, MLBA = Meseta del LBA, NPI = North Patagonian Icefield, CTJ = Chile Triple Junction, and LOFZ = Liquiñe-Ofqui Fault Zone. Geologic units other than the batholith and the glacial deposits are not shown. Extent of the Guivel and Mercer till exposures are not visible at this scale, as the meters-thick units are intercalated with basalt flows and outcrop in narrow bands that follow the contour of the meseta edge. The four sampling locations are marked by stars. Published bedrock AHe data (single samples or sample suites) are shown by squares [24], circles [25], diamonds [17], and pentagons [26]. Large black symbols indicate data that appear in the top panel of Fig. 2.4 and in Table 2.1. Small white symbols indicate other published bedrock ages, which are shown for reference but not used for our analysis. Faults in the region are shown in orange [24].

at the bedrock surface. The vertical sampling method can be used to estimate past erosion rates (e.g., refs. [24, 26]), but it generally provides a short record of erosion rates and it is known to produce biased results, as surface-topography-induced vertical deflections of the closure temperature isotherm will depend on the rate at which surface relief is increasing or decreasing [4]. In contrast, detrital ages provide a more comprehensive sampling of AHe cooling ages at the regional scale, and the interpretation is focused on the transit time from the mean closure depth to the mean surface elevation. As a result, this approach is not influenced by the change-of-topography biases associated with age-elevation transects.

2.3 Geologic setting and sampling locations

Glacial deposits are located along the entire eastern margin of the Patagonian Andes, and generally coincide with the termini of glacial advances (Fig. 2.1). Their exceptional preservation is due to the aridity and low topographic gradient in the eastern Patagonian foreland and, in some cases, due to burial by basalt flows, which are widespread south of 46°S. These deposits are typically conglomeratic, with rounded clasts set in fine-grained matrix. The clasts include volcanic, metamorphic, and granitic material, all of which can be traced to sources in the west within the higher part of the range. The proportion of granitic clasts is 5 to 20% in these deposits. The present surface exposures of the batholith have igneous ages of 155–115 Ma, and igneous pressures indicating initial emplacement at depths of ∼10 km [27]. There are minor intrusions with ages as young as 10 Ma [27], though these were emplaced well below the AHe closure depth. As a result, the AHe ages from these granites are related to cooling during erosion, and are not influenced by post-magmatic cooling. Fig. 2.1 shows ice flow lines, which were determined from a reconstruction of glacial topography during the Last Glacial Maximum (LGM). At its previous LGM size and position, the Patagonian ice sheet transported material from the exposed batholith to the locations of the sampled

deposits.

Our study site is located to the east of the Chile Triple Junction (CTJ) (Fig. 2.1), where the Nazca ridge, which separates the Nazca and Antarctic plates, subducts below the South American plate. Hypotheses regarding the tectonic and thermal effects of the CTJ include "collision deformation" by the Nazca ridge as it subducts [28], heating and/or dynamic uplift caused by an "asthenospheric window" [25], and strike-slip slivering of the forearc north of the triple junction [24]. As of yet, there is little direct evidence to support these ideas. Recent studies [24, 29] infer that there are many local strike-slip faults east of the CTJ, but there is no direct exposure of these structures. One of these faults, located at the southern end of the Liquiñe-Ofqui fault zone (LOFZ), has direct evidence of offset [30]. Most other features ascribed to the LOFZ are based primarily on the linear appearance of fjords.

In contrast to proposed CTJ-associated tectonic and thermal effects, a recent paleotopography study [27] shows that the topography around 46°S, the latitude of the CTJ, has been steady over the last 60 Ma. In another nearby study, the authors demonstrate that the region east of CTJ has been a site of relatively slow erosion and uplift over the last 6 Ma, except for a period of fast valley incision associated with the onset of glaciation [26]. The evidence for glacial incision is widespread, and most markedly demonstrated by the deep fjords and over-deepened lakes that characterize this region, with maximum depths extending to 1468 m below sea level [26]. Current models for glacial erosion show that fjords and over-deepening can form only where the background rate of rock uplift is low [31]. The Patagonian Andes are crisscrossed by a dense network of fjords, and our study area is flanked to the east by Lago Buenos Aires, an over-deepened glacial lake with maximum depth of 586 m. Finally, regional-scale thermochronologic data show that samples south of the CTJ yield older cooling ages relative to those to the north (e.g., ref. [17]). Proposals for ridge collision and dynamic topography predict a northward propagating region of young uplift and erosion, which would yield the opposite of what has been observed. This summary is meant to highlight an ongoing debate in this area about the role of the CTJ.

Based on an assessment of the available information, we conclude that the design of our experiment and the analysis and interpretation of the results are not influenced by the issues outlined above. Our study area lies ∼200 km east of the CTJ, and is east of the easternmost proposed strike-slip fault [24] (Cachet fault, Fig. 2.1). Thermal and thermochronologic modeling [26, 29, 32] indicate that the hot conditions associated with subduction of young lithosphere in the vicinity of the CTJ are too deep and too recent to have affected the shallow thermal field (<65 °C) associated with the AHe cooling ages used in this study. Some authors assume that thermochronologic ages in the Patagonian Andes can be used as a direct record of tectonic uplift [24, 25, 29], and yet it is well known that cooling ages record exhumation not uplift [33]. Erosional exhumation is controlled by surface processes, such as fluvial incision, landsliding, and glacial abrasion. Tectonic processes can play a role in maintaining topography, but are generally not important over the short time scale and modest amounts of erosion documented in our study.

We sampled four glacial deposits in the vicinity of Lago Buenos Aires and compiled published AHe bedrock ages (Fig. 2.1). The two oldest deposits are interbedded within

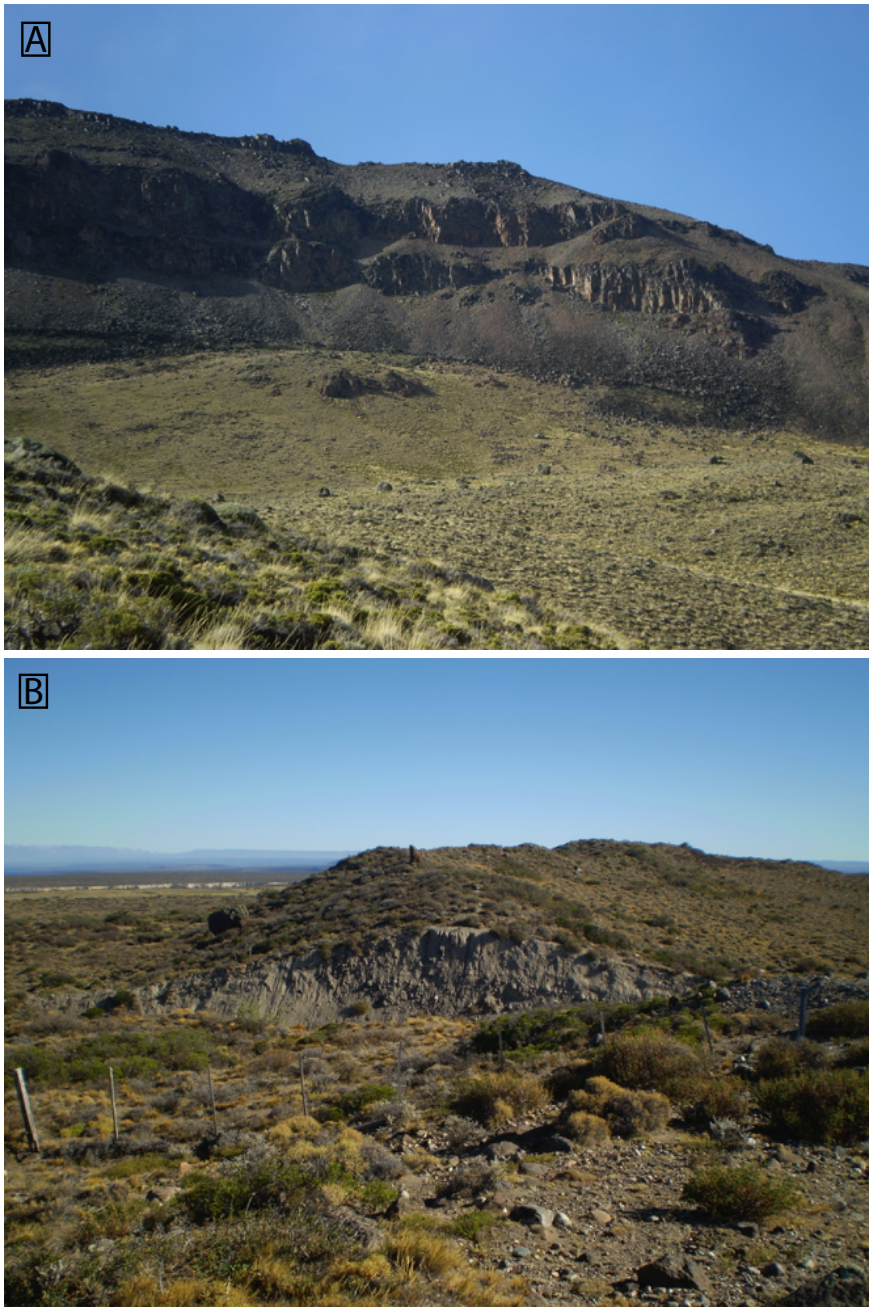

Figure 2.2: Example photos of till and moraine deposit morphology. (A) Outcropping of the Guivel till. Photograph is taken from the southwest. (B) Road cut through Fenix I moraine. Photograph is taken from the south.

a sequence of tabular basaltic flows that underlie the Meseta del Lago Buenos Aires. The oldest, herein referred to as the "Mercer" till (informal name), is exposed on the northwest margin of the Meseta Lago Buenos Aires (MLBA) and is bracketed by basalt flows with ages of 4.7 and 7.3 Ma [34, 35]. The "Guivel" till (informal name, 3.3 ± 0.1 Ma [36]) crops out on the southern margin of the meseta. Cobbles from these deposits were collected well below (>10 m) the overlying basalt flow and with no evidence of nearby feeder dikes or sills, which ensures that the AHe ages from these samples were not thermally reset.

The next youngest deposit is Telken VII (1.016 ± 0.01 Ma), which is exposed as a till-covered hill and marks the largest glacial advance in the area, known as the Great Patagonian Glaciation [37]. The youngest glacial deposit is Fenix I (18.5 ± 0.4 ka), exposed as a sharp-crested moraine with striated and glacially polished cobbles [38, 39]. Note that the four deposits span approximately 75 km north to south and were therefore likely derived from similar source areas within the core of the range (see Fig. 2.1). Examples of the sampled till and moraine morphology are shown in Fig. 2.2. A collection of 51 published bedrock AHe ages (Table 2.1, locations shown in Fig. 2.1) are used here to estimate the distribution of AHe lag times for the modern landscape and extend the lag-time record to the present day.

To better resolve the depositional age of the Mercer till, we use a deep-ocean temperature record [40] (Fig. 2.3), which is based on the global benthic foraminifera δ^{18}O record and corrected for the associated evolution of polar ice volumes. Deep-ocean temperature is a record of time-averaged, high-latitude, sea-surface temperature [41] and provides a useful proxy for cool and warm events in our study area. The three well-dated glacial deposits coincide with extreme cold events in this record. We therefore infer that the Mercer deposit was also associated with an extreme cold event. Given the bracketing ages provided by the basalt flows, the likely event would have been at ∼5.7 Ma (Fig. 2.3).

Fig. 2.1 shows the modern water divide for this portion of the Andes as well as the ice divide and ice flow lines associated with the LGM ice sheet, as determined from ref. [42]. With the modern topography, deeply incised glacial valleys allow westward drainage across the full width of the range, far east of the highest peaks. The older sampled glacial deposits may have been deposited in association with a more western water divide. However, the water divide likely reached its present position by the time that the younger two sample locations were deposited. Therefore, cobbles in the younger deposits could only have been transported from their western sources during glaciations. This conclusion likely holds for all four sampling locations, as each is a glacial deposit. The ice divide depends on the glacier shape and size, but we use the LGM ice divide as an approximation for the location of older ice divides. On this basis, we estimate that the glacial catchments for our sample locations were ∼10,000 km^2 for the older two deposits, and 5,000 km^2 for the younger two. The bedrock sample locations straddle the ice divide, and cover an area of 6,500 km^2.

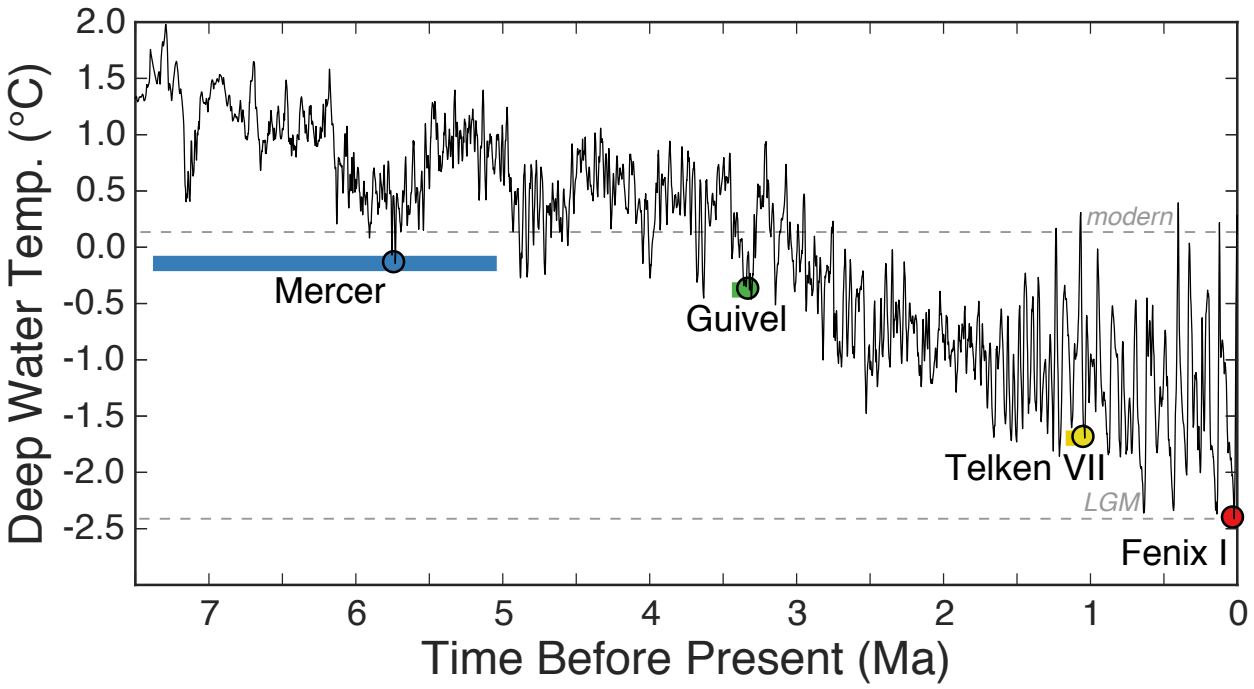

Figure 2.3: Regional climate record and deposit ages. Black curve is deep-ocean water temperature from an ice-volume-corrected model based on the global benthic foraminifera δ^{18}O record [40]. Color rectangles indicate the depositional age constraints on the sampled glacial deposits. Circles indicate intersection of the lowest temperature associated with the depositional age range for each deposit.

2.4 Results

Lag-time results for all samples are shown in Fig. 2.4 (see Materials and Methods for details). Vertical red ticks show AHe ages for each cobble and modern bedrock sample, and the blue curves show probability density distributions for each glacial deposit, as estimated by the kernel density method [43]. Fig. 2.4 and Table 2.2 include estimates of the mean and first quartile lag times for each of the distributions, along with their 2 SE (standard error) uncertainties. We use the harmonic mean for the detrital samples, given that they are sampled by yield and are therefore affected by local variations in erosion rates. The arithmetic mean is used for the bedrock samples given that they are sampled in space (see Materials and Methods for details). Also, note that the means include all lag times in the distribution, including some lag times that are greater than the range shown in the plots. Table 2.3 and Fig. 2.5 provide a full report of all AHe grain ages.

The lag-time distributions show a simple evolution with decreasing age. This pattern suggests that, prior to the onset of alpine glaciation (~6 Ma), rates of erosion were slow. Erosion rates increased by 3.3 Ma, and then returned towards slow at 1.02 Ma, 18.5 ka, and

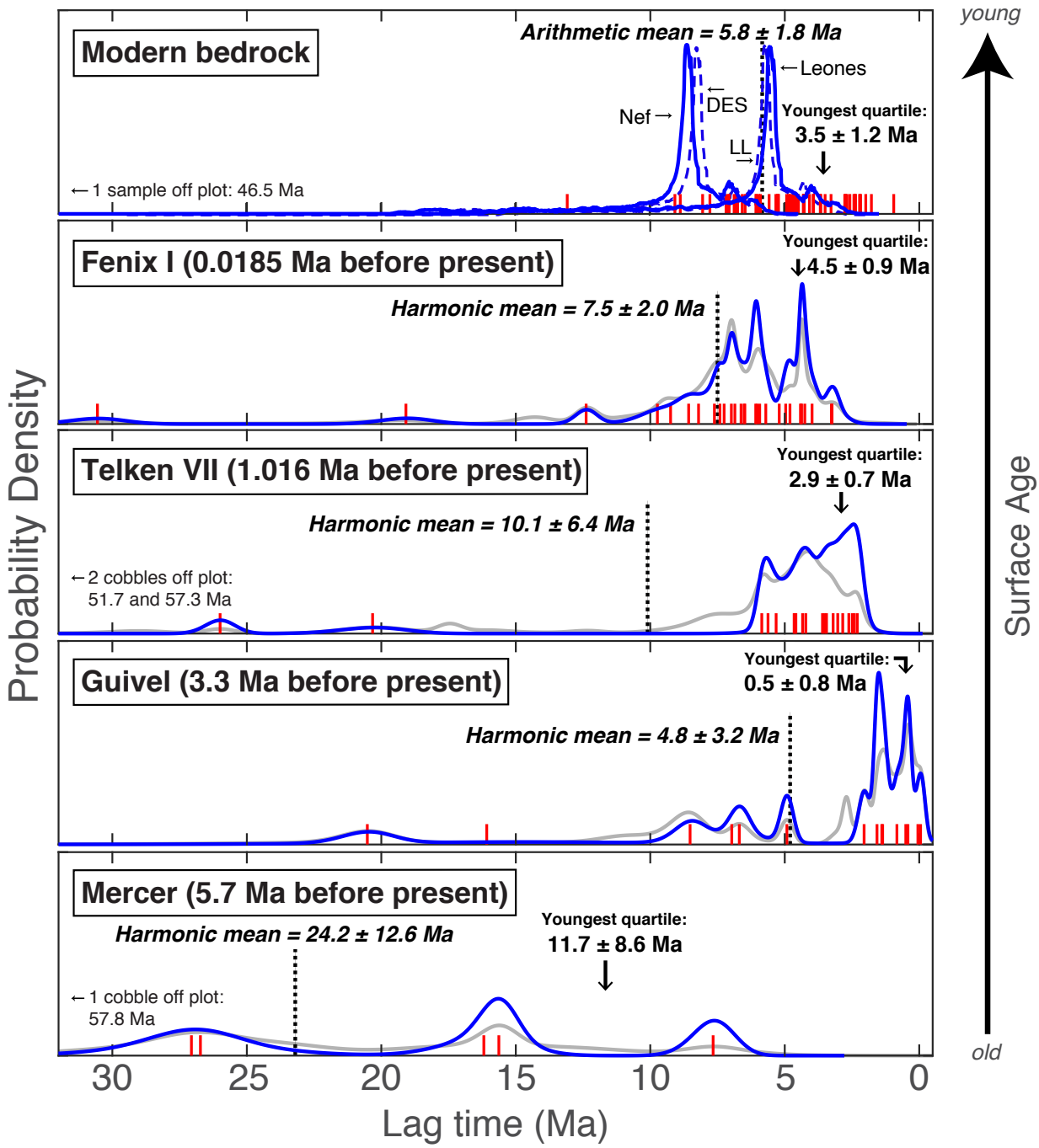

Figure 2.4: (Caption next page.)

Figure 2.4: **(Previous page.)** AHe lag times for samples in this study. Vertical red ticks indicate the lag times of individual cobbles reported herein, and published modern bedrock samples [17, 24, 25]. Blue curves in lower four panels are lag-time probability density plots [43] as estimated by AHe minimum ages for each cobble. Solid blue lines in the top panel represent predicted probability density curves for modern bedrock using Leones and Nef age-elevation relationships (AERs) from ref. [24]; dashed blue lines represent predicted probability density curves for modern bedrock using DES and LL AERs from ref. [25] (see Results and Materials and Methods for details; AER locations shown in Fig. 2.1). Vertical dashed lines indicate relevant mean values, and black arrows indicate first-quartile values for the lag-time distributions. The uncertainties are ±2 standard error, and the uncertainty for first quartile values determined numerically using a bootstrap method.

the present day. The oldest deposit (Mercer) has a mean lag time of 24 Ma and a first-quartile lag time of 12 Ma. In contrast, the distribution for the next deposit, Guivel, has mean and first-quartile lag times of 5 and 0.5 Ma, respectively. The Telken VII distribution has mean and first-quartile lag times of 10 and 3 Ma, and the distribution from Fenix I has mean and first-quartile lag times of 8 Ma and 4.5 Ma. The distribution of the bedrock samples has mean and first-quartile lag times of 6 and 3.5 Ma. The bedrock sample mean is significantly lower than that for the Fenix I deposit, likely because bedrock samples tend to be collected at lower elevations where access is easiest, but where AHe cooling ages tend to be youngest.

We use four published age-elevation transects of modern bedrock samples [24, 25] to provide a more direct comparison with the detrital samples. The transects provide local estimates of the dependence of AHe cooling ages on modern elevation. We used a digital elevation data set paired with sub-icefield bedrock elevation information [44] to extract elevation data for the portion of each ice catchment underlain by batholith (see Fig. 2.1). Similar to ref. [45], we multiplied the resulting hypsometry by each age-elevation relationship, then smooth and normalize to generate probability density curves of AHe lag times for these regions, as shown in the top panel of Fig. 2.4. In comparison, the individual bedrock samples and the cobble samples from the Fenix I deposit show a larger range, both towards smaller and larger lag times, than indicated by these estimated modern bedrock probability density curves. This result suggests that there is a significant spatial variation in erosion rates across the study region.

The black line in Fig. 2.6 (and in Fig. 2.7 at a more optimal scale) shows the evolution of the spatially averaged erosion rates through time. This curve was estimated by first converting the lag-time estimates into an average erosion rate for the age interval covered by that lag time. This conversion was done using a modified version of the *age2edot* program [46], which finds a simultaneous solution for the thermal structure of the upper crust and the erosion rate at the surface as a function of the observed lag time and the thermally sensitive

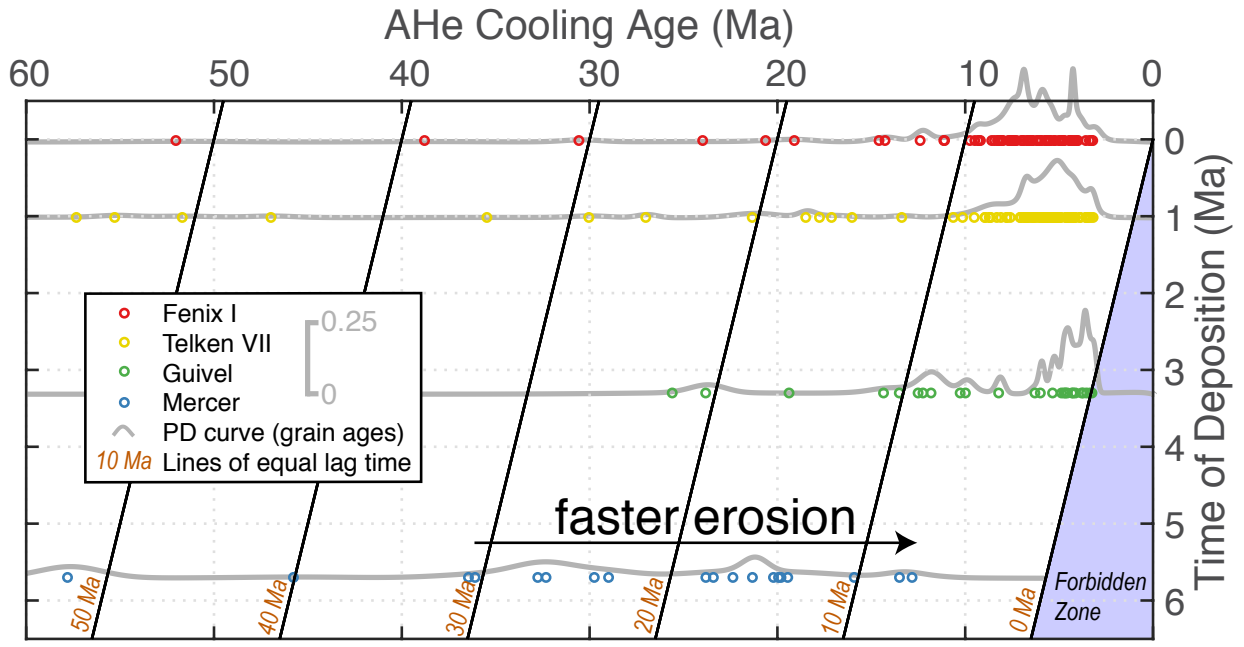

Figure 2.5: Lag-time plot showing all AHe ages (including all replicate ages). Color symbols indicate AHe ages of individual crystals. Gray curves are probability density curves for each deposit, estimated using all of AHe grain ages for the deposit but weighted on a per-cobble basis (i.e., replicate ages for each cobble sum to have a unit sample weight). The diagonal lines show lag-time contours.

diffusion properties of the AHe thermochonometer (see Materials and Methods for details). Sensitivity testing indicates the erosion rates vary by about ±15% over the plausible range of the thermal and diffusive parameters used in the *age2edot* calculation. Note, however, that this source of uncertainty would shift the entire curve. In other words, the relative variations in the erosion rates shown in Fig. 2.6 come from the lag-time data alone, and not from the *age2edot* calculation. Fig. 2.8 shows the erosion rates estimated for all of the cobble lag-time data as a function of geologic age. The spatially averaged erosion rate curve (Figs. 2.6 and 2.7) was determined by averaging the erosion rate estimates from Fig. 2.8 at 0.5-Ma steps along the age axis. The spatially averaged erosion rate curve includes a fair amount of smoothing due to the fact that the individual erosion rate estimates are averages over the duration of the lag-time interval. The smoothing decreases with decreasing lag times and increasing erosion rate. As a result, the temporal resolution of this erosion rate curve tends to increase with decreasing age.

The spatially averaged erosion-rate curve (Figs. 2.6 and 2.7) shows that, prior to the onset of alpine glaciation at ~6 Ma, the spatially averaged erosion rate for the source region was ~0.06 to 0.1 km/Ma. After the start of glaciations, this erosion rate increased to a steady value of ~0.23 km/Ma. This estimate for the mean erosion rate over the past 6 Ma

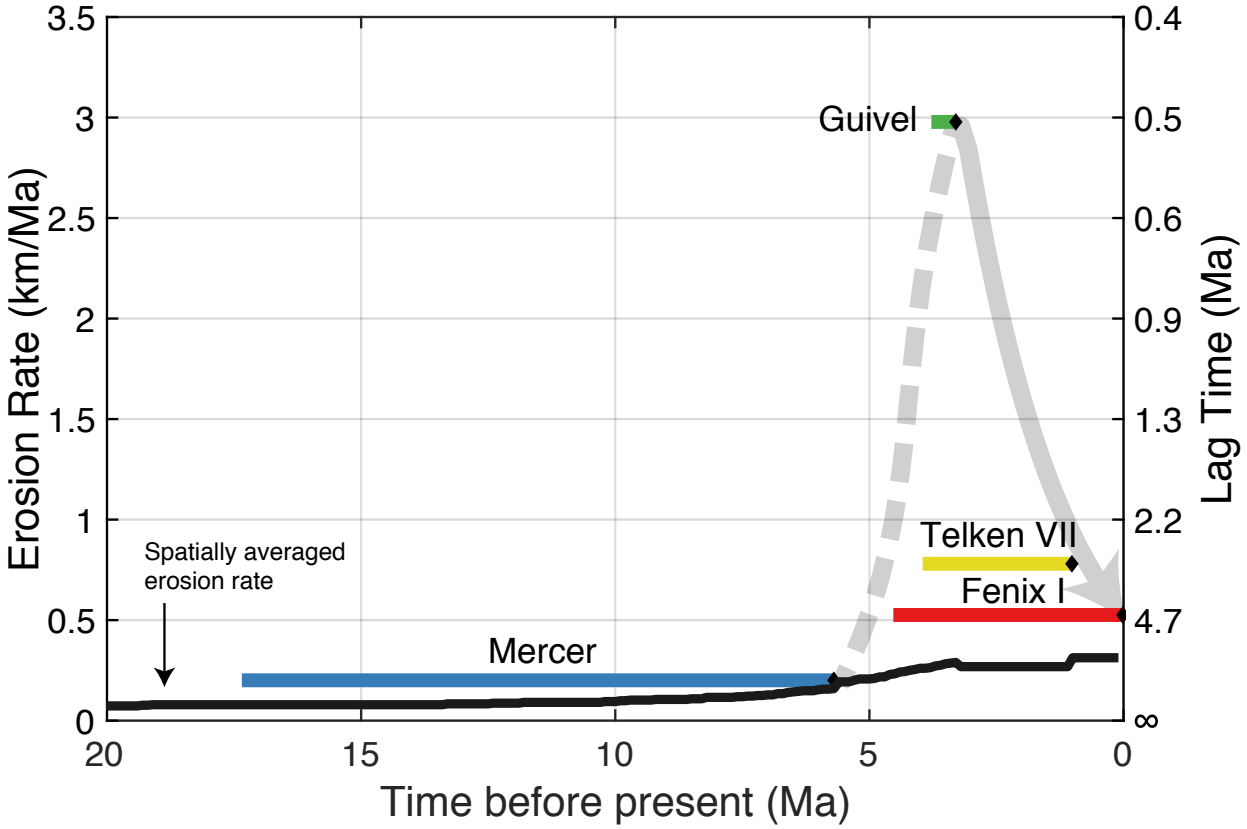

Figure 2.6: Summary of the evolution of erosion rates in the source region sampled by the AHe cobble ages. The black curve shows the evolution of the averaged erosion rate within the source region (Fig. 2.7 shows a larger plot of this curve). The color bars show the fastest rates, as represented by the first-quartile value of the erosion-rate distribution for each deposit. The horizontal extent of each color bar shows the lag interval (AHe closure to deposition) for each of these "fastest erosion" estimates. The gray curve shows, in schematic fashion, the evolution of the fastest eroding part of the source region. The right-hand axis shows the correspondence between lag time and erosion rate, as determined from the *age2edot* program (see Fig. 2.10).

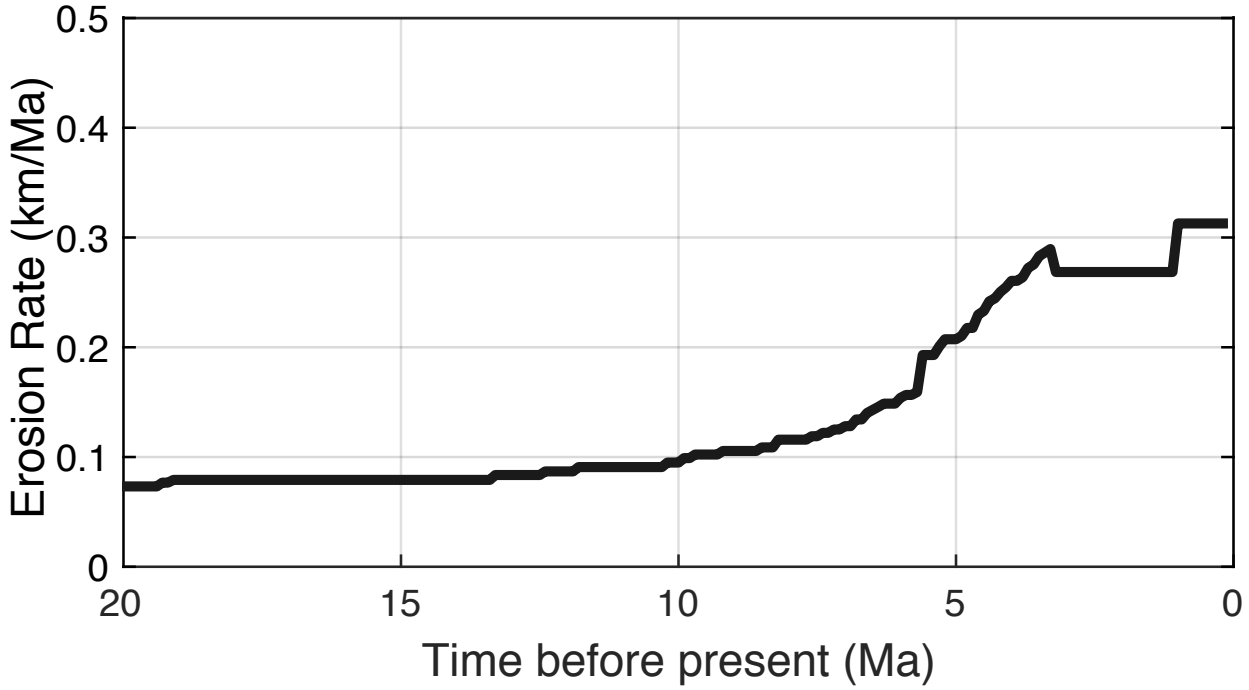

Figure 2.7: Average erosion rate curve from Fig. 2.6.

matches well with previous estimates (0.2 to 0.3 km/Ma) for this time interval, as determined from regional studies of bedrock cooling ages [17, 20].

To gain further insight into the variable rates of erosion across the landscape, we plot the evolution of the *fast*-eroded cobbles from the source region. For this purpose, we use the value at the first quartile for each lag-time distribution (arrows in Fig. 2.4). Fig. 2.6 shows colored bars that indicate the age interval for the first-quartile lag time for each deposit. The gray curve shows an interpretation of the evolution of this "fastest-eroding" component: these estimates begin with a ∼0.2 km/Ma erosion rate prior to the onset of alpine glaciation, increasing to ∼3 km/Ma at 3.3 Ma, and then declining to <0.8 km/Ma between 3.3 and 1.02 Ma, and to 0.5 km/Ma between 1.02 Ma and 18.5 ka. The modern bedrock samples indicate a similar spatially averaged erosion rate of 0.5 km/Ma for the first-quartile lag time (Table 2.2). These data indicate a nearly 15-fold increase in the fastest-eroding component with the onset of glaciation, followed by a return to rates similar to those prior to the onset of glaciation.

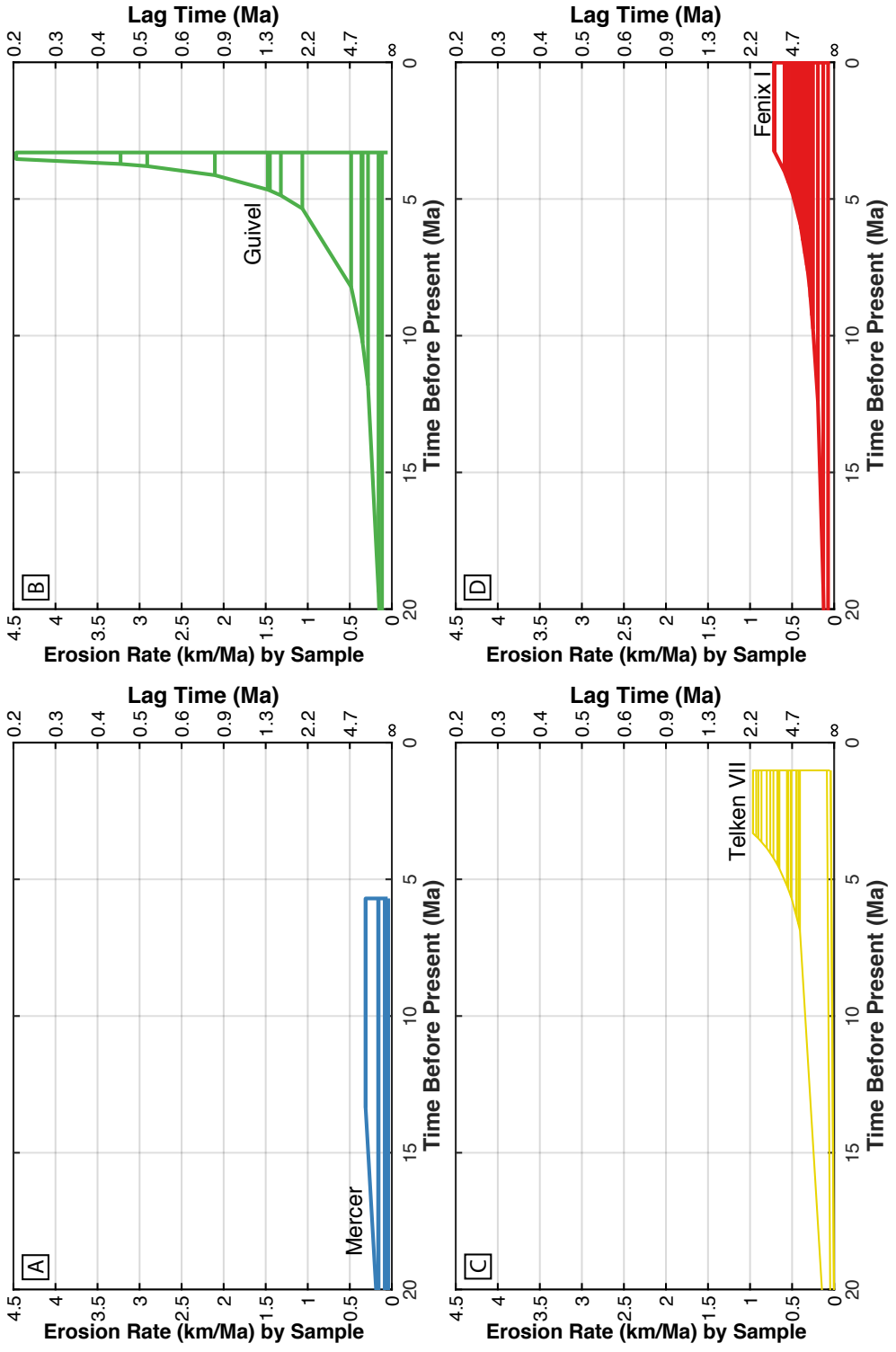

Figure 2.8: (Caption next page.)

Figure 2.8: **(Previous page.)** Color bars showing lag intervals for all AHe cobble ages in our study, plotted separately for each deposit. Each color bar starts at the time of AHe closure and ends at the time of deposition. The vertical position of each color bar represents the estimated erosion rate for that AHe cobble age, as determined by the *age2edot* relationship (Fig. 2.10a). The corresponding lag time is shown on the right axis. These plots illustrate how the spatially averaged erosion rate curve (Fig. 2.6) was calculated. For example, the spatially averaged erosion rate at 10 Ma before present is estimated by calculating the harmonic mean of erosion rates for those color bars that pass over then 10 Ma point on the x-axis, with data for all four plots combined for this estimate.

2.5 Discussion

This study provides a record of the evolution of erosion rates during the transition from fluvial to glacial conditions in the Patagonian Andes. From these observations, we infer that glaciation did not result in uniformly fast erosion, but rather varied spatially across the landscape. We infer that early glaciations would have deepened the pre-existing, fluvial, low-concavity valley profiles. Headward propagation of valley incision along longitudinal profiles is known to cause transient increases in local elevation gradients and relief and will lead to ice sliding velocities driving higher incision rates [16]. However, as erosion propagates headward, the area of the ice catchment above the ELA is reduced, resulting in slower subsequent glacial erosion [14, 16, 39]. Our conclusions are in agreement with ref. [26], which used $^4He/^3He$ apatite data and thermo-kinetic modeling to estimate the formation timing of the exceptionally deep valleys in the Central Patagonian Andes, and concludes that valley incision probably occurred shortly after the onset of glaciations in the Patagonian Andes. Their study indicates incision sometime between 10 and 6 Ma [26], while the results of this study indicate sometime between 6 and 3 Ma.

If our interpretation is correct, then one might expect the initial pulse of fast incision to be followed by decay to rates that balance with rates of rock uplift. In geomorphic systems, a return to steady state commonly occurs in an exponential fashion. Fitting an exponential to the first-quartile erosion rates over the last ∼4 Ma (solid gray curve, Fig. 2.6) indicates an exponential time constant of ∼2 Ma. If correct, this relationship would predict that 95% progress to steady state would take ∼6 Ma (3 times the exponential time constant). As a result, we might expect that the Patagonian Andes are still in transition to a steady state. In comparison, other mid-latitude mountain ranges with more recent glacial onset (e.g., the Alps at 2.6 Ma [47]) may be a few millions of years from balance between erosion and rock uplift. Our finding is consistent with recent modeling results that place landscape response to glaciation between a few tens of thousands and a few millions of years [48].

The fastest rates of erosion in our study, ∼3 km/Ma, are among the highest rates of long-term glacial erosion observed in the geologic record using AHe thermochronometry [13, 49]. Comparably high rates and magnitudes of glacier valley incision occurred in both the

Northern and Southern Hemispheres, but during the Pleistocene: British Columbia, Canada (51°N) >5 km/Ma at ∼1.8 Ma [50]; Rhône Valley, Switzerland (46°N) 1–1.5 km/Ma at ∼1 Ma [51]; Fiordland, New Zealand (45°S) ∼5 km/Ma between ∼2–1 Ma [16]. Rapid incision occurred earlier at higher latitudes in both hemispheres: an increase in glacial erosion rates ∼200 km south of this study area occurred between 10 and 5 Ma [26]. The direct relationship between latitude and glacial onset appears to broadly hold in the Southern Hemisphere, as shown in the Andes and continuing onto the Antarctic Peninsula, where glacial onset was recorded at 33.5 Ma [52]. Study of this long-lived, northward transition to icy conditions over the late Cenozoic helps develop an understanding of the complex interactions between climate, erosion, and tectonics both in the Southern Hemisphere and globally.

2.6 Conclusions

The data set presented in this study resolves systematic changes in mountain-scale erosion rates over a ∼6 Ma response to glacial conditions in a mid-latitude mountain range. We demonstrate that, in one location, glacial erosion takes on a range of rates over space and time and this may not typically be captured by bedrock studies due to sparse sampling. In this study location, a 15-fold increase in the highest (i.e., first quartile) erosion rates during major topographic adjustment, followed by a decrease in these erosion rates, indicates that there is a measurable transient landscape response to the onset of glaciation. The measured erosion rate is not simply due to the presence or absence of actively sliding alpine glaciers, but is a function of the relief and shape of the valley profiles over time and the magnitude of the ice flux. The fastest erosion occurs when flowing ice initially appears on a landscape and the transition time to an equilibrated glacial landscape is on the order of 4 to 6 Ma. As a result, assuming comparable conditions, mountainous landscapes that have been more recently glaciated may still be in a phase of incision and topographic adjustment and may require several million more years of periodic glacial conditions to reach balance between erosion and rock uplift.

2.7 Materials and Methods

2.7.1 AHe thermochronometry

From four deposits, we measured AHe ages for 6 to 29 cobbles per deposit. We collected cobble-sized samples (6–10 kg each) of granite or granodiorite from the deposits to ensure (i) provenance from the Patagonian Batholith and (ii) the occurrence of apatite for AHe dating. The Mercer till yielded only six dated cobbles (due to poor apatite quality), while the other deposits each contained >15 dated cobbles. The uneven sample count might influence our ability to detect the onset of glacial erosion, but we infer that the lack of young lag times (<∼7.5 Ma) in the oldest deposit (Mercer) provides a reasonable sampling of slow erosion

rates prior to the onset of glaciation. That is, the faster erosion associated with glaciation ensures that the onset of glacial erosion should be well represented by the sampled cobbles.

We isolated apatite crystals using conventional mineral separation methods and individual crystals were selected for suitability for AHe analysis (euhedral crystals, free of visible inclusions). Molar abundances of U, Th, Sm and ^{4}He were measured using isotope dilution. A total of 206 crystals from 72 cobbles were analyzed at UC Santa Cruz and the Berkeley Geochronology Center (Table 2.3). Measured AHe ages can yield variance between aliquots that exceeds analytical uncertainty, primarily due to undetected inclusions of U- and Th-bearing minerals, variations in crystal size, and zonation of the parent nuclides. These discordance problems generally introduce an old-side bias to the measured AHe age. When possible, we measured replicate AHe ages in order to screen out older discordant ages. On average, we measured three replicate ages per cobble: some cobbles have up to six replicate ages, and 22% of the cobbles have only one AHe age. The cobbles with replicated ages indicate that discordance was present in only 1 out of 5 cobbles; we therefore believe that issues related to discordance are limited to only about 4% of our cobble ages. Furthermore, AHe data from previous studies in the same region (e.g., refs. [24, 26]) show little discordance in grain ages. For those cobbles with multiple replicate ages, we use a maximum-likelihood method to estimate a minimum age [53], defined as the age of the youngest fraction of grain ages that are statistically concordant as defined by analytical errors. This calculation assumes that the replicate AHe ages are a two-component mixture, consisting of young grain ages free from biasing effects, and older grain ages that are randomly affected by biasing effects.

Helium diffusion in apatite is estimated using numerical integration with time-invariant diffusion parameters [54]. We have not accounted for the potential influence of radiation damage on He diffusivity (more detail on this point below).

2.7.2 Probability density estimates

The probability density curves in Fig. 2.4 and Fig. 2.5 were estimated using the kernel density method [43] with the kernel set to 2.4*SE, where SE is the standard error for the represented discrete observations (e.g., grain ages, minimum ages, etc.). The recommended kernel size is 0.6*SE value [43], but we have selected a larger size for our study in order to emphasize the general features of the probability density distributions. A probability density curve should integrate to unit probability mass. In keeping with this constraint, each probability curve is normalized so that it has the same integrated area as the others.

Fig. 2.9 compares two different estimates of the probability density curves. The blue curve, which is the one shown in Fig. 2.4, is based on the minimum ages from the replicate ages for each of the cobble samples. The gray curve is determined using all of AHe replicate ages with a weighting applied to ensure unit weight for each cobble sample. The comparison shows that these two methods give similar results.

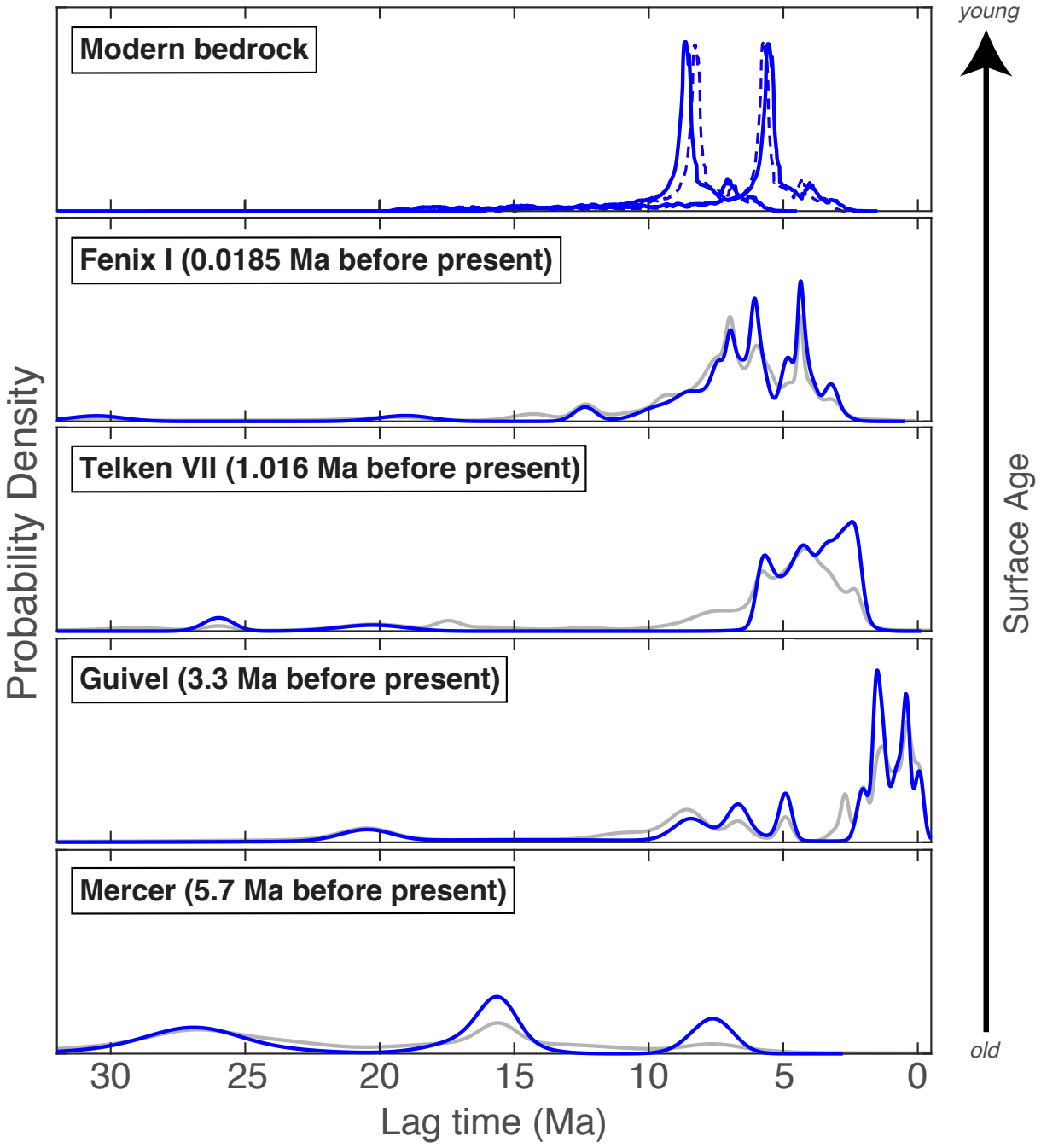

Figure 2.9: (Caption next page.)

Figure 2.9: **(Previous page.)** Simplified version of Fig. 2.4 comparing the technique used to generate the probability density curves in the lower four panels. Blue lines are based on the cobble lag time while gray lines use all individual AHe grain ages, weighted on a per-cobble basis (i.e., replicate ages for each cobble sum to have a unit sample weight). The close agreement between the blue and gray curves demonstrates that our minimum-age estimation has only a minor influence on the estimated distributions. Note that the gray curves in this plot are the same as the gray curves in Fig. 2.5.

2.7.3 Converting lag time to erosion rate

We used the *age2edot* program to convert lag times (i.e., the AHe age minus the deposition age) into erosion rates [46]. The *age2edot* model does not use a prescribed age-elevation relationship, but instead determines an average erosion rate as a function of the cooling age, the closure properties of the AHe thermochronometer, and the 1-D thermal structure of the upper 30 km of Earth's crust, all of which are sensitive to the erosion rate. For this calculation, we assume that the depth to the closure isotherm can be treated in a quasi-steady fashion, which is consistent with the fast response time ($<\sim$1 Ma) of the AHe system to changes in erosion rate [22]. This calculation also accounts for the thermal-magmatic structure of the region, as guided by a recent magmatic arc model [55], which postulates that the thermal structure of the arc is strongly controlled by the emplacement of mantle-derived basaltic melt into the lower crust of the arc. Arc volcanoes occur on a ~100 km spacing across the region, but models of subduction magmatism indicate that there is likely much more widespread melt within the lower crust at depths greater than 20 to 30 km [22, 55]. This effect is accounted for in the *age2edot* calculation. One might anticipate that the shallow crust might be strongly influenced by feeder dikes associated with volcanoes. Thermal analysis, however, shows that, in the shallow crust, potential resetting around a feeder dike would be limited to a region on the order of the thickness of the dike [56]. We therefore conclude that thermal resetting is relatively rare in the shallow crust and our AHe lag-time data is primarily a result of cooling during erosion and can be used to estimate erosion rates.

The *age2edot* program represents the thermal structure of the upper crust using an infinite layer with fixed boundary temperatures. The thermal diffusivity and thermal conductivity of crust are set using a new relationship [57] that accounts for the temperature sensitivity of these properties in typical crustal rocks. The volumetric heat production is set to a uniform value of 2 $\mu W/m^3$, which is the average for the Sierra Nevada Batholith [58]. The upper boundary corresponds to the local mean elevation of the land surface (~1000 m), and is set to a temperature equal to the long-term atmospheric temperature at that elevation (~0 °C). The lower boundary is set at 20 km depth and ~800 °C, the approximate solidus temperature for a granodioritic crust at 20 km [56]. The crust beneath the source region is likely mainly composed of Patagonian Batholith, hence the choice of the granodioritic solidus temperature.

For comparison, the more pelitic composition of the schist belts exposed on the flanks of the range would have a solidus temperature of ∼700 °C at 20 km depth [56]. Erosion is represented by a vertical velocity through the layer. The presence of melt below the basal boundary ensures that material crossing that boundary is always at the solidus temperature. We solve for the lag time of the AHe closure surface as a function of the thermal properties of the crust, the diffusion properties of the AHe system, and the erosion rate.

The depth to the top of the lower-crustal melt zone is controlled by the flux rate of the mantle-derived melt, which in turn is controlled by the subduction velocity and the corner flow velocity within the supra-slab mantle [59]. The top of the melt zone, which marks the shallowest region in the crust with coexisting melt and crust, should remain at a fixed temperature, as defined by the selected solidus curve. The depth of this boundary is mainly controlled by conductive heat transport through the upper crust. Thus, surface erosion will cause the crust to move towards the surface, but the top of the melt zone should remain at a steady depth. This situation is correctly represented in the *age2edot* model by a fixed basal boundary condition, which ensures that as material rises through that boundary, it enters into the model domain at the temperature set for the boundary.

Fig. 2.10A shows that the temperature and depth of the basal boundary condition have little influence on the predicted relationship between erosion rate and AHe cooling age. Fig. 2.10B shows the dependence of closure depth on erosion rate. The estimated closure depth for our cobble samples is between 2.4 km for long lag times and slow erosion and 1.1 km for short lag times and fast erosion. To verify the validity of a quasi-steady state solution for this setting, we have run a full transient calculation of the temperature history of a sample and the evolution of the sample AHe age (Fig. 2.11). The steadiness of the closure depth is measured by the velocity ratio (vertical axis of Fig. 2.11), defined as the ratio of the velocity of the closure surface relative to the vertical material velocity (equal to the erosion rate). The velocity ratio shows high values following the onset of erosion, which indicates unsteady migration of the closure surface, but the ratio drops back down to nearly zero within 2 Ma.

We estimate helium diffusion in apatite using time-invariant diffusion parameters [54]. Radiation damage is unlikely to be a significant source of variance in diffusion parameters given that most AHe ages are relatively young, and all samples are likely to have only experienced cooling (i.e., no reheating) through geologic time. To test this, we use the cooling paths estimated from the first quartile lag times, the alpha damage annealing model (ADAM; ref. [60] and Chapter 3 of this dissertation), and minimum and maximum measured U and Th concentrations (Table 2.3). In the case producing the largest difference (i.e., the Mercer deposit with the slowest apparent erosion rates and the lowest U and Th concentrations; Table 2.3), the corrected AHe age would be no more than 30% less relative to the nominal age. This bias would preferentially influence our estimates of the lowest erosion rates, for example, shifting them upward from 0.2 km/Ma to 0.3 km/Ma. In contrast, our estimated cooling paths for the young Guivel cobble ages would yield a revised erosion rate of 3.2 km/Ma instead of 3 km/Ma. Because these differences are relatively small, we conclude that our use of time-invariant diffusion parameters from ref. [54] is a sufficient approximation in this setting, and eliminates additional computational expense of time-variant diffusivity

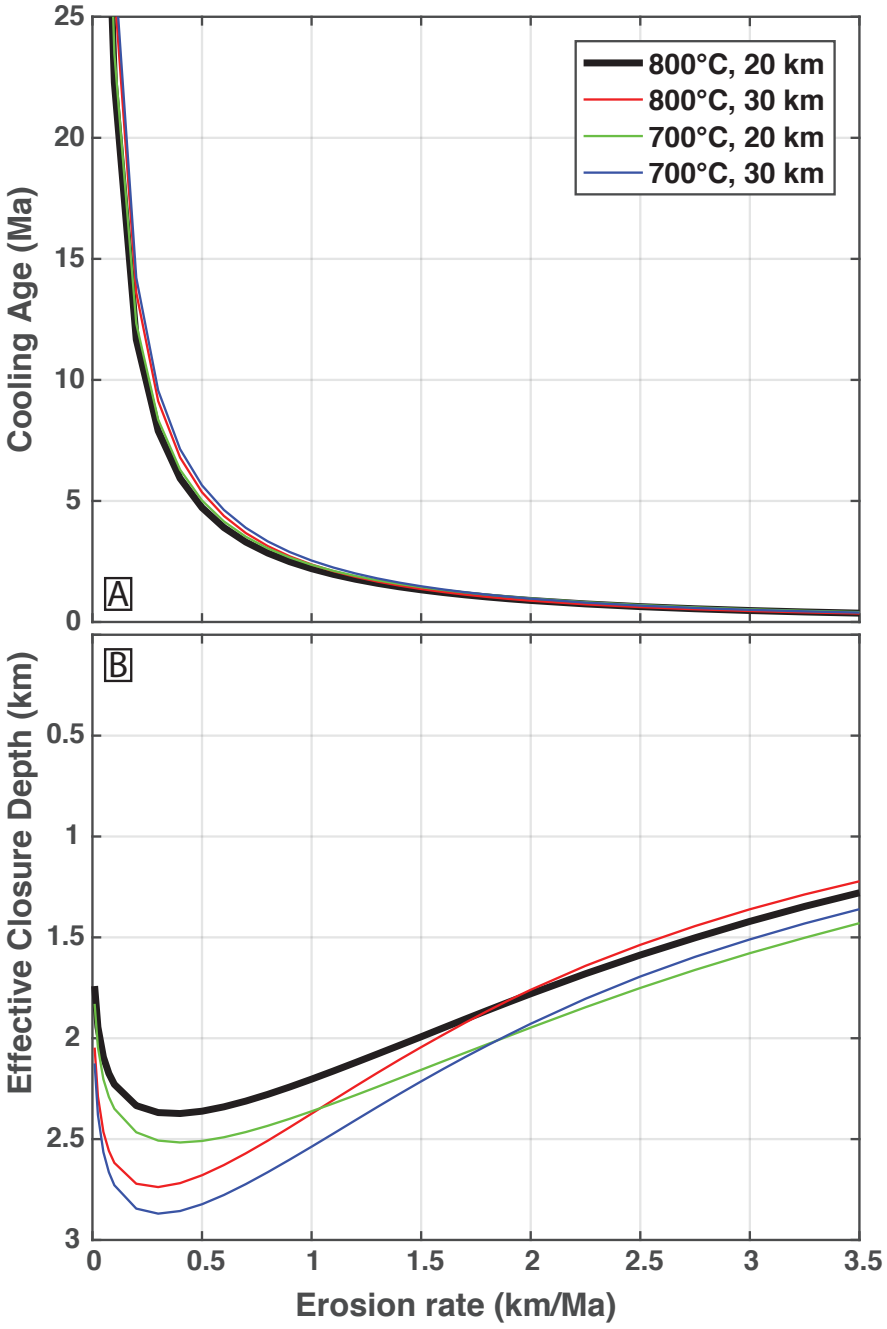

Figure 2.10: (A) Cooling age and (B) effective closure depth for the He apatite system as a function of erosion rate. The four curves show the sensitivities of these functions to different specification of the basal boundary condition for the thermal calculation in the *age2edot* program. He apatite diffusion parameters are from ref. [54] and based on an effective spherical radius of 60 µm.

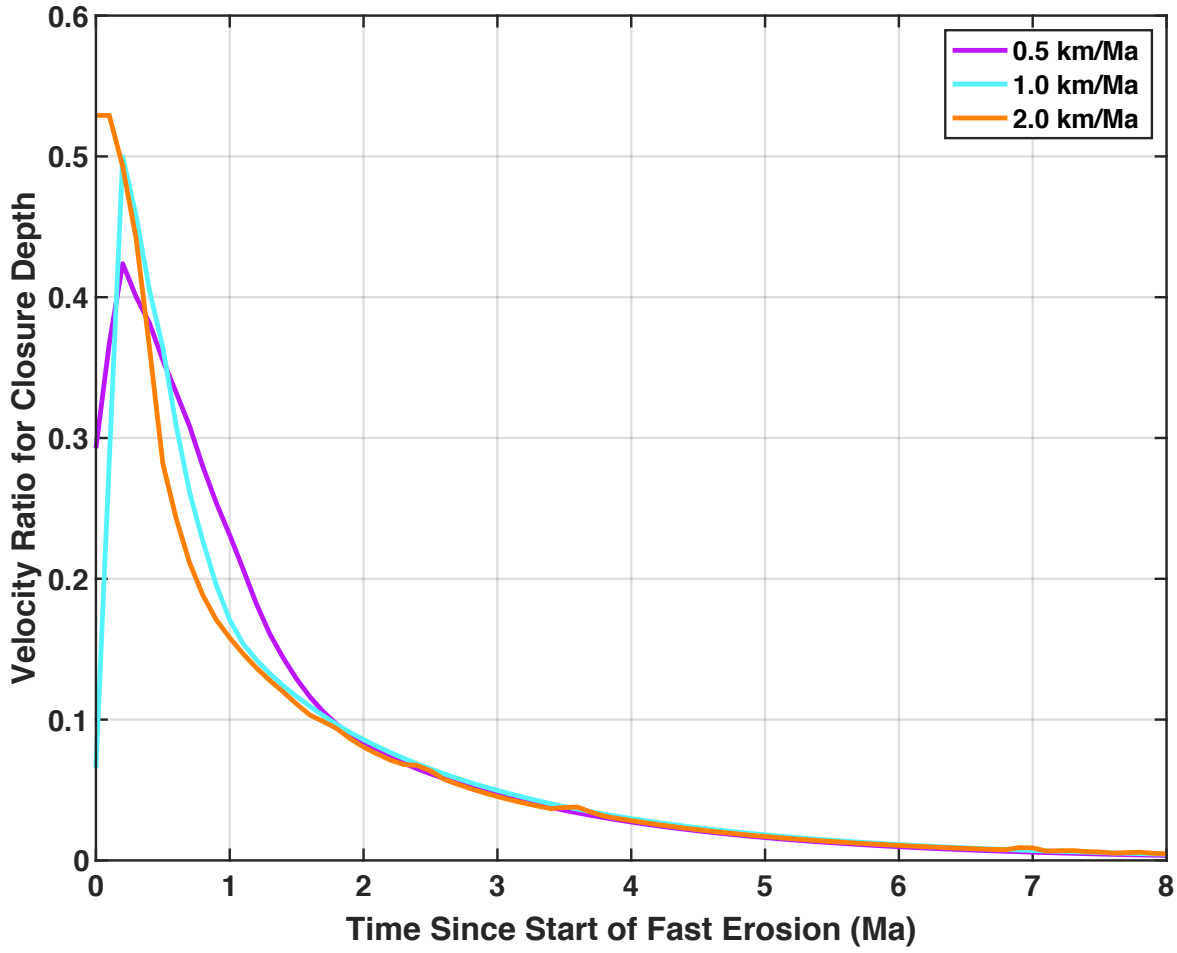

Figure 2.11: Evolution of the closure depth in response to an instantaneous increase in erosion rate. The simulations are based on a long period of slow and steady erosion, at 0.1 km/Ma for time >0 Ma, followed by a transition to faster erosion rates of 0.5, 1, and 2 km/Ma for time <0 Ma. The y-axis is the velocity ratio for the closure depth, defined as the vertical velocity of the closure depth relative to the vertical material velocity caused by erosion, with all velocities relative to a fixed land surface. The velocity ratio peaks just after the onset of erosion and drops to values >0.1 within 2 Ma. These examples demonstrate that quasi-steady solution for cooling ages is appropriate for changes in erosion rate that occur on a time interval longer than ∼1 Ma.

for each of the 206 crystals. Comparable assumptions have been made for bedrock ages measured in the same region [24].

2.7.4 Estimating spatially averaged erosion rates

Each of the cobbles in this study represents an individual bedrock sample from an upland granitic source region "collected" by a glacier in the geologic past. As a result, areas with faster erosion will yield more cobble samples per unit area of the source region than those areas with slower erosion. We employ a method that accounts for this bias and provides spatially averaged erosion rates for the source region. Consider a randomly sampled distribution of erosion rates, e_i where $i = 1$ to n, that are determined, in some fashion, from sediment materials eroded from the source region. The sample mean is defined by

$$\bar{e} = \frac{\sum w_i e_i}{\sum w_i} \tag{2.1}$$

where w_i are weights for each sample. The conventional mean uses uniform weights for the samples ($w_i = 1$). For our problem, this estimate would give mean erosion rate as sampled by the sediment *yield*. Our objective is to estimate the mean erosion rate as sampled by *area*. To do so, we set the weights as $w_i = 1/e_i$, which removes the bias due to spatially varying erosion rates. Substitution into equation 2.1 gives

$$\bar{e} = \left(\frac{\sum (1/e_i)}{n} \right)^{-1}. \tag{2.2}$$

This derivation shows that mean erosion rate by area is simply the reciprocal of the mean of the reciprocal erosion rate. This estimator is called the harmonic mean and is useful when averaging certain kinds of rate measurements, including the use of detrital quartz ^{10}Be measurements to estimate the spatially averaged erosion rate of a river catchment. In the same way, we use the harmonic mean to estimate spatially averaged erosion rates from cobble lag times published in this chapter.

2.8 Acknowledgments

General: The authors thank A. Bryk for assistance with the hypsometry data sets. The authors also greatly appreciate the constructive feedback of three anonymous reviewers and Blair Schoene's useful feedback and thoughtful handling of the manuscript.

Funding: This work was supported by the Yale College Dean's, Von Damm, and Stiles Mellon Forum Research Grants, and NSF Graduate Research Fellowship DGE 1752814 (to C.D.W.); NSF EAR-1650313 (to M.T.B.); the Ann and Gordon Getty Foundation and the Esper Larsen Research Grant (to D.L.S.).

Published in	Sample Name	Age (Ma)	Error (Ma)
Thomson et al. 2010 [17]	anita 2	8.83	0.30
	06PA04	4.25	0.12
	06PA05	4.69	0.18
	06PA06	5.63	0.31
	06PA08	4.26	0.13
	06PA09	3.93	0.12
	06PA16	7.07	0.25
	06PA17	6.04	0.21
	THC16r1	7.23	0.22
	THC17	7.76	0.17
	THC18	46.47	2.04
	THC21r1	2.32	0.06
	THC22r1	6.89	0.55
	THC23r2	4.59	0.09
	THC24	13.08	0.89
	THC25	2.57	0.63
Guillaume et al. 2013 [25]	PATC14-A	7.10	0.40
	DES23	9.10	0.71
	DES25	6.00	0.57
	DES26	2.40	0.09
	DES27	4.80	0.21
	LL01-B	1.80	0.20
	LL02	2.20	0.21
	LL03	3.30	0.10
Georgieva et al., 2016 [24]	AG08_10 (Nef)	5.25	0.51
	AG08_12 (Nef)	6.49	0.74
	AG08_13 (Nef)	6.83	1.16
	AG08_17 (Nef)	8.07	0.27
	AG08_18 (Nef)	5.92	0.45
	AG08_33 (Nef)	6.09	1.88
	AG08_34 (Nef)	4.59	1.10
	LE08_02 (Leones)	4.33	0.70
	11-LL-03 (Leones)	4.32	0.26
	11-LL-04 (Leones)	4.87	0.99
	11-LL-05 (Leones)	3.52	0.39
	11-LL-06 (Leones)	3.95	0.40
	11-LL-07 (Leones)	3.68	0.22
	11-LL-08 (Leones)	2.76	0.80
	11-LL-09 (Leones)	2.24	0.96
	11-LL-10 (Leones)	2.71	0.51
	12-CM-03 (Leones)	6.77	1.12
	12-CM-04 (Leones)	4.51	1.08
	12-CM-05 (Leones)	3.96	1.23
	12-CM-06 (Leones)	5.29	0.68
	12-CM-07 (Leones)	4.95	0.78
	12-CM-08 (Leones)	2.79	0.49
	12-CM-09 (Leones)	2.01	0.64
	12-CM-10 (Leones)	2.45	0.73
	AG08_31 (Colonia)	6.60	0.97
	11-SM-13 (Colonia)	5.29	0.43
	11-SM-14 (Colonia)	5.35	0.46

Table 2.1: Published bedrock ages shown in Fig. 2.4. Errors and precision as reported in the original publications. Thomson et al., 2010 [17]: Ages are from single crystals. Error is 2σ. Guillaume et al., 2013 [25]: Ages are a mix of single crystal and multiple crystal mean ages. Error is 1σ. Georgieva et al., 2016 [24]: Ages are mean ages from three to five single-crystal aliquots from the same sample. Error is the standard deviation of the measured aliquots.

Sample Location	**Deposit Age (Ma)**	**N**	**Mean Lag ±2 SE (Ma)**	**Mean $\dot{E}$ ±2 SE (km/Ma)**	**1st Quart. Lag ±2 SE (Ma)**	**1st Quart. $\dot{E}$ ±2 SE (km/Ma)**
Bedrock	—	51	5.84 ± 1.8	0.3335 (+0.10/–0.08)	3.50 ± 1.2	0.5310 (+0.20/–0.14)
Fenix I	0.0185	29	7.51 ± 2.0	0.3196 (+0.10/–0.08)	4.51 ± 0.92	0.5255 (+0.10/–0.12)
Telken VII	1.016	22	10.09 ± 6.4	0.2419 (+0.22/–0.12)	2.94 ± 0.68	0.7804 (+0.16/–0.18)
Guivel	3.3	15	4.80 ± 3.2	0.4937 (+0.46/–0.24)	0.48 ± 0.82	2.9780 (+2.0/–12.6)
Mercer	5.7	6	24.23 ± 12.6	0.0928 (+0.10/–0.04)	11.65 ± 8.6	0.2006 (+0.08/–0.26)

Table 2.2: Mean and first quartile lag-time and erosion rates for each sample location.

Deposit	Sample Name	#	^{238}U (nmol/g)	^{232}Th (nmol/g)	^{4}He (nmol/g)	FT	Corr. Age (Ma)	Error (Ma)	Min. Age (Ma)	SE (Ma)	Lab
Mercer	M-EB06	A1	42.7	93.2	1.34	0.73	21.33	0.29	21.33	–0.29/+0.29	BGC
		A3	33.8	47.4	1.20	0.66	29.75	0.76			BGC
Mercer	LBA-K52	A3	338.3	1325.1	30.21	0.56	57.80	0.72	57.8	–0.72/+0.72	BGC
Mercer	LBA-N30	A3	13.1	62.0	0.62	0.51	32.76	0.68	32.76	–0.67/+0.69	BGC
Mercer	LBA-K38	A1	30.42	94.79	1.80	0.74	36.10	0.93	32.43	–1.27/+1.32	UCSC
		A2	28.83	111.12	1.25	0.55	32.32	1.16			UCSC
		A3	58.19	243.83	2.99	0.56	36.45	1.02			UCSC
		A5	38.45	134.93	2.68	0.65	45.77	1.41			UCSC
		A6	32.33	145.34	2.59	0.48	63.58	3.60			UCSC
Mercer	LBA-K44	A1	5.79	69.78	0.20	0.44	15.91	2.60	13.36	–0.33/+0.34	UCSC
		A2	17.18	102.68	0.40	0.59	12.83	0.63			UCSC
		A3	13.00	78.50	0.48	0.59	20.21	1.39			UCSC
		A4	12.27	89.78	0.46	0.55	19.81	1.22			UCSC
		A5	331.06	592.09	3.79	0.47	13.50	0.40			UCSC
		A6	39.62	202.80	1.41	0.53	23.81	0.85			UCSC
Mercer	LBA-K47	A1	100.51	271.75	2.42	0.49	23.41	1.00	21.89	–0.64/+0.66	UCSC
		A2	19.15	157.57	0.66	0.46	19.94	1.30			UCSC
		A3	15.78	173.87	1.13	0.54	28.99	1.04			UCSC
		A4	30.38	104.34	0.60	0.44	19.45	1.55			UCSC
		A5	36.33	145.76	0.77	0.38	22.37	1.71			UCSC
Guivel	G-CW04	A1	33.3	128.3	0.65	0.74	10.27	0.58	10.27	–0.56/+0.60	BGC
		A2	3.3	20.0	0.49	0.74	62.59	38.26			BGC
Guivel	G-EB01	A1	29.1	89.0	0.21	0.73	4.57	0.08	4.13	–0.09/+0.09	BGC
		A2	52.2	151.4	0.33	0.71	4.13	0.09			BGC
Guivel	G-EB04	A1	77.8	121.8	1.18	0.72	11.82	0.25	11.82	–0.25/+0.25	BGC
Guivel	G-EB05	A1	93.0	313.1	0.56	0.80	3.25	0.07	3.25	–0.07/+0.07	BGC
Guivel	G-EB06	A1	62.2	126.9	0.86	0.71	9.99	0.16	9.99	–0.16/+0.16	BGC
		A2	29.6	93.0	0.58	0.68	12.25	0.30			BGC
Guivel	G-EB07	A1	74.3	54.5	1.84	0.63	25.60	1.77	19.38	–2.23/+2.53	BGC
		A2	193.5	122.4	3.51	0.61	19.38	2.38			BGC
Guivel	G-EB11	A1	40.8	66.7	0.24	0.67	4.73	0.09	4.69	–0.08/+0.09	BGC
		A2	37.9	100.5	0.23	0.68	4.25	0.28			BGC
		A3	19.6	46.4	0.40	0.69	14.35	0.37			BGC
Guivel	G-EB12	A1	38.8	120.2	0.26	0.71	4.31	0.09	3.72	–0.05/+0.05	BGC
		A2	34.5	93.3	0.20	0.75	3.72	0.05			BGC
Guivel	G-EB15	A1	54.2	166.4	0.53	0.73	6.00	0.06	4.66	–0.07/+0.07	BGC

Deposit	Sample Name	#	^{238}U (nmol/g)	^{232}Th (nmol/g)	^{4}He (nmol/g)	FT	Corr. Age (Ma)	Error (Ma)	Min. Age (Ma)	SE (Ma)	Lab
Guivel	G-EB15	A2	54.8	122.3	0.36	0.71	4.66	0.07			BGC
Guivel	G-EB18	A1	196.4	63.8	0.79	0.79	3.54	0.06	3.54	–0.06/+0.06	BGC
		A2	130.3	13.1	0.48	0.77	3.35	4.07			BGC
Guivel	G-EB19	A1	108.3	384.2	0.88	0.62	5.35	0.09	5.35	–0.09/+0.09	BGC
Guivel	G-KM01	A1	44.0	104.4	0.24	0.70	3.80	0.10	3.80	–0.10/+0.10	BGC
Guivel	G-KM04	A1	43.2	129.2	0.34	0.75	4.87	0.05	4.87	–0.05/+0.05	BGC
		A2	50.7	189.1	1.06	0.62	13.51	0.74			BGC
		A3	44.5	143.6	0.44	0.69	6.29	0.13			BGC
Guivel	G-KM05	A1	42.7	140.3	0.56	0.70	8.22	0.10	8.22	–0.10/+0.10	BGC
		A2	18.4	42.4	0.32	0.69	12.51	0.93			BGC
Guivel	G-KM06	A1	22.5	49.6	0.76	0.68	23.82	0.41	23.82	–0.41/+0.41	BGC
Telken VII	LBA-K16	A1	24.4	92.8	0.22	0.69	5.20	0.17	3.32	–0.09/+0.09	BGC
		A3	53.3	44.6	0.18	0.64	3.32	0.09			BGC
Telken VII	LBA-K19	A1	77.5	142.6	0.48	0.67	5.01	0.34	5.67	–0.16/+0.17	BGC
		A2	59.1	87.2	0.36	0.66	5.29	0.54			BGC
		A3	296.9	425.5	1.82	0.61	5.89	0.20			BGC
Telken VII	LBA-N11	A1	42.5	98.2	0.40	0.70	6.87	0.09	6.87	–0.09/+0.09	BGC
		A2	52.4	148.1	1.32	0.65	18.49	0.19			BGC
Telken VII	LBA-P12	A1	261.5	734.8	7.33	0.59	21.34	0.53	21.34	–0.52/+0.54	BGC
Telken VII	LBA-P13	A1	378.0	509.3	22.25	0.58	57.33	3.88	57.33	–3.75/+4.01	BGC
Telken VII	LBA-P14	A1	14.2	52.7	1.65	0.82	55.29	0.42	51.68	–0.65/+0.66	BGC
		A2	12.7	45.0	1.28	0.78	51.69	0.66			BGC
		A3	250.2	13.0	1.98	0.76	7.80	8.01			BGC
Telken VII	LBA-P15	A1	52.0	183.6	3.70	0.63	46.97	0.51	27.01	–0.23/+0.23	BGC
		A2	11.9	49.9	0.66	0.67	30.04	0.45			BGC
		A3	37.3	127.6	1.85	0.77	27.01	0.23			BGC
Telken VII	LBA-K01	A1	9.75	41.77	4.15	0.57	286.32	11.68	5.35	–0.41/+0.45	UCSC
		A2	10.80	56.61	0.11	0.65	5.35	0.42			UCSC
		A3	36.75	58.26	1.38	0.60	35.47	2.19			UCSC
Telken VII	LBA-K02	A1	184.81	628.03	1.69	0.52	7.60	0.25	4.61	–0.20/+0.21	UCSC
		A2	21.08	57.80	0.16	0.64	5.69	0.29			UCSC
		A3	19.14	99.63	0.27	0.73	6.77	0.19			UCSC
		A4	23.38	75.48	0.17	0.72	4.57	0.18			UCSC
		A5	24.23	73.56	0.18	0.64	5.35	0.29			UCSC
Telken VII	LBA-K04	A1	34.55	126.51	0.26	0.50	6.41	0.62	4.53	–0.23/+0.25	UCSC
		A2	26.73	95.32	0.20	0.60	5.23	0.31			UCSC

Deposit	Sample Name	#	^{238}U (nmol/g)	^{232}Th (nmol/g)	^{4}He (nmol/g)	FT	Corr. Age (Ma)	Error (Ma)	Min. Age (Ma)	SE (Ma)	Lab
Telken VII	LBA-K04	A3	94.22	105.16	0.47	0.59	5.19	0.27			UCSC
		A4	19.55	27.03	0.22	0.75	8.94	0.44			UCSC
		A5	119.64	134.54	0.49	0.56	4.48	0.20			UCSC
Telken VII	LBA-K07	A1	29.00	96.98	0.23	0.68	5.09	0.23	3.63	–0.19/+0.20	UCSC
		A2	19.02	72.34	0.18	0.56	7.05	0.61			UCSC
		A3	21.61	70.62	0.17	0.54	6.34	0.69			UCSC
		A4	22.14	57.02	0.12	0.72	3.58	0.18			UCSC
		A5	15.58	65.99	0.11	0.58	4.60	0.63			UCSC
		A6	16.70	70.34	0.13	0.55	5.49	0.62			UCSC
Telken VII	LBA-K08	A1	38.30	104.87	0.28	0.62	5.58	0.29	5.60	–0.31/+0.33	UCSC
		A2	31.29	120.30	0.34	0.57	7.78	0.38			UCSC
		A3	27.87	73.37	0.63	0.62	17.76	0.86			UCSC
Telken VII	LBA-K08	A4	19.22	60.60	0.25	0.73	8.10	0.27			UCSC
		A5	26.98	71.05	0.38	0.72	9.52	0.33			UCSC
Telken VII	LBA-K10	A1	77.15	76.57	0.38	0.70	4.48	0.15	4.46	–0.14/+0.14	UCSC
		A2	28.51	82.87	0.27	0.68	6.49	0.21			UCSC
		A3	37.72	80.86	0.42	0.66	8.69	0.33			UCSC
		A4	31.07	79.46	0.18	0.63	4.39	0.27			UCSC
		A5	22.75	76.62	0.30	0.70	8.32	0.30			UCSC
Telken VII	LBA-K15	A1	41.38	118.36	0.35	0.64	6.18	0.27	6.34	–0.13/+0.14	UCSC
		A2	40.25	112.34	0.52	0.70	8.72	0.24			UCSC
		A3	34.97	106.37	0.30	0.55	7.04	0.47			UCSC
		A4	50.47	176.11	0.38	0.54	6.01	0.36			UCSC
		A5	37.94	106.93	0.36	0.66	6.70	0.28			UCSC
		A6	37.02	91.57	0.31	0.68	6.02	0.26			UCSC
Telken VII	LBA-K17	A1	47.63	137.96	0.27	0.63	4.13	0.21	4.22	–0.23/+0.25	UCSC
		A2	52.54	143.27	0.36	0.71	4.61	0.12			UCSC
		A3	72.38	134.69	0.50	0.65	5.75	0.20			UCSC
		A4	41.68	81.62	0.34	0.65	6.77	0.22			UCSC
		A5	39.76	128.01	0.34	0.75	5.00	0.12			UCSC
Telken VII	LBA-K20	A1	38.20	96.06	0.28	0.71	5.12	0.16	3.86	–0.12/+0.12	UCSC
		A2	44.22	119.27	0.31	0.64	5.29	0.18			UCSC
		A3	45.88	373.23	0.42	0.64	3.86	0.11			UCSC
Telken VII	LBA-K20	A4	53.59	131.28	0.48	0.63	7.08	0.27			UCSC
		A5	52.28	188.65	1.55	0.73	17.12	0.33			UCSC
Telken VII	LBA-K21	A1	30.64	107.90	0.16	0.56	3.92	0.47	4.05	–0.49/+0.56	UCSC

Deposit	Sample Name	#	^{238}U (nmol/g)	^{232}Th (nmol/g)	^{4}He (nmol/g)	FT	Corr. Age (Ma)	Error (Ma)	Min. Age (Ma)	SE (Ma)	Lab
Telken VII	LBA-K21	A2	314.85	1069.76	2.79	0.38	10.14	0.40			UCSC
		A3	40.51	100.79	0.33	0.67	5.93	0.35			UCSC
		A4	60.73	184.02	0.40	0.53	5.66	0.31			UCSC
		A5	41.62	151.89	0.76	0.48	16.03	0.84			UCSC
Telken VII	LBA-N04	A1	67.95	108.89	0.28	0.66	3.55	0.14	3.43	–0.15/+0.16	UCSC
		A2	55.85	110.14	0.28	0.63	4.20	0.25			UCSC
		A3	50.88	130.91	0.20	0.60	3.19	0.21			UCSC
		A4	55.51	96.91	0.42	0.76	5.42	0.16			UCSC
		A5	31.75	66.42	0.16	0.59	4.56	0.35			UCSC
Telken VII	LBA-N08	A1	18.65	65.12	0.18	0.63	6.62	0.50	5.24	–0.12/+0.12	UCSC
		A2	59.03	105.35	0.98	0.68	13.38	0.27			UCSC
		A3	17.18	85.77	0.11	0.51	4.64	0.92			UCSC
		A4	35.60	118.29	0.25	0.63	4.88	0.22			UCSC
		A5	35.64	111.46	0.30	0.72	5.22	0.15			UCSC
Telken VII	LBA-N09	A1	34.97	92.73	0.39	0.80	6.77	0.14	6.64	–0.10/+0.10	UCSC
		A2	36.38	84.19	0.35	0.71	6.78	0.27			UCSC
		A3	39.38	111.33	0.50	0.69	8.64	0.03			UCSC
		A4	54.39	164.50	0.49	0.65	6.33	0.18			UCSC
		A5	55.83	94.19	0.62	0.70	8.95	0.25			UCSC
Telken VII	LBA-P01	A1	61.15	206.44	0.39	0.49	5.70	0.41	5.63	–0.19/+0.20	UCSC
		A2	47.44	369.20	0.52	0.53	5.77	0.26			UCSC
		A3	55.79	142.42	0.25	0.44	4.98	0.47			UCSC
Telken VII	LBA-P11	A1	25.84	76.37	0.12	0.63	3.43	0.28	3.50	–0.14/+0.15	UCSC
		A2	24.14	66.07	0.33	0.60	10.64	0.57			UCSC
		A3	23.32	69.54	0.17	0.79	4.19	0.11			UCSC
		A4	29.07	84.17	0.21	0.77	4.32	0.10			UCSC
		A5	22.59	80.42	0.14	0.77	3.53	0.16			UCSC
Fenix I	LBA-K22	A1	148.8	142.6	0.50	0.62	3.39	0.21	3.26	–0.10/+0.11	BGC
		A2	697.0	1124.8	2.19	0.56	3.21	0.12			BGC
		A3	708.8	854.8	2.74	0.57	4.04	0.16			BGC
Fenix I	LBA-K28	A1	50.0	156.7	0.40	0.67	5.50	0.08	4.27	–0.06/+0.06	BGC
		A2	63.2	184.5	0.40	0.69	4.27	0.06			BGC
Fenix I	LBA-K28	A3	315.2	794.4	3.04	0.60	8.02	1.82			BGC
Fenix I	LBA-K30	A1	541.5	435.5	3.77	0.57	7.63	0.15	7.63	–0.15/+0.15	BGC
Fenix I	LBA-K33	A1	36.7	99.9	0.35	0.67	6.87	0.11	6.87	–0.11/+0.11	BGC
Fenix I	LBA-K53	A1	47.5	167.1	0.66	0.62	9.26	0.53	9.26	–0.51/+0.55	BGC

Deposit	Sample Name	#	^{238}U (nmol/g)	^{232}Th (nmol/g)	^{4}He (nmol/g)	FT	Corr. Age (Ma)	Error (Ma)	Min. Age (Ma)	SE (Ma)	Lab
Fenix I	LBA-K53	A2	14.9	67.0	0.31	0.63	11.10	0.44			BGC
Fenix I	LBA-K54	A1	1029.6	1064.6	8.24	0.60	8.18	0.40	7.42	–0.09/+0.09	BGC
		A2	288.6	419.6	2.32	0.63	7.40	0.16			BGC
		A3	279.4	500.2	2.48	0.65	7.37	0.11			BGC
Fenix I	LBA-K54	A1	990.2	1453.1	19.56	0.58	19.10	0.42	19.1	–0.42/+0.42	BGC
		A3	628.6	1070.5	15.06	0.55	23.98	2.38			BGC
Fenix I	LBA-K57	A1	52.8	171.0	0.45	0.53	6.64	0.34	6.64	–0.33/+0.35	BGC
Fenix I	LBA-N16	A1	156.6	61.7	1.07	0.68	7.00	0.06	7.00	–0.06/+0.06	BGC
Fenix I	LBA-N20	A1	172.6	443.1	1.29	0.61	5.99	0.10	6.05	–0.10/+0.10	BGC
		A2	154.9	302.3	0.96	0.61	5.46	1.25			BGC
		A3	445.8	1579.9	22.29	0.56	38.79	1.10			BGC
		A4	429.3	1221.4	4.50	0.59	8.44	0.82			BGC
Fenix I	LBA-N21	A1	235.8	1296.4	11.39	0.54	30.57	0.43	30.57	–0.43/+0.43	BGC
		A3	339.1	111.4	2.25	0.52	9.19	0.19			BGC
Fenix I	LBA-N40	A1	8019.3	2401.7	53.00	0.56	8.59	0.18	8.59	–0.18/+0.19	BGC
		A2	154.9	302.3	0.96	0.61	5.46	1.25			BGC
		A4	449.0	103.7	2.38	0.52	7.49	1.93			BGC
Fenix I	LBA-N42	A3	105.7	153.6	0.72	0.68	5.72	0.11	5.72	–0.11/+0.11	BGC
		A5	634.8	1125.1	5.33	0.59	7.56	0.30			BGC
Fenix I	LBA-N43	A2	35.0	80.0	0.45	0.68	9.49	0.12	6.50	–0.14/+0.14	BGC
		A3	115.4	240.1	0.75	0.61	5.59	0.42			BGC
		A4	53.2	145.5	0.47	0.64	6.59	0.15			BGC
Fenix I	LBA-P16	A1	220.9	715.3	2.95	0.58	9.75	0.28	9.75	–0.28/+0.28	BGC
		A2	22.2	80.1	0.50	0.65	14.27	0.28			BGC
Fenix I	LBA-P17	A1	81.1	194.5	0.53	0.68	4.82	0.08	4.82	–0.09/+0.09	BGC
		A2	141.1	363.8	1.05	0.64	5.65	0.16			BGC
		A3	67.6	188.5	0.64	0.66	6.71	0.31			BGC
Fenix I	LBA-P18	A1	84.6	114.1	0.38	0.64	4.16	0.57	4.41	–0.22/+0.23	BGC
		A2	174.0	268.8	0.83	0.62	4.45	0.25			BGC
		A3	30.2	84.9	0.24	0.65	5.75	0.28			BGC
Fenix I	LBA-P19	A1	47.2	93.9	0.32	0.68	5.22	1.06	5.52	–0.95/+1.17	BGC
		A2	349.1	905.4	3.00	0.58	7.26	0.36			BGC
Fenix I	LBA-P20	A1	176.0	481.4	1.58	0.61	6.41	0.41	3.28	–0.22/+0.24	BGC
		A2	1411.1	2109.5	4.99	0.60	3.28	0.23			BGC
Fenix I	LBA-P23	A1	1479.5	1172.1	5.42	0.59	4.00	0.09	4.00	–0.09/+0.09	BGC
		A2	597.8	588.5	2.77	0.61	4.71	0.33			BGC

Deposit	Sample Name	#	^{238}U (nmol/g)	^{232}Th (nmol/g)	^{4}He (nmol/g)	FT	Corr. Age (Ma)	Error (Ma)	Min. Age (Ma)	SE (Ma)	Lab
Fenix I	LBA-P24	A2	45.1	139.3	0.69	0.52	12.40	0.17	12.40	–0.17/+0.17	BGC
Fenix I	LBA-P25	A1	23.0	85.1	0.25	0.70	6.12	0.31	4.43	–0.08/+0.08	BGC
		A2	27.0	95.3	0.21	0.72	4.43	0.08			BGC
		A3	248.9	385.6	2.23	0.61	8.28	0.63			BGC
Fenix I	LBA-P26	A2	42.2	93.9	0.28	0.77	4.39	0.04	4.39	–0.04/+0.04	BGC
Fenix I	LBA-P27	A1	65.6	85.9	0.27	0.69	3.58	1.87	3.58	–1.41/+2.33	BGC
		A2	145.1	371.4	1.07	0.61	5.95	0.10			BGC
Fenix I	LBA-P28	A1	39.6	74.2	0.33	0.71	6.20	0.08	6.09	–0.05/+0.05	BGC
		A2	44.1	93.9	0.36	0.69	6.01	0.07			BGC
		A3	44.6	68.2	0.85	0.73	14.59	0.35			BGC
Fenix I	LBA-P37	A3	780.0	3948.0	10.20	0.57	8.22	0.31	8.22	–0.30/+0.32	BGC
Fenix I	LBA-K24	A1	81.83	241.39	0.51	0.61	4.77	0.17	4.98	–0.09/+0.09	UCSC
		A2	110.61	285.48	0.69	0.60	5.02	0.15			UCSC
		A3	56.04	151.44	0.34	0.52	5.56	0.48			UCSC
		A4	118.29	435.71	0.75	0.54	4.93	0.21			UCSC
Fenix I	LBA-K24	A5	98.45	307.87	0.56	0.49	5.28	0.32			UCSC
Fenix I	LBA-K26	A1	20.06	65.48	0.36	0.71	11.41	0.37	7.27	–0.50/+0.54	UCSC
		A2	24.71	50.28	0.27	0.63	9.31	0.47			UCSC
		A3	44.55	154.72	1.45	0.68	20.63	0.44			UCSC
		A4	60.75	231.19	0.50	0.48	6.97	0.49			UCSC
		A5	27.58	97.00	0.28	0.54	8.00	0.57			UCSC
Fenix I	LBA-K29	A1	458.52	169.29	3.16	0.64	7.71	0.20	6.53	–0.14/+0.15	UCSC
		A2	501.40	104.48	2.62	0.59	6.58	0.18			UCSC
		A3	104.79	83.47	0.60	0.59	6.42	0.25			UCSC
		A4	710.45	88.49	3.50	0.50	7.47	0.18			UCSC
		A5	111.96	81.11	0.91	0.66	8.18	0.21			UCSC

Table 2.3: Measured data for each crystal used in the study.

Chapter 3

A helium-based model for the effects of radiation damage annealing on helium diffusion kinetics in apatite

This chapter was previously published in Willett, C.D., Fox, M.R., and Shuster, D.L., *Earth and Planetary Science Letters* **477**, 195-204 (2017). doi:10.1016/j.epsl.2017.07.047 and in Willett, C.D., Fox, M.R., and Shuster, D.L., *Earth and Planetary Science Letters* **481**, 420 (2018). doi:10.1016/j.epsl.2017.11.017

3.1 Abstract

Widely used to study surface processes and the development of topography through geologic time, (U–Th)/He thermochronometry in apatite depends on a quantitative description of the kinetics of ^{4}He diffusion across a range of temperatures, timescales, and geologic scenarios. Empirical observations demonstrate that He diffusivity in apatite is not solely a function of temperature, but also depends on damage to the crystal structure from radioactive decay processes. Commonly-used models accounting for the influence of thermal annealing of radiation damage on He diffusivity assume the net effects evolve in proportion to the rate of fission track annealing, although the majority of radiation damage results from α-recoil. While existing models adequately quantify the net effects of damage annealing in many geologic scenarios, experimental work suggests different annealing rates for the two damage types. Here, we introduce an alpha-damage annealing model (ADAM) that is independent of fission track annealing kinetics, and directly quantifies the influence of thermal annealing on He diffusivity in apatite. We present an empirical fit to diffusion kinetics data and incorporate this fit into a model that tracks the competing effects of radiation damage accumulation and annealing on He diffusivity in apatite through geologic time. Using time-temperature paths to illustrate differences between models, we highlight the influence of damage annealing on data interpretation. In certain, but not all, geologic scenarios, the

interpretation of low-temperature thermochronometric data can be strongly influenced by which model of radiation damage annealing is assumed. In particular, geologic scenarios involving 1–2 km of sedimentary burial are especially sensitive to the assumed rate of annealing and its influence on He diffusivity. In cases such as basement rocks in Grand Canyon and the Canadian Shield, (U–Th)/He ages predicted from the ADAM can differ by hundreds of Ma from those predicted by other models for a given thermal path involving extended residence between ∼40 and 80 °C.

3.2 Introduction

Over the past two decades, (U–Th)/He thermochronometry in apatite (AHe) has been widely used to study surface processes and topography development through geologic time (e.g., ref. [19]). Because the diffusion of He in apatite is sensitive to temperatures found in the uppermost few kilometers of Earth's crust, the production and diffusion of radiogenic ^{4}He via α-decay of radioactive nuclides (i.e. along the U- and Th-series decay chains) can be used to quantify the timing, rates, and spatial patterns of exhumation over typically >0.1 million year (Ma) timescales (e.g., ref. [61]). A quantitative description of the diffusion kinetics of ^{4}He in apatite is required for accurate interpretation of AHe data. Complexity in the kinetic function has been revealed by empirical observations that He diffusivity in apatite is not solely a function of temperature, but may also evolve as a function of damage to the apatite crystal structure resulting from α-recoil and fission events [6–8, 21]. Damage from α-recoil has recently been mapped in zircon [62], revealing small pockets of damage capable of trapping He [6–8, 21] and other elements. The radiation damage content in a crystal will increase as a function of time, at a rate proportional to parent nuclide concentration, but will also decrease in response to thermal heating [8]. The effects of thermal annealing of radiation damage and its influence on He diffusivity complicates the problem of quantifying ^{4}He diffusivity through time, as the diffusivity at any point in time will be influenced by the sample's prior thermal path. A quantitative understanding of the competing effects of radiation damage accumulation and annealing is necessary to accurately model and interpret the results of all AHe thermochronometric data, but especially in scenarios involving re-heating over geologic time (e.g., due to sedimentary burial).

Previous treatments of the accumulation and annealing of radiation damage in apatite have recently been challenged by observations in certain geologic scenarios, demonstrating the important influence of the assumed rate of annealing on AHe data interpretation (e.g., ref. [63]). Existing models, now commonly used to interpret AHe data, make the fundamental assumption that the net effects of radiation damage in apatite, which primarily result from α-recoil damage, can be quantified using empirical models of apatite fission track (AFT) annealing [6, 7]. This assumption—that fission tracks and α-recoil damage anneal, and in response control He diffusivity, at the same rate—adequately describes the effects of annealing in many geologic scenarios. However, measurements of optical properties suggest that annealing rates of damage resulting from α-recoil and fission events in apatite likely

differ [64]. In the event that fission tracks are less resistant to annealing than α-recoil damage, perhaps a function of damage geometry or size, the previous diffusion models would overpredict the rate of damage annealing and underpredict the AHe age.

Here, we present a new alpha-damage annealing model (ADAM) that quantifies the influence of thermal annealing on He diffusivity without relying on the assumption that α-recoil damage anneals at a rate that is ultimately tied to the annealing of fission tracks. The ADAM instead quantifies the effects of annealing with empirical relationships calibrated by experimentally-controlled damage annealing and He diffusion kinetics data, thus providing an internally consistent and more direct relationship between α-recoil damage annealing and He diffusivity. We present an empirical fit to data of a 2009 study by Shuster and Farley (ref. [8]), which quantify the resulting effects of annealing temperature and duration on He diffusivity. By assuming these experimental results are extrapolatable to longer times and lower temperatures, we incorporate the calibrated functions into a numerical model that tracks the competing effects of radiation damage accumulation and annealing on He diffusivity in apatite; we show evolutions of radiation damage, diffusion kinetics, and the AHe age through geologic time. We compare the results of this new model framework with existing models [6, 54] and demonstrate that in certain, but not all, geologic scenarios, the interpretation of low-temperature thermochronometric data can be strongly influenced by the assumed model of radiation damage annealing.

3.3 A new framework for quantifying the effects of annealing

Predicting AHe ages for a given apatite sample requires specifying the diffusivity of He as it evolves through geologic time and temperature [6–8, 21, 61]. As in previous treatments of this problem, the ADAM calculates the production and diffusion of ^{4}He in a finite crystal domain based on the grain size, U and Th concentrations, temperature, and the damage concentration in the crystal. The ADAM assumes the accumulation of radiation damage causes He diffusivity to decrease, following empirical relationships calibrated in refs. [8] and [6]. However, unlike other models, the ADAM assumes that the annealing of damage from spontaneous fission events and damage from α-recoil do not necessarily occur at the same rate, or even a scaleable rate. Experimental work measuring the effects of thermal annealing conditions in apatite found large differences based on the type of radiation damage (i.e. fission track versus α-recoil), quantified by optical properties [64]. We calibrate the annealing portion of the ADAM using experimentally-determined diffusion kinetics data [8]. Employing an empirical fit to diffusion data produces a simpler, more direct relationship between damage concentration and He diffusion, and—importantly—restores independence between models, and thus interpretations, of AHe and fission track systems in apatite.

The experiments in ref. [8] systematically measure changes in He diffusivity by varying the annealing temperature and duration in Durango apatite; these data provide the basis

for our empirical fits integrated into the ADAM. The authors of ref. [8] present diffusivity or closure temperature [2], both derivative quantities of activation energy (E_a) and the pre-exponential term (D_0/a^2) in the Arrhenius relation for diffusivity. Here, we use the reported values of E_a and $\ln(D_0/a^2)$ in Table 2 of that work. Because we are interested in how diffusion kinetics parameters change in response to annealing conditions, the results are expressed as differences between the measured E_a and $\ln(D_0/a^2)$ values in the suite of annealed samples and the sample with no preheating. Fig. 3.1 shows the results from ref. [8] in this form, plotting the systematic changes in E_a—ΔE_a—in Fig. 3.1A and the changes in $\ln(D_0/a^2)$—$\Delta \ln(D_0/a^2)$—in Fig. 3.1B.

Based on previously published results [6, 8, 21], we sought a mathematical expression to relate temperature, heating duration, and diffusion kinetics with two goals. First, the expression needed to reach maximum and minimum values at low and high temperatures, respectively. That is, no change to diffusion kinetics occurs at very low temperatures, and above some combination of duration and sufficiently high temperature, the parameters reach values characteristic of a fully annealed (or damage-free) crystal: 122.3 kJ/mol for E_a and 9.733 for $\ln(D_0/a^2)$ [6]. Second, we required the ΔE_a and $\Delta \ln(D_0/a^2)$ to depend on both temperature and duration. We thus chose an empirical relationship between annealing temperature, annealing duration, and diffusion kinetics that both adequately describes the available experimental data, and predicts the expected behavior at very low and very high temperatures. We adapted a functional form previously used to quantify similar effects in damage annealing [65], and use two expressions that describe resulting changes in He diffusion kinetics directly: one for ΔE_a and one for $\Delta \ln(D_0/a^2)$:

$$\ln\left[-\ln\left(\frac{\Delta E_a}{c_3\_E_a}\right)+1\right] = c_1\_E_a + \ln(t) + c_2\_E_a * T^{-1} \tag{3.1}$$

$$\ln\left[-\ln\left(\frac{\Delta \ln(D_0/a^2)}{c_3\_D_0}\right)+1\right] = c_1\_D_0 + \ln(t) + c_2\_D_0 * T^{-1} \tag{3.2}$$

where t is duration of thermal annealing at temperature T, c_1 and c_2 (for E_a and D_0) are empirically fit parameters, and $c_3\_E_a$ and $c_3\_D_0$ are calculated values, described below.

To quantify the best-fitting set of parameters for Equations 3.1 and 3.2, we conducted a systematic search of parameter combinations. The tested values for $c_1\_E_a$ and $c_1\_D_0$ range from 55 to 65 and the values for $c_2\_E_a$ and $c_2\_D_0$ range from -25000 to -19000, with both ranges divided into 101 linearly-spaced values. These ranges were selected to encompass combinations of fits that plot near the data and complete the search at an informative resolution. The quantities $c_3\_E_a$ and $c_3\_D_0$ are not fitted values, but rather the differences between the observed values of E_a (141 kJ/mol) and $\ln(D_0/a^2)$ (14.23) for natural (i.e., non-annealed) Durango apatite [8] (Fig. 3.1) and the assumed values of E_a and $\ln(D_0/a^2)$ for fully annealed Durango apatite, as defined above [6]. These c_3 values, effectively vertical scaling coefficients, exert a primary control on the amount of (and maximum possible) change in diffusivity that occurs in response to annealing during each time step and apply specifically to Durango apatite. When extrapolated to non-Durango samples, the values evolve as a

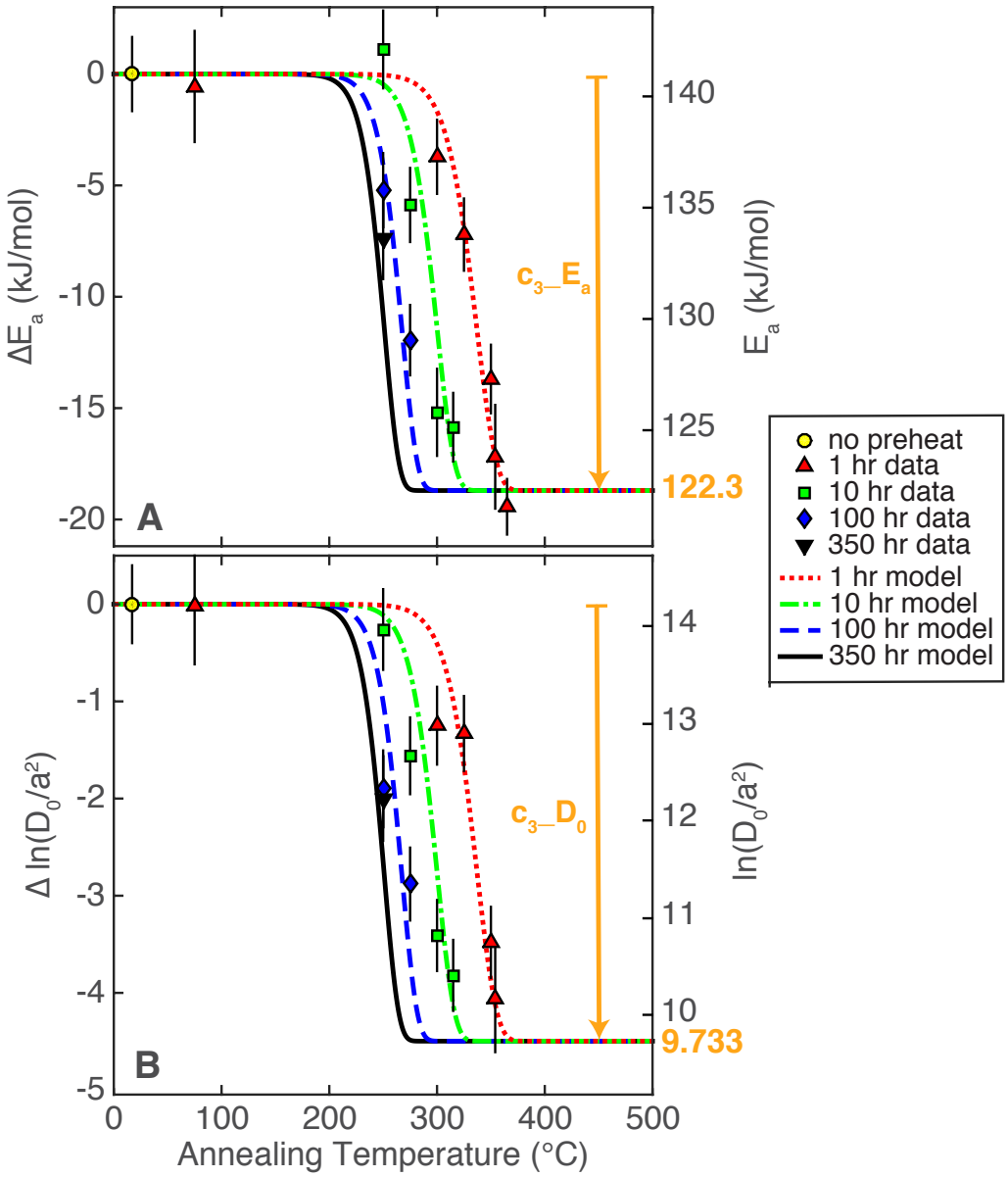

Figure 3.1: Model fits to experimental data for annealed Durango apatite. (A) Measured E_a from ref. [8] (data points), along with the best-fit curves identified by the misfit minimization of Equation 3.1 (lines). (B) Data and best-fit result for $\ln(D_0/a^2)$ and Equation 3.2. (D_0/a^2) values are normalized to s^{-1}. In both panels, the left y-axis is a change in each diffusion parameter relative to unannealed Durango apatite (yellow circle), while the right y-axis is the absolute value of the parameter. The c_3 value shown in each panel is specific to the kinetics of Durango apatite.

function of time and temperature. For the empirical fits, we also required all values to be above the minimum values for fully annealed apatite [6], and thus exclude nine experimental results with lower values. To calibrate our function, we use data of 14 annealing and diffusion experiments conducted between 17 and 365 °C for between 1 to 350 hours.

For each combination of the four parameters, we calculate a χ^2 misfit value between the observed values (i.e., of either ΔE_a or $\Delta \ln(D_0/a^2)$) and their respective model prediction for a given annealing condition. To be consistent with experimental results [8, 21], after modifying E_a and $\ln(D_0/a^2)$ by annealing (i.e., for a given set of parameter values) we also require diffusivity to be the same or higher over modeled temperatures of 0 to 600 °C and up to 10-Ma steps. Each set of four parameters is tested together and must result in increasing (or unchanging) diffusivity; the ΔE_a or $\Delta \ln(D_0/a^2)$ pairs can not be considered independently. As in ref. [6], we use a proxy to track total radiation damage and its annealing. The "effective damage density" (EDD) evolves through model time and provides an empirical relationship between an abundance of radiation damage and the diffusion kinetics of a given sample. At the start of each time step, the ADAM calculates the number of decays from U and Th concentrations and converts those decays into an effective damage value using the damage addition relationship from ref. [6] (Section 3.5). This multiplies the number of decays by the ratio of the fission and α-decay constants and the net length of fission fragments from decay of ^{238}U. This is added to the previous EDD and then used to determine the E_a and $\ln(D_0/a^2)$ of the sample using the relationships between E_a and ETD ("effective track density") and $\ln(D_0/a^2)$ and ETD [6]. Note that ETD and EDD are comparable, but given different names to emphasize that damage in the ADAM is not tied to the AFT system. For a temperature and duration, E_a and $\ln(D_0/a^2)$ are then modified according to Equations 3.1 and 3.2, respectively, using the E_a and $\ln(D_0/a^2)$ at that step to calculate the c_3 values used. The new E_a and $\ln(D_0/a^2)$ values are used to calculate He diffusivity and, in combination with the modeled ^{4}He concentration in the crystal, the model AHe age at that time step. The resultant E_a value is then used to determine the EDD after annealing has taken place, per the relationship described above. The EDD and apparent age at the end of the time step are calculated and stored, and the model moves to the next time interval.

By using Equations 3.1 and 3.2 and calculating c_3 values at each time step as the difference between the EDD-determined kinetics parameter and the corresponding minimum value, we assume that the net change in diffusion parameters at each time step will be greater when the amount of damage present in the crystal is higher. We also assume that these experimentally-calibrated expressions can be extrapolated over geologic timescales. We discuss each assumption and its implications in Section 3.5.

3.4 Results

3.4.1 Best-fit model parameters

Fig. 3.1 shows the best-fit result for the functions for both ΔE_a and $\Delta \ln(D_0/a^2)$ and the data used for calibration. The calculated values for the c_3 parameters are: $c_3\_E_a$ = 18.7068 kJ/mol and $c_3\_D_0$ = 4.497 in natural logarithm units normalized to s^{-1}. The best-fit values for the four parameters are: $c_1\_E_a$ = 58.6, $c_2\_E_a$ = -21820, $c_1\_D_0$ = 58.4, and $c_2\_D_0$ = -21700. The constraint on the tested parameter sets is shown in Fig. 3.2 as a "heat map" of parameter pairs colored by their χ^2 misfit. The parameter pairs for ΔE_a and for $\Delta \ln(D_0/a^2)$ cannot be chosen independently based on misfit values in panel A and panel B; doing so would circumvent the described diffusivity test. Model sensitivity and parameter covariance are discussed in Section 3.5.

3.4.2 Model comparisons and implications

We compare the ADAM with the Radiation Damage Accumulation and Annealing Model (RDAAM; ref. [6]) to illustrate cases where different treatments of radiation damage annealing influence the modeling and interpretation of data. Using five reference time-temperature (t–T) scenarios [66], Fig. 3.3 compares model AHe ages through time for both the ADAM and the RDAAM using an effective uranium concentration value (eU, computed as [U] + 0.235*[Th]; ref. [67]) of 28 parts per million (ppm), 'typical' of apatite samples used in low-temperature thermochronology studies [6]. Unless otherwise specified, the model crystal is unzoned and the grain size is 70 µm for both models throughout this chapter.

The He Partial Retention Zone (HePRZ) is the range of temperatures over which the modeled He age changes rapidly in a particular phase: low temperatures cause near-quantitative He retention whereas high temperatures cause higher rates of diffusive loss of He [66]. At >80 °C or <40 °C for the majority of the model run (i.e., outside the HePRZ), the ADAM and RDAAM predict indistinguishable ages (Fig. 3.3A, 3.3B). For these cases of rapid exhumation or simple cooling, this means that the two models will produce essentially identical results, supporting the conclusions of many published low-temperature thermochronology studies. Scenarios that result in significantly different model ages (Fig. 3.3C–3.3E) are t–T paths that include substantial durations in HePRZ temperatures of 40–80 °C, where the influence of damage annealing is significantly different between the models. In Fig. 3.3E, a slow heating followed by relatively rapid cooling, the ADAM predicts an age 30% older than the age calculated by the RDAAM for the same model inputs. These results demonstrate that the choice of annealing model can greatly influence data interpretation in cases where the temperature of a given sample is thought to increase and then decrease with time, as in cases of deep reburial during sedimentation. Model results for the same t–T paths run at very low and very high temperature are shown in Fig. 3.4 and the implications are discussed in Section 3.4.2.1.

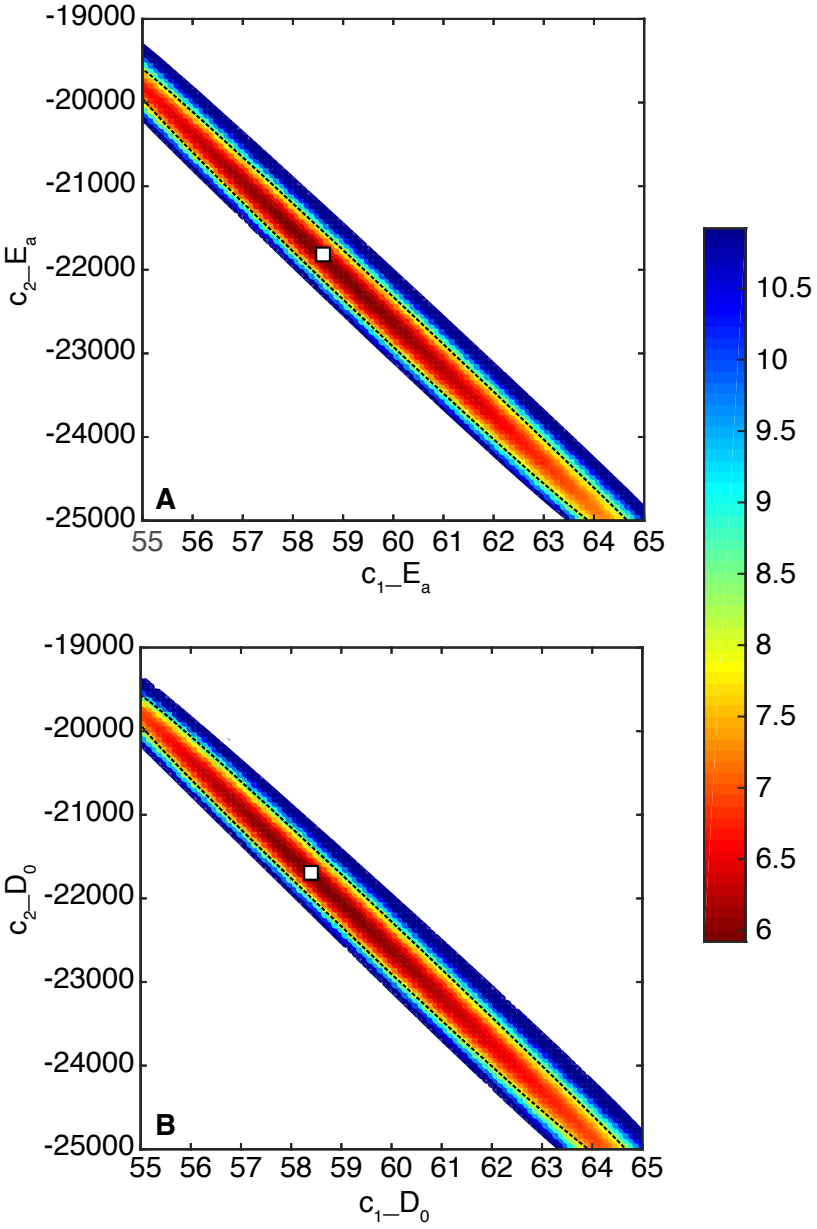

Figure 3.2: Model parameter misfit and optimization. (A) Pairs of $c_1\_E_a$ and $c_2\_E_a$ from Eq. 3.1, colored by reduced χ^2 misfit calculated between the model predictions and data shown in Fig. 3.1. (B) Pairs of $c_1\_D_0$ and $c_2\_D_0$ from Eq. 3.2, colored by reduced χ^2 value. Color bar indicates the reduced χ^2 misfit where red is low and blue is high. White squares indicate the parameter pairs for the best fit. The gray contour in each panel shows the estimated 95% confidence interval. Note that the two pairs of parameters (i.e., for E_a and $\ln(D_0/a^2)$) cannot be selected independently, as all four parameters must be tested together.

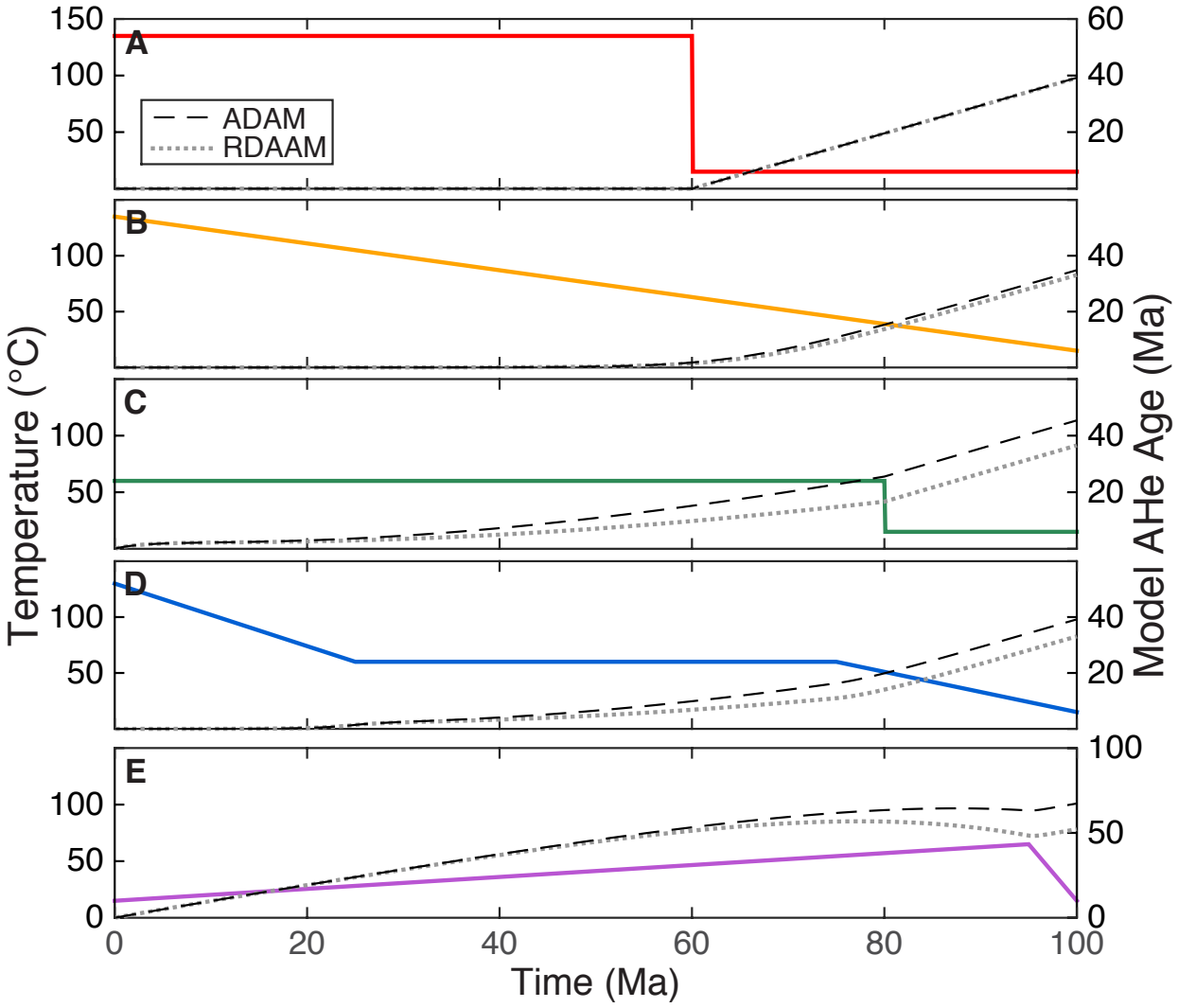

Figure 3.3: Comparisons of the ADAM and the RDAAM using five canonical time-temperature paths from ref. [66] and an eU of 28 ppm. Both models use a 100,000-year time step and predict nearly identical ages through time in cases where temperatures reside mostly outside the HePRZ (A and B). Paths with the longest residence in the HePRZ result in the largest difference between model ages (C, D, and E). See Fig. 3.4 for very low and very high eU values.

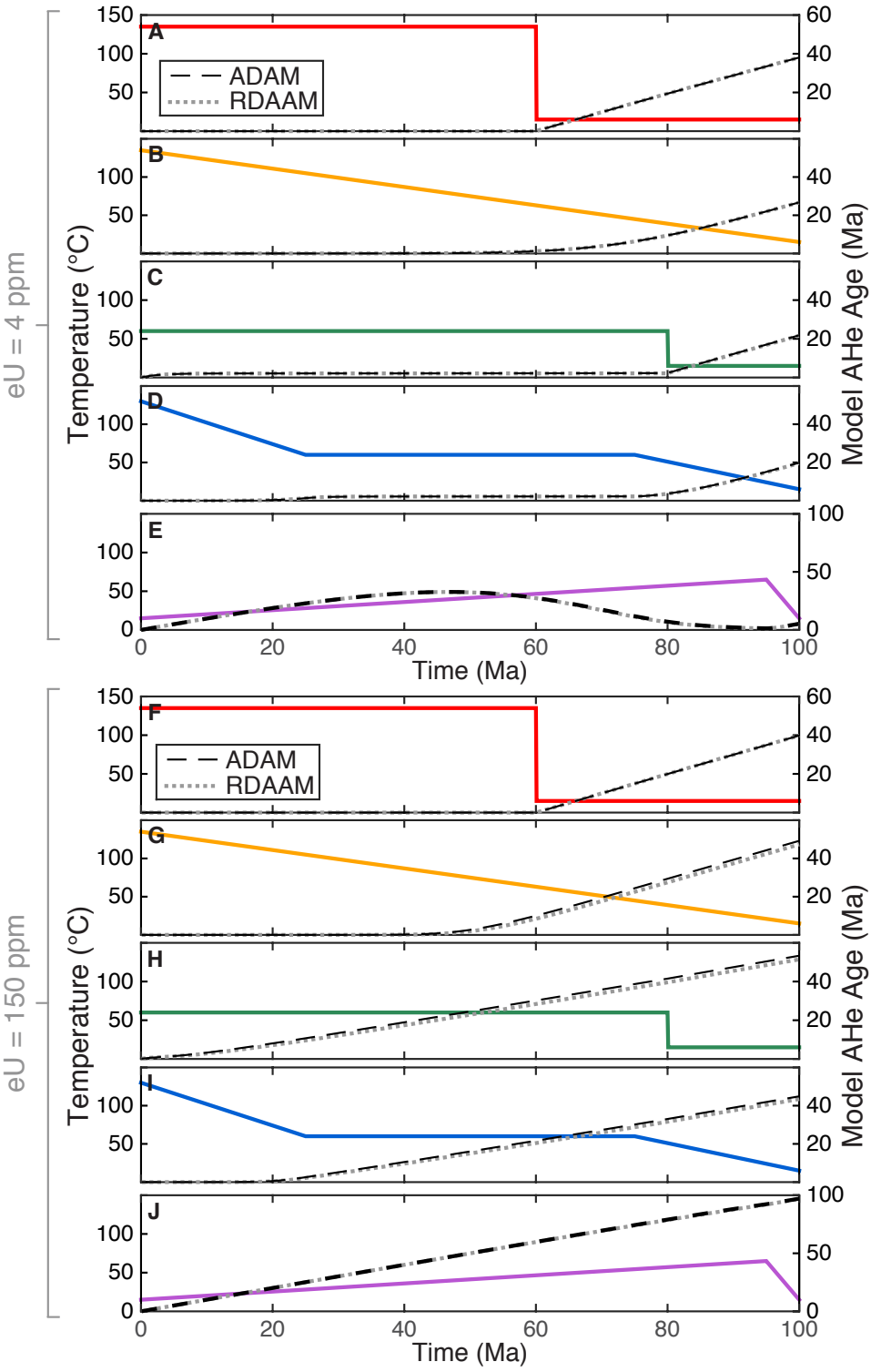

Figure 3.4: (Caption next page.)

Figure 3.4: **(Previous page.)** Comparisons of the ADAM and the RDAAM using five canonical time-temperature paths from ref. [66] with a low eU (4ppm, A–E) and a high eU (150 ppm, F–J). All calculations use a 100,000-year time step. Unlike the results shown for an eU of 28 ppm (Fig. 3.3), in these cases, the models predict similar ages for all paths. At an eU of 4 ppm, both the ADAM and the RDAAM deviate minimally from the initial diffusion kinetics values and remain near fully-annealed. At 150 ppm, the rate of damage accumulation dramatically outpaces the rate of annealing for both models. Damage accumulates steadily, resulting in old ages (J). As a result, the treatment of damage annealing is particularly important when modeling samples with intermediate eU values.

The model results from Fig. 3.3 are shown as a ratio through time in Fig. 3.5, with the ADAM ages normalized to ages calculated by other models. Fig. 3.5A compares the ADAM to model ages calculated assuming the diffusion kinetics of Durango apatite [54], and shows that only the path that begins at surface temperatures followed by reheating predicts an age for the ADAM that is older than that for Durango kinetics. In the other four cases, the ages calculated assuming Durango kinetics are equal to or older than the ages from the ADAM. Fig. 3.5B normalizes the ADAM ages to the RDAAM and demonstrates that the RDAAM predicts a higher rate of increase in diffusivity due to damage annealing (i.e. resulting in younger ages) than does the ADAM for the entirety of these specific t–T scenarios and when eU is 28 ppm. The eU ultimately controls which model will predict an older or younger age for a given t–T scenario, and is explored in the following two sections.

3.4.2.1 The HePRZ and the influence of eU

To illustrate the behavior of the HePRZ using the ADAM, we calculate AHe ages for samples held for 75 Ma at constant temperatures ranging from 0 to 120 °C and eU values from 4 to 150 ppm (Fig. 3.6A). The curves calculated using Durango diffusion kinetics [54] and AFT thermochronometry [68] are included for comparison. The HePRZ for the ADAM shows a similar sigmoidal shape; however, as is the case of the RDAAM, the temperature range of the ADAM HePRZ changes based on the eU in the grain. Samples of low concentration (eU of 4 ppm) will demonstrate this behavior over a temperature range of approximately 30 to 50 °C, while samples whose eU is 150 ppm show a HePRZ between about 70 and 90 °C. Higher parent concentrations lead to more crystal damage, hence greater He retentivity and an older apparent age at a given isothermal holding temperature. The effect of grain size on the calculated HePRZ is secondary to the eU control, as is the case with the RDAAM [6].

A comparison between the ADAM and RDAAM for these isothermal conditions is shown in Fig. 3.6B. For both models, there is a positive, nonlinear correlation between AHe age and eU. This dependence on eU is most strongly pronounced in both models at the middle of the HePRZ temperature range, at 60 °C, where the model age is as low as ∼3 Ma and as high as ∼65 Ma. Under these conditions we also find the largest differences in predicted

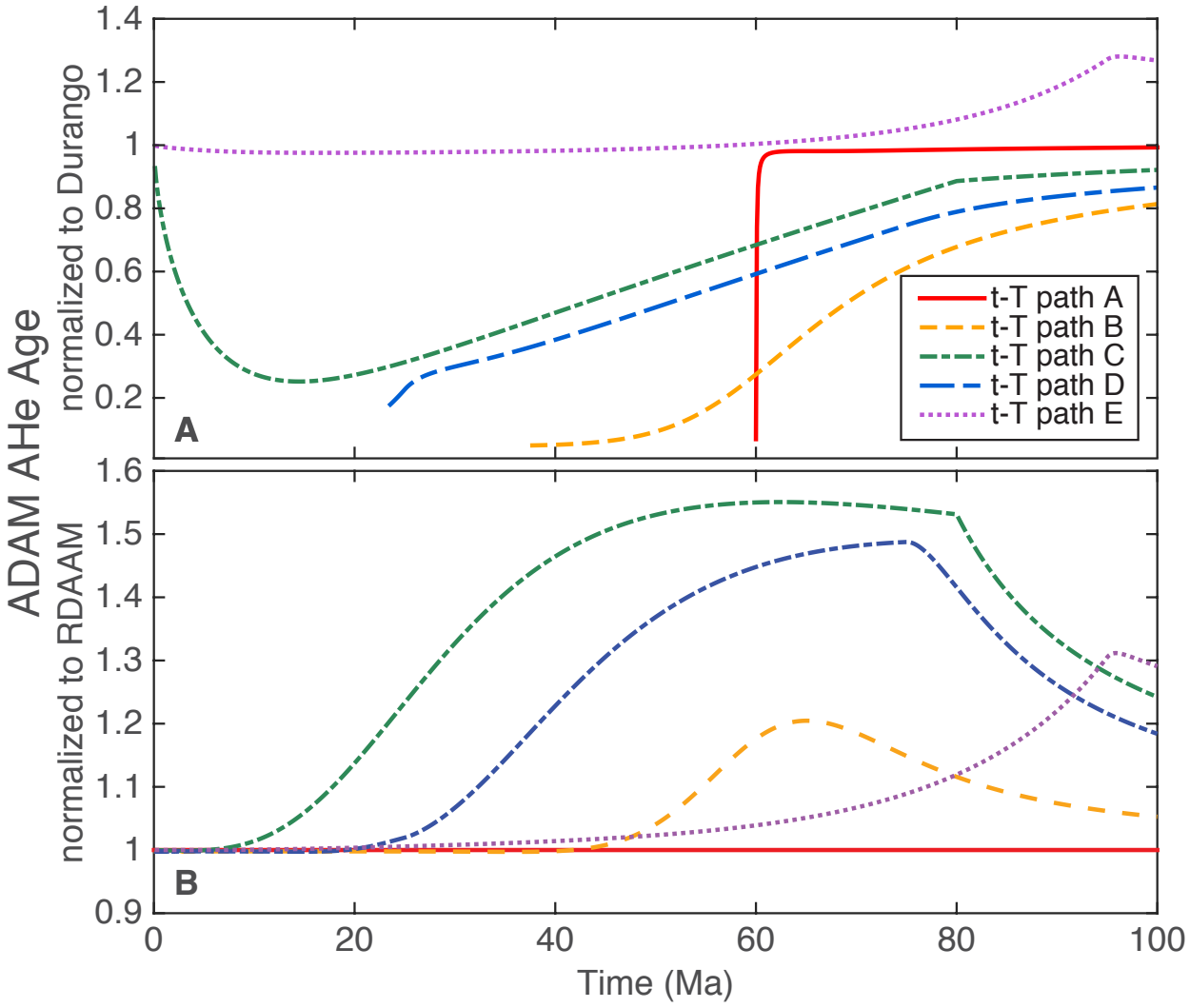

Figure 3.5: Comparisons of model age through time for the five t–T paths used in Fig. 3.3. (A) AHe ages predicted using the ADAM normalized to ages calculated using the kinetics for Durango apatite [54]. (B) ADAM ages normalized to the RDAAM through model time. For eU of 28 ppm, the ADAM consistently predicts an equal or older age than the RDAAM, suggesting that the RDAAM may be over-annealing damage for certain eU values.

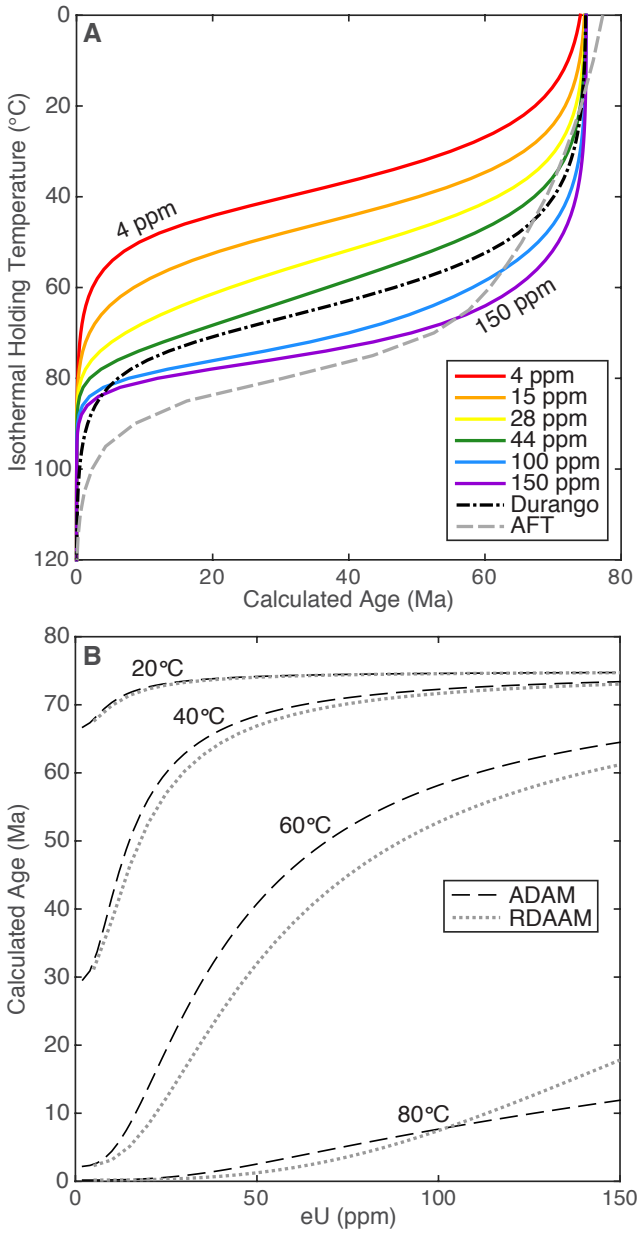

Figure 3.6: Comparisons of model ages for isothermal conditions. (A) Calculated AHe ages for a range temperatures and eU values for 75 Ma of isothermal holding using the ADAM. We also show ages calculated assuming Durango apatite diffusion kinetics (black dash-dot line; ref. [54]) and apatite fission track ages (grey dashed line; ref. [68]) for comparison. (B) Calculated AHe ages for both models as a function of eU for 20, 40, 60, and 80 °C and a hold time of 75 Ma. For the lowest three temperatures, the ADAM predicts ages that are systematically older than those predicted by the RDAAM. In the case of the 80 °C isothermal hold, a crossover in models occurs.

ages between the two models, by as much as 65%. Simulated ages from the two models are the same or older with the ADAM in all cases except for cases of isothermal holding at 80 °C above roughly 100 ppm eU. The ADAM anneals damage at a rate that is proportional to the amount of damage present. Conversely, the evolution of fission track annealing used in the RDAAM is the same for each track, calculated solely as a function of temperature and time, regardless of how many are present. Consequently, there is an eU concentration in certain thermal paths above which the RDAAM predicts an older age than the ADAM, and below which the reverse is true. In cases of low eU, rates of annealing tend to be low in both the ADAM and RDAAM and the model outputs converge. The eU value of 28 ppm used in Fig. 3.3, again chosen as a 'typical' eU value for apatite, produces a significant difference between the two models' ages; however, this difference in modeled age is less pronounced in cases of very low and very high eU values (see Fig. 3.4). At high eU, the rate of damage accumulation far outpaces annealing for both models and damage accumulates steadily, thus resulting in old ages (Fig. 3.4J). At low eU, both the ADAM and RDAAM deviate minimally from damage-free diffusion kinetics over model time, and therefore remain near invariant. For these thermal paths (Fig. 3.3), the competition between damage accumulation and annealing, thus differences between the models, is greatest at intermediate eU values.

3.4.2.2 Continuous thermal path examples

The influence of radiation damage annealing on the AHe system will be most pronounced in scenarios that involve gradual reheating through geologic time (Fig. 3.3). Thus, any inaccuracy in, and differences between, kinetics models are most likely revealed in samples that experienced such conditions. As an example to illustrate the sensitivity of both models to reheating, we consider data collected from basement rocks from the bottom of Grand Canyon [69–72]. The hypothetical t–T path shown in Fig. 3.7A is at Earth surface temperatures for 172 Ma, then increases to 80 °C over roughly 210 Ma, simulating slow reheating via deep sedimentary burial. After residing at 80 °C for 30 Ma, temperature slowly decreases to 60 °C over a 90-Ma period, where it remains until rapidly decreasing from 60 °C to 0 °C in the final 6 Ma of simulated time. This individual path, consistent with a "young canyon" model [70, 73, 74], obeys the constraints used to search potential western Grand Canyon t–T paths in ref. [63]. The predicted AHe ages as they evolve through time are shown in the bottom panel of Fig. 3.7A for both models and two eU values. As with Fig. 3.3 and Fig. 3.4, the eU will influence which model predicts an older age for a given path. At the end of the thermal path, the ADAM predicts an older age than the RDAAM for low eU (10 ppm), while the opposite is true when eU is 40 ppm. This dependence on eU value is explored further below and in Fig. 3.8.

Fig. 3.7B shows a histogram of observed AHe ages from western Grand Canyon [69–71] and histograms of predicted ages for the RDAAM and the ADAM for the thermal path shown in Fig. 3.7A. The models each use the observed U and Th concentrations of the apatites shown in the data panel. For this thermal path, the model ages predicted by the ADAM are in better agreement with the measured ages and have a narrower distribution

than the wide range of ages predicted by the RDAAM. In the ADAM treatment of annealing, where the net change in diffusion kinetics for a given temperature and duration increases with greater amounts of damage present, grains with high eU are predicted to be old assuming the RDAAM kinetics, but significantly younger assuming the ADAM. At low eU, and therefore lower EDD values through all time, the changes in diffusion kinetics due to annealing predicted by the ADAM are smaller than for the RDAAM, thus resulting in slightly higher He retentivity and older ages. The net effect, shown in the lower two panels of Fig. 3.7B, is that for the assumed thermal path, the RDAAM predicts a larger spread in AHe ages, whereas the ADAM predicts a narrower distribution of ages. That is, the young ages predicted by the RDAAM are shifted to older ages, and very old are shifted to much younger ages by the ADAM treatment of damage annealing.

The relationships between eU and both observed and predicted AHe ages from Fig. 3.7 are shown in Fig. 3.8. The ADAM and RDAAM both have distinct age-eU correlation, but this dependence is less dramatic with the ADAM. Both models fail to predict the 50–100 Ma ages for grains with low eU (i.e., <15 ppm). As with the 80 °C isothermal case in Fig. 3.6B, for any given thermal path, there is an eU value that serves as a "crossover point": below a certain value (∼18 ppm in Fig. 3.8 and ∼100 ppm in Fig. 3.6B) the ADAM predicts an older age, whereas the opposite is true above that value.

Previous work in western Grand Canyon calls on the complete resetting of the AFT system to constrain temperature conditions of 110–120 °C between ∼100 and 80 Ma [75]. When used to constrain the thermal history along with AHe ages, these conditions ultimately require an old canyon solution (reaching near-modern topography by ∼70 Ma; ref. [70]) since they predict complete resetting of apatite to maximum He diffusivity (i.e., resetting of both radiogenic 4He and radiation damage content; ref. [63]). Under the 110–120 °C conditions, both models predict virtually the same age distributions, as the influence of damage annealing is negligible at low temperature (e.g., Fig. 3.3A). The example young canyon path whose ADAM ages agree with measured AHe ages, the t–T path shown in Fig. 3.7, does not meet a 110–120 °C criterion during the Paleozoic; however, the model is entirely He-based and internally consistent. Constraining Paleozoic temperatures to 110 °C for a young canyon scenario causes both models to fail to predict the observed AHe ages (Fig. 3.9). However, recent work constrains t–T paths whose maximum temperatures are between 80 and 110 °C, and demonstrates ongoing uncertainty surrounding maximum burial conditions and the timing of western Grand Canyon incision [71].

3.5 Discussion

As with other treatments of He diffusivity in apatite, applications of the ADAM require important assumptions. Here, we discuss model extrapolations from the experimental time and temperature conditions shown in Fig. 3.1, and to different apatite characteristics. We then discuss issues specific to the ADAM and limitations of the model. Finally, we suggest a number of geologic tests that could ultimately help improve our understanding of controls

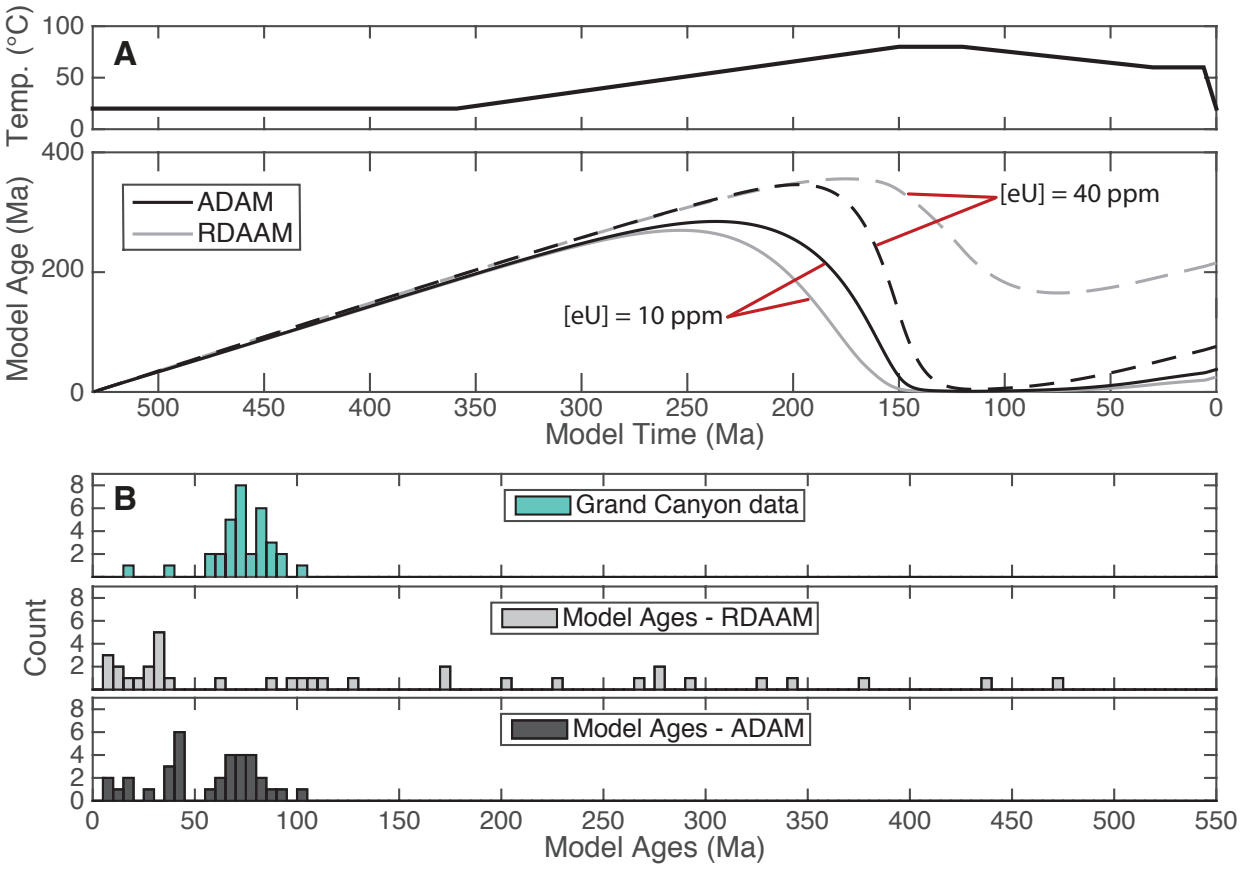

Figure 3.7: A comparison of the ADAM and the RDAAM, using a hypothetical t–T path corresponding to a young-canyon model of western Grand Canyon. Chosen here to illustrate differences between the two kinetic models, Panel A is an example of a young canyon thermal path that is compatible with available data and shows calculated AHe ages through time for eU values of 10 and 40 ppm. Panel B shows a histogram of the measured ages (green, data from refs. [70] and [71]) and the ages predicted by the two different kinetic models (gray and black) using the observed values of eU. While both models are sensitive to eU, this example demonstrates that for this assumed thermal path, the spread of AHe ages calculated by the RDAAM is far broader than that predicted assuming the ADAM.

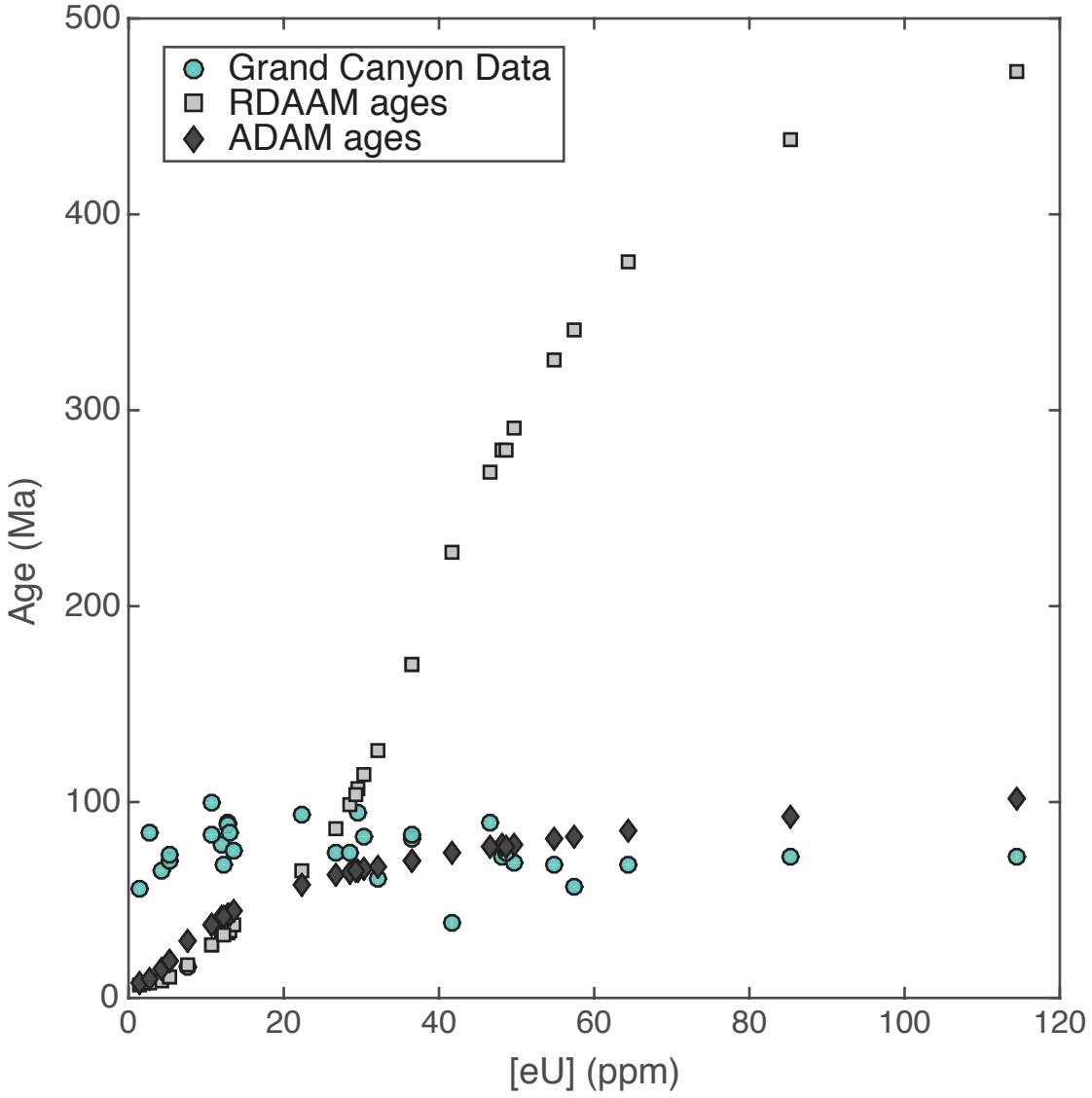

Figure 3.8: A comparison of measured and predicted AHe ages versus the measured eU for published data from western Grand Canyon (green circles, data from refs. [70] and [71]) assuming the hypothetical t–T path shown in Fig. 3.7A. The RDAAM results (black squares) show a stronger age dependence on eU for this t–T path than the modeled ages of this study (gray diamonds). Both models fail to predict the high ages (50–100 Ma) at low eU (<15 ppm).

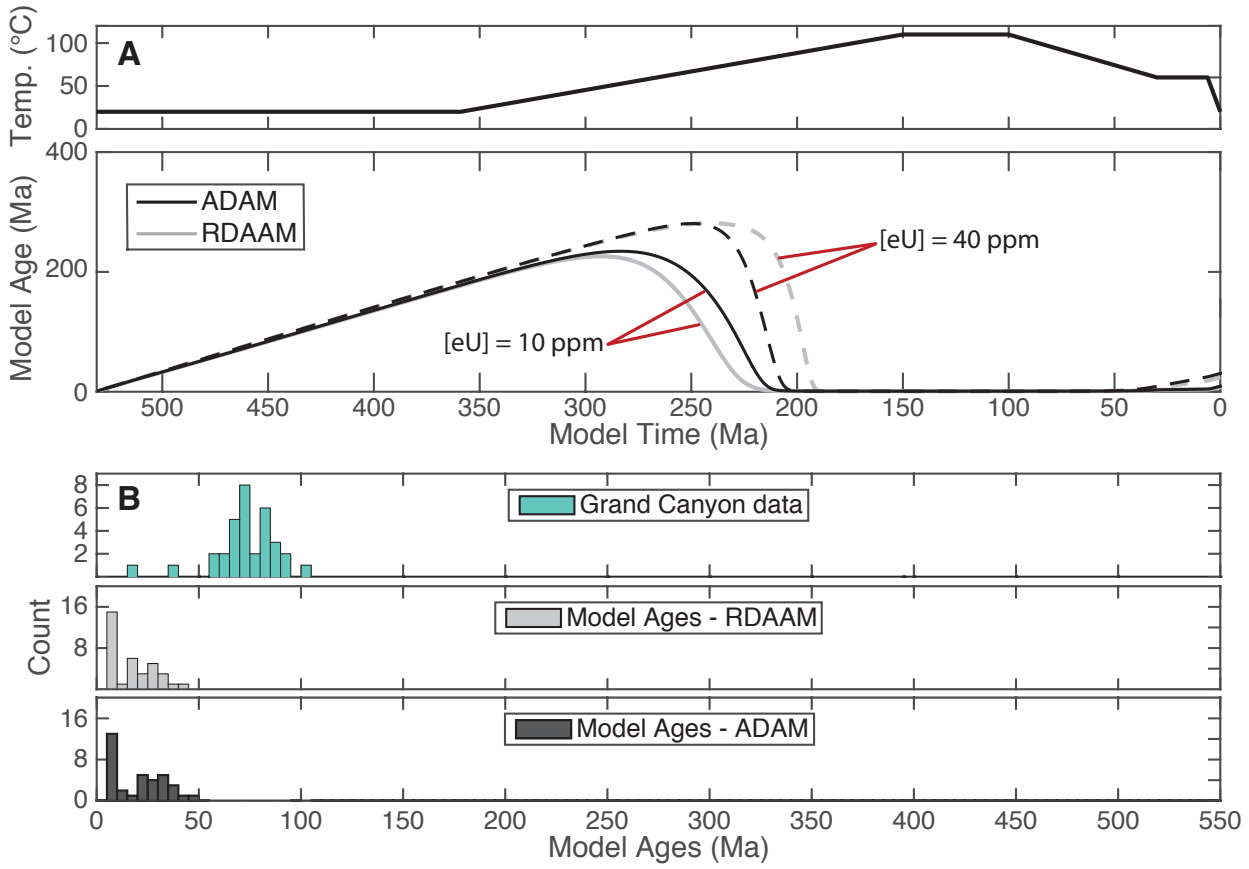

Figure 3.9: A comparison of the ADAM and the RDAAM, using a hypothetical t–T path that reaches the 110 °C condition at 100 Ma proposed in the Flowers and Farley study of western Grand Canyon [70]. Panel A shows the thermal path and calculated AHe ages through time for eU values of 10 and 40 ppm. Panel B is a histogram of the measured ages (green, data from refs. [70] and [71]) and the ages predicted by the two different kinetic models (gray and black) using the observed values of eU. This figure demonstrates that neither diffusion model predicts AHe ages that match the data if the 110 °C temperature condition is included. All predicted ages are too young.

on He diffusivity in apatite, and quantify a model framework that most accurately predicts relatively low-temperature processes near Earth's surface.

3.5.1 Model extrapolations

3.5.1.1 Extrapolating from laboratory conditions to geologic timescales

A somewhat unusual challenge in Earth science is the need to use experimental observations made on laboratory timescales to study processes and phenomena that are active over geologic timescales. While both models discussed in this paper are justified by laboratory data (e.g., refs. [8, 21]), implementing either model, or other models for the AHe system (e.g., ref. [7]), requires the assumption that what has been determined in the lab can be accurately extrapolated to geologic timescales and temperatures. Because laboratory experiments are limited to durations orders of magnitude shorter than geologic timescales, we commonly increase experimental temperatures to achieve a similar net effect. Therefore, implementing the model necessitates extrapolation in both time *and* temperature, which may lead to inaccuracy as the fit proposed in this paper is not based in a physical model, but rather is based on a mathematical function chosen to fit the published data.

Because Equations 3.1 and 3.2 each contain two natural logarithms, the influence of c_1 and c_2 on the shape of the model curves is similar. Decreasing either value results in increased spacing between the duration curves and causes the rollover portion of the curves to be less steep and to begin at higher temperature (Fig. 3.10). The c_2 values have an increased temperature sensitivity due to the multiplication with inverse temperature. The trade off between c_1 and c_2 is shown by the oblong ellipses in Fig. 3.2, a clear indication that the parameters covary.

Experiments with longer annealing times (i.e. months to years, as opposed to hours) at lower temperatures would offer a modest amount of information about model accuracy and c_1 and c_2 values and potentially inform the use of Equations 3.1 and 3.2 in the ADAM. Such longer experiments could serve to validate the quantitative relationship more than provide insight into geological processes and timescales, whereas certain geologic tests, discussed in Section 3.5.3, may offer deeper insight into extrapolation accuracy.

3.5.1.2 Influence of apatite chemistry

The fit shown in Fig. 3.1 was optimized using the only available experimental data on the effects of annealing of Durango apatite [8], which is a fluorapatite with atypically high Th concentration and a measured AHe age of 31.02 ± 1.01 Ma [76]. Apatite, chemical formula $Ca_5(PO_4)_3(OH, Cl, F)$, spans a range of anion chemical compositions, which may influence the rates of both accumulation and annealing of damage in a given apatite [9, 77]. If so, such chemical variability could influence AHe ages in certain thermal histories, and may therefore influence geologic interpretations if such chemical control on annealing is not properly understood. Our framework for fitting an annealing function to directly

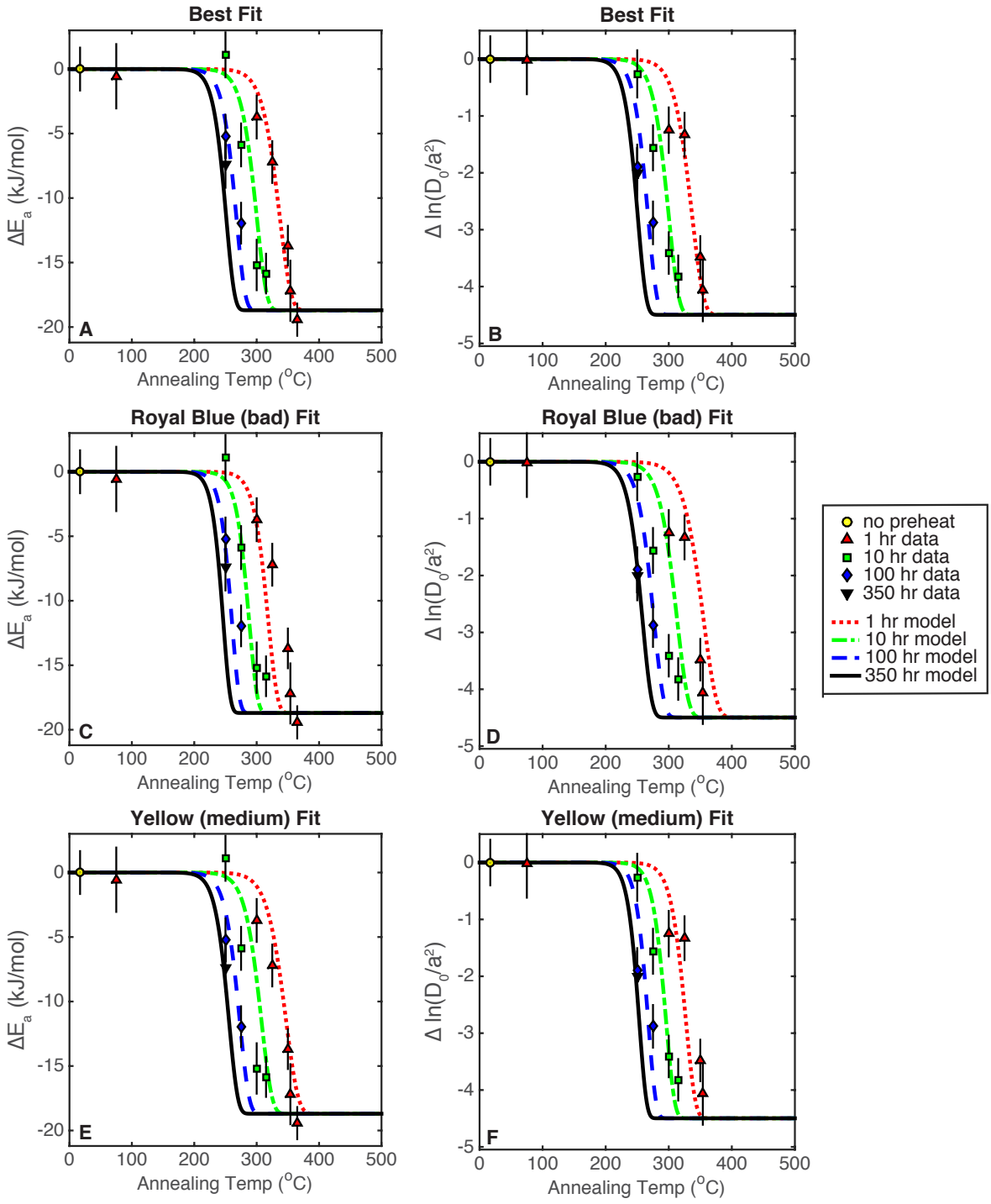

Figure 3.10: (Caption next page.)

Figure 3.10: **(Previous page.)** Alternative model fits to experimental data for annealed Durango apatite. (A–B) Measured diffusion parameters and best-fit model from Fig. 3.1. (C–D) Measured diffusion parameters and poorly fitting model, for misfit of ∼10 (blue color misfit in Fig. 3.2). (E–F) Measured diffusion parameters and selected intermediate fitting model, for misfit of ∼7.75 (yellow color misfit in Fig. 3.2). D_0/a^2 values are normalized to s^{-1}.

calibrate the effects of radiation damage on He diffusivity may require further refinement when additional experimental results on other apatites are collected.

3.5.2 Model limitations

3.5.2.1 Model sensitivity

The set of four parameters used in Equations 3.1 and 3.2 were selected by identifying the lowest total misfit between the calculated model curves and the published diffusion kinetics data. Although Fig. 3.2 shows the parameter pairs and their misfit, it offers little intuition as to how sensitive our "best fit" model is. Fig. 3.10 shows examples of model misfits colored blue and yellow in Fig. 3.2 and confirms that the selected best-fit model appears to better visually match the data. Also note that we are limited to 14 data points in this fit; more data would allow for a better-constrained fit. An effort to collect more data of this type is included in Chapter 4 of this dissertation.

3.5.2.2 E_a-EDD limitations

The chosen relationship between EDD and diffusion kinetics, particularly when determining the EDD after annealing at a given model time step, requires using either the E_a-EDD or the $\ln(D_0/a^2)$-EDD relationship [6]. The determined EDD may be slightly different (<1%) between the two. Here, we use the E_a-EDD relationship because of the unique relationship between the variables, whereas the $\ln(D_0/a^2)$-EDD curve rolls over, with pairs of EDD values corresponding to a single $\ln(D_0/a^2)$ value. Our use of the published E_a-EDD relationship leads to another limitation in the ADAM, since the empirical data of ref. [21] and quantitative relationships in ref. [6] only span E_a values of 122.3–156.3 kJ/mol and EDD values between 10^4 and 10^7 tracks/cm^2.

If a crystal contains much lower or higher damage concentrations, one must extrapolate beyond the available data. If any measured apatite E_a exceeds 156.3 kJ/mol, or if an apatite is believed to be fully annealed and has an E_a much different from 122.3 kJ/mol, a different relationship would be needed to relate these values to the corresponding EDD and the fitting exercise would be re-done. Additionally, these relationships carry their own error [6]; further

experimental work will improve and constrain these relationships, or something similar, and can then be incorporated into this proposed model framework.

3.5.2.3 EDD-dependent annealing

By employing Equations 3.1 and 3.2, the ADAM assumes that the absolute change to the diffusion kinetics parameters, ΔE_a and $\Delta \ln(D_0/a^2)$, is proportional to the amount of damage present at the beginning of that time step. The RDAAM, however, calculates the damage added to the crystal structure and the quantity annealed given a t–T path based on the temperature-dependent length reduction of fission tracks in the AFT system, which is unrelated to the total amount of damage present within the crystal. Other studies have determined that in certain geologic conditions, the RDAAM overestimates the rate of change in diffusion kinetics resulting from fission track annealing [63, 77, 78]. Although damage annealing rates are critical to understanding both the AFT and AHe systems, quantifying the rates and understanding their mechanisms in both apatite and zircon is ongoing work. The rate of damage annealing has been suggested to vary with damage concentration in zircon and to occur by multiple mechanisms [79], supporting this EDD-dependent annealing assumption made in the ADAM, although it is unclear how mechanisms operating at high damage content apply to apatite [80, 81]. Furthermore, others have used empirical data for fitting exercises similar to the one presented in this publication: the authors of ref. [82] employ a linear relationship between track shortening and track density while the authors of ref. [83] fit both hybrid linear and parallel-curvilinear fits for AFT in zircon, demonstrating the diversity in functional form used to quantify radiation damage annealing.

The amount of pre-existing damage in an apatite may influence the relationship between the rate of annealing and He diffusivity. For example, the mechanism of damage annealing may differ in the condition of very little damage or in the condition of approaching a percolation point, where the effective He diffusivity is expected to increase substantially due to intersecting zones of damage [5, 21, 79, 84–86]. Future experiments on the effects of reheating temperature and duration on He diffusion kinetics in a range of apatite samples would test these outlined assumptions, particularly the scaling of the functions via the evolving $c_3\_E_a$ and $c_3\_D_0$ parameters. For example, experiments could be conducted on very young and very old apatite samples or apatites with synthetically-generated radiation damage [21]. Such experiments would help evaluate whether the effects of thermal annealing on He diffusion kinetics depend on the amount of pre-existing damage.

Recent work in atom-probe tomography (APT) suggests that direct visualization of α-recoil damage is possible in apatite. The technique has been used in the mineral zircon [62] and offers the potential to both visualize and quantify damage content. APT has been used to identify nano-crystalline biological apatites [87], but conducting analyses like those if ref. [62] on larger, non-biologic apatite crystals at different stages of thermal annealing could provide a direct means of quantifying the rates of damage addition and thermal annealing, perhaps in tandem with indirect observations of spatial variations in damage obtained through step degassing and spatial mapping of parent nuclides in apatite grains [88].

3.5.3 Model validations

The largest source of uncertainty in the ADAM framework is the extrapolation of kinetic relationships through geologic time. In principle, geologic scenarios with independent knowledge of a reheating and cooling path could provide validation for laboratory-based empirical relationships. However, such scenarios often do not provide sufficient geologic precision for a definitive test. In Fig. 3.7, we use the example of a hypothetical western Grand Canyon thermal path to illustrate differences between the ADAM and the RDAAM. Although Grand Canyon provides a valuable, illustrative case, it does not provide an unambiguous test of thermochronometric model accuracy due to geologic uncertainty in the t–T path of each sample before, during, and after sedimentary burial. Here, we consider the merits of published tests and propose possible tests to validate the ADAM and other models.

3.5.3.1 What tests have been considered in the past?

The authors of ref. [6] use a number of example data sets as plausibility tests of the RDAAM. They use data from eight basement samples collected from the Upper Granite Gorge (UGG) in eastern Grand Canyon to test the hypothesis that the RDAAM should predict correlation between AHe age and eU. While a specified thermal path with the RDAAM successfully predicts the observed data, this test does not necessarily prove that the kinetic model is accurate; another model may also be consistent with the same data and a different, yet geologically permissible, thermal path. In such geologic tests, we commonly lack adequate precision, accuracy, and independent knowledge of a thermal path to confirm model accuracy.

However, the UGG test clearly demonstrates that the RDAAM predicts the data better than the Durango model [54], and also provides a valuable test for the ADAM. Interestingly, using the RDAAM-determined thermal path, the ADAM predicts the measured ages slightly better (Fig. 3.11). Although both models can successfully predict the observations, this scenario does not provide a particularly sensitive test for distinguishing between the two damage models due to the geologic setting, which involves cooling from 120 °C at 80 Ma to 5 °C today. The simple cooling path resembles the test shown in Fig. 3.3B, wherein the two models calculate nearly indistinguishable results. Geologic scenarios that mimic the tests shown in Fig. 3.3E (reheating) or Fig. 3.6B (constant temperature) would provide a better means to test radiation damage models and are described in Section 3.5.3.2.

The authors of ref. [6] also consider seven samples from the Canadian Shield. For this example, the RDAAM predicts an age-eU relationship that matches the data better than the ADAM (Fig. 3.12). However, lowering the temperature of the RDAAM-determined path between 1200 and 720 Ma by $<$12 °C brings the ADAM into better agreement with measured data, and causes the RDAAM to systematically overpredict age. While these natural tests can reveal subtleties of the models, the lack of sufficient precision and independent knowledge of past t–T conditions renders these scenarios unable to test which model more accurately quantifies effects of α-recoil damage annealing.

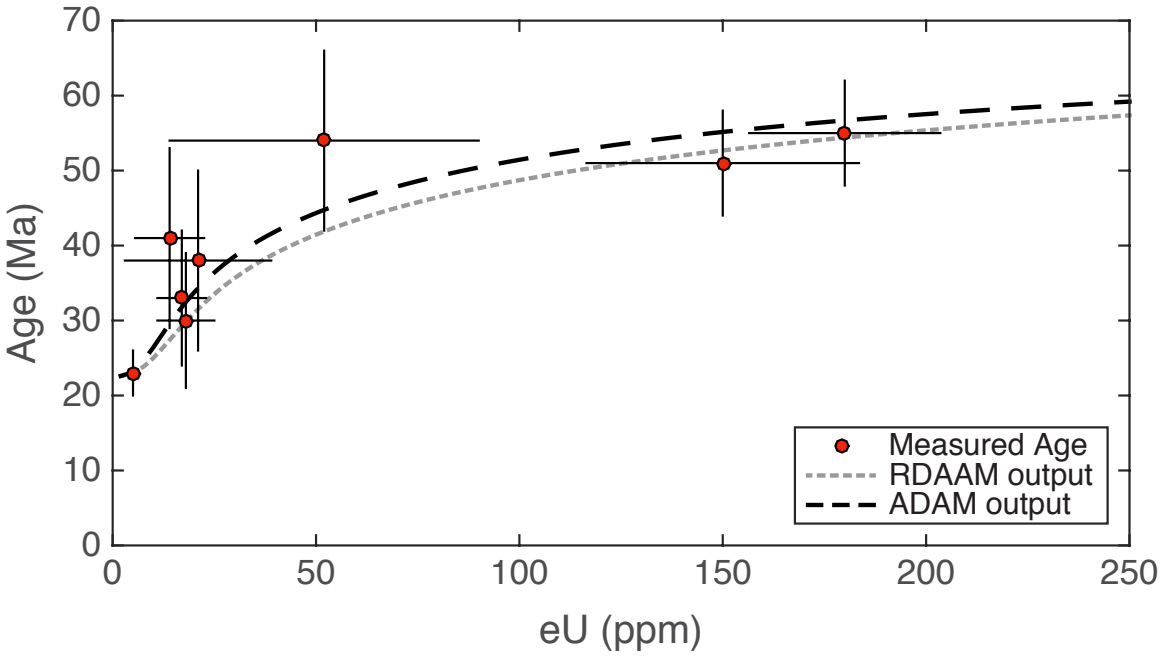

Figure 3.11: Geologic test from the Upper Granite Gorge of eastern Grand Canyon. Individual AHe ages versus eU concentration plotted alongside the model predicted ages using the RDAAM-determined t–T path in ref. [6]. The resulting RDAAM least-squares misfit is ∼378, while the ADAM misfit is ∼254. However, like nearly all geologic tests, this validation is limited, since the true t–T path is not independently known.

3.5.3.2 Proposed additional geologic tests

A natural experiment to test the accuracy of these models over long timescales would be highly informative. However, identifying sites with sufficient and independent knowledge of low-temperature thermal conditions is challenging. One potential test of the ADAM and other models is to use borehole samples, where the relationships between AHe thermochronometric ages, absolute depth, and distances between samples is known and temperatures can be assumed to have been relatively constant for extended durations. For example, apatites collected from the KTB borehole in Germany (e.g. refs. [89, 90]) are assumed to have been at nearly constant temperatures for ∼25 Ma [90]. Fig. 3.6B indicates that analyses of individual crystals spanning a range of eU should provide a sensitive test of the model accuracy. In particular, substantial differences between the ADAM and RDAAM should be resolvable in samples at ∼60 °C. However, existing AHe data from KTB samples were measured on multiple crystals simultaneously [89, 90]. From single crystal observations of borehole—or otherwise isothermal—samples, and correlation between eU and He ages, one can test whether the ADAM, the RDAAM, or some other model is most successful in a plot

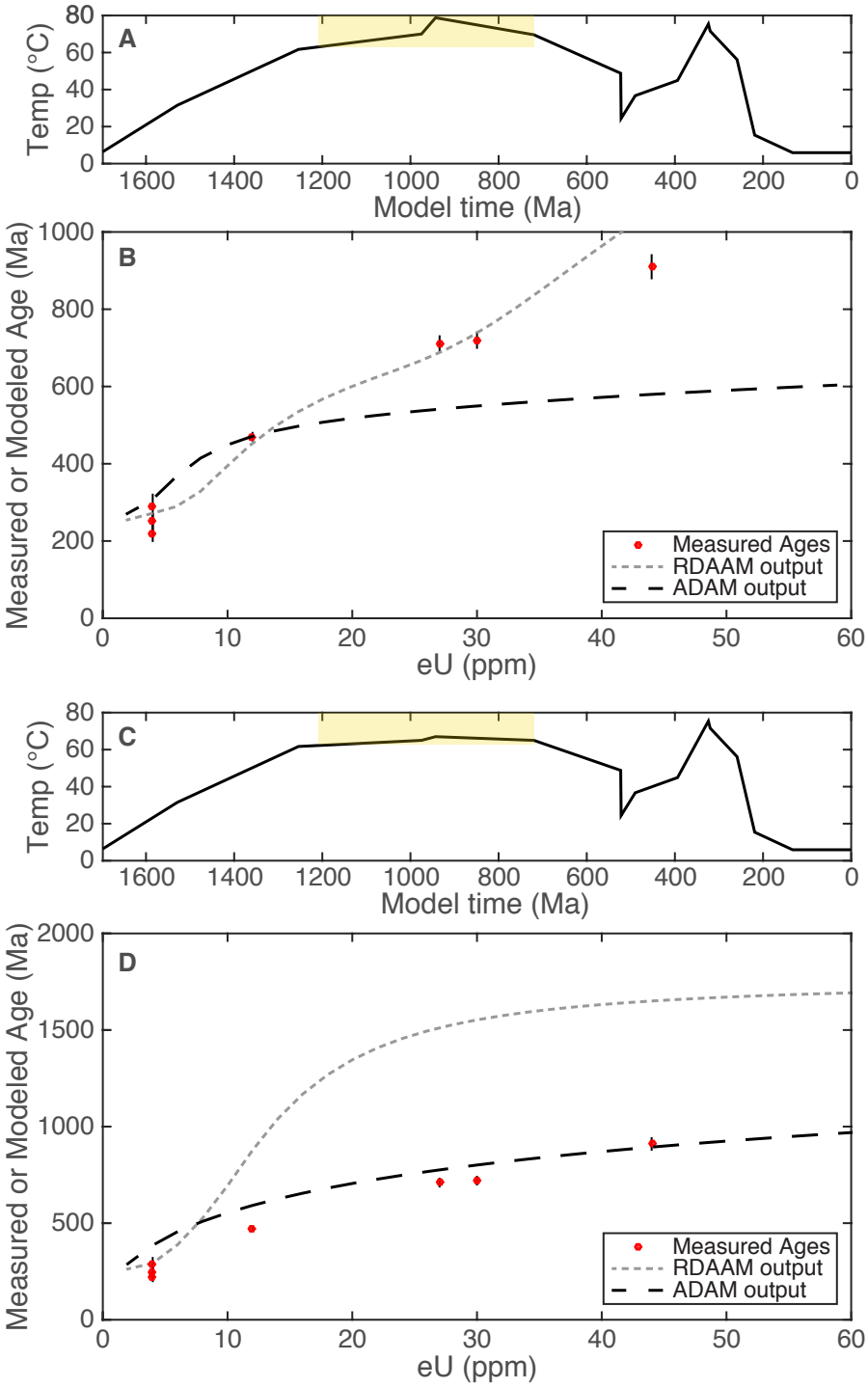

Figure 3.12: (Caption next page.)

Figure 3.12: **(Previous page.)** Geologic test from the Canadian Shield. A comparison of the ADAM and the RDAAM using the thermal path determined using the RDAAM in ref. [6] (A). Panel B shows the measured data and the model outputs for the t–T path shown in (A). The ADAM consistently underestimates the measured ages for this t–T path; however, known constraints for searching t–T space are few (see ref. [6]). The path shown in (C) differs from (A) solely by lowering the maximum temperature between ∼1200 and 800 Ma by <12 °C; the resulting model outputs (D) show the ADAM in better agreement with measured data. The yellow box highlights the only portion of the t–T that differs between (A) and (C). Note the difference in y-axis scaling between (B) and (D). Like nearly all geologic tests, this test is limited in its utility since the true t–T past is not known with sufficient precision to exclude either model.

such as Fig. 3.6B. Such data would not only provide a test of a given model framework, but could also help develop or refine existing model parameters.

Other geologic scenarios can also be used to verify models on timescales that are short by geologic standards but far exceed the constraints laboratory timeframes. Little Devil's Postpile, California, is an ∼8 Ma basalt intrusion into apatite-bearing Sierran granite. Its emplacement caused a thermal perturbation of granite that previously resided at low temperatures for tens of Ma, and can be considered a natural, long-term reheating experiment. The basalt intrusion created a thermal gradient that extended up to 16 m from the contact [91, 92]. Measured and modeled AHe ages in conjunction with diffusion experiments and thermal modeling of the intrusion offers another natural test of the ADAM and other kinetic models of annealing and diffusivity.

3.6 Conclusions

We present a new quantitative treatment of the annealing of radiation damage and its control on He diffusivity in apatite, and illustrate its influence on the modeling and interpretation of low temperature AHe thermochronology data. Instead of assuming that thermal annealing of α-recoil damage must be tied to the annealing of fission tracks in apatite, we fit an empirical set of expressions to published He diffusivity data to more directly, and independently, quantify the effects of thermal annealing on He diffusivity in Durango apatite. The resulting ADAM calculates similar ages to other models in many simple geologic cases but yields different results during extended residence in the HePRZ or when held at low temperatures and subsequently reheated to ∼40–80 °C. The ADAM predicts age-eU correlation, though it is less strong than predicted by the RDAAM in the cases we explore. We use a hypothetical example of burial reheating followed by exhumation that obeys the constraints used in studies of western Grand Canyon [63, 72]. This demonstrates that the new treatment of radiation damage annealing permits at least one young canyon scenario to

be constrained by observed AHe ages. We propose additional experimental work on apatite of differing chemistry, age, and damage content to help confirm or re-evaluate the necessary assumptions made in the construction of this model, and ultimately improve our quantitative understanding of the AHe system.

3.7 Acknowledgments

This work was supported by NSF Graduate Research Fellowship DGE 1752814 (to C.D.W.), the University of California, Berkeley, Esper Larsen Research Fund (to D.L.S.), NERC grant NE/N015479/1 (to M.F.), and NSF Tectonics Program grant EAR 1347990 (to D.L.S.). We acknowledge support of the Ann and Gordon Getty Foundation. We thank An Yin for editorial handling of the manuscript, and Cécile Gautheron and an anonymous reviewer for their helpful suggestions.

Chapter 4

Experimental quantification of radiation damage annealing and helium diffusion kinetics in apatite

4.1 Abstract

The use of (U–Th)/He thermochronology in apatite (AHe) requires a quantitative understanding of He diffusivity as a function of sample temperature and radionuclide concentration over geologic time. Variability in diffusion kinetics between natural apatites has revealed that high concentrations of α-recoil damage correlates with lower He diffusivity. However, few studies have been conducted to experimentally quantify the effects of thermal annealing of radiation damage. We present the results of two suites of experiments aimed at quantifying the effects of radiation damage annealing on He diffusion kinetics, one using apatite from a single sample of granite from Sierra Nevada, CA and another using apatite from an apatite megacryst from Durango, Mexico. Crystals from both samples were heated under vacuum to between 220 and 500 °C for 1, 10, 100 or 1000 hours and then proton-irradiated to produce spallogenic ^{3}He, the diffusant used in subsequent step-heating degassing experiments. Despite low signals (issues with experiments), the data support previously-published work and suggest that an apatite's response to thermal annealing conditions will vary between samples, indicating that the numerical models used to interpret AHe thermochronological data require an update. We fit these data with a previously published radiation damage model equation and demonstrate that the data are not sufficiently precise to improve upon the models that have been published thus far. We conclude with suggestions to further investigate this important problem in low-temperature thermochronology.

4.2 Introduction

The (U–Th)/He system in the mineral apatite (AHe) is sensitive to upper crustal temperatures between ∼90 and 30 °C and is commonly used to quantify the timing, patterns, and rates of topography evolution in the Earth sciences as well as explore potential links between erosion, climate, and tectonics. Critical to correctly interpreting these data, however, is a quantitative understanding of the diffusivity of He within the apatite crystal, which has been demonstrated to be a complicated function of many variables: time, temperature, radionuclide concentration, existing damage, anion chemistry, and potentially other factors [6–8, 21, 77]. Recent insights from the fields of materials science and engineering demonstrate that the problem may be rendered even more complex by α-particle induced annealing (e.g., ref. [93]), in addition to the fission annealing. The effects of thermal annealing of radiation damage complicate the quantification of ^{4}He diffusivity through time because the diffusivity at any time will be influenced by a sample's prior thermal conditions.

AHe thermochronometry has been applied to hundreds of published projects to measure a wide variety of geologic phenomena, ranging from bedrock incision by glaciers or rivers (e.g., ref. [16]) to tectonic compression or extension (e.g., ref. [94]). These geologic interpretations hinge on the quantitative understanding of the competing effects of radiation damage accumulation and annealing, critically necessary to accurately model and interpret AHe thermochronometric data. Detailed models for interpreting AHe data have been available for a decade (e.g., refs. [6, 7, 60]) and are widely used (particularly in the case of the Radiation Damage Accumulation and Annealing Model, or RDAAM [6] with >500 citations in ten years), but in order to confidently apply this technique to questions in the Earth sciences, it is critical that we validate the important assumptions that underlie the models.

Successful progress on this topic will equip the entire thermochronology community with a more accurate tool to process and interpret data. Based on broad use of the RDAAM since publication, it is clear that models are a key component of interpreting AHe data and that an improved model will broadly impact and improve the utility and accuracy of the interpretations from these data. Furthermore, an understanding of the accumulation and annealing of radiation damage in the material apatite may provide useful insights into the long-term viability of materials used to store nuclear waste, which would be subject to the α-decay of heavy parents materials.

A recently published paper (ref. [60] and Chapter 3 of this dissertation) challenged the assumptions underlying each of the commonly used AHe data models that all radiation damage to the apatite crystal lattice responds to thermal annealing in the same way. That is, both the RDAAM [6] and model in ref. [7] quantify the effects of a reduction in radiation damage density based on fission track annealing literature and experimental work. The proposed model, the α-damage annealing model (ADAM; [60]), circumvents this assumption by calibrating the model to experimental data [8] that systematically quantifies the influence of annealing temperature and duration on measured diffusion kinetics in samples of Durango apatite. However, as stated in ref. [60], calibrating a model to data collected from only one apatite sample is likely not sufficient to apply to all apatites.

Quantifying the relationship between thermal annealing conditions and measured diffusion kinetics in multiple apatite samples is critical to the usability and reliability of AHe thermochronometry, but it requires extensive experimental effort. In this chapter, we show the results of two suites of experiments aimed at better quantifying the relationship between thermal conditions and measured changes to He diffusion kinetics. We experiment on apatites from two sources, Durango-B apatite and an apatite from the Sierra Batholith in Yosemite National Park, California, to determine potential sample dependence. We test an experimental procedure modified from the data set of ref. [8], using ^{3}He as the diffusant gas in lieu of radiogenic ^{4}He. We find that sample volumes used were too small to resolve tightly-constrained relationships between annealing conditions and changes to measured He diffusion kinetics. We demonstrate this conclusion by attempting to refit the ADAM using the new data and generating non-realistic model outputs. However, we also find that this relationship between thermal annealing conditions and diffusion kinetics does depend on the sample: the apatite from the Sierra Batholith is more resistant to annealing than the Durango-B. The chapter concludes with a few recommendations for future experimental work to better understand and improve the use of low-temperature thermochronology in apatite.

4.3 Background

4.3.1 Thermochronometry

Many geo- and thermo-chronometers have been developed in the latter half of the 20$^{\text{th}}$ century. Each combination of radioactive decay chain(s) and host mineral provides the ability to measure the timing of a different temperature range for a given sample [19]. The practical applicability of the AHe system as a low-temperature thermochronometer was first demonstrated in ref. [95]. Publications in the following decade (e.g. [66, 89, 96]) explored the potential of this system to be applied in tackling questions in Earth science. Experimental quantification of the diffusion kinetics of He further solidified the viability of the technique in apatite [54] and in other minerals [61].

The AHe system is a low-temperature thermochronometer because the diffusivity of He in apatite transitions from essentially open- to closed-system behavior over an approximate temperature range of ∼90–30 °C. The radiogenic ^{4}He is produced within the crystal via the numerous α-decays that occur along the ^{238}U, ^{235}U, ^{232}Th, and ^{147}Sm decay chains. The low-temperature sensitivity of the system expands the range of geologic problems that can be investigated using apatite-bearing rocks, and can be used both to quantify the timing, patterns, and rates of topography evolution and to examine the potential links between erosion, climate, and tectonics.

As described in Chapter 1 (Equation 1.3), the diffusion of gaseous helium in crystalline apatite has been demonstrated to follow an Arrhenius relationship below roughly 350 °C [54]. That is, the dependence of diffusivity on temperature is as follows:

$$\frac{D}{a^2} = \frac{D_0}{a^2} * exp\Big(\frac{-E_a}{R*T}\Big) \tag{4.1}$$

where D is diffusivity (in area per time), D_0 is the frequency factor, defined as the hypothetical diffusivity at infinite temperature, a is the diffusion domain (the crystal size in the case of apatite), E_a is the activation energy, R is the universal gas constant, and T is temperature. It is common practice in AHe thermochronometry to express the E_a and D_0 values as a single closure temperature [2]. The closure temperature formula, previous described in Chapter 1 (Equation 1.4), is:

$$\frac{E_a}{R*T_c} = ln\Big(\frac{A*R*T_c^2*\frac{D_0}{a^2}}{E_a*\frac{dT}{dt}}\Big) \tag{4.2}$$

where T_c is the closure temperature, A is a geometric constant, and dT/dt is a cooling rate. Ref. [54] uses Durango diffusion kinetics to yield a closure temperature of 68 °C.

A second low-temperature thermochronometer is the apatite fission track (AFT) system. Simply, this low-temperature thermochronometer counts the number of ^{238}U spontaneous fission events that have occurred in an apatite crystal. Each fission event releases energy and the two daughter products damage the structure of the apatite crystal such that each damage zone, or 'track,' can be chemically etched and manually counted on an optical microscope in the laboratory today. When an apatite sample is subjected to heating, however, these tracks visibly shorten and can be annealed completely, thus the measured AFT age reflects time since a sample most recently cooled below ∼110 °C. This technique was developed and implemented as a tool in the Earth sciences decades prior to AHe and provides valuable insight into the complexities of apatite as a mineral.

4.3.2 Radiation damage

Radiation damage, defined as the disruption and distortion of the crystal lattice by the products of radioactive decay, is generated in apatite lattice from two primary processes. First, ^{238}U, ^{235}U, and ^{232}Th all undergo decay chains that involve multiple α-decay events, each time producing a ^{4}He nucleus (α-particle), ejecting it from the parent nucleus, and releasing tens of keV per decay [5]. The heavy daughter product in each decay will recoil as the α-particle is ejected in order to conserve momentum. The second process that introduces radiation damage to a crystal forms the basis of the aforementioned AFT thermochronometer. The ^{238}U spontaneous fission occurs approximately 2 million times less frequently than the α-decay, but each fission event releases energy on the order of tens to hundreds of MeV. The formation of the tracks that forms the foundation of AFT thermochronometry is itself a type of radiation damage.

Due to their respective closure temperatures, one would expect all AFT ages to be greater than AHe ages for crystals analyzed from the same sample. However, the opposite has been observed in some data sets (e.g., ref. [78]), highlighting the importance of the open questions that remain in apatite low-temperature thermochronology.

4.3.3 Prior radiation damage studies

The potential relationship between He diffusion kinetics and the influence of radiation damage on the AHe system was first mentioned in ref. [54]. Noting a deviation from Arrhenius behavior for He diffusion in apatite above 300 °C, the authors of ref. [21] sought to quantify the effect of radiation damage on He diffusivity in apatite crystals using measured ^{4}He concentration as a proxy for the amount of radiation damage, as each α-decay produces one ^{4}He molecule and causes the heavy daughter product to recoil and introduce damage to the crystal. Experimental work from ref. [21] showed an increase in apparent closure temperature with increased measured ^{4}He content in different apatite samples, demonstrating the need for further quantification of the effects of radiation damage on He diffusivity in apatite.

Noting the influence of radiation damage on He diffusion as it pertained to the AHe system, the authors of ref. [8] systematically measured the diffusion kinetics of aliquots of Durango apatite that were subjected to a variety of heating conditions ranging from no preheating to 500 °C for 1 hr to 270 °C for 350 hours. This pre-treatment was followed by stepwise degassing experiments using ^{4}He as the diffusant to constrain the He diffusion kinetics and to calculate closure temperatures. The authors of ref. [8] found that heating above 290 °C lowered the closure temperature of a sample.

Based on these findings, the Radiation Damage Accumulation and Annealing Model [6] was developed. The RDAAM accounts for the accumulation of radiation damage from both α-decay and spontaneous fission as a control on He diffusion and retention over modeled geologic time. In order to quantify the relationship between parent nuclide concentration, time elapsed, temperature, and diffusion kinetics, the RDAAM calls on the well-studied relationship between time, temperature, and fission track length from the AFT literature. This allows the RDAAM to quantify the diffusion kinetics at each timestep for the duration of modeled time. An important consideration, however, is that the RDAAM operates under the assumption that all radiation damage in the apatite crystal will respond to thermal annealing as fission tracks do, despite the damage coming from two different radioactive decay processes. A second model for interpreting AHe data published in the same year [7] also accounts for diffusion kinetics based on radiation damage and makes a comparable assumption about the annealing of radiation damage.

Evidence for the potential difference in radiation damage annealing includes early work that measured optical properties of apatite, which suggest that annealing rates of radiation damage from α-decay and FT differ [64]. Furthermore, the authors of ref. [77] demonstrate an expected difference in radiation damage annealing behavior in apatite as a function of apatite anion chemistry. The experimental work presented in this chapter aims to advance the understanding of radiation damage annealing in apatite and better equip future users of AHe thermochronometry to more accurately interpret data in geologic settings involving reheating, old AHe ages, or both.

4.4 Methods

4.4.1 Sample preparation and irradiation

The Durango apatite used in these experiments ("Durango-B") is a crushed and sieved portion of an apatite megacryst from Durango, Mexico, commonly used as a laboratory age reference standard. The pieces of Durango-B apatite used in the experiment are shards of the once-larger crystal and are therefore not expected to have ^{4}He loss near the surface of the crystal as consequence of ejection during α-decay. The apatite from the Sierra Nevada Batholithic materials near the Little Devil's Postpile in Yosemite National Park (herein called "LDP"), however, was separated from a bedrock sample using conventional mineral separation techniques (e.g., described in ref. [97]). Each sample analyzed was comprised of apatite whole crystals and large crystal fragments and did lose some ^{4}He near the surface of the crystal from α-ejection.

For the majority of the experiments, small aliquots (∼50 crystals) of apatite crystals were placed into 4-mm Al cups and rolled closed. The flattened packet was then mounted onto a K-type thermocouple using a handmade Mo-foil envelope oriented perpendicular to the incident laser beam. This set-up is used to heat each sample while accurately and simultaneously measuring its temperature on the thermocouple. The aliquots were loaded into a diffusion cell and heated under vacuum with either a 30- or 150-W diode laser in a feedback control loop with the thermocouple using a proportional, integral, derivative (PID) temperature controller. The PID set-up maintains a constant setpoint temperature within ∼2 °C. Apatite crystals were heated to temperatures between 220 and 500 °C for 1, 10, 100, or 1000 hours (see Table 4.1 at end of this chapter).

These samples, in addition to at least one aliquot per sample of material that was not heated, were then packed into cylindrical high-density polyethylene capsules and sent to the Francis H. Burr Proton Therapy Center at Massachusetts General Hospital. Samples were irradiated with a total of ∼1x10^{16} protons/cm^2 from a beam of ∼220-MeV protons, producing a uniform distribution of spallogenic ^{3}He from nuclear reactions with various elements in the apatite crystal. We opt for this method because bombardment by high-energy protons produces ^{3}He from virtually all target nuclei and the pre-existing concentrations of ^{3}He in the apatite crystals is expected to be negligible [98]. The ^{3}He then acts as the diffusant in subsequent step-heating diffusion experiments. The use of ^{3}He as a diffusant is sufficient to describe the diffusion kinetics of ^{3}He and ^{4}He in apatite, as demonstrated by previous experimental work [98]. Samples are returned from irradiation and given sufficient time to cool (radioactively) before conducting step-heating diffusion experiments.

4.4.2 Diffusion experimental procedure

For the step-heating diffusion experiments, we selected apatite crystals with a width of >100 microns from each pre-heated aliquot using a Leica MZ16 or M165C stereomicroscope, excluding those with large visible fractures and/or fluid and mineral inclusions. We pho-

tographed and measured the selected crystals using a camera mounted into the calibrated optical microscope before packing them into a Nb packet for degassing. Over the course of this project, we tested different sample sizes for these experiments, ranging from single crystal experiments up to, in two cases, roughly milligram aliquots. Due to inconclusive results from early experiments using ∼10 crystals and single crystals, the majority of experiments presented in this chapter were conducted by simultaneously degassing 2–5 apatite crystals loaded into a single Nb packet. The number of apatite crystals analyzed in each experiment is indicated in Table 4.1 (at end of this chapter) and Appendix A. Each Nb-packed sample was mounted onto a K-type thermocouple using a crimped Pt-Ir alloy tube to hold the sample and thermocouple in contact. The Pt-Ir tube was positioned perpendicular to the incident laser beam to ensure uniform heating and accurate temperature measurements. The assembly was then heated under vacuum by a diode laser (30 or 150 W) or lamp bulb in a feedback control loop with the thermocouple using a PID temperature controller.

The diffusant gas was removed from the crystal using a step-heating procedure based on previous similar analyses performed on other minerals and gases (i.e., the ^{4}He/^{3}He system). The initial heating schedule was developed with the intention of having approximately the same volume of gas released in each step. Following Eq. 4.1, this means longer duration hold times for lower temperature steps and shorter duration hold times for higher temperature steps. All heating schedules begin at 250 °C, follow one retrograde temperature cycle, stepping down to 200 °C and then back up, and ending with a maximum temperature of 900 °C for two to three steps to ensure total gas removal from the sample. Over the course of this work, the heating schedule was modified to improve the resolution of the He diffusivity at temperatures below 300 °C. As more data was collected for this experiment, the heating schedule use was adjusted to provide more resolution for the Arrhenius regressions. Exact heating schedules used for each experiment are listed in Appendix A.

After each heating step, the liberated gas was purified using an automated extraction line. Gas was passed over a SAES Getter pump and then frozen onto a Janis cryogenic trap held at a set point between 12 and 14 K. The cryogenic trap was then heated to 33 K to release the He gas for analysis on an MAP 215-50 sector field mass spectrometer located in the Noble Gas Thermochronometry Laboratory at the Berkeley Geochronology Center. Gas from each step was measured under static vacuum conditions and cycled 4 times through ^{3}He and ^{4}He over the course of approximately one hour. Linear regression through these data provide the time-zero intercept and the standard deviation for each measured nuclide after each heating step.

4.4.3 Data processing

4.4.3.1 Systematizing errors between two instruments

The Noble Gas Thermochronometry Laboratory at the Berkeley Geochronology center (hereafter shortened to 'BGC'), where all reported measurements in this study were made, has two MAP 215-50 sector field mass spectrometers used to measure noble gases. However,

the software on the two instruments calculates the error for each measurement differently. On one instrument (called "MAP2"), the reported error is calculated as Equation 6.15 from ref. [99]:

$$\sigma^2 = \frac{1}{N-2}\sum (y_i - a - bx_i)^2 \tag{4.3}$$

where N is the number of measurements, y is the counts (the dependent variable), x is the measurement time (the independent variable), and a and b are the time-regressed intercept and slope, respectively.

The other instrument (called "Ohio") reports error using the special case of common uncertainties in the dependent variable. The error on the linear fit intercept simplifies to equation 6.23 from ref. [99]:

$$\sigma_a^2 = \frac{\sigma^2}{\Delta'}\sum x_i^2 \tag{4.4}$$

where σ^2 is the error shown in Eq. 4.3 and Δ' is equation 6.13 from ref. [99]:

$$\Delta' = N\sum (x_i^2) - (\sum x_i)^2 \tag{4.5}$$

The data acquisition code on the Ohio instrument records the $\sum x_i^2$ and Δ' values for each experiment. Using a representative set of heating steps and measurements from the two systems, we calculate a pair of correction factors to bring the two systems into agreement. Before completing the regression, errors from the Ohio system are multiplied by 4.8 for ^{3}He measurements and 3.25 for ^{4}He measurements for direct comparison between all results. These correction factors, which were calculated empirically, are the result of both (i) the error calculation programmed into each instrument's data processing software and (ii) each instrument's slight internal variability based on extraction line and measurement components.

4.4.3.2 Blank correction

In each heating schedule, three to four sample chamber blanks were run to quantify the baseline blank measurement for each experiment. These blank measurements inform users how much of the measured signal should subtracted away as background. For most of the experiments described in this chapter, the heating schedule included blank steps of only 30 and 60 minutes in duration, despite some temperature steps lasting three or more hours. To account for this, we calculated a linear regression through the blank measurements for each experiment to generate an experiment-specific, time-dependent blank correction function. For each step within an experiment, we then use the duration of the heating step to calculate the time-dependent blank correction and subtract it from the measured value for each heating step prior to completing the Arrhenius regression. In cases where the time-dependent blank correction linear regression produced a negative slope, we instead used the mean value of the measured blanks and subtracted away a constant value from each step measurement prior to

completing the Arrhenius regression (i.e., the slope of the function is zero and the intercept is the mean of all blanks measured).

4.4.3.3 Arrhenius regressions

Measured ^{3}He fractions from the step-heating experiments are converted into diffusion coefficients using the formulations of ref. [100]. In order to apply these equations, we assume that (i) the diffusant gas has a uniform initial distribution, which we believe to be valid based on the introduction of spallation ^{3}He during the proton irradiation [101], (ii) the diffusion of He gas is isotropic, which has been demonstrated to be true in apatite [54, 102], and (iii) a spherical diffusion domain is sufficient to quantify diffusion in apatite crystals and apatite shards (in the case of Durango B) [101]. The ref. [100] expressions yield the necessary information to create Arrhenius plots (i.e., calculated values of D/a^2 versus $1/T$), through which a line is regressed, giving us both the frequency factor, D_0, and the activation energy, E_a. By systematically comparing the D_0 and E_a values measured in annealed samples to those measured in unheated samples, we can quantify the effects of thermal annealing on measured diffusion kinetics then extrapolate to geologic timescales to understand the implications.

The regressions done for each experiment include gas from temperature steps ranging from 200 °C (the minimum heating temperature in all heating schedules) to 340 °C, based on both observations of deviation from Arrhenius behavior in this data set as well as previously published data [8, 21, 54]. The fraction of the total gas released that was included in the regression is included in Table 4.1 (at end of this chapter) and Appendix A. Furthermore, the regression excludes any measured heating steps whose raw signal is less than 4 times the blank measurement for that experiment (i.e., if the blank correction is greater than 25%, that step is excluded from the regression). The steps excluded on the basis of large blank correction are typically the lowest temperature steps, which exert a notable influence on the slope and intercept of the regression because those points plot farthest to the right in Arrhenius space. In hindsight, these blank corrections have a major influence on the precision of our measurements and overall utility of the data set. Proposed strategies to mitigate this problem in future experiments are outlined in Section 4.6.

4.4.3.4 Departures from previous experimental work

As previously discussed, there exists one previous study which sought to quantify the relationship between thermal conditions and He diffusion kinetics [8]. The work in this study seeks to complement, verify, and build upon those findings in an effort to strengthen AHe thermochronometry as a valuable tool in Earth science. We elected to change some aspects of the previous procedures as we conducted these experiments.

The first difference between the work of ref. [8] and this study is the mass of sample used for each experiment. In ref. [8], measurements were made on aliquots of mass ∼5–30 mg, equivalent to approximately 1,000–10,000 apatite crystals. The experiments presented here

are on samples ranging in size from one to ten crystals, a decision made based on sample availability and the ability to hand-select only high-quality apatite crystals, free of inclusions. The exact sample size for each experiment is indicated in Table 4.1 (at end of this chapter) and Appendix A. We conducted a pair of experiments using higher masses of LDP apatite, on the order of milligrams, but found that the data were not as expected and we opted to continue with the lower mass experiments.

Second, ref. [8] used the naturally-occurring radiogenic ^{4}He as the diffusant in their step-heating experiments. While likely a reasonable assumption, particularly given the volume of sample analyzed in each experiment, the distribution of radiogenic ^{4}He within each crystal depends on the distribution of the parent nuclides (^{238}U, ^{235}U, ^{232}Th, and ^{157}Sm). By using the proton irradiation-generated ^{3}He in these experiments, we can more confidently apply the assumption that the initial distribution of the diffusant gas within a crystal prior to heating is essentially uniform. This change in diffusant, however, comes at a cost, both monetary and time-wise. Using naturally-occurring radiogenic ^{4}He as the diffusant, the authors of ref. [8] would anneal the sample and discard the gas, then conduct the step-heating diffusion experiment in one sample loading step. The ^{3}He procedure requires two loading steps into the vacuum chambers, as well as the time, logistics, and cost associated with sending the samples out for proton irradiation.

4.5 Results

We conducted 116 total experiments for this study. Of these, 19 produced unusable data and were discarded: experiments whose released gas show no semblance of Arrhenius behavior (Fig. 4.1A) are likely a consequence of apatite crystals getting crushed during the packing and loading process or apatite 'dust' clinging to crystals; experiments with one heating step that released >20% of the total He are also excluded from the final data set (Fig. 4.1B).

The remaining 97 experiments underwent the data reduction procedure outlined in Section 4.4. The diffusion data from each individual experiment is included in Appendix A as a data table, an Arrhenius plot, a cumulative release plot, and a residual plot. Fig. 4.2 shows one example of the plots for DurB-240C-1000hr-b, an experiment on six Durango-B crystals that were simultaneously thermally annealed under vacuum at 240 °C for 1000 hours prior to irradiation and degassing (this figure is supplied again as Fig. S53 in Appendix A). In three cases, the temperature of the included steps was adjusted to be different from the 200 °C–340 °C range to isolate the Arrhenius behavior of the released ^{3}He. In three cases, points were manually chosen for exclusion from the Arrhenius regression. For the DurB-300C-1hr-b experiment, one 225 °C step was excluded despite being above the blank criteria for plotting far from the Arrhenius line. For the DurB-240C-1000hr-b experiment, the maximum temperature heating step that was included in the regression was lowered to 315 °C to account for rollover (deviation from Arrhenius behavior) above that temperature. Finally, the regression for the LDP-275C-10hr-c experiment excludes the two 200 °C steps because they plot higher

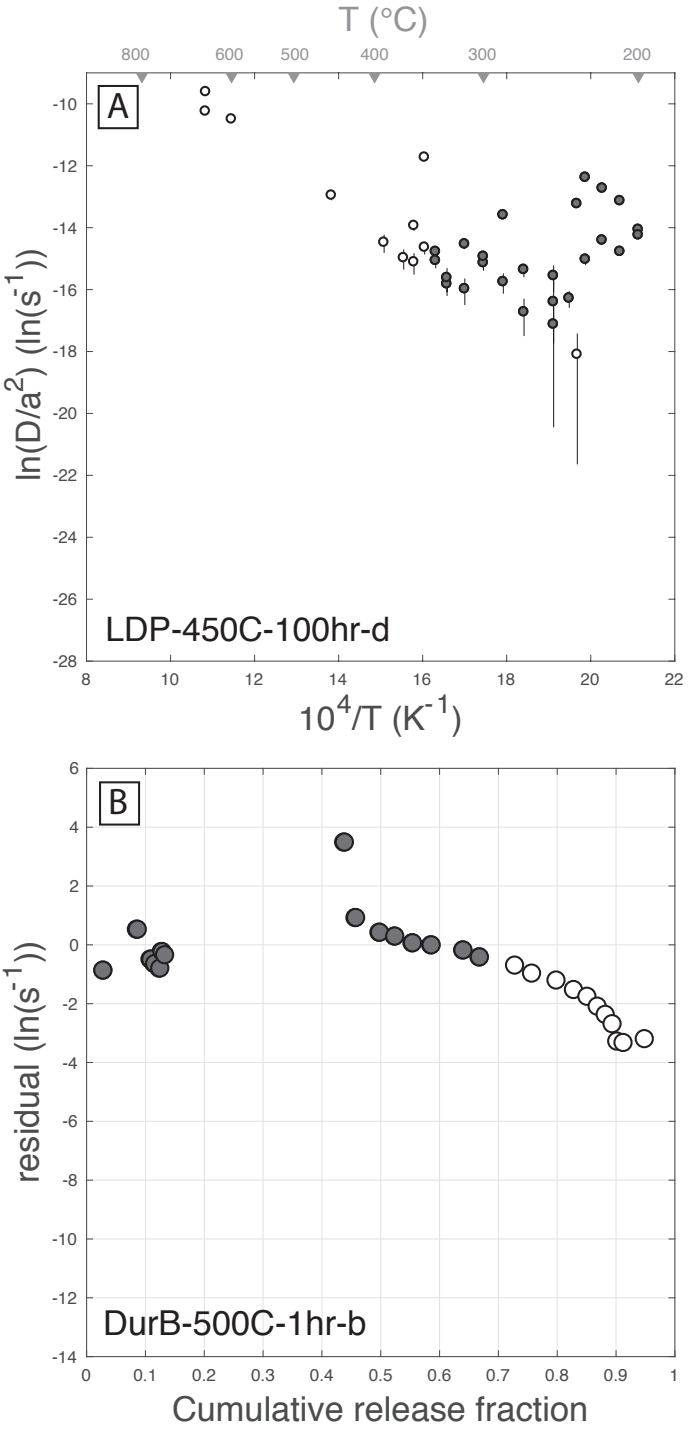

Figure 4.1: (Caption next page.)

Figure 4.1: Two cases for experimental results that are not usable for the subsequent portions of this study. (A) An Arrhenius plot of stepwise degassing behavior that does not exhibit any semblance of Arrhenius behavior (a linear relationship with a negative slope). The measured crystals from LDP were heated to 450 °C for 100 hours prior to irradiation and measurement. Any experiments with this "shotgun" pattern are excluded from further analysis and are likely the consequence of apatite crystal(s) being crushed during the packing and loading process. (B) The residual (between the data and the Arrhenius regression) versus the cumulative ^{3}He gas release for Durango-B apatite crystals that were heated to 500 °C for 1 hour prior to irradiation and measurement. One step contained >20% of the total gas released, thereby disqualifying this experiment from further analysis. In total, 19 experiments demonstrated one of these issues and were excluded from the remainder of this chapter.

than the Arrhenius fit and artificially decrease both the slope and intercept of the line.

The diffusion kinetics information calculated from the stepwise diffusion experimental data are presented in Table 4.1 (Durango-B) and Table 4.2 (LDP) (both at end of this chapter) and in Figs, 4.3 and 4.4. Fig. 4.3 shows plots of E_a and $ln(D_0/a^2)$ and Fig. 4.4 shows the calculated closure temperature of each sample as a function of thermal annealing temperature, separated by annealing duration. Excluded from Figs. 4.3 and 4.4 are data whose normalized misfit exceeds 0.05 or the resulting diffusion kinetics (with error) plot far outside the minimum and maximum value used in the RDAAM. The closure temperatures presented in Table 4.1 use a geometric constant $A = 55$ and a cooling rate $dT/dt = 10$ °C/Ma.

Finally, a critical finding from these experiments is the fact that the "baseline" experiments, those step diffusion experiments on Durango-B and LDP crystals that had not undergone any thermal annealing prior to irradiation and measurement, did not reproduce well, as is shown in Fig. 4.5. The lack of reproducibility may be indicative of some number of issues with the experimental set-up, discussed in Section 4.6.2.

4.6 Discussion

Despite the dramatic differences between the experiments conducted on apatites that were not heated, we are still able to draw some general conclusions from these data. The following section examines the difference between the two studied samples, compares those results to previously published data, then examines the potential for the new data to be used to better calibrate the ADAM model. Upon demonstrating that these data are insufficiently precise, we outline suggestions for improvement and other experimental techniques that may further probe this integral aspect of apatite low-temperature thermochronology.

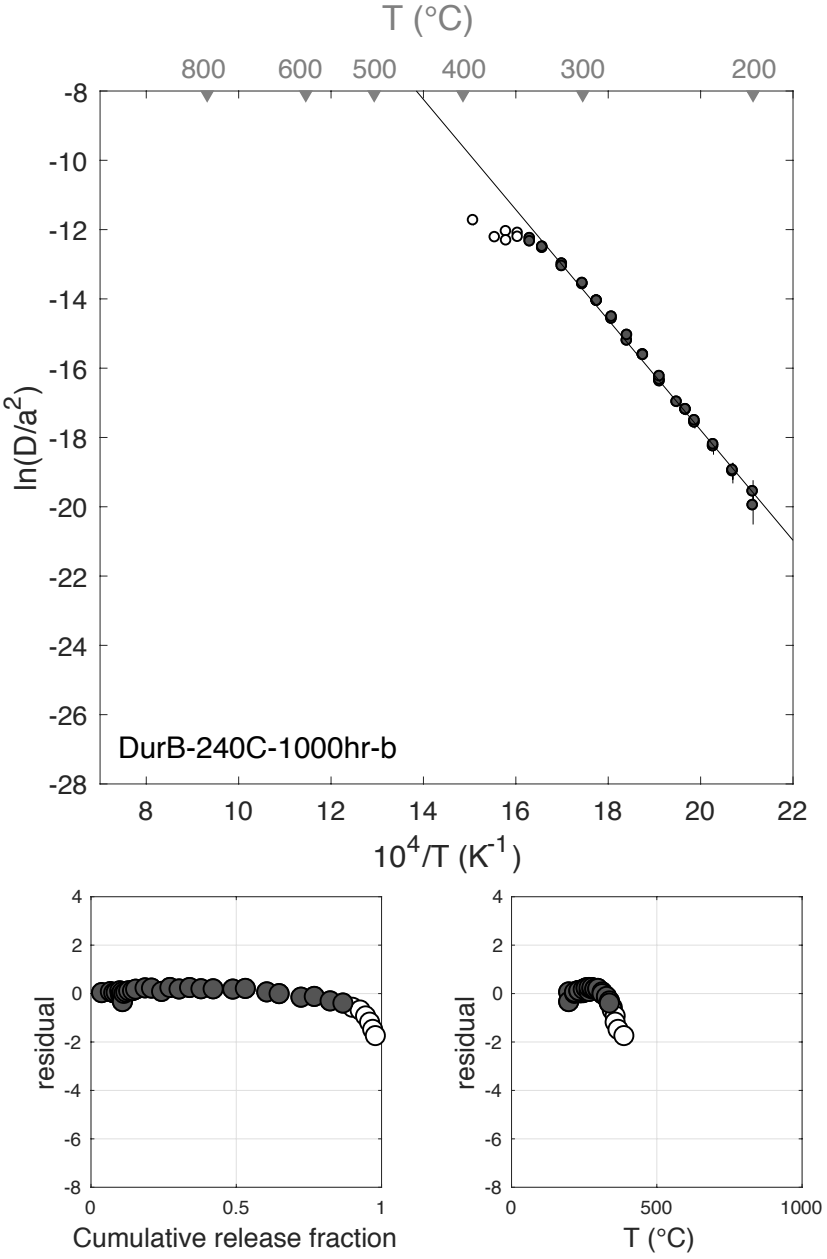

Figure 4.2: Example results from DurB-240C-1000hr-b, an experiment on six Durango-B crystals that were thermally annealed under vacuum at 240 °C for 1000 hours prior to irradiation and degassing. The upper panel shows the Arrhenius plot, while the lower panels show the residual from the Arrhenius regression versus ^{3}He release fraction and step temperature. Vertical error bars are estimated using a Monte Carlo approach (see ref. [103]).

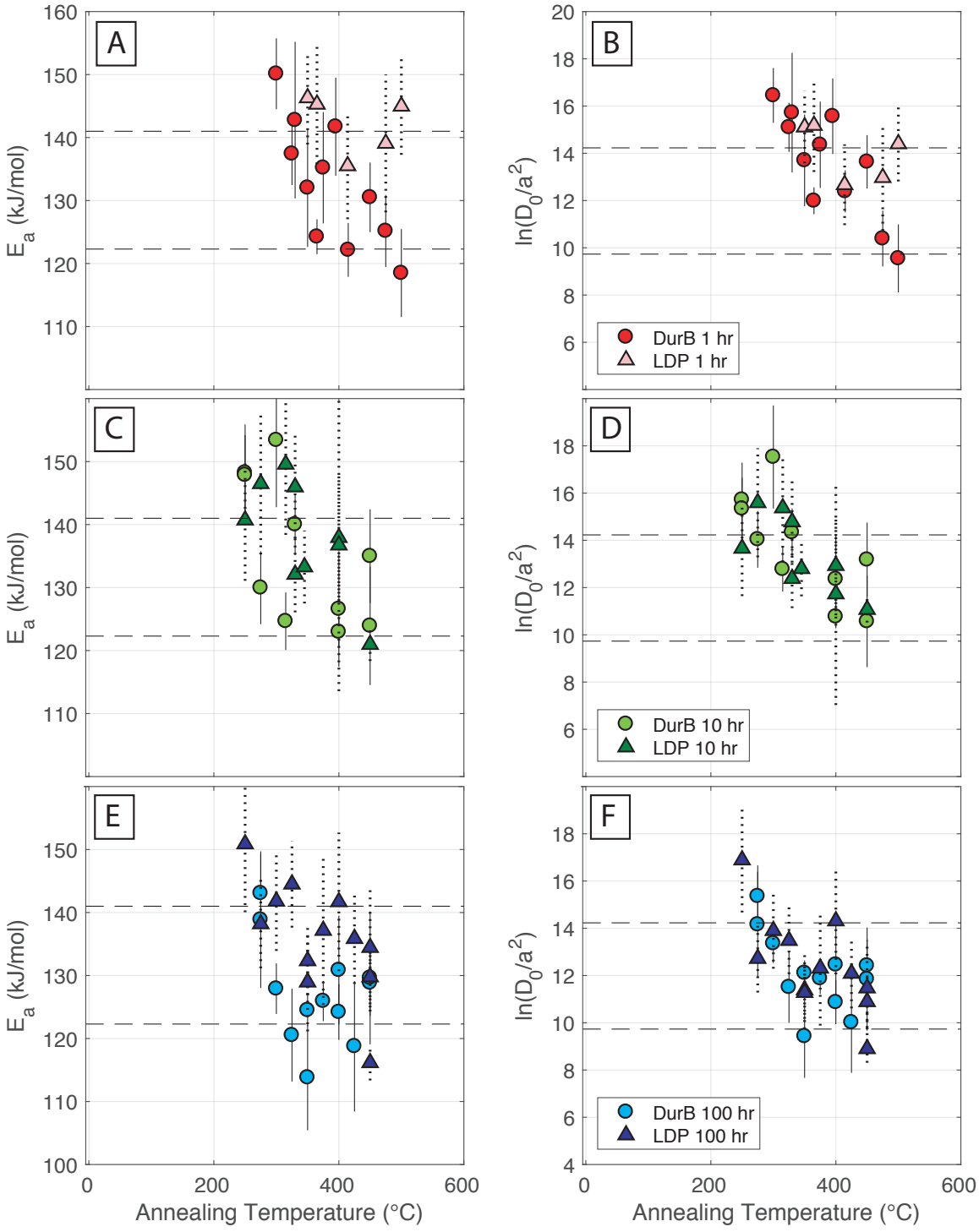

Figure 4.3: (Caption next page.)

Figure 4.3: Compiled results from accepted annealing–diffusion experiments. Panels in the left column (A, C, E) show measured E_a values versus annealing temperature, while panels in the right column (B, D, F) show measured $ln(D_0/a^2)$ values versus annealing temperature. Rows are separated by the annealing heating duration: Panels A and B are 1-hour, C and D are 10-hour, and E and F are 100-hour experiments. The dashed horizontal lines in each panel are the maximum and minimum values for the diffusion kinetics parameter as proposed in the RDAAM [6]. Note that the D_0/a^2 values are normalized to s^{-1}. Error bars are 1σ.

4.6.1 Durango-B and LDP comparison

Based on the experimental data shown in this chapter, the LDP apatite, sourced from the Sierra Nevada Batholith, appears to be generally more resistant to thermal annealing conditions than the Durango-B apatite. This is demonstrated most clearly in Fig. 4.4, where the LDP samples plot consistently higher than Durango-B data for the same annealing conditions. Determining the reason for this different response to annealing conditions requires additional chemical measurements of the LDP sample as well as similar tests on other apatite samples to discern patterns.

4.6.2 Justification for small sample volume experiments

To place the annealing–diffusion experimental results into context, we compare the newly measured data with results from ref. [8] and the ADAM [60]. We conducted experiments with a similar sample mass to ref. [8] (e.g., milligrams of apatite) and found that these experiments did not produce usable results. Data from these two experiments, LDP-NH-f and LDP-300C-100hr-c, are shown in Table 4.2 (at end of this chapter) and Figs. S58 and S89 (in Appendix A). Due to the amount of gas released at each step, the error bars for these experiments are smaller than those from the experiments done on one to ten crystals. However, the measured E_a values are below the minimum measured values on Durango from the RDAAM [6] and well below the other samples in the same batch (i.e., the other non-heated experiments and the other 100-hour experiments). As these trials use significantly more sample volume per experiment, they were dismissed in favor of the small sample volume experiments.

4.6.3 Insufficient data precision to improve diffusion kinetics models

In ref. [60], the authors fit a mathematical function to the data set published in ref. [8], discussed in Section 4.2. To evaluate the utility of the data presented in this work, we replicate that fitting exercise using the following expression for changes to E_a:

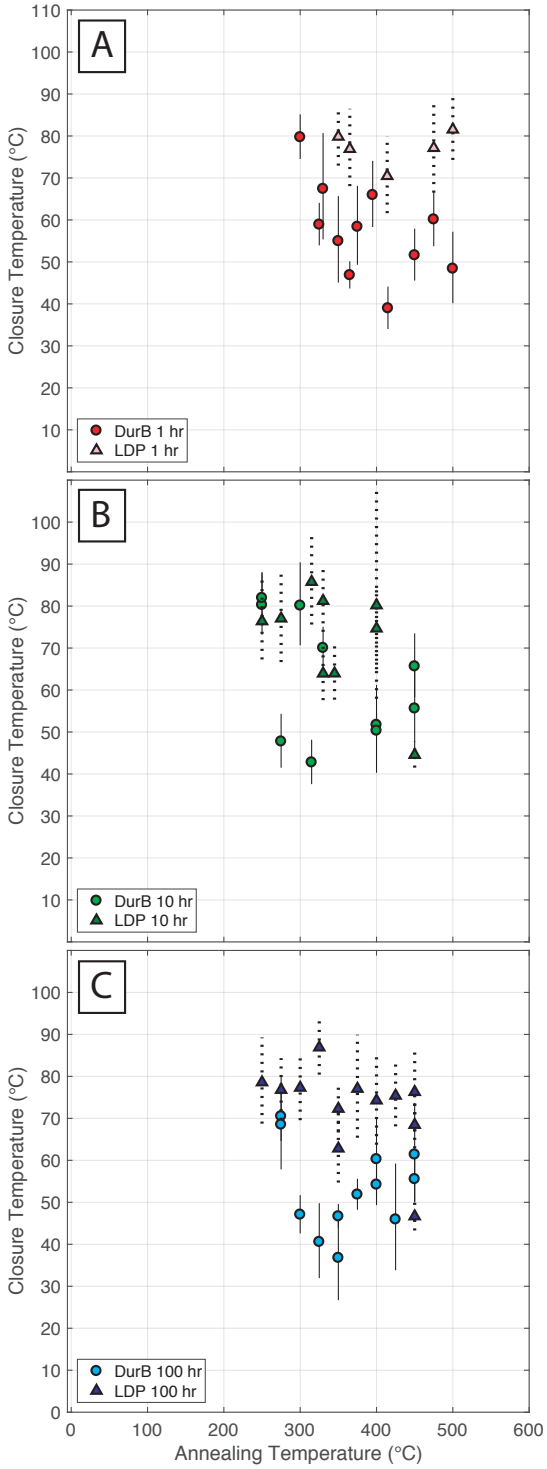

Figure 4.4: (Caption next page.)

Figure 4.4: Compiled closure temperature results calculated from the data shown in Fig. 3. (A) Experiments with a 1-hour thermal annealing step, (B) experiments with a 10-hour thermal annealing step, and (C) experiments with a 100-hour thermal annealing step. The closure temperatures are calculated using Equation 4.2 [2] with a geometric constant of $A = 55$ and a cooling rate of $dT/dt = 10$ °C/Ma. Error bars are calculated using the 1σlower and upper bounds in the E_a and D_0/a^2 values.

$$\ln\left[-\ln\left(\frac{\Delta E_a}{c_3\_E_a}\right)+1\right] = c_1\_E_a + \ln(t) + c_2\_E_a * T^{-1} \tag{4.6}$$

and the following expression for changes to $ln(D_0/a^2)$:

$$\ln\left[-\ln\left(\frac{\Delta \ln(D_0/a^2)}{c_3\_D_0}\right)+1\right] = c_1\_D_0 + \ln(t) + c_2\_D_0 * T^{-1} \tag{4.7}$$

from ref. [60] (and this dissertation Eqs. 4.6 and 4.7), where t is duration of thermal annealing at temperature T, c_1 and c_2 (for E_a and D_0) are empirically fit parameters, and $c_3\_E_a$ and $c_3\_D_0$ are calculated values, described below. When used with the constants discussed below, temperature is in Kelvin and time is in units of 10^6 years (Ma).

4.6.3.1 Re-fitting the ADAM using Durango-B data

To complete this fitting exercise, the model searches over a range of parameters for the c_1 and c_2 values. To quantify the best-fitting set of parameters to plug into equations 4.6 and 4.7 for the Durango-B sample, we conducted a systematic search, first using a wide range of values for each parameter. Upon locating the approximate values wherein the best-fit parameter pair would be, we increased the resolution and completed the fitting exercise once more: the tested values for $c_1\_E_a$ and $c_1\_D_0$ ranged from 88 to 108 (in comparison to 55 to 65 in ref. [60])) and the values for $c_2\_E_a$ and $c_2\_D_0$ ranged from –50000 to –40000 (compared with –25000 to –19000 in ref. [60]), with both ranges divided into 50 linearly-spaced values. The ranges generate fits that yield a best fit solution (i.e., one that minimizes the χ^2 misfit for the set of curves) that does not equal the boundary values.

For Durango-B, the quantities $c_3\_E_a$ and $c_3\_D_0$ are the calculated differences between the mean measured values of E_a and $ln(D_0/a^2)$ for non-annealed Durango-B apatite (Table 4.1) at end of this chapter and the assumed values of E_a and $ln(D_0/a^2)$ for fully annealed apatite, as defined in ref. [6]. When implemented into a forward diffusion kinetics model, the c_3 values, which are essentially vertical scaling coefficients, exert a primary control on the maximum possible change in diffusivity that can occur during each time step. Note that for the empirical fits, we exclude experimental data whose misfit statistic, normalized by the number of points included in the regression, calculated in the Arrhenius regression exceeds a value of 0.025. As in ref. [60], a χ^2 misfit is calculated for each set of four parameters to

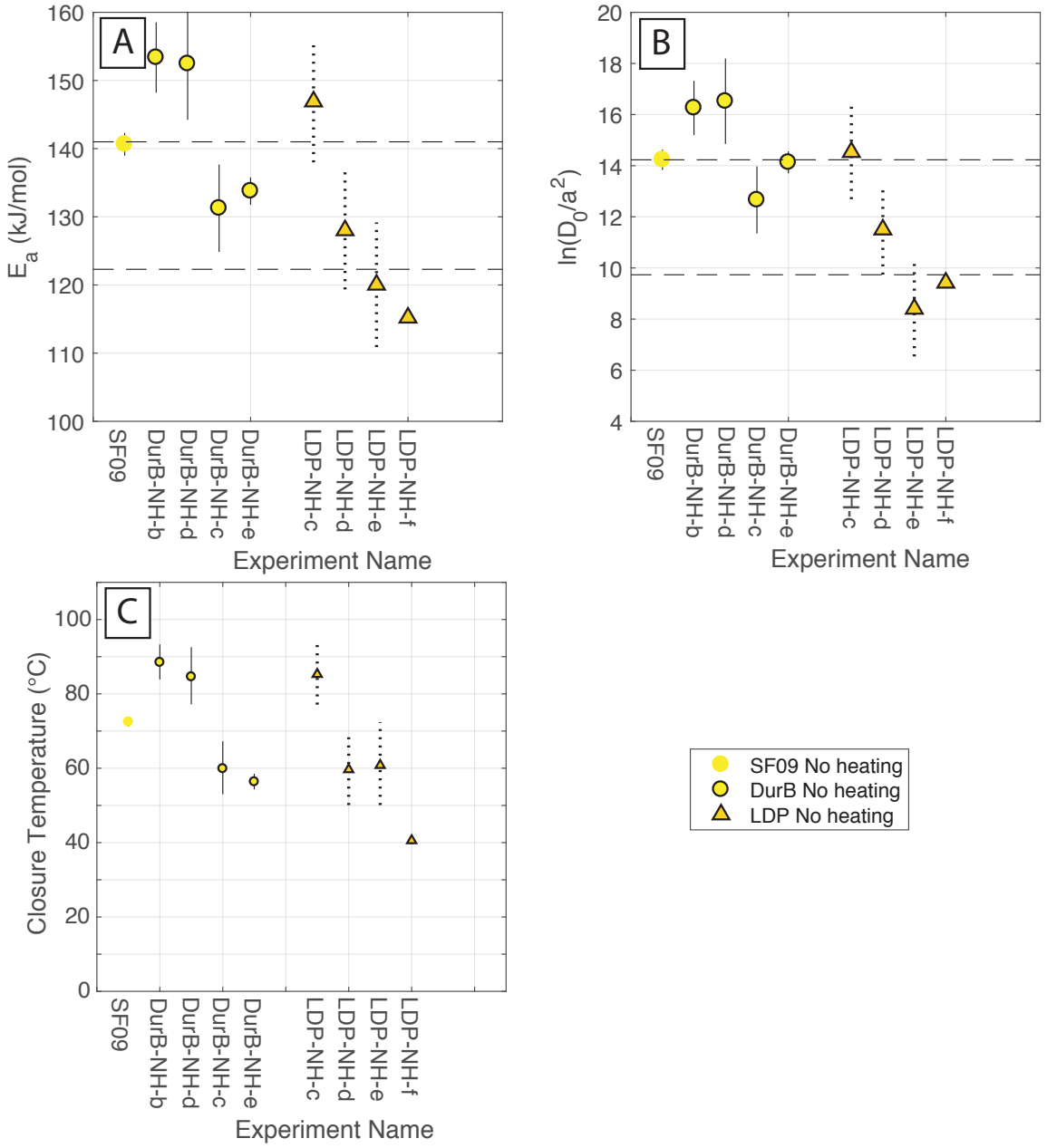

Figure 4.5: Compiled results from annealing–diffusion experiments conducted on Durango-B and LDP apatite crystals that were not subjected to thermal annealing prior to irradiation and measurements. The resulting E_a values (in panel A) and $ln(D_0/a^2)$ values (in panel B) span the expected range of values for the suite of experiments, indicating some flaw in these "baseline" measurements. Panel C shows the calculated closure temperatures for each experiment. Note that the D_0/a^2 values are normalized to s^{-1}. Error bars are 1σ.

determine the best-fit set of parameters. The resulting best fit, where $c_1\_E_a$ = 104.8, $c_2\_E_a$ = –49200, $c_1\_D_0$ = 91.2, and $c_2\_D_0$ = –47400, is shown with the included experimental data in Fig. 4.6 and the misfit values for the E_a and $ln(D_0/a^2)$ parameter pairs is Fig. 4.7. Like previous work using Equations 4.6 and 4.7, there is a covariance between the c_1 and c_2 parameters. The resulting best-fit values are different from the values found in ref. [60] (whose values are: $c_1\_E_a$ = 58.6, $c_2\_E_a$ = -21820, $c_1\_D_0$ = 58.4, and $c_2\_D_0$ = -21700) to a point where the extrapolation to geologic timescales does not reflect the diffusive behavior we know to be true in apatite.

4.6.3.2 Re-fitting the ADAM using LDP data

We repeated the fitting procedure using the LDP data set, using the same 0.025 value for the normalized misfit statistic cutoff. The tested values for $c_1\_E_a$ and $c_1\_D_0$ ranged from 15 to 35 and the values for $c_2\_E_a$ and $c_2\_D_0$ ranged from –10000 to 0, both ranges divided into 51 linearly-spaced values. Due to spread in the measurements of He diffusion kinetics in the no pre-treatment samples (Table 4.2 at end of this chapter and Fig. 4.5), the $c_3\_E_a$ and $c_3\_D_0$ values are not constrained. For illustrative purposes, the fit was done using the c_3 values calculated from the LDP-NH-c experimental results. We again exclude experimental data whose normalized misfit statistic calculated in the Arrhenius regression exceeds 0.025. We calculate a χ^2 misfit for each set of four parameters to determine the best-fit set of parameters. The resulting best fit, where $c_1\_E_a$ = 21.4, $c_2\_E_a$ = –2400, $c_1\_D_0$ = 23.4, and $c_2\_D_0$ = –3600, is shown with the included experimental data in Fig. 4.8 and parameters pairs are shown in Fig. 4.9. Again, the c_1 and c_2 parameters covary.

4.6.3.3 Applicability of the data fits

Figs. 4.6 through 4.9 demonstrate that the data collected through this experimental work are not well-predicted by the model outputs, even those defined as "best-fit" by the misfit minimization. The misfit value is roughly ten times higher than the best-fit misfit value from ref. [60] (included in Chapter 3 of this dissertation). The Durango-B model lines in Fig. 4.6 are tightly spaced, such that a two-value step function might describe the data better than curves. That is, at lower temperatures the model predicts a constant value unchanged from the untreated apatite. Above ∼300 °C, a second value (set to 122.9 kJ/mol for E_a) is the model output. The model lines for LDP samples, shown in Fig. 4.8, instead fan at much higher temperatures. That is, for the majority of the temperature range over which the experiments were conducted, approximately constant diffusion kinetics, equal to the untreated sample results, are produced by the model. While these model predictions are not usable as constructed, the values for their Durango-B and LDP best fits suggest that LDP samples are more resistant to annealing than the Durango-B apatites. Improvements in both the model set-up and measurement techniques will best serve the AHe community in future studies. This chapter concludes that the data herein is insufficient to improve upon the ADAM framework published in ref. [60].

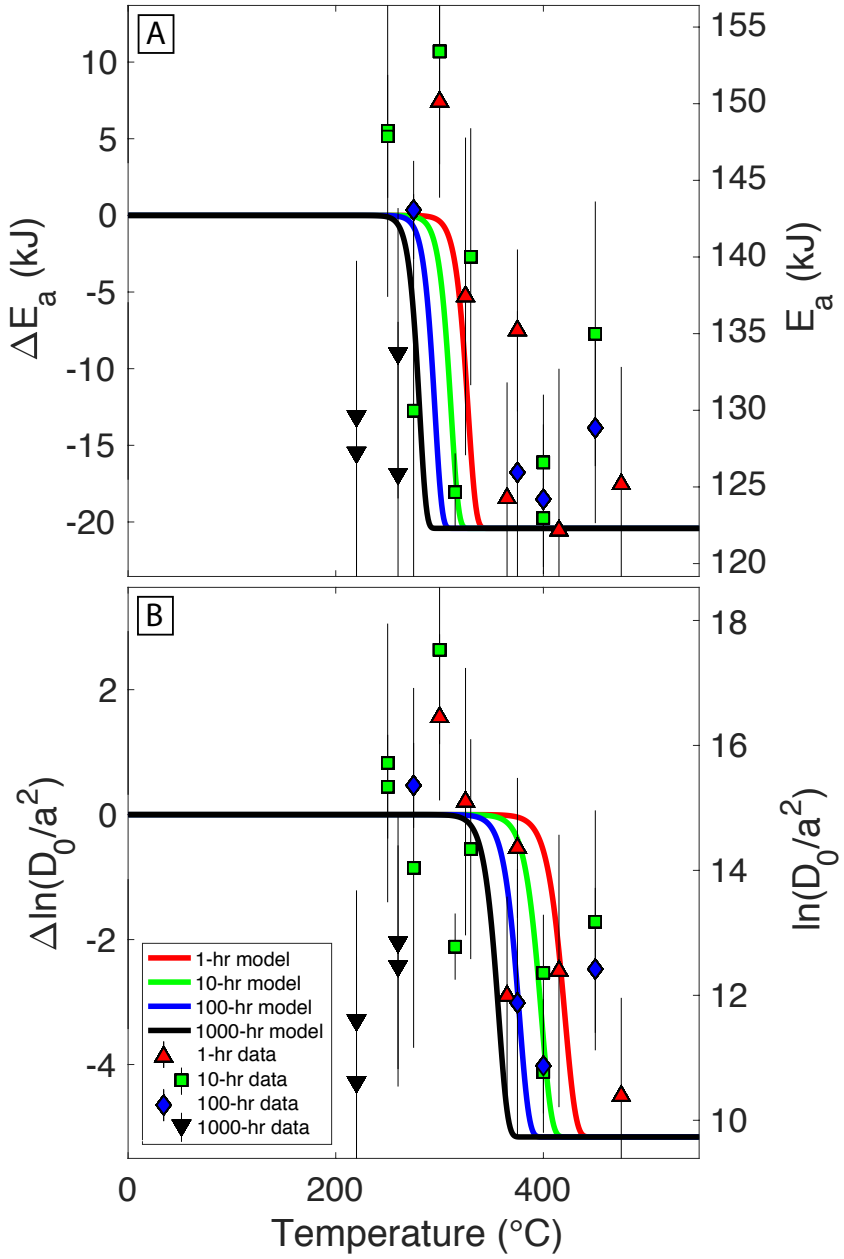

Figure 4.6: ADAM fits to experimental data for annealed Durango-B apatite. (A) Measured E_a from Table 4.1 (at end of this chapter), along with the best-fit curves identified by the misfit minimization of Equation 4.6 (lines). (B) Data and best-fit result for $ln(D_0/a^2)$ using Equation 4.7. D_0/a^2 values are normalized to s^{-1}. In both panels, the left y-axis is a change in each diffusion parameter relative to the mean unannealed Durango-B apatite experiments (Fig. 4.5), while the right y-axis is the absolute value of the parameter.

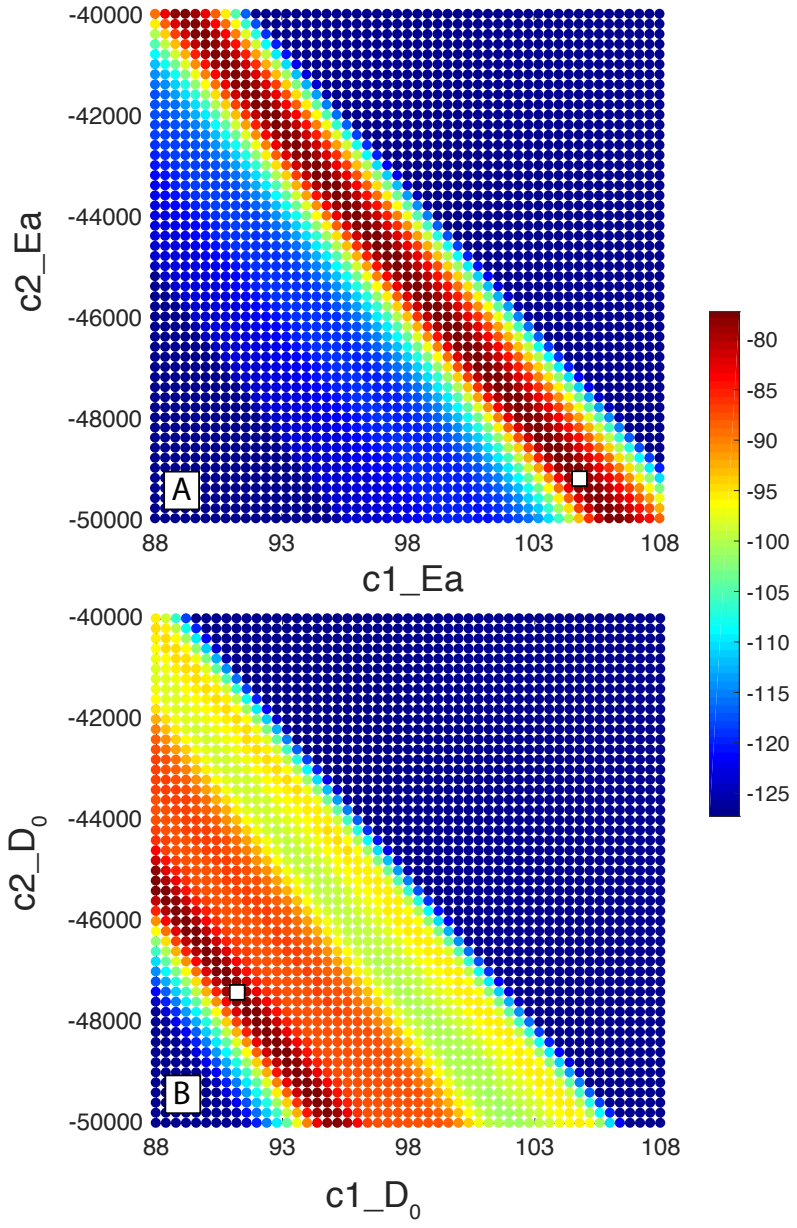

Figure 4.7: ADAM model parameter misfit and optimization for Durango-B apatite. (A) Pairs of $c_1\_E_a$ and $c_2\_E_a$ values from Equation 4.6, colored by reduced χ^2 misfit calculated between the model predictions and data shown in Fig. 4.6. (B) Pairs of $c_1\_D_0$ and $c_2\_D_0$ from Equation 4.7, colored by reduced χ^2 value. Color bar indicates the reduced χ^2 misfit where red is low and blue is high. White squares indicate the parameter pairs for the best fit. The two pairs of parameters (i.e., those for E_a and those for $ln(D_0/a^2)$) cannot be selected independently, as all four parameters must be tested together.

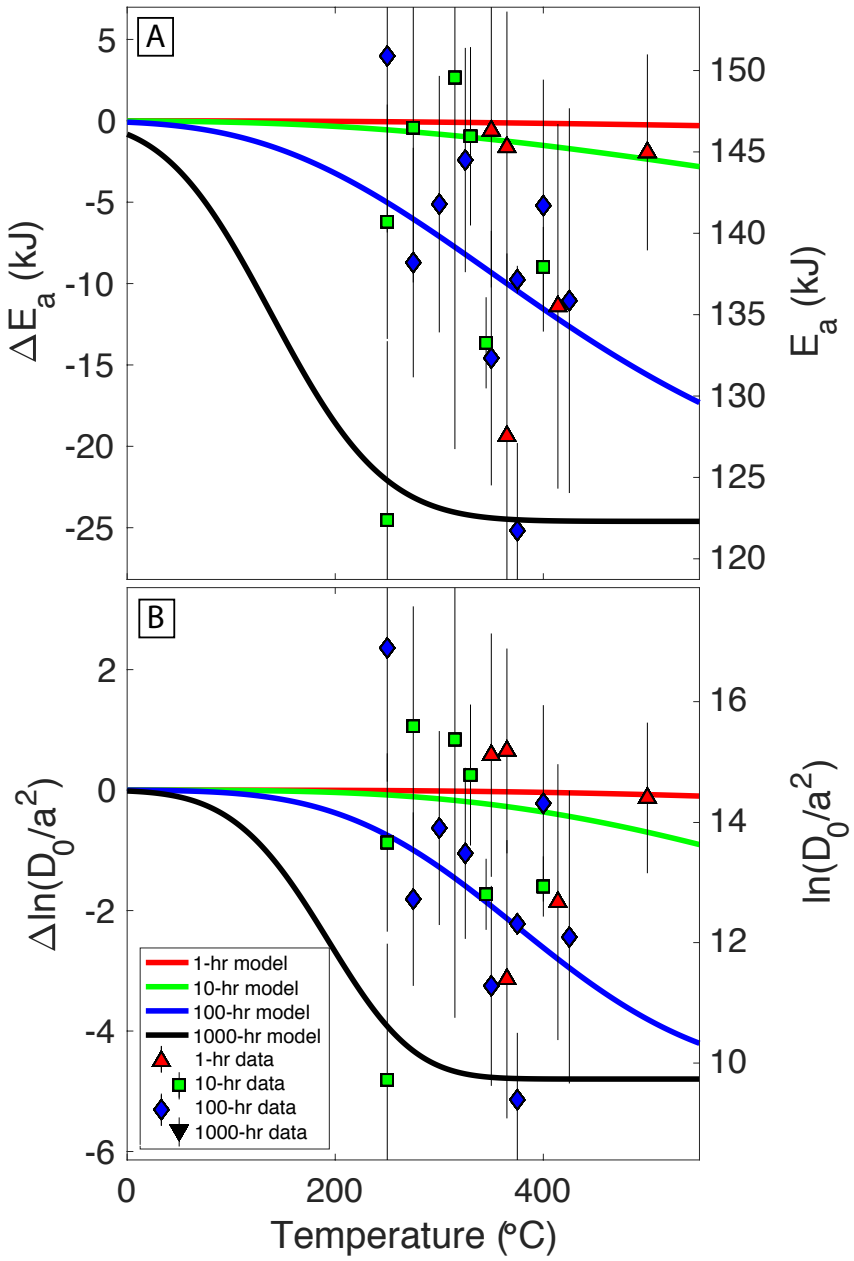

Figure 4.8: ADAM fits to experimental data for annealed LDP apatite. (A) Measured E_a from Table 4.2 (data points), along with the best-fit curves identified by the misfit minimization of Equation 4.6 (lines). (B) Data and best-fit result for $ln(D_0/a^2)$ using Equation 4.7. D_0/a^2 values are normalized to s^{-1}. In both panels, the left y-axis is a change in each diffusion parameter relative to the LDP-NH-c experiment (Table 4.2), while the right y-axis is the absolute value of the parameter.

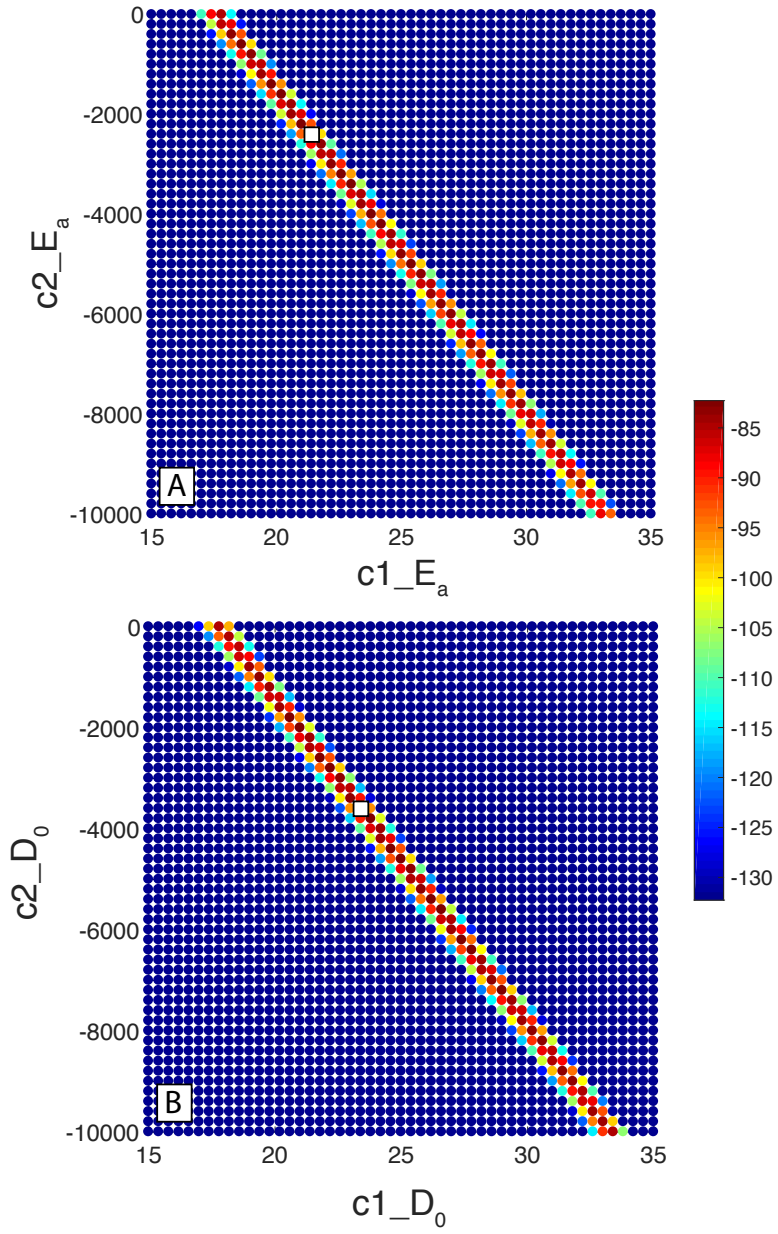

Figure 4.9: ADAM model parameter misfit and optimization for LDP apatite. (A) Pairs of $c_1\_E_a$ and $c_2\_E_a$ values from Equation 4.6, colored by reduced χ^2 misfit calculated between the model predictions and data shown in Fig. 4.6. (B) Pairs of $c_1\_D_0$ and $c_2\_D_0$ from Equation 4.7, colored by reduced χ^2 value. Color bar indicates the reduced χ^2 misfit where red is low and blue is high. White squares indicate the parameter pairs for the best fit. The two pairs of parameters (i.e., those for E_a and those for $ln(D_0/a^2)$) cannot be selected independently, as all four parameters must be tested together.

As with many questions in Earth science, the application of results from experimental work to geologic settings necessitates an extrapolation in timescale. A second critical piece of evidence that points to the unusability of these newly collected data for refining a radiation damage model is this time extrapolation. Using the model results from Section 4.6.3.1 and testing for a geologically-relevant duration of 1 Ma, the model fit from the Durango-B experiments predicts that the diffusion kinetics will evolve rapidly from the unannealed (i.e., damaged) state to a fully annealed state at about ∼200 °C. This contradicts the many measured diffusion kinetics values that populate the values in between. Furthermore, the extrapolation of the model fit to the LDP experiments predicts that the diffusion kinetics for He in apatite would change at temperatures below 0 °C, also contradicted by modern samples. These test cases verify that either the data or the model construction is flawed, or both. For these reasons, it is clear that the data presented in this work are an inadequate basis upon which to build an improved radiation damage model. However, one can still use these results to improve the experimental design and propose ways by which to move this research forward.

4.6.4 Improved imaging of crystals

A recently-published study proposes the use of high-resolution *in-situ* transmission electron spectroscopy (TEM) and crystallinity measurements to quantify the amount of α-recoil radiation damage in an apatite crystal [93]. A potential use of this technique would be to use *in-situ* TEM to image aliquots of apatite crystals from one sample before and after the thermal annealing treatment. Whereas this chapter attempted to measure the effects of radiation damage by measuring the bulk He diffusion kinetics before and after thermal annealing, one may be able to supplement these data by imaging and quantifying the damage directly, akin to the AFT technique, where the size and shape of vision tracks can be seen on an optical microscope.

Another potential technique that may offer the capability of directly measuring radiation damage in an apatite crystal is atom probe tomography (APT), which measures the distribution of chemical species layer by layer in a small piece of material [62, 104]. By identifying species that may migrate into zones of radiation damage, the relative positioning, shape, size of the these damage zones could potentially be mapped in 3-D. The ability to directly measure these damage zones could be used to measure the zone morphology before and after the steps of heating, proton irradiation, and diffusion experiments. Access to this information would confirm and clarify the assumptions upon which the RDAAM and other models depend.

4.6.5 Application of measured diffusion kinetics to Earth science

A challenge that persists in Earth science is the unavoidable extrapolation between laboratory and geologic timescales. In the case of thermochronology, thermo-kinematic models can only truly be tested using data from samples whose geologic and thermal history is ex-

actly known. However, even in the few terrestrial locations where a sample's thermal past is partially known from other indicators, thermochronologists can get stuck in the trap of using a thermal history generated by a thermal model to then test a thermal model and prove its validity. This circular logic means that the tests for validity are not actually test of model validity and should be approached with caution. The other primary approach to testing these models is to conduct laboratory experiments and extrapolate the results to geologic timescales. While this, too, requires some critical and consequential assumptions, it does not suffer from the circular logic problem described above.

4.6.6 Future tests

In order to verify the conclusions drawn from the data presented in this paper, it will be critical to test more apatite samples in a similar and systematic manner. Samples may come from (i) newly acquired bedrock material, (ii) apatite separates acquired from other projects, or (iii) a laboratory setting where apatite with specific chemistry could be synthesized. A major benefit to using sample material leftover from other projects is that the often time-consuming mineral separation steps have already been completed and perhaps some chemical characterization, AFT ages, and/or AHe ages may have already been measured and published.

4.6.6.1 Sample size

To re-run these experiments with increased precision and utility, the most ideal sample candidate will have a larger crystal size. This way, a single crystal can be degassed, avoiding the complications of superimposed gas release from multiple crystal geometries, while providing a sufficient signal to minimize the effects of blank corrections. Barring the availability of larger individual crystals, future experiments should use a higher sample mass than the experiments presented herein, as the blank corrections are so large that, in some cases, they span the range of expected values for all apatite.

4.6.6.2 Heating schedule

An additional lesson learned over the course of these experiments is to conduct the experiments using a heating schedule that spends the majority of its steps measuring He gas release at temperatures below 340 °C. It is above that temperature that we systematically observe deviation from Arrhenius behavior in these, and previous, experiments. This is of particular importance at the lowest temperature steps because these data points exert an outsized control on the slope and intercept of the Arrhenius regression, which determine the measured activation energy and frequency factor for the experiment.

Based on work done in cosmogenic noble gas paleothermometry (e.g., refs. [103, 105]), the addition of more than one retrograde temperature cycle may also be illustrative in the apatite diffusion kinetics. This would serve to indicate any sign of multiple-domain-diffusion

(MDD) behavior (not expected in apatite, but important to rule out) as well as provide internal replicability for steps conducted at the same temperature at different times in the experiment.

4.6.6.3 Apatite geochemistry

The accommodation of AFT models to Cl content of a measured apatite, as well as more recent work pertaining to the AHe system from ref. [77], suggests that the anion chemistry of a particular apatite sample will affect the ability for damage in a crystal to anneal. It is because of this expected anion chemistry dependence that the experiments described in this chapter were conducted on both Durango-B apatite and LDP apatite. Future work will include, first, the measurement of anion chemistry in these two samples and, second, the continuation of diffusion-annealing experiments and anion analysis on additional apatite samples to further constrain the anion chemistry dependence.

4.7 Conclusions

The data presented in this chapter demonstrate a systematic difference between the response to heating between two different apatite samples: Durango-B and Sierran granite collected near the Little Devil's Postpile. As a result of the small sample mass used for these experiments, we have produced a data set whose precision is not sufficient to recalibrate or improve a model used for the interpretation of AHe thermochronologic data. However, the data presented here indicate that the behavior shown in ref. [8] is replicated. That is, there is a combination of temperature (between 200 and 500 °C) and heating duration above which the diffusion kinetics for He in apatite change measurably, with both the activation energy and frequency factor decreasing. The extrapolation of these laboratory results to geologic timescales indicates that He diffusion kinetics will likely change at temperatures found in the top few kilometers of Earth's crust, which is particularly important in settings with reheating due to burial or local magmatism. These findings reinforce the nature of the complex relationship between the accumulation and annealing of radiation damage in the mineral apatite and the interpretation of AHe ages to solve geologic problems.

4.8 Acknowledgements

This work was supported by an NSF Graduate Research Fellowship DGE 1752814 (to C.D.W.) and the Esper Larsen Research Grant (to D.L.S.). We acknowledge the support of the Ann and Gordon Getty Foundation.

Sample Name	Instr.	# cryst.	E_a kJ/mol	$ln(D_0/a^2)$	T_c (°C)	Tot. ^{3}He (Matoms)	% gas incl.	Regr. MF
DurB-NH-a	Map2	3	112.94 ± 3.81	9.94 ± 0.81	31.1 (–4.7/+4.9)	238.4	0.76	0.107
DurB-NH-b	Map2	3	153.37 ± 5.17	16.26 ± 1.06	88.5 (–4.6/+4.8)	140.8	0.43	0.032
DurB-NH-c	Map2	1	152.45 ± 8.22	16.52 ± 1.67	84.6 (–7.4/+7.9)	63.4	0.49	0.017
DurB-NH-d	Map2	1	131.26 ± 6.42	12.66 ± 1.31	59.9 (–6.9/+7.3)	55.0	0.55	0.013
DurB-NH-e	OH	15	133.78 ± 2.02	14.13 ± 0.43	56.4 (–2.1/+2.1)	498.0	0.84	0.093
DurB-300C-1hr-a	Map2	4	150.13 ± 5.63	16.45 ± 1.16	79.7 (–5.2/+5.4)	89.3	0.59	0.012
DurB-300C-1hr-b	OH	2	121.02 ± 10.78	11.49 ± 2.22	41.9 (–12.4/+13.6)	53.4	0.75	0.055
DurB-300C-1hr-c	Map2	2	141.4 ± 48.93	15.31 ± 9.91	66.9 (–42.4/+62.9)	17.3	0.69	0.030
DurB-325C-1hr-b	Map2	4	137.43 ± 4.96	15.10 ± 1.04	58.9 (–5.0/+5.2)	75.4	0.85	0.018
DurB-330C-1hr-a	Map2	1	142.76 ± 12.43	15.72 ± 2.53	67.4 (–12.0/+13.3)	16.0	0.77	0.034
DurB-350C-1hr-a	Map2	3	132.03 ± 9.40	13.70 ± 1.94	55.0 (–9.9/+10.7)	44.6	0.78	0.040
DurB-365C-1hr-a	Map2	2	124.26 ± 2.77	11.99 ± 0.57	46.9 (–3.2/+3.2)	132.1	0.73	0.019
DurB-375C-1hr-a	Map2	1	135.21 ± 8.84	14.36 ± 1.83	58.4 (–9.1/+9.7)	32.9	0.77	0.015
DurB-395C-1hr-a	Map2	2	98.86 ± 5.60	7.63 ± 1.17	7.9 (–7.9/+8.4)	22.5	0.89	0.033
DurB-395C-1hr-b	Map2	4	141.73 ± 7.79	15.57 ± 1.60	66.0 (–7.6/+8.1)	33.4	0.75	0.027
DurB-415C-1hr-a	Map2	3	122.16 ± 4.27	12.39 ± 0.89	39.0 (–5.0/+5.2)	45.7	0.91	0.024
DurB-450C-1hr-b	Map2	3	130.51 ± 5.53	13.64 ± 1.13	51.6 (–6.1/+6.3)	41.5	0.82	0.047
DurB-475C-1hr-a	OH	1	125.17 ± 5.71	10.39 ± 1.18	60.1 (–6.4/+6.7)	103.7	0.37	0.017
DurB-500C-1hr-c	Map2	2	118.49 ± 6.98	9.55 ± 1.44	48.4 (–8.2/+8.8)	116.9	0.45	0.031
DurB-250C-10hr-a	Map2	3	148.24 ± 7.66	15.72 ± 1.57	80.3 (–7.1/+7.6)	65.0	0.51	0.011
DurB-250C-10hr-b	Map2	2	147.87 ± 6.33	15.34 ± 1.31	82.0 (–5.9/+6.2)	100.6	0.45	0.014
DurB-275C-10hr-a	Map2	3	129.98 ± 5.79	14.04 ± 1.20	47.8 (–6.3/+6.6)	44.6	0.92	0.024
DurB-275C-10hr-b	OH	2	109.69 ± 7.99	10.01 ± 1.70	22.1 (–9.9/+10.7)	25.3	0.91	0.132
DurB-300C-10hr-a	Map2	3	153.41 ± 10.65	17.53 ± 2.18	80.1 (–9.5/+10.3)	56.5	0.66	0.012
DurB-315C-10hr-a	Map2	3	124.66 ± 4.57	12.78 ± 0.95	42.8 (–5.2/+5.4)	58.3	0.88	0.019
DurB-330C-10hr-a	Map2	3	140.02 ± 4.87	14.34 ± 1.01	70.0 (–4.8/+5.0)	149.6	0.55	0.013
DurB-330C-10hr-b	Map2	3	95.49 ± 2.51	6.51 ± 0.52	5.5 (–3.8/+3.8)	62.3	0.81	0.095
DurB-345C-10hr-a	Map2	3	116.1 ± 4.42	10.52 ± 0.91	35.6 (–5.4/+5.6)	51.2	0.77	0.039
DurB-400C-10hr-a	OH	2	122.97 ± 2.37	10.77 ± 0.49	51.7 (–2.8/+2.8)	222.5	0.52	0.007
DurB-400C-10hr-b	Map2	2	126.6 ± 9.15	12.36 ± 1.89	50.3 (–10.0/+10.9)	58.5	0.71	0.024

Sample Name	**Instr.**	**# cryst.**	E_a **kJ/mol**	$ln(D_0/a^2)$	T_c **(°C)**	**Tot. ^{3}He (Matoms)**	**% gas incl.**	**Regr. MF**
DurB-450C-10hr-a	OH	2	134.99 ± 7.43	13.18 ± 1.57	65.7 (–7.4/+7.9)	123.8	0.51	0.010
DurB-450C-10hr-b	Map2	2	123.93 ± 9.40	10.57 ± 1.94	55.6 (–10.5/+11.4)	89.0	0.44	0.033
DurB-275C-100hr-a	Map2	3	143.07 ± 6.21	15.36 ± 1.30	70.5 (–5.9/+6.2)	81.3	0.62	0.025
DurB-275C-100hr-c	Map2	2	138.87 ± 10.84	14.16 ± 2.23	68.5 (–10.7/+11.7)	73.0	0.58	0.028
DurB-300C-100hr-b	Map2	3	127.91 ± 4.01	13.36 ± 0.83	47.1 (–4.5/+4.6)	56.1	0.86	0.058
DurB-325C-100hr-a	Map2	3	196.58 ± 14.12	25.84 ± 2.88	117.7 (–9.2/+10.1)	30.3	0.65	0.206
DurB-325C-100hr-b	Map2	3	120.53 ± 7.36	11.51 ± 1.51	40.6 (–8.6/+9.2)	24.7	0.78	0.052
DurB-350C-100hr-a	OH	3	124.5 ± 2.53	12.11 ± 0.53	46.7 (–2.8/+2.9)	245.5	0.74	0.034
DurB-350C-100hr-b	Map2	2	113.81 ± 8.38	9.43 ± 1.76	36.8 (–10.1/+11.0)	104.4	0.62	0.033
DurB-375C-100hr-a	OH	3	125.95 ± 3.19	11.88 ± 0.66	51.9 (–3.6/+3.7)	113.0	0.63	0.006
DurB-400C-100hr-a	OH	2	124.2 ± 4.42	10.87 ± 0.93	54.2 (–4.9/+5.1)	244.2	0.50	0.011
DurB-400C-100hr-b	Map2	2	130.86 ± 8.63	12.46 ± 1.78	60.3 (–9.1/+9.8)	112.5	0.54	0.033
DurB-425C-100hr-a	OH	2	116.52 ± 6.26	9.55 ± 1.33	43.2 (–7.3/+7.8)	151.8	0.53	0.032
DurB-425C-100hr-d	Map2	2	118.77 ± 10.36	10.02 ± 2.14	46.0 (–12.1/+13.3)	74.2	0.54	0.055
DurB-425C-100hr-e	Map2	2	110.44 ± 7.56	9.27 ± 1.59	28.9 (–9.4/+10.1)	84.73	0.74	0.042
DurB-450C-100hr-a	OH	2	128.85 ± 5.28	12.42 ± 1.12	55.5 (–5.6/+5.9)	150.8	0.62	0.009
DurB-450C-100hr-b	Map2	2	129.63 ± 10.55	11.85 ± 2.18	61.4 (–11.2/+12.3)	83.3	0.46	0.040
DurB-220C-1000hr-a	Map2	1	129.61 ± 10.14	11.60 ± 2.08	63.0 (–10.9/+11.8)	53.3	0.42	0.024
DurB-220C-1000hr-b	Map2	1	127.24 ± 9.84	10.61 ± 2.01	64.0 (–10.8/+11.8)	49.6	0.33	0.006
DurB-220C-1000hr-c	Map2	1	131.35 ± 9.47	11.65 ± 1.93	67.2 (–10.1/+11.0)	45.1	0.40	0.085
DurB-240C-1000hr-a	Map2	1	136.66 ± 9.91	13.16 ± 2.03	69.9 (–10.0/+10.9)	50.3	0.46	0.032
DurB-240C-1000hr-b	OH	6	132.25 ± 3.20	14.03 ± 0.68	53.4 (–3.3/+3.4)	248.8	0.87	0.028
DurB-260C-1000hr-a	Map2	1	133.72 ± 10.52	12.47 ± 2.14	67.4 (–10.9/+11.9)	34.0	0.43	0.011
DurB-260C-1000hr-b	OH	6	125.86 ± 4.88	12.85 ± 1.07	45.3 (–5.1/+5.3)	185.4	0.61	0.019

Table 4.1: Measured diffusion kinetics values for each Durango-B sample. The annealing temperature precedes "C" in the sample name (NH = no pre-heating) and the annealing duration in hours precedes the "hr" the in sample name. The $ln(D_0/a^2)$ values are in natural logarithm units normalized to s^{-1}. Closure temperature calculated using ref. [2] with a cooling rate of 10 °C/Ma and geometric constant of $A = 55$.

Sample Name	Instr.	# cryst.	E_a kJ/mol	$ln(D_0/a^2)$	T_c (°C)	Tot. ^{3}He (Matoms)	% gas incl.	Regr. MF
LDP-NH-c	OH	2	146.91 ± 8.92	14.53 ± 1.84	85.3 (–8.2/+8.8)	106.7	0.34	0.022
LDP-NH-d	Map2	1	128.01 ± 8.66	11.5 ± 1.76	59.7 (–9.5/+10.3)	44.5	0.48	0.038
LDP-NH-e	Map2	2	120.03 ± 9.14	8.4 ± 1.86	60.8 (–10.7/+11.6)	65.9	0.25	0.072
LDP-NH-f	Map2	mg	115.2 ± 0.80	9.42 ± 0.17	40.6 (–1/+1)	9774.2	0.54	0.086
LDP-NH-g	OH	15	112.33 ± 4.92	9.2 ± 1.04	34.4 (–6.1/+6.4)	610.6	0.63	0.125
LDP-NH-j	OH	15	110.27 ± 3.14	8.08 ± 0.66	36.4 (–4/+4.1)	476.6	0.54	0.202
LDP-350C-1hr-a	Map2	5	146.3 ± 7.40	15.11 ± 1.53	79.8 (–6.9/+7.3)	109.1	0.45	0.016
LDP-365C-1hr-a	Map2	9	127.53 ± 6.61	11.39 ± 1.34	59.2 (–7.4/+7.8)	88.9	0.57	0.024
LDP-365C-1hr-b	OH	2	145.28 ± 9.50	15.18 ± 1.97	76.9 (–8.9/+9.6)	58.0	0.50	0.022
LDP-375C-1hr-a	OH	3	110.63 ± 8.53	7.59 ± 1.73	40.8 (–11/+11.9)	43.5	0.36	0.018
LDP-397C-1hr-a	OH	2	113.74 ± 18.29	9.05 ± 3.7	39.2 (–22.1/+26.1)	16.5	0.44	0.007
LDP-414C-1hr-a	OH	10	135.51 ± 8.47	12.67 ± 1.71	70.5 (–8.9/+9.5)	73.5	0.50	0.004
LDP-450C-1hr-a	OH	3	235.19 ± 20.23	33.24 ± 4.05	143.8 (–10.5/+11.9)	21.1	0.51	0.181
LDP-475C-1hr-a	OH	3	139.07 ± 10.94	12.97 ± 2.25	77.1 (–10.6/+11.7)	69.8	0.34	0.044
LDP-500C-1hr-a	OH	10	130.37 ± 10.54	11.27 ± 2.16	67.3 (–11.1/+12.2)	62.2	0.34	0.045
LDP-500C-1hr-b	OH	2	144.97 ± 7.71	14.4 ± 1.59	81.5 (–7.2/+7.7)	106.8	0.37	0.008
LDP-250C-10hr-a	OH	10	122.38 ± 2.46	9.72 ± 0.5	57.5 (–2.9/+3)	400.8	0.44	0.011
LDP-250C-10hr-b	OH	3	140.71 ± 9.63	13.66 ± 2.02	76.4 (–9.1/+9.9)	75.6	0.42	0.015
LDP-275C-10hr-c	OH	3	146.49 ± 11.23	15.59 ± 2.31	77 (–10.4/+11.4)	41.8	0.53	0.024
LDP-300C-10hr-a	OH	2	117.02 ± 8.34	8.95 ± 1.7	48.7 (–10.1/+10.9)	139.9	0.49	1.518
LDP-315C-10hr-b	OH	2	149.57 ± 11.20	15.37 ± 2.29	85.8 (–10.2/+11.1)	54.4	0.38	0.014
LDP-330C-10hr-a	OH	3	132.09 ± 6.02	12.38 ± 1.25	63.9 (–6.3/+6.7)	103.5	0.48	0.047
LDP-330C-10hr-b	OH	2	145.96 ± 8.17	14.78 ± 1.72	81.2 (–7.4/+7.9)	156.8	0.41	0.017
LDP-345C-10hr-a	Map2	1	128.46 ± 28.54	12.05 ± 5.77	57.1 (–29.3/+37.3)	7.6	0.68	0.044
LDP-345C-10hr-b	OH	10	133.27 ± 5.79	12.8 ± 1.17	64 (–6.3/+6.6)	78.4	0.63	0.008
LDP-400C-10hr-a	OH	2	137.93 ± 10.04	12.93 ± 2.1	74.7 (–9.7/+10.6)	76.6	0.39	0.017
LDP-400C-10hr-b	Map2	1	136.74 ± 23.18	11.73 ± 4.7	80.2 (–22.3/+27.2)	25.7	0.25	0.142
LDP-450C-10hr-a	OH	2	120.97 ± 2.63	11.07 ± 0.55	44.6 (–3/+3.1)	250.1	0.65	0.046

Sample Name	**Instr.**	**# cryst.**	E_a **kJ/mol**	$ln(D_0/a^2)$	T_c **(°C)**	**Tot. ^{3}He (Matoms)**	**% gas incl.**	**Regr. MF**
LDP-250C-100hr-a	OH	4	150.89 ± 10.84	16.89 ± 2.22	78.6 (–9.8/+10.7)	50.4	0.62	0.019
LDP-275C-100hr-a	OH	5	138.20 ± 7.05	12.72 ± 1.44	76.8 (–7.1/+7.6)	110.8	0.32	0.003
LDP-300C-100hr-a	OH	4	141.79 ± 7.88	13.9 ± 1.61	77.3 (–7.7/+8.3)	89.8	0.39	0.003
LDP-325C-100hr-a	OH	2	144.50 ± 6.89	13.48 ± 1.42	86.9 (–6.5/+6.9)	180.0	0.27	0.020
LDP-350C-100hr-a	OH	2	128.95 ± 7.82	11.39 ± 1.66	62.8 (–8.1/+8.7)	172.5	0.39	0.029
LDP-350C-100hr-b	OH	2	132.33 ± 5.38	11.28 ± 1.11	72.3 (–5.7/+5.9)	168.8	0.29	0.018
LDP-350C-100hr-c	Map2	mg	115.61 ± 0.85	8.38 ± 0.18	48.9 (–1/+1.1)	5349.8	0.34	0.105
LDP-375C-100hr-a	OH	2	121.73 ± 7.74	9.39 ± 1.63	58.1 (–8.6/+9.2)	136.3	0.32	0.016
LDP-375C-100hr-b	OH	2	137.15 ± 11.82	12.31 ± 2.43	77 (–11.7/+12.9)	58.6	0.30	0.017
LDP-400C-100hr-a	OH	2	141.70 ± 10.99	14.31 ± 2.26	74.3 (–10.5/+11.5)	45.9	0.48	0.022
LDP-425C-100hr-a	OH	2	135.86 ± 7.2	12.09 ± 1.48	75.4 (–7.3/+7.8)	104.4	0.31	0.007
LDP-450C-100hr-a	OH	2	134.44 ± 9.51	11.47 ± 1.99	76.3 (–9.4/+10.2)	122.2	0.27	0.027
LDP-450C-100hr-b	OH	2	114.30 ± 22.83	7.75 ± 4.62	49.9 (–26.7/+33.1)	57.1	0.29	0.084
LDP-450C-100hr-c	OH	15	129.77 ± 5.48	10.89 ± 1.17	68.5 (–5.6/+5.9)	877.5	0.30	0.073
LDP-450C-100hr-e	Map2	15	116.15 ± 2.80	8.9 ± 0.59	46.7 (–3.4/+3.5)	315.4	0.46	0.047

Table 4.2: Measured diffusion kinetics values for each LDP sample. The annealing temperature precedes "C" in the sample name (NH = no pre-heating) and the annealing duration in hours precedes the "hr" the in sample name. The "mg" indicates experiments conducted on hundreds of apatite crystals, described in Section 4.4.2. The $ln(D_0/a^2)$ values are in natural logarithm units normalized to s^{-1}. Closure temperature calculated using ref. [2] with a cooling rate of 10 °C/Ma and geometric constant of $A = 55$.

Chapter 5

Conclusions

Using the production and diffusion of radiogenic ^{4}He in the mineral apatite provides those who study it the opportunity to quantify and comprehend vast spatial and temporal scales. Taken together, the chapters in this dissertation demonstrate both the value and responsibility that comes with applying apatite (U–Th)/He thermochronology to Earth science.

Much of the work presented in this dissertation is empirical and would greatly benefit from being informed by true mechanism, both for radiation damage accumulation and its annealing, as well as the temperature-dependent diffusion of He in apatite. Future analyses, such as those outlined in Section 4.6.6, in tandem with physics-based modeling will ultimately be the key to understanding the connection between radiogenic ^{4}He in apatite and the Earth science questions one hopes to address using low-temperature thermochronometry.

Bibliography

1. Schoene, B. in *Treatise on Geochemistry (Second Edition)* (eds Holland, H. D. & Turekian, K. K.) Second Edition, 341–378 (Oxford, 2014).
2. Dodson, M. H. Closure temperature in cooling geochronological and petrological systems. *Contrib. Mineral. Petrol.* **40,** 259–274 (1973).
3. Bernet, M., Brandon, M., Garver, J., Balestieri, M. L., Ventura, B. & Zattin, M. Exhuming the Alps through time: clues from detrital zircon fission-track thermochronology. *Basin Res.* **21,** 781–798 (2009).
4. Braun, J. Quantifying the effect of recent relief changes on age–elevation relationships. *Earth Planet. Sci. Lett.* **200,** 331–343 (2002).
5. Trachenko, K., Dove, M. T. & Salje, E. K. H. Large swelling and percolation in irradiated zircon. *J. Phys. Condens. Matter* **15,** L1–L7 (2002).
6. Flowers, R. M., Ketcham, R. A., Shuster, D. L. & Farley, K. A. Apatite (U–Th)/He thermochronometry using a radiation damage accumulation and annealing model. *Geochim. Cosmochim. Acta* **73,** 2347–2365 (2009).
7. Gautheron, C., Tassan-Got, L., Barbarand, J. & Pagel, M. Effect of alpha-damage annealing on apatite (U–Th)/He thermochronology. *Chem. Geol.* **266,** 157–170 (2009).
8. Shuster, D. L. & Farley, K. A. The influence of artificial radiation damage and thermal annealing on helium diffusion kinetics in apatite. *Geochim. Cosmochim. Acta* **73,** 183–196 (2009).
9. Ketcham, R. A., Donelick, R. A. & Carlson, W. D. Variability of apatite fission-track annealing kinetics: III. Extrapolation to geological time scales. *Am. Mineral.* **84,** 1235–1255 (1999).
10. Hallet, B., Hunter, L. & Bogen, J. Rates of erosion and sediment evacuation by glaciers: A review of field data and their implications. *Global and Planetary Change* **12,** 213–235 (1996).
11. Peizhen, Z., Molnar, P. & Downs, W. R. Increased sedimentation rates and grain sizes 2±4 Myr ago due to the influence of climate change on erosion rates. *Nature* **410,** 891–897 (2001).

12. Willenbring, J. K. & von Blanckenburg, F. Long-term stability of global erosion rates and weathering during late-Cenozoic cooling. *Nature* **465,** 211–214 (2010).

13. Herman, F., Seward, D., Valla, P. G., Carter, A., Kohn, B., Willett, S. D. & Ehlers, T. A. Worldwide acceleration of mountain erosion under a cooling climate. *Nature* **504,** 423–426 (2013).

14. Oerlemans, J. Numerical experiments on large-scale glacial erosion. *Z. Gletscherkd. Glazialgeol.* **20,** 107–126 (1984).

15. Kaplan, M. R., Hein, A. S., Hubbard, A. & Lax, S. M. Can glacial erosion limit the extent of glaciation? *Geomorphology* **103,** 172–179 (2009).

16. Shuster, D. L., Cuffey, K. M., Sanders, J. W. & Balco, G. Thermochronometry reveals headward propagation of erosion in an alpine landscape. *Science* **332,** 84–88 (2011).

17. Thomson, S. N., Brandon, M. T., Tomkin, J. H., Reiners, P. W., Vásquez, C. & Wilson, N. J. Glaciation as a destructive and constructive control on mountain building. *Nature* **467,** 313–317 (2010).

18. Schildgen, T. F., van der Beek, P. A., Sinclair, H. D. & Thiede, R. C. Spatial correlation bias in late-Cenozoic erosion histories derived from thermochronology. *Nature* **559,** 89–93 (2018).

19. Reiners, P. W. & Brandon, M. T. Using thermochronology to understand orogenic erosion. *Annu. Rev. Earth Planet. Sci.* **34,** 419–466 (2006).

20. Herman, F. & Brandon, M. Mid-latitude glacial erosion hotspot related to equatorial shifts in southern Westerlies. *Geology* **43,** 987–990 (2015).

21. Shuster, D. L., Flowers, R. M. & Farley, K. A. The influence of natural radiation damage on helium diffusion kinetics in apatite. *Earth Planet. Sci. Lett.* **249,** 148–161 (2006).

22. Garver, J. I., Brandon, M. T., Roden-Tice, M. & Kamp, P. J. J. Exhumation history of orogenic highlands determined by detrital fission-track thermochronology. *Geological Society, London, Special Publications* **154,** 283–304 (1999).

23. McPhillips, D. & Brandon, M. Using tracer thermochronology to measure modern relief change in the Sierra Nevada, California. *Earth Planet. Sci. Lett.* **296,** 373–383 (2010).

24. Georgieva, V., Melnick, D., Schildgen, T. F., Ehlers, T. A., Lagabrielle, Y., Enkelmann, E. & Strecker, M. R. Tectonic control on rock uplift, exhumation, and topography above an oceanic ridge collision: Southern Patagonian Andes (47°S), Chile. *Tectonics* **35,** 1317–1341 (2016).

25. Guillaume, B., Gautheron, C., Simon-Labric, T., Martinod, J., Roddaz, M. & Douville, E. Dynamic topography control on Patagonian relief evolution as inferred from low temperature thermochronology. *Earth Planet. Sci. Lett.* **364,** 157–167 (2013).

26. Christeleit, E. C., Brandon, M. T. & Shuster, D. L. Miocene development of alpine glacial relief in the Patagonian Andes, as revealed by low-temperature thermochronometry. *Earth Planetary Science Letters* **460,** 152–163 (2017).

27. Colwyn, D. A., Brandon, M. T., Hren, M. T., Hourigan, J., Pacini, A., Cosgrove, M. G., Midzik, M., Garreaud, R. D. & Metzger, C. Growth and steady state of the Patagonian Andes. *Am. J. Sci.* **319,** 431–472 (2019).

28. Ramos, V. A. & Ghiglione, M. C. in *The Late Cenozoic of Patagonia and Tierra del Fuego* 57–71 (Elsevier, 2008).

29. Georgieva, V., Gallagher, K., Sobczyk, A., Sobel, E. R., Schildgen, T. F., Ehlers, T. A. & Strecker, M. R. Effects of slab-window, alkaline volcanism, and glaciation on thermochronometer cooling histories, Patagonian Andes. *Earth Planet. Sci. Lett.* **511,** 164–176 (2019).

30. De Pascale, G. P., Penna, I., Hermanns, R. L., Froude, M. & Sepulveda, S. A. *First steps towards a fast slip rate along the Liquiñe-Ofqui Fault Zone in Chilean Patagonia* in (AGU San Francisco, 2016).

31. Headley, R. M., Roe, G. & Hallet, B. Glacier longitudinal profiles in regions of active uplift. *Earth Planet. Sci. Lett.* **317-318,** 354–362 (2012).

32. Stevens Goddard, A. L. & Fosdick, J. C. Multichronometer thermochronologic modeling of migrating spreading ridge subduction in southern Patagonia. *Geology* (2019).

33. England, P. & Molnar, P. Surface uplift, uplift of rocks, and exhumation of rocks. *Geology* **18,** 1173–1177 (1990).

34. Mercer, J. H. & Sutter, J. F. Late Miocene–earliest Pliocene glaciation in southern Argentina: Implications for global ice-sheet history. *Palaeogeography, Palaeoclimatology, Palaeoecology* **38,** 185–206 (1982).

35. Ton-That, T., Singer, B., Mörner, N.-A. & Rabassa, J. Datación de lavas basálticas por $^{40}Ar/^{39}Ar$ y geología glacial de la región del lago Buenos Aires, provincia de Santa Crux, Argentina. *Revista de la Asociación Geológica Argentina* **54,** 333–352 (1999).

36. Guivel, C. *et al.* Miocene to Late Quaternary Patagonian basalts (46–47°S): Geochronometric and geochemical evidence for slab tearing due to active spreading ridge subduction. *Journal of Volcanology and Geothermal Research* **149,** 346–370 (2006).

37. Singer, B. S., Ackert, R. P. & Guillou, H. $^{40}Ar/^{39}Ar$ and K–Ar chronology of Pleistocene glaciations in Patagonia. *Geological Society of America Bulletin* **116,** 434–450 (2004).

38. Douglass, D. C., Singer, B. S., Kaplan, M. R., Mickelson, D. M. & Caffee, M. W. Cosmogenic nuclide surface exposure dating of boulders on last-glacial and late-glacial moraines, Lago Buenos Aires, Argentina: Interpretive strategies and paleoclimate implications. *Quat. Geochronol.* **1,** 43–58 (2006).

39. Kaplan, M. R. *et al.* In-situ cosmogenic ^{10}Be production rate at Lago Argentino, Patagonia: Implications for late-glacial climate chronology. *Earth Planet. Sci. Lett.* **309,** 21–32 (2011).

40. De Boer, B., van de Wal, R. S. W., Bintanja, R., Lourens, L. J. & Tuenter, E. Cenozoic global ice-volume and temperature simulations with 1-D ice-sheet models forced by benthic δ^{18}O records. *Annals of Glaciology* **51,** 23–33 (2010).

41. Gordon, A. L. in *Encyclopedia of Ocean Sciences* (ed Steele, J. H.) 334–340 (Academic Press, Oxford, 2001).

42. Hulton, N. R. J., Purves, R. S., McCulloch, R. D., Sugden, D. E. & Bentley, M. J. *The Last Glacial Maximum and deglaciation in southern South America* 2002.

43. Brandon, M. T. Probability density plot for fission-track grain-age sample. *Radiat. Meas.* **26,** 663–676 (1996).

44. Millan, R. *Ice thickness and bed elevation of the Patagonian Icefields* 2019.

45. Stock, G. M., Ehlers, T. A. & Farley, K. A. Where does sediment come from? Quantifying catchment erosion with detrital apatite (U–Th)/He thermochronometry. *Geology* **34,** 725–728 (2006).

46. Ehlers, T. A. *et al.* in. 1, 589–622 (Min. Soc. of Amer., 2005).

47. Preusser, F. Quaternary glaciation history of northern Switzerland. *Quat. Int.* **60,** 282–305 (2012).

48. Herman, F., Braun, J., Deal, E. & Prasicek, G. The response time of glacial erosion. *J. Geophys. Res. Earth Surf.* **123,** 801–817 (2018).

49. Willenbring, J. K., Codilean, A. T. & McElroy, B. Earth is (mostly) flat: Apportionment of the flux of continental sediment over millennial time scales. *Geology* **41,** 343–346 (2013).

50. Shuster, D. L., Ehlers, T. A., Rusmore, M. E. & Farley, K. A. Rapid glacial erosion at 1.8 Ma revealed by ^{4}He/^{3}He thermochronometry. *Science* **310** (2005).

51. Valla, P. G., Shuster, D. L. & van der Beek, P. A. Significant increase in relief of the European Alps during mid-Pleistocene glaciations. *Nature Geoscience* **4,** 688–692 (2011).

52. Ivany, L. C., Van Simaeys, S., Domack, E. W. & Samson, S. D. Evidence for an earliest Oligocene ice sheet on the Antarctic Peninsula. *Geology* **34,** 377–380 (2006).

53. Galbraith, R. *Statistics for Fission Track Analysis* (Taylor & Francis Group, Boca Raton, FL, 2005).

54. Farley, K. A. Helium diffusion from apatite: General behavior as illustrated by Durango fluorapatite. *Journal of Geophysical Research* **105,** 2903–2914 (2000).

55. Annen, C., Blundy, J. D. & Sparks, R. S. J. The genesis of intermediate and silicic magmas in deep crustal hot zones. *J. Petrol.* **47,** 505–539 (2006).

56. Jaeger, J. C. Thermal effects of intrusions. *Rev. Geophys.* **2,** 443 (1964).

57. Nabelek, P. I., Whittington, A. G. & Hofmeister, A. M. Strain heating as a mechanism for partial melting and ultrahigh temperature metamorphism in convergent orogens: Implications of temperature-dependent thermal diffusivity and rheology. *J. Geophys. Res.* **115,** 1–17 (2010).

58. Saltus, R. W. & Lachenbruch, A. H. Thermal evolution of the Sierra Nevada: Tectonic implications of new heat flow data. *Tectonics* **10,** 325–344 (1991).

59. England, P. C. & Katz, R. F. Melting above the anhydrous solidus controls the location of volcanic arcs. *Nature* **467,** 700–703 (2010).

60. Willett, C. D., Fox, M. & Shuster, D. L. A helium-based model for the effects of radiation damage annealing on helium diffusion kinetics in apatite. *Earth Planet. Sci. Lett.* **477,** 195–204 (2017).

61. Farley, K. A. (U–Th)/He Dating: Techniques, Calibrations, and Applications. *Rev. Mineral. Geochem.* **47,** 819–844 (2002).

62. Valley, J. W. *et al.* Hadean age for a post-magma-ocean zircon confirmed by atom-probe tomography. *Nat. Geosci.* **7,** 219–223 (2014).

63. Fox, M. & Shuster, D. L. The influence of burial heating on the (U–Th)/He system in apatite: Grand Canyon case study. *Earth Planet. Sci. Lett.* **397,** 174–183 (2014).

64. Ritter, W. & Märk, T. D. Radiation damage and its annealing in apatite. *Nuclear Instruments and Methods in Physics Research* **814,** 314–322 (1986).

65. Laslett, G. M., Green, P. F., Duddy, I. R. & Gleadow, A. J. W. Thermal Annealing of Fission Tracks in Apatite 2. A Quantitative Analysis. *Chem. Geol.* **65,** 1–13 (1987).

66. Wolf, R. A., Farley, K. A. & Kass, D. M. Modeling of the temperature sensitivity of the apatite (U–Th)/He thermochronometer. *Chemical Geology* **148,** 105–114 (1998).

67. Gastil, R. G., DeLisle, M. & Morgan, J. R. Some effects of progressive metamorphism on zircons. *Geol. Soc. Am. Bull.* **78,** 879–906 (1967).

68. Ketcham, R. A., Carter, A., Donelick, R. A., Barbarand, J. & Hurford, A. J. Improved modeling of fission-track annealing in apatite. *Am. Mineral.* **92,** 799–810 (2007).

69. Flowers, R. M., Wernicke, B. P. & Farley, K. A. Unroofing, incision, and uplift history of the southwestern Colorado Plateau from apatite (U–Th)/He thermochronometry. *Geol. Soc. Am. Bull.* **120,** 571–587 (2008).

70. Flowers, R. M. & Farley, K. A. Apatite ^{4}He/^{3}He and (U–Th)/He Evidence for an Ancient Grand Canyon. *Science* **338,** 1616–1619 (2012).

71. Winn, C., Karlstrom, K. E., Shuster, D. L., Kelley, S. & Fox, M. 6 Ma age of carving Westernmost Grand Canyon: Reconciling geologic data with combined AFT, (U–Th)/He, and ^{4}He/^{3}He thermochronologic data. *Earth Planet. Sci. Lett.* **474,** 257–271 (2017).

72. Fox, M., Tripathy-Lang, A., Shuster, D. L., Winn, C., Karlstrom, K. & Kelley, S. Westernmost Grand Canyon incision: Testing thermochronometric resolution. *Earth Planet. Sci. Lett.* **474,** 248–256 (2017).

73. Karlstrom, K. E., Crow, R., Crossey, L. J., Coblentz, D. & Van Wijk, J. W. Model for tectonically driven incision of the younger than 6 Ma Grand Canyon. *Geology* **36,** 835–838 (2008).

74. Karlstrom, K. E. *et al.* Formation of the Grand Canyon 5 to 6 million years ago through integration of older palaeocanyons. *Nat. Geosci.* **7,** 239–244 (2014).

75. Dumitru, T. A., Duddy, I. R. & Green, P. F. Mesozoic–Cenozoic burial, uplift, and erosion history of the west-central Colorado Plateau. *Geology* **22,** 499–502 (1994).

76. McDowell, F. W., McIntosh, W. C. & Farley, K. A. A precise ^{40}Ar–^{39}Ar reference age for the Durango apatite (U–Th)/He and fission-track dating standard. *Am. J. Sci.* **312,** 90–116 (2012).

77. Gautheron, C., Barbarand, J., Ketcham, R. A., Tassan-Got, L., van der Beek, P., Pagel, M., Pinna-Jamme, R., Couffignal, F. & Fialin, M. Chemical influence on alpha-recoil damage annealing in apatite: Implications for (U–Th)/He dating. *Chem. Geol.* **351,** 257–267 (2013).

78. Ault, A. K., Reiners, P. W., Thomson, S. N. & Miller, G. H. *Inverted Apatite (U–Th)/He and Fission-track Dates from the Rae craton, Baffin Island, Canada and Implications for Apatite Radiation Damage-He Diffusivity Models* in (AGU San Francisco, 2015).

79. Ewing, R. C., Meldrum, A., Wang, L., Weber, W. J. & René Corrales, L. Radiation Effects in Zircon. *Rev. Mineral. Geochem.* **53,** 387–425 (2003).

80. Zhang, M., Salje, E. K. H., Farnan, I., Graeme-Barber, A., Danield, P., Ewing, R. C., Clark, A. M. & Leroux, H. Metamictization of zircon: Raman spectroscopic study. *J. Phys. Condens. Matter* **12,** 1915–1925 (2000).

81. Marsellos, A. E. & Garver, J. I. Radiation damage and uranium concentration in zircon as assessed by Raman spectroscopy and neutron irradiation. *Am. Mineral.* **95,** 1192–1201 (2010).

82. Tagami, T., Ito, H. & Nishimura, S. Thermal annealing characteristics of spontaneous fission tracks in zircon. *Chemical Geology: Isotope Geoscience section* **80,** 159–169 (1990).

83. Yamada, R., Murakami, M. & Tagami, T. Statistical modelling of annealing kinetics of fission tracks in zircon; Reassessment of laboratory experiments. *Chem. Geol.* **236,** 75–91 (2007).

84. Trachenko, K. Understanding resistance to amorphization by radiation damage. *J. Phys. Condens. Matter* **16,** R1491–R1515 (2004).

85. Ketcham, R. A., Guenthner, W. R. & Reiners, P. W. Geometric analysis of radiation damage connectivity in zircon, and its implications for helium diffusion. *Am. Mineral.* **98,** 350–360 (2013).

86. Guenthner, W. R., Reiners, P. W., Ketcham, R. A., Nasdala, L. & Giester, G. Helium diffusion in natural zircon: Radiation damage, anisotropy, and the interpretation of zircon (U–Th)/He thermochronology. *Am. J. Sci.* **313,** 145–198 (2013).

87. Gordon, L. M., Tran, L. & Joester, D. Atom probe tomography of apatites and bone-type mineralized tissues. *ACS Nano* **6,** 10667–10675 (2012).

88. Fox, M., McKeon, R. E. & Shuster, D. L. Incorporating 3-D parent nuclide zonation for apatite ^{4}He/^{3}He thermochronometry: An example from the Appalachian Mountains. *Geochem. Geophys. Geosyst.* **15,** 4217–4229 (2014).

89. Warnock, A. C., Zeitler, P. K., Wolf, R. A. & Bergman, S. C. An evaluation of low-temperature apatite U–Th/He thermochronometry. *Geochim. Cosmochim. Acta* **61,** 5371–5377 (1997).

90. Guralnik, B. *et al.* OSL-thermochronometry of feldspar from the KTB borehole, Germany. *Earth Planet. Sci. Lett.* **423,** 232–243 (2015).

91. Calk, L. C. & Naeser, C. W. The thermal effect of a basalt intrusion on fission tracks in quartz monzonite. *J. Geol.* **81,** 189–198 (1973).

92. Shuster, D. L., Reiners, P. W., Schmidt, J. L., Zeitler, P. K., Ketcham, R. A. & Karlstrom, L. *Intercalibration of multiple thermochonometric systems at the Little Devil's Postpile contact aureole* in (AGU, San Francisco, 2012).

93. Li, W., Shen, Y., Zhou, Y., Nan, S., Chen, C.-H. & Ewing, R. C. In situ TEM observation of alpha-particle induced annealing of radiation damage in Durango apatite. *Sci. Rep.* **7,** 1–10 (2017).

94. Abbey, A. L. & Niemi, N. A. Low-temperature thermochronometric constraints on fault initiation and growth in the northern Rio Grande rift, upper Arkansas River valley, Colorado, USA. *Geology* **46,** 627–630 (2018).

95. Zeitler, P. K., Herczeg, A. L., Mcdougall, I. & Honda, M. U–Th–He dating of apatite: A potential thermochronometer. *Geochim. Cosmochim. Acta* **51,** 2865–2868 (1987).

96. Farley, K. A., Wolf, R. A. & Silver, L. T. The effects of long alpha-stopping distances on (U–Th)/He ages. *Geochim. Cosmochim. Acta* **60,** 4223–4229 (1996).

97. Tremblay, M. M., Fox, M., Schmidt, J. L., Tripathy-Lang, A., Wielicki, M. M., Harrison, T. M., Zeitler, P. K. & Shuster, D. L. Erosion in southern Tibet shut down at ∼10 Ma due to enhanced rock uplift within the Himalaya. *Proceedings of the National Academy of Sciences* **112,** 12030–12035 (2015).

98. Shuster, D. L., Farley, K. A., Sisterson, J. M. & Burnett, D. S. Quantifying the diffusion kinetics and spatial distributions of radiogenic ^{4}He in minerals containing proton-induced ^{3}He. *Earth Planet. Sci. Lett.* **217,** 19–32 (2004).

99. Bevington, P. R. & Robinson, D. K. *Data Reduction and Error Analysis for the Physical Sciences* (McGraw Hill, New York, NY 10020, 2003).

100. Fechtig, H. & Kalbitzer, S. in *Potassium Argon Dating* (eds Schaeffer, O. A. & Zähringer, J.) 68–107 (Springer, Berlin and Heidelberg, 1966).

101. Shuster, D. L. & Farley, K. A. ^{4}He/^{3}He thermochronometry. *Earth Planet. Sci. Lett.* **217,** 1–17 (2004).

102. Cherniak, D. J., Watson, E. B. & Thomas, J. B. Diffusion of helium in zircon and apatite. *Chem. Geol.* **268,** 155–166 (2009).

103. Tremblay, M. M., Shuster, D. L. & Balco, G. Diffusion kinetics of ^{3}He and ^{21}Ne in quartz and implications for cosmogenic noble gas paleothermometry. *Geochim. Cosmochim. Acta* **142,** 186–204 (2014).

104. Saxey, D. W., Moser, D. E., Piazolo, S., Reddy, S. M. & Valley, J. W. Atomic worlds: Current state and future of atom probe tomography in geoscience. *Scr. Mater.* **148,** 115–121 (2018).

105. Tremblay, M. M., Shuster, D. L., Balco, G. & Cassata, W. S. Neon diffusion kinetics and implications for cosmogenic neon paleothermometry in feldspars. *Geochim. Cosmochim. Acta* **205,** 14–30 (2017).

Appendix A

Annealing-diffusion experimental results from Chapter 4

The following Appendix includes the experimental results from the 97 annealing–diffusion experiments discussed in Chapter 4 of this dissertation. For each experiment, there is a data table that includes the heating schedule (i.e., the temperature a duration for each heating step), the measured ^{3}He and ^{4}He and their errors (all in Matoms), as well as the calculated ^{4}He/^{3}He and all associated error for each step. A numeral in the final column indicates if step was included ("1") or not included ("0") in the Arrhenius regression.

Across the top of each data table is the information included in Tables 4.1 and 4.2: the resultant E_a (in kJ/mol), D_0 (in natural logarithm units normalized to s^{-1}), and T_c (closure temperature in °C) and their errors, as well as the the total measured ^{3}He (in Matoms), the fraction included in the regression, and regular and normalized misfits (normalized by number of included heating steps).

Following each data table is a set of three plots, showing the data listed in the preceding table. These plots comprise an Arrhenius plot of calculated values of D/a^2 versus $1/T$ (top) and two residual plots below—one against the cumulative release fraction of the ^{3}He gas and the other against the temperature of the heating step.

DurB-NH-a

E_a	+/-	D_0	+/-	T_c	-	+	Total ^{3}He	Incl.	Misfit	Norm. Misfit
112.94	3.81	9.94	0.81	31.13	4.68	4.85	238.42	0.761	2.034	0.107

Step #	°C	t (hrs)	^{3}He	Error	^{4}He	Error	^{4}He/^{3}He	Err	In ^{3}He Reg.
1	250	0.25	10.40	0.58	9795.9	59.4	931.6	0.06	1
2	250	0.50	5.00	0.36	4691.7	40.9	929.0	0.07	1
3	250	1.00	9.61	0.55	9205.1	67.1	947.9	0.06	1
4	225	1.50	1.89	0.25	1809.5	37.8	945.7	0.13	1
5	225	2.50	2.12	0.28	2089.7	40.5	976.8	0.13	1
6	200	3.00	0.49	0.19	490.3	41.5	984.9	0.40	1
7	200	4.00	0.71	0.24	658.0	43.4	920.0	0.34	1
8	235	2.00	3.68	0.34	3376.5	49.9	908.3	0.09	1
9	235	3.00	5.50	0.41	5242.1	59.8	943.5	0.08	1
10	270	1.91	16.52	0.62	15756.2	96.0	943.6	0.04	1
11	270	1.57	6.54	0.44	6427.0	56.9	973.1	0.07	1
12	285	1.25	14.60	0.74	14328.5	83.4	971.7	0.05	1
13	285	1.56	9.54	0.49	9368.6	63.3	971.9	0.05	1
14	300	1.91	14.36	0.75	14346.6	72.7	989.1	0.05	1
15	300	1.45	13.33	0.65	13251.2	74.4	984.4	0.05	1
16	325	1.74	27.97	1.02	27641.7	140.3	978.1	0.04	1
17	325	1.32	10.81	0.56	11118.7	66.9	1018.5	0.05	1
18	340	1.58	15.28	0.66	15484.1	73.7	1003.3	0.04	1
19	340	1.89	13.14	0.60	13485.7	83.4	1016.1	0.05	1
20	350	1.48	5.89	0.39	6174.6	57.8	1039.2	0.07	0
21	350	1.82	5.93	0.39	6381.4	53.3	1066.7	0.07	0
22	360	1.50	3.23	0.30	3321.9	37.9	1018.7	0.09	0
23	360	1.98	2.51	0.28	2815.8	40.9	1113.3	0.11	0
24	370	1.88	2.46	0.25	2539.2	31.1	1022.7	0.10	0
25	390	1.47	2.70	0.25	2661.6	42.0	976.3	0.09	0
26	450	1.00	3.97	0.36	3970.0	43.3	990.0	0.09	0
27	600	1.00	11.34	0.56	9201.1	67.6	801.7	0.05	0
28	900	1.00	14.43	1.95	4417.7	42.1	296.2	0.14	0
29	900	1.00	4.49	0.32	56.0	33.7	2.5	0.61	0

Figure S1

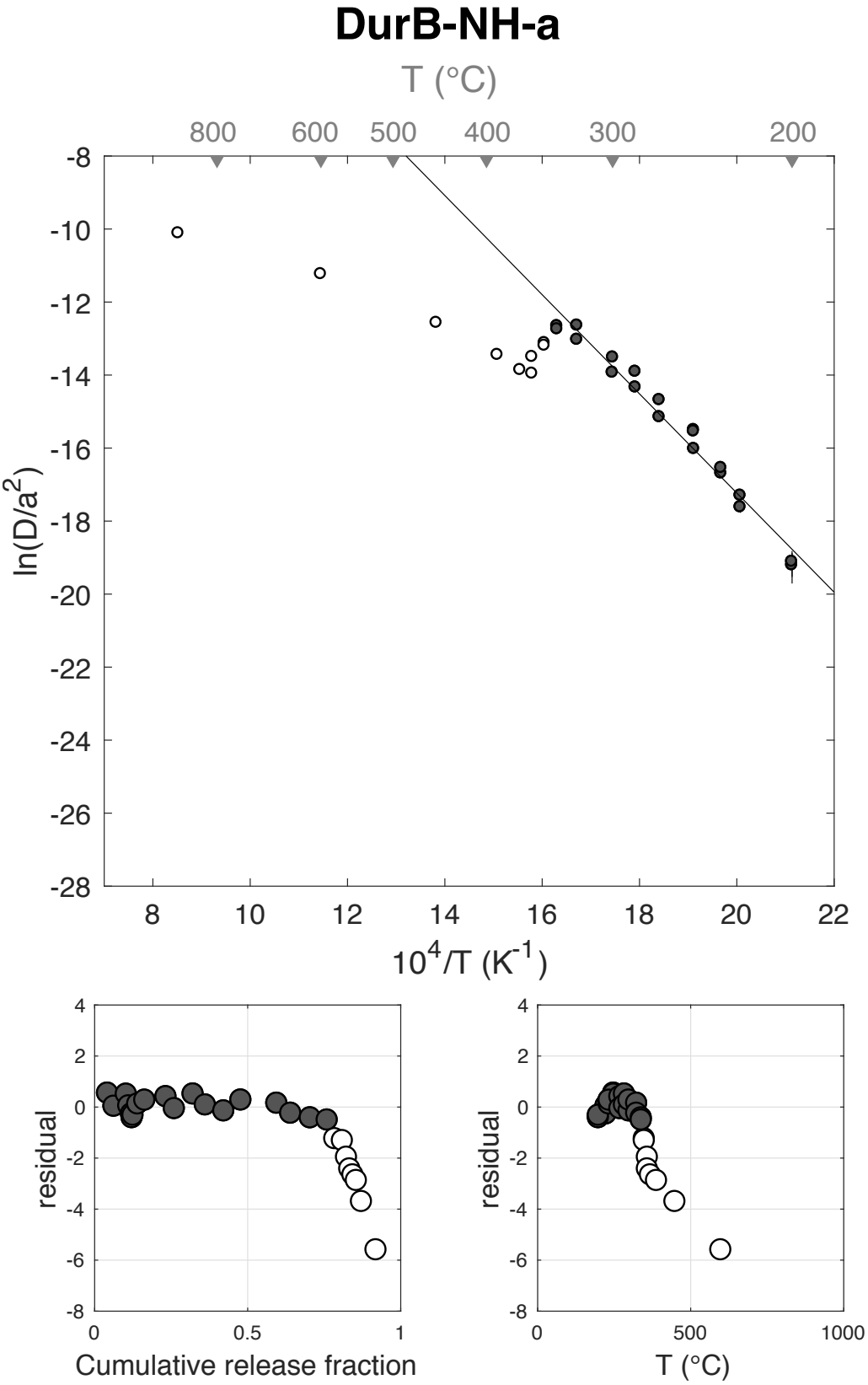
DurB-NH-a
T (°C)
800
600
500
400
300
200
-8
-10
-12
-14
-16
-18
-20
-22
-24
-26
-28
ln(D/a²)
8
10
12
14
16
18
20
22
10⁴/T (K⁻¹)
4
2
0
-2
-4
-6
-8
residual
0
0.5
1
Cumulative release fraction
0
500
1000
T (°C)

DurB-NH-b

E_a	+/-	D_0	+/-	T_c	-	+	Total ^{3}He	Incl.	Misfit	Norm. Misfit
153.37	5.17	16.26	1.06	88.50	4.62	4.81	140.77	0.427	0.541	0.032

Step #	°C	t (hrs)	^{3}He	Error	^{4}He	Error	^{4}He/^{3}He	Err	In ^{3}He Reg.
1	250	0.25	1.28	0.17	1264.5	43.3	977.8	0.14	1
2	250	0.50	0.62	0.13	677.9	41.2	1080.5	0.22	1
3	250	1.00	0.71	0.14	765.9	33.9	1064.3	0.20	1
4	225	1.50	0.20	0.08	197.2	43.1	952.0	0.45	1
5	225	2.50	0.41	0.11	381.8	35.4	919.9	0.28	1
6	200	3.00	0.06	0.07	54.0	29.8	866.1	1.31	0
7	200	4.00	0.07	0.08	60.6	35.4	826.4	1.20	0
8	235	2.00	0.44	0.10	431.9	33.7	968.4	0.24	1
9	235	3.00	0.82	0.14	788.7	40.0	952.9	0.18	1
10	270	1.91	2.52	0.23	2494.2	60.5	977.8	0.09	1
11	270	1.57	1.76	0.20	1676.6	50.9	942.3	0.12	1
12	285	1.25	2.34	0.25	2388.2	57.5	1012.1	0.11	1
13	285	1.56	2.22	0.23	2333.1	54.8	1039.1	0.11	1
14	300	1.91	4.99	0.29	4966.3	102.4	985.9	0.06	1
15	300	1.45	3.39	0.25	3348.3	62.0	978.0	0.08	1
16	325	1.74	10.09	0.51	9940.2	163.0	975.6	0.05	1
17	325	1.32	6.30	0.39	6297.4	117.1	990.1	0.06	1
18	340	1.58	11.03	0.56	10812.7	173.3	970.5	0.05	1
19	340	1.89	10.94	0.50	10666.4	176.2	964.7	0.05	1
20	350	1.48	10.14	0.46	9682.6	161.5	944.8	0.05	0
21	350	1.82	10.07	0.44	9682.9	152.9	951.9	0.05	0
22	360	1.50	8.01	0.53	8012.9	145.6	990.2	0.07	0
23	360	1.98	9.67	0.46	9198.5	165.4	941.4	0.05	0
24	370	1.88	9.26	0.49	8403.6	135.1	897.4	0.06	0
25	390	1.47	9.97	0.50	9085.5	158.1	901.1	0.05	0
26	450	1.00	15.41	0.54	14204.2	243.8	911.8	0.04	0
27	600	1.00	7.99	0.46	7318.1	129.2	906.0	0.06	0
28	900	1.00	0.05	0.06	55.6	33.0	1042.1	1.31	0
29	900	1.00	0.00	0.00	0.0	0.0	NaN	NaN	0

Figure S2

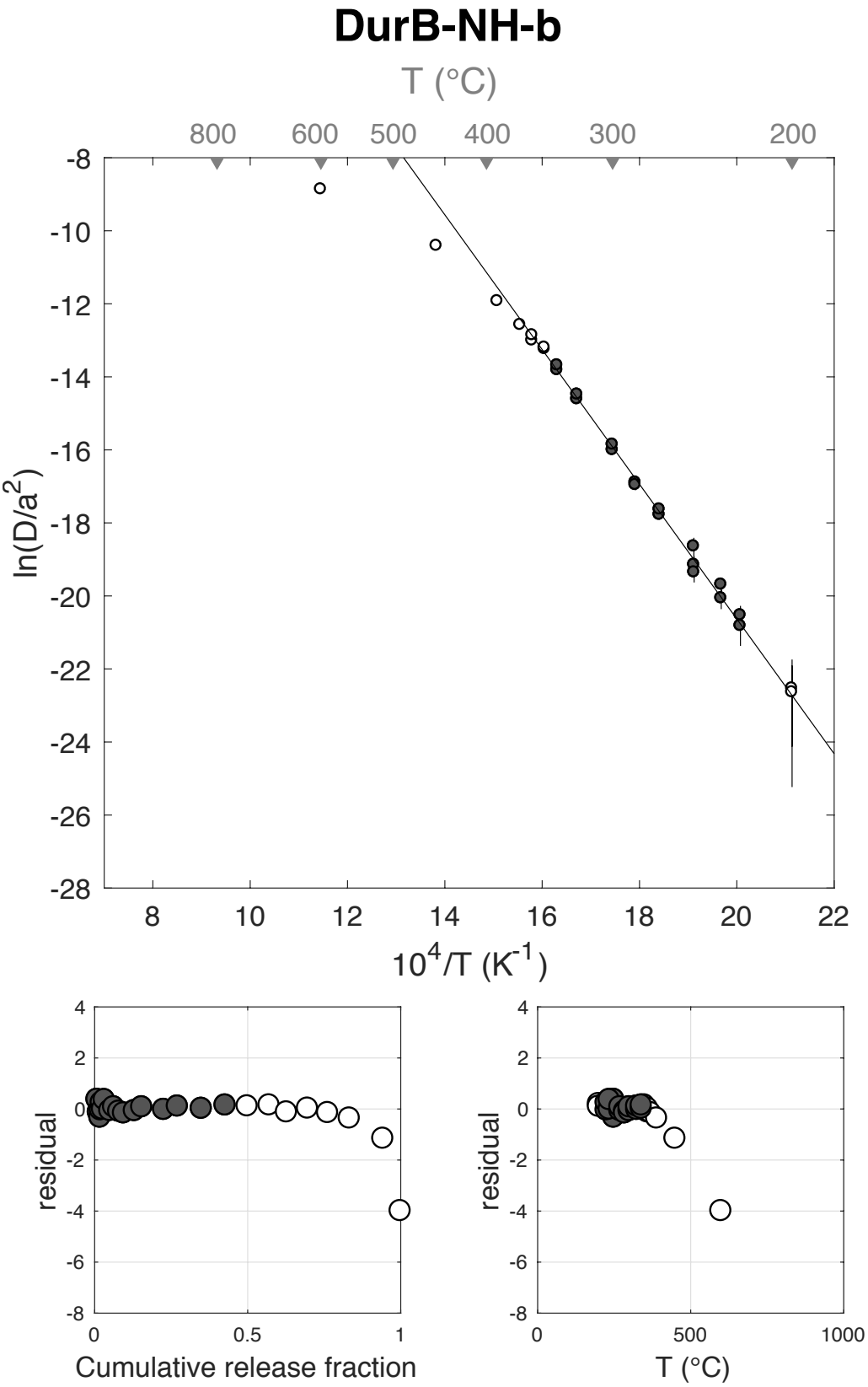
DurB-NH-b
T (°C)
800
600
500
400
300
200
-8
-10
-12
-14
-16
-18
-20
-22
-24
-26
-28
ln(D/a²)
8
10
12
14
16
18
20
22
10⁴/T (K⁻¹)
4
2
0
-2
-4
-6
-8
residual
0
0.5
1
Cumulative release fraction
0
500
1000
T (°C)

DurB-NH-c

E_a	+/-	D_0	+/-	T_c	-	+	Total ^{3}He	Incl.	Misfit	Norm. Misfit
152.45	8.22	16.52	1.67	84.62	7.44	7.93	63.43	0.494	0.215	0.017

Step #	°C	t (hrs)	^{3}He	Error	^{4}He	Error	^{4}He/^{3}He	Err	In ^{3}He Reg.
1	250	0.25	0.64	0.14	868.3	26.4	1342.0	0.22	1
2	250	0.50	0.49	0.12	617.8	23.0	1258.9	0.24	1
3	250	1.00	0.58	0.13	740.5	18.2	1273.0	0.23	1
4	225	1.50	0.09	0.07	69.6	18.2	802.1	0.87	0
5	225	2.50	0.13	0.09	101.5	34.9	743.7	0.77	0
6	200	3.00	0.00	0.00	0.0	0.0	NaN	NaN	0
7	200	4.00	0.00	0.00	0.0	0.0	NaN	NaN	0
8	235	2.00	0.24	0.11	261.7	27.1	1078.8	0.46	0
9	235	3.00	0.21	0.12	252.5	43.7	1176.4	0.60	0
10	270	1.91	1.34	0.19	2055.9	34.6	1526.7	0.14	1
11	270	1.57	1.00	0.17	1323.6	26.1	1311.5	0.17	1
12	285	1.25	1.32	0.19	2082.0	22.3	1568.6	0.14	1
13	285	1.56	1.35	0.21	2168.9	36.1	1594.8	0.15	1
14	300	1.91	3.27	0.29	4850.9	45.5	1473.5	0.09	1
15	300	1.45	1.95	0.27	3001.5	31.5	1525.6	0.14	1
16	325	1.74	5.78	0.43	8586.7	61.5	1475.0	0.07	1
17	325	1.32	3.28	0.31	4995.5	30.8	1510.7	0.10	1
18	340	1.58	4.81	0.45	8333.2	70.2	1722.6	0.09	1
19	340	1.89	5.49	0.33	8112.7	56.1	1467.3	0.06	1
20	350	1.48	4.07	0.41	6707.3	41.1	1637.6	0.10	0
21	350	1.82	4.74	0.34	6901.8	59.9	1445.8	0.07	0
22	360	1.50	4.01	0.33	6108.3	46.1	1511.7	0.08	0
23	360	1.98	4.14	0.32	6410.4	59.5	1539.6	0.08	0
24	370	1.88	3.98	0.33	6001.7	43.9	1496.9	0.08	0
25	390	1.47	3.58	0.28	5328.1	35.4	1478.8	0.08	0
26	450	1.00	6.78	0.43	10788.4	63.2	1581.1	0.06	0
27	600	1.00	0.10	0.07	30.9	11.0	300.2	0.82	0
28	900	1.00	0.00	0.00	8.1	9.8	Inf	NaN	0
29	900	1.00	0.04	0.06	8.5	10.4	181.1	1.84	0

Figure S3

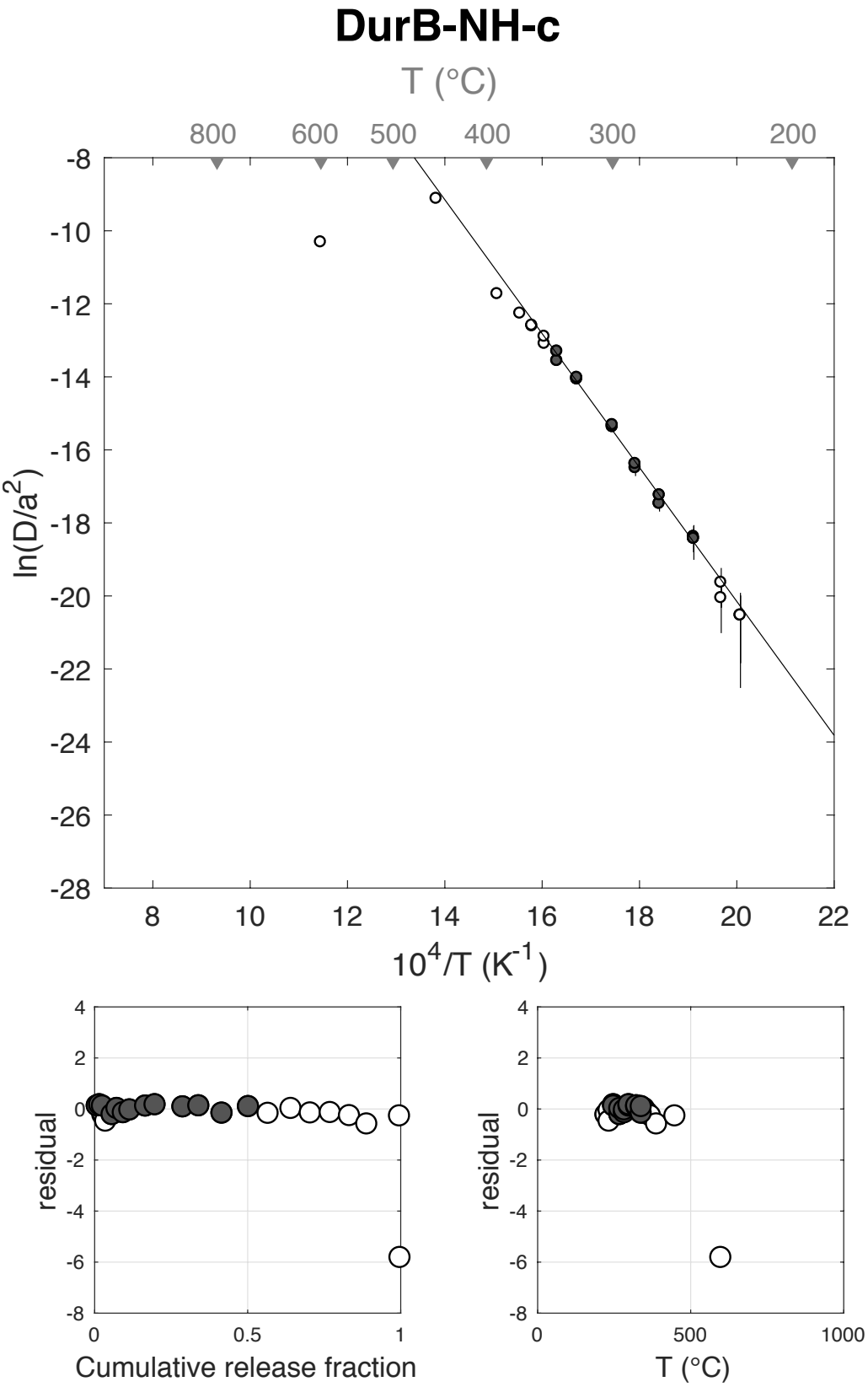
DurB-NH-c
T (°C)
800
600
500
400
300
200
-8
-10
-12
-14
-16
-18
-20
-22
-24
-26
-28
ln(D/a2)
8
10
12
14
16
18
20
22
10^4/T (K^-1)
4
2
0
-2
-4
-6
-8
residual
0
0.5
1
Cumulative release fraction
0
500
1000
T (°C)

E_a	+/-	D_0	+/-	T_c	-	+	Total ^{3}He	Incl.	Misfit	Norm. Misfit
131.26	6.42	12.66	1.31	59.92	6.94	7.32	55.02	0.549	0.174	0.013

Step #	°C	t (hrs)	^{3}He	Error	^{4}He	Error	^{4}He/^{3}He	Err	In ^{3}He Reg.
1	250	0.25	0.88	0.14	1068.3	43.4	1206.2	0.16	1
2	250	0.50	0.65	0.14	670.7	27.2	1025.4	0.21	1
3	250	1.00	0.72	0.16	805.5	17.3	1108.0	0.22	1
4	225	1.50	0.15	0.09	103.2	28.0	656.7	0.64	0
5	225	2.50	0.22	0.10	119.3	58.6	529.2	0.66	0
6	200	3.00	0.02	0.08	0.0	0.0	NaN	NaN	0
7	200	4.00	0.01	0.10	0.0	0.0	NaN	NaN	0
8	235	2.00	0.33	0.14	212.2	41.3	635.9	0.46	0
9	235	3.00	0.44	0.15	369.5	75.6	825.3	0.40	0
10	270	1.91	1.88	0.26	2342.2	47.3	1235.6	0.14	1
11	270	1.57	1.13	0.18	1510.0	36.3	1328.0	0.16	1
12	285	1.25	1.86	0.21	2216.8	30.8	1183.1	0.11	1
13	285	1.56	1.70	0.23	2106.0	33.4	1230.5	0.14	1
14	300	1.91	3.22	0.32	4006.1	48.7	1235.3	0.10	1
15	300	1.45	2.14	0.28	2628.1	38.4	1219.3	0.13	1
16	325	1.74	4.95	0.38	6193.2	58.1	1240.7	0.08	1
17	325	1.32	2.89	0.29	3826.7	40.1	1313.3	0.10	1
18	340	1.58	4.17	0.31	5640.4	47.4	1343.3	0.07	1
19	340	1.89	4.06	0.35	5248.5	55.8	1284.3	0.09	1
20	350	1.48	3.20	0.28	4273.9	42.4	1323.6	0.09	0
21	350	1.82	2.91	0.38	4127.3	50.8	1408.0	0.13	0
22	360	1.50	2.87	0.29	3665.5	38.3	1267.6	0.10	0
23	360	1.98	2.69	0.28	3447.9	46.4	1271.9	0.10	0
24	370	1.88	2.34	0.23	3156.1	46.8	1337.1	0.10	0
25	390	1.47	2.55	0.27	3245.8	44.4	1263.9	0.11	0
26	450	1.00	2.82	0.31	3886.7	31.5	1370.5	0.11	0
27	600	1.00	3.60	0.29	5239.6	58.5	1447.1	0.08	0
28	900	1.00	0.60	0.13	740.4	18.0	1229.8	0.22	0
29	900	1.00	0.04	0.06	0.0	0.0	NaN	NaN	0

Figure S4

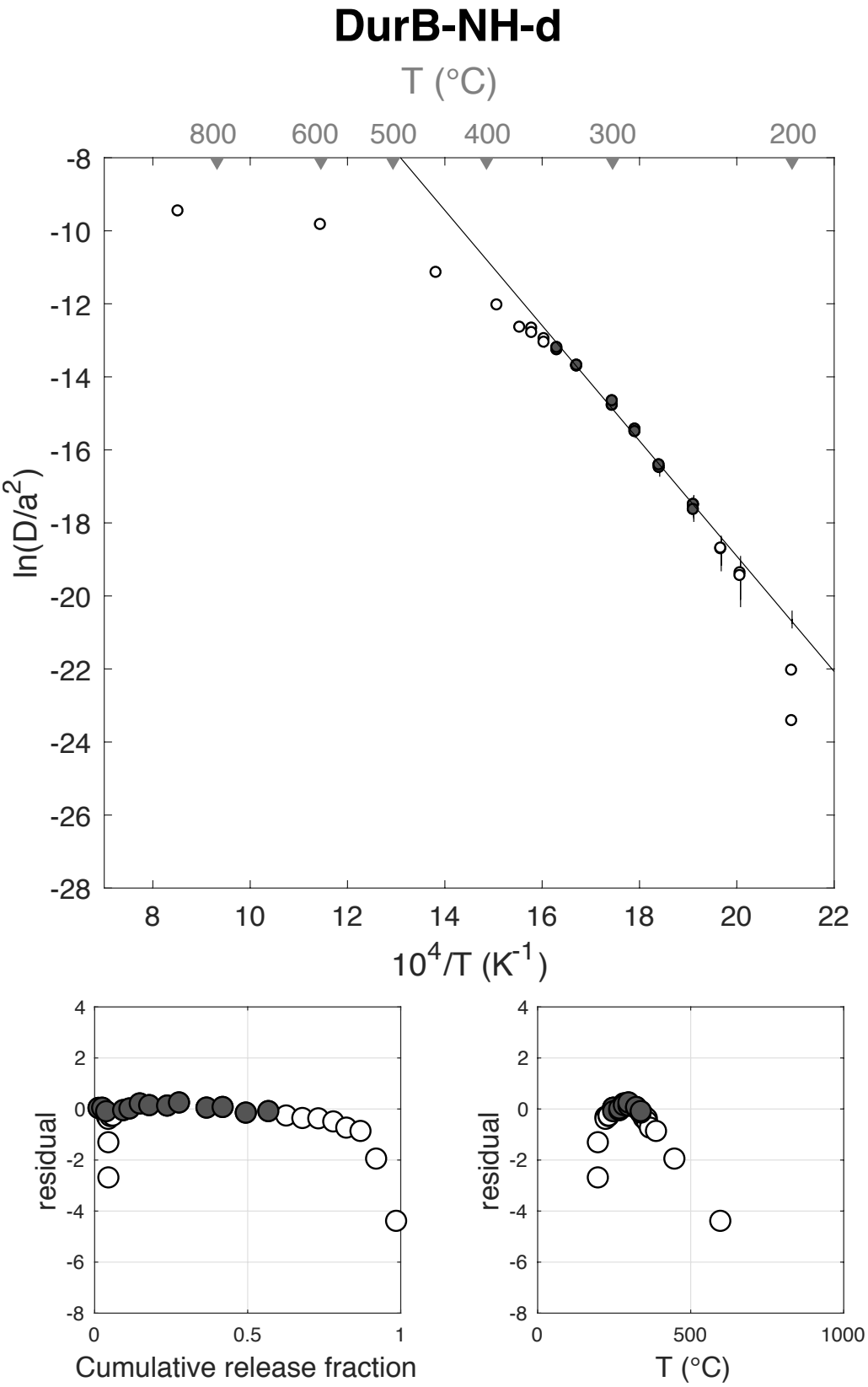
DurB-NH-d
T (°C)
800
600
500
400
300
200
-8
-10
-12
-14
-16
-18
-20
-22
-24
-26
-28
ln(D/a2)
8
10
12
14
16
18
20
22
10^4/T (K^-1)
4
2
0
-2
-4
-6
-8
residual
0
0.5
1
Cumulative release fraction
500
1000
T (°C)

DurB-NH-e

E_a	+/-	D_0	+/-	T_c	-	+	Total ^{3}He	Incl.	Misfit	Norm. Misfit
133.78	2.02	14.13	0.43	56.39	2.08	2.12	497.98	0.836	2.780	0.093

Step #	°C	t (hrs)	^{3}He	Error	^{4}He	Error	^{4}He/^{3}He	Err	In ^{3}He Reg.
1	250	0.50	16.30	0.74	25087.5	215.9	1529.5	0.05	1
2	250	1.00	11.85	0.72	18069.6	198.8	1514.5	0.06	1
3	240	1.00	4.73	0.39	7295.7	90.4	1532.2	0.08	1
4	230	1.50	3.31	0.36	5086.5	55.0	1528.2	0.11	1
5	230	2.50	5.03	0.45	7619.2	135.0	1503.3	0.09	1
6	210	2.50	1.23	0.25	1870.2	42.2	1505.8	0.20	1
7	210	3.50	1.79	0.27	2580.2	59.3	1430.1	0.15	1
8	200	3.00	0.66	0.20	1053.9	40.8	1586.4	0.30	1
9	200	4.00	0.82	0.22	1427.8	54.0	1732.4	0.27	1
10	220	2.50	2.23	0.30	3396.5	67.3	1515.1	0.14	1
11	220	3.50	2.64	0.35	4583.4	95.2	1725.7	0.13	1
12	235	2.00	5.35	0.47	7957.7	93.1	1477.7	0.09	1
13	235	3.00	21.47	0.99	33690.3	180.5	1559.4	0.05	1
14	250	1.00	3.56	0.41	5715.9	70.9	1596.7	0.12	1
15	260	1.91	11.13	0.65	17837.4	150.2	1593.3	0.06	1
16	260	1.57	8.15	0.56	13106.6	102.0	1597.5	0.07	1
17	270	1.91	15.34	0.86	24580.2	170.3	1592.6	0.06	1
18	270	1.57	11.30	0.61	18052.9	118.2	1587.2	0.05	1
19	280	1.25	13.47	0.76	21519.2	218.5	1587.2	0.06	1
20	280	1.57	15.30	0.81	24607.9	168.9	1598.1	0.05	1
21	290	1.25	16.68	0.79	27540.7	185.3	1641.0	0.05	1
22	290	1.57	18.63	0.82	30319.9	191.5	1617.1	0.04	1
23	300	1.91	29.43	1.11	48722.4	428.0	1645.5	0.04	1
24	300	1.45	18.94	0.83	31061.2	319.3	1630.3	0.05	1
25	315	1.74	35.11	1.03	58459.4	327.6	1655.2	0.03	1
26	315	1.32	21.69	0.85	35537.4	249.3	1628.3	0.04	1
27	330	1.74	39.70	1.28	67439.5	376.5	1688.6	0.03	1
28	330	1.32	23.82	1.06	40004.0	245.3	1669.4	0.04	1
29	340	1.58	30.24	1.08	52563.2	575.5	1728.5	0.04	1
30	340	1.89	26.59	0.94	46285.5	234.5	1730.5	0.04	1
31	350	1.48	21.32	0.89	36800.2	466.5	1716.4	0.04	0
32	350	1.82	0.00	0.00	0.0	0.0	NaN	NaN	0
33	360	1.50	23.80	1.74	31284.8	1332.6	1304.6	0.08	0
34	360	1.98	12.02	0.67	19560.9	335.3	1617.3	0.06	0
35	370	1.88	8.77	0.54	14629.5	174.1	1657.4	0.06	0
36	390	1.47	6.25	0.50	10651.7	93.3	1693.3	0.08	0
37	450	1.00	9.32	0.53	14006.7	101.0	1492.3	0.06	0

Figure S5

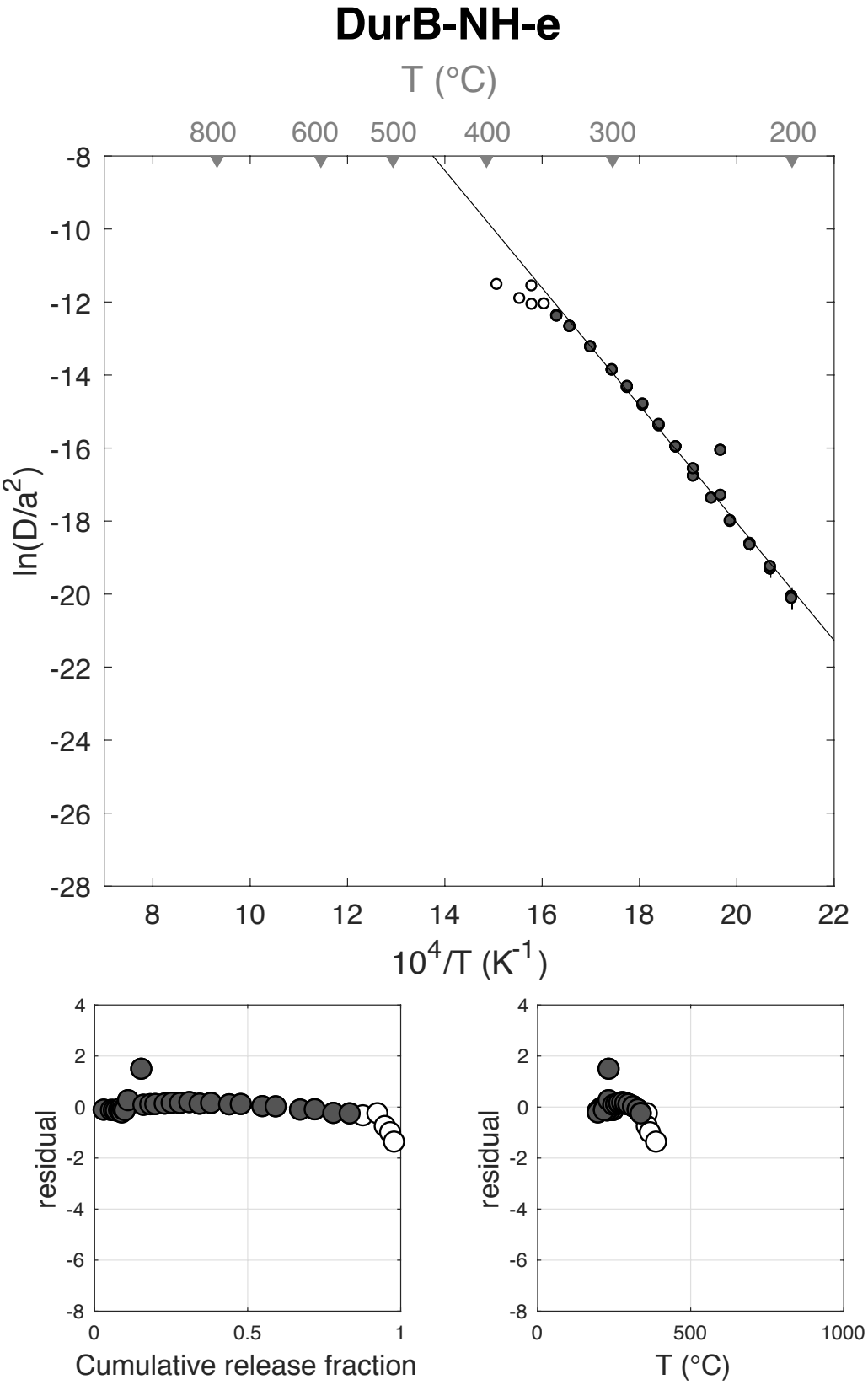
DurB-NH-e
T (°C)
800
600
500
400
300
200
-8
-10
-12
-14
-16
-18
-20
-22
-24
-26
-28
ln(D/a²)
8
10
12
14
16
18
20
22
10⁴/T (K⁻¹)
4
2
0
-2
-4
-6
-8
residual
0
0.5
1
Cumulative release fraction
0
500
1000
T (°C)

DurB-300C-1hr-a

E_a	+/-	D_0	+/-	T_c	-	+	Total ^{3}He	Incl.	Misfit	Norm. Misfit
150.13	5.63	16.45	1.16	79.72	5.20	5.43	89.27	0.585	0.204	0.012

Step #	°C	t (hrs)	^{3}He	Error	^{4}He	Error	^{4}He/^{3}He	Err	In ^{3}He Reg.
1	250	0.25	1.00	0.18	175.6	28.0	165.9	0.24	1
2	250	0.50	0.72	0.16	297.6	34.4	401.6	0.25	1
3	250	1.00	0.99	0.17	562.2	40.1	557.3	0.19	1
4	225	1.50	0.29	0.10	165.7	31.7	569.8	0.39	1
5	225	2.50	0.35	0.13	262.7	37.2	746.4	0.39	1
6	200	3.00	0.10	0.10	24.0	40.0	223.0	1.94	0
7	200	4.00	0.11	0.12	33.1	36.2	304.1	1.58	0
8	235	2.00	0.51	0.12	405.3	30.4	783.2	0.24	1
9	235	3.00	0.65	0.15	605.1	31.8	921.2	0.24	1
10	270	1.91	2.55	0.26	2847.8	33.7	1108.8	0.10	1
11	270	1.57	1.66	0.24	2151.9	35.1	1285.0	0.14	1
12	285	1.25	2.25	0.31	3344.9	36.1	1476.0	0.14	1
13	285	1.56	2.39	0.26	3706.3	39.4	1539.3	0.11	1
14	300	1.91	5.02	0.39	7842.0	75.9	1550.6	0.08	1
15	300	1.45	3.22	0.31	5110.1	42.5	1578.2	0.10	1
16	325	1.74	9.40	0.55	14731.4	82.1	1556.6	0.06	1
17	325	1.32	5.03	0.34	8662.5	82.5	1713.1	0.07	1
18	340	1.58	8.71	0.49	14592.8	104.2	1665.5	0.06	1
19	340	1.89	7.45	0.44	12987.8	105.7	1734.3	0.06	1
20	350	1.48	6.44	0.48	10899.4	89.2	1682.0	0.07	0
21	350	1.82	6.03	0.43	10342.6	74.1	1706.4	0.07	0
22	360	1.50	5.03	0.37	8928.6	71.1	1766.7	0.07	0
23	360	1.98	4.81	0.37	8743.1	70.3	1806.1	0.08	0
24	370	1.88	4.08	0.37	7614.7	69.8	1855.6	0.09	0
25	390	1.47	3.56	0.32	6729.9	57.5	1879.9	0.09	0
26	450	1.00	4.16	0.32	8172.2	71.6	1956.7	0.08	0
27	600	1.00	1.96	0.29	4018.6	50.0	2036.0	0.15	0
28	900	1.00	0.81	0.16	1502.3	35.9	1842.3	0.20	0
29	900	1.00	0.00	0.07	0.0	0.0	NaN	NaN	0

Figure S6

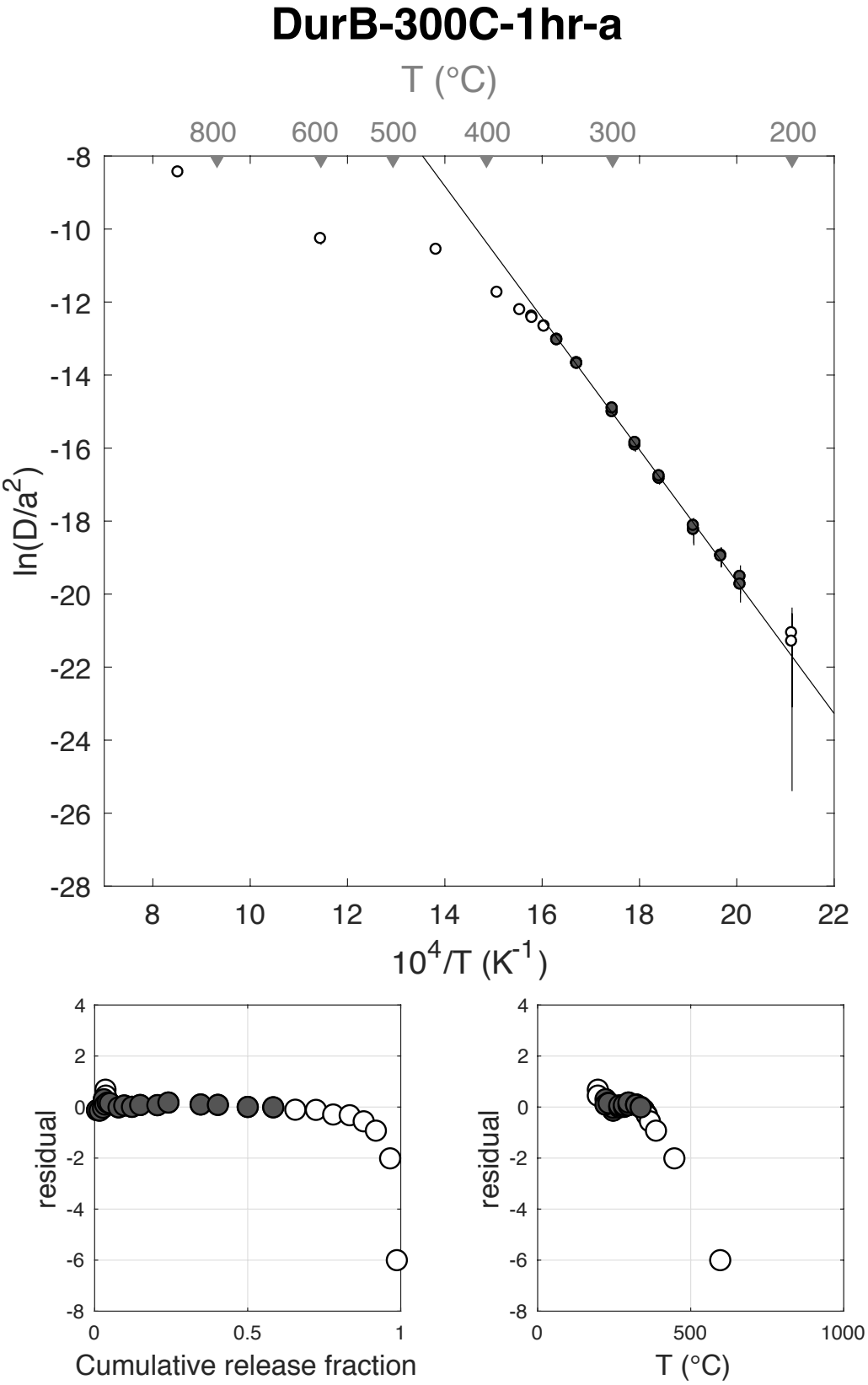
DurB-300C-1hr-a
T (°C)
800
600
500
400
300
200
-8
-10
-12
-14
-16
-18
-20
-22
-24
-26
-28
ln(D/a2)
8
10
12
14
16
18
20
22
10^4/T (K^-1)
4
2
0
-2
-4
-6
-8
residual
0
0.5
1
Cumulative release fraction
0
500
1000
T (°C)

DurB-300C-1hr-b

E_a	+/-	D_0	+/-	T_c	-	+	Total ^{3}He	Incl.	Misfit	Norm. Misfit
121.02	10.78	11.49	2.22	41.93	12.40	13.63	53.43	0.749	0.823	0.055

Step #	°C	t (hrs)	^{3}He	Error	^{4}He	Error	^{4}He/^{3}He	Err	In ^{3}He Reg.
1	250	0.25	1.66	0.38	588.6	106.7	344.9	0.29	1
2	250	0.50	1.07	0.36	863.8	76.4	794.7	0.35	1
3	250	1.00	1.59	0.36	1773.5	132.2	1107.2	0.24	1
4	225	1.50	0.69	0.37	799.8	143.8	1148.5	0.57	0
5	225	2.50	1.87	0.59	2730.6	265.9	1449.6	0.33	0
6	200	3.00	0.12	0.61	193.7	335.0	1547.5	5.21	0
7	200	4.00	0.65	0.84	1040.9	480.4	1599.4	1.38	0
8	235	2.00	0.91	0.50	1498.0	196.5	1638.8	0.56	1
9	235	3.00	0.74	0.53	208.7	324.0	270.3	1.71	1
10	270	1.91	1.69	0.49	3060.8	188.6	1796.9	0.29	1
11	270	1.57	1.16	0.43	2323.8	157.1	1994.2	0.37	1
12	285	1.25	1.98	0.37	3789.2	124.0	1900.8	0.19	1
13	285	1.57	1.76	0.51	3780.4	183.6	2139.5	0.30	1
14	300	1.91	4.02	0.61	7800.8	269.5	1929.8	0.15	1
15	300	1.45	2.49	0.49	5275.4	163.7	2107.4	0.20	1
16	325	1.74	7.10	0.63	13740.7	279.4	1925.9	0.09	1
17	325	1.32	4.07	0.52	7925.8	116.0	1935.4	0.13	1
18	340	1.58	5.35	0.58	11078.7	159.2	2061.2	0.11	1
19	340	1.89	4.44	0.60	9028.0	196.5	2024.5	0.14	1
20	350	1.48	3.25	0.46	6812.5	150.8	2085.4	0.14	0
21	350	1.82	2.53	0.51	5280.7	203.3	2074.6	0.20	0
22	360	1.50	1.43	0.44	3252.6	151.7	2259.2	0.31	0
23	360	1.98	1.25	0.48	2546.8	201.8	2028.0	0.39	0
24	370	1.88	0.62	0.48	1624.0	200.0	2629.4	0.78	0
25	390	1.47	0.41	0.40	33.6	352.5	72.6	10.54	0
26	450	1.00	0.37	0.35	1239.2	117.5	3299.9	0.93	0
27	600	1.00	0.20	0.39	820.9	110.1	4188.6	1.98	0
28	900	1.00	0.00	0.00	0.0	0.0	NaN	NaN	0
29	900	1.00	0.00	0.00	28.8	103.2	Inf	NaN	0

Figure S7

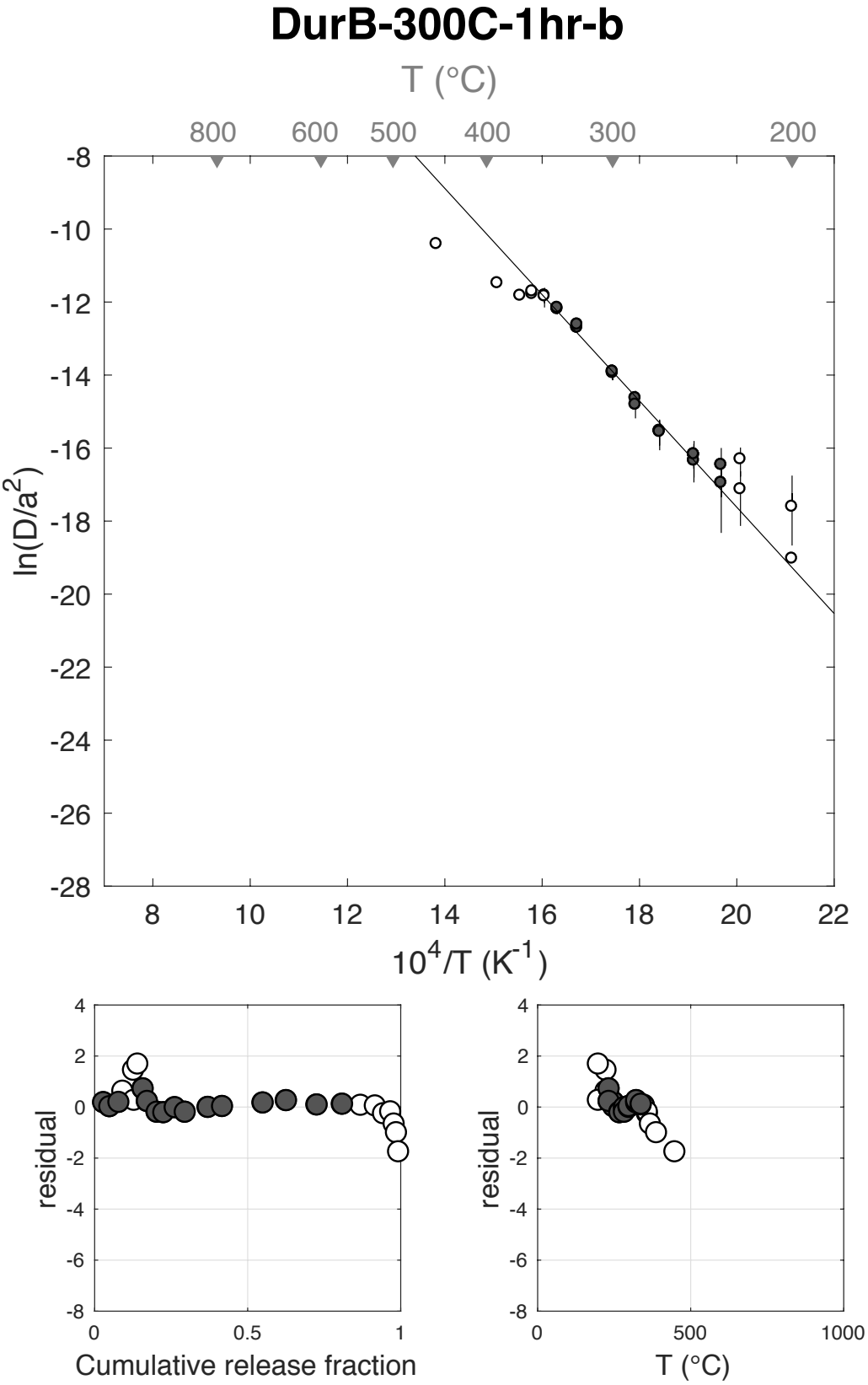
DurB-300C-1hr-b
T (°C)
800
600
500
400
300
200
-8
-10
-12
-14
-16
-18
-20
-22
-24
-26
-28
ln(D/a2)
8
10
12
14
16
18
20
22
10^4/T (K^-1)
4
2
0
-2
-4
-6
-8
residual
0
0.5
1
Cumulative release fraction
500
1000
T (°C)

DurB-300C-1hr-c

E_a	+/-	D_0	+/-	T_c	-	+	Total ^{3}He	Incl.	Misfit	Norm. Misfit
141.40	48.93	15.31	9.91	66.90	42.39	62.85	17.30	0.685	0.273	0.030

Step #	°C	t (hrs)	^{3}He	Error	^{4}He	Error	^{4}He/^{3}He	Err	In ^{3}He Reg.
1	250	0.25	0.41	0.58	557.0	21.4	1340.7	1.42	0
2	250	0.50	0.16	0.35	371.8	14.3	2297.7	2.16	0
3	250	1.00	0.20	0.23	464.4	25.0	2264.4	1.12	0
4	225	1.50	0.00	0.00	133.6	9.1	Inf	NaN	0
5	225	2.50	0.00	0.00	204.9	13.6	Inf	NaN	0
6	200	3.00	0.00	0.00	44.3	9.3	Inf	NaN	0
7	200	4.00	0.00	0.00	55.1	9.8	Inf	NaN	0
8	235	2.00	0.01	1.12	269.5	16.0	26030.6	107.85	0
9	235	3.00	0.11	2.07	369.0	16.1	3318.7	18.63	0
10	270	1.91	1.04	1.07	1725.2	39.9	1648.8	1.03	1
11	270	1.57	0.33	0.73	1032.5	20.8	3099.2	2.19	0
12	285	1.25	0.64	0.45	1601.6	30.8	2491.3	0.71	1
13	285	1.56	0.67	0.73	1680.4	32.2	2499.9	1.09	1
14	300	1.91	1.45	1.07	3456.2	43.3	2378.9	0.74	1
15	300	1.45	0.88	0.65	2028.8	35.8	2298.3	0.74	1
16	325	1.74	2.60	0.97	5606.0	65.7	2145.2	0.37	1
17	325	1.32	1.29	0.58	3184.1	36.3	2459.0	0.45	1
18	340	1.58	1.86	0.81	4732.6	44.0	2531.8	0.44	1
19	340	1.89	1.42	1.06	3665.4	57.3	2570.2	0.75	1
20	350	1.48	1.15	0.69	2667.9	36.5	2312.7	0.60	0
21	350	1.82	0.91	0.98	2132.6	37.6	2337.8	1.08	0
22	360	1.50	0.58	0.69	1571.8	40.5	2703.7	1.19	0
23	360	1.98	0.50	1.11	1246.1	30.7	2486.1	2.22	0
24	370	1.88	0.25	1.01	1016.5	24.6	3998.6	3.98	0
25	390	1.47	0.27	0.63	897.3	23.4	3348.9	2.34	0
26	450	1.00	0.41	0.28	1450.2	32.4	3507.3	0.68	0
27	600	1.00	0.15	0.21	756.1	24.0	5034.4	1.41	0
28	900	1.00	0.00	0.00	88.5	9.8	Inf	NaN	0
29	900	1.00	0.00	0.00	4.0	4.8	Inf	NaN	0

Figure S8

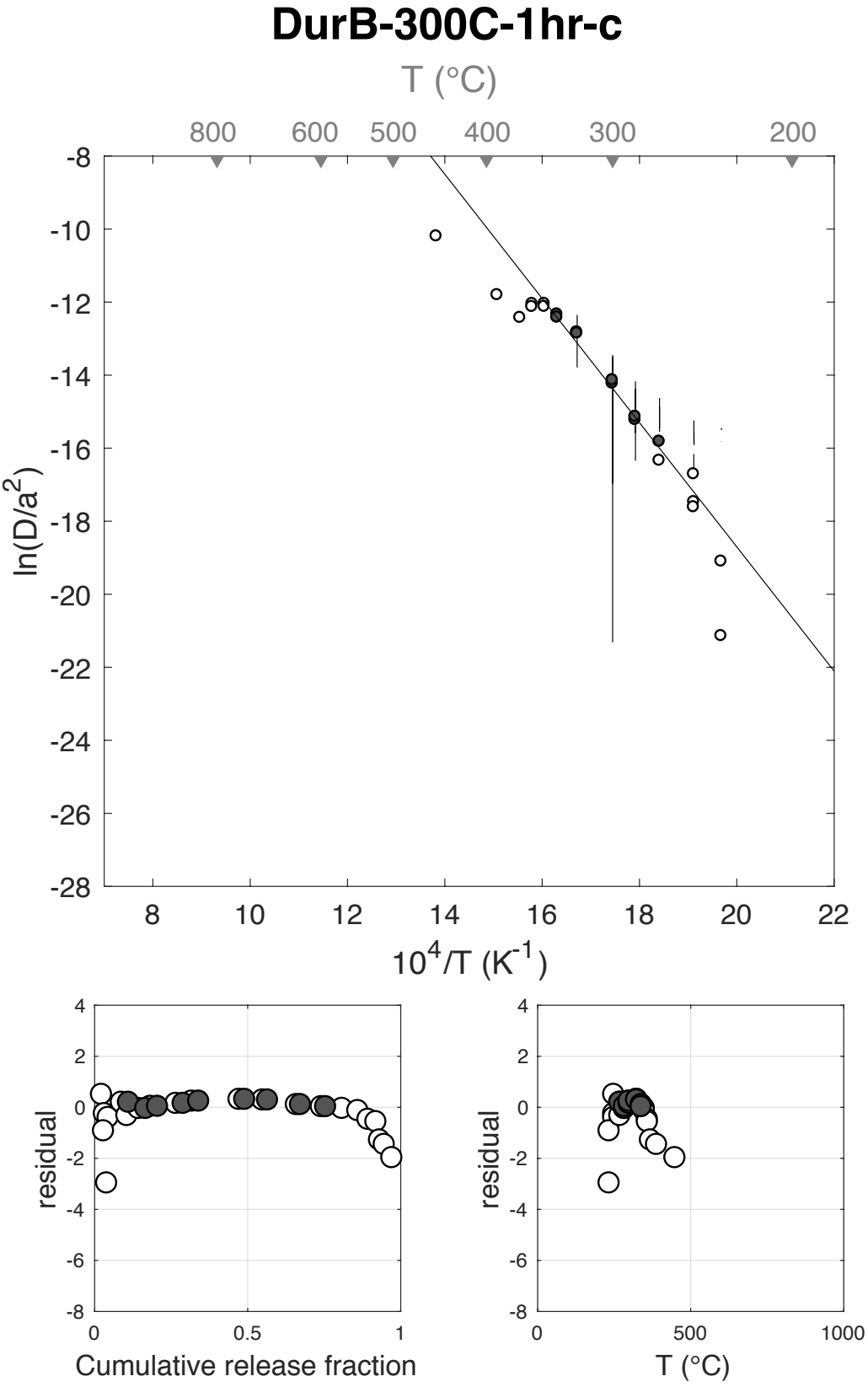
DurB-300C-1hr-c
T (°C)
800
600
500
400
300
200
-8
-10
-12
-14
-16
-18
-20
-22
-24
-26
-28
ln(D/a²)
8
10
12
14
16
18
20
22
10⁴/T (K⁻¹)
4
2
0
-2
-4
-6
-8
residual
0
0.5
1
Cumulative release fraction
500
1000
T (°C)

DurB-325C-1hr-b

E_a	+/-	D_0	+/-	T_c	-	+	Total ^{3}He	Incl.	Misfit	Norm. Misfit
137.43	4.96	15.10	1.04	58.90	4.96	5.17	75.36	0.848	0.324	0.018

Step #	°C	t (hrs)	^{3}He	Error	^{4}He	Error	^{4}He/^{3}He	Err	In ^{3}He Reg.
1	250	0.25	2.00	0.21	399.1	33.2	189.2	0.13	1
2	250	0.50	1.31	0.18	317.2	33.7	232.7	0.17	1
3	250	1.00	1.61	0.23	448.2	31.7	268.2	0.16	1
4	225	1.50	0.41	0.09	119.7	39.0	282.6	0.39	1
5	225	2.50	0.76	0.13	238.1	44.9	305.3	0.26	1
6	200	3.00	0.17	0.08	40.7	53.8	227.1	1.39	1
7	200	4.00	0.17	0.08	51.5	68.5	294.7	1.41	0
8	235	2.00	0.92	0.15	336.4	35.5	355.2	0.20	1
9	235	3.00	1.20	0.17	465.4	58.1	379.1	0.19	1
10	270	1.91	4.53	0.30	2062.5	59.6	445.4	0.07	1
11	270	1.57	2.68	0.25	1495.8	51.0	548.5	0.10	1
12	285	1.25	2.81	0.37	2305.8	58.6	810.0	0.13	1
13	285	1.56	3.89	0.27	2560.0	70.9	648.6	0.08	1
14	300	1.91	7.49	0.36	5172.3	95.7	680.4	0.05	1
15	300	1.45	4.32	0.31	3145.1	71.1	717.8	0.08	1
16	325	1.74	10.85	0.48	7979.7	135.4	725.3	0.05	1
17	325	1.32	5.59	0.49	4150.6	90.6	732.2	0.09	1
18	340	1.58	7.91	0.43	5986.1	110.0	746.8	0.06	1
19	340	1.89	5.48	0.34	4311.5	93.5	777.4	0.07	1
20	350	1.48	3.73	0.25	2905.7	64.9	768.4	0.07	0
21	350	1.82	2.74	0.24	2175.8	61.7	783.2	0.09	0
22	360	1.50	1.58	0.19	1325.9	44.0	827.6	0.12	0
23	360	1.98	1.08	0.16	917.5	40.3	842.2	0.16	0
24	370	1.88	0.68	0.15	550.1	37.1	801.9	0.23	0
25	390	1.47	0.42	0.10	347.7	31.7	823.1	0.26	0
26	450	1.00	0.49	0.12	374.3	30.9	748.5	0.26	0
27	600	1.00	0.47	0.11	422.2	32.7	894.3	0.25	0
28	900	1.00	0.07	0.07	53.3	25.7	737.2	1.06	0
29	900	1.00	0.00	0.00	0.0	0.0	NaN	NaN	0

Figure S9

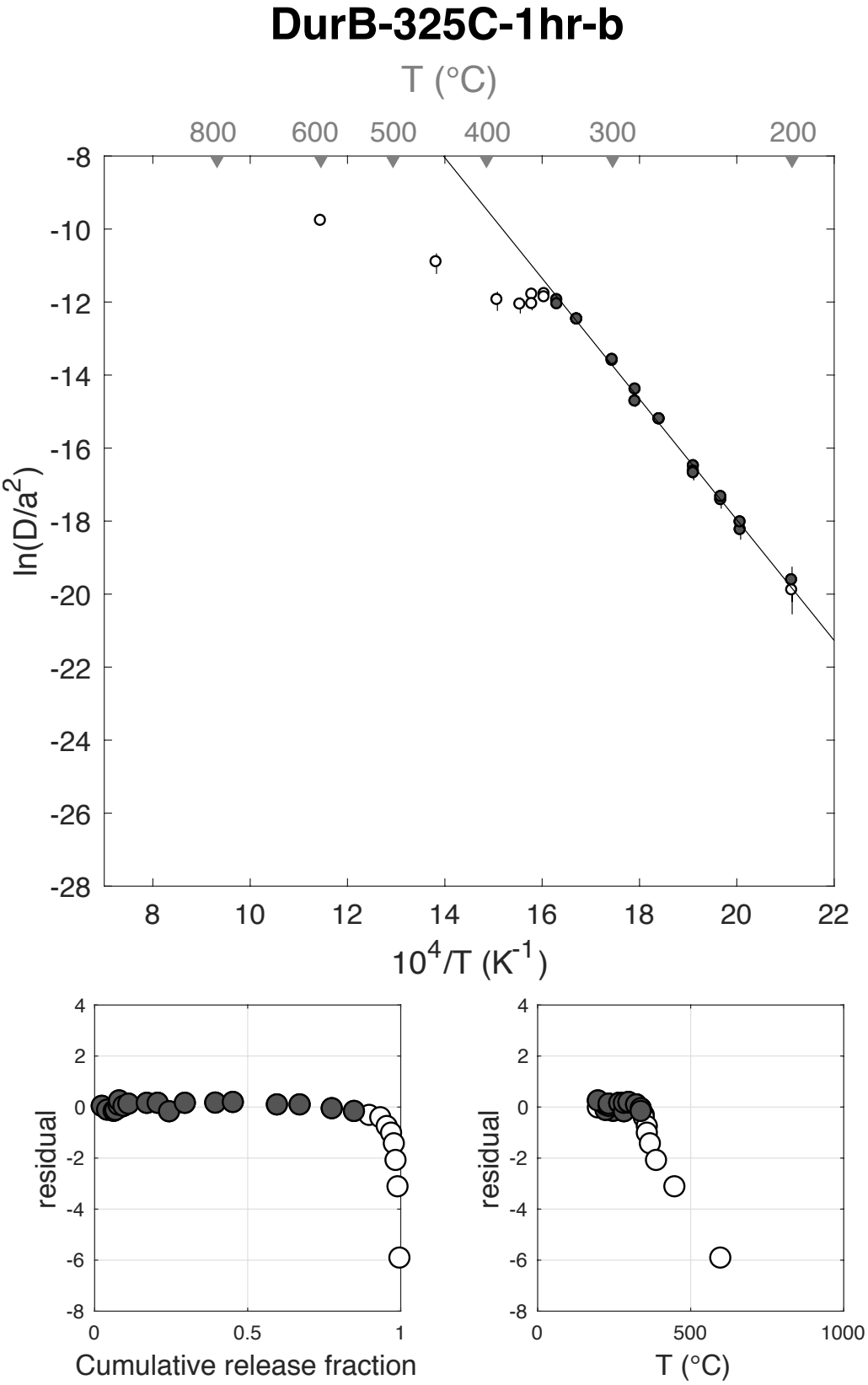
DurB-325C-1hr-b
T (°C)
800
600
500
400
300
200
-8
-10
-12
-14
-16
-18
-20
-22
-24
-26
-28
ln(D/a2)
8
10
12
14
16
18
20
22
10^4/T (K^-1)
4
2
0
-2
-4
-6
-8
residual
0
0.5
1
Cumulative release fraction
500
1000
T (°C)

DurB-330C-1hr-a

E_a	+/-	D_0	+/-	T_c	-	+	Total ^{3}He	Incl.	Misfit	Norm. Misfit
142.76	12.43	15.72	2.53	67.41	12.04	13.29	16.03	0.770	0.444	0.034

Step #	°C	t (hrs)	^{3}He	Error	^{4}He	Error	^{4}He/^{3}He	Err	In ^{3}He Reg.
1	250	0.25	0.39	0.11	64.2	31.2	156.1	0.56	1
2	250	0.50	0.25	0.09	90.0	19.8	354.9	0.44	1
3	250	1.00	0.30	0.09	150.0	14.7	484.5	0.32	1
4	225	1.50	0.04	0.07	44.6	34.6	1205.2	2.02	0
5	225	2.50	0.04	0.08	65.0	85.1	1490.6	2.25	0
6	200	3.00	0.00	0.00	15.0	109.4	Inf	NaN	0
7	200	4.00	0.00	0.00	19.1	159.6	Inf	NaN	0
8	235	2.00	0.07	0.07	65.7	60.1	975.3	1.41	0
9	235	3.00	0.03	0.09	153.2	109.6	4586.1	2.83	0
10	270	1.91	0.62	0.16	949.2	56.8	1514.5	0.26	1
11	270	1.57	0.41	0.10	653.0	45.7	1575.0	0.26	1
12	285	1.25	0.64	0.14	1175.1	33.5	1826.2	0.22	1
13	285	1.56	0.66	0.14	1247.2	40.8	1891.3	0.22	1
14	300	1.91	1.27	0.22	2595.0	58.4	2034.5	0.18	1
15	300	1.45	0.68	0.12	1397.3	36.8	2035.0	0.18	1
16	325	1.74	2.41	0.27	4848.7	61.5	2001.5	0.11	1
17	325	1.32	1.09	0.17	2393.2	39.8	2195.2	0.16	1
18	340	1.58	1.85	0.21	3814.6	52.3	2050.6	0.11	1
19	340	1.89	1.78	0.24	3852.0	61.2	2157.4	0.14	1
20	350	1.48	1.13	0.16	2450.0	41.3	2149.4	0.15	0
21	350	1.82	0.86	0.17	1916.3	54.1	2213.3	0.20	0
22	360	1.50	0.53	0.12	1119.2	39.7	2088.6	0.23	0
23	360	1.98	0.39	0.12	813.6	59.8	2086.9	0.32	0
24	370	1.88	0.24	0.10	510.1	55.1	2133.5	0.44	0
25	390	1.47	0.15	0.09	300.6	34.8	1967.6	0.59	0
26	450	1.00	0.15	0.09	223.4	13.5	1513.2	0.62	0
27	600	1.00	0.03	0.05	30.8	12.7	912.7	1.56	0
28	900	1.00	0.00	0.05	0.0	0.0	NaN	NaN	0
29	900	1.00	0.02	0.05	0.0	0.0	NaN	NaN	0

Figure S10

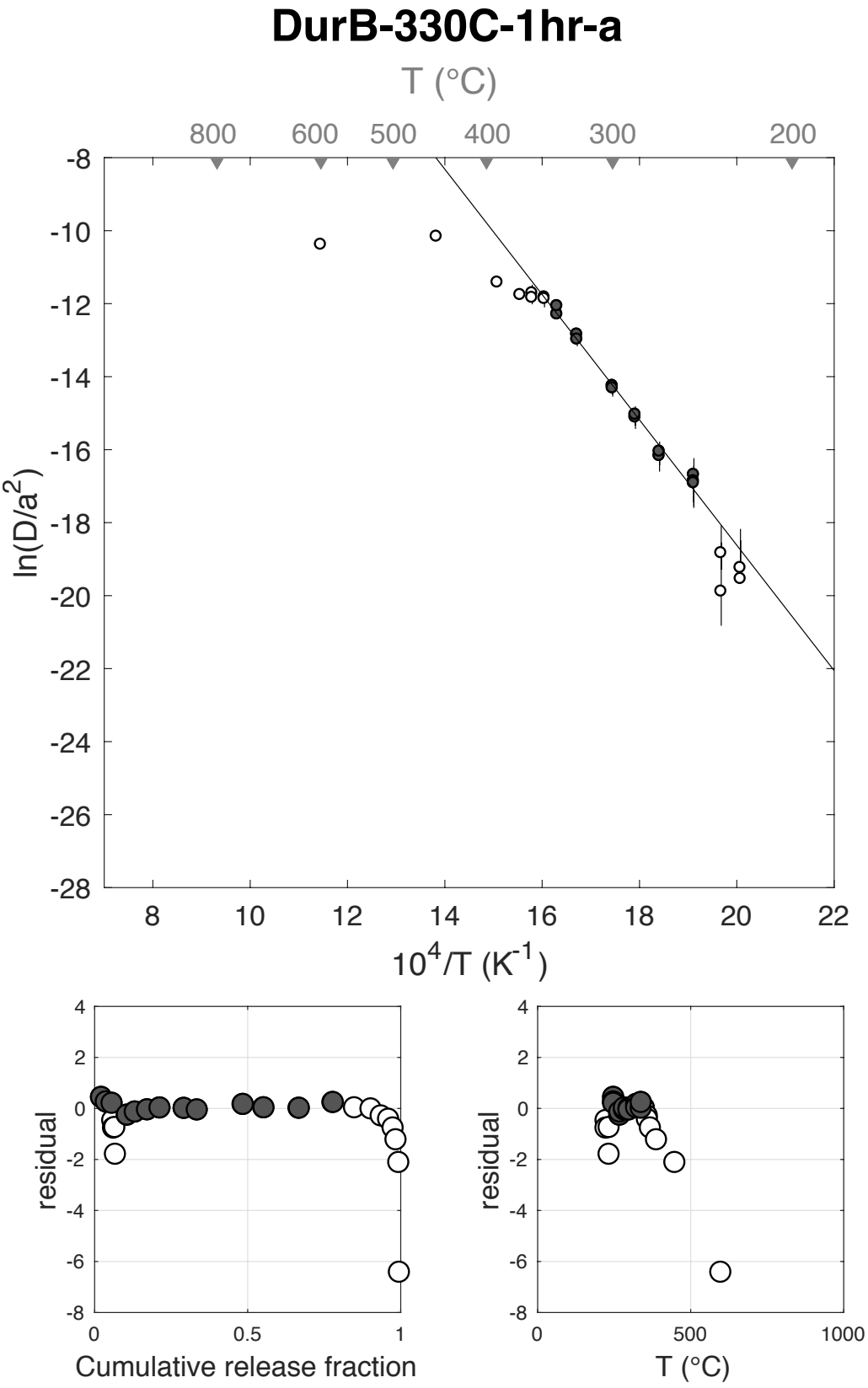
DurB-330C-1hr-a
T (°C)
800
600
500
400
300
200
ln(D/a²)
10⁴/T (K⁻¹)
residual
Cumulative release fraction
residual
T (°C)

DurB-350C-1hr-a

E_a	+/-	D_0	+/-	T_c	-	+	Total ^{3}He	Incl.	Misfit	Norm. Misfit
132.03	9.40	13.70	1.94	54.97	9.89	10.70	44.58	0.778	0.639	0.040

Step #	°C	t (hrs)	^{3}He	Error	^{4}He	Error	^{4}He/^{3}He	Err	In ^{3}He Reg.
1	250	0.25	1.20	0.21	179.6	30.7	139.6	0.25	1
2	250	0.50	0.84	0.18	160.8	28.2	182.0	0.27	1
3	250	1.00	1.13	0.19	209.5	31.0	174.9	0.23	1
4	225	1.50	0.19	0.16	72.8	35.1	374.6	0.96	0
5	225	2.50	0.41	0.24	106.5	39.4	247.5	0.69	1
6	200	3.00	0.10	0.27	27.6	45.2	267.2	3.21	0
7	200	4.00	0.08	0.40	26.7	56.9	320.5	5.37	0
8	235	2.00	0.47	0.20	143.1	34.3	296.9	0.48	1
9	235	3.00	0.61	0.30	200.8	40.2	320.1	0.53	1
10	283	1.91	2.18	0.31	814.6	33.7	363.5	0.15	1
11	270	1.57	1.35	0.21	599.8	27.2	435.2	0.16	1
12	285	1.25	1.97	0.24	928.5	28.5	461.1	0.13	1
13	285	1.56	1.93	0.24	1090.1	31.4	554.6	0.13	1
14	300	1.91	3.86	0.35	2417.6	36.1	616.7	0.09	1
15	300	1.45	2.16	0.29	1611.5	41.9	737.5	0.14	1
16	325	1.74	5.80	0.43	4581.1	50.8	779.7	0.07	1
17	325	1.32	3.01	0.28	2678.4	40.8	879.7	0.09	1
18	340	1.58	4.36	0.40	4185.7	40.5	950.4	0.09	1
19	340	1.89	3.42	0.33	3490.7	51.7	1011.7	0.10	1
20	350	1.48	2.10	0.27	2658.4	41.8	1253.2	0.13	0
21	350	1.82	2.07	0.27	2218.0	37.6	1063.9	0.13	0
22	360	1.50	1.48	0.21	1661.2	34.6	1114.9	0.14	0
23	360	1.98	1.19	0.24	1322.4	37.2	1102.0	0.20	0
24	370	1.88	0.83	0.22	992.5	38.0	1183.8	0.27	0
25	390	1.47	0.67	0.17	765.3	35.2	1126.7	0.26	0
26	450	1.00	0.77	0.17	1021.2	32.0	1314.5	0.22	0
27	600	1.00	0.41	0.13	664.0	26.2	1593.0	0.32	0
28	900	1.00	0.00	0.00	6.8	35.9	Inf	NaN	0
29	899	1.00	0.00	0.00	2.0	32.9	Inf	NaN	0

Figure S11

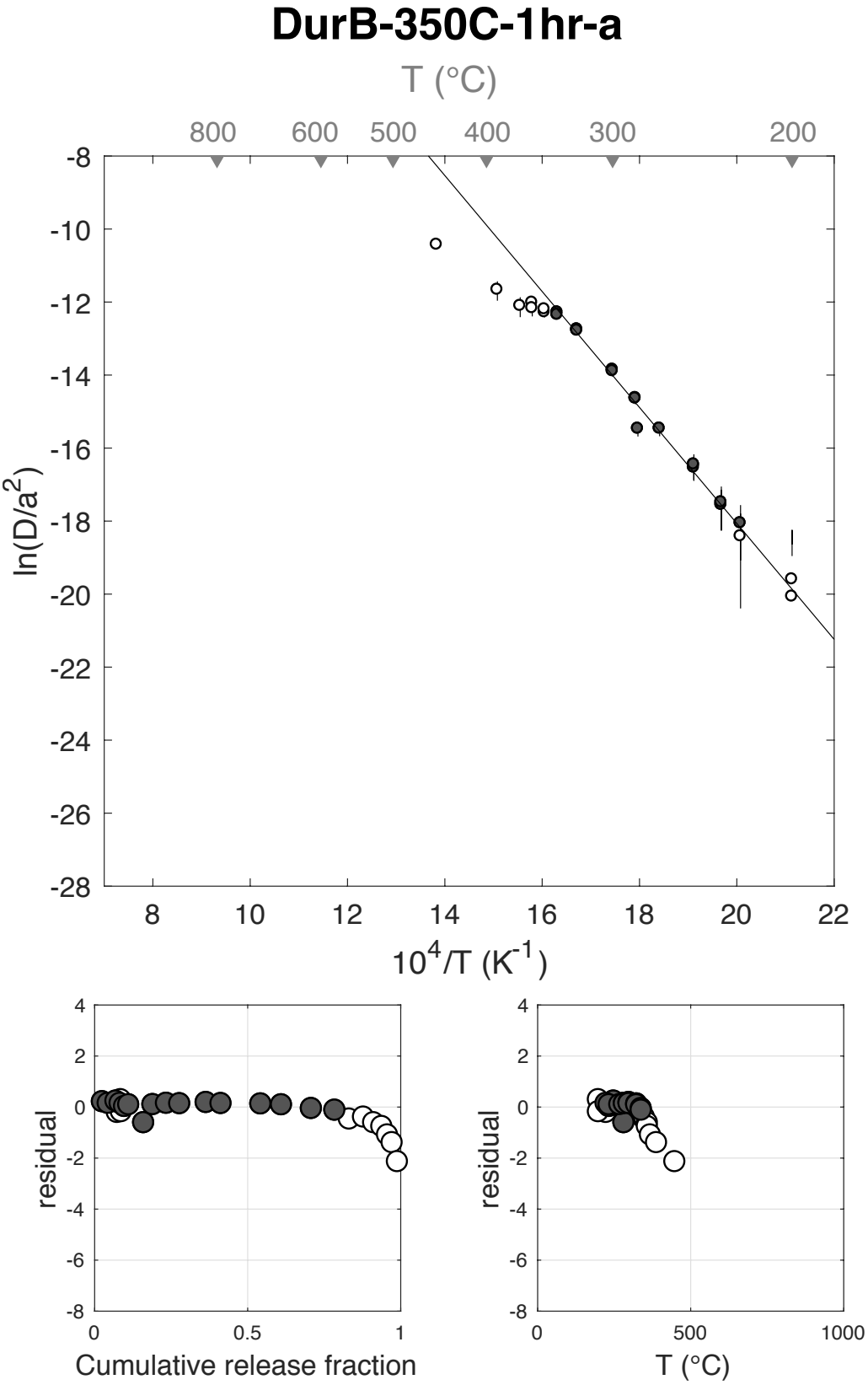
DurB-350C-1hr-a
T (°C)
800
600
500
400
300
200
-8
-10
-12
-14
-16
-18
-20
-22
-24
-26
-28
ln(D/a²)
8
10
12
14
16
18
20
22
10⁴/T (K⁻¹)
4
2
0
-2
-4
-6
-8
residual
0
0.5
1
Cumulative release fraction
500
1000
T (°C)

DurB-365C-1hr-a

E_a	+/-	D_0	+/-	T_c	-	+	Total ^{3}He	Incl.	Misfit	Norm. Misfit
124.26	2.77	11.99	0.57	46.86	3.19	3.27	132.10	0.731	0.322	0.019

Step #	°C	t (hrs)	^{3}He	Error	^{4}He	Error	^{4}He/^{3}He	Err	In ^{3}He Reg.
1	250	0.25	3.91	0.26	704.0	28.8	170.1	0.08	1
2	250	0.50	2.50	0.26	493.5	29.6	187.3	0.12	1
3	250	1.00	3.06	0.30	682.8	30.1	213.2	0.11	1
4	225	1.50	0.71	0.16	197.2	30.6	265.9	0.27	1
5	225	2.50	1.07	0.19	290.1	41.2	260.5	0.22	1
6	200	3.00	0.22	0.11	52.2	51.3	224.5	1.10	0
7	200	4.00	0.25	0.12	86.4	53.3	338.8	0.78	0
8	235	2.00	1.35	0.20	376.0	33.3	269.3	0.17	1
9	235	3.00	1.76	0.23	515.0	47.2	282.5	0.16	1
10	270	1.91	6.53	0.50	2037.8	38.0	302.0	0.08	1
11	270	1.57	3.99	0.36	1487.6	30.1	362.6	0.09	1
12	285	1.25	5.61	0.42	2257.6	38.1	392.6	0.08	1
13	285	1.56	5.70	0.42	2605.1	41.0	446.7	0.08	1
14	300	1.91	10.17	0.53	5493.9	48.6	530.0	0.05	1
15	300	1.45	6.10	0.39	3596.2	48.0	579.9	0.06	1
16	325	1.74	14.72	0.62	9547.6	73.3	638.6	0.04	1
17	325	1.32	7.88	0.51	5514.0	62.7	690.0	0.07	1
18	340	1.58	11.44	0.60	8779.2	69.8	757.4	0.05	1
19	340	1.89	10.06	0.54	7528.5	69.6	738.0	0.05	1
20	350	1.48	7.78	0.46	6023.4	46.1	763.9	0.06	0
21	350	1.82	6.68	0.44	5303.4	51.9	783.9	0.07	0
22	360	1.50	5.14	0.38	4169.1	44.7	801.3	0.07	0
23	360	1.98	4.62	0.41	3673.2	62.4	784.4	0.09	0
24	370	1.88	3.42	0.33	2898.0	48.7	836.2	0.10	0
25	390	1.47	2.71	0.22	2216.1	44.9	806.3	0.08	0
26	450	1.00	2.65	0.25	2215.3	39.7	826.2	0.10	0
27	600	1.00	1.56	0.23	1623.7	30.4	1028.2	0.15	0
28	900	1.00	0.13	0.11	0.0	0.0	NaN	NaN	0
29	900	1.00	0.34	0.12	326.5	28.8	939.8	0.36	0

Figure S12

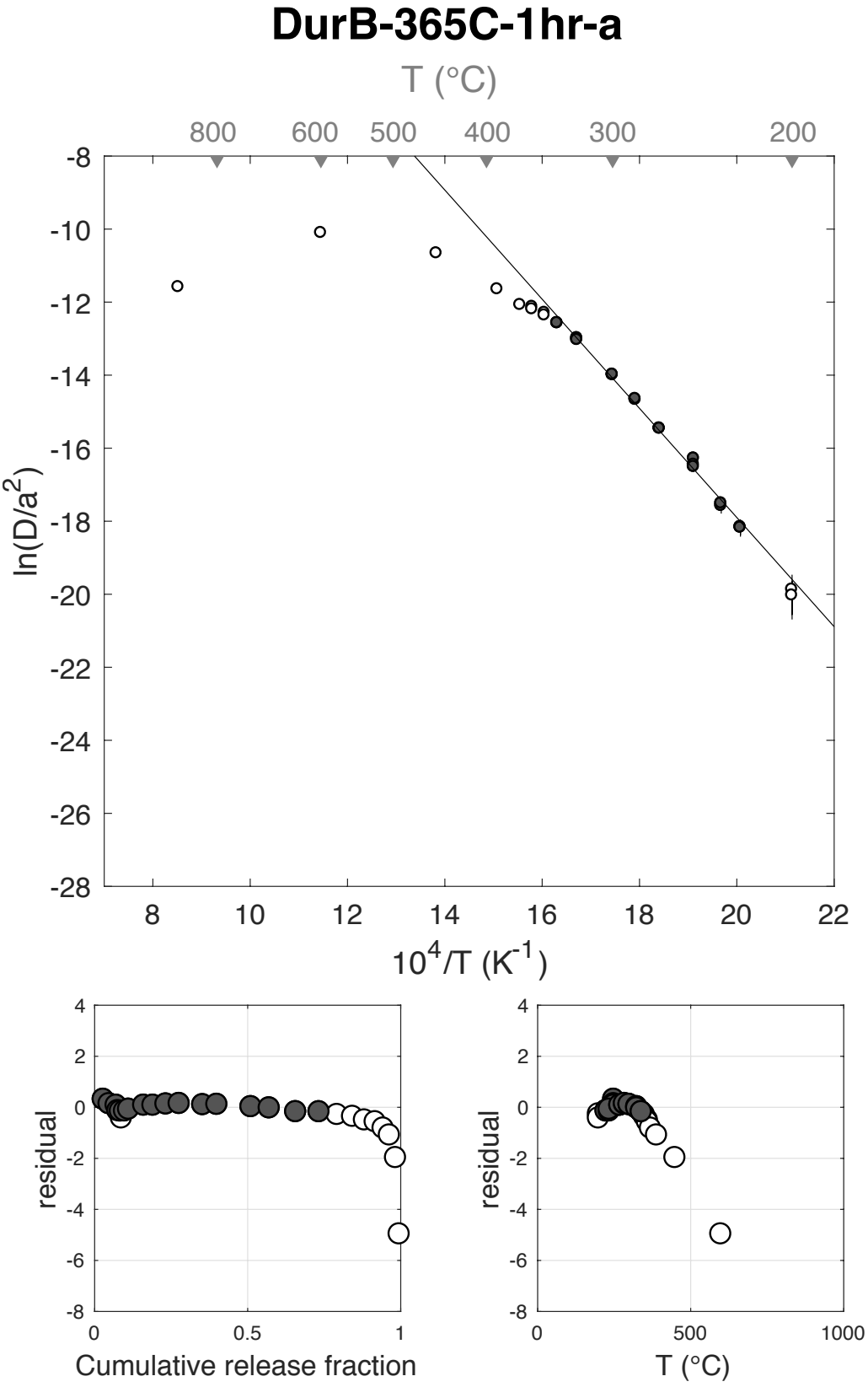
DurB-365C-1hr-a
T (°C)
800
600
500
400
300
200
ln(D/a²)
10⁴/T (K⁻¹)
residual
Cumulative release fraction
residual
T (°C)

DurB-375C-1hr-a

E_a	+/-	D_0	+/-	T_c	-	+	Total ^{3}He	Incl.	Misfit	Norm. Misfit
135.21	8.84	14.36	1.83	58.38	9.05	9.74	32.88	0.772	0.251	0.015

Step #	°C	t (hrs)	^{3}He	Error	^{4}He	Error	^{4}He/^{3}He	Err	In ^{3}He Reg.
1	250	0.25	0.89	0.16	151.9	43.0	160.5	0.34	1
2	250	0.50	0.57	0.14	109.2	32.8	180.0	0.38	1
3	250	1.00	0.67	0.15	136.6	39.5	195.4	0.36	1
4	225	1.50	0.19	0.11	42.6	37.6	217.1	1.06	1
5	225	2.50	0.27	0.14	57.0	39.8	202.2	0.87	1
6	200	3.00	0.07	0.14	17.7	40.9	255.5	3.12	0
7	200	4.00	0.07	0.19	18.5	47.6	238.0	3.64	0
8	235	2.00	0.34	0.13	81.3	36.7	231.1	0.60	1
9	235	3.00	0.44	0.17	102.5	43.6	222.6	0.58	1
10	270	1.91	1.57	0.22	378.7	34.9	230.9	0.17	1
11	270	1.57	1.03	0.16	254.0	34.6	237.1	0.21	1
12	285	1.25	1.44	0.20	361.5	32.8	241.5	0.17	1
13	285	1.56	1.46	0.22	408.9	33.9	271.0	0.17	1
14	300	1.91	2.73	0.29	841.4	42.9	298.7	0.12	1
15	300	1.45	1.58	0.23	564.4	32.0	348.2	0.16	1
16	325	1.74	4.37	0.39	1600.0	32.4	356.5	0.09	1
17	325	1.32	2.16	0.23	958.7	34.1	434.6	0.11	1
18	340	1.58	3.26	0.31	1527.6	33.7	458.3	0.10	1
19	340	1.89	2.44	0.27	1271.2	36.6	511.4	0.11	1
20	350	1.48	1.78	0.23	946.5	31.7	522.0	0.13	0
21	350	1.82	1.42	0.21	768.0	37.6	529.5	0.16	0
22	360	1.50	0.96	0.17	570.0	37.5	585.6	0.19	0
23	373	1.98	0.64	0.18	447.3	37.2	690.0	0.30	0
24	370	1.88	0.51	0.15	340.3	35.2	659.5	0.32	0
25	390	1.47	0.42	0.13	313.7	35.4	736.2	0.32	0
26	450	1.00	0.75	0.16	689.3	32.4	907.7	0.22	0
27	600	1.00	0.72	0.17	624.4	36.8	851.9	0.25	0
28	900	1.00	0.07	0.07	28.6	38.9	390.6	1.69	0
29	900	1.00	0.09	0.08	13.9	39.9	148.7	3.02	0

Figure S13

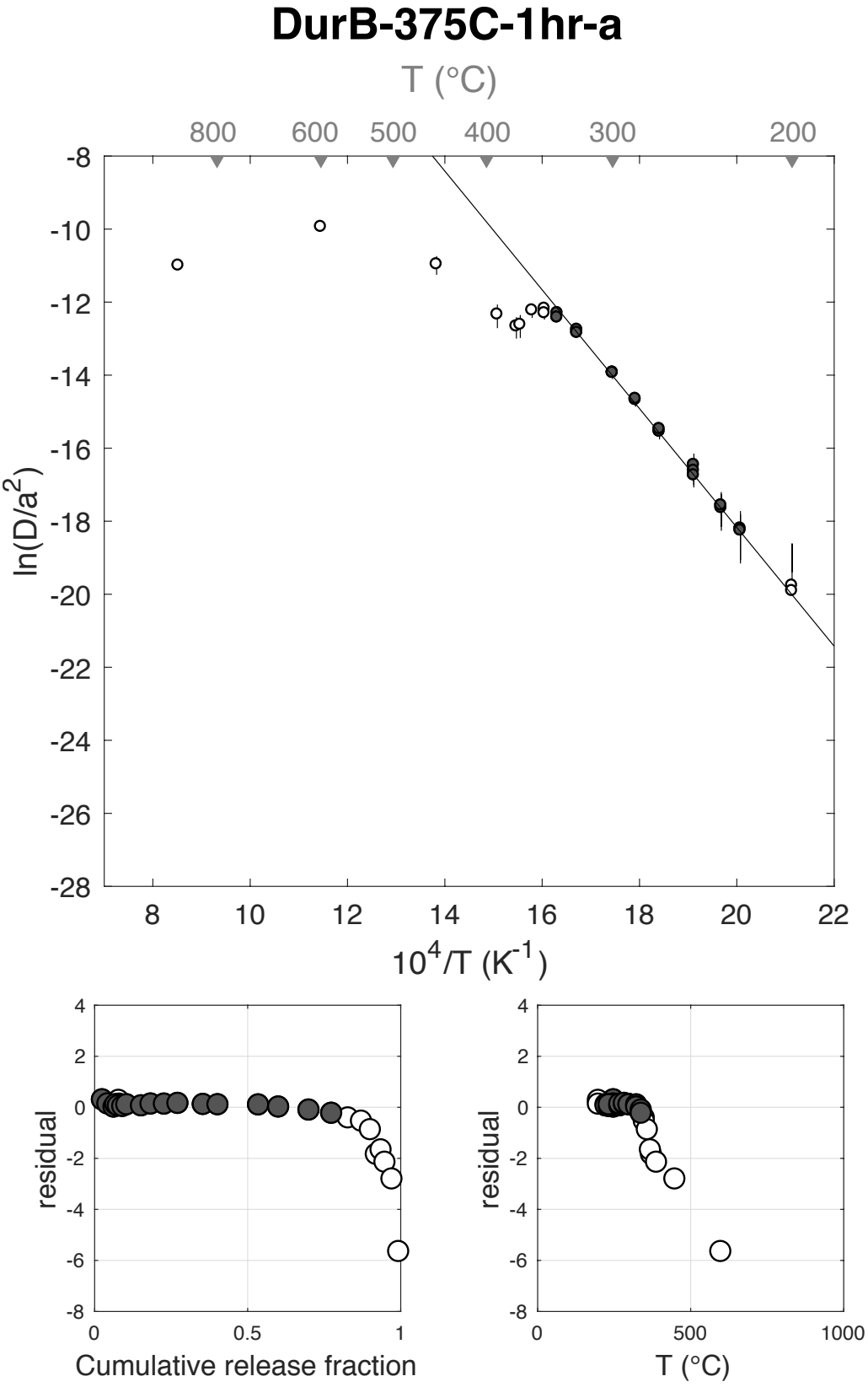
DurB-375C-1hr-a
T (°C)
800
600
500
400
300
200
-8
-10
-12
-14
-16
-18
-20
-22
-24
-26
-28
ln(D/a²)
8
10
12
14
16
18
20
22
10⁴/T (K⁻¹)
4
2
0
-2
-4
-6
-8
residual
0
0.5
1
Cumulative release fraction
500
1000
T (°C)

DurB-395C-1hr-a

E_a	+/-	D_0	+/-	T_c	-	+	Total ^{3}He	Incl.	Misfit	Norm. Misfit
98.86	5.60	7.63	1.17	7.92	7.91	8.35	22.47	0.894	0.561	0.033

Step #	°C	t (hrs)	^{3}He	Error	^{4}He	Error	^{4}He/^{3}He	Err	In ^{3}He Reg.
1	250	0.25	1.43	0.21	100.4	39.5	60.2	0.42	1
2	250	0.50	0.93	0.17	82.4	43.1	78.4	0.55	1
3	250	1.00	1.10	0.17	102.7	40.9	82.9	0.43	1
4	225	1.50	0.29	0.11	41.6	37.2	133.7	0.97	1
5	225	2.50	0.40	0.12	63.3	52.5	150.3	0.88	1
6	200	3.00	0.07	0.08	25.7	61.8	357.9	2.69	0
7	200	4.00	0.13	0.09	23.7	88.5	170.7	3.80	0
8	235	2.00	0.44	0.13	77.6	48.4	165.4	0.69	1
9	235	3.00	0.66	0.16	121.5	63.1	175.5	0.57	1
10	270	1.91	1.94	0.23	380.7	40.2	186.1	0.16	1
11	270	1.57	1.04	0.17	259.9	38.1	240.7	0.22	1
12	285	1.25	1.26	0.20	361.1	34.1	275.5	0.19	1
13	285	1.56	1.16	0.19	416.9	37.8	350.4	0.19	1
14	300	1.91	2.04	0.23	824.9	42.6	395.2	0.13	1
15	300	1.45	1.14	0.21	542.2	38.0	465.4	0.20	1
16	325	1.74	2.42	0.32	1327.3	38.5	538.5	0.14	1
17	325	1.32	1.14	0.17	728.5	37.5	626.3	0.16	1
18	340	1.58	1.64	0.25	1045.6	45.6	628.2	0.16	1
19	340	1.89	1.07	0.26	807.5	40.1	745.7	0.25	1
20	350	1.48	0.75	0.16	510.1	39.1	672.6	0.22	0
21	350	1.82	0.54	0.14	370.8	43.6	679.3	0.29	0
22	360	1.50	0.29	0.11	251.8	36.9	857.0	0.39	0
23	360	1.98	0.20	0.10	162.8	43.7	807.9	0.56	0
24	370	1.88	0.15	0.09	99.4	41.6	644.7	0.73	0
25	390	1.47	0.07	0.08	68.2	30.2	985.2	1.25	0
26	450	1.00	0.04	0.08	60.3	35.4	1334.3	1.91	0
27	600	1.00	0.12	0.09	109.5	37.1	892.8	0.79	0
28	900	1.00	0.02	0.06	0.0	0.0	NaN	NaN	0
29	900	1.00	0.00	0.00	0.0	0.0	NaN	NaN	0

Figure S14

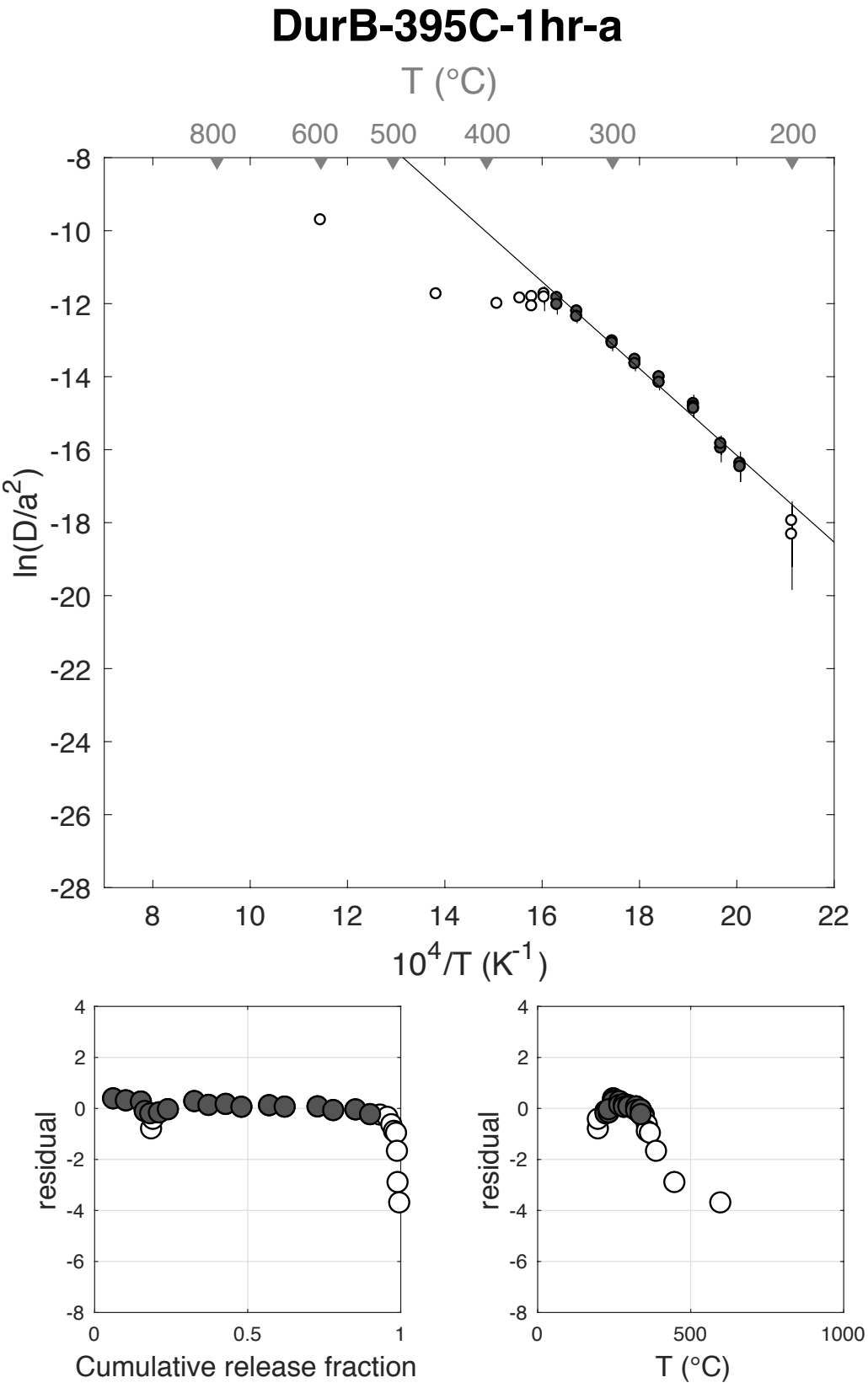
DurB-395C-1hr-a
T (°C)
800
600
500
400
300
200
-8
-10
-12
-14
-16
-18
-20
-22
-24
-26
-28
ln(D/a²)
8
10
12
14
16
18
20
22
10⁴/T (K⁻¹)
4
2
0
-2
-4
-6
-8
residual
0
0.5
1
Cumulative release fraction
4
2
0
-2
-4
-6
-8
residual
0
500
1000
T (°C)

DurB-395C-1hr-b

E_a	+/-	D_0	+/-	T_c	-	+	Total ^{3}He	Incl.	Misfit	Norm. Misfit
141.73	7.79	15.57	1.60	65.95	7.63	8.12	33.43	0.748	0.435	0.027

Step #	°C	t (hrs)	^{3}He	Error	^{4}He	Error	^{4}He/^{3}He	Err	In ^{3}He Reg.
1	250	0.25	0.69	0.12	23.5	19.0	24.0	0.83	1
2	250	0.50	0.42	0.10	10.6	27.4	15.2	2.59	1
3	250	1.00	0.54	0.12	24.3	22.4	35.2	0.95	1
4	225	1.50	0.19	0.09	17.4	23.2	83.4	1.42	0
5	225	2.50	0.29	0.13	12.4	31.6	32.4	2.58	1
6	200	3.00	0.03	0.13	3.6	33.6	131.5	10.80	0
7	200	4.00	0.00	0.00	2.5	43.2	Inf	NaN	0
8	235	2.00	0.33	0.12	17.7	27.9	43.5	1.62	1
9	235	3.00	0.43	0.16	22.0	35.4	41.2	1.65	1
10	270	1.91	1.68	0.20	92.1	26.2	44.7	0.31	1
11	270	1.57	0.97	0.16	65.3	24.9	57.4	0.42	1
12	285	1.25	1.49	0.19	104.6	24.6	60.0	0.27	1
13	285	1.56	1.41	0.20	136.3	28.4	86.7	0.25	1
14	300	1.91	2.80	0.24	352.7	31.3	115.9	0.12	1
15	300	1.45	1.62	0.18	246.9	35.2	142.7	0.18	1
16	325	1.74	4.31	0.34	830.1	36.4	182.5	0.09	1
17	325	1.32	2.25	0.25	553.6	30.8	236.2	0.13	1
18	340	1.58	3.18	0.32	967.7	41.7	294.0	0.11	1
19	340	1.89	2.60	0.23	904.0	38.5	338.0	0.10	1
20	350	1.48	1.75	0.20	728.4	33.6	406.1	0.12	0
21	350	1.82	1.52	0.21	687.9	36.4	442.8	0.15	0
22	360	1.50	1.12	0.18	588.0	33.7	516.2	0.17	0
23	360	1.98	1.02	0.16	531.7	38.1	512.7	0.17	0
24	370	1.88	0.82	0.14	454.9	27.9	545.7	0.18	0
25	390	1.47	0.66	0.12	369.0	31.2	550.8	0.20	0
26	450	1.00	0.65	0.13	435.9	27.3	659.5	0.21	0
27	600	1.00	0.39	0.11	328.1	29.1	840.0	0.29	0
28	899	1.00	0.27	0.08	276.0	33.3	1001.1	0.33	0
29	900	1.00	0.01	0.06	6.0	18.0	526.2	6.05	0

Figure S15

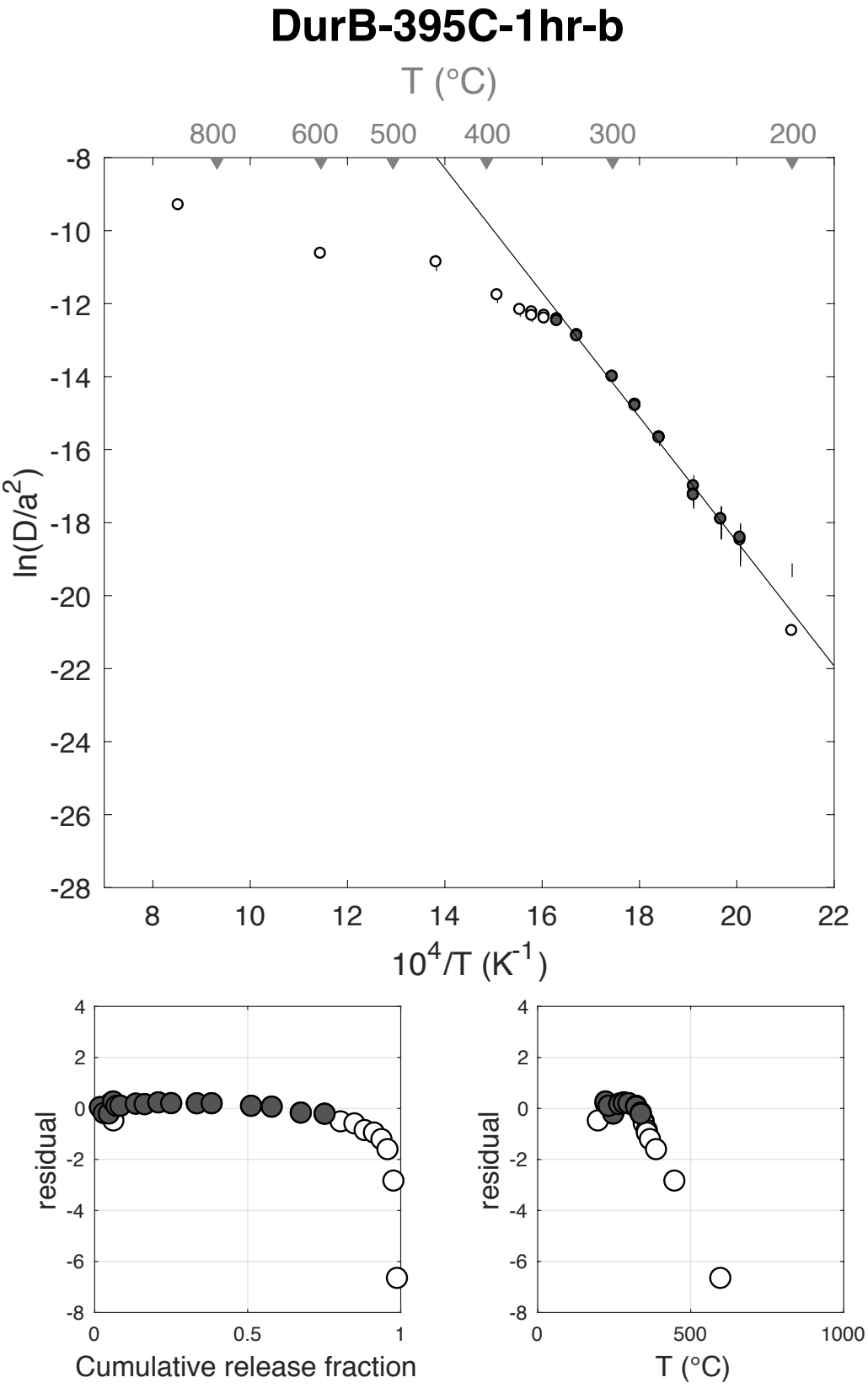
DurB-395C-1hr-b
T (°C)
800
600
500
400
300
200
-8
-10
-12
-14
-16
-18
-20
-22
-24
-26
-28
ln(D/a2)
8
10
12
14
16
18
20
22
10^4/T (K^-1)
4
2
0
-2
-4
-6
-8
residual
0
0.5
1
Cumulative release fraction
0
500
1000
T (°C)

DurB-415C-1hr-a

E_a	+/-	D_0	+/-	T_c	-	+	Total ^{3}He	Incl.	Misfit	Norm. Misfit
122.16	4.27	12.39	0.89	38.97	4.96	5.15	45.74	0.905	0.405	0.024

Step #	°C	t (hrs)	^{3}He	Error	^{4}He	Error	^{4}He/^{3}He	Err	In ^{3}He Reg.
1	250	0.25	1.84	0.22	30.4	33.5	6.5	1.11	1
2	250	0.50	1.31	0.19	21.8	32.4	6.6	1.50	1
3	250	1.00	1.75	0.20	23.9	29.7	3.7	1.25	1
4	225	1.50	0.39	0.12	8.2	40.8	11.1	4.97	1
5	225	2.50	0.65	0.18	21.1	58.3	22.7	2.77	1
6	200	3.00	0.13	0.15	24.9	66.8	182.5	2.91	0
7	200	4.00	0.04	0.19	0.0	0.0	NaN	NaN	0
8	235	2.00	0.71	0.17	14.6	50.3	10.5	3.47	1
9	235	3.00	0.95	0.22	42.2	65.3	34.6	1.56	1
10	270	1.91	3.32	0.32	65.6	40.0	9.7	0.62	1
11	270	1.57	2.19	0.23	37.0	41.7	6.9	1.13	1
12	285	1.25	2.80	0.27	48.8	32.4	7.4	0.67	1
13	285	1.56	2.89	0.32	42.2	37.7	4.6	0.90	1
14	300	1.91	4.90	0.36	90.0	45.5	8.4	0.51	1
15	300	1.45	2.92	0.26	52.2	35.0	7.9	0.68	1
16	325	1.74	6.00	0.39	102.8	38.0	7.1	0.38	1
17	325	1.32	2.95	0.25	69.8	32.4	13.6	0.47	1
18	340	1.58	3.47	0.32	82.5	39.5	13.8	0.49	1
19	340	1.89	2.34	0.28	69.1	42.1	19.5	0.62	1
20	350	1.48	1.21	0.21	40.8	40.4	23.8	1.00	0
21	350	1.82	0.82	0.15	35.0	45.1	32.8	1.30	0
22	360	1.50	0.52	0.14	40.3	31.5	67.8	0.83	0
23	360	1.98	0.36	0.12	42.0	40.1	106.7	1.01	0
24	370	1.88	0.30	0.13	34.3	43.9	103.0	1.35	0
25	390	1.47	0.28	0.12	14.1	48.3	41.1	3.46	0
26	450	1.00	0.42	0.13	68.9	31.0	153.2	0.55	0
27	600	1.00	0.29	0.11	134.4	33.0	456.6	0.45	0
28	900	1.00	0.00	0.00	8.6	30.7	Inf	NaN	0
29	900	1.00	0.00	0.00	1.1	35.1	Inf	NaN	0

Figure S16

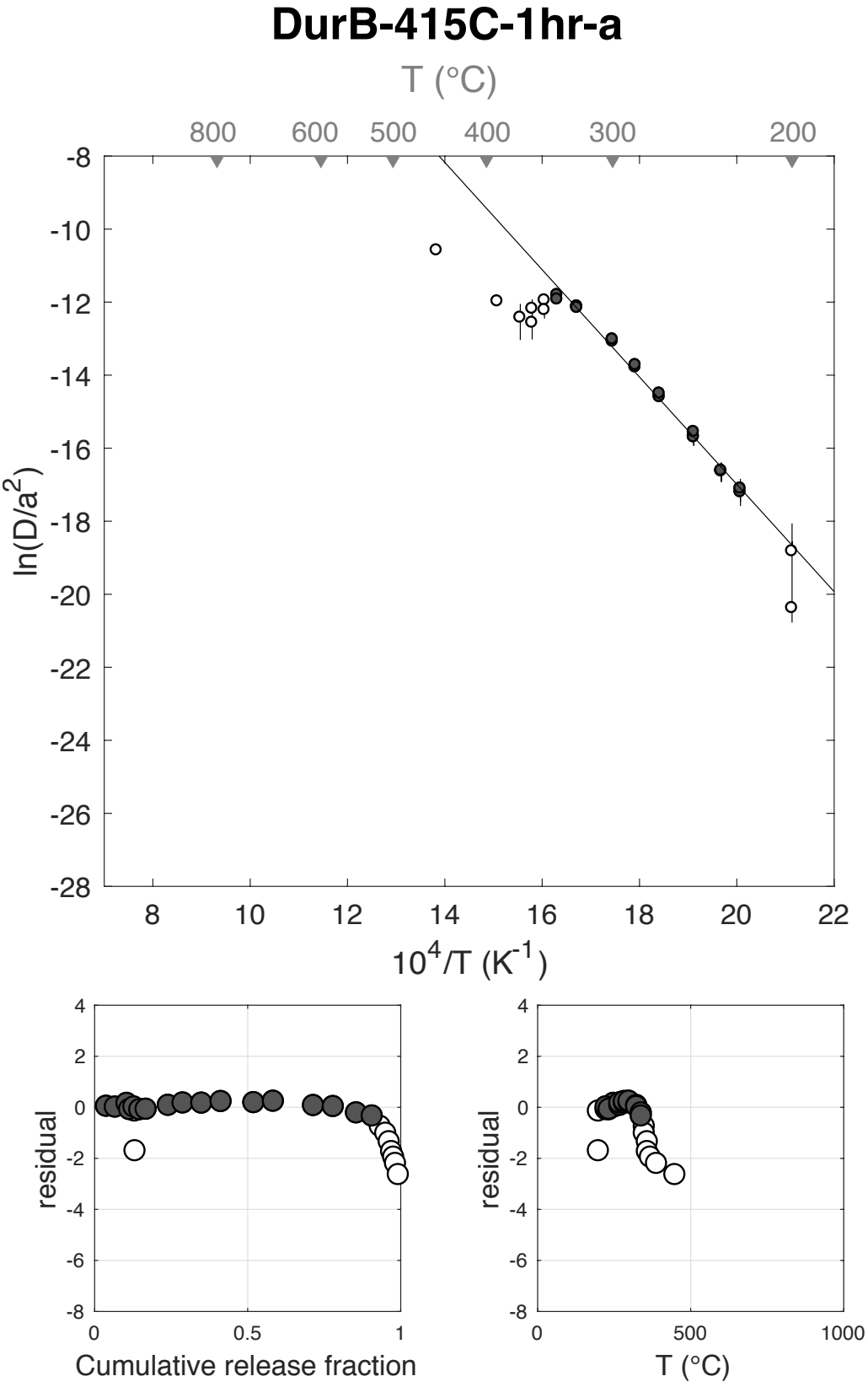
DurB-415C-1hr-a
T (°C)
800
600
500
400
300
200
-8
-10
-12
-14
-16
-18
-20
-22
-24
-26
-28
ln(D/a²)
8
10
12
14
16
18
20
22
10⁴/T (K⁻¹)
4
2
0
-2
-4
-6
-8
residual
0
0.5
1
Cumulative release fraction
500
1000
T (°C)

DurB-450C-1hr-b

E_a	+/-	D_0	+/-	T_c	-	+	Total ^{3}He	Incl.	Misfit	Norm. Misfit
130.51	5.53	13.64	1.13	51.60	6.05	6.34	41.52	0.822	0.797	0.047

Step #	°C	t (hrs)	^{3}He	Error	^{4}He	Error	^{4}He/^{3}He	Err	In ^{3}He Reg.
1	250	0.25	1.06	0.25	20.9	23.7	9.7	1.16	1
2	250	0.50	0.69	0.14	12.2	25.6	7.5	2.11	1
3	250	1.00	0.92	0.14	21.1	19.2	13.0	0.92	1
4	225	1.50	0.33	0.11	19.4	23.5	49.7	1.26	1
5	225	2.50	0.53	0.15	19.0	38.5	25.7	2.05	1
6	200	3.00	0.08	0.13	12.9	45.8	144.9	3.86	0
7	200	4.00	0.13	0.18	27.7	60.1	210.6	2.59	0
8	235	2.00	0.59	0.14	19.4	28.6	23.1	1.49	1
9	235	3.00	0.80	0.17	23.4	45.8	19.2	1.97	1
10	270	1.91	2.80	0.25	47.0	28.1	6.8	0.61	1
11	270	1.57	1.69	0.17	20.2	30.4	2.0	1.51	1
12	285	1.25	1.98	0.21	24.6	24.8	2.4	1.01	1
13	285	1.56	2.10	0.22	24.8	28.4	1.8	1.15	1
14	300	1.91	4.12	0.31	54.2	29.9	3.2	0.56	1
15	300	1.45	2.31	0.22	37.1	23.3	6.0	0.64	1
16	325	1.74	4.90	0.33	77.6	25.9	5.8	0.34	1
17	325	1.32	2.54	0.27	38.5	24.4	5.2	0.64	1
18	340	1.58	3.71	0.37	56.2	32.6	5.2	0.59	1
19	340	1.89	3.06	0.24	53.1	32.0	7.3	0.61	1
20	350	1.48	2.01	0.22	47.7	25.2	13.8	0.54	0
21	350	1.82	1.45	0.18	45.2	28.4	21.1	0.64	0
22	360	1.50	1.05	0.15	33.5	29.4	22.0	0.89	0
23	360	1.98	0.78	0.15	34.6	30.9	34.2	0.91	0
24	370	1.88	0.54	0.12	38.2	29.3	61.0	0.80	0
25	390	1.47	0.32	0.11	34.6	21.7	98.6	0.72	0
26	450	1.00	0.53	0.10	96.6	24.9	172.7	0.33	0
27	600	1.00	0.48	0.12	156.6	29.8	313.0	0.32	0
28	900	1.00	0.02	0.05	1.7	24.5	77.4	14.26	0
29	900	1.00	0.00	0.00	0.0	0.0	NaN	NaN	0

Figure S17

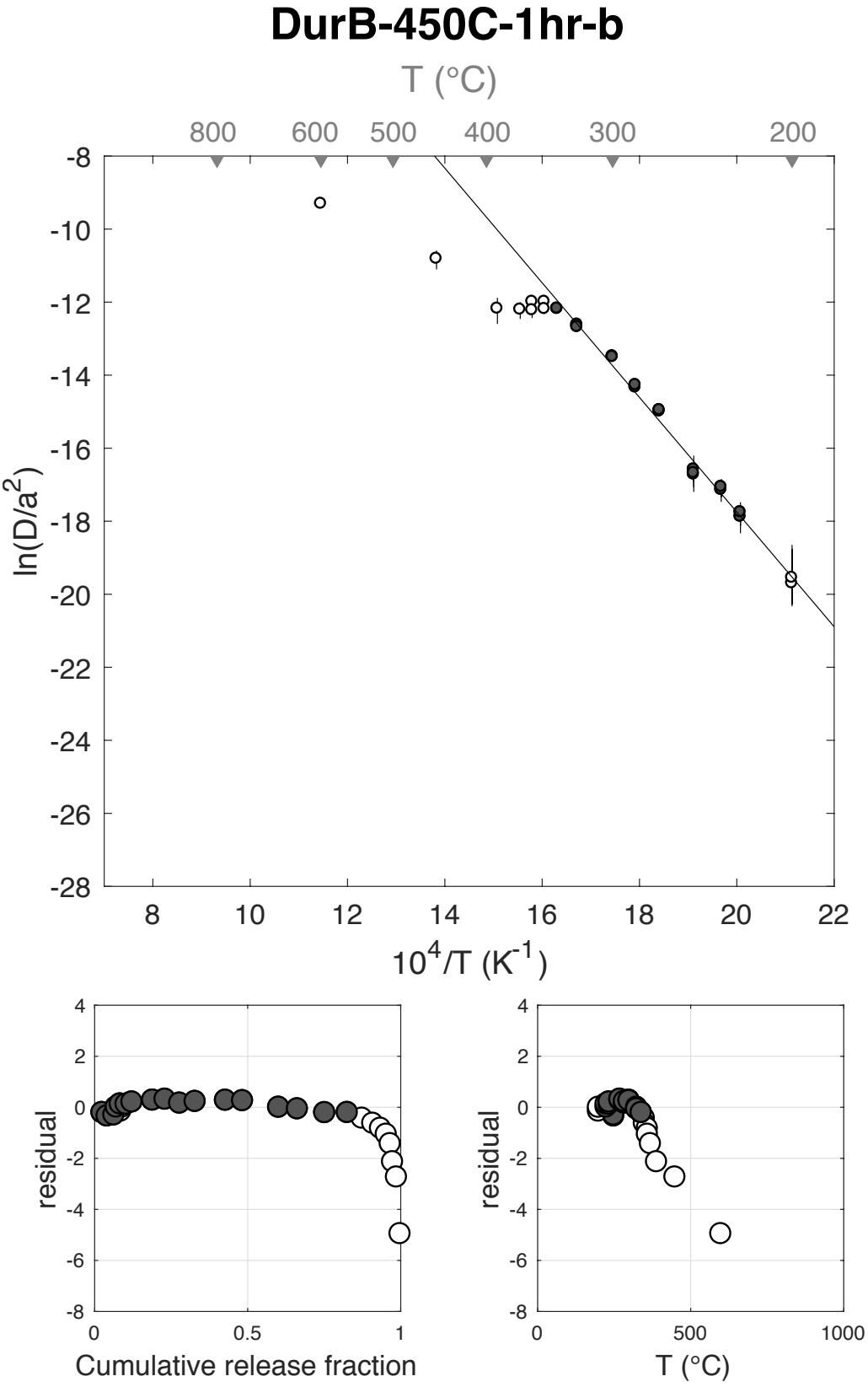
DurB-450C-1hr-b
T (°C)
800
600
500
400
300
200
ln(D/a²)
10⁴/T (K⁻¹)
residual
Cumulative release fraction
residual
T (°C)

DurB-475C-1hr-a

E_a	+/-	D_0	+/-	T_c	-	+	Total ^{3}He	Incl.	Misfit	Norm. Misfit
125.17	5.71	10.39	1.18	60.14	6.40	6.74	103.73	0.370	0.285	0.017

Step #	°C	t (hrs)	^{3}He	Error	^{4}He	Error	^{4}He/^{3}He	Err	In ^{3}He Reg.
1	250	0.25	1.30	0.18	132.8	21.0	91.8	0.21	1
2	250	0.50	0.81	0.15	92.0	16.6	103.2	0.26	1
3	250	1.00	1.04	0.16	107.9	13.7	94.2	0.20	1
4	225	1.50	0.25	0.11	36.7	19.6	138.0	0.69	1
5	225	2.50	0.36	0.12	51.8	35.7	134.5	0.77	1
6	200	3.00	0.03	0.09	17.9	45.0	503.3	3.58	0
7	200	4.00	0.06	0.11	10.2	66.2	157.4	6.73	0
8	235	2.00	0.43	0.11	59.7	28.7	127.5	0.54	1
9	235	3.00	0.55	0.13	86.2	46.9	145.8	0.59	1
10	270	1.91	2.05	0.23	264.8	26.8	119.1	0.15	1
11	270	1.57	1.38	0.16	200.9	22.4	136.0	0.16	1
12	285	1.25	1.92	0.20	305.9	19.0	149.6	0.12	1
13	285	1.57	1.87	0.20	326.6	22.4	164.9	0.13	1
14	300	1.91	3.56	0.26	697.0	30.4	185.9	0.09	1
15	300	1.45	2.09	0.22	509.0	25.0	233.8	0.12	1
16	325	1.74	5.83	0.39	1573.2	32.6	259.8	0.07	1
17	325	1.32	3.46	0.26	1133.9	26.1	317.9	0.08	1
18	340	1.58	5.90	0.39	2198.5	33.3	362.5	0.07	1
19	340	1.89	5.61	0.33	2459.5	38.8	428.7	0.06	1
20	350	1.48	4.81	0.33	2436.1	29.9	496.2	0.07	0
21	350	1.82	5.10	0.34	2757.5	33.9	530.9	0.07	0
22	360	1.50	4.95	0.32	2892.3	35.8	574.7	0.07	0
23	360	1.98	5.23	0.36	3333.8	39.8	627.6	0.07	0
24	370	1.88	5.50	0.34	3760.8	40.5	674.2	0.06	0
25	390	1.47	6.02	0.37	4389.1	36.6	719.1	0.06	0
26	450	1.00	12.15	0.55	10071.0	50.1	818.7	0.05	0
27	600	1.00	19.99	0.63	25083.4	92.4	1244.8	0.03	0
28	900	1.00	1.49	0.20	2757.0	27.8	1843.2	0.13	0
29	900	1.00	0.00	0.00	68.9	16.6	Inf	NaN	0

Figure S18

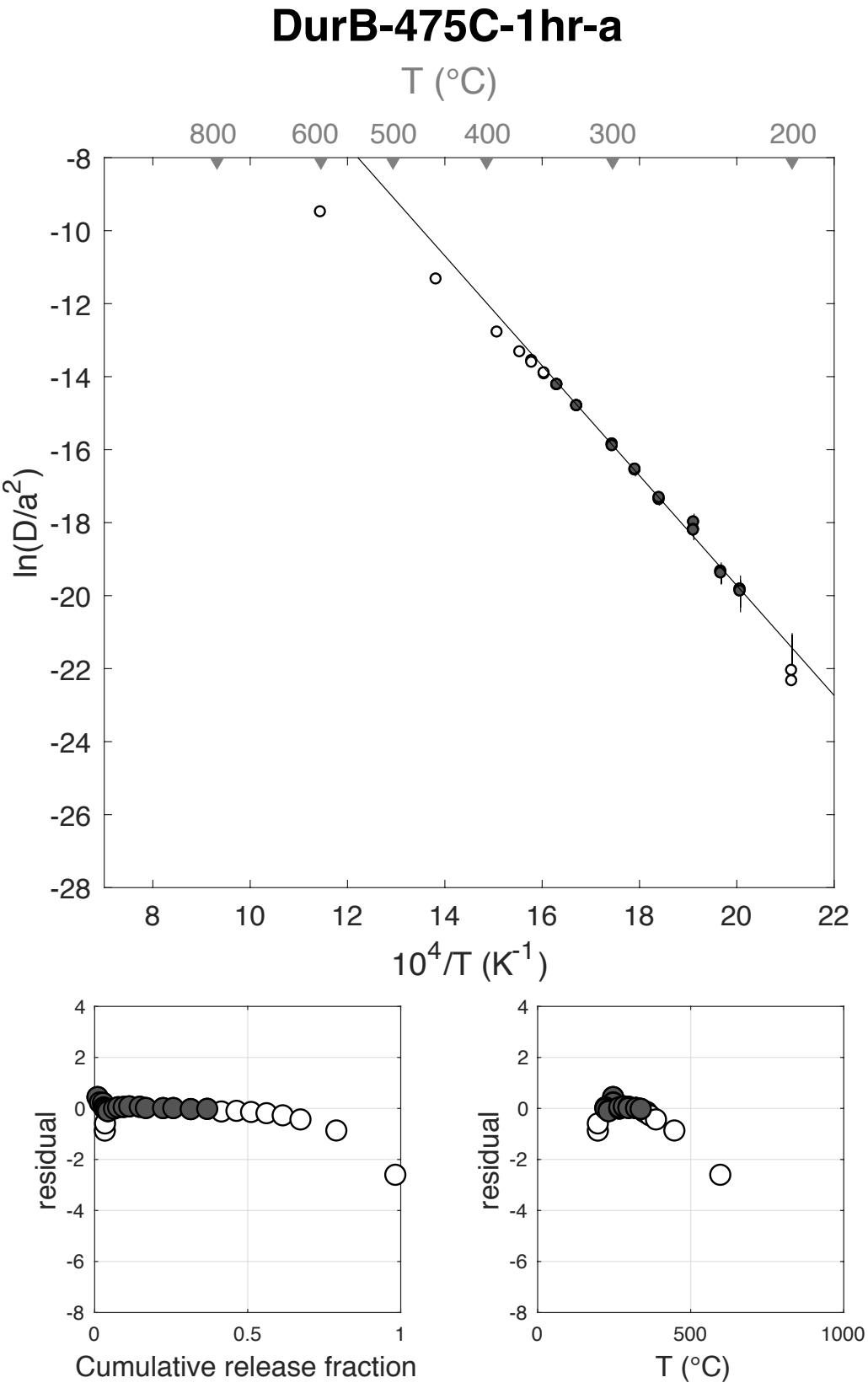
DurB-475C-1hr-a
T (°C)
800
600
500
400
300
200
-8
-10
-12
-14
-16
-18
-20
-22
-24
-26
-28
ln(D/a²)
8
10
12
14
16
18
20
22
10⁴/T (K⁻¹)
4
2
0
-2
-4
-6
-8
residual
0
0.5
1
Cumulative release fraction
0
500
1000
T (°C)

DurB-500C-1hr-c

E_a	+/-	D_0	+/-	T_c	-	+	Total ^{3}He	Incl.	Misfit	Norm. Misfit
118.49	6.98	9.55	1.44	48.41	8.24	8.78	116.92	0.449	0.531	0.031

Step #	°C	t (hrs)	^{3}He	Error	^{4}He	Error	^{4}He/^{3}He	Err	In ^{3}He Reg.
1	250	0.25	2.13	0.37	53.0	8.1	14.8	0.23	1
2	250	0.50	1.35	0.30	19.8	6.1	4.6	0.38	1
3	250	1.00	1.55	0.32	0.0	0.0	NaN	NaN	1
4	225	1.50	0.35	0.17	0.0	0.0	NaN	NaN	1
5	225	2.50	0.59	0.21	0.0	0.0	NaN	NaN	1
6	200	3.00	0.04	0.12	0.0	0.0	NaN	NaN	0
7	200	4.00	0.12	0.12	0.0	0.0	NaN	NaN	0
8	235	2.00	0.73	0.24	0.0	0.0	NaN	NaN	1
9	235	3.00	1.03	0.30	315.1	26.7	295.7	0.30	1
10	270	1.91	3.71	0.46	0.0	0.0	NaN	NaN	1
11	270	1.57	1.98	0.39	0.0	0.0	NaN	NaN	1
12	285	1.25	2.81	0.45	16.8	9.2	NaN	NaN	1
13	285	1.56	2.80	0.50	0.0	0.0	NaN	NaN	1
14	300	1.91	5.23	0.63	0.0	0.0	NaN	NaN	1
15	300	1.45	3.07	0.49	1.7	10.6	NaN	NaN	1
16	325	1.74	7.82	0.76	18.5	11.8	NaN	NaN	1
17	325	1.32	4.30	0.66	37.6	9.6	NaN	NaN	1
18	340	1.58	6.73	0.61	15.3	11.4	NaN	NaN	1
19	340	1.89	6.31	0.69	7.8	13.0	NaN	NaN	1
20	350	1.48	5.51	0.76	22.9	10.7	NaN	NaN	0
21	350	1.82	5.10	0.64	0.0	0.0	NaN	NaN	0
22	360	1.50	5.05	0.59	4.2	11.5	NaN	NaN	0
23	360	1.98	4.33	0.66	0.0	0.0	NaN	NaN	0
24	370	1.88	5.38	0.58	0.0	0.0	NaN	NaN	0
25	390	1.47	5.58	0.70	1.6	11.3	NaN	NaN	0
26	450	1.00	11.76	0.94	117.2	14.5	NaN	NaN	0
27	600	1.00	21.30	1.38	862.4	27.1	30.5	0.07	0
28	900	1.00	0.28	0.16	274.3	15.6	972.2	0.56	0
29	900	1.00	0.00	0.00	0.0	0.0	NaN	NaN	0

Figure S19

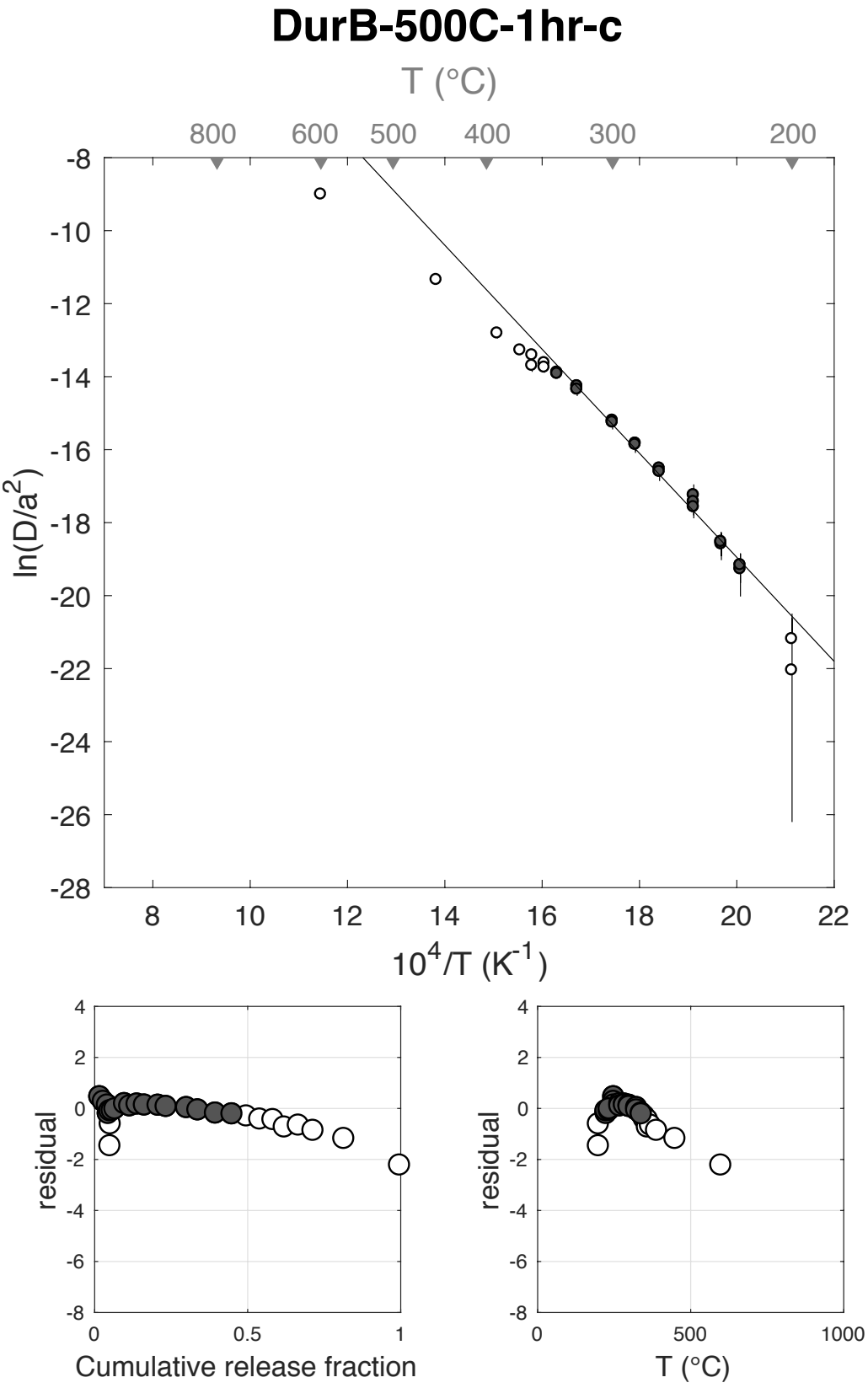
DurB-500C-1hr-c
T (°C)
800
600
500
400
300
200
-8
-10
-12
-14
-16
-18
-20
-22
-24
-26
-28
ln(D/a2)
8
10
12
14
16
18
20
22
10^4/T (K^-1)
4
2
0
-2
-4
-6
-8
residual
0
0.5
1
Cumulative release fraction
500
1000
T (°C)

DurB-250C-10hr-a

E_a	+/-	D_0	+/-	T_c	-	+	Total ^{3}He	Incl.	Misfit	Norm. Misfit
148.24	7.66	15.72	1.57	80.28	7.12	7.57	65.04	0.509	0.176	0.011

Step #	°C	t (hrs)	^{3}He	Error	^{4}He	Error	^{4}He/^{3}He	Err	In ^{3}He Reg.
1	250	0.25	0.77	0.16	58.2	24.1	65.6	0.46	1
2	250	0.50	0.49	0.13	83.5	27.0	160.7	0.42	1
3	250	1.00	0.60	0.14	155.3	24.8	248.5	0.28	1
4	225	1.50	0.17	0.10	35.7	31.2	204.0	1.05	0
5	225	2.50	0.24	0.09	61.2	28.2	250.2	0.61	1
6	200	3.00	0.04	0.08	0.0	0.0	NaN	NaN	0
7	200	4.00	0.06	0.09	0.5	37.5	NaN	NaN	0
8	235	2.00	0.24	0.11	109.3	28.6	441.1	0.52	1
9	235	3.00	0.43	0.13	190.5	34.7	431.4	0.35	1
10	270	1.91	1.55	0.20	898.3	29.4	569.5	0.13	1
11	270	1.57	0.95	0.16	658.5	31.1	684.9	0.17	1
12	285	1.25	1.34	0.19	1105.9	32.7	812.6	0.15	1
13	285	1.56	1.46	0.19	1376.1	37.5	935.6	0.13	1
14	300	1.91	3.08	0.29	2991.1	41.1	962.5	0.10	1
15	300	1.45	1.75	0.23	1912.7	30.1	1080.9	0.13	1
16	325	1.74	5.78	0.36	6268.3	76.6	1075.4	0.06	1
17	325	1.32	3.38	0.31	3910.5	51.8	1147.0	0.09	1
18	340	1.58	5.81	0.41	6778.0	118.6	1156.1	0.07	1
19	340	1.89	5.25	0.39	6295.8	62.8	1189.2	0.08	1
20	350	1.48	4.48	0.34	5403.0	51.3	1195.7	0.08	0
21	350	1.82	4.42	0.35	5267.1	55.3	1181.2	0.08	0
22	360	1.50	4.03	0.32	4758.6	55.9	1170.0	0.08	0
23	360	1.98	4.03	0.33	4735.5	59.0	1165.9	0.08	0
24	370	1.88	3.72	0.27	4487.1	73.6	1195.4	0.08	0
25	390	1.47	3.63	0.32	4251.2	65.4	1160.6	0.09	0
26	450	1.00	4.98	0.39	6092.8	72.0	1212.8	0.08	0
27	600	1.00	2.24	0.25	2864.8	57.2	1269.4	0.11	0
28	900	1.00	0.12	0.07	150.2	5.4	1274.0	0.65	0
29	900	1.00	0.00	0.00	0.0	0.0	NaN	NaN	0

Figure S20

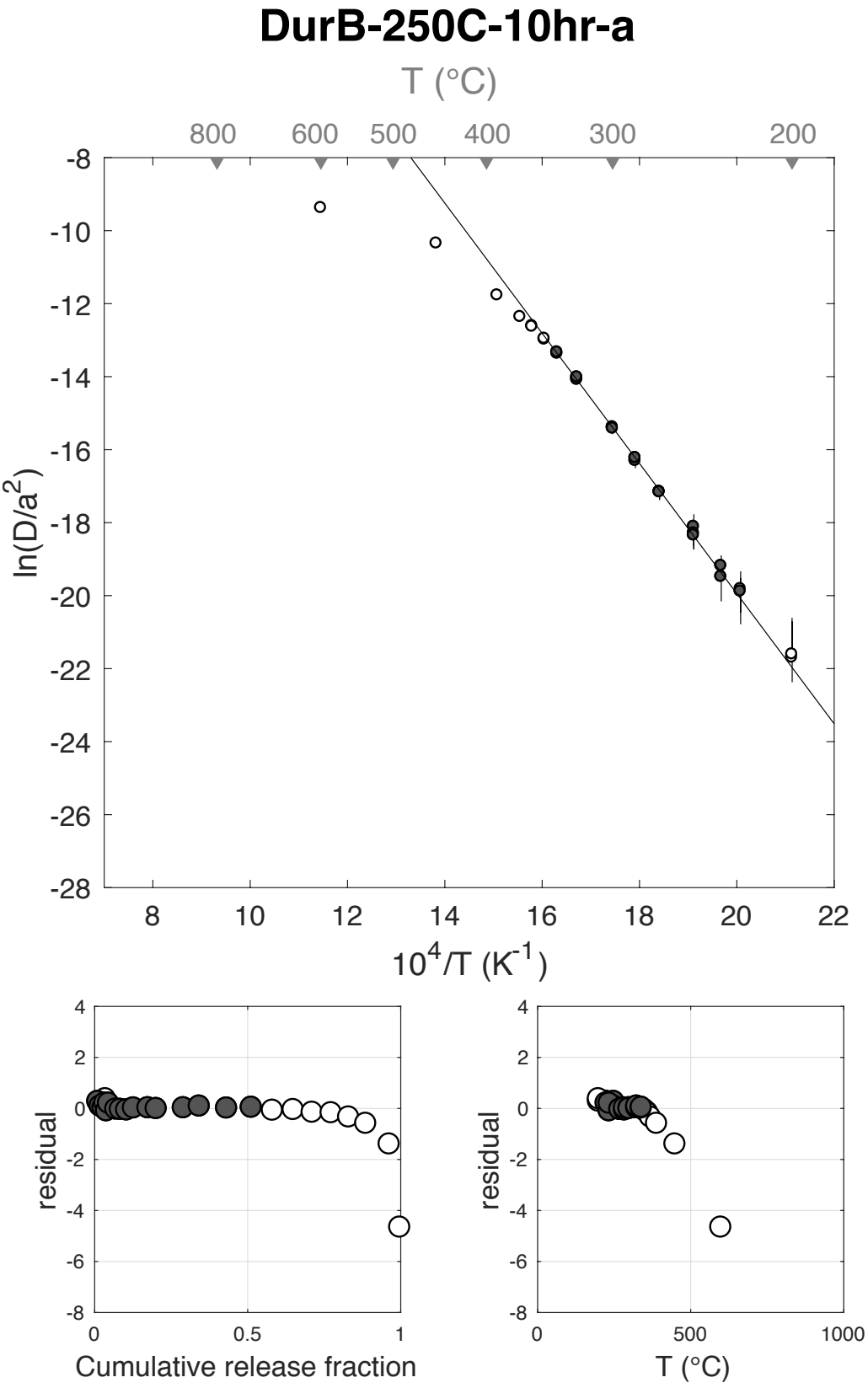
DurB-250C-10hr-a
T (°C)
800
600
500
400
300
200
-8
-10
-12
-14
-16
-18
-20
-22
-24
-26
-28
ln(D/a²)
8
10
12
14
16
18
20
22
10⁴/T (K⁻¹)
4
2
0
-2
-4
-6
-8
residual
0
0.5
1
Cumulative release fraction
500
1000
T (°C)

DurB-250C-10hr-b

E_a	+/-	D_0	+/-	T_c	-	+	Total ^{3}He	Incl.	Misfit	Norm. Misfit
147.87	6.33	15.34	1.31	81.95	5.86	6.16	100.62	0.454	0.244	0.014

Step #	°C	t (hrs)	^{3}He	Error	^{4}He	Error	^{4}He/^{3}He	Err	In ^{3}He Reg.
1	250	0.25	0.91	0.14	87.3	21.9	86.4	0.30	1
2	250	0.50	0.62	0.11	123.6	19.1	189.6	0.23	1
3	250	1.00	0.82	0.14	223.6	26.9	261.8	0.21	1
4	225	1.50	0.21	0.10	75.3	22.1	351.4	0.55	1
5	225	2.50	0.34	0.12	112.7	30.5	322.8	0.44	1
6	200	3.00	0.03	0.11	8.6	33.5	258.9	5.29	0
7	200	4.00	0.09	0.16	13.1	43.5	129.4	3.73	0
8	235	2.00	0.42	0.11	174.3	25.3	409.1	0.31	1
9	235	3.00	0.56	0.16	246.0	39.1	429.5	0.32	1
10	270	1.91	2.21	0.24	1256.7	42.1	559.6	0.11	1
11	270	1.57	1.33	0.18	907.9	37.4	672.7	0.14	1
12	285	1.25	2.02	0.21	1571.9	44.7	770.1	0.11	1
13	285	1.56	1.38	0.29	1852.8	53.8	1332.2	0.21	1
14	300	1.91	4.39	0.31	4178.6	96.9	941.6	0.07	1
15	300	1.45	2.71	0.22	2695.8	73.3	984.8	0.08	1
16	325	1.74	8.05	0.45	8369.4	179.7	1029.4	0.06	1
17	325	1.32	4.49	0.30	4988.3	123.0	1101.8	0.07	1
18	340	1.58	7.92	0.36	8772.6	205.7	1097.0	0.05	1
19	340	1.89	7.27	0.38	8089.3	193.9	1101.9	0.06	1
20	350	1.48	5.80	0.51	7085.3	172.4	1212.4	0.09	0
21	350	1.82	6.11	0.40	6879.0	152.9	1115.0	0.07	0
22	360	1.50	5.64	0.31	6400.2	161.2	1125.1	0.06	0
23	360	1.98	5.96	0.37	6778.0	161.9	1127.5	0.07	0
24	370	1.88	6.00	0.37	6884.7	170.8	1136.7	0.07	0
25	390	1.47	6.17	0.42	7009.4	171.4	1125.9	0.07	0
26	450	1.00	10.26	0.45	12266.7	267.1	1185.6	0.05	0
27	600	1.00	8.79	0.47	10897.3	258.4	1229.9	0.06	0
28	900	1.00	0.08	0.06	6.0	22.1	64.5	3.73	0
29	900	1.00	0.04	0.06	2.4	19.1	50.2	8.15	0

Figure S21

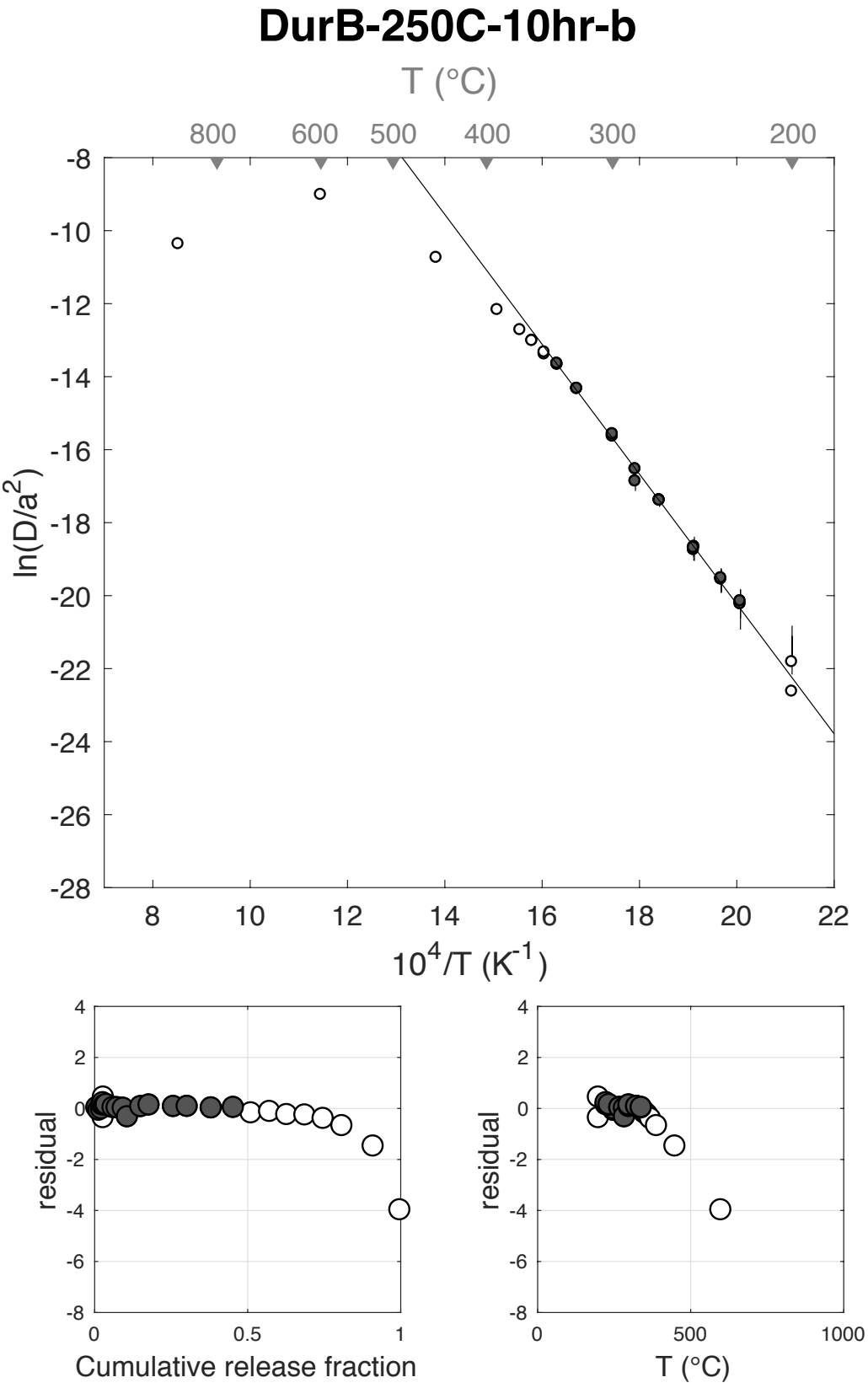
DurB-250C-10hr-b
T (°C)
800
600
500
400
300
200
-8
-10
-12
-14
-16
-18
-20
-22
-24
-26
-28
ln(D/a2)
8
10
12
14
16
18
20
22
10^4/T (K^-1)
4
2
0
-2
-4
-6
-8
residual
0
0.5
1
Cumulative release fraction
0
500
1000
T (°C)

DurB-275C-10hr-a

E_a	+/-	D_0	+/-	T_c	-	+	Total ^{3}He	Incl.	Misfit	Norm. Misfit
129.98	5.79	14.04	1.20	47.76	6.26	6.58	44.60	0.915	0.413	0.024

Step #	°C	t (hrs)	^{3}He	Error	^{4}He	Error	^{4}He/^{3}He	Err	In ^{3}He Reg.
1	250	0.25	1.59	0.23	72.8	35.7	35.8	0.51	1
2	250	0.50	1.32	0.21	88.3	20.4	57.0	0.28	1
3	250	1.00	1.45	0.20	109.1	24.4	65.2	0.26	1
4	225	1.50	0.38	0.13	31.6	38.8	72.9	1.27	1
5	225	2.50	0.50	0.21	60.8	71.3	111.2	1.24	1
6	200	3.00	0.12	0.20	25.4	88.1	201.6	3.85	0
7	200	4.00	0.14	0.28	34.3	127.5	232.5	4.22	0
8	235	2.00	0.65	0.17	68.6	53.1	95.0	0.82	1
9	235	3.00	0.92	0.25	114.1	87.9	113.7	0.82	1
10	270	1.91	3.23	0.30	445.7	50.1	128.1	0.15	1
11	270	1.57	2.12	0.22	337.8	38.2	149.2	0.15	1
12	285	1.25	2.91	0.26	530.9	29.5	172.2	0.10	1
13	285	1.56	2.81	0.29	653.6	37.3	223.0	0.12	1
14	300	1.91	5.03	0.34	1394.9	51.9	267.1	0.08	1
15	300	1.45	2.67	0.27	917.3	42.2	333.2	0.11	1
16	325	1.74	6.25	0.46	2369.3	48.6	369.3	0.08	1
17	325	1.32	2.87	0.28	1220.9	43.0	415.8	0.10	1
18	340	1.58	4.05	0.31	2013.7	44.6	487.6	0.08	1
19	340	1.89	2.06	0.27	1147.6	54.6	546.0	0.14	1
20	350	1.48	1.18	0.20	710.6	39.4	592.2	0.18	0
21	350	1.82	0.63	0.16	474.7	43.7	747.9	0.27	0
22	360	1.50	0.35	0.12	306.9	35.5	874.6	0.35	0
23	360	1.98	0.33	0.15	265.6	52.4	799.6	0.49	0
24	370	1.88	0.21	0.14	199.2	50.0	943.7	0.70	0
25	390	1.47	0.12	0.11	166.1	41.2	1398.6	0.93	0
26	450	1.00	0.21	0.09	233.8	29.7	1122.0	0.48	0
27	600	1.00	0.51	0.12	534.7	34.2	1044.1	0.25	0
28	900	1.00	0.00	0.00	20.0	24.4	Inf	NaN	0
29	900	1.00	0.00	0.00	0.0	0.0	NaN	NaN	0

Figure S22

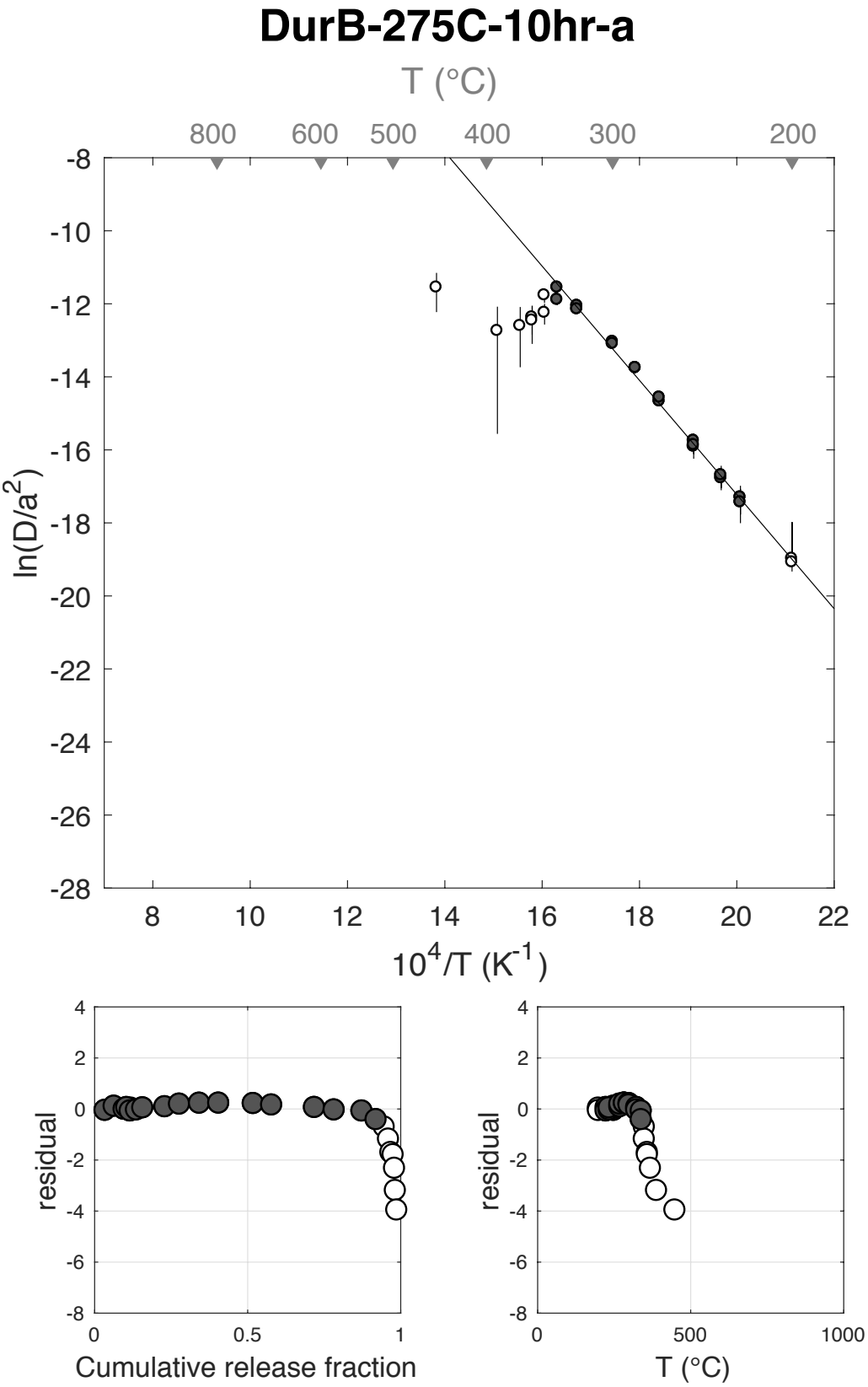
DurB-275C-10hr-a
T (°C)
800
600
500
400
300
200
ln(D/a²)
10⁴/T (K⁻¹)
residual
Cumulative release fraction
residual
T (°C)

DurB-275C-10hr-b

E_a	+/-	D_0	+/-	T_c	-	+	Total ^{3}He	Incl.	Misfit	Norm. Misfit
109.69	7.99	10.01	1.70	22.13	9.93	10.70	25.25	0.912	2.505	0.132

Step #	°C	t (hrs)	^{3}He	Error	^{4}He	Error	^{4}He/^{3}He	Err	In ^{3}He Reg.
1	250	0.25	2.03	0.23	307.7	20.2	141.6	0.13	1
2	250	0.50	1.07	0.17	180.2	22.9	158.5	0.20	1
3	250	1.00	1.24	0.17	227.3	27.1	172.8	0.18	1
4	225	1.50	0.29	0.09	59.6	24.7	197.1	0.52	1
5	225	2.50	0.37	0.11	88.6	46.8	231.5	0.61	1
6	200	3.00	0.06	0.08	5.5	58.5	81.3	10.79	1
7	200	4.00	0.12	0.09	31.1	82.0	242.6	2.73	1
8	235	2.00	0.45	0.10	92.7	35.6	195.4	0.45	1
9	235	3.00	0.64	0.13	120.1	59.2	179.0	0.53	1
10	270	1.91	2.05	0.25	431.1	37.2	199.8	0.15	1
11	270	1.57	1.12	0.16	266.5	26.4	228.3	0.17	1
12	285	1.25	1.54	0.19	401.7	21.3	250.7	0.13	1
13	285	1.57	1.41	0.20	436.4	25.9	298.8	0.15	1
14	300	1.91	2.40	0.24	874.2	38.2	354.2	0.11	1
15	300	1.45	1.29	0.18	573.6	27.3	434.2	0.15	1
16	325	1.74	2.94	0.28	1493.7	36.7	497.7	0.10	1
17	325	1.32	1.33	0.16	764.2	20.4	563.3	0.12	1
18	340	1.58	1.62	0.20	1024.2	28.4	624.1	0.13	1
19	340	1.89	1.04	0.16	697.7	36.1	661.5	0.16	1
20	350	1.48	0.58	0.12	446.7	26.9	759.8	0.22	0
21	350	1.82	0.39	0.12	315.2	30.8	802.0	0.32	0
22	360	1.50	0.24	0.10	238.7	28.1	982.9	0.45	0
23	360	1.98	0.21	0.10	196.2	35.1	934.9	0.51	0
24	370	1.88	0.17	0.09	197.7	33.4	1168.7	0.56	0
25	390	1.47	0.19	0.09	214.1	23.1	1108.9	0.46	0
26	450	1.00	0.34	0.10	340.7	18.0	1001.8	0.30	0
27	600	1.00	0.12	0.09	127.1	14.2	1076.8	0.76	0
28	900	1.00	0.00	0.06	12.1	15.5	3507.7	18.07	0
29	899	1.00	0.00	0.00	10.8	15.9	Inf	NaN	0

Figure S23

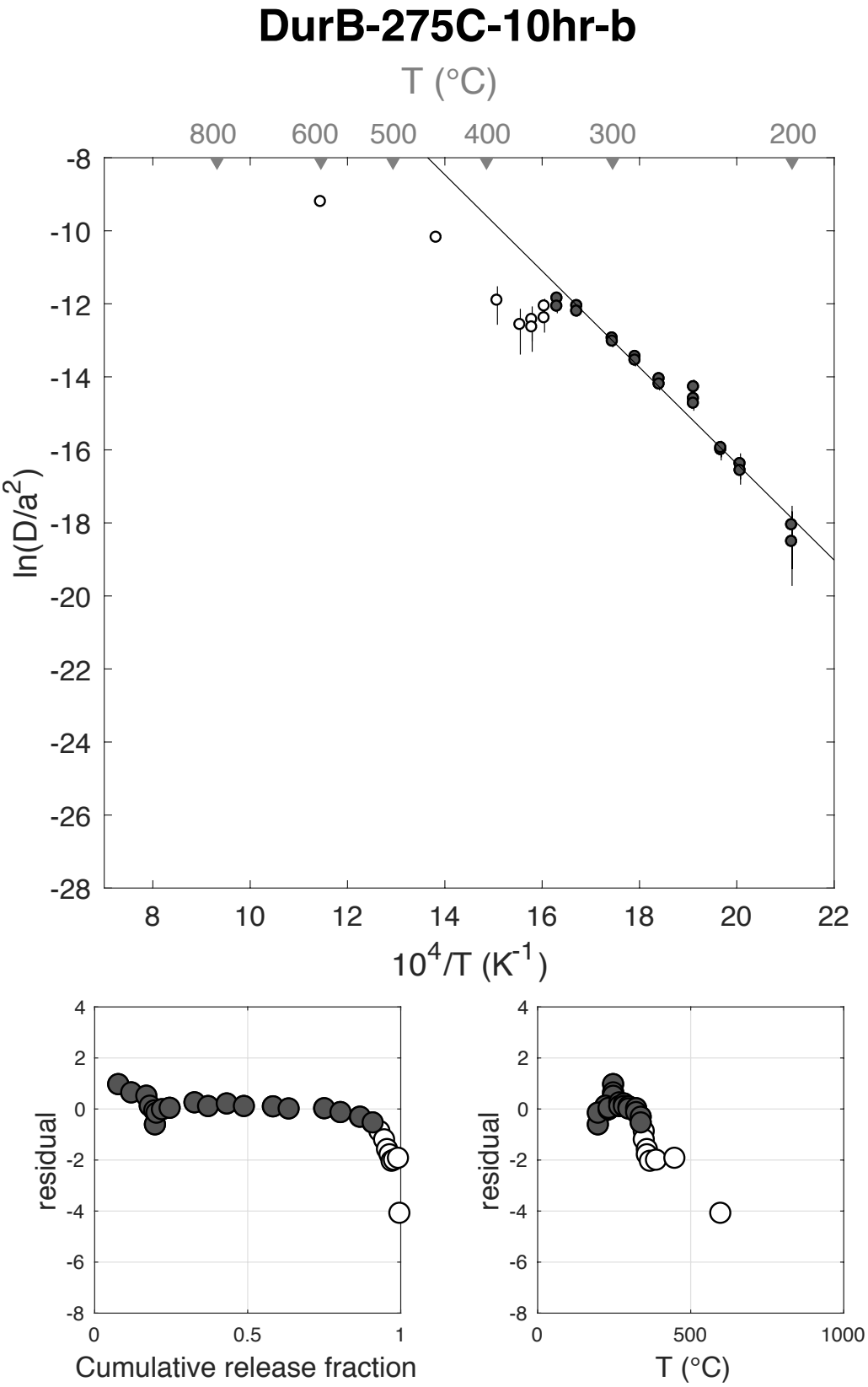
DurB-275C-10hr-b
T (°C)
800
600
500
400
300
200
ln(D/a²)
10⁴/T (K⁻¹)
residual
Cumulative release fraction
residual
T (°C)

DurB-300C-10hr-a

E_a	+/-	D_0	+/-	T_c	-	+	Total ^{3}He	Incl.	Misfit	Norm. Misfit
153.41	10.65	17.53	2.18	80.13	9.48	10.29	56.47	0.664	0.167	0.012

Step #	°C	t (hrs)	^{3}He	Error	^{4}He	Error	^{4}He/^{3}He	Err	In ^{3}He Reg.
1	250	0.25	0.91	0.19	74.9	89.4	72.0	1.21	1
2	250	0.50	0.54	0.15	21.5	54.0	29.8	2.53	1
3	250	1.00	0.77	0.16	63.4	30.0	72.8	0.52	1
4	225	1.50	0.23	0.14	29.0	101.2	114.7	3.54	0
5	225	2.50	0.30	0.23	26.6	249.5	77.4	9.41	0
6	200	3.00	0.09	0.27	27.0	323.5	288.3	12.33	0
7	200	4.00	0.11	0.39	0.0	0.0	NaN	NaN	0
8	235	2.00	0.30	0.19	9.1	174.9	20.2	19.25	0
9	235	3.00	0.44	0.29	20.4	323.8	36.5	15.89	1
10	270	1.91	1.74	0.28	71.2	162.7	30.9	2.29	1
11	270	1.57	1.33	0.24	83.2	112.0	52.3	1.36	1
12	285	1.25	1.57	0.21	104.0	66.4	56.3	0.65	1
13	285	1.56	1.82	0.22	138.0	110.7	65.6	0.81	1
14	300	1.91	3.81	0.32	390.2	162.7	92.3	0.43	1
15	300	1.45	2.18	0.26	271.4	98.4	114.4	0.38	1
16	325	1.74	6.59	0.45	791.1	211.7	110.1	0.28	1
17	325	1.32	4.16	0.34	966.7	75.2	222.6	0.11	1
18	340	1.58	6.41	0.44	1506.5	120.4	225.2	0.11	1
19	340	1.89	5.22	0.39	1626.2	160.2	301.8	0.12	1
20	350	1.48	3.80	0.26	1312.1	103.0	335.7	0.10	0
21	350	1.82	3.16	0.29	1243.8	153.2	383.2	0.15	0
22	360	1.50	2.59	0.29	1063.0	106.8	400.2	0.15	0
23	360	1.98	2.13	0.27	1021.5	174.7	469.8	0.21	0
24	370	1.88	1.61	0.26	810.1	159.9	492.9	0.26	0
25	390	1.47	1.25	0.18	88.1	367.3	60.4	4.17	0
26	450	1.00	1.47	0.21	1082.4	45.5	725.7	0.15	0
27	600	1.00	1.77	0.27	1579.9	53.4	883.9	0.16	0
28	900	1.00	0.17	0.09	173.4	32.2	1036.3	0.59	0
29	900	1.00	0.00	0.00	0.0	0.0	NaN	NaN	0

Figure S24

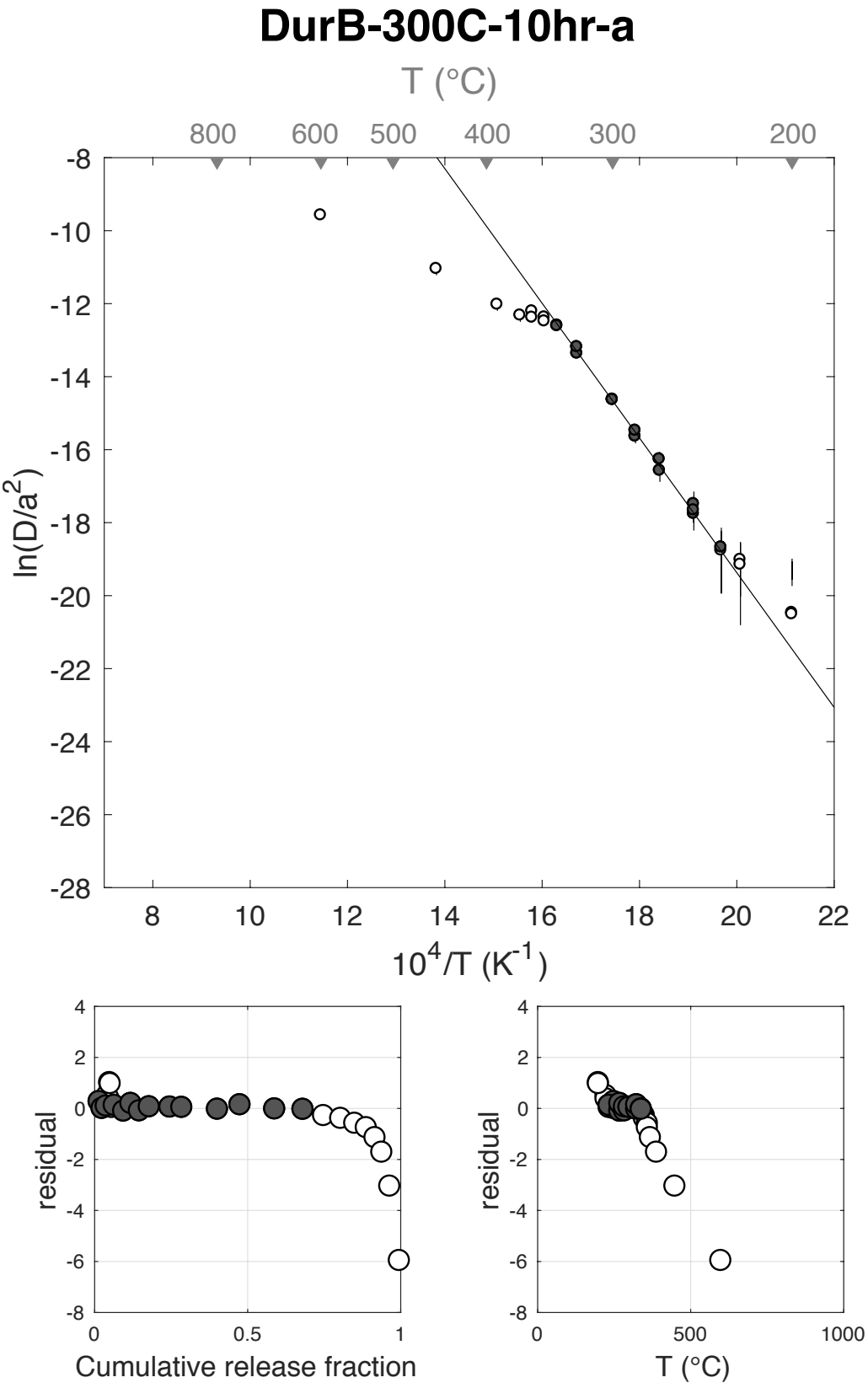
DurB-300C-10hr-a
T (°C)
800
600
500
400
300
200
-8
-10
-12
-14
-16
-18
-20
-22
-24
-26
-28
ln(D/a2)
8
10
12
14
16
18
20
22
10^4/T (K^-1)
4
2
0
-2
-4
-6
-8
residual
0
0.5
1
Cumulative release fraction
500
1000
T (°C)

DurB-315C-10hr-a

E_a	+/-	D_0	+/-	T_c	-	+	Total ^{3}He	Incl.	Misfit	Norm. Misfit
124.66	4.57	12.78	0.95	42.77	5.19	5.40	58.25	0.881	0.317	0.019

Step #	°C	t (hrs)	^{3}He	Error	^{4}He	Error	^{4}He/^{3}He	Err	In ^{3}He Reg.
1	250	0.25	2.14	0.23	62.3	76.4	19.1	1.23	1
2	250	0.50	1.57	0.20	61.9	46.3	29.4	0.76	1
3	250	1.00	1.97	0.24	50.2	25.1	15.5	0.51	1
4	225	1.50	0.47	0.15	37.9	86.5	70.3	2.30	1
5	225	2.50	0.66	0.21	43.0	210.8	55.7	4.91	1
6	200	3.00	0.18	0.21	175.6	315.0	942.7	2.14	0
7	200	4.00	0.23	0.30	13.4	399.6	47.9	29.87	0
8	235	2.00	0.79	0.18	14.2	148.7	8.0	10.45	1
9	235	3.00	1.19	0.26	18.4	273.8	5.4	14.90	1
10	270	1.91	4.25	0.39	82.1	137.1	9.3	1.67	1
11	270	1.57	2.56	0.26	44.0	95.7	7.2	2.18	1
12	285	1.25	3.09	0.29	62.0	59.4	10.0	0.96	1
13	285	1.56	3.11	0.32	86.6	94.2	17.8	1.09	1
14	300	1.91	6.13	0.40	196.7	138.7	22.1	0.71	1
15	300	1.45	3.56	0.29	131.0	81.6	26.8	0.63	1
16	325	1.74	7.89	0.51	296.0	135.2	27.5	0.46	1
17	325	1.32	3.75	0.35	205.4	65.6	44.8	0.33	1
18	340	1.58	4.73	0.38	324.0	98.3	58.5	0.31	1
19	340	1.89	3.45	0.34	298.5	135.6	76.6	0.46	1
20	350	1.48	1.88	0.21	216.6	85.6	105.5	0.41	0
21	350	1.82	1.39	0.21	213.2	127.1	143.3	0.61	0
22	360	1.50	0.74	0.16	155.3	87.6	198.9	0.61	0
23	360	1.98	0.45	0.16	137.7	148.2	294.3	1.14	0
24	370	1.88	0.31	0.15	136.2	133.8	426.3	1.10	0
25	390	1.47	0.21	0.12	244.3	81.7	1132.9	0.67	0
26	450	1.00	0.39	0.12	233.9	31.8	586.2	0.33	0
27	600	1.00	1.13	0.20	933.5	43.9	813.7	0.18	0
28	900	1.00	0.00	0.00	0.0	0.0	NaN	NaN	0
29	900	1.00	0.00	0.00	0.0	0.0	NaN	NaN	0

Figure S25

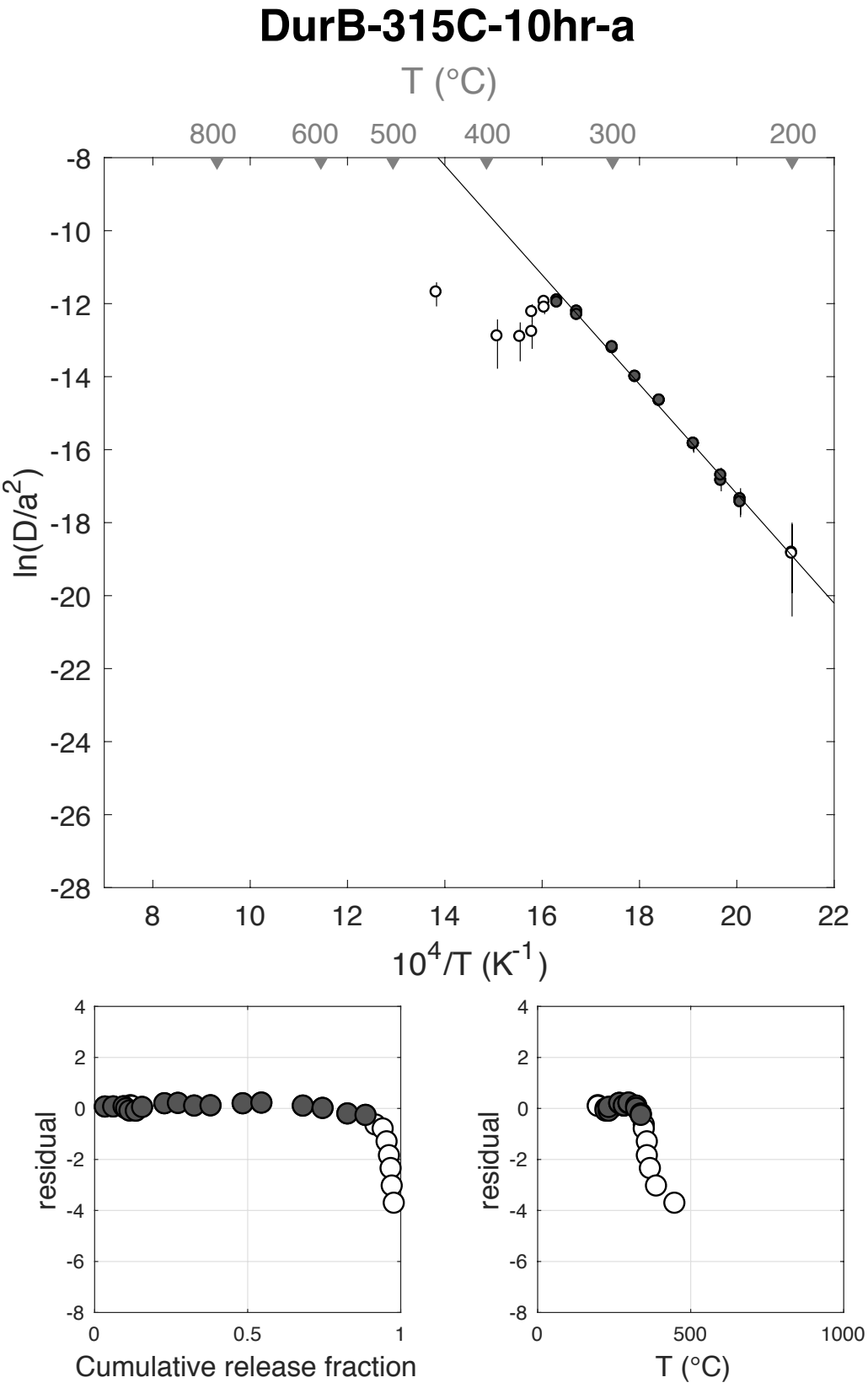
DurB-315C-10hr-a
T (°C)
800
600
500
400
300
200
-8
-10
-12
-14
-16
-18
-20
-22
-24
-26
-28
ln(D/a²)
8
10
12
14
16
18
20
22
10⁴/T (K⁻¹)
4
2
0
-2
-4
-6
-8
residual
0
0.5
1
Cumulative release fraction
500
1000
T (°C)

DurB-330C-10hr-a

E_a	+/-	D_0	+/-	T_c	-	+	Total ^{3}He	Incl.	Misfit	Norm. Misfit
140.02	4.87	14.34	1.01	70.05	4.83	5.03	149.58	0.554	0.217	0.013

Step #	°C	t (hrs)	^{3}He	Error	^{4}He	Error	^{4}He/^{3}He	Err	In ^{3}He Reg.
1	250	0.25	2.38	0.23	76.3	23.3	22.0	0.32	1
2	250	0.50	1.55	0.21	58.9	22.6	28.0	0.41	1
3	250	1.00	1.68	0.24	58.5	19.9	24.8	0.37	1
4	225	1.50	0.39	0.16	0.0	0.0	NaN	NaN	1
5	225	2.50	0.62	0.17	0.0	0.0	NaN	NaN	1
6	200	3.00	0.00	0.00	0.0	0.0	NaN	NaN	0
7	200	4.00	0.00	0.00	0.0	0.0	NaN	NaN	0
8	235	2.00	0.79	0.17	15.6	21.9	9.7	1.41	1
9	235	3.00	1.18	0.19	20.6	20.6	7.5	1.01	1
10	270	1.91	4.74	0.39	211.9	27.3	34.7	0.15	1
11	270	1.57	2.63	0.34	154.6	29.5	48.7	0.23	1
12	285	1.25	3.68	0.34	236.3	24.4	54.2	0.14	1
13	285	1.56	4.23	0.35	303.7	33.3	61.8	0.14	1
14	300	1.91	8.39	0.56	715.4	41.8	75.2	0.09	1
15	300	1.45	4.87	0.40	509.6	38.5	94.7	0.11	1
16	325	1.74	13.45	0.62	1748.3	78.3	119.9	0.06	1
17	325	1.32	8.06	0.59	1207.1	59.3	139.9	0.09	1
18	340	1.58	13.19	0.70	2425.2	117.8	173.8	0.07	1
19	340	1.89	11.04	0.62	2467.6	107.8	213.5	0.07	1
20	350	1.48	9.38	0.48	2430.3	118.9	249.0	0.07	0
21	350	1.82	8.87	0.64	2576.5	121.9	280.3	0.09	0
22	360	1.50	7.66	0.48	2475.9	130.5	313.3	0.08	0
23	360	1.98	7.56	0.45	2700.0	134.5	346.9	0.08	0
24	370	1.88	7.14	0.39	2777.1	144.8	378.7	0.08	0
25	390	1.47	6.47	0.45	2865.3	151.4	432.8	0.09	0
26	450	1.00	9.76	0.56	5051.6	239.0	507.4	0.07	0
27	600	1.00	7.98	0.51	6141.0	298.7	759.6	0.08	0
28	900	1.00	0.96	0.34	874.9	54.8	900.0	0.36	0
29	900	1.00	0.90	0.16	23.7	23.3	16.4	1.00	0

Figure S26

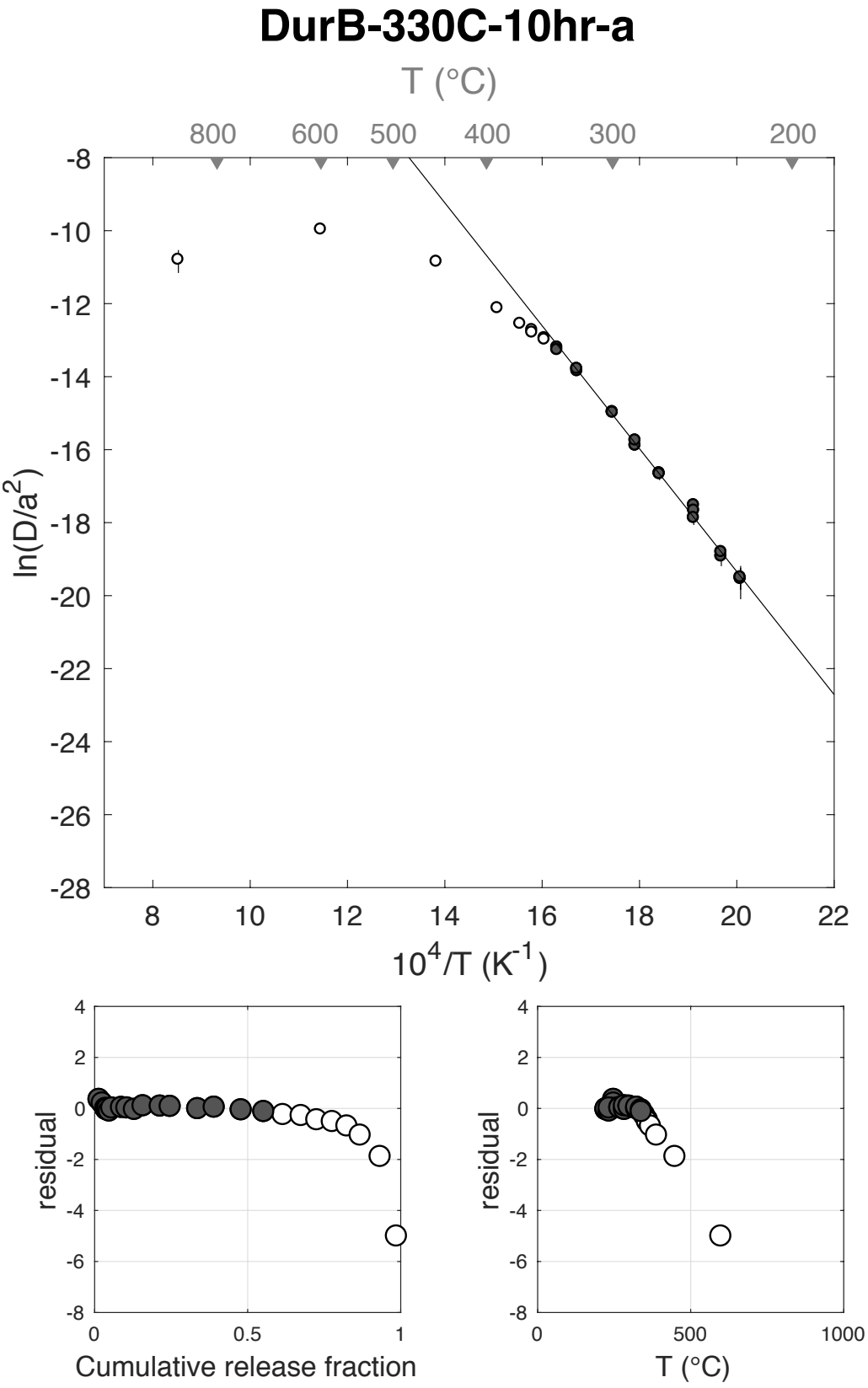
DurB-330C-10hr-a
T (°C)
800
600
500
400
300
200
-8
-10
-12
-14
-16
-18
-20
-22
-24
-26
-28
ln(D/a2)
8
10
12
14
16
18
20
22
10^4/T (K^-1)
4
2
0
-2
-4
-6
-8
residual
0
0.5
1
Cumulative release fraction
0
500
1000
T (°C)

DurB-330C-10hr-b

E_a	+/-	D_0	+/-	T_c	-	+	Total ^{3}He	Incl.	Misfit	Norm. Misfit
95.49	2.51	6.51	0.52	5.54	3.75	3.84	62.33	0.813	1.618	0.095

Step #	°C	t (hrs)	^{3}He	Error	^{4}He	Error	^{4}He/^{3}He	Err	In ^{3}He Reg.
1	250	0.25	4.49	0.28	247.3	24.1	45.1	0.12	1
2	250	0.50	2.04	0.21	123.1	25.0	50.3	0.23	1
3	250	1.00	2.33	0.23	116.2	20.7	39.8	0.20	1
4	225	1.50	0.61	0.12	16.4	16.9	16.9	1.05	1
5	225	2.50	0.80	0.12	3.7	23.3	NaN	NaN	1
6	200	3.00	0.05	0.08	0.0	0.0	NaN	NaN	0
7	200	4.00	0.01	0.08	0.0	0.0	NaN	NaN	0
8	235	2.00	1.04	0.15	31.7	20.7	20.5	0.67	1
9	235	3.00	1.15	0.16	9.1	20.5	NaN	NaN	1
10	270	1.91	4.31	0.27	223.9	20.0	42.0	0.11	1
11	270	1.57	2.21	0.23	129.1	23.6	48.5	0.21	1
12	285	1.25	2.87	0.24	191.6	21.8	56.6	0.14	1
13	285	1.56	2.91	0.25	212.3	20.9	63.0	0.13	1
14	300	1.91	5.19	0.37	431.4	30.1	73.2	0.10	1
15	300	1.45	2.63	0.22	259.1	22.5	88.5	0.12	1
16	325	1.74	6.06	0.33	727.3	33.0	110.1	0.07	1
17	325	1.32	3.21	0.24	475.8	31.4	138.2	0.10	1
18	340	1.58	4.87	0.29	817.3	40.7	157.7	0.08	1
19	340	1.89	3.94	0.30	738.2	40.5	177.4	0.09	1
20	350	1.48	2.95	0.21	637.3	39.3	206.2	0.09	0
21	350	1.82	2.42	0.22	648.6	35.5	258.1	0.11	0
22	360	1.50	1.77	0.18	477.6	33.6	259.1	0.13	0
23	360	1.98	1.38	0.19	417.5	32.3	293.6	0.16	0
24	370	1.88	0.99	0.13	353.4	26.6	345.6	0.15	0
25	390	1.47	0.70	0.15	329.8	28.7	460.4	0.22	0
26	450	1.00	0.93	0.14	588.7	36.6	621.8	0.16	0
27	600	1.00	0.46	0.10	591.4	36.7	1276.6	0.24	0
28	900	1.00	0.00	0.00	10.0	18.8	Inf	NaN	0
29	900	1.00	0.00	0.05	0.0	0.0	NaN	NaN	0

Figure S27

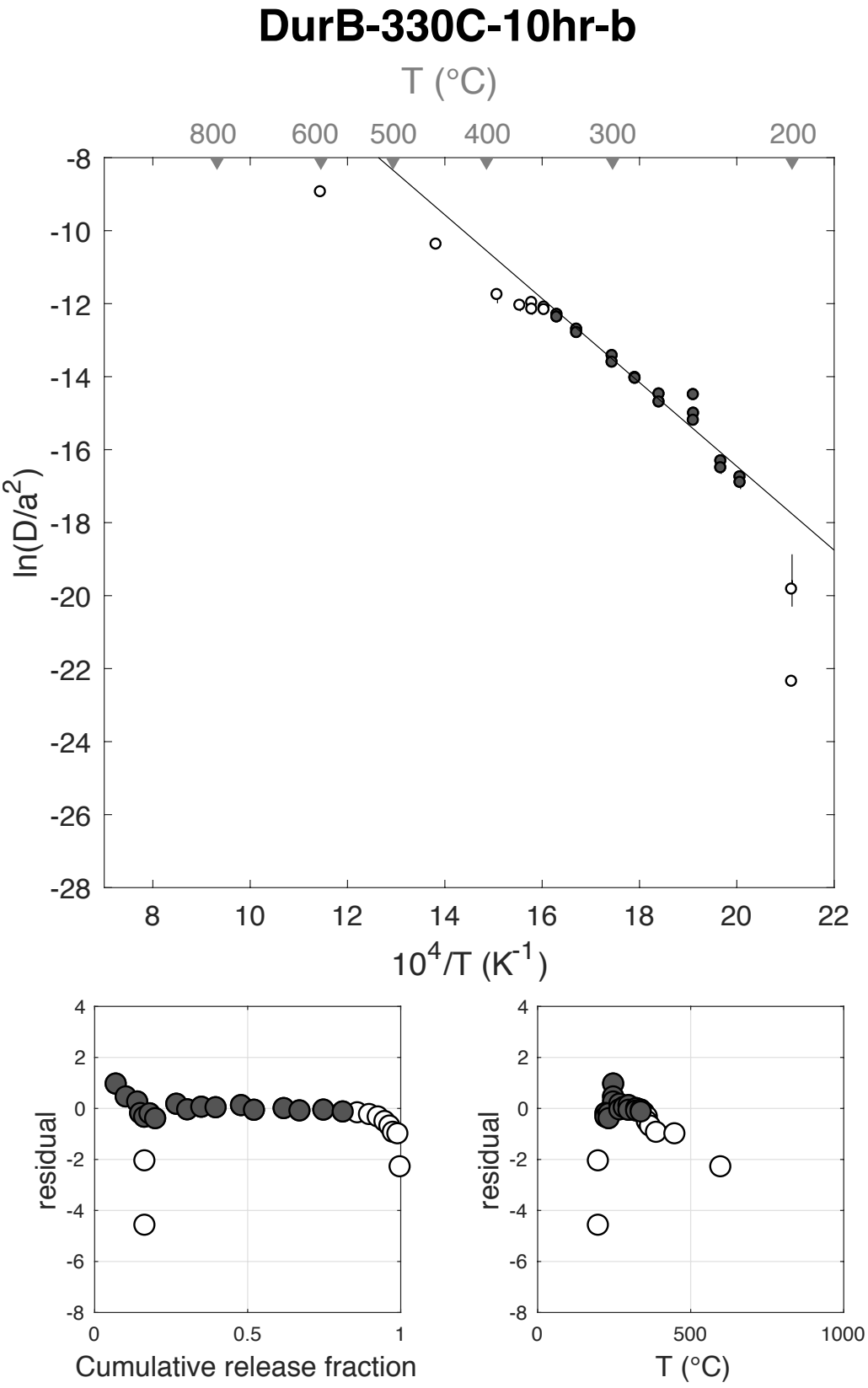
DurB-330C-10hr-b
T (°C)
800
600
500
400
300
200
-8
-10
-12
-14
-16
-18
-20
-22
-24
-26
-28
ln(D/a2)
8
10
12
14
16
18
20
22
10^4/T (K^-1)
4
2
0
-2
-4
-6
-8
residual
0
0.5
1
Cumulative release fraction
0
500
1000
T (°C)

DurB-345C-10hr-a

E_a	+/-	D_0	+/-	T_c	-	+	Total ^{3}He	Incl.	Misfit	Norm. Misfit
116.10	4.42	10.52	0.91	35.58	5.41	5.63	51.22	0.768	0.660	0.039

Step #	°C	t (hrs)	^{3}He	Error	^{4}He	Error	^{4}He/^{3}He	Err	In ^{3}He Reg.
1	250	0.25	1.81	0.22	40.1	19.9	12.1	0.51	1
2	250	0.50	1.05	0.17	18.4	18.0	7.5	0.99	1
3	250	1.00	1.29	0.20	14.7	21.2	1.4	1.46	1
4	225	1.50	0.40	0.12	0.0	0.0	NaN	NaN	1
5	225	2.50	0.57	0.15	0.0	0.0	NaN	NaN	1
6	200	3.00	0.08	0.11	0.0	0.0	NaN	NaN	0
7	200	4.00	0.04	0.13	0.0	0.0	NaN	NaN	0
8	235	2.00	0.74	0.15	0.0	0.0	NaN	NaN	1
9	235	3.00	0.89	0.19	0.0	0.0	NaN	NaN	1
10	270	1.91	3.45	0.32	38.7	23.8	1.2	0.62	1
11	270	1.57	1.87	0.26	25.7	18.2	3.7	0.72	1
12	285	1.25	2.48	0.30	41.3	19.1	6.7	0.48	1
13	285	1.56	2.64	0.25	44.0	21.9	6.7	0.51	1
14	300	1.91	4.55	0.36	82.8	30.9	8.2	0.38	1
15	300	1.45	2.25	0.27	61.1	20.7	17.2	0.36	1
16	325	1.74	5.93	0.37	180.2	24.6	20.4	0.15	1
17	325	1.32	2.52	0.28	108.1	24.1	32.9	0.25	1
18	340	1.58	3.73	0.32	167.4	27.7	34.9	0.19	1
19	340	1.89	3.19	0.29	167.6	28.4	42.5	0.19	1
20	350	1.48	2.10	0.26	161.1	23.4	66.7	0.19	0
21	350	1.82	1.56	0.23	155.4	28.6	89.9	0.24	0
22	360	1.50	1.08	0.19	144.4	25.8	123.5	0.25	0
23	360	1.98	0.81	0.15	152.4	30.4	178.5	0.28	0
24	370	1.88	0.58	0.13	143.1	29.4	238.4	0.31	0
25	390	1.47	0.46	0.12	173.8	22.2	365.3	0.30	0
26	450	1.00	0.79	0.15	476.7	34.1	590.1	0.20	0
27	600	1.00	2.30	0.25	1791.4	96.7	769.2	0.12	0
28	900	1.00	2.05	0.26	1726.0	95.7	830.6	0.14	0
29	900	0.76	0.01	0.06	3.4	17.6	234.1	6.62	0

Figure S28

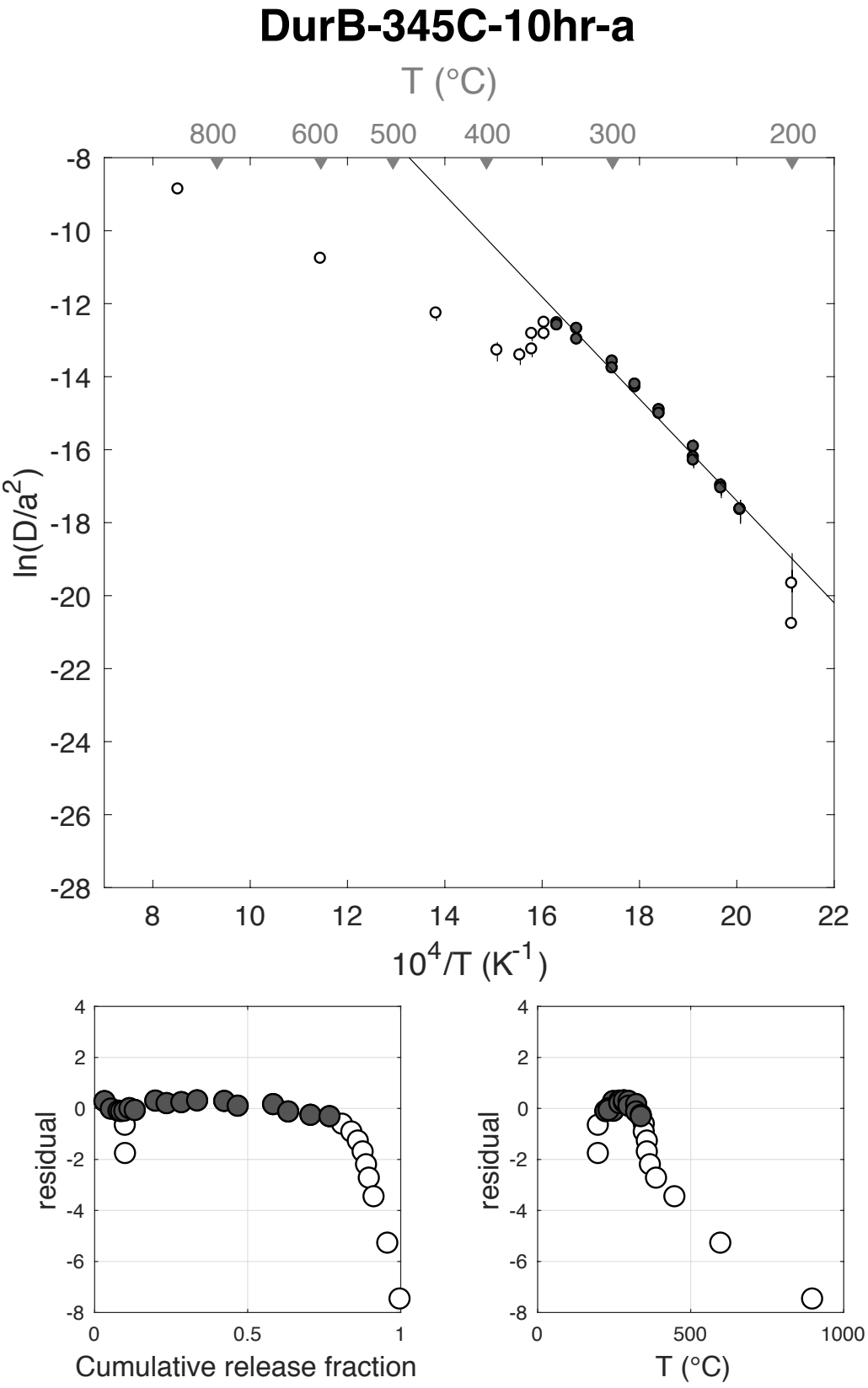
DurB-345C-10hr-a
T (°C)
800
600
500
400
300
200
-8
-10
-12
-14
-16
-18
-20
-22
-24
-26
-28
ln(D/a2)
8
10
12
14
16
18
20
22
10^4/T (K^-1)
4
2
0
-2
-4
-6
-8
residual
0
0.5
1
Cumulative release fraction
0
500
1000
T (°C)

DurB-400C-10hr-a

E_a	+/-	D_0	+/-	T_c	-	+	Total ^{3}He	Incl.	Misfit	Norm. Misfit
122.97	2.37	10.77	0.49	51.72	2.77	2.83	222.47	0.523	0.121	0.007

Step #	°C	t (hrs)	^{3}He	Error	^{4}He	Error	^{4}He/^{3}He	Err	In ^{3}He Reg.
1	250	0.25	4.00	0.30	36.9	18.1	NaN	NaN	1
2	250	0.50	2.64	0.24	34.7	14.4	3.2	0.42	1
3	250	1.00	3.28	0.29	60.1	18.2	8.3	0.32	1
4	225	1.50	0.88	0.16	14.3	24.9	6.2	1.75	1
5	225	2.50	1.23	0.19	29.3	32.2	13.8	1.11	1
6	200	3.00	0.22	0.11	0.0	0.0	NaN	NaN	0
7	200	4.00	0.25	0.14	0.0	0.0	NaN	NaN	0
8	235	2.00	1.56	0.21	52.8	27.1	23.8	0.53	1
9	235	3.00	1.96	0.25	58.9	42.1	20.0	0.73	1
10	270	1.91	6.77	0.41	196.6	27.1	19.1	0.15	1
11	270	1.57	4.24	0.31	155.5	20.7	26.6	0.15	1
12	285	1.25	5.94	0.37	220.7	17.4	27.1	0.10	1
13	285	1.57	6.04	0.40	277.0	24.3	35.9	0.11	1
14	300	1.91	11.14	0.55	583.4	26.9	42.4	0.07	1
15	300	1.45	7.07	0.41	409.9	21.3	48.0	0.08	1
16	325	1.74	17.49	0.65	1261.9	27.5	62.2	0.04	1
17	325	1.32	10.29	0.47	901.6	24.2	77.6	0.05	1
18	340	1.58	16.50	0.60	1724.4	27.0	94.5	0.04	1
19	340	1.89	15.22	0.64	1874.5	29.6	113.2	0.05	1
20	350	1.48	13.09	0.54	1816.7	25.9	128.8	0.04	0
21	350	1.82	13.14	0.45	1978.7	32.5	140.6	0.04	0
22	360	1.50	11.84	0.51	1935.6	26.0	153.4	0.04	0
23	360	1.98	12.18	0.55	2128.9	36.1	164.8	0.05	0
24	370	1.88	11.83	0.58	2213.8	35.4	177.1	0.05	0
25	390	1.47	11.90	0.56	2419.2	30.3	193.2	0.05	0
26	450	1.00	19.87	0.65	4752.7	36.4	229.2	0.03	0
27	600	1.00	11.89	0.56	3642.2	36.2	296.5	0.05	0
28	900	1.00	0.00	0.00	0.0	0.0	NaN	NaN	0
29	900	1.00	0.00	0.07	8.7	18.0	2862.2	23.57	0

Figure S29

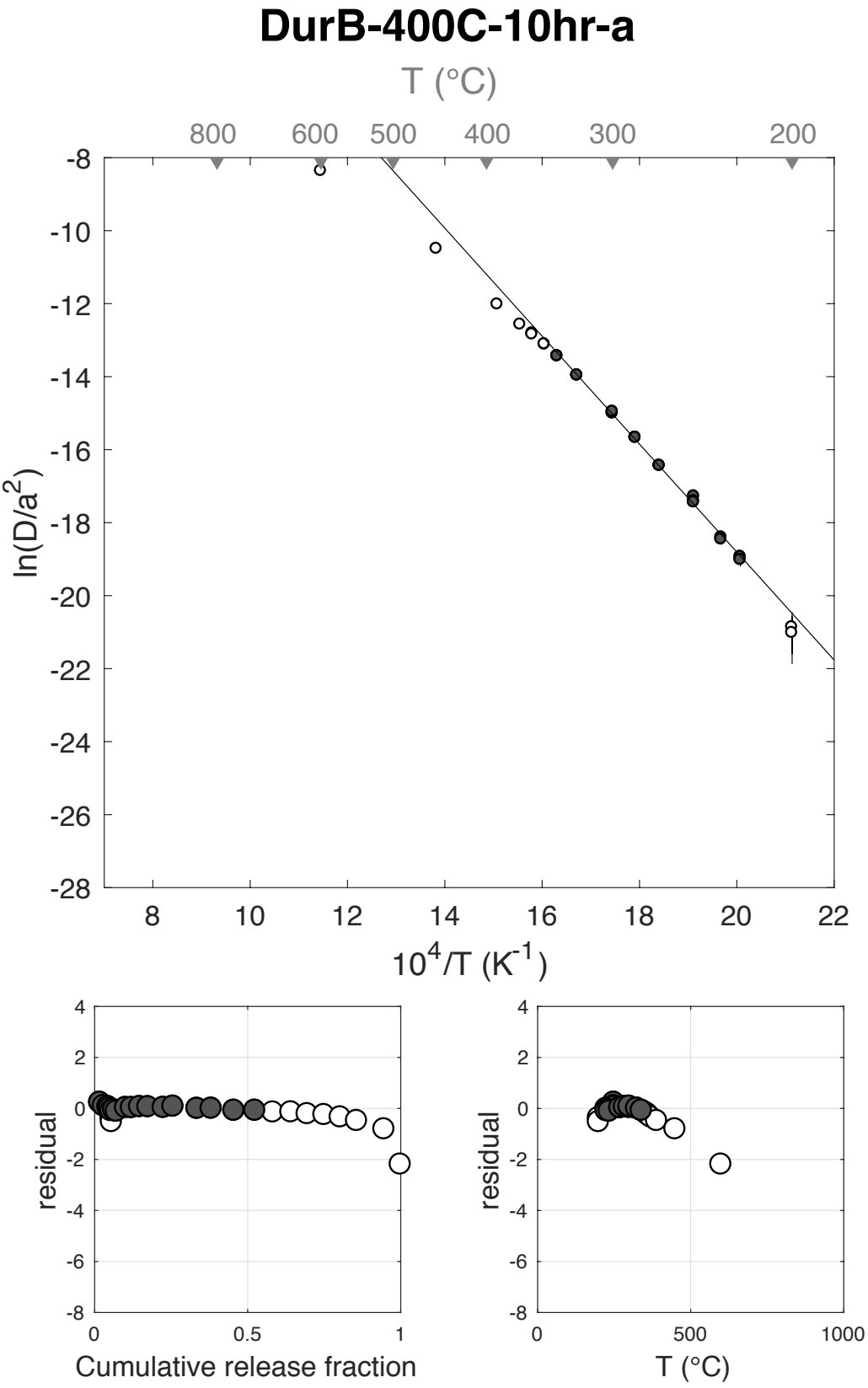
DurB-400C-10hr-a
T (°C)
800
600
500
400
300
200
-8
-10
-12
-14
-16
-18
-20
-22
-24
-26
-28
ln(D/a2)
8
10
12
14
16
18
20
22
10^4/T (K^-1)
4
2
0
-2
-4
-6
-8
residual
0
0.5
1
Cumulative release fraction
0
500
1000
T (°C)

DurB-400C-10hr-b

E_a	+/-	D_0	+/-	T_c	-	+	Total ^{3}He	Incl.	Misfit	Norm. Misfit
126.60	9.15	12.36	1.89	50.33	10.04	10.86	58.45	0.714	0.402	0.024

Step #	°C	t (hrs)	^{3}He	Error	^{4}He	Error	^{4}He/^{3}He	Err	In ^{3}He Reg.
1	250	0.25	1.60	0.37	19.7	7.2	2.3	0.43	1
2	250	0.50	1.05	0.30	15.3	6.1	4.5	0.49	1
3	250	1.00	1.33	0.33	13.9	6.4	0.5	0.52	1
4	225	1.50	0.29	0.19	7.2	6.2	14.3	1.08	1
5	225	2.50	0.43	0.20	9.1	13.1	10.9	1.51	1
6	200	3.00	0.05	0.14	3.2	15.9	48.5	5.62	0
7	200	4.00	0.10	0.16	3.1	22.3	21.1	7.43	0
8	235	2.00	0.66	0.26	10.4	9.3	5.8	0.97	1
9	235	3.00	0.85	0.27	13.8	15.7	6.3	1.18	1
10	270	1.91	2.57	0.50	29.9	11.0	1.6	0.42	1
11	270	1.57	1.79	0.41	19.2	7.4	0.7	0.45	1
12	285	1.25	2.40	0.42	27.7	9.1	1.5	0.37	1
13	285	1.56	1.89	0.47	28.4	9.8	5.0	0.43	1
14	300	1.91	4.35	0.60	52.8	10.8	2.1	0.25	1
15	300	1.45	2.94	0.49	35.2	8.0	2.0	0.28	1
16	325	1.74	5.69	0.75	88.1	10.5	5.5	0.18	1
17	325	1.32	3.32	0.51	51.9	8.8	5.6	0.23	1
18	340	1.58	6.36	0.73	85.6	10.7	3.5	0.17	1
19	340	1.89	4.19	0.71	82.9	11.3	9.8	0.22	1
20	350	1.48	3.31	0.52	62.4	10.5	8.8	0.23	0
21	350	1.82	3.23	0.54	66.2	9.9	10.5	0.22	0
22	360	1.50	2.20	0.45	52.2	8.1	13.8	0.26	0
23	360	1.98	2.01	0.42	56.7	12.2	18.2	0.30	0
24	370	1.88	1.51	0.33	54.0	10.3	25.7	0.29	0
25	390	1.47	1.11	0.34	61.8	9.2	45.7	0.34	0
26	450	1.00	1.99	0.39	192.7	10.3	86.9	0.20	0
27	600	1.00	1.21	0.36	330.5	21.3	262.3	0.31	0
28	900	1.00	0.00	0.00	25.2	5.9	Inf	NaN	0
29	900	1.00	0.00	0.00	0.0	0.0	NaN	NaN	0

Figure S30

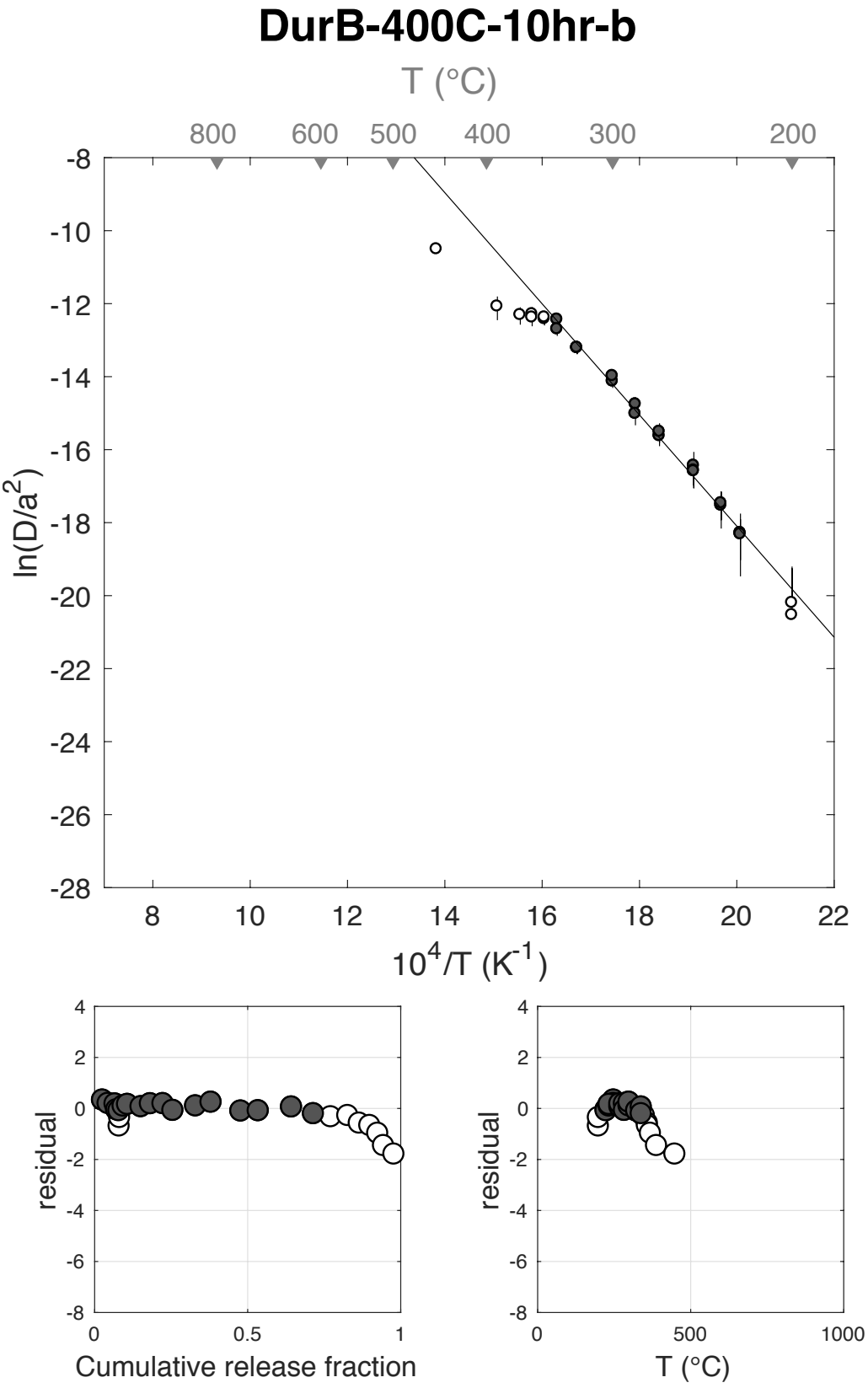
DurB-400C-10hr-b
T (°C)
800
600
500
400
300
200
-8
-10
-12
-14
-16
-18
-20
-22
-24
-26
-28
ln(D/a2)
8
10
12
14
16
18
20
22
10^4/T (K^-1)
4
2
0
-2
-4
-6
-8
residual
0
0.5
1
Cumulative release fraction
500
1000
T (°C)

DurB-450C-10hr-a

E_a	+/-	D_0	+/-	T_c	-	+	Total ^{3}He	Incl.	Misfit	Norm. Misfit
134.99	7.43	13.18	1.57	65.65	7.36	7.85	123.77	0.513	0.191	0.010

Step #	°C	t (hrs)	^{3}He	Error	^{4}He	Error	^{4}He/^{3}He	Err	In ^{3}He Reg.
1	250	0.25	1.72	0.19	13.4	20.9	NaN	NaN	1
2	250	0.50	1.28	0.16	18.2	14.2	4.2	0.79	1
3	250	1.00	1.58	0.18	27.5	17.6	7.4	0.65	1
4	225	1.50	0.42	0.11	0.0	0.0	NaN	NaN	1
5	225	2.50	0.61	0.13	11.4	26.9	8.7	2.38	1
6	200	3.00	0.12	0.09	0.0	0.0	NaN	NaN	1
7	200	4.00	0.15	0.11	2.0	39.5	3.9	19.56	1
8	235	2.00	0.73	0.15	10.9	20.6	4.9	1.89	1
9	235	3.00	0.94	0.17	10.9	28.8	1.5	2.65	1
10	270	1.91	3.73	0.31	42.2	17.1	1.3	0.41	1
11	270	1.57	2.21	0.20	23.1	15.7	0.4	0.68	1
12	285	1.25	3.08	0.26	32.7	16.8	0.6	0.52	1
13	285	1.57	3.29	0.30	43.9	19.1	3.3	0.44	1
14	300	1.91	6.54	0.39	72.5	21.4	1.1	0.30	1
15	300	1.45	4.04	0.33	48.3	18.5	2.0	0.39	1
16	325	1.74	9.20	0.71	103.2	19.3	1.2	0.20	1
17	325	1.32	5.84	0.33	62.4	19.2	0.7	0.31	1
18	340	1.58	9.29	0.45	97.7	22.5	0.5	0.24	1
19	340	1.89	8.66	0.47	85.3	19.3	NaN	NaN	1
20	350	1.48	7.05	0.41	88.8	18.1	2.6	0.21	0
21	350	1.82	6.50	0.35	79.6	17.6	2.2	0.23	0
22	360	1.50	5.73	0.36	70.2	17.7	2.3	0.26	0
23	360	1.98	6.34	0.39	78.4	21.4	2.4	0.28	0
24	370	1.88	6.52	0.41	87.9	19.4	3.5	0.23	0
25	390	1.47	6.72	0.40	92.2	14.4	3.7	0.17	0
26	450	1.00	11.82	0.46	212.3	18.8	8.0	0.10	0
27	600	1.00	9.53	0.42	1110.4	22.6	106.5	0.05	0
28	900	1.00	0.13	0.09	118.6	17.8	904.5	0.71	0
29	900	1.00	0.00	0.00	4.1	12.4	Inf	NaN	0

Figure S31

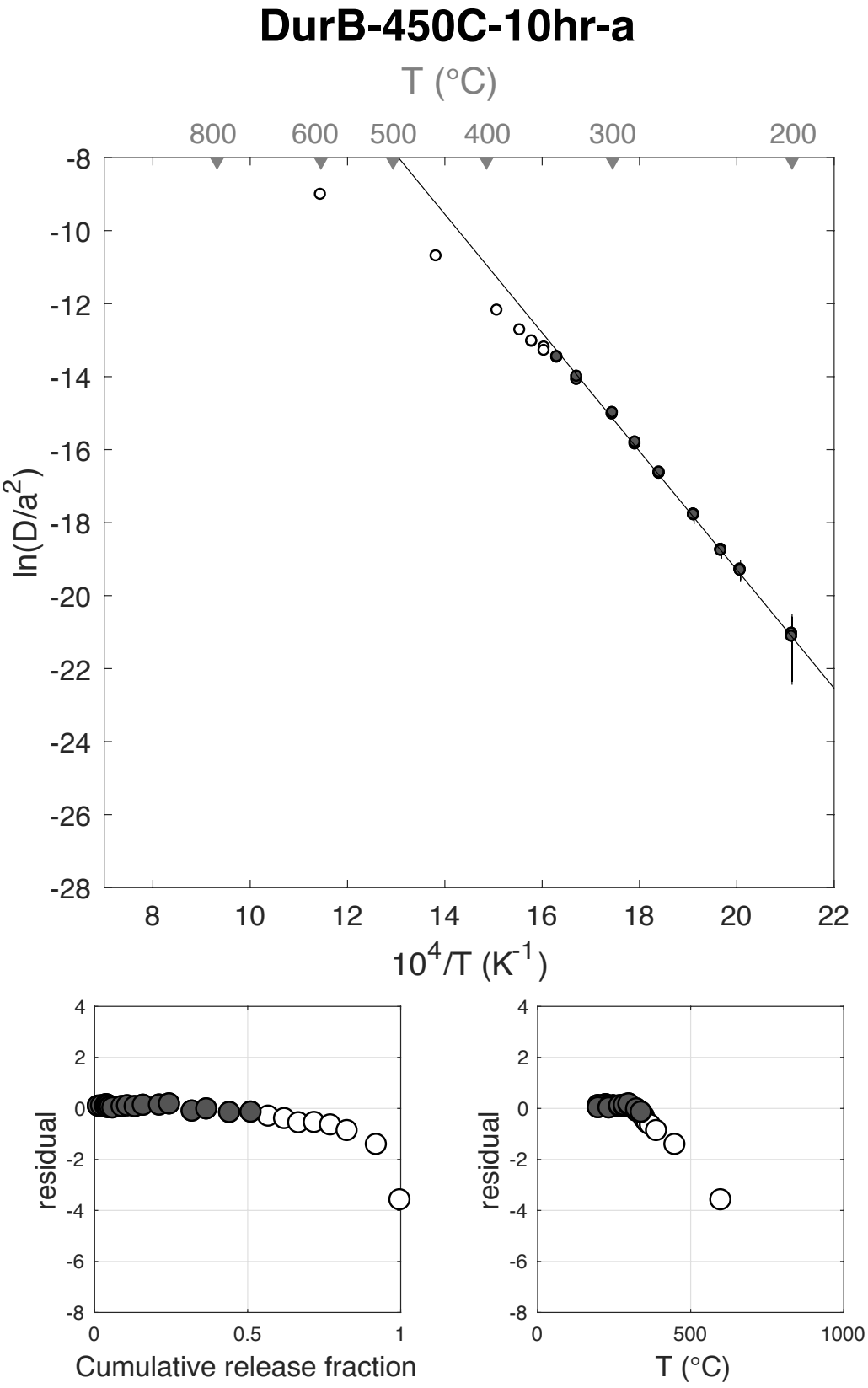
DurB-450C-10hr-a
T (°C)
800
600
500
400
300
200
-8
-10
-12
-14
-16
-18
-20
-22
-24
-26
-28
ln(D/a²)
8
10
12
14
16
18
20
22
10⁴/T (K⁻¹)
4
2
0
-2
-4
-6
-8
residual
0
0.5
1
Cumulative release fraction
500
1000
T (°C)

DurB-450C-10hr-b

E_a	+/-	D_0	+/-	T_c	-	+	Total ^{3}He	Incl.	Misfit	Norm. Misfit
123.93	9.40	10.57	1.94	55.62	10.51	11.43	89.04	0.436	0.525	0.033

Step #	°C	t (hrs)	^{3}He	Error	^{4}He	Error	^{4}He/^{3}He	Err	In ^{3}He Reg.
1	250	0.25	1.26	0.29	25.7	6.4	10.4	0.34	1
2	250	0.50	1.03	0.28	17.9	6.6	7.5	0.46	1
3	250	1.00	1.17	0.29	36.0	6.4	20.7	0.30	1
4	225	1.50	0.29	0.15	13.1	7.5	34.6	0.76	1
5	225	2.50	0.34	0.21	37.1	9.1	98.4	0.67	0
6	200	3.00	0.00	0.00	28.6	10.7	Inf	NaN	0
7	200	4.00	0.00	0.00	38.0	11.8	Inf	NaN	0
8	235	2.00	0.55	0.20	25.6	6.9	36.6	0.46	1
9	235	3.00	0.56	0.30	37.2	9.7	56.2	0.60	1
10	270	1.91	1.93	0.46	48.9	10.4	15.3	0.32	1
11	270	1.57	1.80	0.35	30.0	7.3	6.7	0.31	1
12	285	1.25	1.96	0.43	34.6	6.8	7.6	0.30	1
13	285	1.56	2.14	0.41	39.6	10.0	8.5	0.32	1
14	300	1.91	3.93	0.56	68.2	9.0	7.3	0.19	1
15	300	1.45	2.65	0.43	36.9	6.5	4.0	0.24	1
16	325	1.74	6.27	0.83	97.7	11.2	5.6	0.17	1
17	325	1.32	3.56	0.51	57.0	6.1	6.0	0.18	1
18	340	1.58	5.21	0.68	96.0	10.7	8.4	0.17	1
19	340	1.89	4.48	0.57	100.0	10.6	12.3	0.17	1
20	350	1.48	4.09	0.63	86.5	10.6	11.2	0.20	0
21	350	1.82	3.79	0.62	88.4	12.7	13.3	0.22	0
22	360	1.50	3.60	0.58	93.0	9.5	15.8	0.19	0
23	360	1.98	3.48	0.54	113.2	9.7	22.6	0.18	0
24	370	1.88	3.25	0.52	138.3	10.8	32.6	0.18	0
25	390	1.47	3.94	0.57	179.7	9.7	35.6	0.15	0
26	450	1.00	7.51	0.75	498.6	21.9	56.4	0.11	0
27	600	1.00	16.06	1.18	12351.9	117.5	759.3	0.07	0
28	900	1.00	4.19	0.59	5518.4	71.5	1305.5	0.14	0
29	900	1.00	0.00	0.00	1.8	5.8	Inf	NaN	0

Figure S32

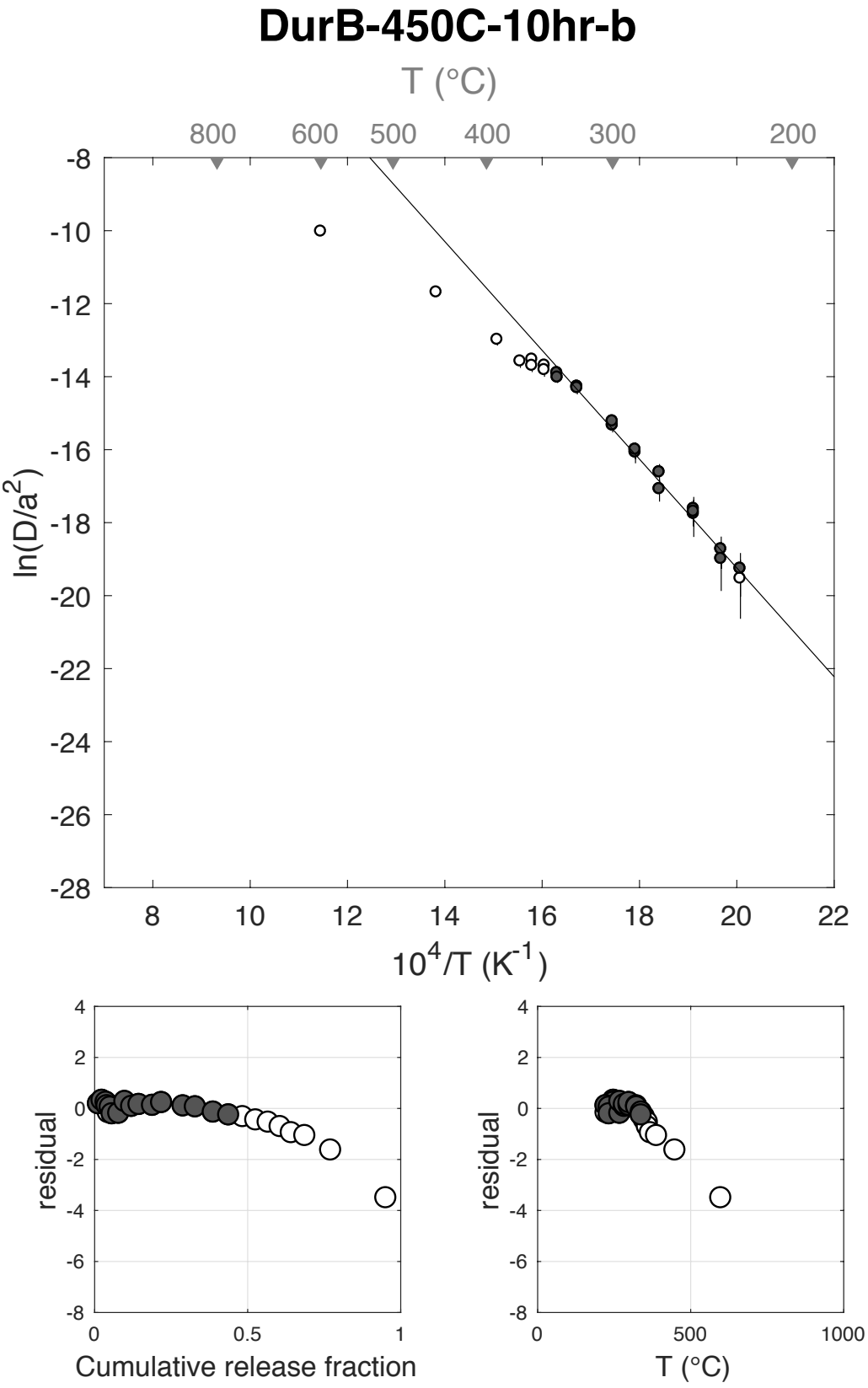
DurB-450C-10hr-b
T (°C)
800
600
500
400
300
200
-8
-10
-12
-14
-16
-18
-20
-22
-24
-26
-28
ln(D/a2)
8
10
12
14
16
18
20
22
10^4/T (K^-1)
4
2
0
-2
-4
-6
-8
residual
0
0.5
1
Cumulative release fraction
0
500
1000
T (°C)

DurB-275C-100hr-a

E_a	+/-	D_0	+/-	T_c	-	+	Total ^{3}He	Incl.	Misfit	Norm. Misfit
143.07	6.21	15.36	1.30	70.50	5.89	6.20	81.26	0.616	0.399	0.025

Step #	°C	t (hrs)	^{3}He	Error	^{4}He	Error	^{4}He/^{3}He	Err	In ^{3}He Reg.
1	250	0.25	1.26	0.20	9.6	23.5	NaN	NaN	1
2	250	0.50	0.86	0.16	10.5	14.5	2.2	1.39	1
3	250	1.00	0.95	0.19	30.5	17.4	22.3	0.60	1
4	225	1.50	0.33	0.13	8.4	24.7	15.9	2.96	1
5	225	2.50	0.51	0.15	14.9	43.7	19.3	2.94	1
6	200	3.00	0.12	0.10	0.0	0.0	NaN	NaN	0
7	200	4.00	0.14	0.11	0.0	0.0	NaN	NaN	0
8	235	2.00	0.53	0.13	15.2	34.5	18.9	2.28	1
9	235	3.00	0.85	0.16	27.4	57.1	22.4	2.09	1
10	270	1.91	3.16	0.34	177.3	37.2	46.1	0.24	1
11	270	1.57	1.87	0.26	144.5	32.0	67.4	0.26	1
12	285	1.25	2.57	0.30	247.4	32.0	86.3	0.17	1
13	285	1.56	2.78	0.28	356.8	39.8	118.3	0.15	1
14	300	1.91	5.51	1.67	854.9	64.6	145.2	0.31	1
15	300	1.45	3.50	0.31	642.1	47.8	173.5	0.12	1
16	325	1.74	9.24	0.73	2242.1	144.4	232.5	0.10	1
17	325	1.32	0.00	0.00	0.0	0.0	NaN	NaN	0
18	340	1.58	7.71	0.45	2800.3	153.3	353.1	0.08	1
19	340	1.89	8.44	0.51	3716.2	215.2	430.5	0.08	1
20	350	1.48	5.72	0.38	3047.4	194.3	522.6	0.09	0
21	350	1.82	6.54	0.47	3461.1	213.2	519.2	0.09	0
22	360	1.50	5.03	0.33	3005.2	197.5	586.9	0.09	0
23	360	1.98	4.04	1.30	2738.4	176.1	668.5	0.33	0
24	370	1.88	3.48	0.30	2370.6	152.8	671.7	0.11	0
25	390	1.47	2.83	0.29	2170.0	136.9	757.7	0.12	0
26	450	1.00	2.19	0.29	2096.8	131.4	946.2	0.15	0
27	600	1.00	1.05	0.17	1252.2	89.8	1178.2	0.18	0
28	900	1.00	0.05	0.08	63.4	22.1	1256.8	1.58	0
29	900	1.00	0.00	0.07	0.0	0.0	NaN	NaN	0

Figure S33

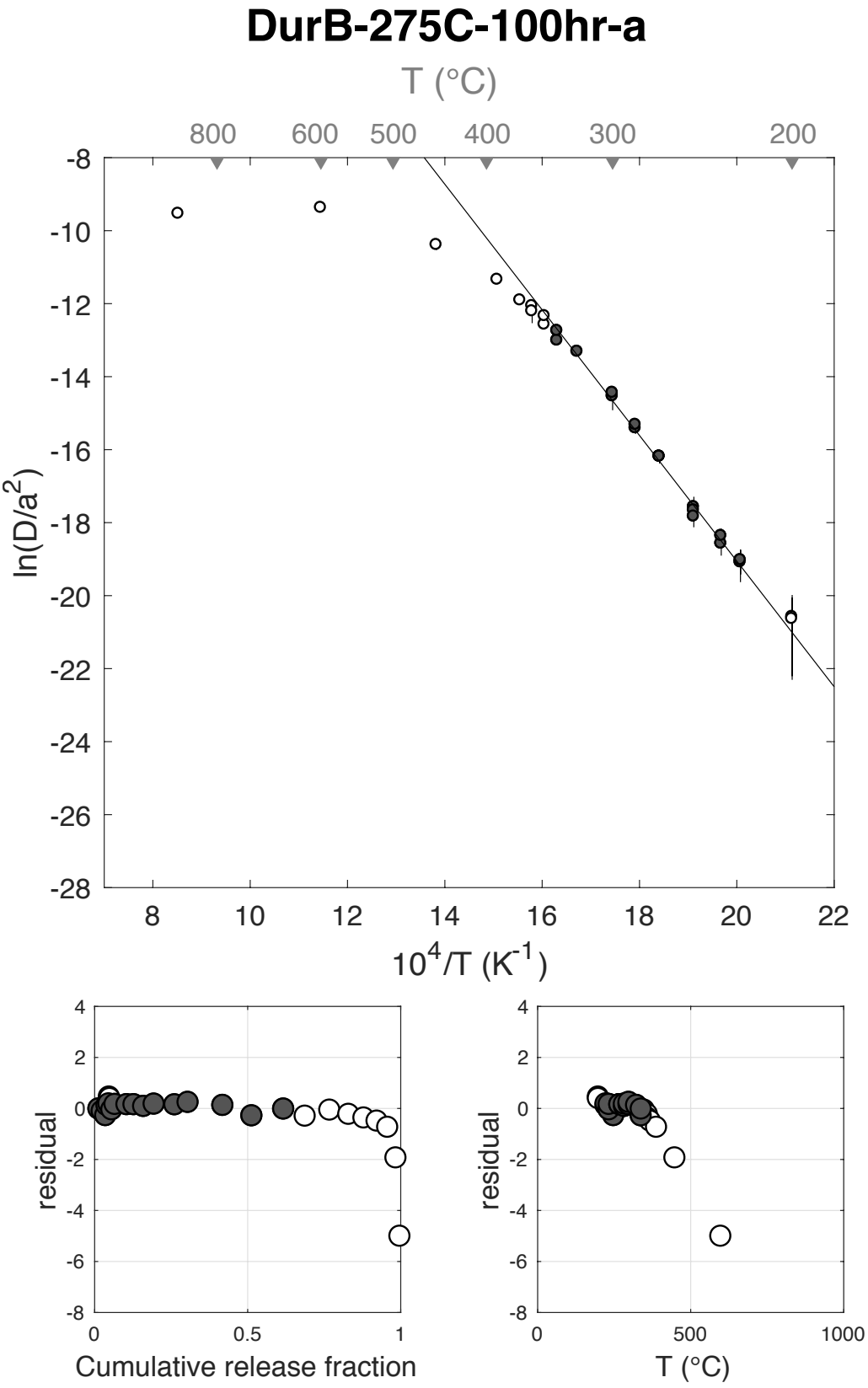
DurB-275C-100hr-a
T (°C)
800
600
500
400
300
200
-8
-10
-12
-14
-16
-18
-20
-22
-24
-26
-28
ln(D/a2)
8
10
12
14
16
18
20
22
10^4/T (K^-1)
4
2
0
-2
-4
-6
-8
residual
0
0.5
1
Cumulative release fraction
0
500
1000
T (°C)

DurB-275C-100hr-c

E_a	+/-	D_0	+/-	T_c	-	+	Total ^{3}He	Incl.	Misfit	Norm. Misfit
138.87	10.84	14.16	2.23	68.52	10.68	11.68	73.04	0.575	0.473	0.028

Step #	°C	t (hrs)	^{3}He	Error	^{4}He	Error	^{4}He/^{3}He	Err	In ^{3}He Reg.
1	250	0.25	1.15	0.31	22.8	7.8	9.8	0.44	1
2	250	0.50	0.85	0.32	21.0	7.5	14.7	0.52	1
3	250	1.00	1.08	0.28	29.6	7.7	17.4	0.37	1
4	225	1.50	0.20	0.14	14.2	8.1	61.9	0.92	1
5	225	2.50	0.36	0.23	12.7	12.6	25.2	1.18	1
6	200	3.00	0.04	0.18	6.2	16.5	159.6	5.62	0
7	200	4.00	0.09	0.25	10.4	23.1	108.8	3.64	0
8	235	2.00	0.57	0.24	21.7	10.3	28.2	0.63	1
9	235	3.00	0.60	0.30	33.5	16.9	45.6	0.71	1
10	270	1.91	1.84	0.40	130.3	13.0	60.9	0.24	1
11	270	1.57	1.34	0.37	81.7	12.1	51.1	0.31	1
12	285	1.25	1.90	0.45	170.2	12.3	79.4	0.25	1
13	285	1.56	1.86	0.39	213.6	16.4	104.6	0.22	1
14	300	1.91	4.57	0.65	536.8	22.2	107.6	0.15	1
15	300	1.45	2.72	0.55	396.7	18.2	135.8	0.21	1
16	325	1.74	6.73	0.78	1425.5	38.7	201.8	0.12	1
17	325	1.32	3.32	0.59	984.5	28.5	286.6	0.18	1
18	340	1.58	6.60	0.95	1972.6	47.2	288.7	0.15	1
19	340	1.89	6.32	0.70	2128.6	35.3	326.7	0.11	1
20	350	1.48	4.86	0.74	2060.0	49.7	413.7	0.15	0
21	350	1.82	4.97	0.78	2145.4	42.6	421.5	0.16	0
22	360	1.50	4.08	0.62	2087.4	50.6	501.8	0.15	0
23	360	1.98	4.19	0.58	2215.9	44.4	518.9	0.14	0
24	370	1.88	4.09	0.60	2115.5	55.3	507.4	0.15	0
25	390	1.47	3.34	0.59	1942.4	30.7	571.1	0.18	0
26	450	1.00	4.04	0.64	2471.4	54.9	602.4	0.16	0
27	600	1.00	1.32	0.35	818.8	34.4	608.5	0.27	0
28	900	1.00	0.00	0.08	11.3	5.8	3612.3	24.67	0
29	900	1.00	0.01	0.08	0.0	0.0	NaN	NaN	0

Figure S34

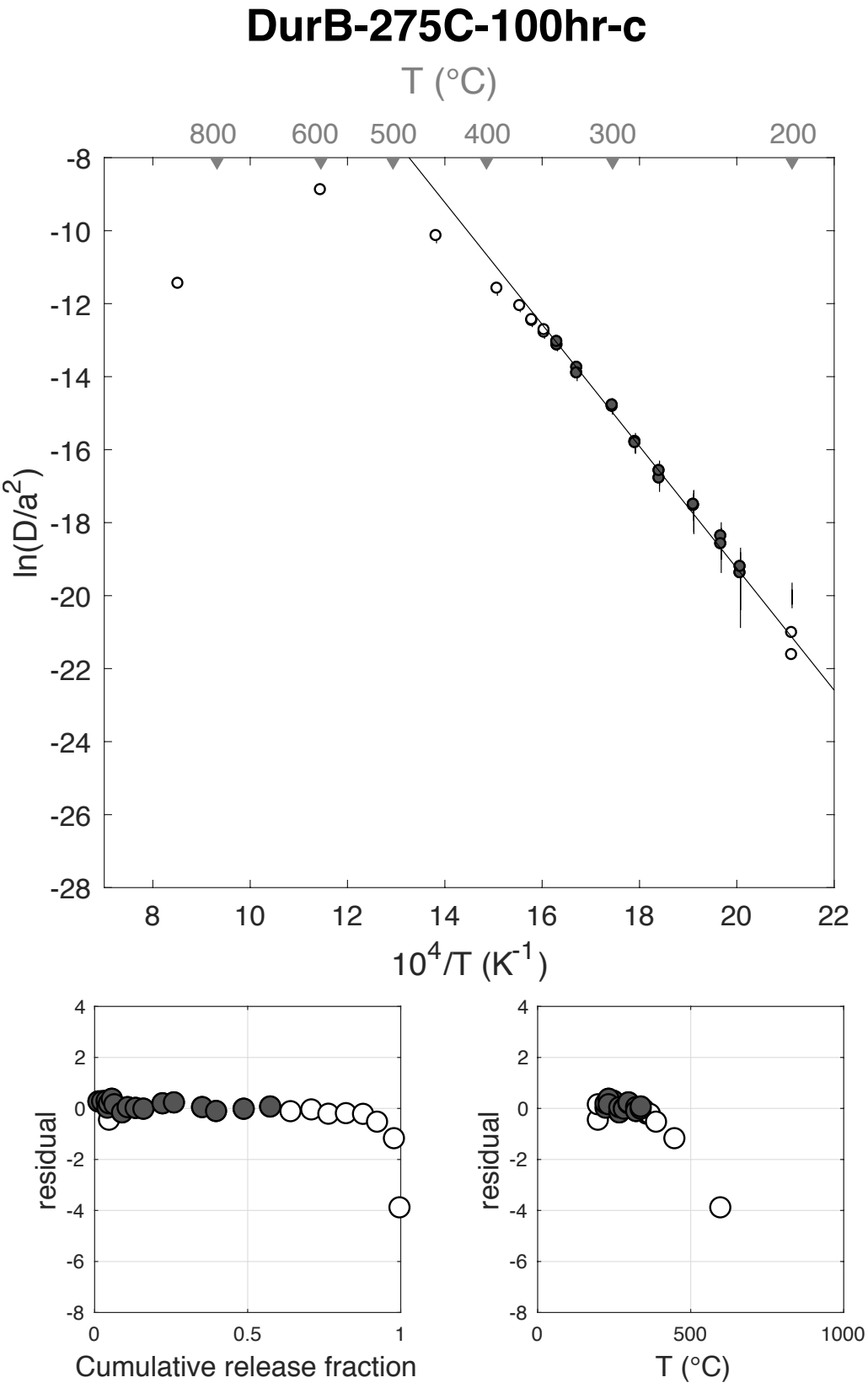
DurB-275C-100hr-c
T (°C)
800
600
500
400
300
200
-8
-10
-12
-14
-16
-18
-20
-22
-24
-26
-28
ln(D/a2)
8
10
12
14
16
18
20
22
10^4/T (K^-1)
4
2
0
-2
-4
-6
-8
residual
0
0.5
1
Cumulative release fraction
500
1000
T (°C)

DurB-300C-100hr-b

E_a	+/-	D_0	+/-	T_c	-	+	Total ^{3}He	Incl.	Misfit	Norm. Misfit
127.91	4.01	13.36	0.83	47.08	4.48	4.63	56.08	0.864	0.994	0.058

Step #	°C	t (hrs)	^{3}He	Error	^{4}He	Error	^{4}He/^{3}He	Err	In ^{3}He Reg.
1	250	0.25	1.97	0.21	21.8	20.3	1.1	0.94	1
2	250	0.50	1.36	0.16	8.7	24.7	NaN	NaN	1
3	250	1.00	1.55	0.18	8.2	21.2	NaN	NaN	1
4	225	1.50	0.49	0.11	1.7	19.6	NaN	NaN	1
5	225	2.50	0.70	0.13	0.0	0.0	NaN	NaN	1
6	200	3.00	0.15	0.08	0.0	0.0	NaN	NaN	0
7	200	4.00	0.17	0.08	0.0	0.0	NaN	NaN	0
8	235	2.00	0.83	0.15	6.6	24.6	NaN	NaN	1
9	235	3.00	0.55	0.21	0.0	0.0	NaN	NaN	1
10	270	1.91	3.85	0.29	23.5	26.7	NaN	NaN	1
11	270	1.57	2.49	0.25	20.5	23.2	NaN	NaN	1
12	285	1.25	3.25	0.25	30.1	24.6	NaN	NaN	1
13	285	1.56	3.33	0.31	37.4	22.7	1.2	0.61	1
14	300	1.91	6.12	0.34	77.4	26.5	2.6	0.35	1
15	300	1.45	3.36	0.26	27.9	24.6	NaN	NaN	1
16	325	1.74	7.60	0.50	128.8	24.1	6.9	0.20	1
17	325	1.32	3.41	0.23	73.1	20.4	11.4	0.29	1
18	340	1.58	4.59	0.32	142.0	25.4	20.9	0.19	1
19	340	1.89	3.02	0.25	152.7	26.2	40.6	0.19	1
20	350	1.48	1.61	0.18	125.3	22.5	67.7	0.21	0
21	350	1.82	1.32	0.17	156.9	26.3	108.6	0.21	0
22	360	1.50	0.89	0.15	152.1	23.2	160.2	0.23	0
23	360	1.98	0.72	0.13	186.9	26.5	248.8	0.22	0
24	370	1.88	0.59	0.10	220.5	24.3	362.0	0.20	0
25	390	1.47	0.55	0.13	283.5	26.6	506.2	0.25	0
26	450	1.00	0.85	0.15	610.3	34.0	705.8	0.18	0
27	600	1.00	0.74	0.13	618.6	37.2	822.6	0.18	0
28	900	1.00	0.01	0.05	0.0	0.0	NaN	NaN	0
29	900	1.00	0.01	0.05	0.0	0.0	NaN	NaN	0

Figure S35

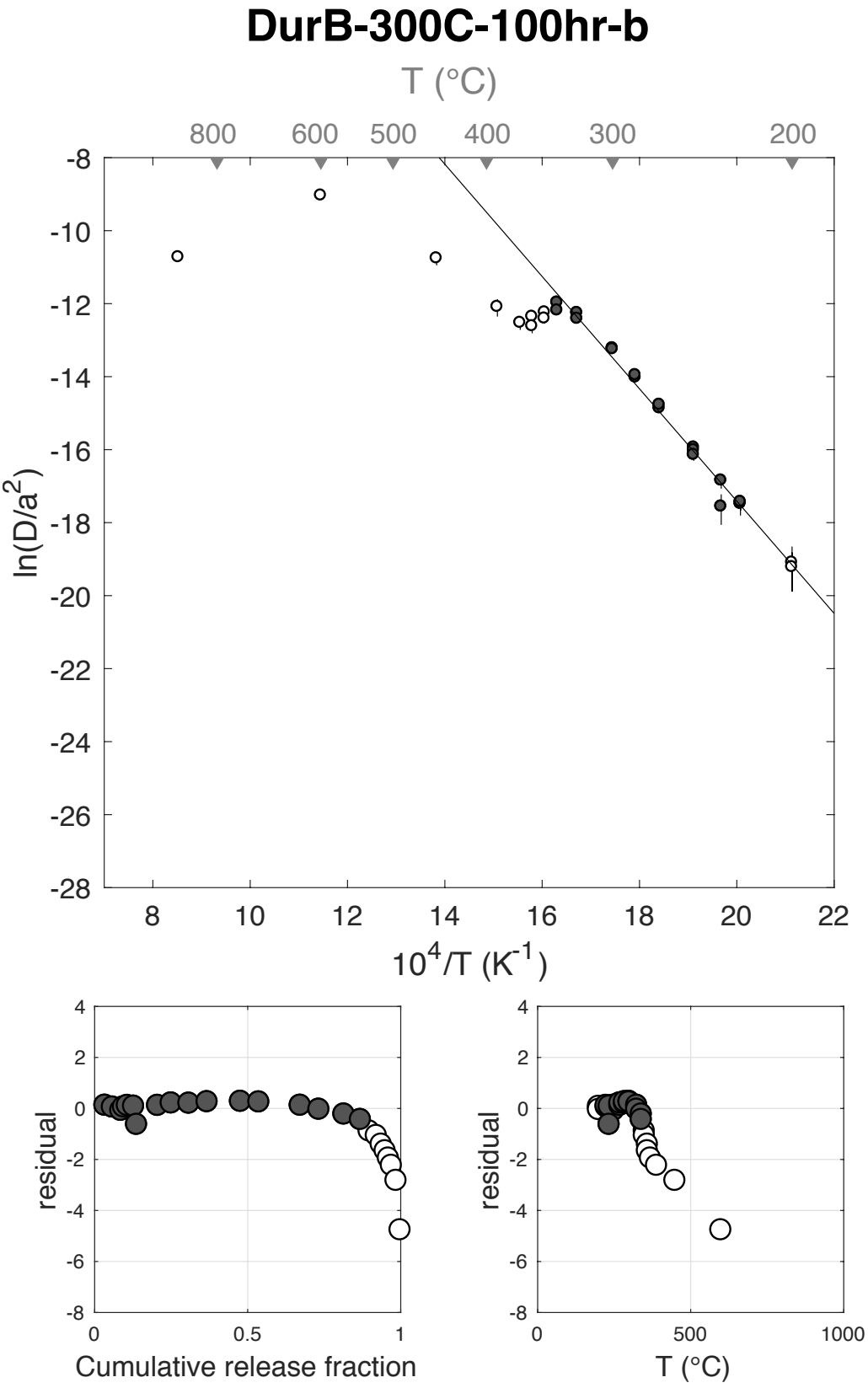
DurB-300C-100hr-b
T (°C)
800
600
500
400
300
200
-8
-10
-12
-14
-16
-18
-20
-22
-24
-26
-28
ln(D/a2)
8
10
12
14
16
18
20
22
10^4/T (K^-1)
4
2
0
-2
-4
-6
-8
residual
0
0.5
1
Cumulative release fraction
0
500
1000
T (°C)

DurB-325C-100hr-a

E_a	+/-	D_0	+/-	T_c	-	+	Total ^{3}He	Incl.	Misfit	Norm. Misfit
196.58	14.12	25.84	2.88	117.71	9.18	10.09	30.34	0.646	2.890	0.206

Step #	°C	t (hrs)	^{3}He	Error	^{4}He	Error	^{4}He/^{3}He	Err	In ^{3}He Reg.
1	250	0.25	0.21	0.06	25.1	65.7	112.5	2.63	1
2	250	0.50	0.13	0.05	27.6	39.3	198.1	1.47	1
3	250	1.00	0.23	0.05	24.2	16.1	97.2	0.71	1
4	225	1.50	0.06	0.05	24.0	67.6	381.4	2.94	0
5	225	2.50	0.10	0.10	21.0	173.5	193.9	8.31	0
6	200	3.00	0.02	0.12	20.2	226.4	1316.6	13.68	0
7	200	4.00	0.03	0.17	18.3	332.5	689.4	19.29	0
8	235	2.00	0.09	0.08	25.4	120.5	279.5	4.82	0
9	235	3.00	0.15	0.13	22.4	226.4	141.1	10.15	1
10	270	1.91	0.57	0.10	26.8	110.9	36.9	4.14	1
11	270	1.57	0.32	0.07	23.5	75.0	63.7	3.20	1
12	285	1.25	0.43	0.08	25.5	41.9	49.1	1.65	1
13	285	1.56	0.40	0.08	23.7	74.1	49.1	3.14	1
14	300	1.91	1.03	0.17	34.2	111.1	23.1	3.25	1
15	300	1.45	2.14	0.20	20.2	64.8	NaN	NaN	1
16	325	1.74	4.08	0.41	23.0	98.2	NaN	NaN	1
17	325	1.32	2.70	0.21	3.0	56.4	NaN	NaN	1
18	340	1.58	4.05	0.26	30.9	81.7	NaN	NaN	1
19	340	1.89	3.18	0.26	26.2	113.1	NaN	NaN	1
20	350	1.48	2.27	0.24	9.8	72.6	NaN	NaN	0
21	350	1.82	1.99	0.23	20.8	106.5	0.5	5.12	0
22	360	1.50	1.51	0.20	20.7	75.2	3.7	3.63	0
23	360	1.98	1.32	0.18	21.1	121.6	5.9	5.76	0
24	370	1.88	0.77	0.15	15.1	111.5	9.5	7.38	0
25	390	1.47	1.02	0.16	49.4	71.6	38.3	1.46	0
26	450	1.00	1.16	0.16	184.8	30.1	149.8	0.21	0
27	600	1.00	0.35	0.11	86.3	34.0	239.0	0.50	0
28	900	1.00	0.03	0.05	0.0	0.0	NaN	NaN	0
29	900	1.00	0.01	0.05	0.0	0.0	NaN	NaN	0

Figure S36

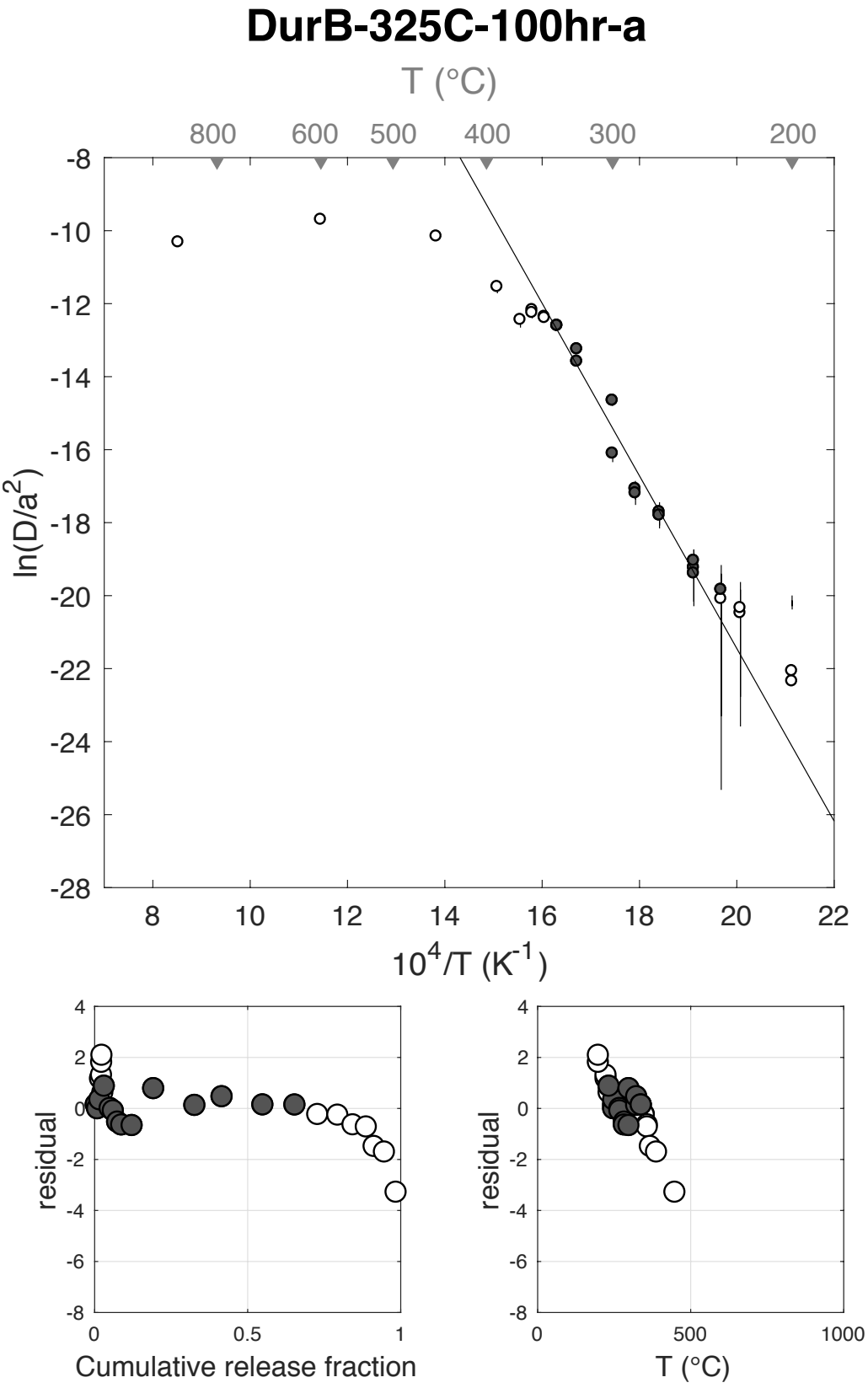
DurB-325C-100hr-a
T (°C)
800
600
500
400
300
200
-8
-10
-12
-14
-16
-18
-20
-22
-24
-26
-28
ln(D/a2)
8
10
12
14
16
18
20
22
10^4/T (K^-1)
4
2
0
-2
-4
-6
-8
residual
0
0.5
1
Cumulative release fraction
0
500
1000
T (°C)

DurB-325C-100hr-b

E_a	+/-	D_0	+/-	T_c	-	+	Total ^{3}He	Incl.	Misfit	Norm. Misfit
120.53	7.36	11.51	1.51	40.58	8.64	9.22	24.66	0.784	0.878	0.052

Step #	°C	t (hrs)	^{3}He	Error	^{4}He	Error	^{4}He/^{3}He	Err	In ^{3}He Reg.
1	250	0.25	0.76	0.15	21.3	20.2	17.9	0.97	1
2	250	0.50	0.52	0.11	0.4	21.3	NaN	NaN	1
3	250	1.00	0.55	0.24	9.7	18.5	7.6	1.95	1
4	225	1.50	0.21	0.08	0.0	0.0	NaN	NaN	1
5	225	2.50	0.26	0.11	0.0	0.0	NaN	NaN	1
6	200	3.00	0.10	0.08	0.0	0.0	NaN	NaN	0
7	200	4.00	0.03	0.10	0.0	0.0	NaN	NaN	0
8	235	2.00	0.44	0.10	0.0	0.0	NaN	NaN	1
9	235	3.00	0.49	0.12	0.0	0.0	NaN	NaN	1
10	270	1.91	1.74	0.20	16.5	23.7	NaN	NaN	1
11	270	1.57	1.02	0.15	12.9	22.4	2.6	1.75	1
12	285	1.25	1.17	0.14	14.3	20.5	2.3	1.44	1
13	285	1.56	1.22	0.17	2.6	26.9	NaN	NaN	1
14	300	1.91	2.25	0.24	33.4	25.5	4.9	0.77	1
15	300	1.45	1.28	0.15	16.3	19.6	2.7	1.21	1
16	325	1.74	2.48	0.22	44.8	22.0	8.1	0.50	1
17	325	1.32	1.42	0.17	27.3	18.4	9.3	0.68	1
18	340	1.58	1.98	0.20	46.1	23.0	13.3	0.51	1
19	340	1.89	1.53	0.19	48.7	26.0	21.8	0.55	1
20	350	1.48	1.03	0.13	62.3	20.0	50.3	0.35	0
21	350	1.82	0.84	0.14	58.2	25.9	59.6	0.47	0
22	360	1.50	0.58	0.10	70.3	17.9	110.6	0.31	0
23	360	1.98	0.51	0.11	79.5	27.6	147.3	0.41	0
24	370	1.88	0.42	0.11	109.8	24.1	253.9	0.35	0
25	390	1.47	0.45	0.09	136.5	24.9	293.5	0.27	0
26	450	1.00	0.75	0.13	396.1	30.6	515.3	0.19	0
27	600	1.00	0.62	0.11	512.8	40.3	812.1	0.20	0
28	900	1.00	0.00	0.00	5.3	16.1	Inf	NaN	0
29	900	1.00	0.00	0.05	0.7	15.3	909.3	68.06	0

Figure S37

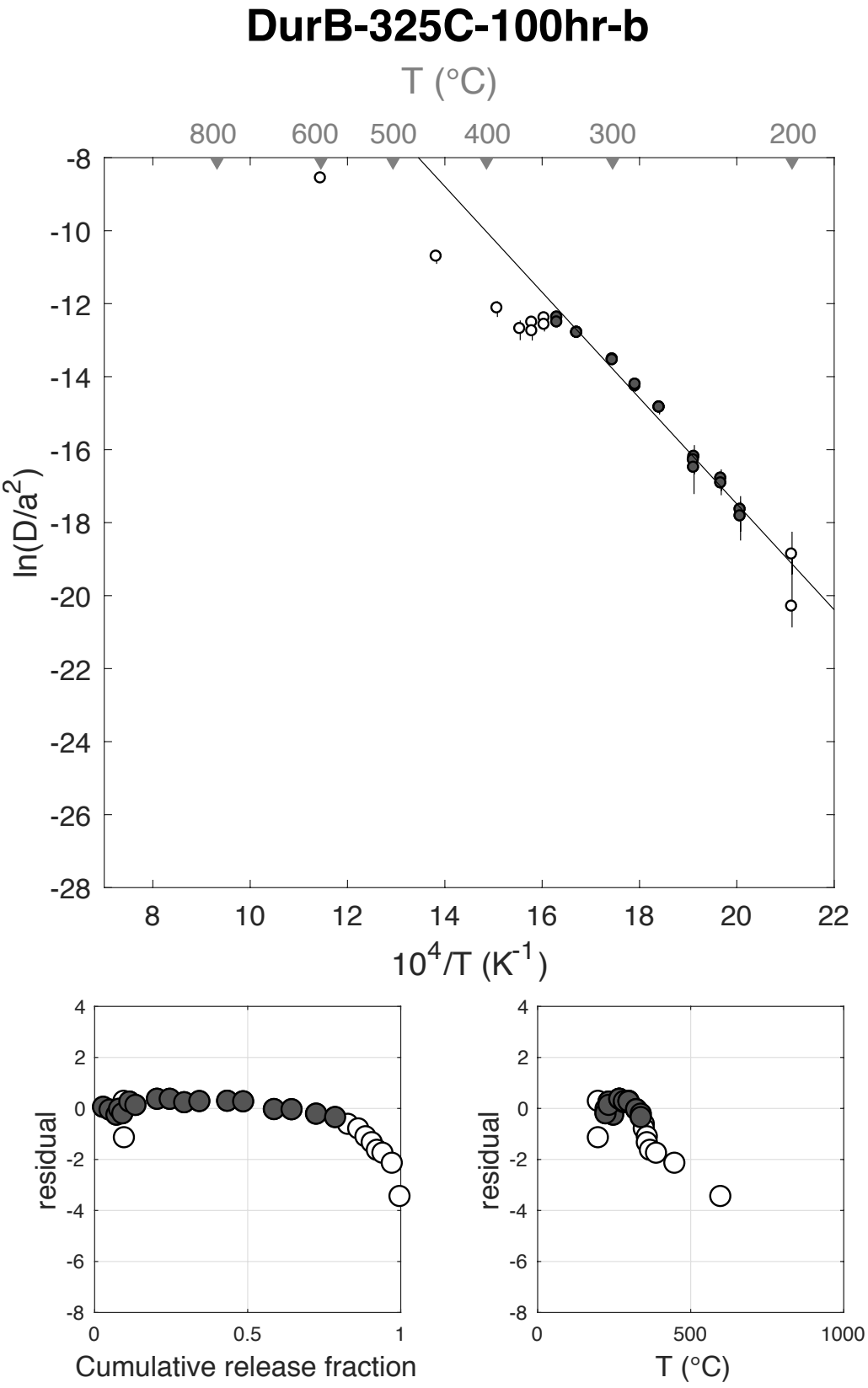
DurB-325C-100hr-b
T (°C)
800
600
500
400
300
200
-8
-10
-12
-14
-16
-18
-20
-22
-24
-26
-28
ln(D/a2)
8
10
12
14
16
18
20
22
10^4/T (K^-1)
4
2
0
-2
-4
-6
-8
residual
0
0.5
1
Cumulative release fraction
500
1000
T (°C)

E_a	+/-	D_0	+/-	T_c	-	+	Total ^{3}He	Incl.	Misfit	Norm. Misfit
124.50	2.53	12.11	0.53	46.67	2.84	2.91	245.49	0.742	0.655	0.034

Step #	°C	t (hrs)	^{3}He	Error	^{4}He	Error	^{4}He/^{3}He	Err	In ^{3}He Reg.
1	250	0.25	7.21	0.39	69.1	20.5	NaN	NaN	1
2	250	0.50	3.90	0.28	57.9	15.6	4.9	0.28	1
3	250	1.00	5.11	0.34	71.4	19.5	4.0	0.28	1
4	225	1.50	1.36	0.21	33.4	22.4	14.5	0.69	1
5	225	2.50	2.08	0.23	53.2	41.6	15.5	0.79	1
6	200	3.00	0.62	0.15	34.5	52.2	45.9	1.54	1
7	200	4.00	0.77	0.20	46.2	74.6	50.3	1.64	1
8	235	2.00	3.42	0.28	77.6	33.7	12.7	0.44	1
9	235	3.00	4.25	0.33	92.2	53.9	11.7	0.59	1
10	270	1.91	14.14	0.56	233.5	31.7	6.5	0.14	1
11	270	1.57	8.60	0.49	140.0	23.3	6.3	0.18	1
12	285	1.25	10.24	0.51	181.0	18.6	7.7	0.11	1
13	285	1.57	11.65	0.52	216.6	24.0	8.6	0.12	1
14	300	1.91	20.54	0.76	414.2	30.4	10.2	0.08	1
15	300	1.45	11.38	0.55	266.4	22.3	13.4	0.10	1
16	325	1.74	23.93	0.79	663.6	27.9	17.7	0.05	1
17	325	1.32	14.14	0.57	503.4	23.8	25.6	0.06	1
18	340	1.58	21.65	0.66	858.0	26.2	29.6	0.04	1
19	340	1.89	17.28	0.58	859.4	31.7	39.7	0.05	1
20	350	1.48	13.10	0.56	824.6	27.9	52.9	0.05	0
21	350	1.82	11.38	0.46	859.6	32.2	65.6	0.06	0
22	360	1.50	8.31	0.40	737.7	25.6	78.8	0.06	0
23	360	1.98	7.38	0.43	800.3	32.2	98.4	0.07	0
24	370	1.88	5.55	0.38	727.6	30.9	121.0	0.08	0
25	390	1.47	4.14	0.33	768.9	22.6	175.5	0.09	0
26	450	1.00	3.79	0.33	1679.3	30.3	432.6	0.09	0
27	600	1.00	6.25	0.40	9064.4	54.2	1439.9	0.06	0
28	900	1.00	3.29	0.29	4952.8	42.7	1496.7	0.09	0
29	900	1.00	0.01	0.07	0.0	0.0	NaN	NaN	0

Figure S38

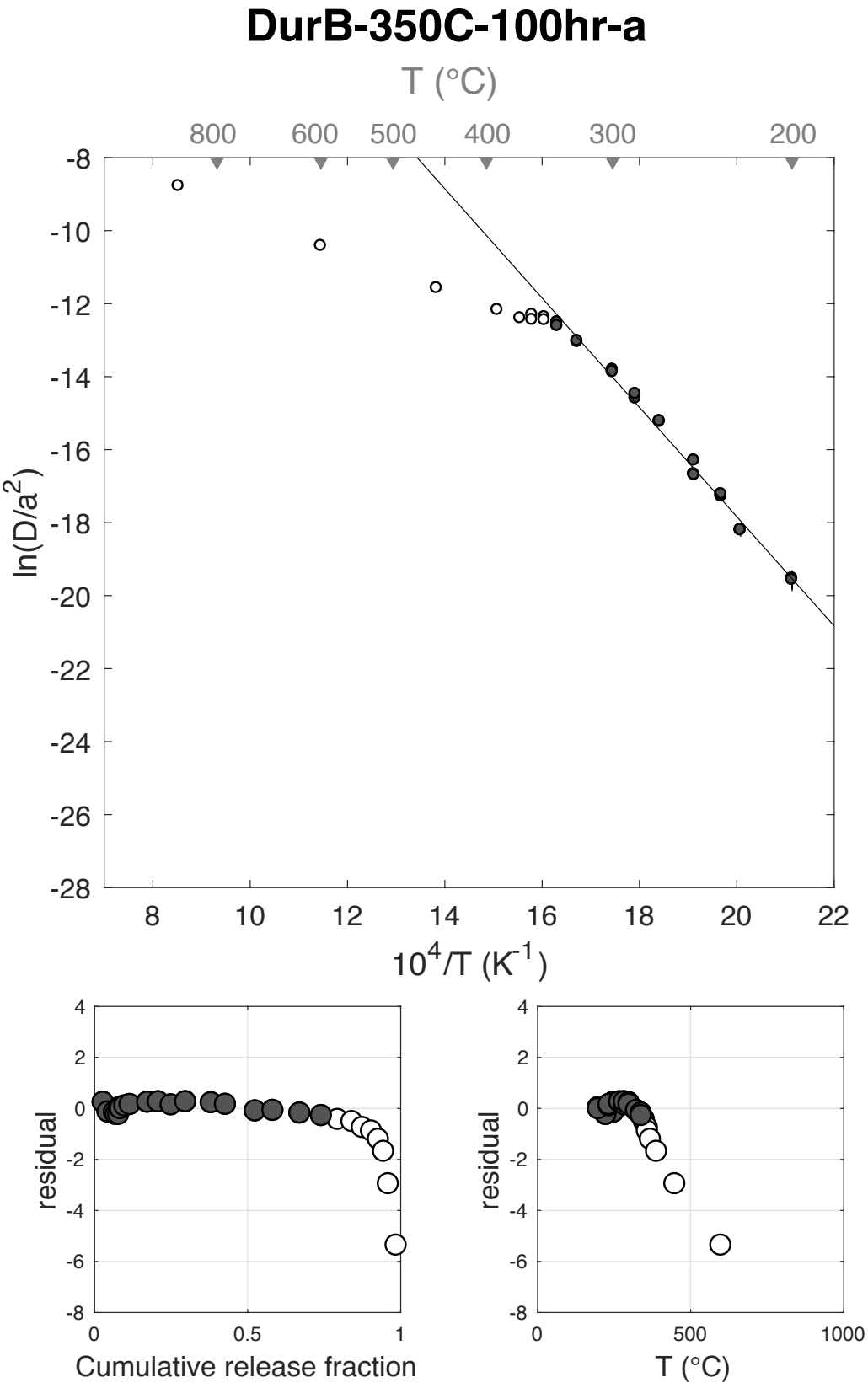
DurB-350C-100hr-a
T (°C)
800
600
500
400
300
200
-8
-10
-12
-14
-16
-18
-20
-22
-24
-26
-28
ln(D/a2)
8
10
12
14
16
18
20
22
10^4/T (K^-1)
4
2
0
-2
-4
-6
-8
residual
0
0.5
1
Cumulative release fraction
0
500
1000
T (°C)

DurB-350C-100hr-b

E_a	+/-	D_0	+/-	T_c	-	+	Total ^{3}He	Incl.	Misfit	Norm. Misfit
113.81	8.38	9.43	1.76	36.78	10.10	10.92	104.41	0.618	0.588	0.033

Step #	°C	t (hrs)	^{3}He	Error	^{4}He	Error	^{4}He/^{3}He	Err	In ^{3}He Reg.
1	250	0.25	2.94	0.49	57.2	7.9	9.4	0.22	1
2	250	0.50	2.15	0.39	27.2	7.0	2.7	0.32	1
3	250	1.00	2.42	0.43	28.3	8.3	1.7	0.34	1
4	225	1.50	0.52	0.24	8.4	6.6	6.2	0.91	1
5	225	2.50	0.99	0.32	10.8	7.2	0.9	0.74	1
6	200	3.00	0.22	0.20	0.0	0.0	NaN	NaN	1
7	200	4.00	0.18	0.25	0.0	0.0	NaN	NaN	0
8	235	2.00	1.09	0.32	12.2	7.8	1.2	0.70	1
9	235	3.00	1.39	0.42	16.0	8.2	1.5	0.60	1
10	270	1.91	4.72	0.64	62.1	7.4	3.1	0.18	1
11	270	1.57	2.79	0.53	40.6	7.7	4.6	0.27	1
12	285	1.25	3.33	0.57	47.5	6.9	4.3	0.23	1
13	285	1.56	3.70	0.63	51.3	10.9	3.9	0.27	1
14	300	1.91	5.76	0.55	93.0	12.9	6.1	0.17	1
15	300	1.45	3.90	0.57	59.3	7.8	5.2	0.20	1
16	325	1.74	9.08	0.81	167.4	11.6	8.4	0.11	1
17	325	1.32	5.29	0.61	101.4	10.2	9.2	0.15	1
18	340	1.58	7.83	0.78	203.4	15.5	16.0	0.13	1
19	340	1.89	6.39	0.72	207.9	13.2	22.5	0.13	1
20	350	1.48	4.77	0.72	218.8	16.7	35.9	0.17	0
21	350	1.82	5.85	0.65	231.0	13.0	29.5	0.12	0
22	360	1.50	4.94	0.65	248.9	14.6	40.4	0.14	0
23	360	1.98	5.77	0.66	285.7	17.3	39.5	0.13	0
24	370	1.88	4.43	0.70	326.2	12.5	63.7	0.16	0
25	390	1.47	4.33	0.60	420.4	22.7	87.2	0.15	0
26	450	1.00	6.08	0.75	1095.6	30.5	170.2	0.13	0
27	600	1.00	3.50	0.55	1187.2	35.2	329.0	0.16	0
28	900	1.00	0.03	0.07	14.5	6.3	461.5	2.30	0
29	900	1.00	0.02	0.08	0.0	0.0	NaN	NaN	0

Figure S39

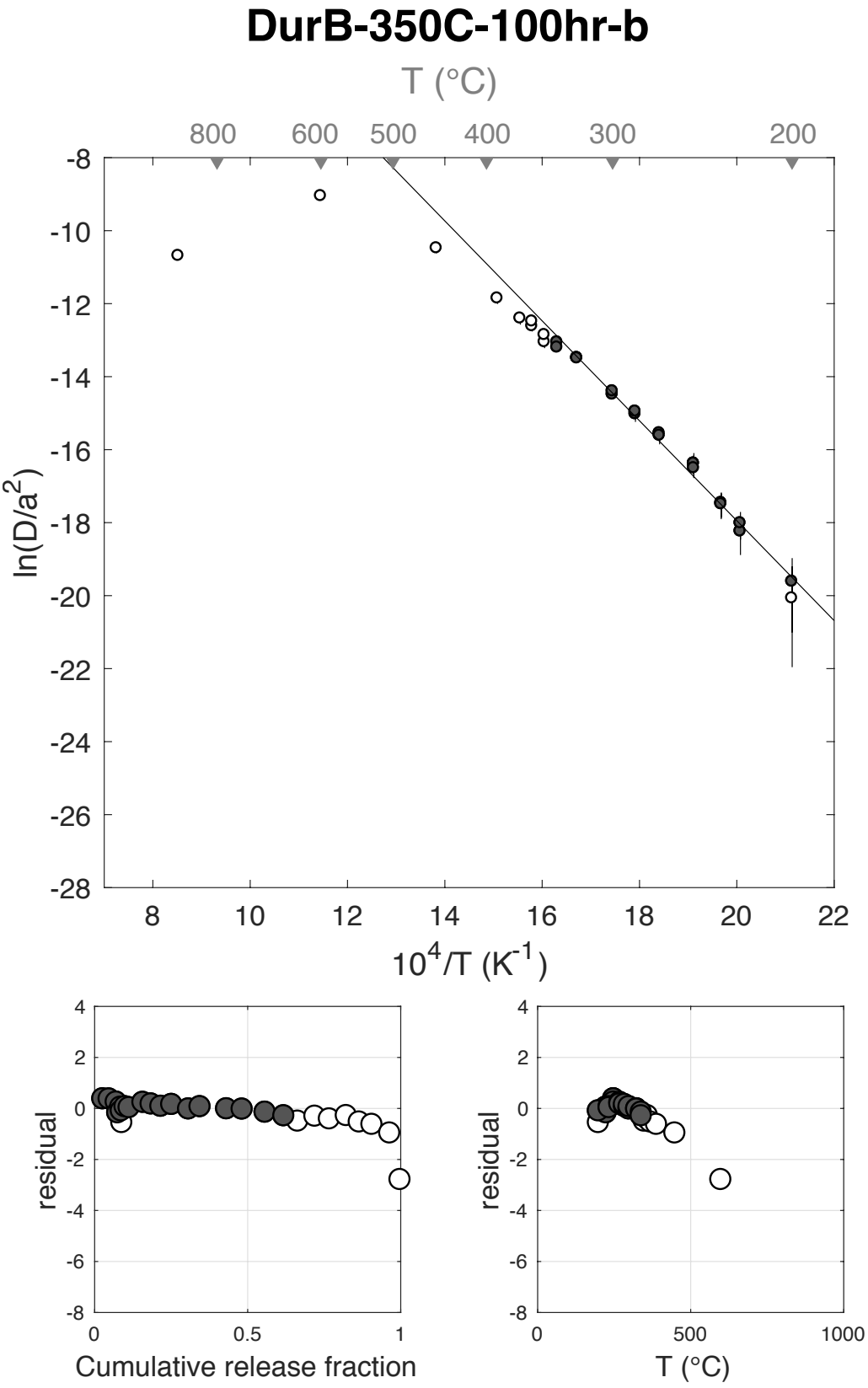
DurB-350C-100hr-b
T (°C)
800
600
500
400
300
200
ln(D/a²)
10⁴/T (K⁻¹)
residual
Cumulative release fraction
residual
T (°C)

E_a	+/-	D_0	+/-	T_c	-	+	Total ^{3}He	Incl.	Misfit	Norm. Misfit
125.95	3.19	11.88	0.66	51.86	3.62	3.73	112.98	0.633	0.096	0.006

Step #	°C	t (hrs)	^{3}He	Error	^{4}He	Error	^{4}He/^{3}He	Err	In ^{3}He Reg.
1	250	0.25	2.31	0.24	23.2	20.8	0.0	0.90	1
2	250	0.50	1.71	0.21	0.0	0.0	NaN	NaN	1
3	250	1.00	2.03	0.23	0.0	0.0	NaN	NaN	1
4	225	1.50	0.53	0.13	0.0	0.0	NaN	NaN	1
5	225	2.50	0.83	0.16	0.0	0.0	NaN	NaN	1
6	200	3.00	0.12	0.11	0.0	0.0	NaN	NaN	0
7	200	4.00	0.15	0.12	0.0	0.0	NaN	NaN	0
8	235	2.00	1.00	0.18	0.0	0.0	NaN	NaN	1
9	235	3.00	1.30	0.18	0.0	0.0	NaN	NaN	1
10	270	1.91	4.24	0.34	10.9	33.0	NaN	NaN	1
11	270	1.57	2.80	0.26	21.5	25.4	NaN	NaN	1
12	285	1.25	3.73	0.31	22.8	19.4	NaN	NaN	1
13	285	1.57	4.03	0.28	24.2	26.4	NaN	NaN	1
14	300	1.91	7.28	0.41	55.8	33.2	NaN	NaN	1
15	300	1.45	4.51	0.36	26.3	27.5	NaN	NaN	1
16	325	1.74	11.07	0.52	75.0	29.1	NaN	NaN	1
17	325	1.32	6.25	0.42	37.4	24.8	NaN	NaN	1
18	340	1.58	9.36	0.49	82.9	24.6	NaN	NaN	1
19	340	1.89	8.51	0.47	72.2	33.9	NaN	NaN	1
20	350	1.48	6.86	0.45	63.4	24.6	NaN	NaN	0
21	350	1.82	6.49	0.37	61.8	31.2	NaN	NaN	0
22	360	1.50	5.49	0.37	69.4	24.1	2.6	0.35	0
23	360	1.98	5.27	0.38	73.1	36.5	3.9	0.50	0
24	370	1.88	4.60	0.34	68.8	32.9	4.9	0.48	0
25	390	1.47	4.06	0.28	105.1	27.2	15.9	0.27	0
26	450	1.00	5.78	0.36	337.2	17.0	48.4	0.08	0
27	600	1.00	2.66	0.25	357.0	16.4	124.2	0.11	0
28	899	1.00	0.00	0.00	0.0	0.0	NaN	NaN	0
29	900	1.00	0.01	0.07	0.0	0.0	NaN	NaN	0

Figure S40

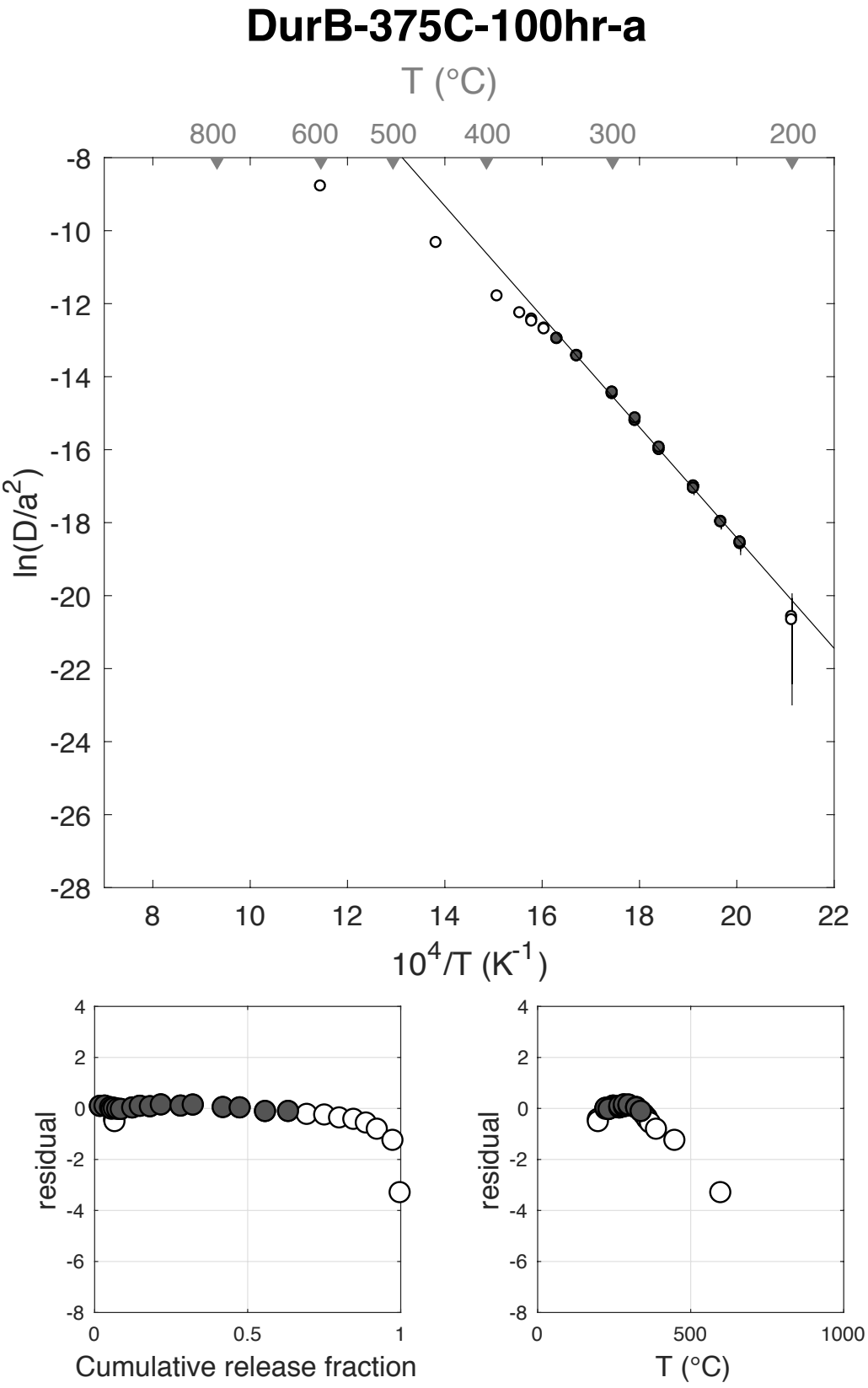
DurB-375C-100hr-a
T (°C)
800
600
500
400
300
200
-8
-10
-12
-14
-16
-18
-20
-22
-24
-26
-28
ln(D/a2)
8
10
12
14
16
18
20
22
10^4/T (K^-1)
4
2
0
-2
-4
-6
-8
residual
0
0.5
1
Cumulative release fraction
500
1000
T (°C)

DurB-400C-100hr-a

E_a	+/-	D_0	+/-	T_c	-	+	Total ^{3}He	Incl.	Misfit	Norm. Misfit
124.20	4.42	10.87	0.93	54.23	4.89	5.09	244.18	0.496	0.201	0.011

Step #	°C	t (hrs)	^{3}He	Error	^{4}He	Error	^{4}He/^{3}He	Err	In ^{3}He Reg.
1	249	0.25	4.12	0.32	48.2	20.6	1.7	0.43	1
2	250	0.50	2.71	0.28	25.3	18.4	NaN	NaN	1
3	250	1.00	3.36	0.31	29.0	20.0	NaN	NaN	1
4	225	1.50	0.85	0.16	7.3	25.2	NaN	NaN	1
5	225	2.50	1.29	0.20	0.0	0.0	NaN	NaN	1
6	200	3.00	0.30	0.12	0.0	0.0	NaN	NaN	1
7	200	4.00	0.40	0.15	0.0	0.0	NaN	NaN	1
8	235	2.00	1.66	0.23	0.0	0.0	NaN	NaN	1
9	235	3.00	2.28	0.25	0.0	0.0	NaN	NaN	1
10	270	1.91	5.75	0.35	37.3	25.1	NaN	NaN	1
11	270	1.57	4.17	0.33	13.9	20.9	NaN	NaN	1
12	285	1.25	5.88	0.37	51.0	17.3	NaN	NaN	1
13	285	1.57	5.55	0.36	20.3	21.7	NaN	NaN	1
14	300	1.91	11.64	0.52	80.8	26.1	NaN	NaN	1
15	300	1.45	7.31	0.41	55.2	23.5	NaN	NaN	1
16	325	1.74	18.65	0.72	143.9	25.0	NaN	NaN	1
17	325	1.32	11.01	0.50	85.0	22.7	NaN	NaN	1
18	340	1.58	17.85	0.72	134.6	24.6	NaN	NaN	1
19	340	1.89	16.40	0.69	132.9	24.9	NaN	NaN	1
20	350	1.48	14.94	0.54	120.4	18.3	NaN	NaN	0
21	350	1.82	12.95	0.51	92.0	24.1	NaN	NaN	0
22	360	1.50	12.46	0.58	106.1	19.0	NaN	NaN	0
23	360	1.98	12.35	0.59	92.2	27.6	NaN	NaN	0
24	370	1.88	12.41	0.55	79.3	27.1	NaN	NaN	0
25	390	1.47	12.75	0.54	112.3	19.5	NaN	NaN	0
26	450	1.00	23.29	0.71	248.7	16.5	0.7	0.07	0
27	600	1.00	21.88	0.77	487.6	18.2	12.3	0.05	0
28	900	1.00	0.00	0.06	0.0	0.0	NaN	NaN	0
29	900	1.00	0.00	0.00	9.0	18.0	Inf	NaN	0

Figure S41

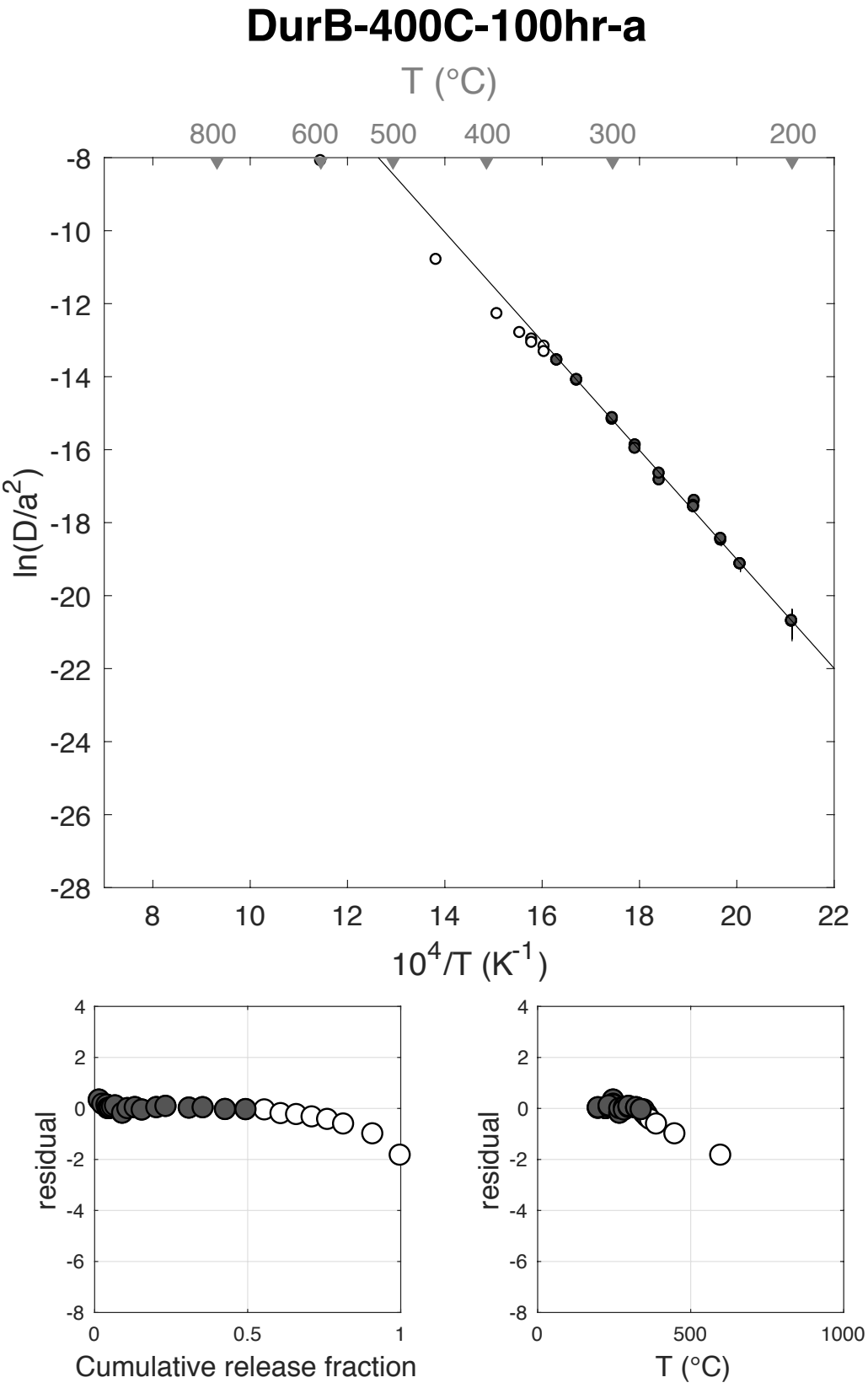
DurB-400C-100hr-a
T (°C)
800
600
500
400
300
200
-8
-10
-12
-14
-16
-18
-20
-22
-24
-26
-28
ln(D/a2)
8
10
12
14
16
18
20
22
10^4/T (K^-1)
4
2
0
-2
-4
-6
-8
residual
0
0.5
1
Cumulative release fraction
0
500
1000
T (°C)

DurB-400C-100hr-b

E_a	+/-	D_0	+/-	T_c	-	+	Total ^{3}He	Incl.	Misfit	Norm. Misfit
130.86	8.63	12.46	1.78	60.29	9.12	9.82	112.49	0.542	0.531	0.033

Step #	°C	t (hrs)	^{3}He	Error	^{4}He	Error	^{4}He/^{3}He	Err	In ^{3}He Reg.
1	250	0.25	2.12	0.39	26.4	8.4	2.5	0.37	1
2	250	0.50	1.32	0.32	16.2	6.2	2.3	0.45	1
3	250	1.00	1.76	0.37	15.5	6.7	NaN	NaN	1
4	225	1.50	0.40	0.22	3.8	6.9	NaN	NaN	1
5	225	2.50	0.29	0.23	6.2	6.8	11.2	1.35	0
6	200	3.00	0.00	0.00	2.8	8.0	Inf	NaN	0
7	200	4.00	0.00	0.00	0.0	0.0	NaN	NaN	0
8	235	2.00	0.65	0.29	5.1	8.0	NaN	NaN	1
9	235	3.00	0.79	0.28	8.8	8.7	1.2	1.05	1
10	270	1.91	3.43	0.49	39.9	7.7	1.6	0.24	1
11	270	1.57	2.35	0.43	22.2	7.2	NaN	NaN	1
12	285	1.25	2.84	0.50	35.7	6.1	2.6	0.24	1
13	285	1.56	2.99	0.61	37.1	8.9	2.4	0.32	1
14	300	1.91	6.81	0.75	67.2	10.1	NaN	NaN	1
15	300	1.45	3.66	0.75	33.7	7.3	NaN	NaN	1
16	325	1.74	9.83	0.82	113.9	11.5	1.6	0.13	1
17	325	1.32	5.45	0.55	59.8	11.0	1.0	0.21	1
18	340	1.58	8.39	0.84	97.7	8.6	1.6	0.13	1
19	340	1.89	8.15	0.76	92.7	10.8	1.4	0.15	1
20	350	1.48	5.56	0.74	75.4	10.7	3.5	0.19	0
21	350	1.82	5.34	0.73	74.9	9.4	4.0	0.19	0
22	360	1.50	5.15	0.65	56.2	8.7	0.9	0.20	0
23	360	1.98	5.07	0.62	63.8	7.8	2.6	0.17	0
24	370	1.88	4.83	0.72	54.7	9.4	1.3	0.23	0
25	390	1.47	5.25	0.55	77.9	7.5	4.8	0.14	0
26	450	1.00	8.01	0.78	204.8	16.1	15.6	0.12	0
27	600	1.00	12.02	1.66	1037.9	21.1	76.3	0.14	0
28	900	1.00	0.02	0.10	23.5	5.3	1216.8	5.05	0
29	900	1.00	0.00	0.00	0.9	3.8	Inf	NaN	0

Figure S42

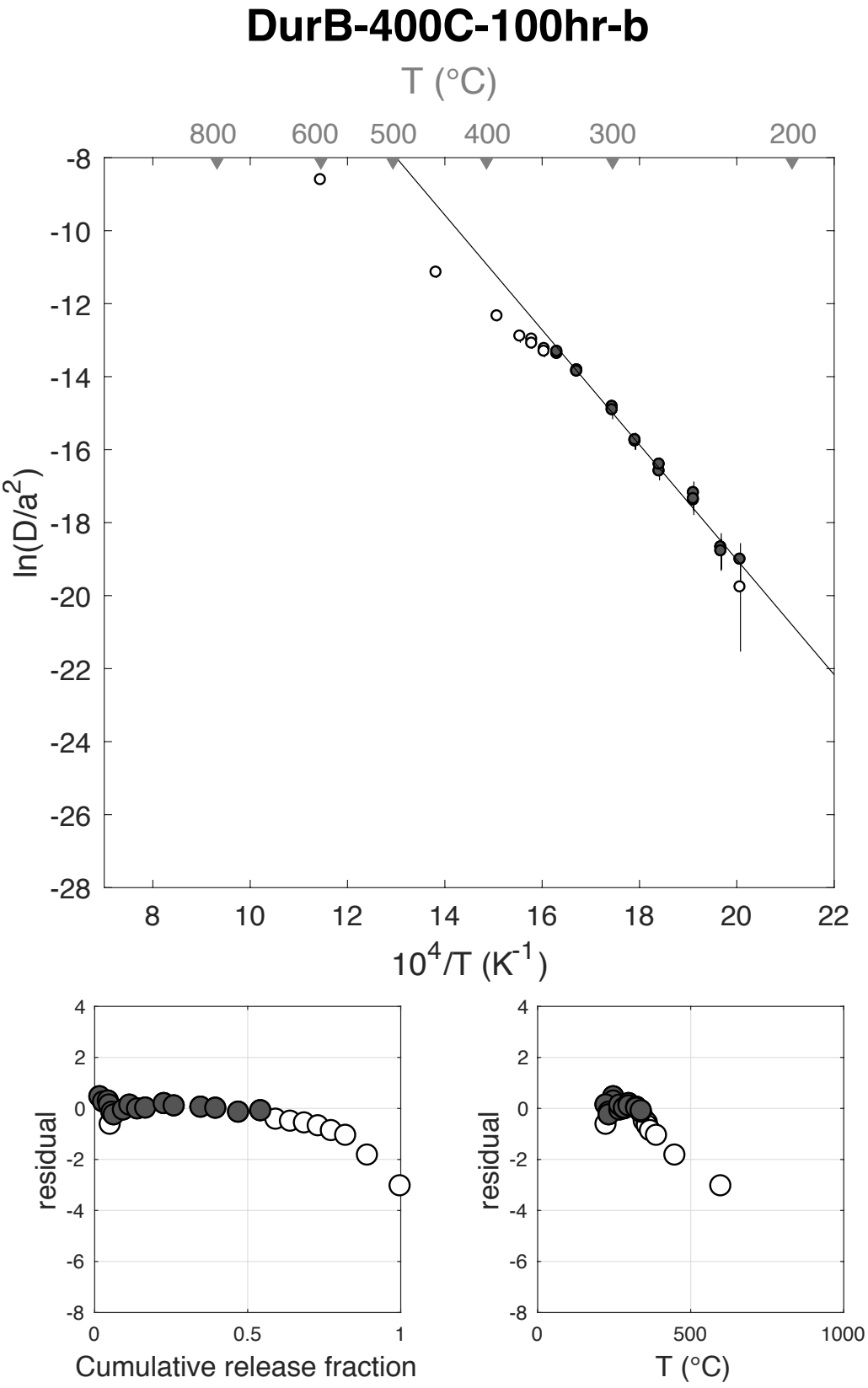
DurB-400C-100hr-b
T (°C)
800
600
500
400
300
200
-8
-10
-12
-14
-16
-18
-20
-22
-24
-26
-28
ln(D/a2)
8
10
12
14
16
18
20
22
10^4/T (K^-1)
4
2
0
-2
-4
-6
-8
residual
0
0.5
1
Cumulative release fraction
0
500
1000
T (°C)

DurB-425C-100hr-a

E_a	+/-	D_0	+/-	T_c	-	+	Total ^{3}He	Incl.	Misfit	Norm. Misfit
116.52	6.26	9.55	1.33	43.20	7.34	7.79	151.82	0.527	0.607	0.032

Step #	°C	t (hrs)	^{3}He	Error	^{4}He	Error	^{4}He/^{3}He	Err	In ^{3}He Reg.
1	250	0.25	3.31	0.31	71.3	14.3	11.5	0.22	1
2	250	0.50	2.06	0.23	30.0	20.4	4.5	0.69	1
3	250	1.00	2.69	0.27	36.2	18.3	3.4	0.52	1
4	225	1.50	0.75	0.16	11.2	22.8	5.1	2.04	1
5	225	2.50	0.95	0.20	0.0	0.0	NaN	NaN	1
6	200	3.00	0.25	0.14	0.0	0.0	NaN	NaN	1
7	200	4.00	0.34	0.19	0.0	0.0	NaN	NaN	1
8	235	2.00	1.32	0.20	12.4	18.5	NaN	NaN	1
9	235	3.00	1.81	0.25	2.3	23.7	NaN	NaN	1
10	270	1.91	5.66	0.37	50.9	20.7	NaN	NaN	1
11	270	1.57	3.83	0.36	36.3	16.5	NaN	NaN	1
12	285	1.25	4.06	0.30	32.7	19.5	NaN	NaN	1
13	285	1.57	3.52	0.31	26.4	13.9	NaN	NaN	1
14	300	1.91	5.82	0.41	48.4	18.1	NaN	NaN	1
15	300	1.45	5.31	0.35	48.8	16.2	NaN	NaN	1
16	325	1.74	9.75	0.77	87.1	19.8	NaN	NaN	1
17	325	1.32	7.65	0.48	72.0	21.8	NaN	NaN	1
18	340	1.58	11.86	0.55	101.4	18.0	NaN	NaN	1
19	340	1.89	9.00	0.48	76.4	14.4	NaN	NaN	1
20	350	1.48	9.72	0.46	109.2	21.1	1.2	0.20	0
21	350	1.82	9.12	2.05	80.4	16.1	NaN	NaN	0
22	360	1.50	8.45	0.41	77.3	22.6	NaN	NaN	0
23	360	1.98	7.32	0.41	67.3	17.4	NaN	NaN	0
24	370	1.88	6.87	0.41	66.4	18.7	NaN	NaN	0
25	390	1.47	6.21	0.39	69.0	19.3	1.1	0.29	0
26	450	1.00	10.45	0.53	173.6	14.8	6.6	0.10	0
27	600	1.00	11.90	1.67	1683.9	26.0	131.5	0.14	0
28	899	1.00	1.83	0.21	2220.8	23.4	1201.0	0.12	0
29	900	1.00	0.00	0.00	0.0	0.0	NaN	NaN	0

Figure S43

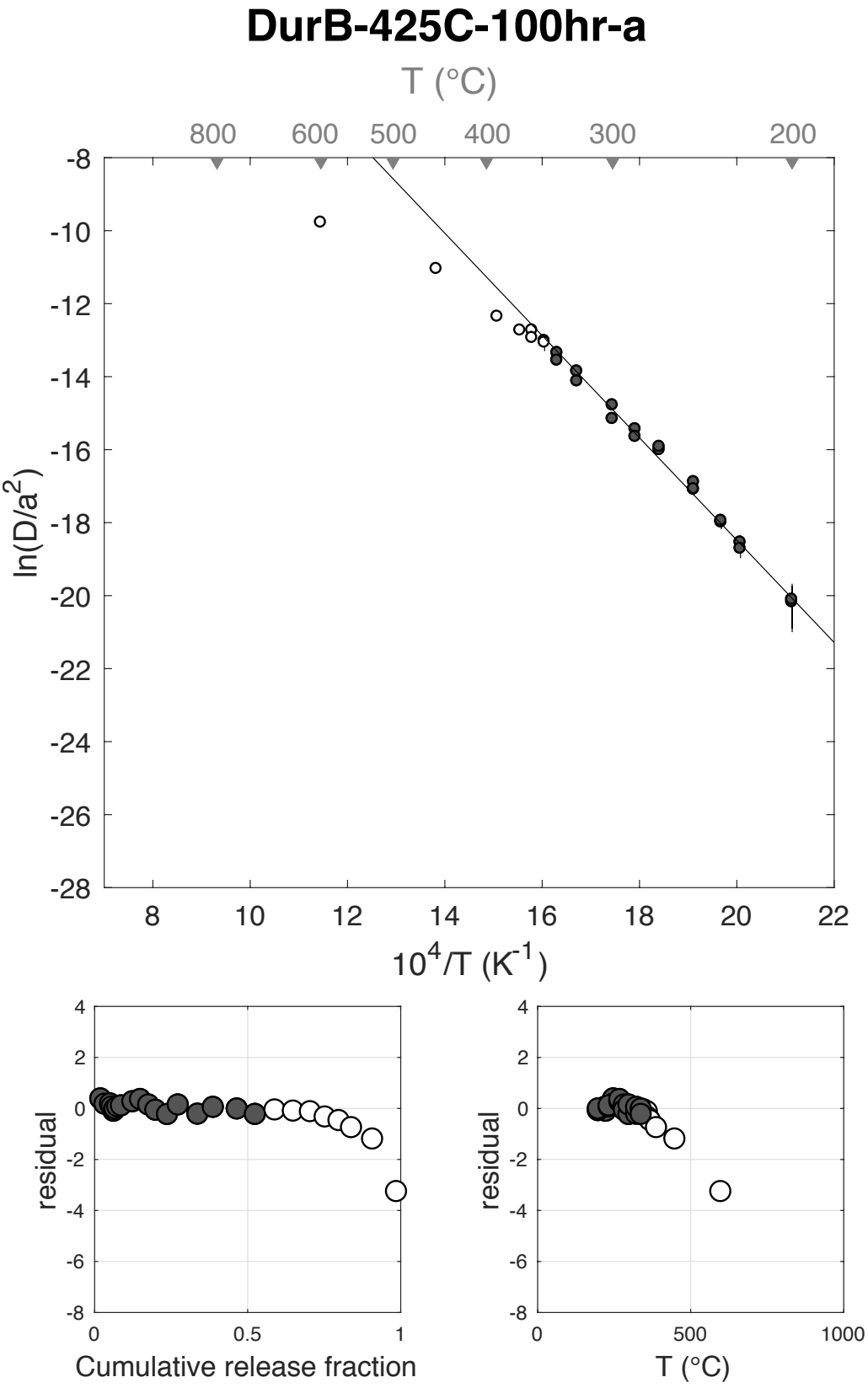
DurB-425C-100hr-a
T (°C)
800
600
500
400
300
200
-8
-10
-12
-14
-16
-18
-20
-22
-24
-26
-28
ln(D/a²)
8
10
12
14
16
18
20
22
10⁴/T (K⁻¹)
4
2
0
-2
-4
-6
-8
residual
0
0.5
1
Cumulative release fraction
500
1000
T (°C)

DurB-425C-100hr-d

E_a	+/-	D_0	+/-	T_c	-	+	Total ^{3}He	Incl.	Misfit	Norm. Misfit
118.77	10.36	10.02	2.14	45.94	12.11	13.29	74.19	0.541	0.887	0.055

Step #	°C	t (hrs)	^{3}He	Error	^{4}He	Error	^{4}He/^{3}He	Err	In ^{3}He Reg.
1	250	0.25	1.93	0.44	23.6	8.5	2.2	0.43	1
2	250	0.50	1.03	0.35	12.9	7.5	2.6	0.67	1
3	250	1.00	1.14	0.40	20.8	6.6	8.2	0.47	1
4	225	1.50	0.33	0.20	10.3	8.7	21.3	1.03	1
5	225	2.50	0.34	0.20	13.9	11.8	31.1	1.03	0
6	200	3.00	0.00	0.00	10.8	13.2	Inf	NaN	0
7	200	4.00	0.00	0.00	15.7	18.9	Inf	NaN	0
8	235	2.00	0.48	0.26	11.2	10.1	13.2	1.05	1
9	235	3.00	0.73	0.27	17.4	15.0	13.9	0.94	1
10	270	1.91	2.63	0.52	33.6	11.4	2.8	0.39	1
11	270	1.57	1.48	0.42	18.5	9.0	2.5	0.56	1
12	285	1.25	2.28	0.45	26.0	8.4	1.4	0.38	1
13	285	1.56	1.91	0.47	23.4	7.7	2.2	0.41	1
14	300	1.91	3.66	0.56	44.7	10.2	2.2	0.27	1
15	300	1.45	2.34	0.51	22.1	8.5	NaN	NaN	1
16	325	1.74	5.91	0.76	63.1	10.6	0.7	0.21	1
17	325	1.32	3.16	0.66	41.3	9.8	3.1	0.32	1
18	340	1.58	6.14	0.72	66.5	10.4	0.8	0.20	1
19	340	1.89	5.00	0.62	66.0	10.9	3.2	0.21	1
20	350	1.48	3.97	0.56	41.1	10.5	0.4	0.29	0
21	350	1.82	3.77	0.65	47.5	10.9	2.6	0.29	0
22	360	1.50	3.37	0.53	40.6	8.0	2.0	0.25	0
23	360	1.98	3.93	0.62	43.7	10.8	1.1	0.29	0
24	370	1.88	3.88	0.62	45.9	9.6	1.8	0.26	0
25	390	1.47	3.75	0.63	45.0	9.6	2.0	0.27	0
26	450	1.00	6.28	0.78	102.3	10.8	6.3	0.16	0
27	600	1.00	4.47	0.66	438.4	20.4	88.0	0.16	0
28	900	1.00	0.26	0.17	271.6	20.2	1046.2	0.67	0
29	900	1.00	0.00	0.00	0.0	0.0	NaN	NaN	0

Figure S44

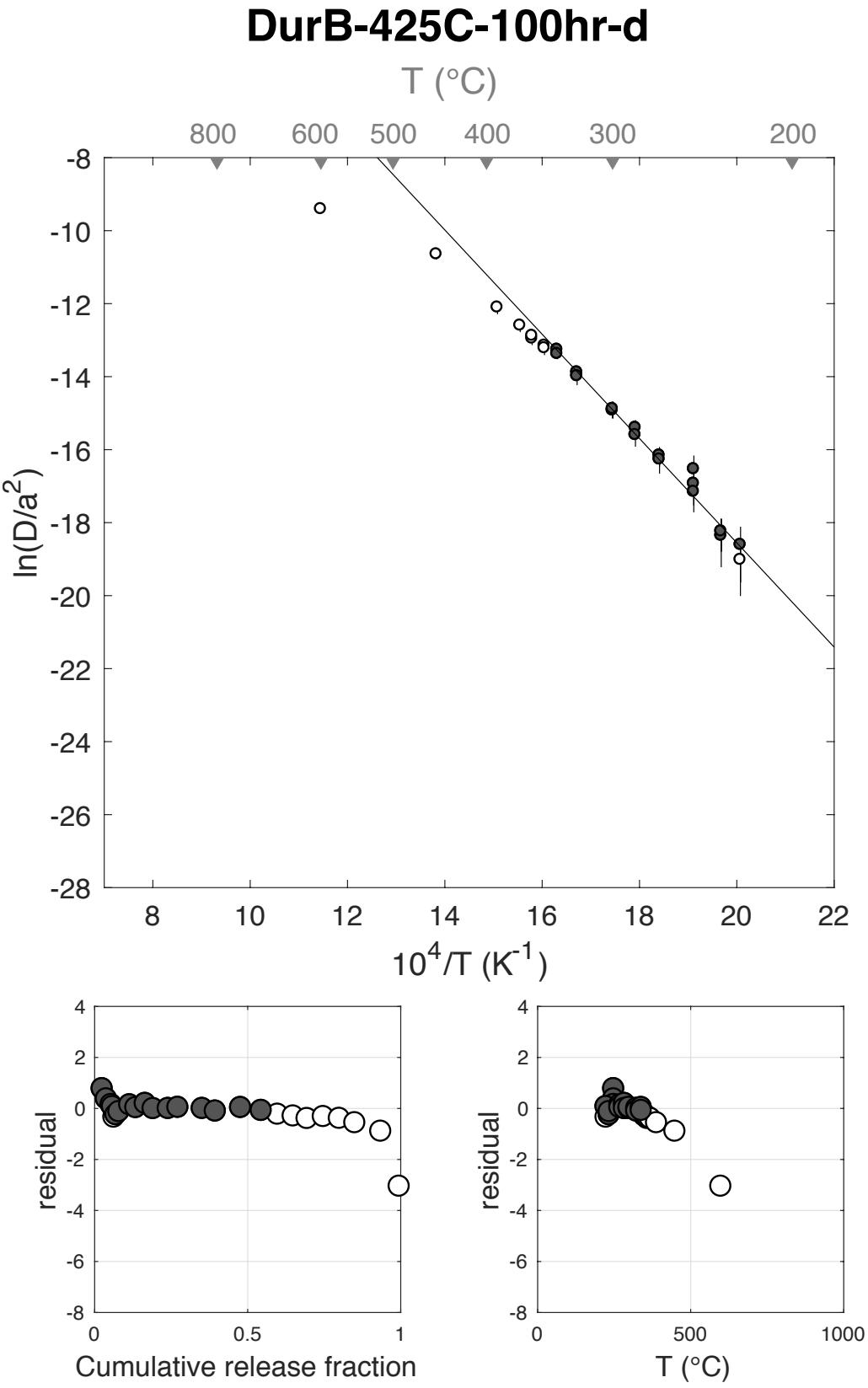
DurB-425C-100hr-d
T (°C)
800
600
500
400
300
200
-8
-10
-12
-14
-16
-18
-20
-22
-24
-26
-28
ln(D/a2)
8
10
12
14
16
18
20
22
10^4/T (K^-1)
4
2
0
-2
-4
-6
-8
residual
0
0.5
1
Cumulative release fraction
0
500
1000
T (°C)

DurB-425C-100hr-e

E_a	+/-	D_0	+/-	T_c	-	+	Total ^{3}He	Incl.	Misfit	Norm. Misfit
110.44	7.56	9.27	1.59	28.85	9.43	10.13	84.73	0.738	0.789	0.042

Step #	°C	t (hrs)	^{3}He	Error	^{4}He	Error	^{4}He/^{3}He	Err	In ^{3}He Reg.
1	250	0.25	3.34	0.50	45.6	18.0	3.7	0.42	1
2	250	0.50	2.53	0.51	40.6	13.0	6.0	0.38	1
3	250	1.00	2.51	0.48	19.9	8.8	NaN	NaN	1
4	225	1.50	0.65	0.26	1.5	15.2	NaN	NaN	1
5	225	2.50	1.03	0.33	6.4	36.1	NaN	NaN	1
6	200	3.00	0.26	0.15	0.0	0.0	NaN	NaN	1
7	200	4.00	0.28	0.19	0.0	0.0	NaN	NaN	1
8	235	2.00	1.11	0.37	4.2	26.1	NaN	NaN	1
9	235	3.00	1.57	0.40	6.7	46.7	NaN	NaN	1
10	270	1.91	4.87	0.76	43.3	25.1	NaN	NaN	1
11	270	1.57	3.18	0.49	18.8	18.7	NaN	NaN	1
12	285	1.25	3.60	0.56	23.3	14.1	NaN	NaN	1
13	285	1.56	3.19	0.54	21.0	16.8	NaN	NaN	1
14	300	1.91	6.01	0.74	54.1	25.0	NaN	NaN	1
15	300	1.45	3.60	0.59	23.7	17.2	NaN	NaN	1
16	325	1.74	7.17	0.85	80.3	20.9	1.2	0.29	1
17	325	1.32	4.82	0.62	43.2	14.1	NaN	NaN	1
18	340	1.58	6.57	1.01	66.7	19.8	0.1	0.33	1
19	340	1.89	6.19	0.84	61.2	25.0	NaN	NaN	1
20	350	1.48	4.10	0.62	50.5	16.2	2.3	0.35	0
21	350	1.82	4.19	0.56	42.6	24.0	0.2	0.58	0
22	360	1.50	3.93	0.62	35.0	17.6	NaN	NaN	0
23	360	1.98	3.58	0.58	29.3	26.1	NaN	NaN	0
24	370	1.88	2.38	0.46	20.0	23.6	NaN	NaN	0
25	390	1.47	1.53	0.40	24.0	17.4	5.7	0.77	0
26	450	1.00	1.42	0.35	56.9	11.3	30.2	0.32	0
27	600	1.00	1.07	0.34	13.5	9.6	2.6	0.79	0
28	900	1.00	0.00	0.01	0.0	0.0	NaN	NaN	0
29	900	1.00	0.03	0.06	0.0	0.0	NaN	NaN	0

Figure S45

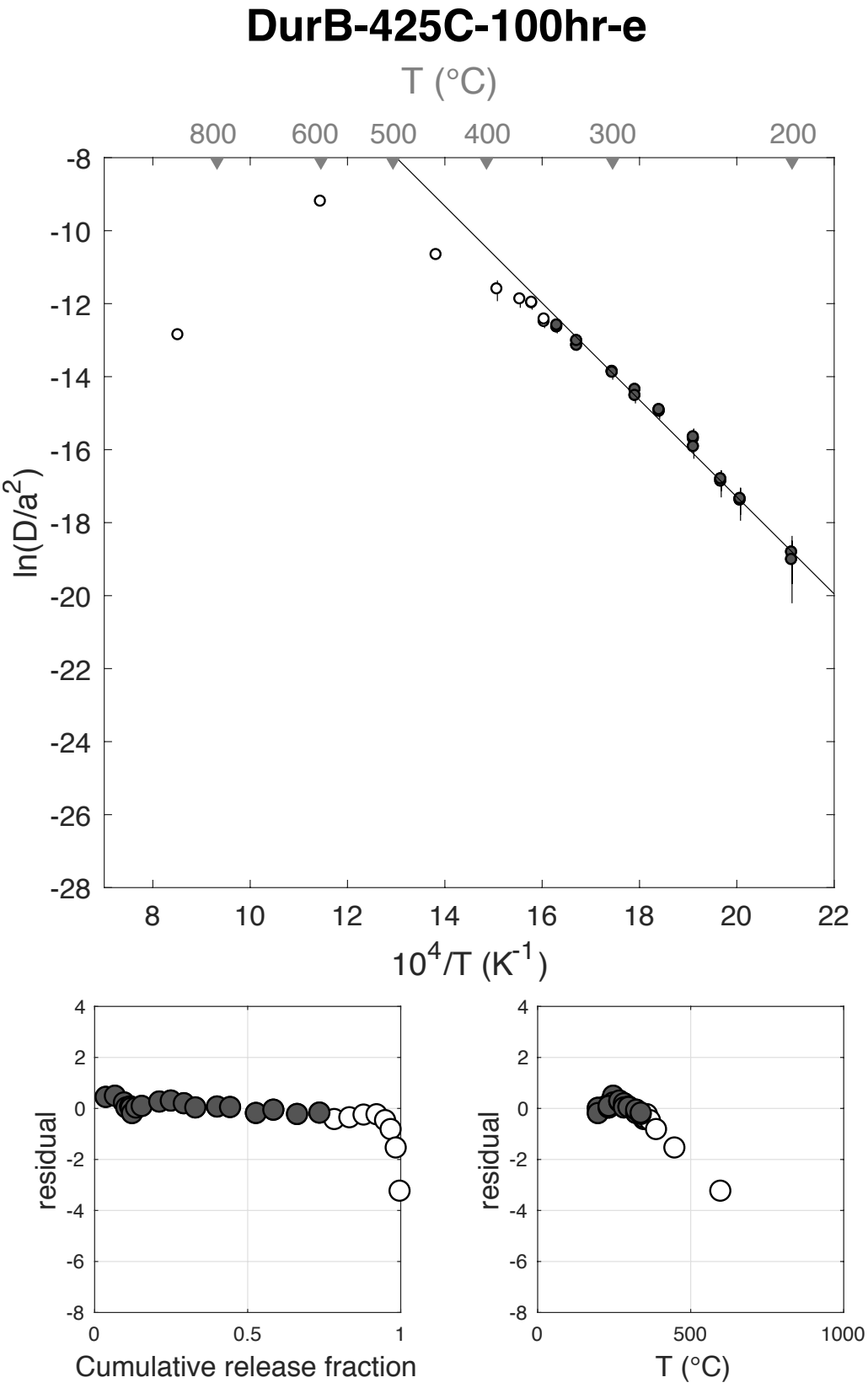
DurB-425C-100hr-e
T (°C)
800
600
500
400
300
200
-8
-10
-12
-14
-16
-18
-20
-22
-24
-26
-28
ln(D/a2)
8
10
12
14
16
18
20
22
10^4/T (K^-1)
4
2
0
-2
-4
-6
-8
residual
0
0.5
1
Cumulative release fraction
0
500
1000
T (°C)

DurB-450C-100hr-a

E_a	+/-	D_0	+/-	T_c	-	+	Total ^{3}He	Incl.	Misfit	Norm. Misfit
128.85	5.28	12.42	1.12	55.54	5.59	5.86	150.80	0.620	0.166	0.009

Step #	°C	t (hrs)	^{3}He	Error	^{4}He	Error	^{4}He/^{3}He	Err	In ^{3}He Reg.
1	250	0.25	3.09	0.26	21.0	19.1	NaN	NaN	1
2	250	0.50	2.01	0.25	19.4	15.9	NaN	NaN	1
3	250	1.00	2.40	0.26	3.6	17.3	NaN	NaN	1
4	225	1.50	0.67	0.14	0.0	0.0	NaN	NaN	1
5	225	2.50	1.02	0.18	0.0	0.0	NaN	NaN	1
6	200	3.00	0.24	0.12	0.0	0.0	NaN	NaN	1
7	200	4.00	0.28	0.12	0.0	0.0	NaN	NaN	1
8	235	2.00	1.34	0.19	0.0	0.0	NaN	NaN	1
9	235	3.00	1.81	0.22	0.0	0.0	NaN	NaN	1
10	270	1.91	5.71	0.35	34.1	19.8	NaN	NaN	1
11	270	1.57	3.44	0.28	17.2	20.2	NaN	NaN	1
12	285	1.25	4.71	0.36	25.7	19.8	NaN	NaN	1
13	285	1.57	4.82	0.32	28.3	19.1	NaN	NaN	1
14	300	1.91	9.60	0.48	47.1	16.5	NaN	NaN	1
15	300	1.45	5.63	0.37	37.8	17.4	NaN	NaN	1
16	325	1.74	15.86	0.58	120.8	16.5	NaN	NaN	1
17	325	1.32	7.81	0.44	48.6	13.2	NaN	NaN	1
18	340	1.58	11.86	0.52	85.1	20.0	NaN	NaN	1
19	340	1.89	11.16	0.55	77.5	16.6	NaN	NaN	1
20	350	1.48	9.60	0.50	62.2	15.4	NaN	NaN	0
21	350	1.82	8.67	0.45	46.5	19.6	NaN	NaN	0
22	360	1.50	4.24	0.30	16.4	13.6	NaN	NaN	0
23	360	1.98	8.46	0.43	40.5	21.1	NaN	NaN	0
24	370	1.88	7.21	0.46	40.0	18.9	NaN	NaN	0
25	390	1.47	6.08	0.38	37.5	16.7	NaN	NaN	0
26	450	1.00	9.79	0.52	78.4	15.0	NaN	NaN	0
27	600	1.00	3.26	0.28	55.6	17.1	7.0	0.32	0
28	900	1.00	0.01	0.07	2.5	18.7	471.7	15.57	0
29	900	1.00	0.00	0.00	0.0	0.0	NaN	NaN	0

Figure S46

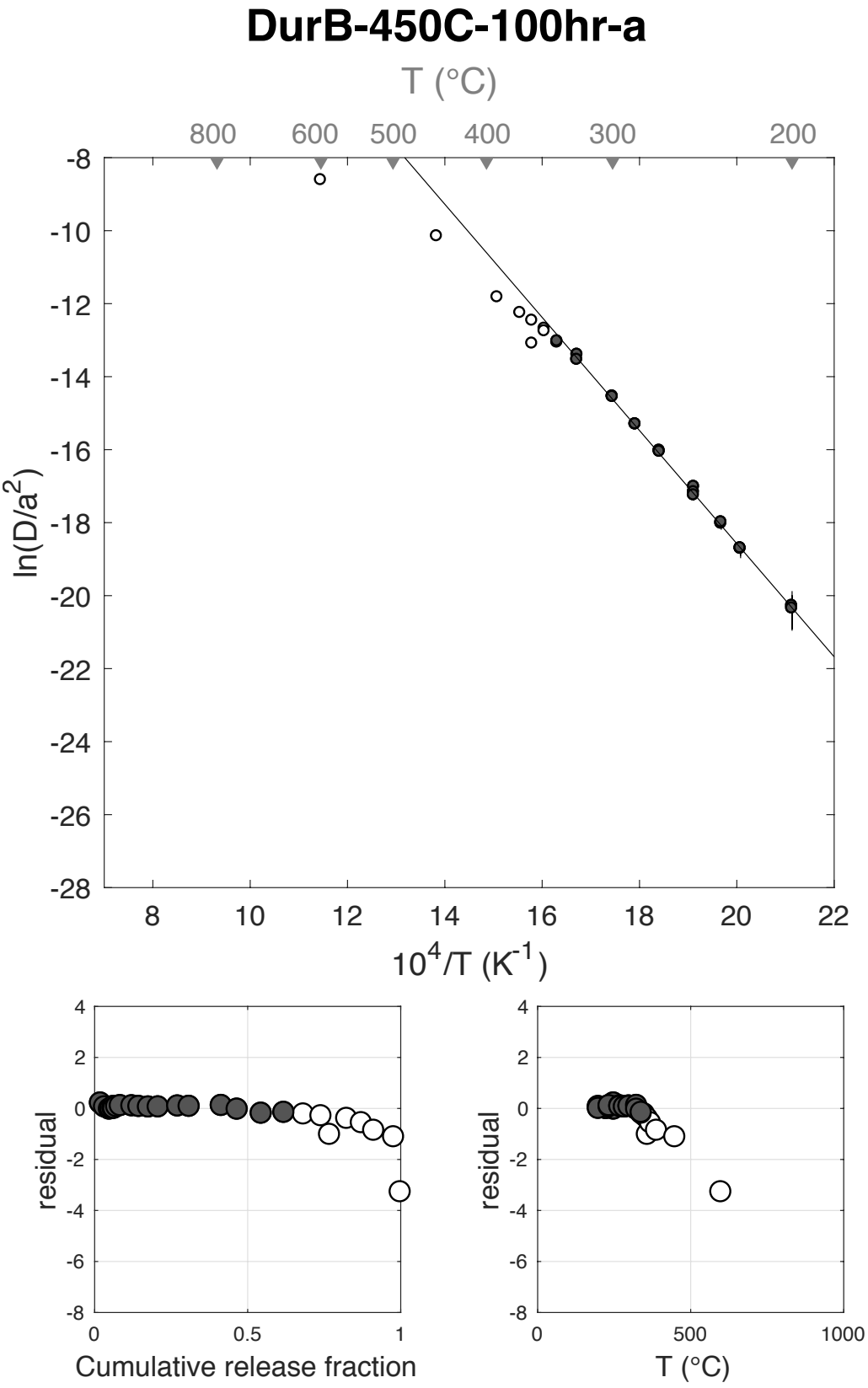
DurB-450C-100hr-a
T (°C)
800
600
500
400
300
200
-8
-10
-12
-14
-16
-18
-20
-22
-24
-26
-28
ln(D/a2)
8
10
12
14
16
18
20
22
10^4/T (K^-1)
4
2
0
-2
-4
-6
-8
residual
0
0.5
1
Cumulative release fraction
0
500
1000
T (°C)

DurB-450C-100hr-b

E_a	+/-	D_0	+/-	T_c	-	+	Total ^{3}He	Incl.	Misfit	Norm. Misfit
129.63	10.55	11.85	2.18	61.40	11.19	12.27	83.25	0.455	0.676	0.040

Step #	°C	t (hrs)	^{3}He	Error	^{4}He	Error	^{4}He/^{3}He	Err	In ^{3}He Reg.
1	250	0.25	1.03	0.33	24.0	13.1	13.2	0.63	1
2	250	0.50	0.88	0.28	14.0	9.6	6.0	0.75	1
3	250	1.00	1.02	0.29	16.5	8.1	6.2	0.56	1
4	225	1.50	0.22	0.17	15.9	13.9	63.3	1.19	1
5	225	2.50	0.38	0.22	34.7	29.4	82.1	1.03	1
6	200	3.00	0.07	0.16	40.5	38.2	543.0	2.41	0
7	200	4.00	0.09	0.22	54.8	55.4	577.1	2.52	0
8	235	2.00	0.57	0.22	28.7	22.0	40.3	0.86	1
9	235	3.00	0.73	0.24	43.3	38.0	49.5	0.94	1
10	270	1.91	2.80	0.44	33.6	20.7	2.0	0.64	1
11	270	1.57	1.52	0.33	19.2	14.9	2.6	0.81	1
12	285	1.25	1.99	0.44	36.4	12.2	8.3	0.40	1
13	285	1.56	2.04	0.38	29.2	14.1	4.3	0.52	1
14	300	1.91	3.98	0.54	52.2	21.1	3.1	0.43	1
15	300	1.45	2.58	0.43	32.0	13.2	2.4	0.44	1
16	325	1.74	5.43	0.77	63.4	18.3	1.7	0.32	1
17	325	1.32	2.82	0.59	30.7	11.6	0.9	0.43	1
18	340	1.58	5.31	0.66	69.4	15.5	3.1	0.26	1
19	340	1.89	4.58	0.51	57.2	20.3	2.5	0.37	1
20	350	1.48	3.70	0.71	45.7	14.3	2.3	0.37	0
21	350	1.82	4.01	0.61	47.9	19.2	2.0	0.43	0
22	360	1.50	3.73	0.54	60.0	13.7	6.1	0.27	0
23	360	1.98	4.13	0.57	59.4	22.0	4.4	0.40	0
24	370	1.88	3.93	0.55	61.3	20.4	5.6	0.36	0
25	390	1.47	4.21	0.59	50.5	13.6	2.0	0.30	0
26	450	1.00	6.72	0.71	120.7	12.2	8.0	0.15	0
27	600	1.00	9.38	0.85	1547.2	35.6	154.9	0.09	0
28	900	1.00	5.42	0.73	5349.7	58.6	977.4	0.14	0
29	900	1.00	0.00	0.07	13.8	8.0	30181.0	160.88	0

Figure S47

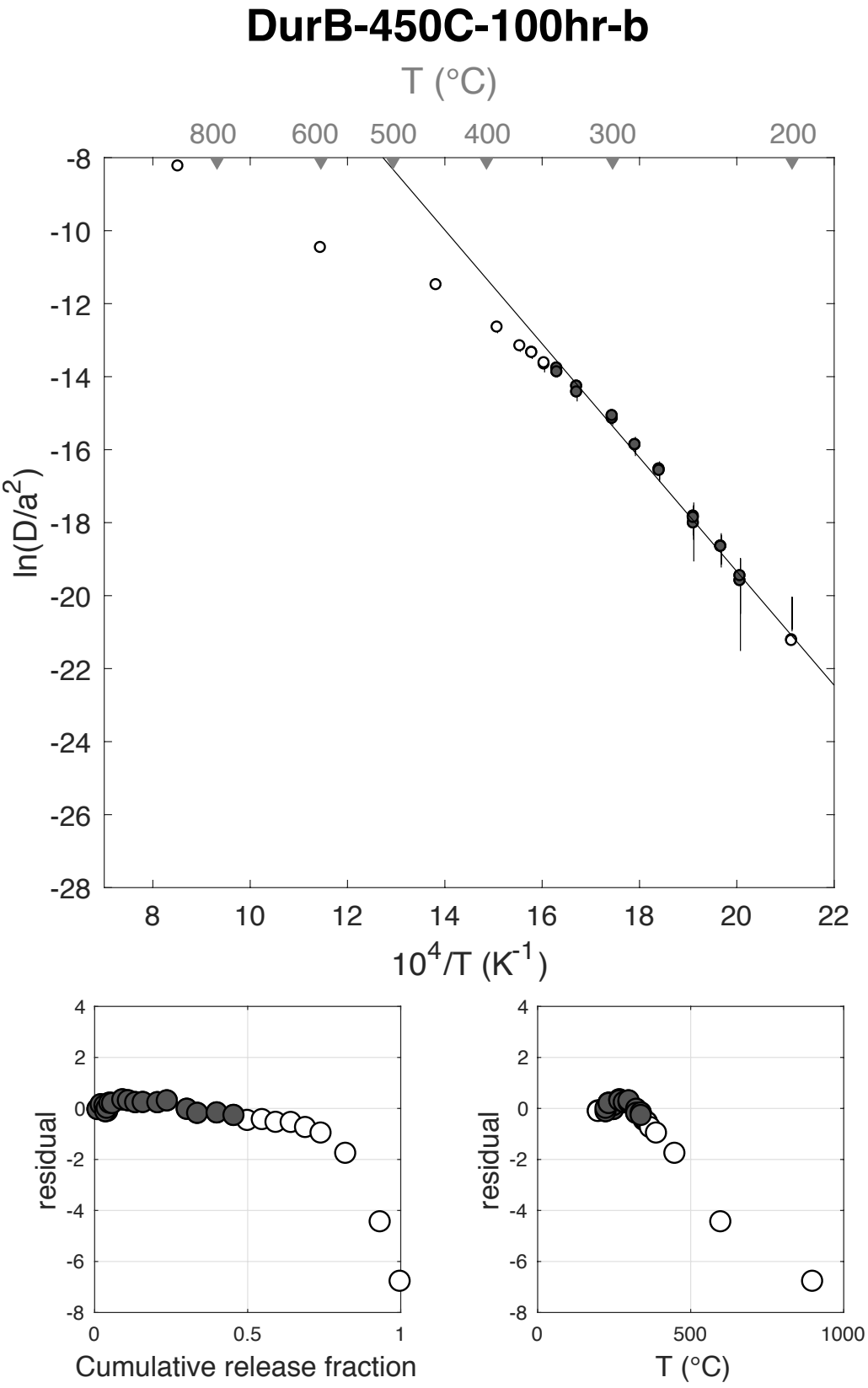
DurB-450C-100hr-b
T (°C)
800
600
500
400
300
200
-8
-10
-12
-14
-16
-18
-20
-22
-24
-26
-28
ln(D/a2)
8
10
12
14
16
18
20
22
10^4/T (K^-1)
4
2
0
-2
-4
-6
-8
residual
0
0.5
1
Cumulative release fraction
residual
0
500
1000
T (°C)

DurB-220C-1000hr-a

E_a	+/-	D_0	+/-	T_c	-	+	Total ^{3}He	Incl.	Misfit	Norm. Misfit
129.61	10.14	11.60	2.08	63.03	10.85	11.84	53.25	0.419	0.336	0.024

Step #	°C	t (hrs)	^{3}He	Error	^{4}He	Error	^{4}He/^{3}He	Err	In ^{3}He Reg.
1	250	0.25	0.79	0.15	95.3	14.9	110.6	0.25	1
2	250	0.50	0.40	0.11	57.1	11.4	133.6	0.35	1
3	250	1.00	0.52	0.12	69.4	14.1	123.0	0.30	1
4	225	1.50	0.17	0.09	0.0	0.0	NaN	NaN	0
5	225	2.50	0.18	0.14	0.0	0.0	NaN	NaN	0
6	200	3.00	0.07	0.17	0.0	0.0	NaN	NaN	0
7	200	4.00	0.12	0.24	0.0	0.0	NaN	NaN	0
8	235	2.00	0.24	0.13	0.0	0.0	NaN	NaN	0
9	235	3.00	0.30	0.18	0.0	0.0	NaN	NaN	1
10	270	1.91	1.34	0.21	451.8	17.6	326.4	0.16	1
11	270	1.57	0.76	0.17	280.3	13.8	358.8	0.23	1
12	285	1.25	0.99	0.16	676.5	14.8	673.6	0.17	1
13	285	1.56	1.03	0.21	797.3	16.9	764.9	0.20	1
14	300	1.91	2.09	0.23	1999.2	28.0	948.3	0.11	1
15	300	1.45	1.23	0.19	1385.1	20.5	1112.1	0.15	1
16	325	1.74	3.48	0.31	4730.2	36.4	1349.9	0.09	1
17	325	1.32	2.24	0.20	3085.1	33.0	1365.4	0.09	1
18	340	1.58	3.64	0.30	5736.0	37.9	1567.8	0.08	1
19	340	1.89	3.53	0.32	5648.3	41.3	1591.5	0.09	1
20	350	1.48	3.27	0.31	5325.3	43.4	1620.0	0.09	0
21	350	1.82	3.22	0.30	5415.3	45.6	1670.9	0.09	0
22	360	1.50	2.90	0.27	5231.0	37.1	1794.7	0.09	0
23	360	1.98	3.45	0.34	5887.0	41.6	1698.8	0.10	0
24	370	1.88	3.46	0.27	6006.2	48.2	1727.3	0.08	0
25	390	1.47	3.67	0.31	6394.3	41.3	1734.3	0.09	0
26	450	1.00	6.50	0.50	11649.0	62.9	1783.3	0.08	0
27	600	1.00	3.67	0.34	6956.9	38.7	1883.2	0.09	0
28	900	1.00	0.01	0.06	0.0	0.0	NaN	NaN	0
29	900	1.00	0.01	0.06	0.0	0.0	NaN	NaN	0

Figure S48

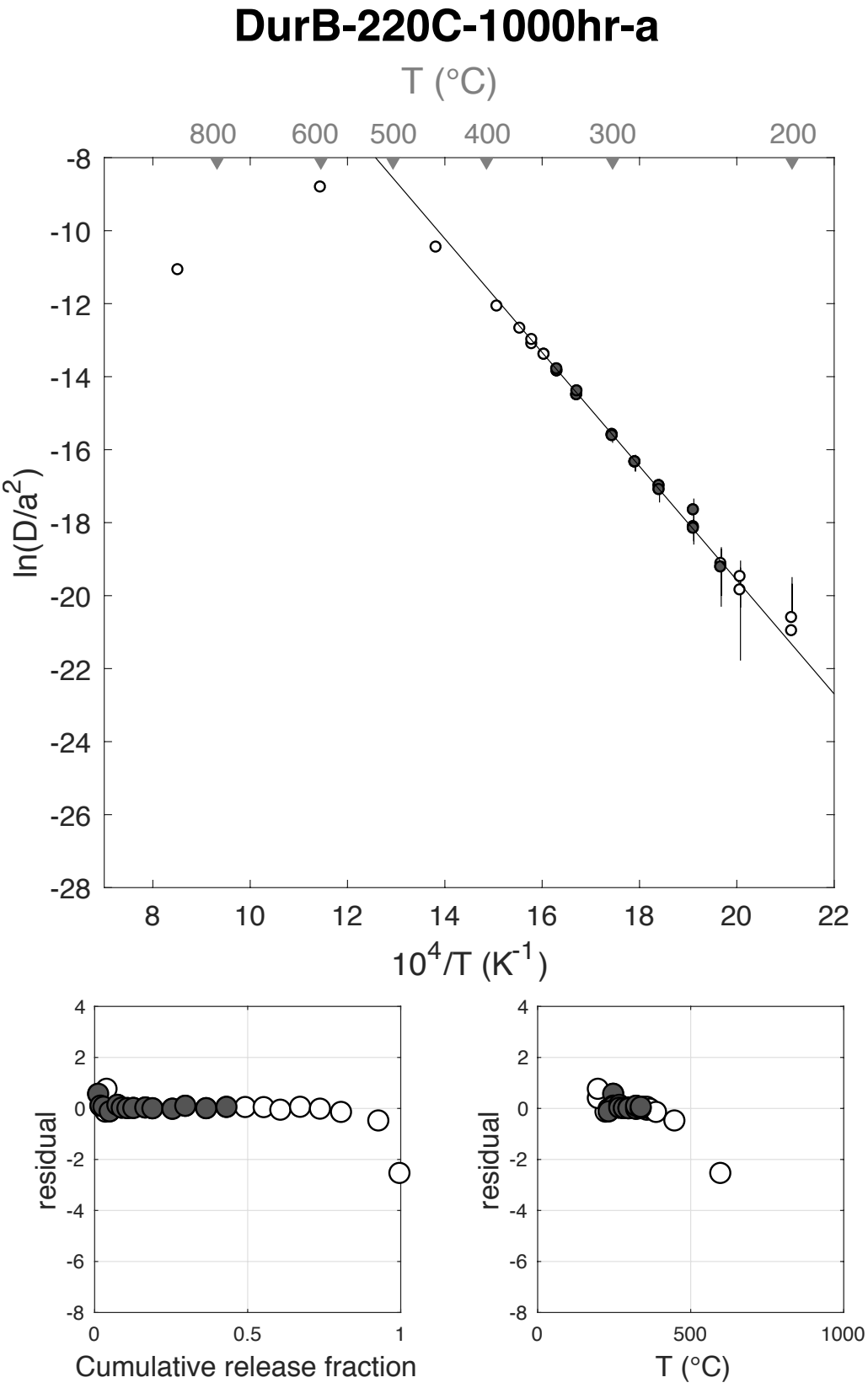
DurB-220C-1000hr-a
T (°C)
800
600
500
400
300
200
-8
-10
-12
-14
-16
-18
-20
-22
-24
-26
-28
ln(D/a2)
8
10
12
14
16
18
20
22
10^4/T (K^-1)
4
2
0
-2
-4
-6
-8
residual
0
0.5
1
Cumulative release fraction
500
1000
T (°C)

DurB-220C-1000hr-b

E_a	+/-	D_0	+/-	T_c	-	+	Total ^{3}He	Incl.	Misfit	Norm. Misfit
127.24	9.84	10.61	2.01	63.95	10.78	11.76	49.61	0.328	0.081	0.006

Step #	°C	t (hrs)	^{3}He	Error	^{4}He	Error	^{4}He/^{3}He	Err	In ^{3}He Reg.
1	250	0.25	0.50	0.12	30.2	9.6	50.7	0.40	1
2	250	0.50	0.31	0.10	29.6	8.2	85.7	0.43	1
3	250	1.00	0.40	0.09	0.0	0.0	NaN	NaN	1
4	225	1.50	0.11	0.07	0.0	0.0	NaN	NaN	0
5	225	2.50	0.14	0.08	0.0	0.0	NaN	NaN	0
6	200	3.00	0.08	0.08	0.0	0.0	NaN	NaN	0
7	200	4.00	0.04	0.09	0.0	0.0	NaN	NaN	0
8	235	2.00	0.21	0.10	0.0	0.0	NaN	NaN	0
9	235	3.00	0.21	0.10	0.0	0.0	NaN	NaN	0
10	270	1.91	0.90	0.16	178.7	16.7	187.7	0.20	1
11	270	1.57	0.61	0.13	175.7	11.3	280.0	0.23	1
12	285	1.25	0.85	0.15	426.3	25.9	489.9	0.18	1
13	285	1.56	0.74	0.14	488.5	17.1	646.8	0.20	1
14	300	1.91	1.56	0.19	1284.9	21.1	812.5	0.12	1
15	300	1.45	1.07	0.17	1016.8	14.4	944.0	0.16	1
16	325	1.74	2.61	0.28	3162.3	46.4	1201.5	0.11	1
17	325	1.32	1.65	0.20	2166.8	25.6	1299.6	0.12	1
18	340	1.58	2.67	0.28	3934.4	33.9	1465.6	0.10	1
19	340	1.89	2.42	0.24	3683.9	39.8	1514.5	0.10	1
20	350	1.48	2.09	0.24	3408.8	33.9	1619.9	0.11	0
21	350	1.82	2.12	0.23	3432.8	31.4	1609.3	0.11	0
22	360	1.50	2.02	0.23	3262.6	45.2	1604.4	0.11	0
23	360	1.98	2.07	0.24	3446.0	25.8	1652.3	0.11	0
24	370	1.88	2.20	0.26	3457.1	39.6	1562.0	0.12	0
25	390	1.47	2.27	0.25	3769.6	33.1	1653.5	0.11	0
26	450	1.00	3.80	0.30	6513.8	44.5	1702.9	0.08	0
27	600	1.00	3.62	0.32	5763.2	38.9	1583.8	0.09	0
28	880	1.00	12.31	0.66	1199.2	21.5	87.4	0.06	0
29	900	1.00	0.01	0.05	36.4	14.8	2958.9	4.03	0
30	900	1.00	0.02	0.04	18.9	10.8	1223.7	2.86	0

Figure S49

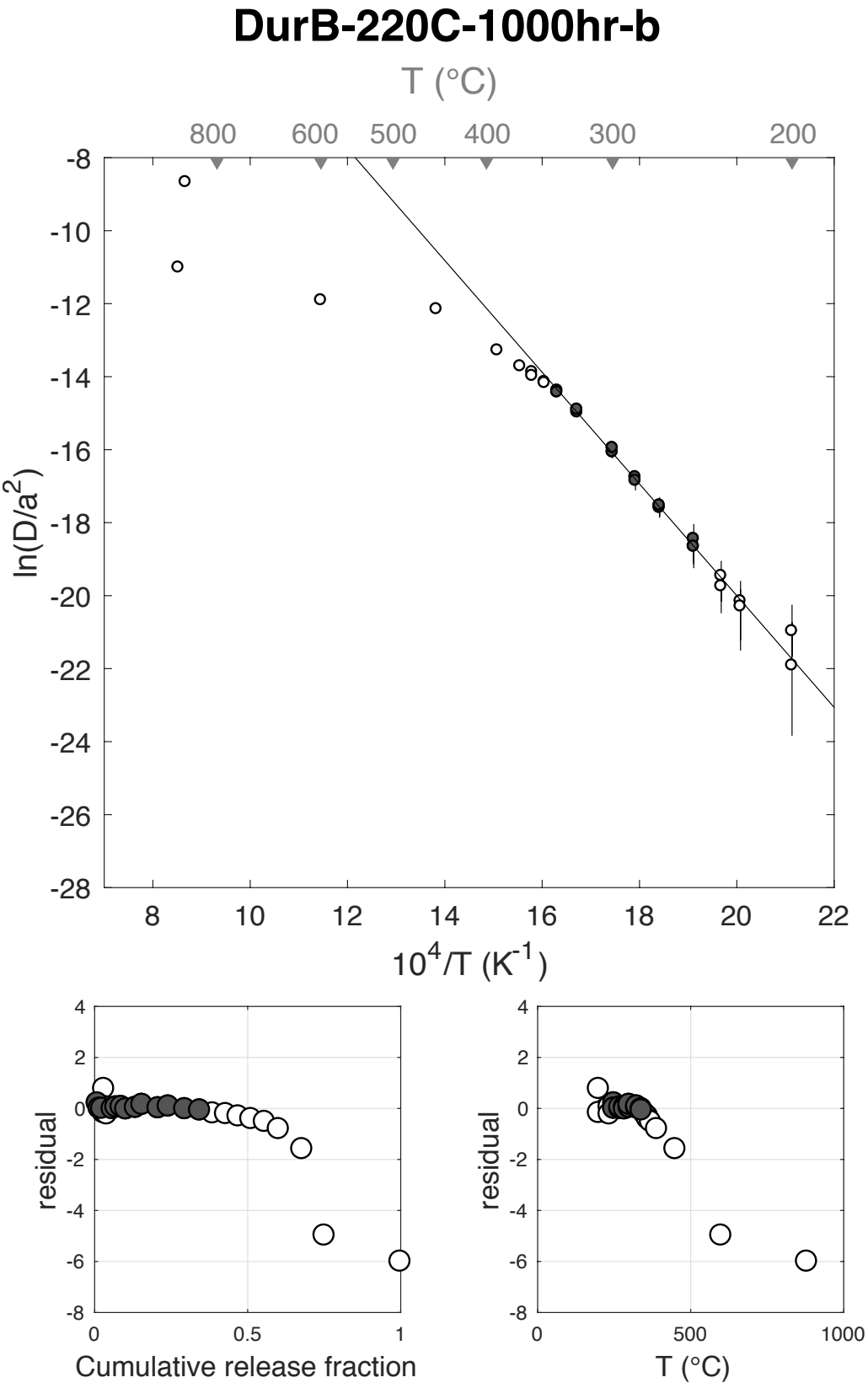
DurB-220C-1000hr-b
T (°C)
800
600
500
400
300
200
-8
-10
-12
-14
-16
-18
-20
-22
-24
-26
-28
ln(D/a2)
8
10
12
14
16
18
20
22
10^4/T (K^-1)
4
2
0
-2
-4
-6
-8
residual
0
0.5
1
Cumulative release fraction
0
500
1000
T (°C)

DurB-220C-1000hr-c

E_a	+/-	D_0	+/-	T_c	-	+	Total ^{3}He	Incl.	Misfit	Norm. Misfit
131.35	9.47	11.65	1.93	67.15	10.08	10.94	45.06	0.396	1.109	0.085

Step #	°C	t (hrs)	^{3}He	Error	^{4}He	Error	^{4}He/^{3}He	Err	In ^{3}He Reg.
1	250	0.25	0.58	0.12	27.0	29.4	36.8	1.11	1
2	250	0.50	0.33	0.10	23.7	19.7	61.4	0.89	1
3	250	1.00	0.44	0.12	1.1	13.2	NaN	NaN	1
4	225	1.50	0.04	0.07	0.0	0.0	NaN	NaN	0
5	225	2.50	0.03	0.08	0.0	0.0	NaN	NaN	0
6	200	3.00	0.00	0.00	0.0	0.0	NaN	NaN	0
7	200	4.00	0.00	0.00	0.0	0.0	NaN	NaN	0
8	235	2.00	0.03	0.09	0.0	0.0	NaN	NaN	0
9	235	3.00	0.01	0.09	0.0	0.0	NaN	NaN	0
10	270	1.91	0.70	0.17	130.8	49.4	177.6	0.45	1
11	270	1.57	0.50	0.13	138.4	34.1	265.6	0.36	1
12	285	1.25	0.80	0.14	378.4	26.4	460.5	0.19	1
13	285	1.56	0.82	0.17	461.3	35.4	553.2	0.22	1
14	300	1.91	1.67	0.25	1350.1	1.9	799.7	0.15	1
15	300	1.45	0.99	0.20	925.2	34.0	926.9	0.20	1
16	325	1.74	2.98	0.31	3646.0	51.8	1215.2	0.10	1
17	325	1.32	1.90	0.24	2609.4	34.6	1360.9	0.13	1
18	340	1.58	3.21	0.28	4861.0	47.5	1503.3	0.09	1
19	340	1.89	2.93	0.35	4774.8	64.9	1617.8	0.12	1
20	350	1.48	2.85	0.29	4695.4	48.4	1638.1	0.10	0
21	350	1.82	2.81	0.29	4729.5	55.8	1671.0	0.10	0
22	360	1.50	2.54	0.25	4652.5	47.0	1819.1	0.10	0
23	360	1.98	2.92	0.30	5055.7	60.8	1720.5	0.10	0
24	370	1.88	2.92	0.28	5108.3	60.0	1742.3	0.10	0
25	390	1.47	3.05	0.33	5638.0	49.0	1841.1	0.11	0
26	450	1.00	5.87	0.35	10257.2	40.7	1736.2	0.06	0
27	600	1.00	4.10	0.33	8154.1	43.1	1981.2	0.08	0
28	900	1.00	0.00	0.00	11.5	12.5	Inf	NaN	0
29	900	1.00	0.04	0.07	9.9	11.0	251.3	2.08	0

Figure S50

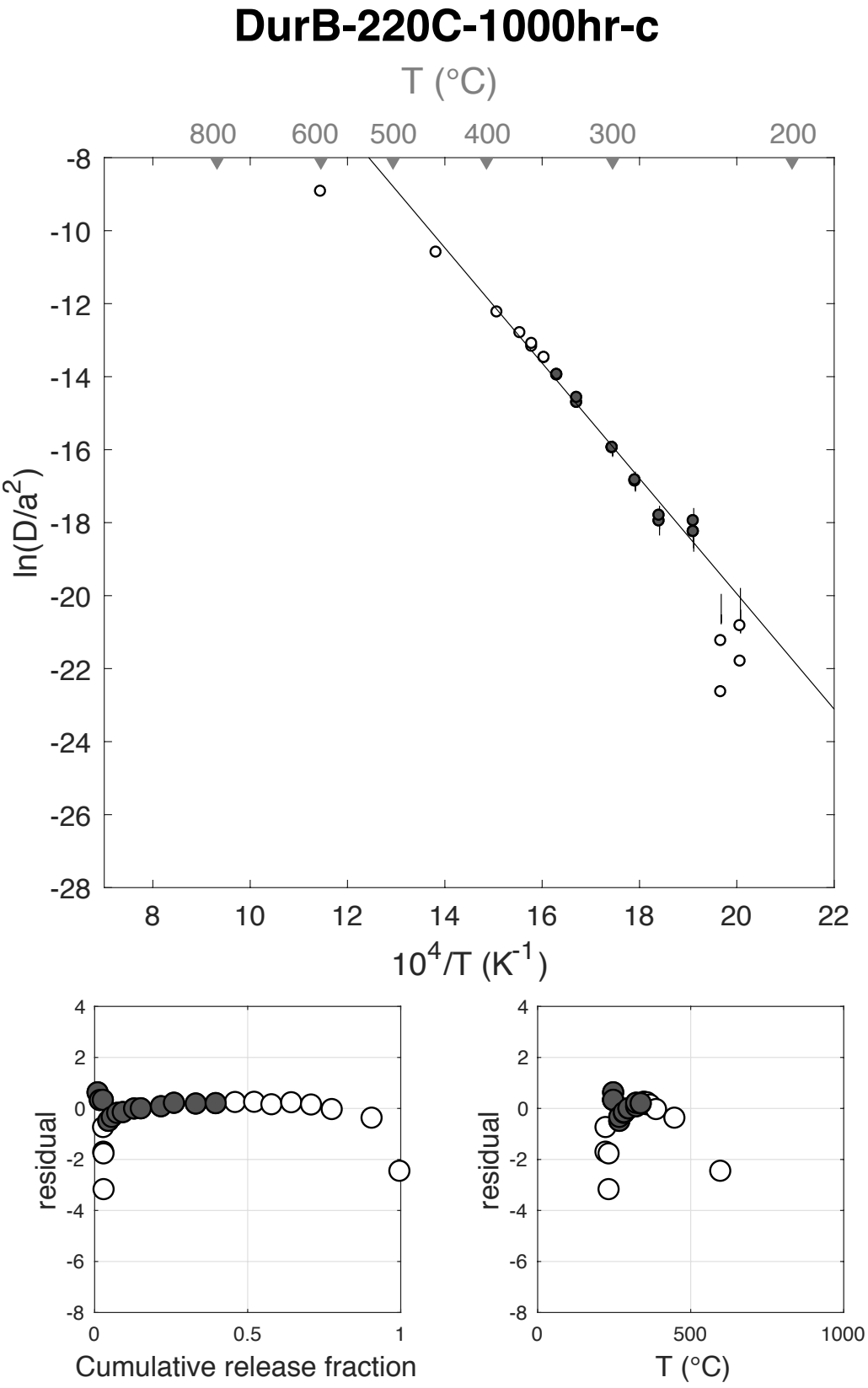
DurB-220C-1000hr-c
T (°C)
800
600
500
400
300
200
-8
-10
-12
-14
-16
-18
-20
-22
-24
-26
-28
ln(D/a2)
8
10
12
14
16
18
20
22
10^4/T (K^-1)
4
2
0
-2
-4
-6
-8
residual
0
0.5
1
Cumulative release fraction
0
500
1000
T (°C)

E_a	+/-	D_0	+/-	T_c	-	+	Total ^{3}He	Incl.	Misfit	Norm. Misfit
136.66	9.91	13.16	2.03	69.87	10.02	10.89	50.34	0.460	0.476	0.032

Step #	°C	t (hrs)	^{3}He	Error	^{4}He	Error	^{4}He/^{3}He	Err	In ^{3}He Reg.
1	250	0.25	0.55	0.15	37.8	19.9	59.0	0.59	1
2	250	0.50	0.39	0.10	17.2	14.2	33.7	0.86	1
3	250	1.00	0.52	0.12	0.0	0.0	NaN	NaN	1
4	225	1.50	0.13	0.07	0.0	0.0	NaN	NaN	0
5	225	2.50	0.33	0.15	0.0	0.0	NaN	NaN	1
6	200	3.00	0.04	0.14	0.0	0.0	NaN	NaN	0
7	200	4.00	0.09	0.20	0.0	0.0	NaN	NaN	0
8	235	2.00	0.22	0.12	0.0	0.0	NaN	NaN	0
9	235	3.00	0.32	0.16	0.0	0.0	NaN	NaN	1
10	270	1.91	1.12	0.21	69.8	32.1	52.1	0.50	1
11	270	1.57	0.60	0.15	75.3	23.3	115.0	0.40	1
12	285	1.25	1.01	0.18	248.2	16.9	235.0	0.19	1
13	285	1.56	1.10	0.17	310.8	23.5	272.5	0.17	1
14	300	1.91	2.23	0.28	896.9	37.6	392.3	0.13	1
15	300	1.45	1.45	0.18	730.0	26.0	492.2	0.13	1
16	325	1.74	3.83	0.34	2819.0	38.8	726.9	0.09	1
17	325	1.32	2.34	0.29	2025.4	28.1	854.1	0.12	1
18	340	1.58	3.85	0.39	3959.1	33.7	1017.6	0.10	1
19	340	1.89	3.50	0.28	3968.4	47.3	1123.9	0.08	1
20	350	1.48	2.85	0.27	3524.4	31.5	1227.5	0.10	0
21	350	1.82	3.07	0.32	3960.3	47.3	1278.2	0.10	0
22	360	1.50	2.91	0.29	3628.5	43.0	1236.4	0.10	0
23	360	1.98	3.23	0.29	4339.8	50.7	1333.1	0.09	0
24	370	1.88	3.29	0.28	4358.7	49.2	1316.7	0.08	0
25	390	1.47	3.09	0.28	4379.9	41.1	1407.8	0.09	0
26	450	1.00	5.10	0.35	7336.3	56.5	1428.7	0.07	0
27	600	1.00	3.16	0.31	5003.0	41.9	1572.4	0.10	0
28	900	1.00	0.01	0.05	0.0	0.0	NaN	NaN	0
29	900	1.00	0.00	0.00	0.0	0.0	NaN	NaN	0

Figure S51

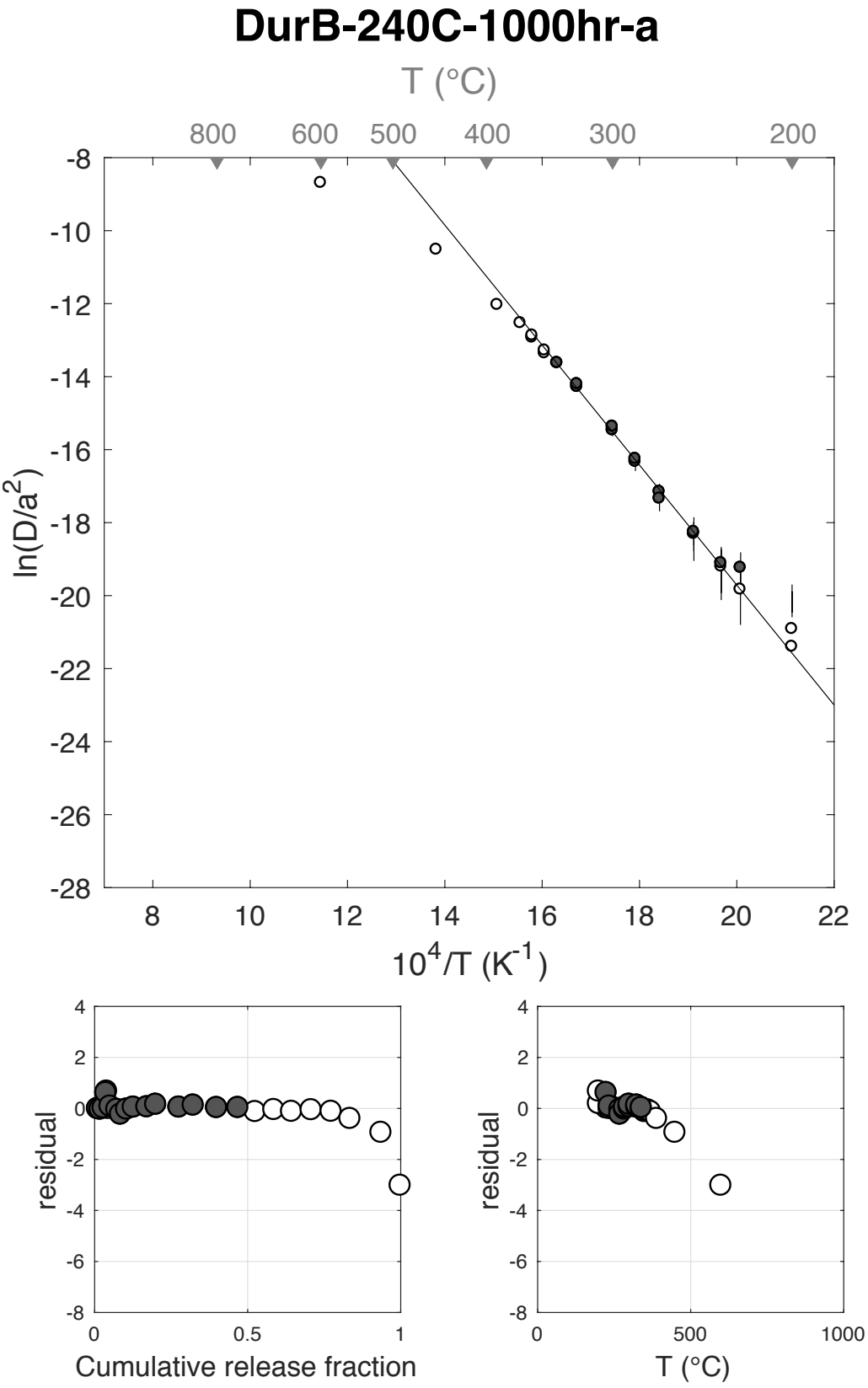
DurB-240C-1000hr-a
T (°C)
800
600
500
400
300
200
-8
-10
-12
-14
-16
-18
-20
-22
-24
-26
-28
ln(D/a2)
8
10
12
14
16
18
20
22
10^4/T (K^-1)
4
2
0
-2
-4
-6
-8
residual
0
0.5
1
Cumulative release fraction
0
500
1000
T (°C)

DurB-240C-1000hr-b

E_a	+/-	D_0	+/-	T_c	-	+	Total ^{3}He	Incl.	Misfit	Norm. Misfit
132.25	3.20	14.03	0.68	53.37	3.33	3.42	248.79	0.870	0.844	0.028

Step #	°C	t (hrs)	^{3}He	Error	^{4}He	Error	^{4}He/^{3}He	Err	In ^{3}He Reg.
1	250	0.50	9.89	0.64	987.4	28.5	89.9	0.07	1
2	250	1.00	7.50	0.53	1399.3	25.7	176.6	0.07	1
3	240	1.00	2.86	0.35	705.9	20.1	236.5	0.12	1
4	230	1.50	2.09	0.29	564.9	21.9	260.1	0.14	1
5	230	2.50	3.05	0.34	902.6	29.4	285.5	0.12	1
6	210	2.50	0.65	0.18	230.9	21.6	345.3	0.30	1
7	210	3.50	0.91	0.21	331.2	35.1	354.0	0.25	1
8	200	3.00	0.41	0.16	123.1	25.2	290.1	0.44	1
9	200	4.00	0.36	0.15	162.5	35.9	440.1	0.47	1
10	220	2.50	1.20	0.24	455.0	26.2	369.2	0.21	1
11	220	3.50	1.68	0.27	612.0	33.6	354.1	0.17	1
12	235	2.00	2.43	0.32	949.7	29.7	381.0	0.14	1
13	235	3.00	3.34	0.33	1410.2	32.6	412.5	0.10	1
14	250	1.00	2.63	0.33	1150.1	29.4	426.9	0.13	1
15	260	1.91	8.08	0.59	3894.3	52.0	472.0	0.07	1
16	260	1.57	5.51	0.43	3067.7	36.3	546.3	0.08	1
17	270	1.91	8.66	0.56	6312.4	53.1	719.3	0.07	1
18	270	1.57	7.09	0.48	5145.5	70.4	715.9	0.07	1
19	280	1.25	7.85	0.57	6365.5	86.7	800.7	0.07	1
20	280	1.57	9.00	0.62	7595.5	106.7	834.2	0.07	1
21	290	1.25	9.76	0.60	9158.3	89.3	928.6	0.06	1
22	290	1.57	10.44	0.65	10480.0	90.0	993.5	0.06	1
23	300	1.91	16.80	0.72	17287.0	176.9	1019.2	0.04	1
24	300	1.45	10.76	0.58	11494.9	130.1	1058.2	0.06	1
25	315	1.74	18.36	0.81	21898.8	168.3	1182.7	0.04	1
26	315	1.32	10.56	0.86	13886.4	99.6	1305.2	0.08	1
27	330	1.74	18.74	0.93	25593.5	180.5	1355.5	0.05	1
28	330	1.32	11.38	0.65	15031.6	174.9	1311.4	0.06	1
29	340	1.58	13.56	0.74	19085.7	169.8	1397.3	0.06	1
30	340	1.89	10.97	0.62	15407.9	290.4	1394.3	0.06	1
31	350	1.48	8.13	0.54	11651.1	145.5	1422.3	0.07	0
32	350	1.82	6.59	0.48	9168.6	106.5	1381.1	0.07	0
33	360	1.50	4.66	0.41	6549.9	164.8	1395.8	0.09	0
34	360	1.98	3.47	0.38	5219.6	71.8	1495.9	0.11	0
35	370	1.88	2.62	0.31	3882.5	52.7	1471.5	0.12	0
36	390	1.47	2.31	0.29	3365.2	48.1	1444.1	0.13	0
37	450	1.00	4.49	0.39	6201.7	69.3	1372.5	0.09	0

Figure S52

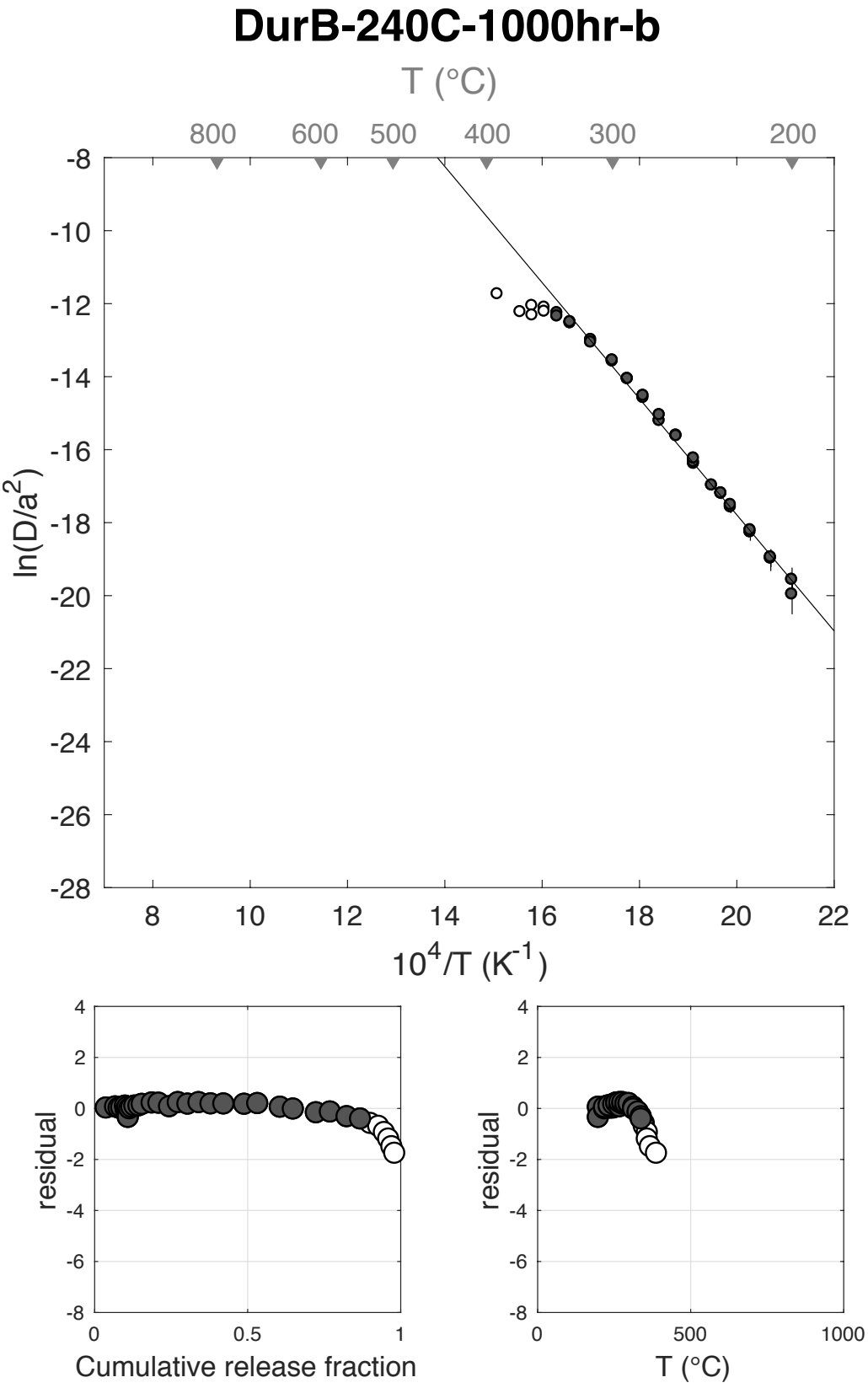
DurB-240C-1000hr-b
T (°C)
800
600
500
400
300
200
-8
-10
-12
-14
-16
-18
-20
-22
-24
-26
-28
ln(D/a2)
8
10
12
14
16
18
20
22
10^4/T (K^-1)
4
2
0
-2
-4
-6
-8
residual
0
0.5
1
Cumulative release fraction
500
1000
T (°C)

DurB-260C-1000hr-a

E_a	+/-	D_0	+/-	T_c	-	+	Total ^{3}He	Incl.	Misfit	Norm. Misfit
133.72	10.52	12.47	2.14	67.38	10.93	11.94	34.01	0.425	0.149	0.011

Step #	°C	t (hrs)	^{3}He	Error	^{4}He	Error	^{4}He/^{3}He	Err	In ^{3}He Reg.
1	250	0.25	0.42	0.10	58.1	22.6	129.3	0.46	1
2	250	0.50	0.29	0.10	30.5	14.8	95.3	0.59	1
3	250	1.00	0.33	0.10	0.0	0.0	NaN	NaN	1
4	225	1.50	0.14	0.07	0.0	0.0	NaN	NaN	0
5	225	2.50	0.14	0.07	0.0	0.0	NaN	NaN	0
6	200	3.00	0.02	0.05	0.0	0.0	NaN	NaN	0
7	200	4.00	0.04	0.06	0.0	0.0	NaN	NaN	0
8	235	2.00	0.14	0.08	0.0	0.0	NaN	NaN	0
9	235	3.00	0.21	0.08	0.0	0.0	NaN	NaN	0
10	270	1.91	0.66	0.15	0.0	0.0	NaN	NaN	1
11	270	1.57	0.52	0.12	2.4	23.5	NaN	NaN	1
12	285	1.25	0.60	0.12	28.1	15.6	36.8	0.59	1
13	285	1.56	0.73	0.15	44.4	24.1	50.6	0.58	1
14	300	1.91	1.43	0.22	155.3	36.7	98.9	0.28	1
15	300	1.45	0.90	0.14	160.9	23.3	168.0	0.21	1
16	325	1.74	2.43	0.26	679.9	32.1	269.9	0.12	1
17	325	1.32	1.37	0.20	503.9	21.8	357.7	0.15	1
18	340	1.58	2.50	0.24	1101.8	27.8	430.7	0.10	1
19	340	1.89	2.29	0.22	1146.8	39.8	491.3	0.10	1
20	350	1.48	2.02	0.24	1234.0	27.1	600.6	0.12	0
21	350	1.82	1.97	0.24	1326.3	33.8	661.7	0.13	0
22	360	1.50	1.78	0.24	1438.4	29.2	799.9	0.13	0
23	360	1.98	2.01	0.24	1678.3	39.3	824.2	0.12	0
24	370	1.88	1.73	0.23	1849.1	39.8	1057.5	0.13	0
25	390	1.47	2.12	0.25	2202.5	30.5	1030.1	0.12	0
26	450	1.00	3.81	0.31	4562.3	35.1	1186.9	0.08	0
27	599	1.00	3.27	0.28	4625.7	41.8	1406.7	0.09	0
28	900	1.00	0.02	0.05	299.8	14.6	14169.6	2.43	0
29	900	1.00	0.11	0.07	46.7	12.2	408.1	0.67	0

Figure S53

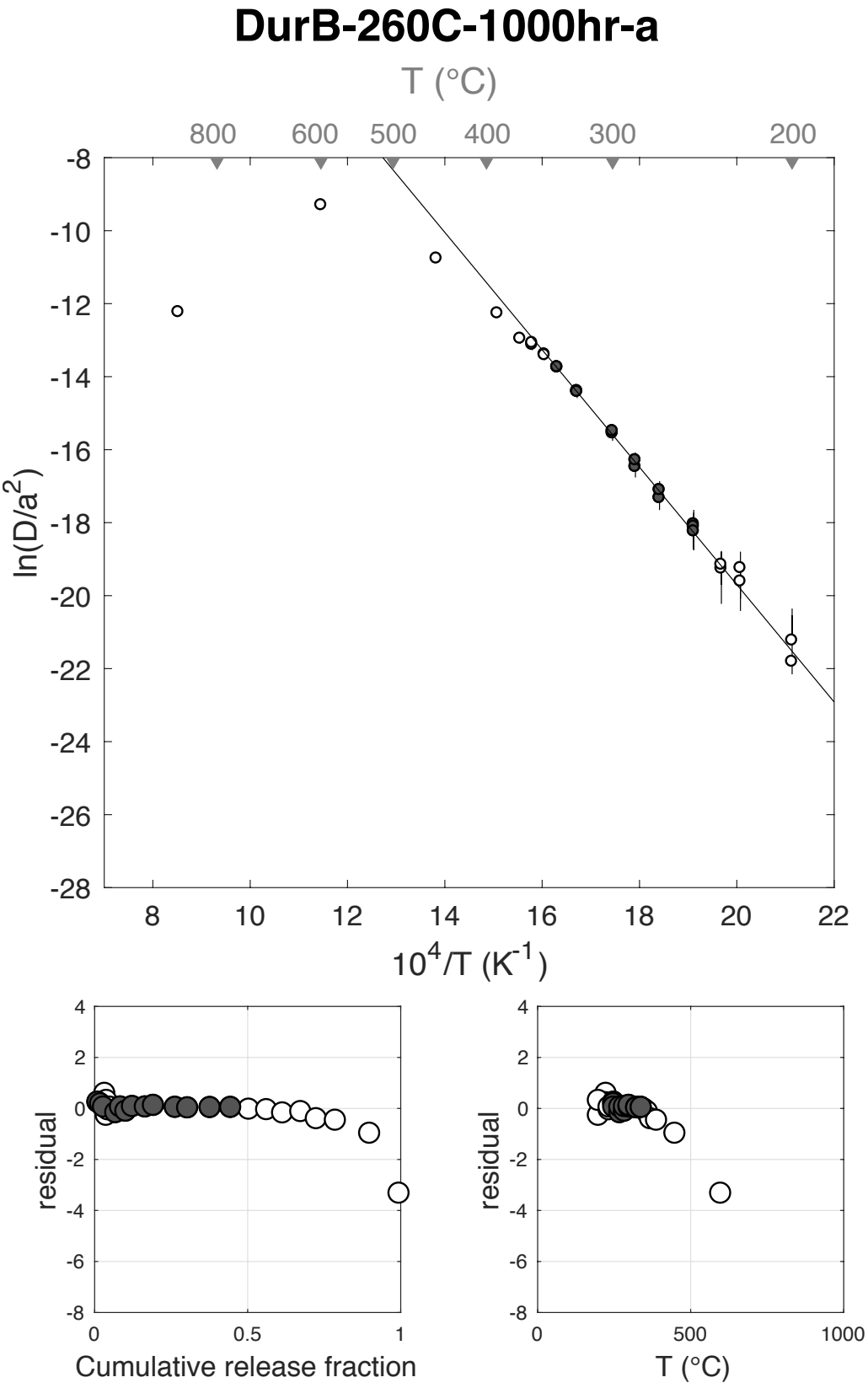
DurB-260C-1000hr-a
T (°C)
800
600
500
400
300
200
-8
-10
-12
-14
-16
-18
-20
-22
-24
-26
-28
ln(D/a2)
8
10
12
14
16
18
20
22
10^4/T (K^-1)
4
2
0
-2
-4
-6
-8
residual
0
0.5
1
Cumulative release fraction
0
500
1000
T (°C)

DurB-260C-1000hr-b

E_a	+/-	D_0	+/-	T_c	-	+	Total ^{3}He	Incl.	Misfit	Norm. Misfit
125.86	4.88	12.85	1.07	45.28	5.11	5.34	185.35	0.612	0.422	0.019

Step #	°C	t (hrs)	^{3}He	Error	^{4}He	Error	^{4}He/^{3}He	Err	In ^{3}He Reg.
1	250	0.50	9.63	0.60	276.4	23.1	18.7	0.10	1
2	250	1.00	6.37	0.48	368.7	35.0	47.9	0.12	1
3	240	1.00	2.54	0.33	201.0	19.5	69.2	0.16	1
4	230	1.50	1.64	0.27	160.7	22.0	88.0	0.21	1
5	230	2.50	2.52	0.32	248.5	21.3	88.7	0.15	1
6	210	2.50	0.71	0.19	68.4	16.4	85.7	0.35	1
7	210	3.50	0.82	0.21	104.1	19.4	116.5	0.31	1
8	200	3.00	0.37	0.17	49.6	18.0	124.4	0.58	1
9	200	4.00	0.43	0.19	64.4	20.3	139.2	0.54	1
10	220	2.50	1.07	0.23	132.5	23.2	113.5	0.28	1
11	220	3.50	1.55	0.26	183.0	24.5	107.7	0.22	1
12	235	2.00	2.19	0.29	253.9	18.7	105.7	0.15	1
13	235	3.00	2.54	0.35	395.0	20.4	145.7	0.15	1
14	250	1.00	2.07	0.27	318.8	23.3	144.1	0.15	1
15	270	1.91	10.08	0.63	1716.8	34.8	160.3	0.07	1
16	270	1.57	6.43	0.50	1349.8	49.2	200.0	0.09	1
17	285	1.25	8.75	0.54	2164.5	34.2	237.4	0.06	1
18	285	1.57	8.91	0.58	2629.3	41.3	285.1	0.07	1
19	300	1.91	15.08	2.20	5753.3	85.7	371.4	0.15	1
20	300	1.45	8.25	0.64	4089.5	95.9	485.8	0.08	1
21	315	1.74	13.82	0.73	7593.7	94.3	539.3	0.05	1
22	315	1.32	7.62	0.53	4968.8	83.0	642.4	0.07	1
23	330	1.74	13.66	0.71	9805.7	122.6	707.6	0.05	0
24	330	1.32	7.72	0.60	6089.2	56.8	778.5	0.08	0
25	340	1.58	9.05	0.61	7891.4	97.6	861.9	0.07	0
26	340	1.89	7.82	0.56	7098.4	76.6	897.9	0.07	0
27	350	1.48	5.99	0.48	5783.0	76.4	956.0	0.08	0
28	350	1.82	4.83	0.39	4836.9	83.8	992.3	0.08	0
29	360	1.50	3.66	0.36	3948.5	54.4	1069.2	0.10	0
30	360	1.98	3.06	0.33	3464.0	41.3	1122.8	0.11	0
31	370	1.88	2.85	0.32	3291.2	35.6	1143.5	0.11	0
32	390	1.47	2.69	0.32	3273.5	44.4	1205.7	0.12	0
33	450	1.00	4.05	0.39	4932.8	60.8	1206.9	0.10	0
34	600	1.00	3.97	0.39	4743.3	66.8	1183.8	0.10	0
35	900	1.00	2.53	0.27	4024.0	37.4	1582.4	0.11	0
36	900	1.00	0.04	0.09	4.8	13.8	98.0	3.60	0
37	900	1.00	0.02	0.09	0.1	11.7	NaN	NaN	0

Figure S54

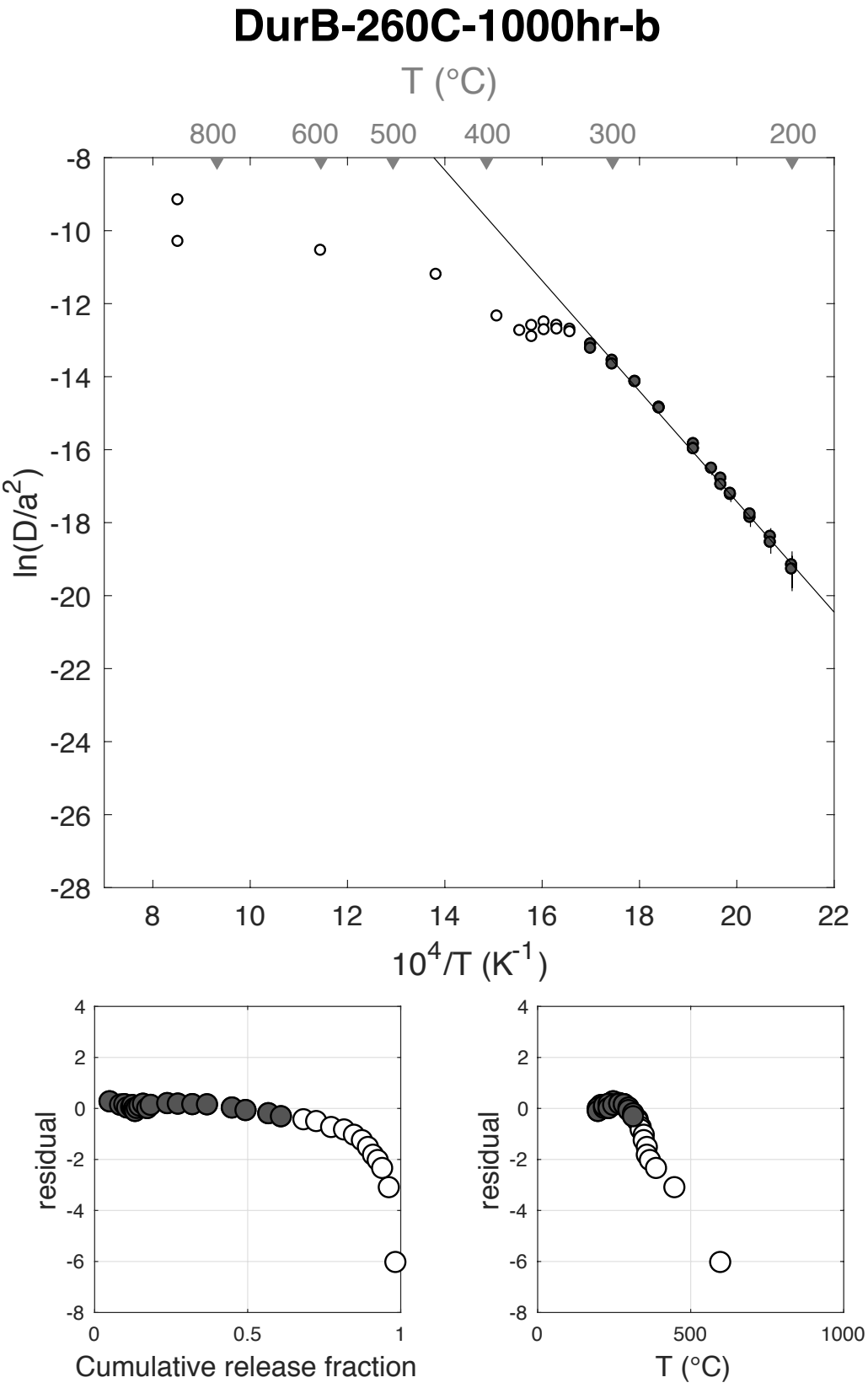
DurB-260C-1000hr-b
T (°C)
800
600
500
400
300
200
-8
-10
-12
-14
-16
-18
-20
-22
-24
-26
-28
ln(D/a2)
8
10
12
14
16
18
20
22
10^4/T (K^-1)
4
2
0
-2
-4
-6
-8
residual
0
0.5
1
Cumulative release fraction
0
500
1000
T (°C)

LDP-NH-c

E_a	+/-	D_0	+/-	T_c	-	+	Total ^{3}He	Incl.	Misfit	Norm. Misfit
146.91	8.92	14.53	1.84	85.27	8.16	8.78	106.73	0.335	0.373	0.022

Step #	°C	t (hrs)	^{3}He	Error	^{4}He	Error	^{4}He/^{3}He	Err	In ^{3}He Reg.
1	250	0.25	0.91	0.16	421.9	21.3	454.4	0.19	1
2	250	0.50	0.57	0.12	396.0	18.1	681.1	0.22	1
3	250	1.00	0.65	0.15	545.6	21.3	829.1	0.23	1
4	225	1.50	0.13	0.09	144.0	17.9	1134.5	0.71	1
5	225	2.50	0.20	0.11	203.0	29.7	1003.9	0.57	1
6	200	3.00	0.02	0.07	33.5	35.9	1531.2	3.54	0
7	200	4.00	0.04	0.09	45.9	52.0	1141.3	2.53	0
8	235	2.00	0.29	0.11	288.0	27.2	995.1	0.40	1
9	235	3.00	0.37	0.10	386.5	39.2	1030.3	0.29	1
10	270	1.91	1.71	0.21	1634.8	36.0	943.4	0.12	1
11	270	1.57	1.11	0.18	1081.4	22.3	964.0	0.16	1
12	285	1.25	1.61	0.19	1599.3	26.2	982.0	0.12	1
13	285	1.57	1.55	0.21	1702.6	30.1	1086.9	0.14	1
14	300	1.91	3.14	0.27	3640.5	38.4	1147.6	0.09	1
15	300	1.45	2.00	0.22	2393.3	33.3	1185.8	0.11	1
16	325	1.74	5.79	0.39	7545.8	52.1	1292.3	0.07	1
17	325	1.32	3.55	0.29	4803.2	34.2	1341.6	0.08	1
18	340	1.58	6.26	0.39	9101.9	60.7	1442.9	0.06	1
19	340	1.89	5.89	0.39	8999.3	56.8	1517.9	0.07	1
20	350	1.48	5.62	0.33	8834.4	50.6	1560.7	0.06	0
21	350	1.82	5.70	0.38	9242.5	54.7	1610.1	0.07	0
22	360	1.50	5.59	0.34	9283.7	47.2	1649.6	0.06	0
23	360	1.98	5.92	0.33	10214.8	67.6	1715.2	0.06	0
24	370	1.88	6.40	0.38	11230.9	67.8	1745.9	0.06	0
25	390	1.47	7.47	0.41	13075.2	62.0	1740.9	0.06	0
26	450	1.00	15.31	0.65	27452.6	95.6	1783.2	0.04	0
27	600	1.00	18.76	0.66	34885.9	148.8	1850.0	0.04	0
28	900	1.00	0.14	0.08	253.8	20.6	1758.9	0.59	0
29	900	1.00	0.00	0.00	10.2	19.3	Inf	NaN	0

Figure S55

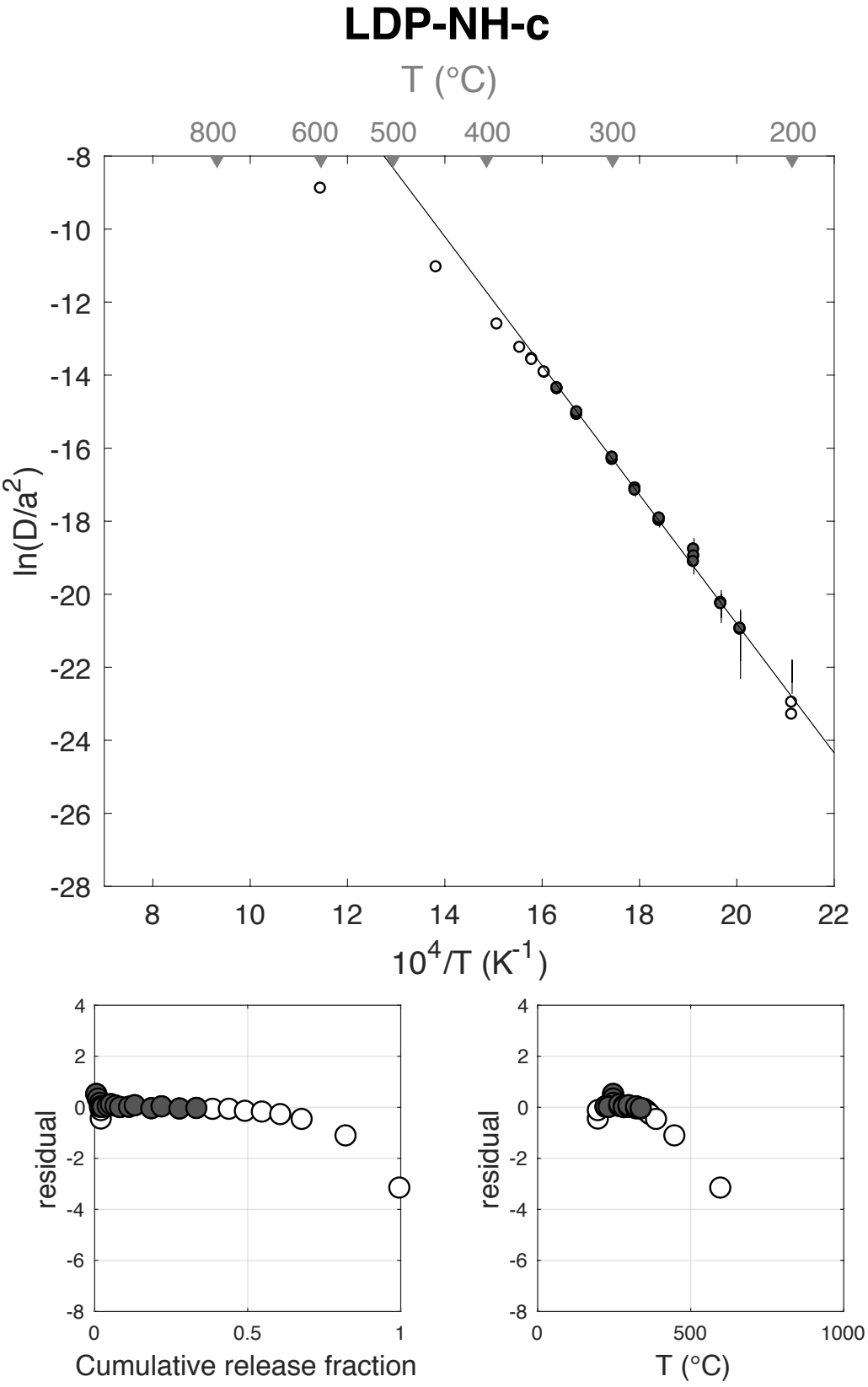
LDP-NH-c
T (°C)
800
600
500
400
300
200
-8
-10
-12
-14
-16
-18
-20
-22
-24
-26
-28
ln(D/a2)
8
10
12
14
16
18
20
22
10^4/T (K^-1)
4
2
0
-2
-4
-6
-8
residual
0
0.5
1
Cumulative release fraction
0
500
1000
T (°C)

LDP-NH-d

E_a	+/-	D_0	+/-	T_c	-	+	Total ^{3}He	Incl.	Misfit	Norm. Misfit
128.01	8.66	11.50	1.76	59.65	9.54	10.28	44.52	0.479	0.489	0.038

Step #	°C	t (hrs)	^{3}He	Error	^{4}He	Error	^{4}He/^{3}He	Err	In ^{3}He Reg.
1	250	0.25	0.66	0.15	259.4	25.4	381.5	0.25	1
2	250	0.50	0.53	0.13	242.1	22.7	450.2	0.26	1
3	250	1.00	0.50	0.12	352.5	16.2	696.9	0.24	1
4	225	1.50	0.07	0.10	0.0	0.0	NaN	NaN	0
5	225	2.50	0.06	0.13	0.0	0.0	NaN	NaN	0
6	200	3.00	0.00	0.00	0.0	0.0	NaN	NaN	0
7	200	4.00	0.00	0.00	0.0	0.0	NaN	NaN	0
8	235	2.00	0.19	0.12	68.5	28.5	358.8	0.75	0
9	235	3.00	0.02	0.17	73.8	50.9	3040.1	7.19	0
10	270	1.91	1.01	0.22	1160.1	33.2	1139.1	0.22	1
11	270	1.57	0.69	0.15	792.8	23.2	1136.4	0.22	1
12	285	1.25	1.07	0.19	1353.7	22.7	1252.2	0.18	1
13	285	1.56	1.12	0.20	1477.3	25.2	1314.6	0.18	1
14	300	1.91	2.13	0.28	3204.1	42.8	1494.5	0.13	1
15	300	1.45	1.29	0.19	2031.5	23.4	1562.4	0.15	1
16	325	1.74	3.46	0.30	6043.0	38.7	1736.3	0.09	1
17	325	1.32	1.97	0.22	3516.7	33.2	1774.5	0.11	1
18	340	1.58	3.54	0.35	6404.1	42.8	1796.9	0.10	1
19	340	1.89	3.37	0.32	6259.3	68.8	1848.7	0.09	1
20	350	1.48	2.79	0.32	5604.4	44.0	1998.3	0.11	0
21	350	1.82	2.94	0.26	5671.6	63.2	1918.6	0.09	0
22	360	1.50	2.80	0.31	5499.6	60.9	1957.3	0.11	0
23	360	1.98	2.70	0.30	5676.4	49.7	2090.9	0.11	0
24	370	1.88	2.72	0.26	5695.2	67.0	2084.1	0.10	0
25	390	1.47	2.83	0.32	5870.0	41.2	2064.1	0.11	0
26	450	1.00	4.53	0.39	9325.9	46.6	2048.5	0.09	0
27	600	1.00	1.49	0.22	3264.4	37.9	2186.0	0.15	0
28	900	1.00	0.00	0.00	0.0	0.0	NaN	NaN	0
29	900	1.00	0.04	0.06	0.0	0.0	NaN	NaN	0

Figure S56

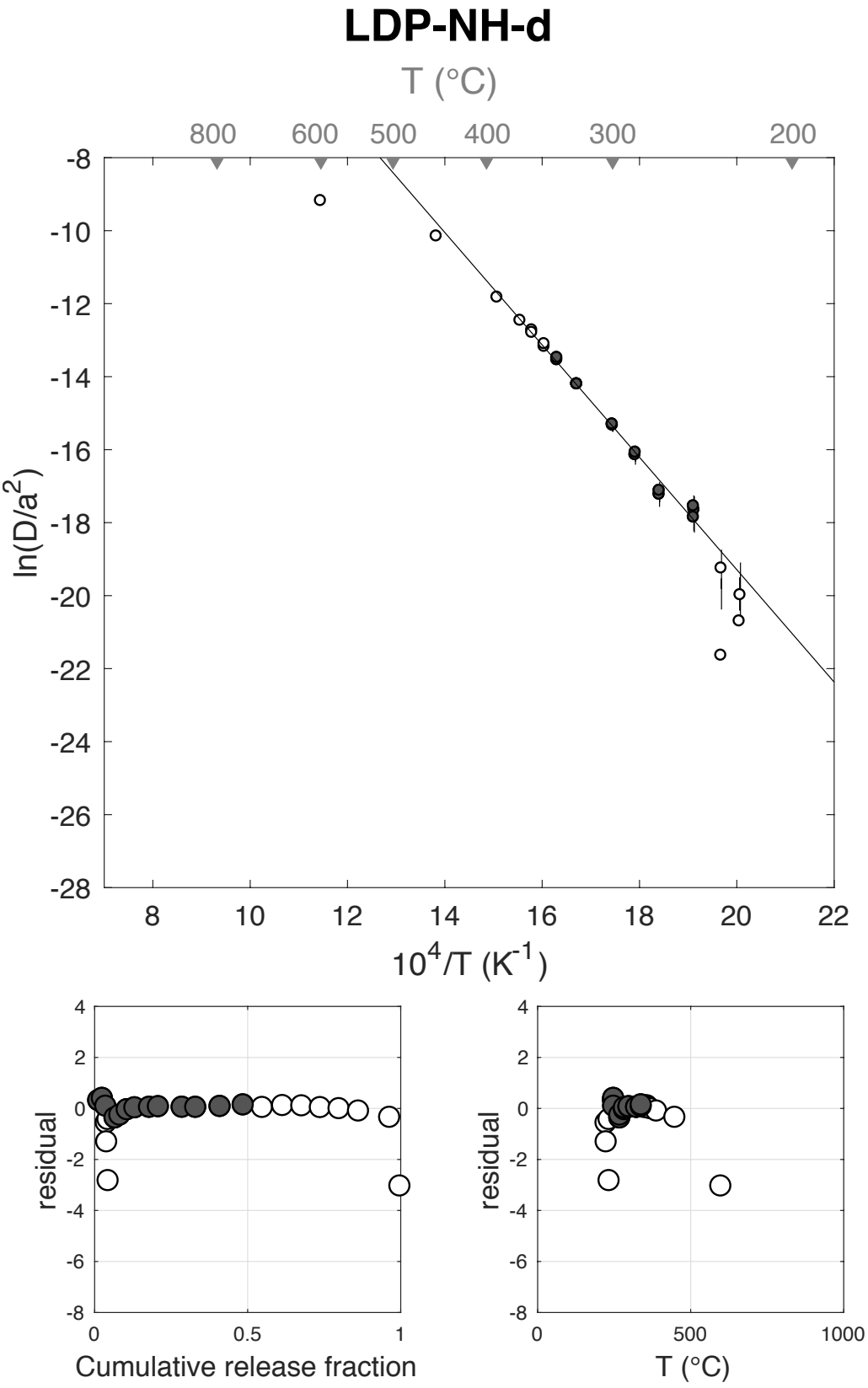
LDP-NH-d
T (°C)
800
600
500
400
300
200
-8
-10
-12
-14
-16
-18
-20
-22
-24
-26
-28
ln(D/a2)
8
10
12
14
16
18
20
22
10^4/T (K^-1)
4
2
0
-2
-4
-6
-8
residual
0
0.5
1
Cumulative release fraction
0
500
1000
T (°C)

E_a	+/-	D_0	+/-	T_c	-	+	Total ^{3}He	Incl.	Misfit	Norm. Misfit
120.03	9.14	8.40	1.86	60.79	10.68	11.62	65.93	0.254	0.930	0.072

Step #	°C	t (hrs)	^{3}He	Error	^{4}He	Error	^{4}He/^{3}He	Err	In ^{3}He Reg.
1	250	0.25	0.60	0.13	266.6	15.9	431.2	0.22	1
2	250	0.50	0.38	0.11	193.8	13.6	503.9	0.29	1
3	250	1.00	0.39	0.12	280.8	14.4	704.2	0.32	1
4	225	1.50	0.08	0.08	0.0	0.0	NaN	NaN	0
5	225	2.50	0.00	0.00	0.0	0.0	NaN	NaN	0
6	200	3.00	0.00	0.00	0.0	0.0	NaN	NaN	0
7	200	4.00	0.00	0.00	0.0	0.0	NaN	NaN	0
8	235	2.00	0.06	0.09	9.6	15.1	155.4	2.22	0
9	235	3.00	0.02	0.11	0.0	0.0	NaN	NaN	0
10	270	1.91	0.76	0.14	869.6	23.1	1133.1	0.18	1
11	270	1.57	0.49	0.13	594.6	15.5	1214.9	0.28	1
12	285	1.25	0.81	0.16	1084.9	18.1	1323.3	0.20	1
13	285	1.56	0.78	0.17	1032.4	20.5	1319.5	0.22	1
14	300	1.91	1.47	0.21	2143.3	31.2	1445.1	0.15	1
15	300	1.45	1.01	0.19	1432.9	23.6	1407.4	0.19	1
16	325	1.74	2.49	0.29	4101.4	41.0	1636.7	0.12	1
17	325	1.32	1.79	0.22	2844.9	28.8	1580.2	0.12	1
18	340	1.58	3.06	0.34	5128.1	46.0	1668.0	0.11	1
19	340	1.89	2.69	0.30	4746.6	66.7	1752.3	0.11	1
20	350	1.48	2.99	0.29	5222.6	40.6	1736.9	0.10	0
21	350	1.82	2.73	0.29	4850.9	37.0	1764.8	0.11	0
22	360	1.50	2.62	0.27	5004.8	55.8	1902.6	0.10	0
23	360	1.98	2.89	0.32	5408.8	36.4	1863.8	0.11	0
24	370	1.88	3.01	0.29	6073.8	39.6	2009.9	0.10	0
25	390	1.47	3.85	0.30	7778.3	44.3	2008.0	0.08	0
26	450	1.00	9.45	0.51	18789.9	116.2	1979.2	0.05	0
27	600	1.00	19.70	0.80	36600.0	220.6	1848.1	0.04	0
28	900	1.00	1.80	0.21	3974.2	41.4	2192.2	0.12	0
29	900	1.00	0.01	0.06	11.9	8.8	914.5	5.06	0

Figure S57

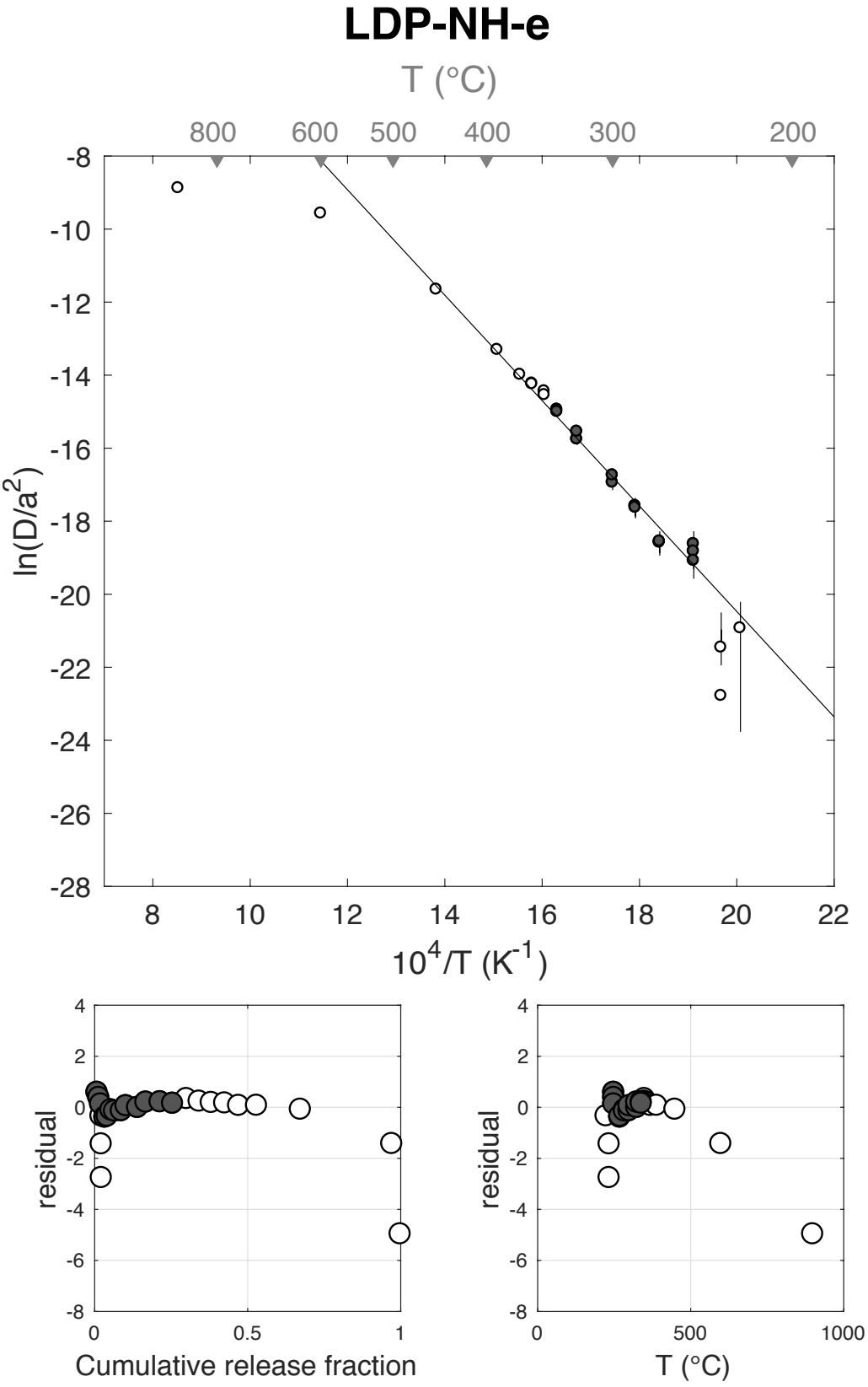
LDP-NH-e
T (°C)
800
600
500
400
300
200
-8
-10
-12
-14
-16
-18
-20
-22
-24
-26
-28
ln(D/a2)
8
10
12
14
16
18
20
22
10^4/T (K^-1)
4
2
0
-2
-4
-6
-8
residual
0
0.5
1
Cumulative release fraction
0
500
1000
T (°C)

LDP-NH-f

E_a	+/-	D_0	+/-	T_c	-	+	Total ^{3}He	Incl.	Misfit	Norm. Misfit
115.20	0.80	9.42	0.17	40.56	0.97	0.98	9774.18	0.543	1.633	0.086

Step #	°C	t (hrs)	^{3}He	Error	^{4}He	Error	^{4}He/^{3}He	Err	In ^{3}He Reg.
1	250	0.25	298.94	3.66	0.0	0.0	NaN	NaN	1
2	250	0.50	151.10	3.32	0.0	0.0	NaN	NaN	1
3	250	1.00	172.89	2.78	0.0	0.0	NaN	NaN	1
4	225	1.50	46.65	1.93	48901.7	286.4	1038.2	0.04	1
5	225	2.50	68.05	2.20	69610.9	194.7	1012.9	0.03	1
6	200	3.00	13.42	1.19	17948.8	63.4	1327.8	0.09	1
7	200	4.00	16.19	1.77	21956.8	106.3	1345.8	0.11	1
8	235	2.00	73.04	1.79	0.0	0.0	NaN	NaN	1
9	235	3.00	102.84	2.24	0.0	0.0	NaN	NaN	1
10	270	1.91	380.46	4.17	0.0	0.0	NaN	NaN	1
11	270	1.57	206.65	4.15	0.0	0.0	NaN	NaN	1
12	285	1.25	282.85	3.52	0.0	0.0	NaN	NaN	1
13	285	1.56	289.47	4.15	0.0	0.0	NaN	NaN	1
14	300	1.91	570.84	5.97	0.0	0.0	NaN	NaN	1
15	300	1.45	283.35	3.80	0.0	0.0	NaN	NaN	1
16	325	1.74	833.73	6.29	0.0	0.0	NaN	NaN	1
17	325	1.32	388.93	4.15	0.0	0.0	NaN	NaN	1
18	340	1.58	599.70	4.69	0.0	0.0	NaN	NaN	1
19	340	1.89	529.53	4.17	0.0	0.0	NaN	NaN	1
20	350	1.48	413.52	4.13	0.0	0.0	NaN	NaN	0
21	350	1.82	467.44	4.16	0.0	0.0	NaN	NaN	0
22	360	1.50	353.10	3.77	0.0	0.0	NaN	NaN	0
23	360	1.98	362.57	4.16	0.0	0.0	NaN	NaN	0
24	370	1.88	355.14	4.38	0.0	0.0	NaN	NaN	0
25	390	1.47	355.97	3.92	0.0	0.0	NaN	NaN	0
26	450	1.00	594.61	6.25	0.0	0.0	NaN	NaN	0
27	600	1.00	869.59	7.38	0.0	0.0	NaN	NaN	0
28	880	30.00	691.90	14.52	0.0	0.0	NaN	NaN	0
29	900	1.00	1.57	0.29	3811.04	0.5	2418.3	0.19	0
30	900	1.00	0.00	0.00	2787.8	27.9	Inf	NaN	0
31	899	1.00	0.09	0.11	2157.0	24.8	24795.7	1.30	0
32	900	1.00	0.03	0.12	2133.4	29.2	64392.2	3.74	0

Figure S58

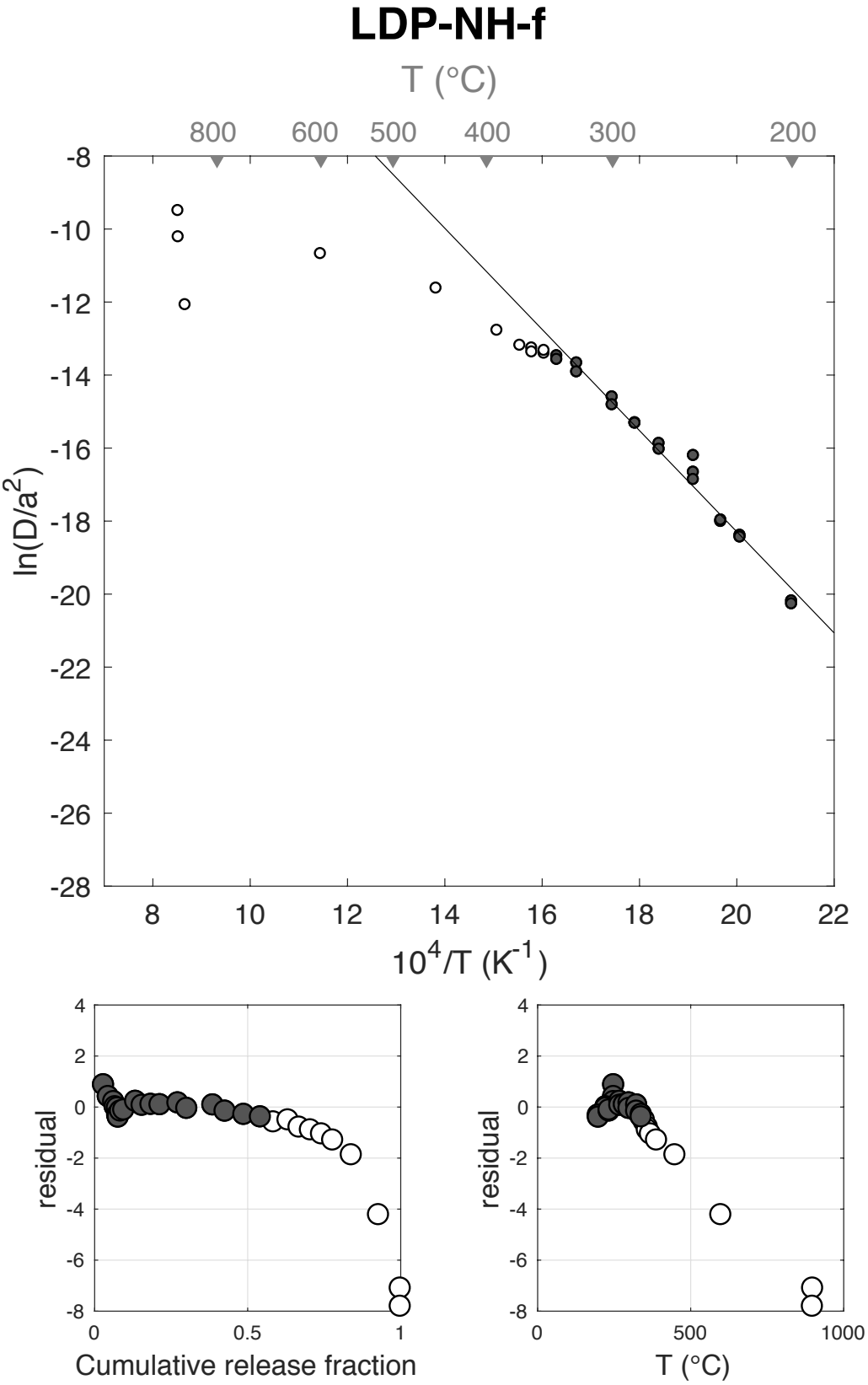
LDP-NH-f
T (°C)
800
600
500
400
300
200
-8
-10
-12
-14
-16
-18
-20
-22
-24
-26
-28
ln(D/a2)
8
10
12
14
16
18
20
22
10^4/T (K^-1)
4
2
0
-2
-4
-6
-8
residual
0
0.5
1
Cumulative release fraction
0
500
1000
T (°C)

E_a	+/-	D_0	+/-	T_c	-	+	Total ^{3}He	Incl.	Misfit	Norm. Misfit
112.33	4.92	9.20	1.04	34.36	6.09	6.37	610.55	0.627	2.252	0.125

Step #	°C	t (hrs)	^{3}He	Error	^{4}He	Error	^{4}He/^{3}He	Err	In ^{3}He Reg.
1	250	0.25	17.64	0.80	14540.6	152.5	814.3	0.05	1
2	250	0.50	11.03	0.62	11647.2	102.7	1046.1	0.06	1
3	250	1.00	13.36	0.69	15318.5	176.2	1136.2	0.05	1
4	225	1.50	2.79	0.34	3404.8	55.1	1208.3	0.12	1
5	225	2.50	4.42	0.43	5886.6	94.9	1322.7	0.10	1
6	200	3.00	0.95	0.23	1569.9	56.6	1643.3	0.25	1
7	200	4.00	4.44	2.63	2652.9	83.4	587.5	0.59	1
8	235	3.00	16.40	0.87	23256.6	323.6	1408.4	0.05	1
9	270	1.91	22.17	0.90	30833.5	239.9	1380.7	0.04	1
10	270	1.57	20.03	0.80	29119.2	372.1	1443.6	0.04	1
11	285	1.25	25.10	0.97	38194.4	343.0	1511.4	0.04	1
12	285	1.57	25.69	1.00	38702.8	373.4	1496.7	0.04	1
13	300	1.91	41.81	1.28	62575.2	565.2	1486.6	0.03	1
14	300	1.45	25.41	1.07	40900.4	602.6	1599.5	0.04	1
15	325	1.74	51.10	1.47	81168.4	2519.1	1578.4	0.04	1
16	325	1.32	27.60	1.03	47064.0	334.8	1695.0	0.04	1
17	340	1.58	41.33	1.26	70222.4	552.7	1689.2	0.03	1
18	340	1.89	31.63	1.26	55573.8	458.6	1747.2	0.04	1
19	350	1.48	26.89	0.97	47094.8	573.5	1741.2	0.04	0
20	350	1.82	25.77	1.06	46301.4	317.9	1786.6	0.04	0
21	360	1.50	24.00	1.00	43920.6	373.3	1819.8	0.04	0
22	360	1.98	19.47	0.84	37272.3	201.3	1904.6	0.04	0
23	370	1.88	18.59	0.86	35683.6	339.5	1909.5	0.05	0
24	390	1.47	21.61	0.90	39869.2	426.7	1834.6	0.04	0
25	450	1.00	32.87	1.05	64366.8	480.9	1948.1	0.03	0
26	600	1.00	33.45	1.10	61726.8	266.8	1835.2	0.03	0
27	900	1.00	24.52	0.93	45970.1	581.5	1864.8	0.04	0
28	899	1.00	0.46	0.14	1135.3	33.8	2446.1	0.31	0

Figure S59

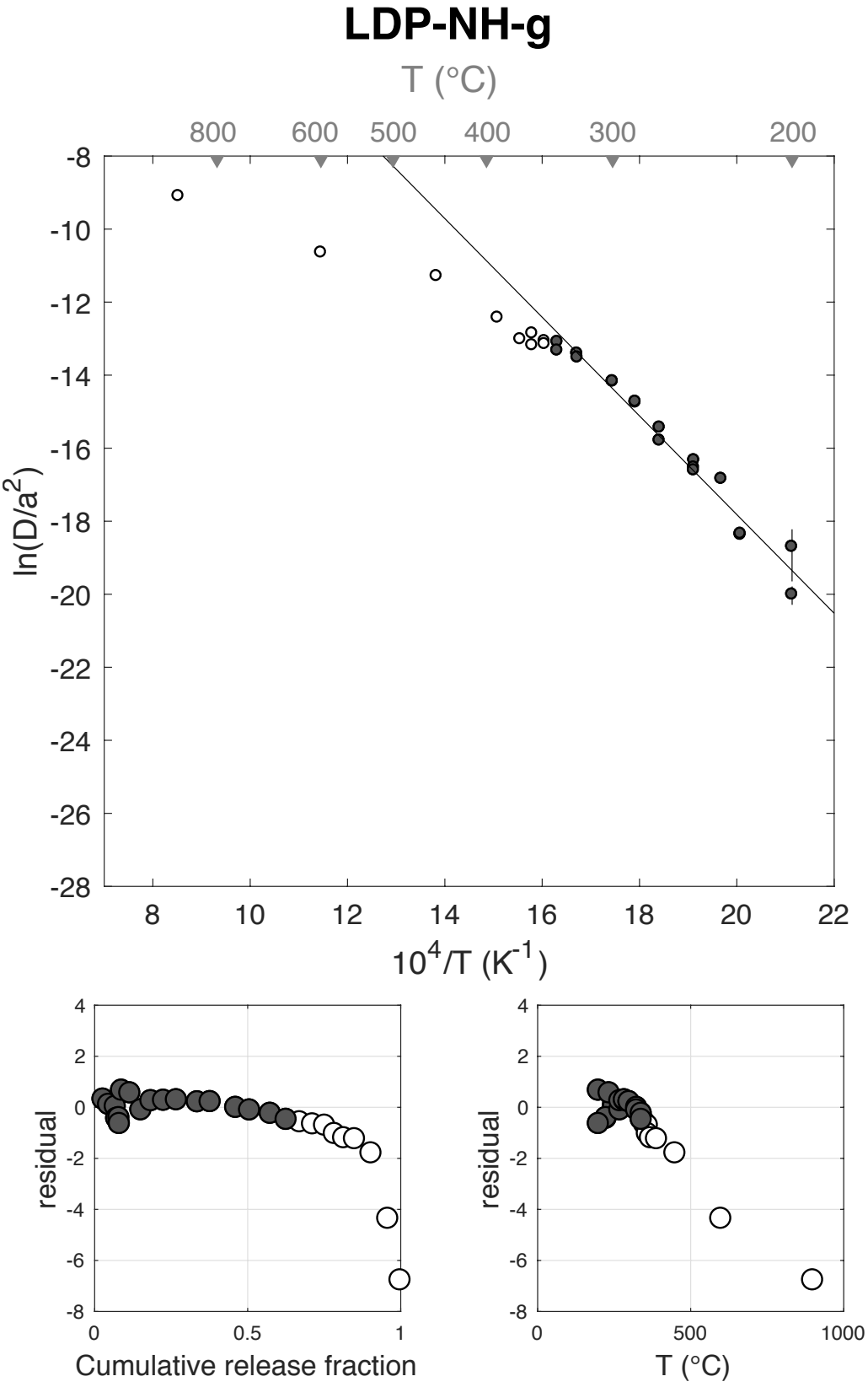
LDP-NH-g
T (°C)
800
600
500
400
300
200
-8
-10
-12
-14
-16
-18
-20
-22
-24
-26
-28
ln(D/a2)
8
10
12
14
16
18
20
22
10^4/T (K^-1)
4
2
0
-2
-4
-6
-8
residual
0
0.5
1
Cumulative release fraction
0
500
1000
T (°C)

E_a	+/-	D_0	+/-	T_c	-	+	Total ^{3}He	Incl.	Misfit	Norm. Misfit
110.27	3.14	8.08	0.66	36.44	4.00	4.12	476.55	0.543	5.252	0.202

Step #	°C	t (hrs)	^{3}He	Error	^{4}He	Error	^{4}He/^{3}He	Err	In ^{3}He Reg.
1	250	0.50	16.22	0.89	12608.2	98.3	767.5	0.06	1
2	250	1.00	9.72	0.61	9848.1	65.8	1002.9	0.06	1
3	240	1.00	3.44	0.46	4000.0	44.5	1152.1	0.13	1
4	230	1.50	2.22	0.39	2623.0	54.9	1170.3	0.18	1
5	230	2.50	3.60	0.49	4453.2	126.4	1225.8	0.14	1
6	210	2.50	0.66	0.30	911.7	136.5	1381.6	0.49	1
7	210	3.50	2.28	0.32	4768.7	61.8	2085.4	0.14	1
8	200	3.00	4.46	0.43	4567.0	71.1	1013.4	0.10	1
9	200	4.00	0.48	0.21	584.6	44.1	1198.6	0.44	1
10	220	2.50	1.17	0.25	1492.3	37.3	1264.8	0.21	1
11	220	3.50	1.67	0.24	1980.0	48.2	1175.4	0.15	1
12	235	2.00	2.26	0.36	2910.1	51.0	1276.7	0.16	1
13	235	3.00	3.16	0.34	3884.0	59.6	1220.2	0.11	1
14	250	1.00	2.38	0.34	3052.1	51.6	1269.8	0.14	1
15	270	1.91	12.90	0.77	15653.7	124.3	1203.5	0.06	1
16	270	1.57	7.88	0.56	10121.9	92.7	1274.3	0.07	1
17	285	1.25	10.88	0.72	14770.1	259.0	1347.7	0.07	1
18	285	1.57	11.59	0.74	15345.1	226.0	1313.9	0.07	1
19	300	1.91	25.06	1.04	33391.5	412.6	1322.6	0.04	1
20	300	1.45	11.08	0.91	17047.8	297.4	1528.1	0.08	1
21	315	1.74	20.95	1.18	33879.6	354.5	1607.0	0.06	1
22	315	1.32	12.89	0.77	20782.7	221.2	1602.6	0.06	1
23	330	1.74	26.07	1.07	43536.8	580.1	1660.0	0.04	1
24	330	1.32	19.00	0.87	28334.6	475.8	1481.0	0.05	1
25	340	1.58	24.19	1.45	39566.3	289.2	1625.4	0.06	1
26	340	1.89	22.72	1.06	38313.6	256.4	1676.0	0.05	1
27	350	1.48	20.51	0.87	34727.0	230.5	1683.4	0.04	0
28	350	1.82	20.22	1.11	34935.8	460.7	1717.8	0.06	0
29	360	1.50	20.26	0.97	34920.6	458.0	1713.8	0.05	0
30	360	1.98	20.70	0.84	35218.4	279.1	1691.5	0.04	0
31	370	1.88	21.00	1.01	36537.1	261.1	1730.2	0.05	0
32	390	1.47	21.76	0.96	39304.5	353.2	1796.3	0.05	0
33	450	1.00	39.21	1.29	69672.6	656.9	1766.8	0.03	0
34	600	1.00	44.57	1.54	81622.7	327.8	1821.3	0.03	0
35	900	1.00	9.38	0.60	18479.2	97.1	1961.0	0.06	0
36	900	1.00	0.00	0.13	59.5	20.1	19571.2	42.24	0
37	900	1.00	0.00	0.00	0.4	13.7	Inf	NaN	0

Figure S60

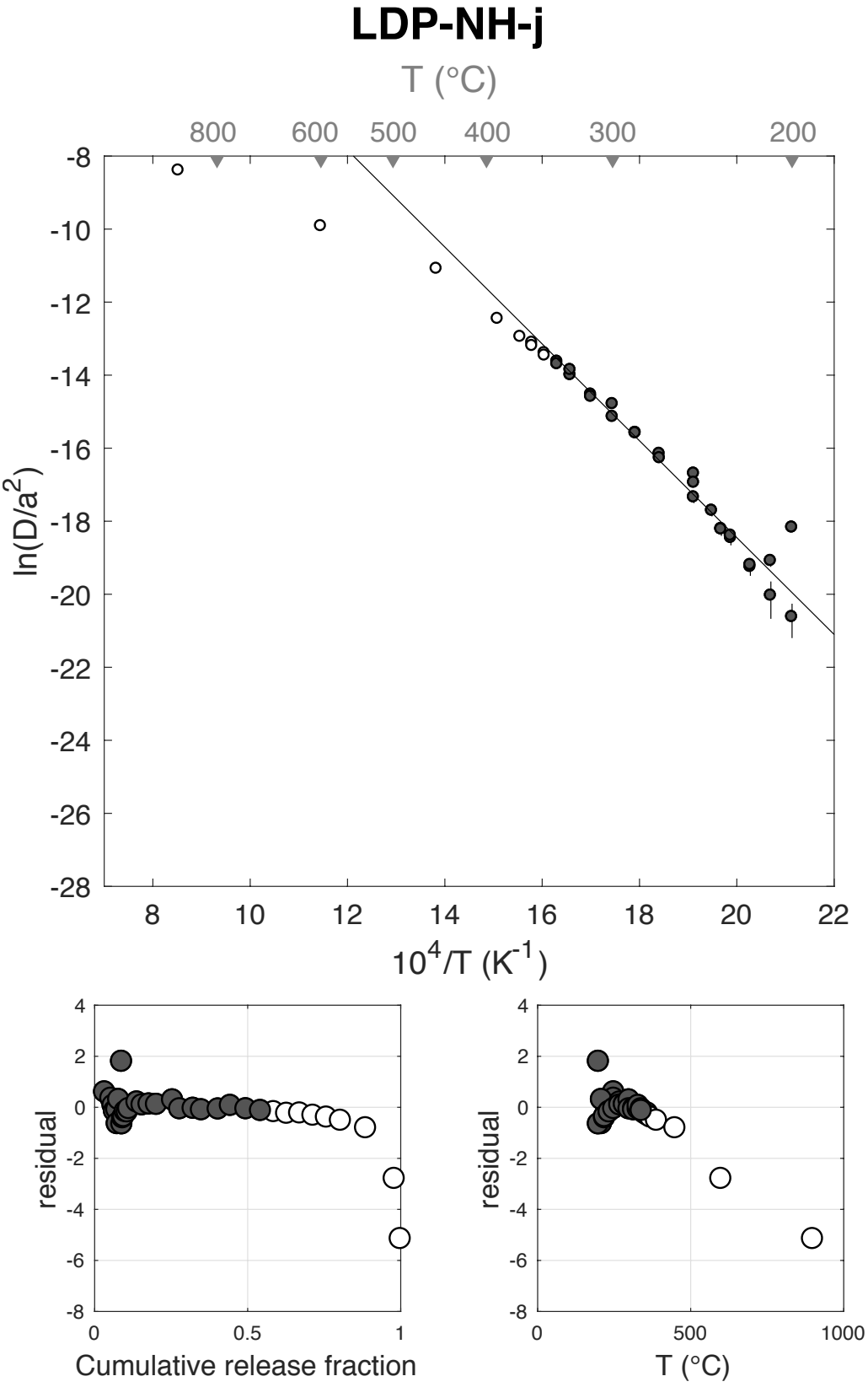
LDP-NH-j
T (°C)
800
600
500
400
300
200
-8
-10
-12
-14
-16
-18
-20
-22
-24
-26
-28
ln(D/a2)
8
10
12
14
16
18
20
22
10^4/T (K^-1)
4
2
0
-2
-4
-6
-8
residual
0
0.5
1
Cumulative release fraction
0
500
1000
T (°C)

LDP-350C-1hr-a

E_a	+/-	D_0	+/-	T_c	-	+	Total ^{3}He	Incl.	Misfit	Norm. Misfit
146.30	7.40	15.11	1.53	79.83	6.90	7.33	109.05	0.449	0.277	0.016

Step #	°C	t (hrs)	^{3}He	Error	^{4}He	Error	^{4}He/^{3}He	Err	In ^{3}He Reg.
1	250	0.25	1.08	0.18	56.3	43.4	42.1	0.79	1
2	250	0.50	0.77	0.14	85.3	40.0	101.2	0.50	1
3	250	1.00	0.97	0.19	136.7	37.4	130.3	0.34	1
4	225	1.50	0.17	0.11	57.9	45.0	324.1	0.99	1
5	225	2.50	0.39	0.14	110.7	60.2	272.4	0.65	1
6	200	3.00	0.11	0.13	32.4	75.7	275.1	2.62	0
7	200	4.00	0.10	0.16	39.5	102.7	399.0	3.07	0
8	235	2.00	0.54	0.14	122.2	54.3	215.2	0.51	1
9	235	3.00	0.52	0.18	176.5	76.3	329.6	0.56	1
10	270	1.91	2.56	0.26	737.6	62.2	278.2	0.13	1
11	270	1.57	1.67	0.22	607.5	57.6	353.1	0.16	1
12	285	1.25	2.22	0.28	1008.3	54.9	443.9	0.14	1
13	285	1.56	2.51	0.25	1249.6	61.8	488.2	0.11	1
14	300	1.91	4.78	0.37	3039.9	101.5	625.5	0.08	1
15	300	1.45	2.82	0.26	2089.9	73.4	732.4	0.10	1
16	325	1.74	8.45	0.44	7221.9	145.9	844.2	0.06	1
17	325	1.32	4.55	0.36	4653.1	104.3	1011.8	0.08	1
18	340	1.58	8.00	0.89	8888.6	173.8	1101.5	0.11	1
19	340	1.89	6.94	0.46	8917.2	183.1	1275.4	0.07	1
20	350	1.48	6.06	0.57	8346.7	147.6	1368.1	0.10	0
21	350	1.82	5.93	0.53	8396.5	178.5	1405.6	0.09	0
22	360	1.50	6.01	0.41	8068.1	166.8	1332.2	0.07	0
23	360	1.98	5.83	0.38	8566.8	215.6	1458.2	0.07	0
24	370	1.88	6.09	0.45	8446.2	171.5	1376.1	0.08	0
25	390	1.47	5.91	0.57	8987.6	171.0	1509.6	0.10	0
26	450	1.00	8.97	0.48	14767.0	270.4	1636.6	0.06	0
27	600	1.00	11.78	0.56	17964.2	340.9	1514.5	0.05	0
28	900	1.00	3.27	0.59	5276.4	128.4	1602.3	0.18	0
29	900	1.00	0.02	0.05	0.0	0.0	NaN	NaN	0

Figure S61

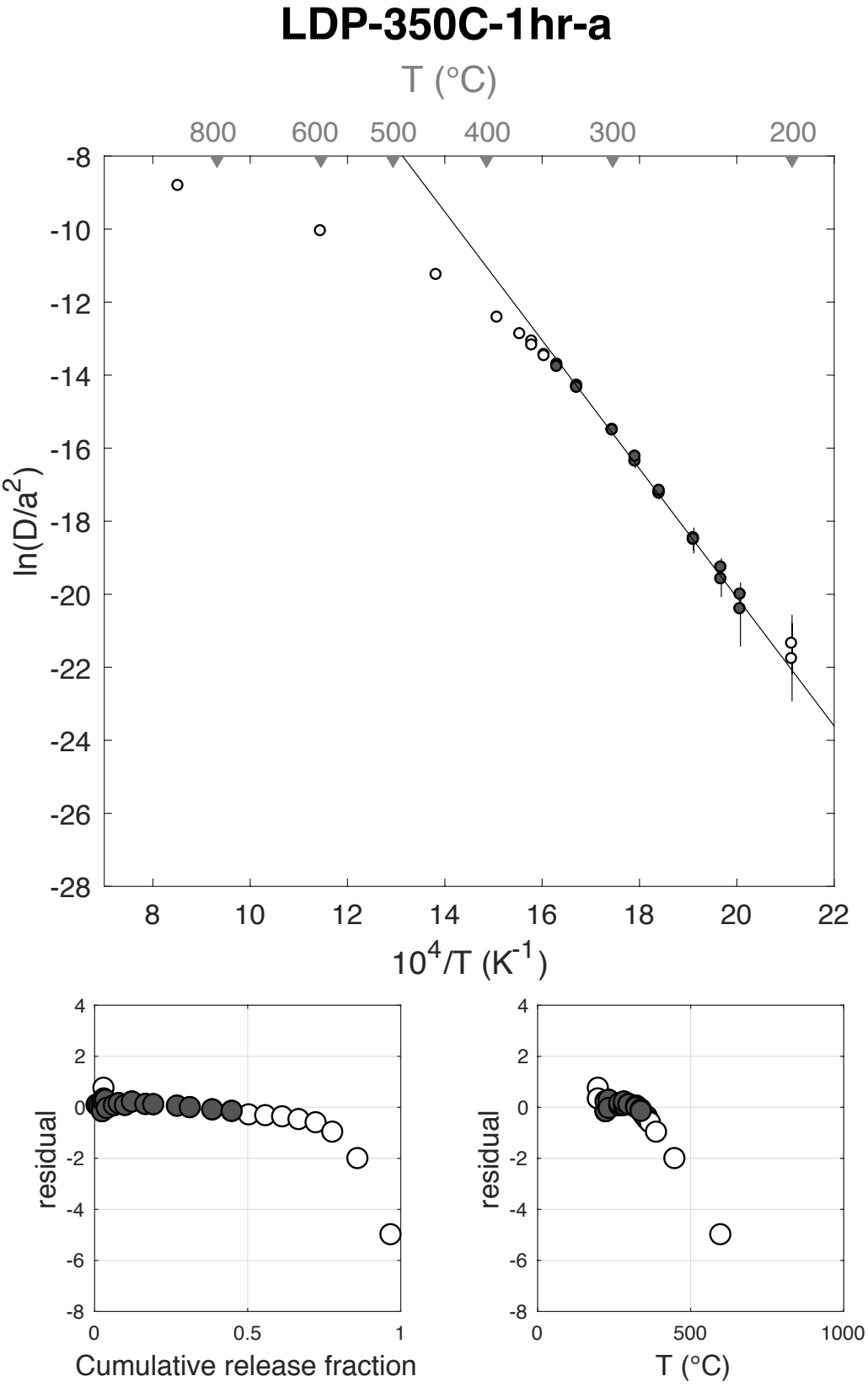
LDP-350C-1hr-a
T (°C)
800
600
500
400
300
200
-8
-10
-12
-14
-16
-18
-20
-22
-24
-26
-28
ln(D/a2)
8
10
12
14
16
18
20
22
10^4/T (K^-1)
4
2
0
-2
-4
-6
-8
residual
0
0.5
1
Cumulative release fraction
0
500
1000
T (°C)

LDP-365C-1hr-a

E_a	+/-	D_0	+/-	T_c	-	+	Total ^{3}He	Incl.	Misfit	Norm. Misfit
127.53	6.61	11.39	1.34	59.23	7.38	7.82	88.90	0.566	0.437	0.024

Step #	°C	t (hrs)	^{3}He	Error	^{4}He	Error	^{4}He/^{3}He	Err	In ^{3}He Reg.
1	250	0.25	1.48	0.19	590.3	42.1	389.5	0.15	1
2	250	0.50	0.87	0.16	401.9	47.5	453.8	0.22	1
3	250	1.00	0.77	0.18	497.9	41.1	633.3	0.25	1
4	225	1.50	0.26	0.11	131.4	43.5	504.9	0.55	1
5	200	2.50	0.07	0.11	0.0	0.0	NaN	NaN	0
6	235	2.50	0.66	0.17	341.4	57.5	507.9	0.31	1
7	270	1.16	1.79	0.21	833.3	45.1	456.5	0.13	1
8	290	1.17	3.27	0.29	1603.5	66.7	479.9	0.10	1
9	300	1.30	3.77	0.28	2083.8	73.9	543.0	0.08	1
10	300	1.91	4.18	0.32	2520.7	79.0	593.0	0.08	1
11	310	1.57	3.97	0.33	2716.5	83.8	673.9	0.09	1
12	310	1.25	2.41	0.26	1781.8	67.8	728.2	0.11	1
13	320	1.56	4.21	0.35	3361.8	92.6	788.6	0.09	1
14	320	1.91	4.21	0.27	3642.8	92.3	854.4	0.07	1
15	330	1.45	3.51	0.33	3757.5	114.5	1059.3	0.10	1
16	330	1.74	3.93	0.33	4013.2	105.8	1011.3	0.09	1
17	340	1.32	3.66	0.32	3962.7	103.2	1073.6	0.09	1
18	340	1.58	3.50	0.30	4034.3	98.3	1141.8	0.09	1
19	340	1.89	3.87	0.29	4417.5	108.4	1132.1	0.08	1
20	350	1.48	3.87	0.34	4323.3	113.3	1105.7	0.09	0
21	350	1.82	3.43	0.27	4754.4	120.7	1377.6	0.08	0
22	360	1.50	3.33	0.25	4662.5	125.4	1392.0	0.08	0
23	360	1.98	3.62	0.55	5101.5	113.0	1399.4	0.15	0
24	370	1.88	3.85	0.32	5713.5	128.0	1473.2	0.09	0
25	390	1.47	4.19	0.36	6494.5	136.1	1540.1	0.09	0
26	450	1.00	6.63	1.26	14597.8	293.7	2192.8	0.19	0
27	600	1.00	9.11	0.51	17901.9	366.5	1956.1	0.06	0
28	879	1.00	0.49	0.16	1009.9	58.7	2056.0	0.34	0
29	874	1.00	0.00	0.00	72.3	39.8	Inf	NaN	0

Figure S62

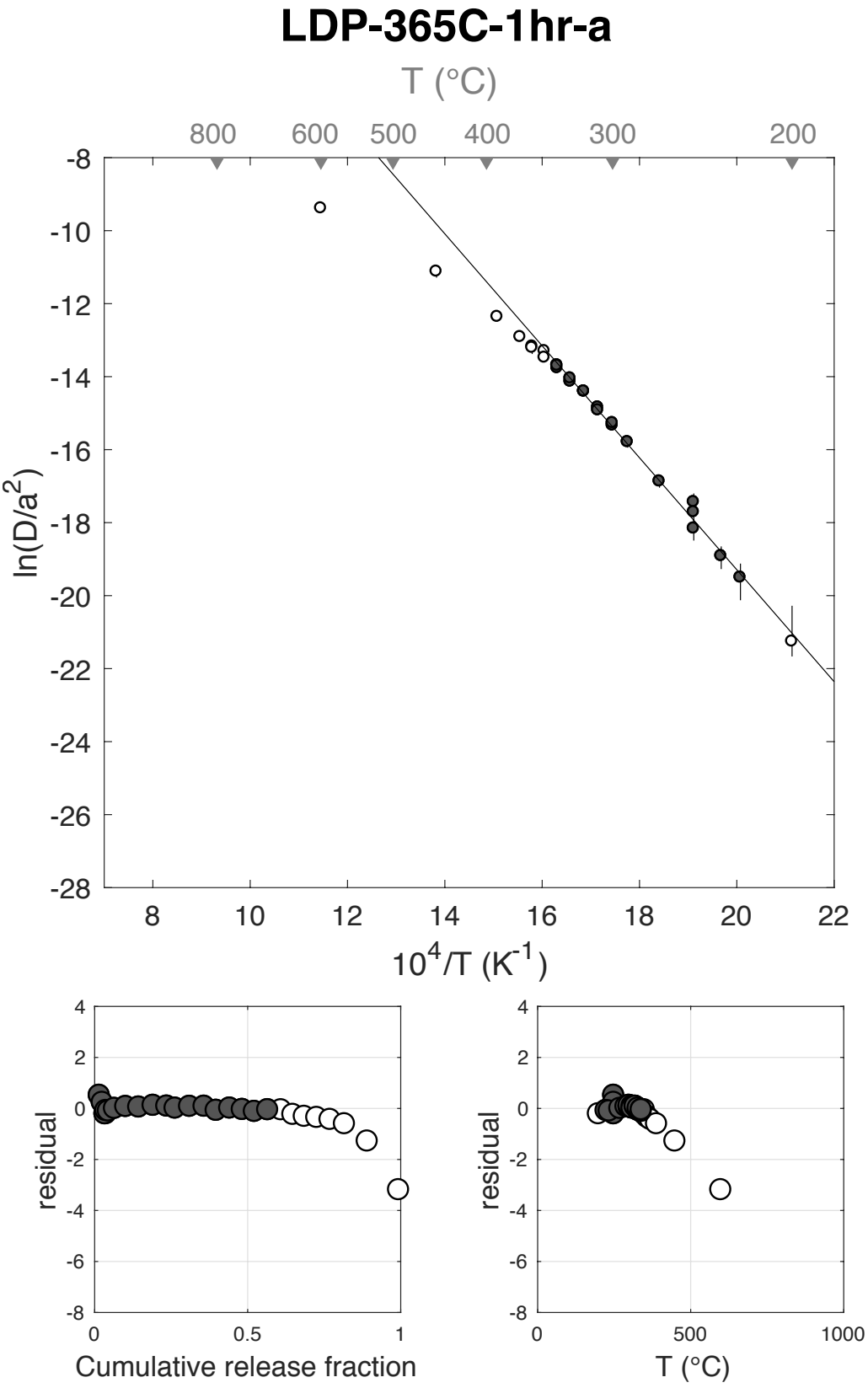
LDP-365C-1hr-a
T (°C)
800
600
500
400
300
200
-8
-10
-12
-14
-16
-18
-20
-22
-24
-26
-28
ln(D/a2)
8
10
12
14
16
18
20
22
10^4/T (K^-1)
4
2
0
-2
-4
-6
-8
residual
0
0.5
1
Cumulative release fraction
0
500
1000
T (°C)

LDP-365C-1hr-b

E_a	+/-	D_0	+/-	T_c	-	+	Total ^{3}He	Incl.	Misfit	Norm. Misfit
145.28	9.50	15.18	1.97	76.91	8.86	9.57	57.96	0.502	0.352	0.022

Step #	°C	t (hrs)	^{3}He	Error	^{4}He	Error	^{4}He/^{3}He	Err	In ^{3}He Reg.
1	250	0.25	0.77	0.13	107.8	19.3	129.9	0.25	1
2	250	0.50	0.53	0.11	100.6	19.4	178.6	0.28	1
3	250	1.00	0.65	0.13	136.0	15.7	198.0	0.23	1
4	225	1.50	0.11	0.09	40.5	16.6	370.9	0.98	1
5	225	2.50	0.17	0.10	60.5	22.6	347.1	0.68	0
6	200	3.00	0.00	0.00	23.0	30.6	Inf	NaN	0
7	200	4.00	0.00	0.00	4.4	39.4	Inf	NaN	0
8	235	2.00	0.25	0.11	80.1	18.5	308.9	0.48	1
9	235	3.00	0.33	0.11	116.2	31.0	340.3	0.43	1
10	270	1.91	1.54	0.17	505.1	23.6	317.9	0.12	1
11	270	1.57	0.92	0.18	376.2	18.7	398.7	0.20	1
12	285	1.25	1.41	0.19	603.0	21.5	418.6	0.14	1
13	285	1.57	1.44	0.19	708.2	22.3	482.5	0.13	1
14	300	1.91	2.77	0.23	1574.8	31.3	558.0	0.09	1
15	300	1.45	1.84	0.22	1073.0	19.2	572.3	0.12	1
16	325	1.74	5.00	0.29	3353.9	34.3	660.5	0.06	1
17	325	1.32	2.81	0.29	2089.8	24.7	732.8	0.10	1
18	340	1.58	4.71	0.36	3799.8	29.4	796.8	0.08	1
19	340	1.89	4.00	0.32	3640.4	42.1	900.0	0.08	1
20	350	1.48	3.60	0.28	3337.1	37.9	916.0	0.08	0
21	350	1.82	3.39	0.26	3353.0	33.2	978.5	0.08	0
22	360	1.50	3.07	0.23	3168.2	32.2	1020.9	0.08	0
23	360	1.98	3.03	0.29	3242.1	28.8	1060.2	0.10	0
24	370	1.88	2.96	0.30	3234.3	41.8	1081.7	0.10	0
25	390	1.47	3.00	0.26	3386.9	28.1	1119.8	0.09	0
26	450	1.00	5.19	0.34	5920.1	35.8	1130.1	0.06	0
27	600	1.00	4.12	0.27	4329.5	35.3	1041.9	0.07	0
28	900	1.00	0.31	0.12	299.8	16.9	972.4	0.40	0
29	899	1.00	0.03	0.06	0.1	15.5	NaN	NaN	0

Figure S63

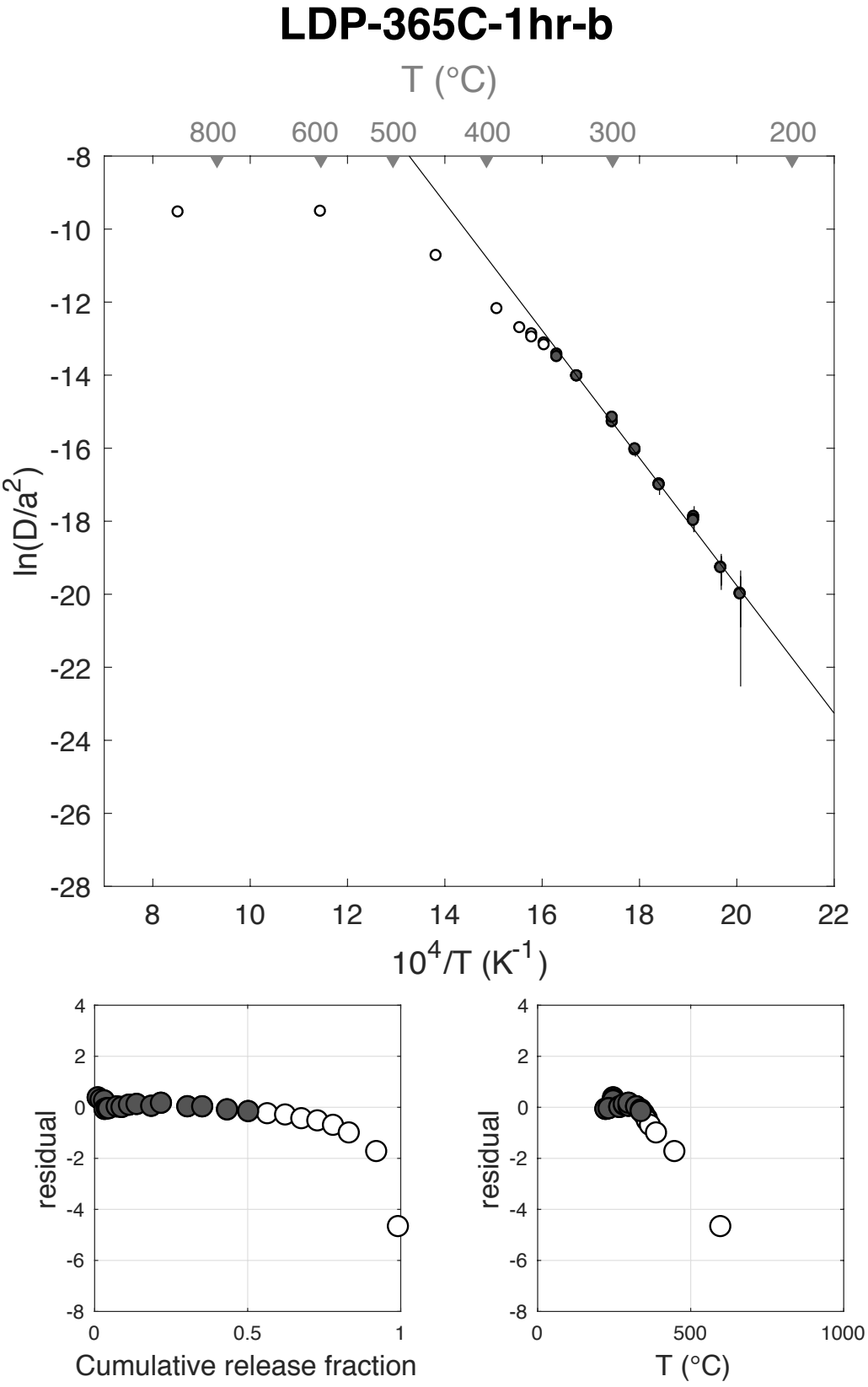
LDP-365C-1hr-b
T (°C)
800
600
500
400
300
200
ln(D/a²)
10⁴/T (K⁻¹)
residual
Cumulative release fraction
residual
T (°C)

LDP-375C-1hr-a

E_a	+/-	D_0	+/-	T_c	-	+	Total ^{3}He	Incl.	Misfit	Norm. Misfit
110.63	8.53	7.59	1.73	40.81	10.96	11.87	43.47	0.364	0.194	0.018

Step #	°C	t (hrs)	^{3}He	Error	^{4}He	Error	^{4}He/^{3}He	Err	In Reg.
1	250	0.25	0.70	0.15	4315.4	1327.7	6132.9	0.37	1
2	250	0.50	0.42	0.12	1720.3	715.1	4076.7	0.51	0
3	250	1.00	0.41	0.13	4354.4	538.4	10652.7	0.33	0
4	225	1.50	0.12	0.10	6218.2	1746.3	53671.6	0.87	0
5	225	2.50	0.18	0.11	9740.7	4194.7	54663.9	0.73	0
6	200	3.00	0.04	0.10	10521.7	5410.0	260020.7	2.41	0
7	200	4.00	0.10	0.11	12621.9	7860.1	126654.2	1.31	0
8	235	2.00	0.18	0.11	4609.8	2963.0	25518.1	0.88	0
9	235	3.00	0.33	0.13	8168.8	5409.7	24573.7	0.77	0
10	270	1.91	0.98	0.18	3880.8	2749.4	3934.0	0.73	1
11	270	1.57	0.65	0.13	2716.0	1918.6	4142.8	0.74	1
12	285	1.25	0.85	0.17	1871.1	1137.4	2187.2	0.64	1
13	285	1.57	0.84	0.19	2697.2	1916.2	3192.6	0.74	1
14	300	1.91	1.58	0.22	3501.9	2749.7	2204.8	0.80	1
15	300	1.45	1.01	0.16	1459.7	1619.2	1441.4	1.12	1
16	325	1.74	2.80	0.29	1977.4	2325.7	695.5	1.18	1
17	325	1.32	1.41	0.22	109.5	1297.5	67.9	11.85	1
18	340	1.58	2.67	0.25	808.4	1939.1	292.5	2.40	1
19	340	1.89	2.33	0.22	2904.6	2698.1	1237.5	0.93	1
20	350	1.48	2.07	0.25	2123.6	1698.0	1017.4	0.81	0
21	350	1.82	1.94	0.23	2934.5	2524.9	1505.4	0.87	0
22	360	1.50	1.73	0.27	2050.5	1739.7	1177.4	0.86	0
23	360	1.50	1.80	0.21	2050.5	1739.7	1131.6	0.86	0
24	360	1.98	1.84	0.24	1594.2	2924.7	857.7	1.84	0
25	370	1.88	1.90	0.23	958.0	2671.0	493.7	2.79	0
26	390	1.47	2.20	0.22	2096.6	1671.2	942.9	0.80	0
27	449	1.00	4.83	0.37	4255.8	523.3	871.5	0.14	0
28	599	1.00	6.93	0.44	8573.8	571.0	1228.1	0.09	0
29	900	1.00	0.65	0.15	8756.3	527.9	13477.3	0.24	0
30	899	0.50	0.00	0.00	4476.3	720.9	Inf	NaN	0

Figure S64

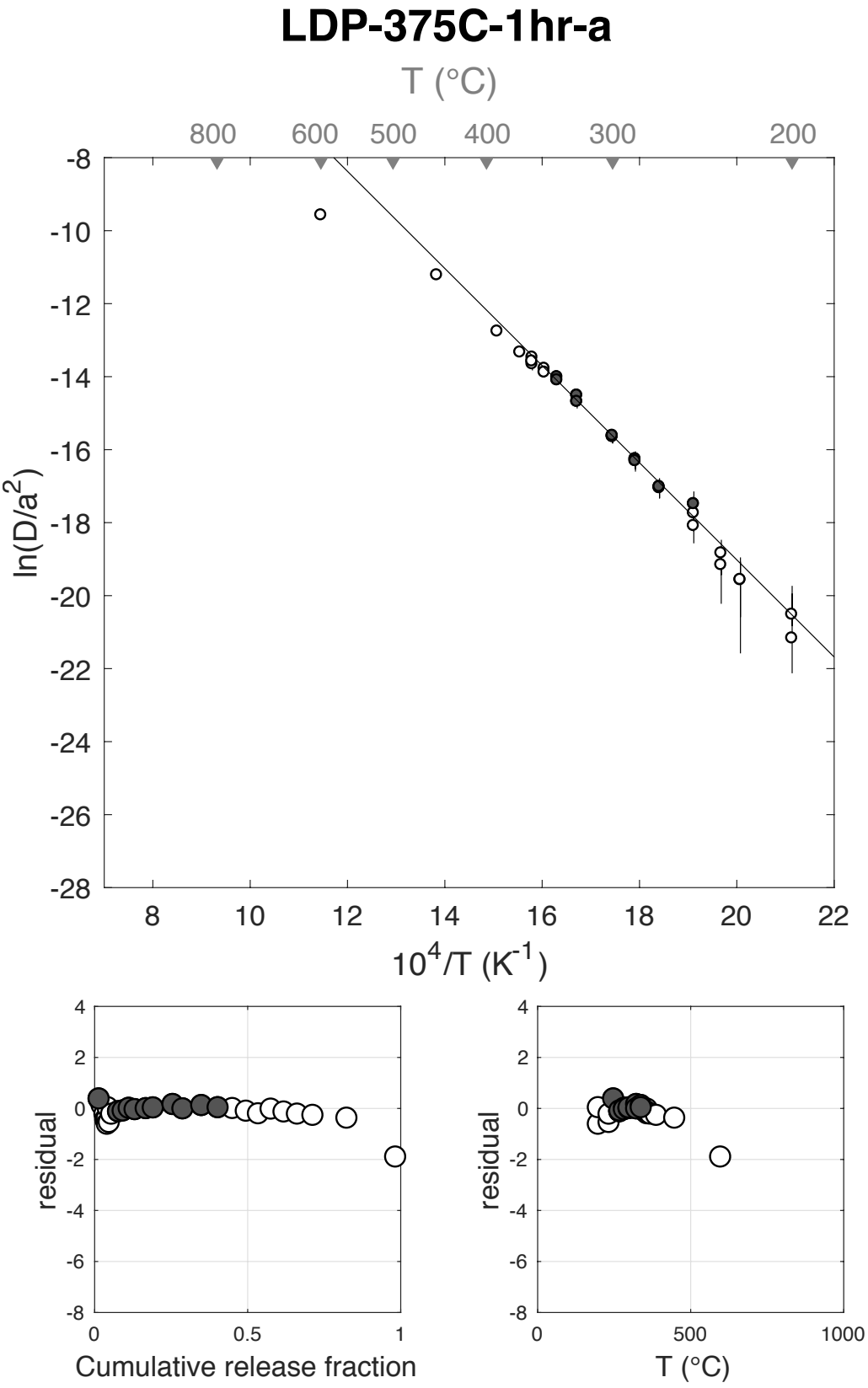
LDP-375C-1hr-a
T (°C)
800
600
500
400
300
200
ln(D/a²)
10⁴/T (K⁻¹)
residual
Cumulative release fraction
residual
T (°C)

LDP-397C-1hr-a

E_a	+/-	D_0	+/-	T_c	-	+	Total ^{3}He	Incl.	Misfit	Norm. Misfit
113.74	18.29	9.05	3.70	39.18	22.07	26.05	16.49	0.435	0.059	0.007

Step #	°C	t (hrs)	^{3}He	Error	^{4}He	Error	^{4}He/^{3}He	Err	In ^{3}He Reg.
1	250	0.25	0.35	0.11	32.4	18.1	82.2	0.64	1
2	250	0.50	0.21	0.10	31.7	12.8	139.7	0.62	0
3	250	1.00	0.27	0.11	35.3	14.1	120.4	0.58	0
4	225	1.50	0.06	0.09	28.3	24.5	489.4	1.74	0
5	225	2.50	0.05	0.11	48.7	48.5	1015.0	2.45	0
6	200	3.00	0.00	0.00	97.4	68.8	Inf	NaN	0
7	200	4.00	0.00	0.00	31.4	89.6	Inf	NaN	0
8	235	2.00	0.08	0.10	25.3	38.9	291.4	1.92	0
9	235	3.00	0.09	0.12	29.1	61.8	315.7	2.53	0
10	270	1.91	0.55	0.15	108.2	36.8	188.2	0.44	0
11	270	1.57	0.34	0.10	68.2	25.2	191.2	0.48	0
12	285	1.25	0.51	0.15	100.2	22.8	185.0	0.37	1
13	285	1.57	0.47	0.14	112.3	24.9	226.5	0.36	0
14	300	1.91	1.00	0.16	228.3	35.8	219.4	0.23	1
15	300	1.45	0.54	0.13	148.2	23.3	262.1	0.29	1
16	325	1.74	1.47	0.20	435.6	29.2	286.1	0.15	1
17	325	1.32	0.81	0.17	283.6	22.0	338.1	0.22	1
18	340	1.58	1.40	0.20	570.7	29.6	396.5	0.15	1
19	340	1.89	1.08	0.19	571.3	37.1	519.0	0.18	1
20	350	1.48	0.98	0.20	565.0	43.0	566.6	0.22	0
21	350	1.82	0.93	0.19	566.4	35.4	598.4	0.21	0
22	360	1.50	0.80	0.16	530.6	27.7	656.0	0.21	0
23	360	1.98	0.77	0.16	555.3	39.0	714.2	0.22	0
24	370	1.88	0.74	0.17	571.1	34.5	766.2	0.23	0
25	390	1.47	0.78	0.15	589.2	30.2	746.1	0.20	0
26	450	1.00	1.27	0.18	1020.7	23.0	793.4	0.14	0
27	600	1.00	0.88	0.15	882.6	27.6	993.2	0.18	0
28	900	1.00	0.04	0.08	58.4	14.0	1347.4	1.88	0
29	899	0.50	0.01	0.07	9.8	15.8	683.7	5.54	0

Figure S65

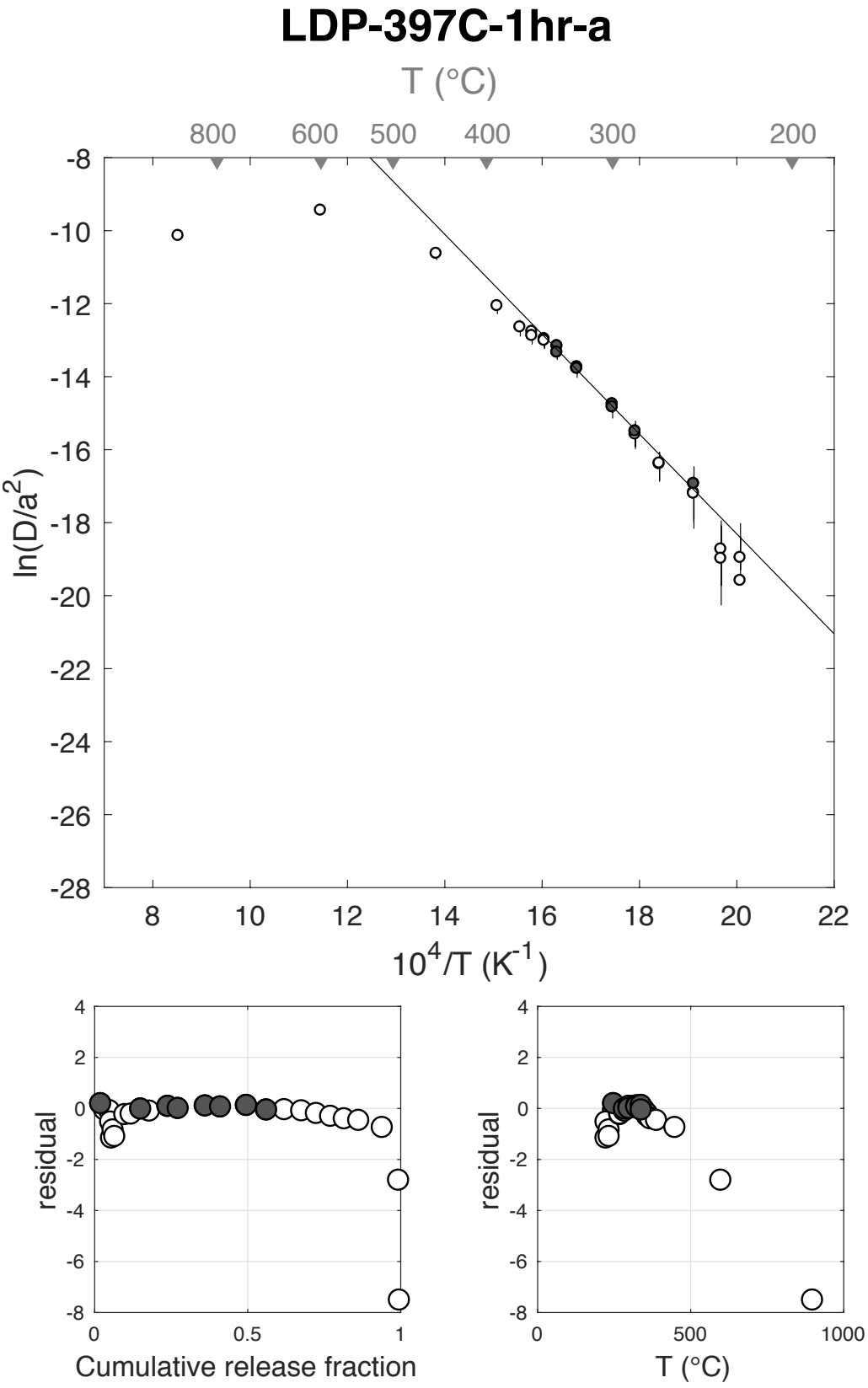
LDP-397C-1hr-a
T (°C)
800
600
500
400
300
200
-8
-10
-12
-14
-16
-18
-20
-22
-24
-26
-28
ln(D/a2)
8
10
12
14
16
18
20
22
10^4/T (K^-1)
4
2
0
-2
-4
-6
-8
residual
0
0.5
1
Cumulative release fraction
0
500
1000
T (°C)

LDP-414C-1hr-a

E_a	+/-	D_0	+/-	T_c	-	+	Total ^{3}He	Incl.	Misfit	Norm. Misfit
135.51	8.47	12.67	1.71	70.46	8.85	9.49	73.45	0.501	0.071	0.004

Step #	°C	t (hrs)	^{3}He	Error	^{4}He	Error	^{4}He/^{3}He	Err	In ^{3}He Reg.
1	250	0.25	0.75	0.16	5.2	31.4	NaN	NaN	1
2	250	0.50	0.58	0.14	12.4	21.0	11.3	1.70	1
3	250	1.00	0.61	0.15	51.3	17.4	73.6	0.42	1
4	225	1.50	0.11	0.10	85.5	41.9	757.3	1.03	0
5	200	2.50	0.00	0.00	123.7	94.9	Inf	NaN	0
6	235	2.50	0.33	0.13	134.4	94.6	400.7	0.80	0
7	270	1.16	1.18	0.19	52.4	24.7	34.3	0.50	1
8	290	1.17	2.19	0.24	91.7	27.1	32.0	0.32	1
9	300	1.30	2.69	0.25	149.9	30.7	45.7	0.22	1
10	300	1.91	2.88	0.25	179.2	63.9	52.3	0.37	1
11	310	1.57	2.76	0.28	182.3	48.0	56.1	0.28	1
12	310	1.25	1.81	0.22	127.3	30.8	60.5	0.27	1
13	320	1.56	3.09	0.30	244.9	45.3	69.2	0.21	1
14	320	1.91	2.91	0.28	305.2	63.4	94.9	0.23	1
15	330	1.45	2.93	0.27	317.4	41.0	98.2	0.16	1
16	330	1.74	3.32	0.30	394.6	56.2	108.9	0.17	1
17	340	1.32	3.12	0.32	424.8	33.0	126.4	0.13	1
18	340	1.58	3.05	0.29	471.2	46.5	144.7	0.14	1
19	340	1.89	2.93	0.27	507.2	63.6	163.1	0.16	1
20	350	1.48	3.03	0.29	543.2	45.7	169.1	0.13	0
21	350	1.82	3.02	0.28	635.6	61.7	200.4	0.13	0
22	360	1.50	3.13	0.30	665.3	44.0	202.2	0.12	0
23	360	1.98	3.20	0.31	777.0	68.8	233.0	0.13	0
24	370	1.88	3.53	0.31	959.3	62.5	261.8	0.11	0
25	390	1.47	4.32	0.31	1164.4	44.6	259.5	0.08	0
26	450	1.00	8.90	0.50	2901.2	34.1	315.9	0.06	0
27	600	1.00	6.38	0.45	3297.1	39.1	507.1	0.07	0
28	900	1.00	0.70	0.16	630.1	21.9	888.3	0.23	0
29	899	0.50	0.00	0.06	0.0	0.0	NaN	NaN	0

Figure S66

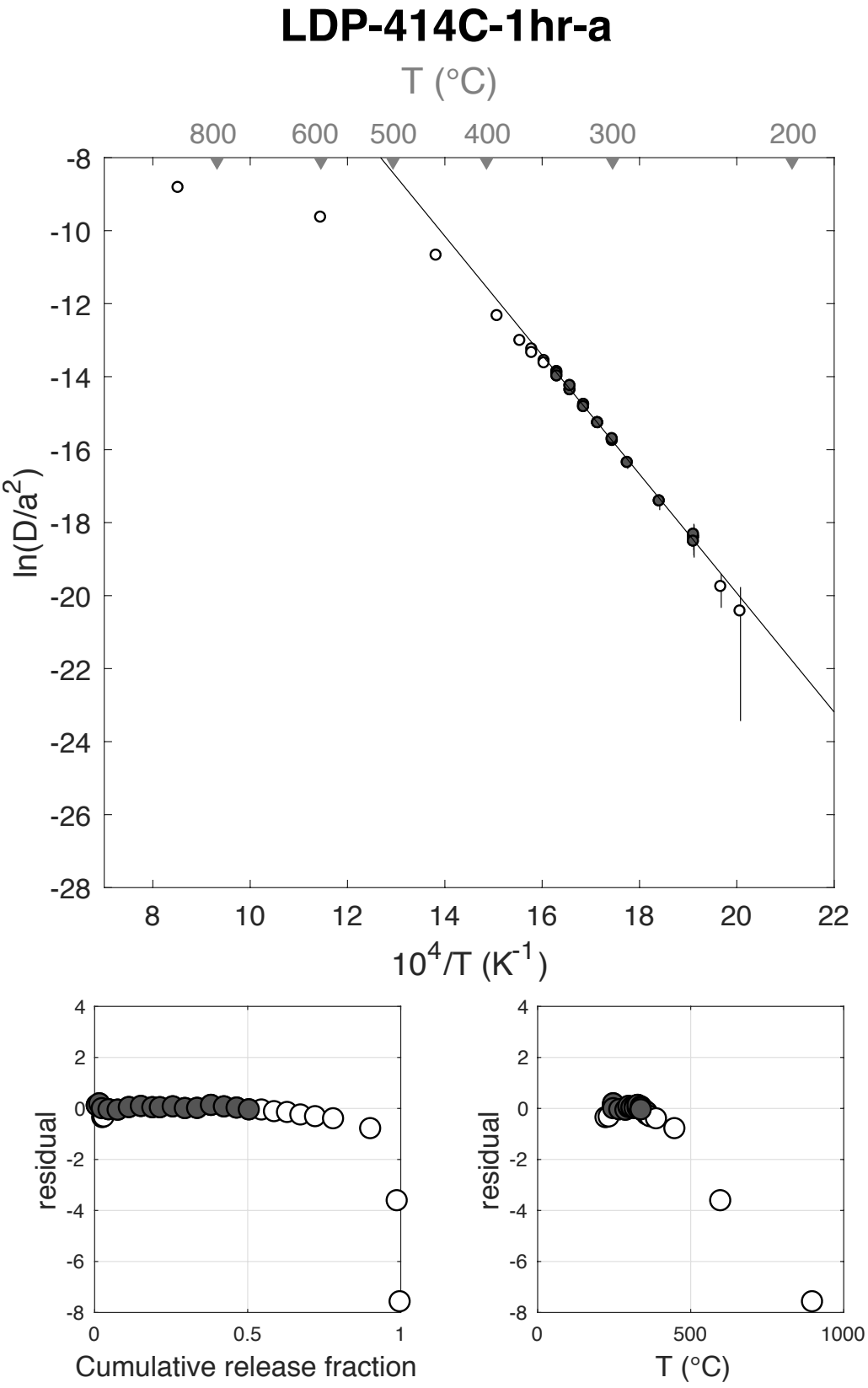
LDP-414C-1hr-a
T (°C)
800
600
500
400
300
200
ln(D/a²)
10⁴/T (K⁻¹)
residual
Cumulative release fraction
residual
T (°C)

LDP-414C-1hr-c

E_a	+/-	D_0	+/-	T_c	-	+	Total ^{3}He	Incl.	Misfit	Norm. Misfit
235.19	20.23	33.24	4.05	143.84		10.54	11.87	21.06	0.512	1.811	0.181

Step #	°C	t (hrs)	^{3}He	Error	^{4}He	Error	^{4}He/^{3}He	Err	In ^{3}He Reg.
1	250	0.25	0.09	0.05	26.4	70.2	274.5	2.71	0
2	250	0.50	0.04	0.04	21.6	42.5	475.7	2.16	0
3	250	1.00	0.08	0.04	22.1	16.8	257.9	0.88	0
4	225	1.50	0.03	0.04	23.3	72.2	802.1	3.41	0
5	225	2.50	0.06	0.07	29.0	185.5	516.3	6.51	0
6	200	3.00	0.01	0.08	24.0	242.2	3512.6	15.90	0
7	200	4.00	0.02	0.12	23.0	355.6	1210.5	16.72	0
8	235	2.00	0.04	0.05	20.9	128.9	578.0	6.36	0
9	235	3.00	0.08	0.09	27.5	242.2	332.6	8.87	0
10	270	1.91	0.24	0.07	35.9	118.7	142.7	3.32	1
11	270	1.57	0.14	0.06	32.2	80.1	212.5	2.52	1
12	285	1.25	0.19	0.06	34.1	44.5	171.1	1.34	1
13	285	1.56	0.24	0.07	37.2	79.2	142.2	2.15	1
14	300	1.91	1.46	0.20	87.1	123.5	49.5	1.42	1
15	300	1.45	0.89	0.14	34.3	73.4	28.4	2.15	1
16	325	1.74	2.28	0.25	235.4	107.5	93.5	0.47	1
17	325	1.32	1.30	0.17	168.9	63.2	119.9	0.40	1
18	340	1.58	2.15	0.20	326.7	92.6	142.3	0.30	1
19	340	1.89	1.89	0.21	389.7	121.4	196.5	0.33	1
20	350	1.48	1.51	0.20	387.9	78.0	247.0	0.24	0
21	350	1.82	1.50	0.19	416.0	115.5	267.8	0.30	0
22	360	1.50	1.21	0.18	392.5	80.4	314.0	0.25	0
23	360	1.98	1.26	0.26	452.9	131.3	349.7	0.36	0
24	370	1.88	0.98	0.16	362.9	120.3	360.8	0.37	0
25	390	1.47	1.02	0.15	436.9	77.5	416.4	0.23	0
26	450	1.00	1.34	0.19	664.2	43.0	484.6	0.16	0
27	600	1.00	0.95	0.14	784.5	46.2	812.3	0.16	0
28	900	1.00	0.06	0.07	39.1	34.4	662.2	1.43	0
29	900	1.00	0.00	0.00	0.0	0.0	NaN	NaN	0

Figure S67

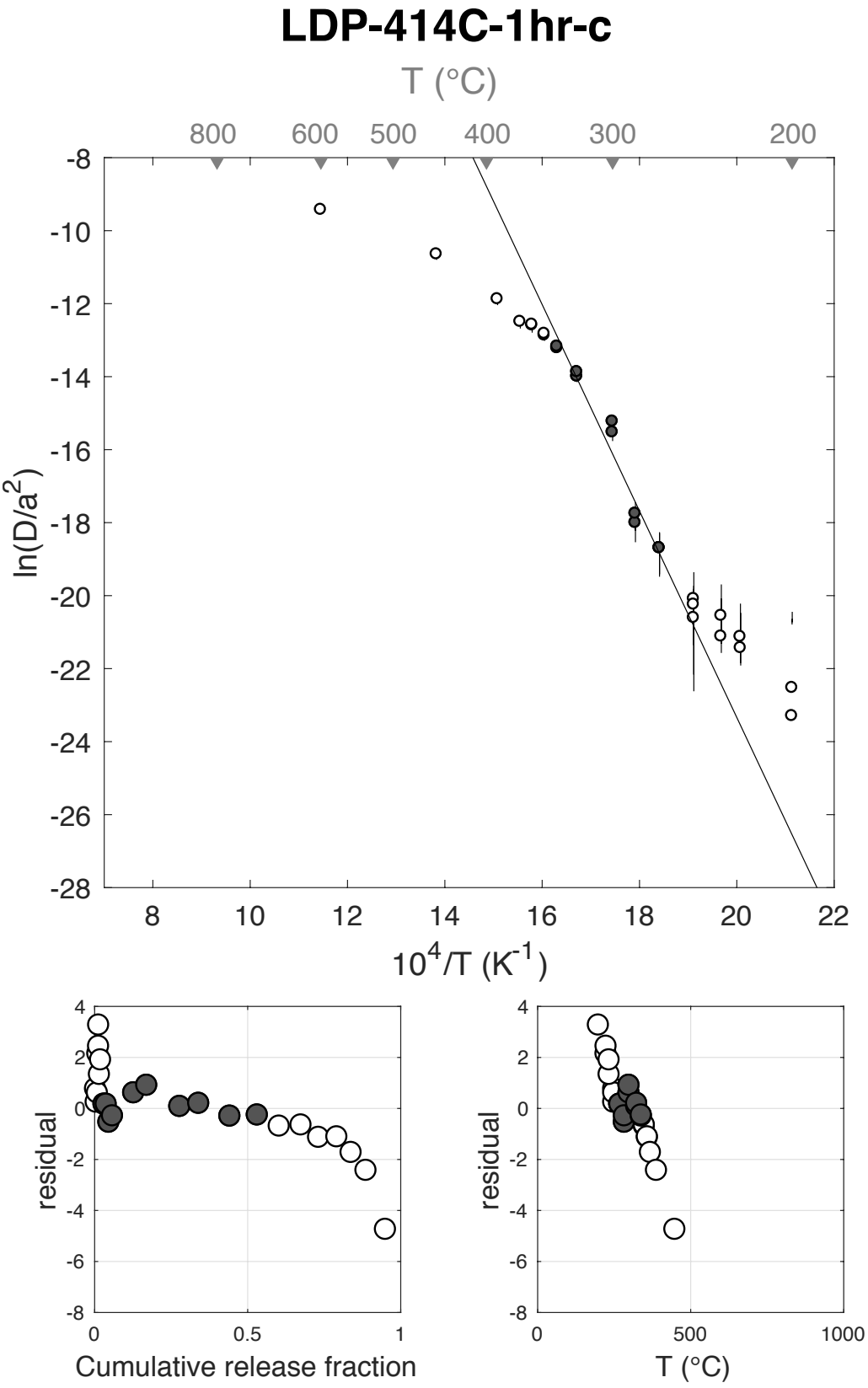
LDP-414C-1hr-c
T (°C)
800
600
500
400
300
200
-8
-10
-12
-14
-16
-18
-20
-22
-24
-26
-28
ln(D/a2)
8
10
12
14
16
18
20
22
10^4/T (K^-1)
residual
4
2
0
-2
-4
-6
-8
0
0.5
1
Cumulative release fraction
residual
0
500
1000
T (°C)

LDP-450C-1hr-a

E_a	+/-	D_0	+/-	T_c	-	+	Total ^{3}He	Incl.	Misfit	Norm. Misfit
139.07	10.94	12.97	2.25	77.14	10.64	11.67	69.78	0.335	0.660	0.044

Step #	°C	t (hrs)	^{3}He	Error	^{4}He	Error	^{4}He/^{3}He	Err	In ^{3}He Reg.
1	250	0.25	0.72	0.13	31.2	16.1	33.6	0.55	1
2	250	0.50	0.43	0.11	36.6	14.4	74.4	0.47	1
3	250	1.00	0.48	0.13	26.0	16.5	43.7	0.69	1
4	225	1.50	0.11	0.09	2.8	15.1	16.3	5.42	0
5	225	2.50	0.13	0.13	0.0	0.0	NaN	NaN	0
6	200	3.00	0.00	0.00	0.0	0.0	NaN	NaN	0
7	200	4.00	0.04	0.16	0.0	0.0	NaN	NaN	0
8	235	2.00	0.16	0.12	0.0	0.0	NaN	NaN	1
9	235	3.00	0.27	0.14	0.0	0.0	NaN	NaN	1
10	270	1.91	1.20	0.18	66.3	23.1	45.3	0.38	1
11	270	1.57	0.72	0.16	45.9	17.5	53.9	0.44	1
12	285	1.25	1.09	0.17	100.7	17.1	82.8	0.23	1
13	285	1.57	1.12	0.17	104.5	16.3	83.1	0.22	1
14	300	1.91	2.20	0.25	259.9	18.3	107.9	0.14	1
15	300	1.45	1.33	0.17	188.6	19.6	131.6	0.17	1
16	325	1.74	3.85	0.29	697.3	23.9	171.3	0.08	1
17	325	1.32	2.14	0.25	506.2	18.7	226.7	0.12	1
18	340	1.58	3.92	0.35	1102.8	25.2	271.6	0.09	1
19	340	1.89	3.72	0.31	1274.7	21.6	332.6	0.09	1
20	350	1.48	3.51	0.33	1450.3	28.9	402.9	0.10	0
21	350	1.82	3.62	0.28	1675.9	25.7	453.0	0.08	0
22	360	1.50	3.58	0.29	1853.8	29.3	508.2	0.08	0
23	360	1.98	3.80	0.32	2242.1	31.4	579.6	0.09	0
24	370	1.88	4.31	0.34	2797.8	30.3	639.5	0.08	0
25	390	1.47	5.01	0.32	3632.7	27.9	714.5	0.06	0
26	450	1.00	8.63	4.15	9618.8	55.5	1105.1	0.48	0
27	600	1.00	13.40	0.58	15678.4	83.6	1159.6	0.04	0
28	900	1.00	0.27	0.11	454.1	19.5	1645.3	0.39	0
29	900	1.00	0.01	0.06	0.0	0.0	NaN	NaN	0

Figure S68

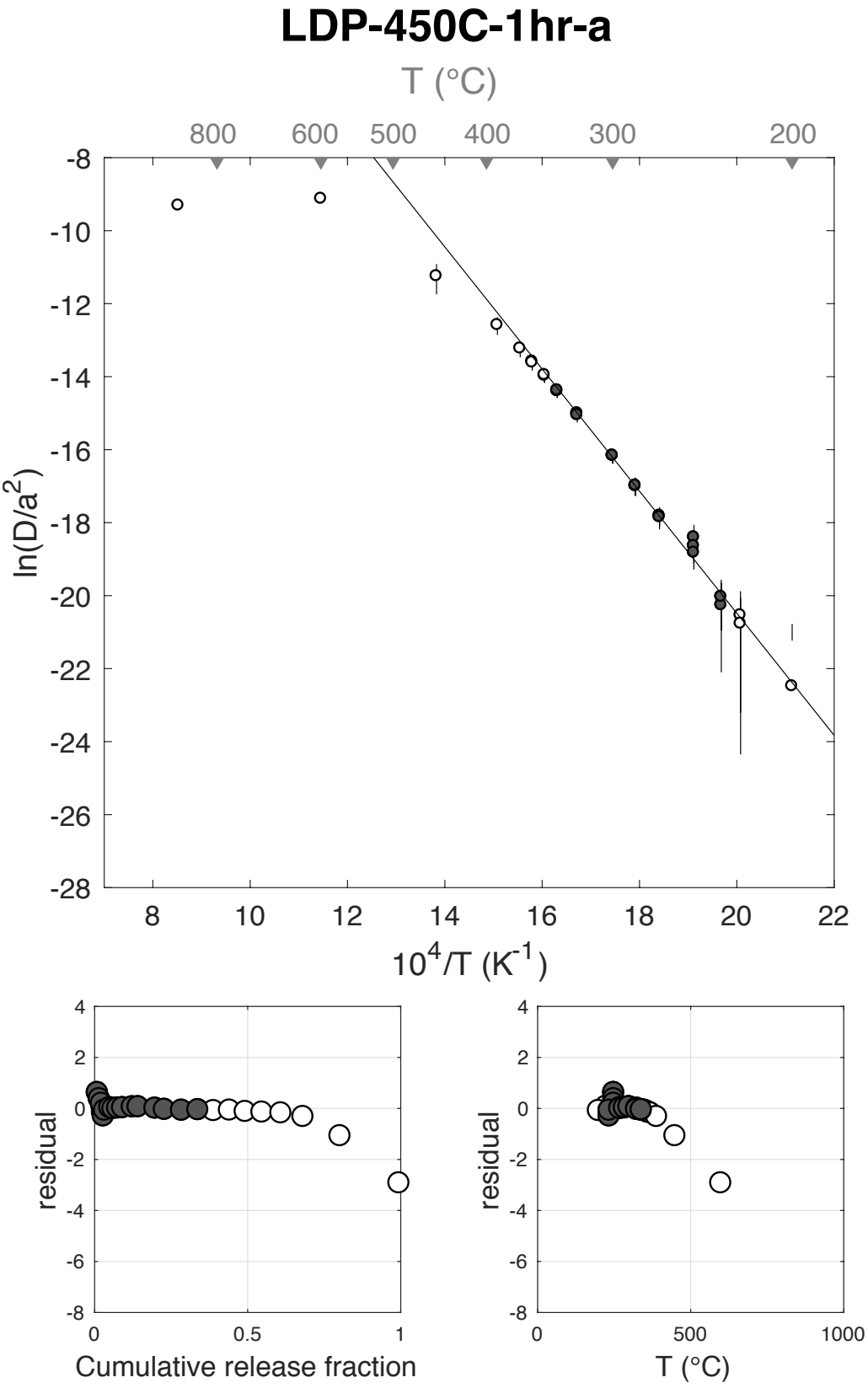
LDP-450C-1hr-a
T (°C)
800
600
500
400
300
200
ln(D/a²)
10⁴/T (K⁻¹)
residual
Cumulative release fraction
residual
T (°C)

LDP-475C-1hr-a

E_a	+/-	D_0	+/-	T_c	-	+	Total ^{3}He	Incl.	Misfit	Norm. Misfit
130.37	10.54	11.27	2.16	67.29	11.11	12.18	62.22	0.338	0.719	0.045

Step #	°C	t (hrs)	^{3}He	Error	^{4}He	Error	^{4}He/^{3}He	Err	In ^{3}He Reg.
1	250	0.25	0.69	0.16	12.0	22.2	7.5	1.85	1
2	250	0.50	0.44	0.13	19.1	19.2	33.9	1.04	1
3	250	1.00	0.54	0.15	26.5	18.2	38.7	0.74	1
4	225	1.50	0.11	0.09	24.6	23.3	220.4	1.26	0
5	225	2.50	0.20	0.11	19.6	41.6	88.7	2.19	1
6	200	3.00	0.00	0.00	0.0	0.0	NaN	NaN	0
7	200	4.00	0.00	0.00	18.9	75.8	Inf	NaN	0
8	235	2.00	0.18	0.12	15.0	34.6	74.5	2.39	1
9	235	3.00	0.28	0.14	13.4	53.1	37.8	3.98	1
10	270	1.91	1.36	0.21	93.8	33.2	58.7	0.39	1
11	270	1.57	0.78	0.15	55.2	24.2	60.9	0.48	1
12	285	1.25	1.02	0.16	88.5	18.3	77.2	0.26	1
13	285	1.57	1.16	0.17	116.0	24.3	90.4	0.26	1
14	300	1.91	2.14	0.24	286.0	31.2	123.5	0.16	1
15	300	1.45	1.18	0.18	212.8	25.3	169.6	0.19	1
16	325	1.74	3.26	0.27	690.6	27.4	201.6	0.09	1
17	325	1.32	1.53	0.20	407.2	25.2	256.8	0.14	1
18	340	1.58	3.31	0.28	1028.6	27.4	300.6	0.09	1
19	340	1.89	2.96	0.26	1151.2	35.7	379.2	0.09	1
20	350	1.48	2.96	0.29	1391.3	24.8	460.7	0.10	0
21	350	1.82	2.66	0.28	1517.1	39.4	561.1	0.11	0
22	360	1.50	2.71	0.26	1763.1	33.4	639.7	0.10	0
23	360	1.98	2.75	0.26	2040.3	41.1	731.2	0.10	0
24	370	1.88	3.08	0.26	2553.4	38.9	819.5	0.08	0
25	390	1.47	4.02	0.33	3573.6	54.7	878.5	0.08	0
26	450	1.00	8.85	0.45	9317.4	53.3	1042.3	0.05	0
27	600	1.00	12.83	0.55	19502.7	70.9	1509.9	0.04	0
28	900	1.00	1.22	0.18	2716.8	44.3	2220.7	0.15	0
29	899	1.00	0.00	0.00	11.2	20.0	Inf	NaN	0

Figure S69

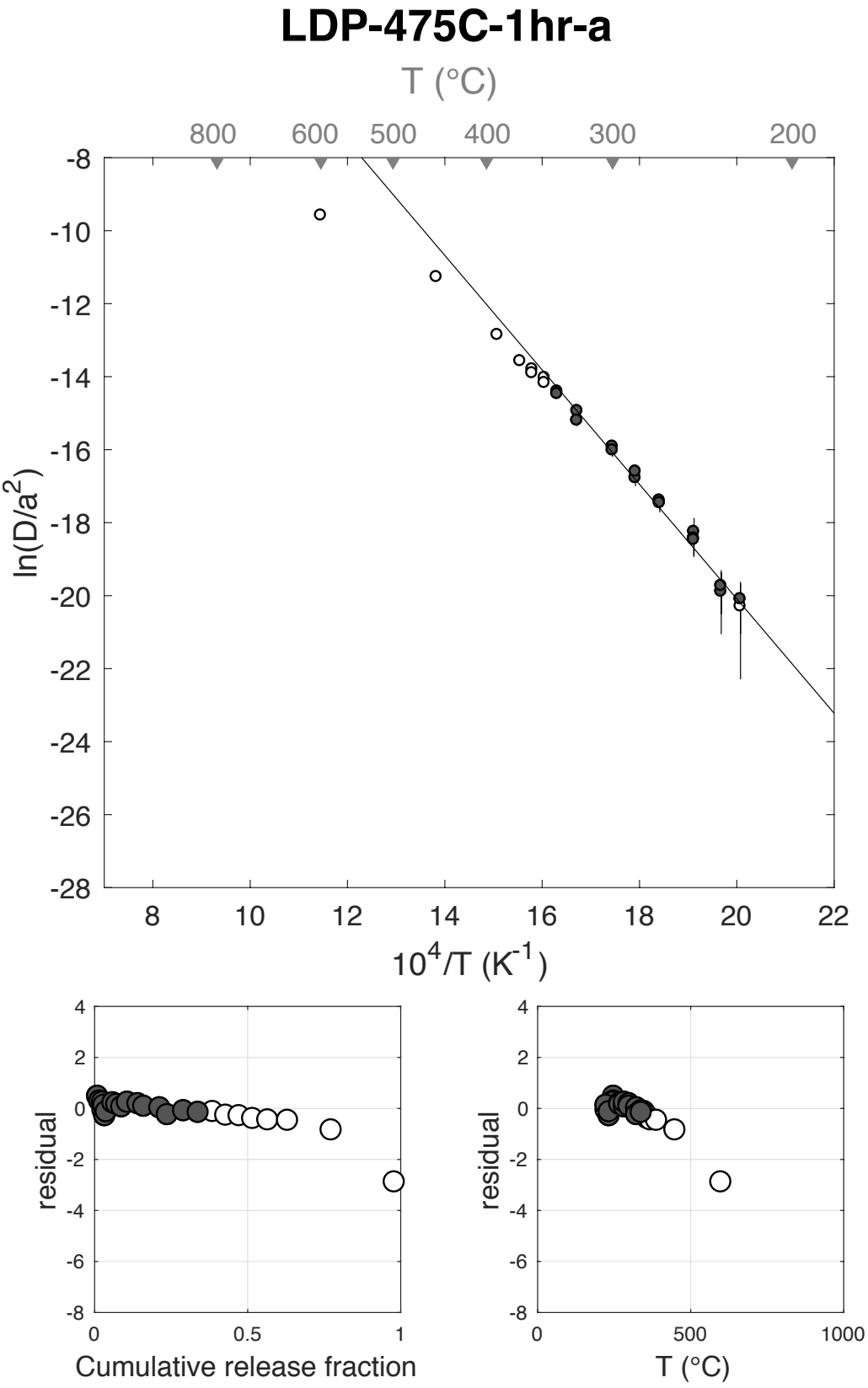
LDP-475C-1hr-a
T (°C)
800
600
500
400
300
200
-8
-10
-12
-14
-16
-18
-20
-22
-24
-26
-28
ln(D/a2)
8
10
12
14
16
18
20
22
10^4/T (K^-1)
4
2
0
-2
-4
-6
-8
residual
0
0.5
1
Cumulative release fraction
0
500
1000
T (°C)

LDP-500C-1hr-b

E_a	+/-	D_0	+/-	T_c	-	+	Total ^{3}He	Incl.	Misfit	Norm. Misfit
144.97	7.71	14.40	1.59	81.53	7.24	7.71	106.82	0.373	0.132	0.008

Step #	°C	t (hrs)	^{3}He	Error	^{4}He	Error	^{4}He/^{3}He	Err	In ^{3}He Reg.
1	250	0.25	0.89	0.16	60.5	22.2	58.3	0.41	1
2	250	0.50	0.61	0.13	48.7	21.9	70.4	0.50	1
3	250	1.00	0.83	0.16	67.4	17.5	71.4	0.33	1
4	225	1.50	0.18	0.10	25.7	20.1	132.8	0.95	1
5	225	2.50	0.26	0.12	26.4	38.7	91.9	1.53	1
6	200	3.00	0.02	0.08	12.1	46.8	494.3	5.19	0
7	200	4.00	0.01	0.08	23.0	68.6	1772.5	7.07	0
8	235	2.00	0.37	0.12	28.1	28.1	65.4	1.05	1
9	235	3.00	0.46	0.14	21.3	48.8	36.3	2.31	1
10	270	1.91	2.05	0.25	126.0	28.2	51.6	0.25	1
11	270	1.57	1.33	0.19	83.2	23.3	52.8	0.31	1
12	285	1.25	2.02	0.25	114.3	17.4	46.4	0.20	1
13	285	1.57	1.92	0.22	141.2	25.0	63.7	0.21	1
14	300	1.91	3.72	0.30	264.2	32.7	60.9	0.15	1
15	300	1.45	2.25	0.25	174.9	20.1	67.6	0.16	1
16	325	1.74	6.27	0.36	545.2	30.5	77.0	0.08	1
17	325	1.32	3.95	0.31	377.3	21.8	85.4	0.10	1
18	340	1.58	6.83	0.39	719.7	30.9	95.4	0.07	1
19	340	1.89	5.96	0.38	752.1	28.9	116.2	0.08	1
20	350	1.48	4.89	0.40	770.7	28.2	147.6	0.09	0
21	350	1.82	4.90	0.35	837.4	29.8	161.0	0.08	0
22	360	1.50	4.65	0.37	894.1	27.5	182.4	0.08	0
23	360	1.98	4.77	0.36	1084.2	33.4	217.3	0.08	0
24	370	1.88	5.40	0.37	1307.7	34.0	232.0	0.07	0
25	390	1.47	6.08	0.36	1657.1	27.9	262.6	0.06	0
26	450	1.00	12.71	0.56	4234.8	32.8	323.1	0.04	0
27	600	1.00	19.94	0.77	11572.6	95.0	570.3	0.04	0
28	900	1.00	3.54	0.30	5412.5	41.5	1519.5	0.09	0
29	900	1.00	0.02	0.08	113.3	17.0	5816.9	4.00	0

Figure S70

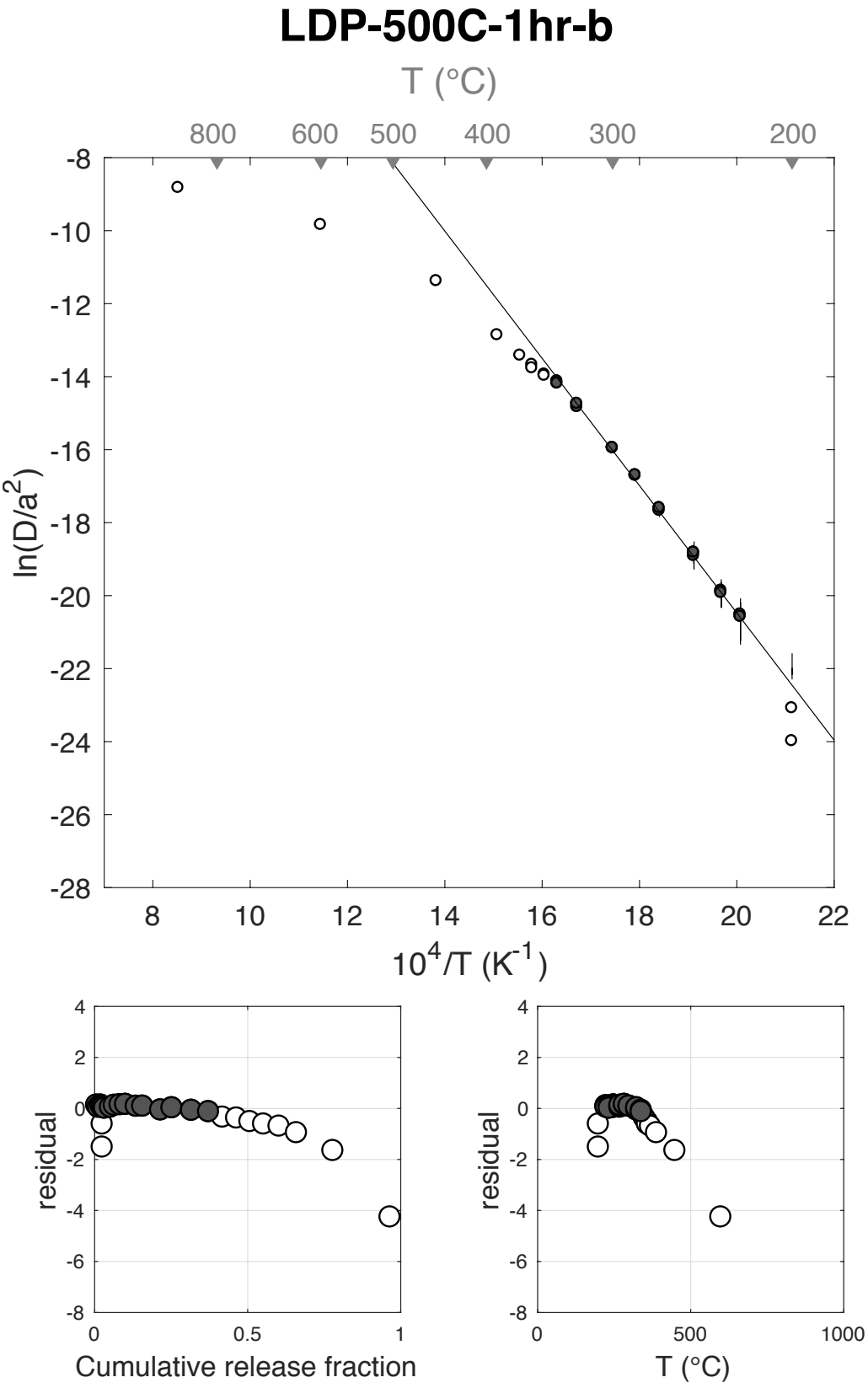
LDP-500C-1hr-b
T (°C)
800
600
500
400
300
200
ln(D/a²)
10⁴/T (K⁻¹)
residual
Cumulative release fraction
residual
T (°C)

LDP-250C-10hr-a

E_a	+/-	D_0	+/-	T_c	-	+	Total ^{3}He	Incl.	Misfit	Norm. Misfit
122.38	2.46	9.72	0.50	57.51	2.93	2.99	400.82	0.436	0.191	0.011

Step #	°C	t (hrs)	^{3}He	Error	^{4}He	Error	^{4}He/^{3}He	Err	In ^{3}He Reg.
1	250	0.25	4.63	0.32	1593.7	37.0	334.0	0.07	1
2	250	0.50	3.01	0.28	1121.5	30.0	362.2	0.10	1
3	250	1.00	3.31	0.31	1367.0	32.6	402.8	0.10	1
4	225	1.50	0.93	0.14	370.6	42.6	389.5	0.19	1
5	200	2.50	0.26	0.12	147.0	89.8	552.9	0.76	0
6	235	2.50	2.31	0.27	1010.9	92.6	427.3	0.15	1
7	270	1.16	6.29	0.39	2783.7	38.4	432.2	0.06	1
8	290	1.17	11.37	0.57	5558.0	47.2	478.7	0.05	1
9	300	1.30	13.47	0.55	7523.2	80.3	548.6	0.04	1
10	300	1.91	13.55	0.55	8310.2	75.2	603.4	0.04	1
11	310	1.57	12.99	0.59	8868.5	65.0	672.7	0.05	1
12	310	1.25	8.75	0.47	6045.1	42.9	680.8	0.05	1
13	320	1.56	14.18	0.58	10342.4	66.1	719.2	0.04	1
14	320	1.91	13.72	0.55	10394.0	75.0	747.7	0.04	1
15	330	1.45	13.44	0.61	10366.7	66.3	761.6	0.05	1
16	330	1.74	13.19	0.64	10658.3	83.1	798.3	0.05	1
17	340	1.32	13.08	0.64	10603.5	59.9	800.9	0.05	1
18	340	1.58	13.23	0.59	10979.6	86.4	820.0	0.05	1
19	340	1.89	13.31	0.57	11282.6	83.9	837.9	0.04	1
20	350	1.48	13.56	0.56	11470.0	86.2	836.1	0.04	0
21	350	1.82	14.14	0.56	12126.4	141.4	847.8	0.04	0
22	360	1.50	14.41	0.68	12444.2	114.8	853.5	0.05	0
23	360	1.98	15.85	0.59	13854.6	105.0	864.0	0.04	0
24	370	1.88	17.76	0.63	15485.0	156.1	861.8	0.04	0
25	545	1.47	21.13	0.76	18860.2	173.4	882.6	0.04	0
26	450	1.00	46.96	1.08	42445.7	194.9	893.8	0.02	0
27	600	1.00	68.00	1.38	62680.2	515.5	911.8	0.02	0
28	900	1.00	14.00	0.57	12083.5	115.1	853.1	0.04	0
29	899	0.50	0.00	0.00	38.1	18.0	Inf	NaN	0

Figure S71

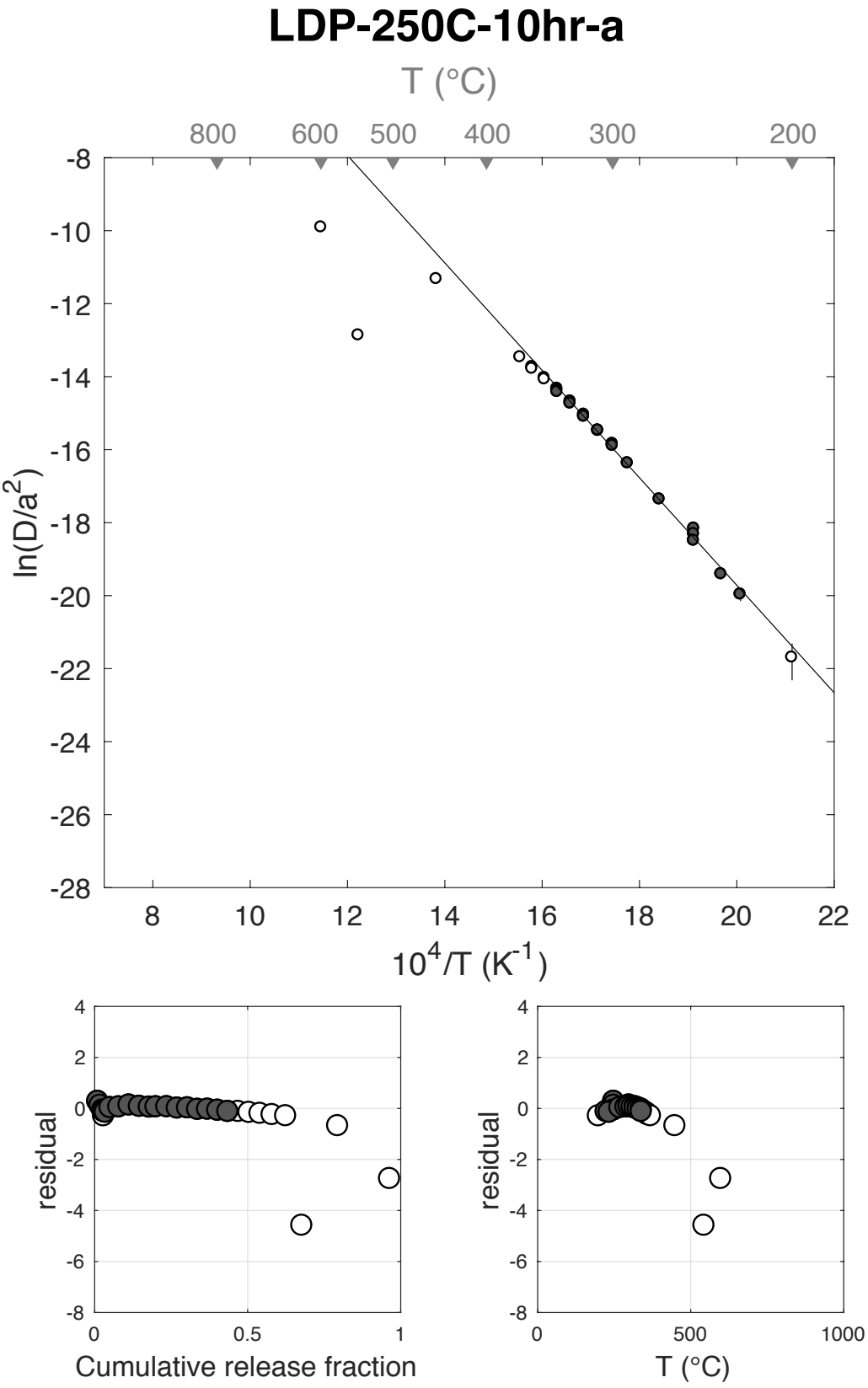
LDP-250C-10hr-a
T (°C)
800
600
500
400
300
200
-8
-10
-12
-14
-16
-18
-20
-22
-24
-26
-28
ln(D/a2)
8
10
12
14
16
18
20
22
10^4/T (K^-1)
4
2
0
-2
-4
-6
-8
residual
0
0.5
1
Cumulative release fraction
0
500
1000
T (°C)

LDP-250C-10hr-b

E_a	+/-	D_0	+/-	T_c	-	+	Total ^{3}He	Incl.	Misfit	Norm. Misfit
140.71	9.63	13.66	2.02	76.38	9.10	9.87	75.56	0.415	0.277	0.015

Step #	°C	t (hrs)	^{3}He	Error	^{4}He	Error	^{4}He/^{3}He	Err	In ^{3}He Reg.
1	250	0.25	0.75	0.16	175.5	17.5	224.1	0.23	1
2	250	0.50	0.42	0.11	221.8	14.1	514.5	0.27	1
3	250	1.00	0.53	0.13	362.3	20.5	679.9	0.26	1
4	225	1.50	0.14	0.07	87.5	15.9	624.6	0.57	1
5	225	2.50	0.24	0.11	126.4	20.2	519.0	0.49	1
6	200	3.00	0.05	0.09	0.0	0.0	NaN	NaN	1
7	200	4.00	0.08	0.11	0.0	0.0	NaN	NaN	1
8	235	2.00	0.28	0.11	193.8	19.2	690.4	0.40	1
9	235	3.00	0.38	0.13	265.4	20.8	688.1	0.34	1
10	270	1.91	1.52	0.20	1409.0	25.0	919.4	0.13	1
11	270	1.57	0.97	0.17	956.6	20.2	978.4	0.17	1
12	285	1.25	1.38	0.19	1555.5	28.1	1119.0	0.14	1
13	285	1.57	1.36	0.19	1662.7	24.8	1213.5	0.14	1
14	300	1.91	2.84	0.30	3652.2	37.2	1274.3	0.10	1
15	300	1.45	1.66	0.24	2365.9	35.3	1418.6	0.15	1
16	325	1.74	5.19	0.37	7552.7	52.1	1445.4	0.07	1
17	325	1.32	3.10	0.30	4713.1	35.5	1509.4	0.10	1
18	340	1.58	5.43	0.37	8893.7	40.1	1626.4	0.07	1
19	340	1.89	5.02	0.34	8521.9	55.2	1688.5	0.07	1
20	350	1.48	4.69	0.34	7967.2	62.3	1688.4	0.07	0
21	350	1.82	4.43	0.32	7848.9	53.2	1761.9	0.07	0
22	360	1.50	4.25	0.33	7638.4	49.0	1787.0	0.08	0
23	360	1.98	4.41	0.33	8027.3	36.9	1812.2	0.08	0
24	370	1.88	4.57	0.33	8303.0	54.3	1806.5	0.07	0
25	390	1.47	4.89	0.38	8965.1	65.3	1823.7	0.08	0
26	450	1.00	8.74	0.42	16076.1	75.8	1828.6	0.05	0
27	600	1.00	7.74	0.41	14548.6	76.5	1870.8	0.05	0
28	900	1.00	0.52	0.12	1010.3	28.2	1933.8	0.24	0
29	900	1.00	0.00	0.06	5.3	14.7	2304.5	26.53	0

Figure S72

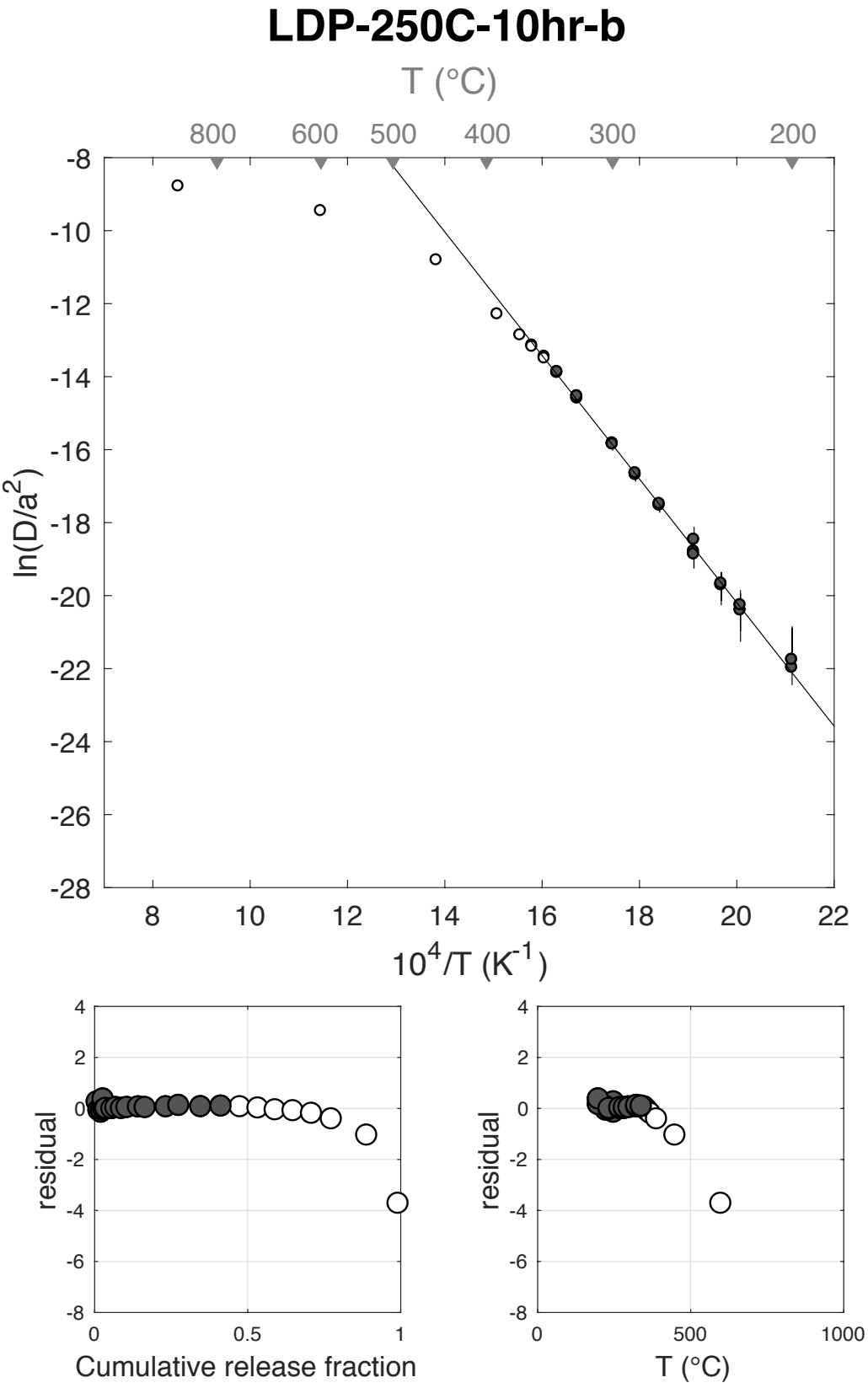
LDP-250C-10hr-b
T (°C)
800
600
500
400
300
200
-8
-10
-12
-14
-16
-18
-20
-22
-24
-26
-28
ln(D/a2)
8
10
12
14
16
18
20
22
10^4/T (K^-1)
4
2
0
-2
-4
-6
-8
residual
0
0.5
1
Cumulative release fraction
500
1000
T (°C)

E_a	+/-	D_0	+/-	T_c	-	+	Total ^{3}He	Incl.	Misfit	Norm. Misfit
146.49	11.23	15.59	2.31	77.03	10.38	11.36	41.81	0.532	0.407	0.024

Step #	°C	t (hrs)	^{3}He	Error	^{4}He	Error	^{4}He/^{3}He	Err	In ^{3}He Reg.
1	250	0.25	0.61	0.14	142.3	17.7	222.9	0.26	1
2	250	0.50	0.36	0.11	107.0	15.6	286.8	0.33	1
3	250	1.00	0.43	0.12	147.7	12.4	330.9	0.28	1
4	225	1.50	0.11	0.09	40.5	18.4	374.9	0.98	1
5	225	2.50	0.18	0.13	75.1	35.6	418.7	0.88	1
6	200	3.00	0.12	0.15	77.6	44.5	662.8	1.41	0
7	200	4.00	0.18	0.20	32.6	63.9	174.2	2.28	0
8	235	2.00	0.22	0.11	92.4	26.7	408.4	0.59	1
9	235	3.00	0.22	0.16	91.1	44.8	399.6	0.89	1
10	270	1.91	1.18	0.18	551.4	26.8	458.2	0.16	1
11	270	1.57	0.72	0.15	363.0	21.4	495.3	0.21	1
12	285	1.25	1.11	0.18	634.1	18.4	562.2	0.16	1
13	285	1.57	1.06	0.20	726.2	23.7	673.8	0.19	1
14	300	1.91	2.20	0.23	1620.6	28.1	727.1	0.11	1
15	300	1.45	1.32	0.17	1079.8	26.6	809.2	0.13	1
16	325	1.74	3.87	0.31	3534.2	45.0	903.2	0.08	1
17	325	1.32	2.07	0.23	2093.0	31.9	1000.3	0.11	1
18	340	1.58	3.55	0.33	3997.2	46.0	1117.5	0.09	1
19	340	1.89	3.05	0.32	3707.6	35.0	1205.7	0.11	1
20	350	1.48	2.67	0.26	3278.1	33.0	1216.1	0.10	0
21	350	1.82	0.00	0.00	1.5	22.8	Inf	NaN	0
22	360	1.50	2.35	0.24	3107.7	30.7	1312.7	0.10	0
23	360	1.98	2.25	0.25	3030.9	38.3	1339.3	0.11	0
24	370	1.88	2.24	0.27	3120.6	40.3	1381.9	0.12	0
25	390	1.47	2.19	0.21	3149.3	32.4	1426.0	0.10	0
26	450	1.00	3.46	0.30	5099.1	35.6	1464.6	0.09	0
27	599	1.00	3.43	0.29	5401.5	44.2	1566.1	0.09	0
28	900	1.00	0.64	0.15	1190.8	28.1	1863.1	0.24	0
29	899	0.50	0.05	0.07	22.8	17.3	470.0	1.68	0

Figure S73

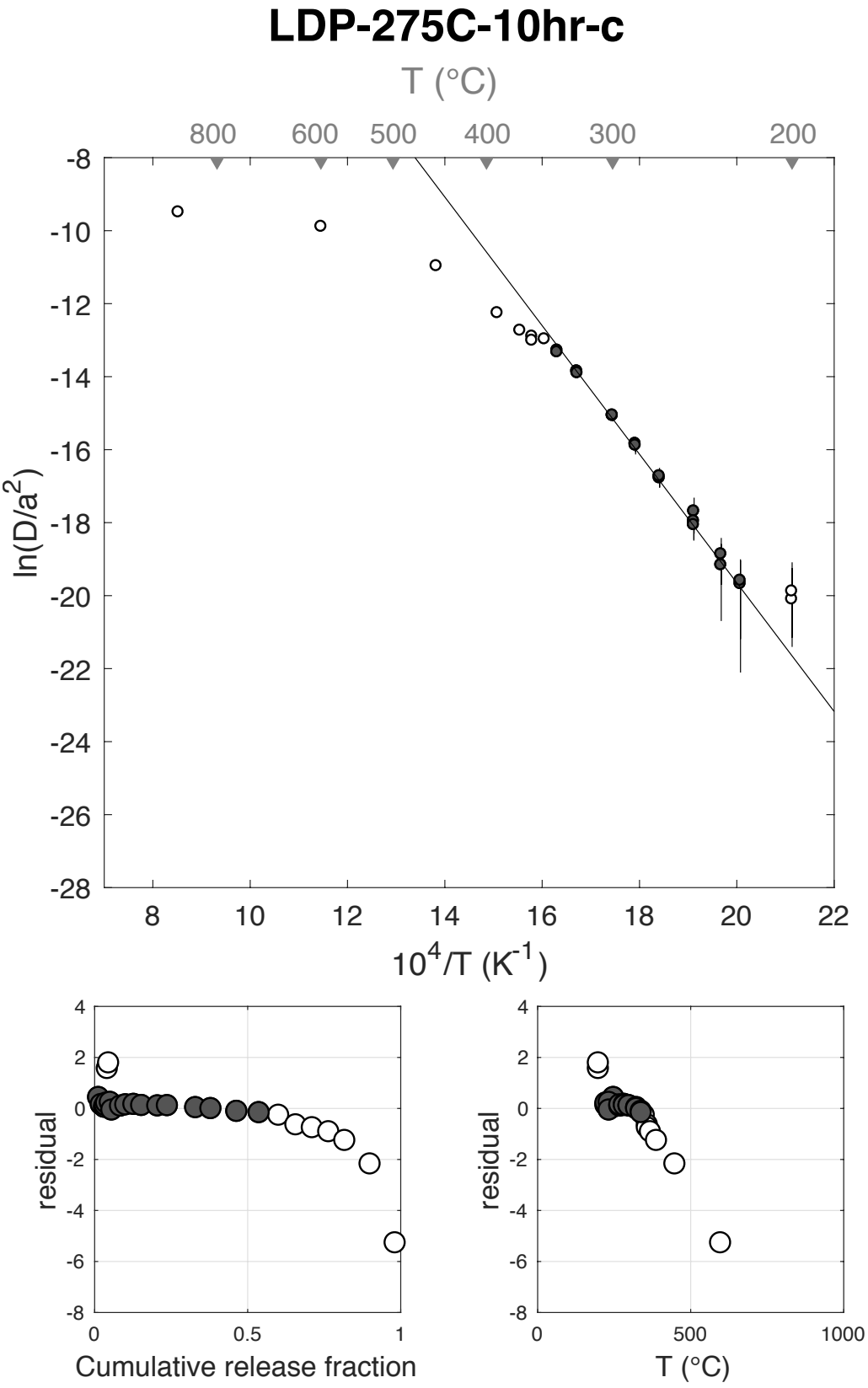
LDP-275C-10hr-c
T (°C)
800
600
500
400
300
200
-8
-10
-12
-14
-16
-18
-20
-22
-24
-26
-28
ln(D/a2)
8
10
12
14
16
18
20
22
10^4/T (K^-1)
4
2
0
-2
-4
-6
-8
residual
0
0.5
1
Cumulative release fraction
0
500
1000
T (°C)

E_a	+/-	D_0	+/-	T_c	-	+	Total ^{3}He	Incl.	Misfit	Norm. Misfit
117.02	8.34	8.95	1.70	48.69	10.13	10.93	139.92	0.487	18.22	1.518

Step #	°C	t (hrs)	^{3}He	Error	^{4}He	Error	^{4}He/^{3}He	Err	In ^{3}He Reg.
1	250	0.25	0.80	0.19	3942.2	3735.4	4925.3	0.98	1
2	250	0.50	0.49	0.15	4646.6	2009.0	9406.7	0.53	0
3	250	1.00	0.60	0.18	10090.9	1454.9	16815.9	0.33	0
4	225	1.50	0.19	0.18	18915.3	4903.3	101791.6	1.01	0
5	225	2.50	0.20	0.36	28837.6	11809.8	144304.9	1.83	0
6	200	3.00	0.67	0.47	0.0	0.0	NaN	NaN	0
7	200	4.00	2.04	0.68	0.0	0.0	NaN	NaN	1
8	235	2.00	0.10	0.26	5191.3	8356.1	51948.8	3.07	0
9	235	3.00	0.27	0.46	13175.3	15264.0	47986.9	2.02	0
10	270	1.91	1.45	0.31	7976.1	7733.8	5484.5	0.99	1
11	270	1.57	0.90	0.22	6394.3	5384.9	7073.0	0.88	1
12	285	1.25	1.70	0.20	7116.2	3175.7	4174.7	0.46	1
13	285	1.57	25.58	0.95	0.0	0.0	NaN	NaN	1
14	300	1.91	2.99	0.37	5981.5	7733.8	1993.5	1.30	1
15	300	1.45	1.94	0.28	4691.5	4556.5	2402.2	0.98	1
16	325	1.74	16.29	0.73	0.0	0.0	NaN	NaN	1
17	325	1.32	3.64	0.36	22178.2	3660.3	6076.3	0.19	1
18	340	1.58	5.77	0.47	0.0	0.0	NaN	NaN	1
19	340	1.89	4.98	0.45	4585.7	7595.4	911.1	1.66	1
20	350	1.48	4.77	0.41	2888.7	4763.2	595.7	1.65	0
21	350	1.82	4.77	0.43	5366.5	7112.0	1114.4	1.33	0
22	360	1.50	4.70	0.37	3911.3	4901.3	821.4	1.26	0
23	360	1.98	5.18	0.44	7026.6	8217.3	1347.4	1.17	0
24	370	1.88	5.93	0.48	7510.6	7526.5	1257.4	1.01	0
25	390	1.47	7.05	0.50	6708.1	4696.2	942.2	0.70	0
26	450	1.00	16.48	0.69	16493.6	1452.1	990.7	0.10	0
27	600	1.00	19.29	0.77	17632.1	1449.4	904.1	0.09	0
28	900	1.00	1.14	0.22	12615.2	1449.0	11087.6	0.22	0
29	900	0.50	0.00	0.00	15770.0	2010.6	Inf	NaN	0

Figure S74

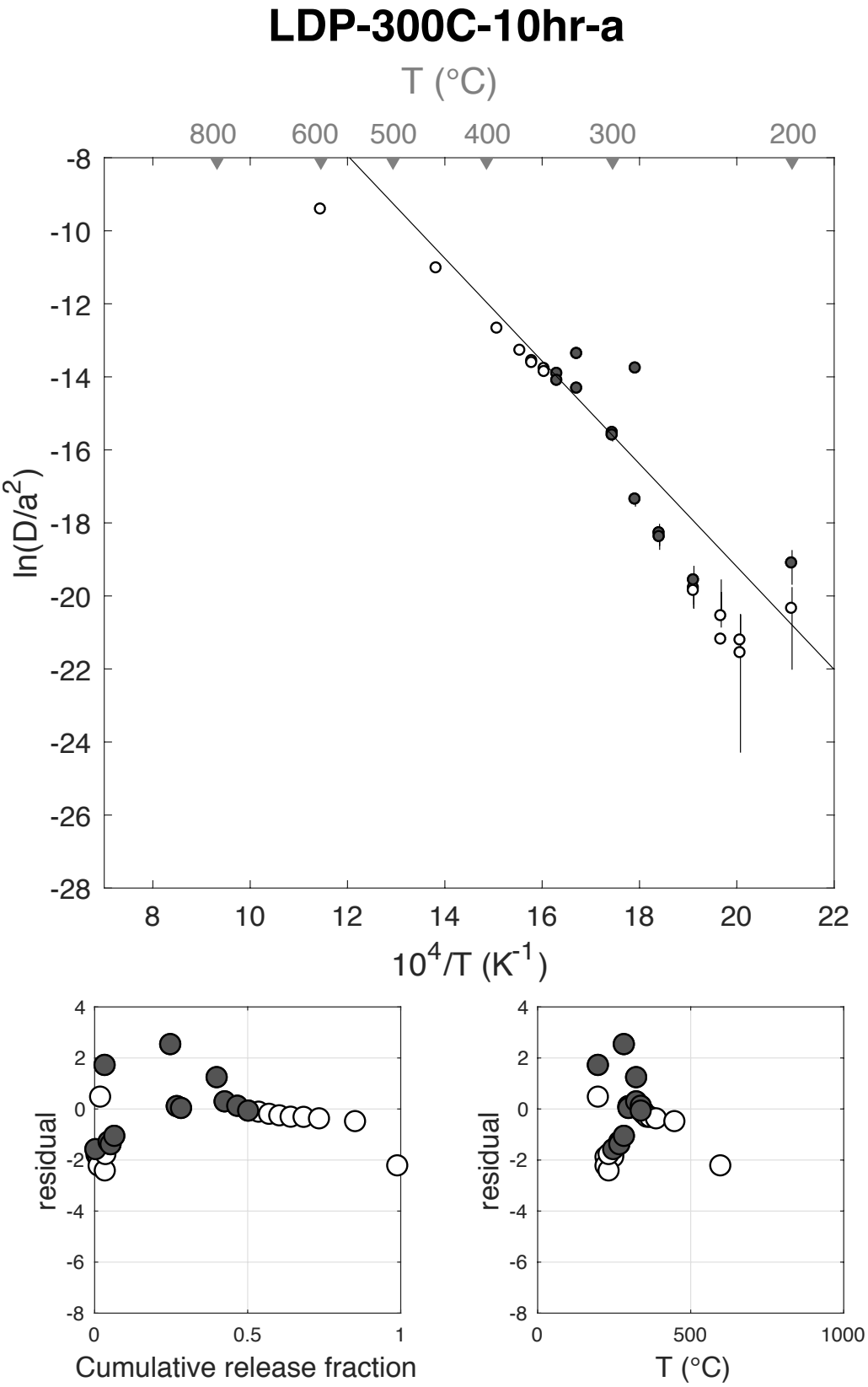
LDP-300C-10hr-a
T (°C)
800
600
500
400
300
200
-8
-10
-12
-14
-16
-18
-20
-22
-24
-26
-28
ln(D/a2)
8
10
12
14
16
18
20
22
10^4/T (K^-1)
4
2
0
-2
-4
-6
-8
residual
0
0.5
1
Cumulative release fraction
0
500
1000
T (°C)

LDP-315C-10hr-b

E_a	+/-	D_0	+/-	T_c	-	+	Total ^{3}He	Incl.	Misfit	Norm. Misfit
149.57	11.20	15.37	2.29	85.76	10.16	11.11	54.36	0.383	0.210	0.014

Step #	°C	t (hrs)	^{3}He	Error	^{4}He	Error	^{4}He/^{3}He	Err	In ^{3}He Reg.
1	250	0.25	0.47	0.13	33.5	16.9	61.8	0.57	1
2	250	0.50	0.33	0.11	36.2	16.8	98.9	0.56	1
3	250	1.00	0.39	0.13	48.8	15.9	114.7	0.47	1
4	225	1.50	0.08	0.08	5.4	12.9	61.0	2.60	0
5	225	2.50	0.10	0.10	8.8	17.3	77.4	2.18	0
6	200	3.00	0.00	0.00	0.0	0.0	NaN	NaN	0
7	200	4.00	0.01	0.10	0.0	0.0	NaN	NaN	0
8	235	2.00	0.15	0.09	11.2	19.4	62.5	1.83	1
9	235	3.00	0.23	0.11	17.7	17.5	65.9	1.09	1
10	270	1.91	1.02	0.18	288.8	23.4	274.0	0.20	1
11	270	1.57	0.63	0.14	221.1	14.7	339.9	0.23	1
12	285	1.25	0.93	0.15	412.6	16.3	432.0	0.16	1
13	285	1.57	1.01	0.16	495.7	18.4	481.7	0.16	1
14	300	1.91	1.95	0.23	1221.1	25.5	615.2	0.12	1
15	300	1.45	1.27	0.19	874.0	27.8	680.5	0.16	1
16	325	1.74	3.45	0.29	3051.9	34.7	874.9	0.08	1
17	325	1.32	2.03	0.26	2070.1	28.1	1011.3	0.13	1
18	340	1.58	3.63	0.32	4029.3	43.9	1099.1	0.09	1
19	340	1.89	3.31	0.32	3935.3	39.3	1180.1	0.10	1
20	350	1.48	2.94	0.26	3774.1	38.0	1275.4	0.09	0
21	350	1.82	2.83	0.28	3829.0	31.0	1341.9	0.10	0
22	360	1.50	2.65	0.26	3824.6	40.2	1433.0	0.10	0
23	360	1.98	2.82	0.28	4076.7	38.5	1435.3	0.10	0
24	370	1.88	2.81	0.28	4324.1	43.0	1528.7	0.10	0
25	390	1.47	3.15	0.30	4890.7	37.3	1544.5	0.10	0
26	450	1.00	6.30	0.44	9867.4	68.1	1555.5	0.07	0
27	600	1.00	8.84	0.43	15409.6	57.8	1732.4	0.05	0
28	900	1.00	1.01	0.16	1751.9	26.7	1723.3	0.16	0
29	900	1.00	0.02	0.07	0.0	0.0	NaN	NaN	0

Figure S75

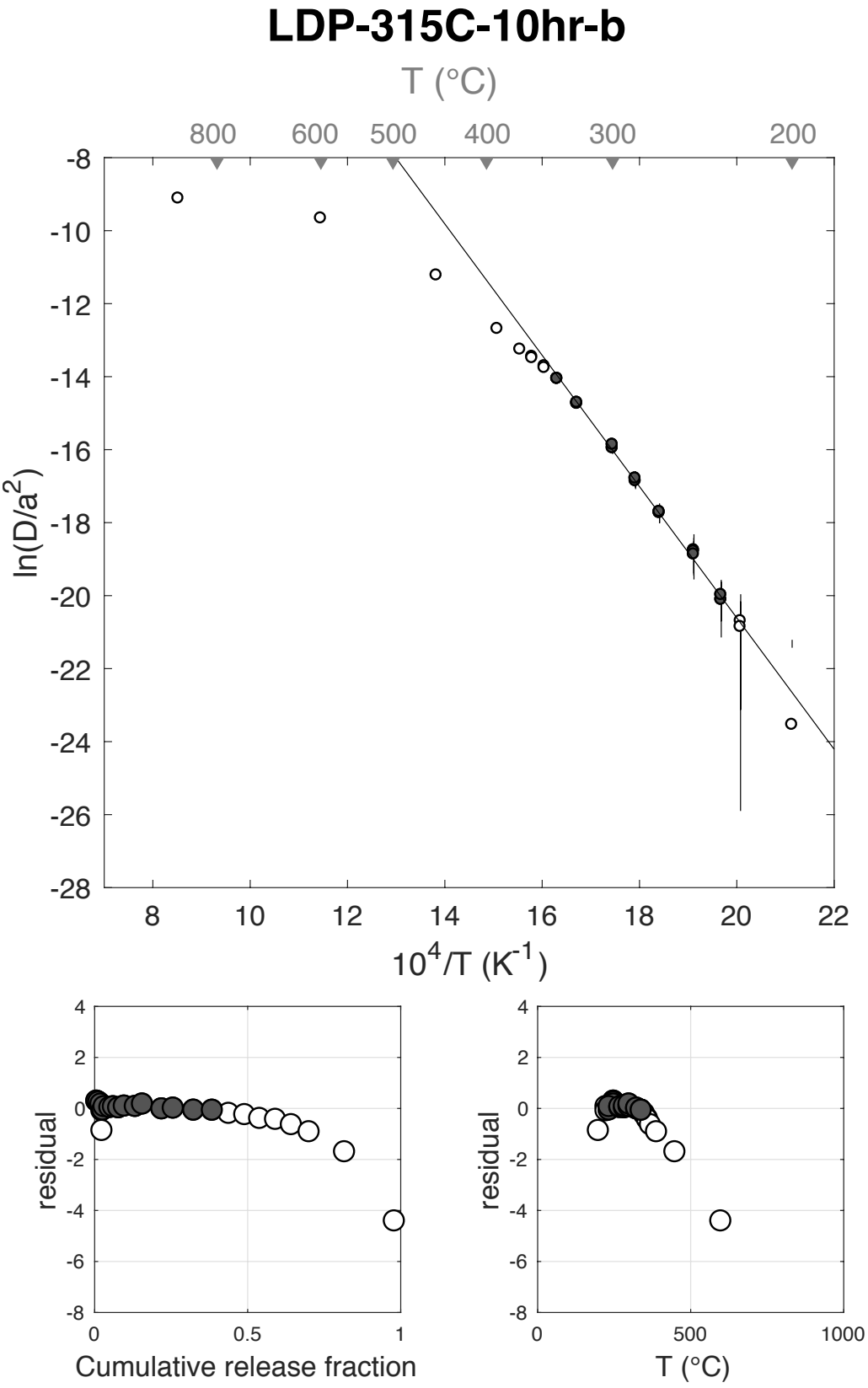
LDP-315C-10hr-b
T (°C)
800
600
500
400
300
200
ln(D/a²)
10⁴/T (K⁻¹)
residual
Cumulative release fraction
residual
T (°C)

LDP-330C-10hr-a

E_a	+/-	D_0	+/-	T_c	-	+	Total ^{3}He	Incl.	Misfit	Norm. Misfit
132.09	6.02	12.38	1.25	63.92	6.33	6.67	103.53	0.476	0.797	0.047

Step #	°C	t (hrs)	^{3}He	Error	^{4}He	Error	^{4}He/^{3}He	Err	In ^{3}He Reg.
1	250	0.25	1.70	0.20	662.3	18.1	379.7	0.12	1
2	250	0.50	1.30	0.15	559.4	15.9	421.1	0.12	1
3	250	1.00	1.15	0.16	320.4	18.3	269.6	0.15	1
4	225	1.50	0.20	0.11	99.3	16.2	480.6	0.59	1
5	225	2.50	0.36	0.10	125.3	17.4	336.1	0.32	1
6	200	3.00	0.06	0.10	121.5	16.3	2107.4	1.69	0
7	200	4.00	0.04	0.12	35.4	22.7	958.8	3.45	0
8	235	2.00	0.51	0.13	167.4	16.8	317.4	0.27	1
9	235	3.00	0.66	0.14	228.7	20.9	337.9	0.23	1
10	270	1.91	2.70	0.22	1039.4	22.7	375.6	0.08	1
11	270	1.57	1.54	0.18	692.5	16.3	439.7	0.12	1
12	285	1.25	2.27	0.21	1110.2	20.4	479.3	0.09	1
13	285	1.57	2.33	0.20	1292.1	19.5	544.8	0.09	1
14	300	1.91	4.50	0.30	2888.3	31.9	631.7	0.07	1
15	300	1.45	2.85	0.24	2306.2	22.7	798.8	0.09	1
16	325	1.74	7.89	0.37	6362.3	34.9	796.3	0.05	1
17	325	1.32	4.48	0.29	4244.5	36.5	938.4	0.07	1
18	340	1.58	7.75	0.40	7864.2	77.9	1004.6	0.05	1
19	340	1.89	7.14	0.38	7732.4	57.4	1073.6	0.05	1
20	350	1.48	6.52	0.40	7466.7	27.9	1135.3	0.06	0
21	350	1.82	5.85	0.35	7187.5	49.3	1217.7	0.06	0
22	360	1.50	5.91	0.36	7469.9	41.8	1254.5	0.06	0
23	360	1.98	6.01	0.34	7894.2	53.7	1302.6	0.06	0
24	370	1.88	6.14	0.34	8256.6	59.9	1334.9	0.06	0
25	390	1.47	6.41	0.38	8719.2	47.0	1349.8	0.06	0
26	450	1.00	10.84	0.49	15088.3	96.5	1382.0	0.05	0
27	600	1.00	6.40	0.32	9574.1	62.6	1487.1	0.05	0
28	900	1.00	0.04	0.07	85.6	15.9	2116.2	1.64	0
29	900	1.00	0.00	0.00	0.0	0.0	NaN	NaN	0

Figure S76

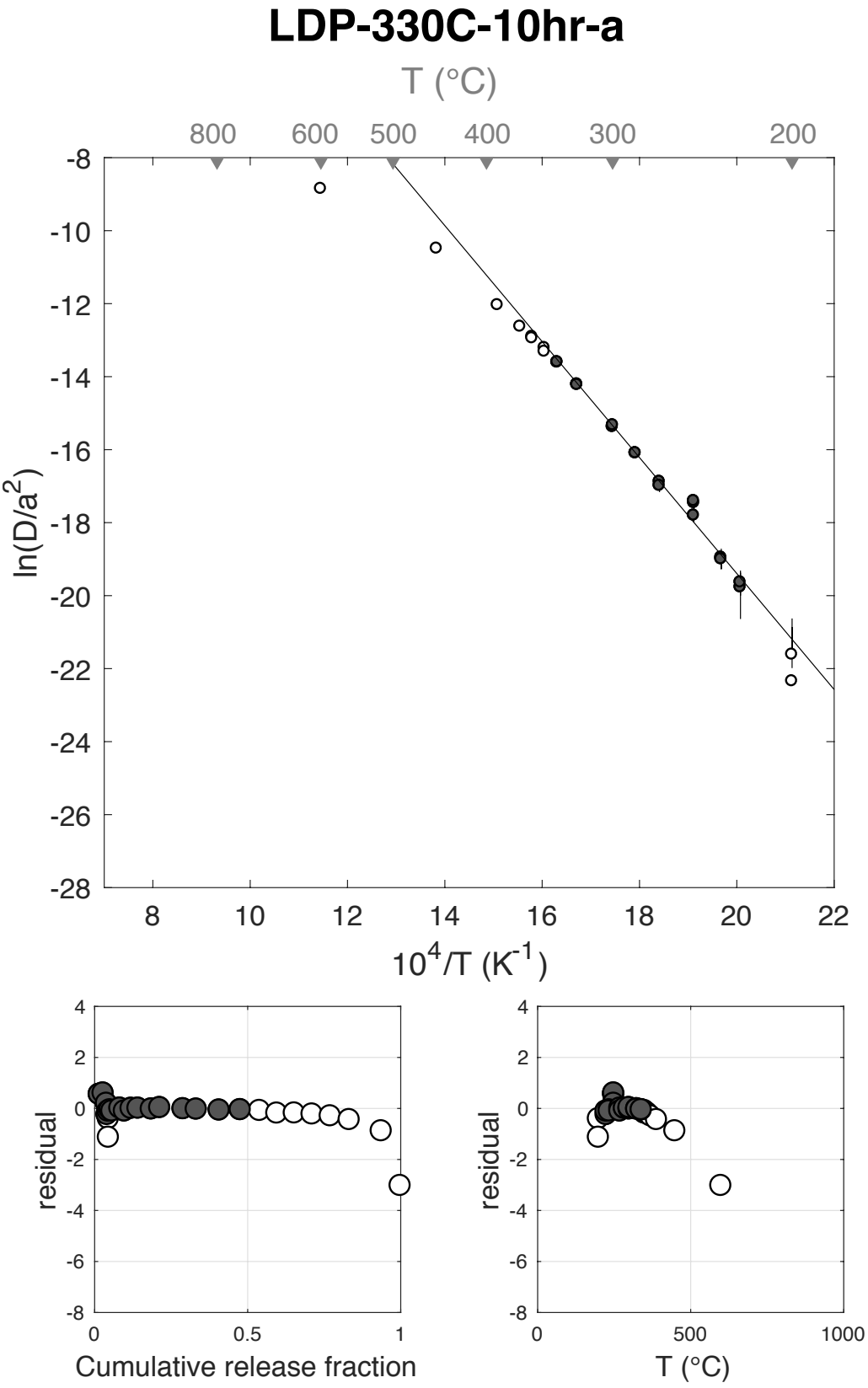
LDP-330C-10hr-a
T (°C)
800
600
500
400
300
200
-8
-10
-12
-14
-16
-18
-20
-22
-24
-26
-28
ln(D/a2)
8
10
12
14
16
18
20
22
10^4/T (K^-1)
4
2
0
-2
-4
-6
-8
residual
0
0.5
1
Cumulative release fraction
0
500
1000
T (°C)

E_a	+/-	D_0	+/-	T_c	-	+	Total ^{3}He	Incl.	Misfit	Norm. Misfit
145.96	8.17	14.78	1.72	81.22	7.37	7.89	156.80	0.412	0.321	0.017

Step #	°C	t (hrs)	^{3}He	Error	^{4}He	Error	^{4}He/^{3}He	Err	In ^{3}He Reg.
1	250	0.25	1.42	0.20	58.3	16.7	31.1	0.32	1
2	250	0.50	0.95	0.16	98.4	18.6	94.1	0.25	1
3	250	1.00	1.22	0.18	158.8	15.8	120.1	0.17	1
4	225	1.50	0.25	0.11	50.2	15.4	193.4	0.54	1
5	225	2.50	0.40	0.13	69.1	17.6	164.4	0.42	1
6	200	3.00	0.11	0.08	0.0	0.0	NaN	NaN	1
7	200	4.00	0.11	0.10	5.1	24.0	37.1	4.77	1
8	235	2.00	0.56	0.13	101.9	17.0	171.6	0.29	1
9	235	3.00	0.78	0.16	144.4	19.5	174.3	0.25	1
10	270	1.91	3.02	0.26	817.7	25.3	260.7	0.09	1
11	270	1.57	2.00	0.24	654.1	17.9	317.5	0.12	1
12	285	1.25	2.87	0.28	1140.6	20.0	387.8	0.10	1
13	285	1.57	3.02	0.29	1404.1	20.9	455.6	0.10	1
14	300	1.91	6.16	0.42	3338.8	29.5	531.6	0.07	1
15	300	1.45	3.90	0.30	2406.8	26.4	607.7	0.08	1
16	325	1.74	10.95	0.51	7936.1	42.6	714.8	0.05	1
17	325	1.32	6.34	0.39	5093.3	46.5	793.7	0.06	1
18	340	1.58	10.71	0.52	9885.5	56.3	913.4	0.05	1
19	340	1.89	9.90	0.46	9693.5	54.7	969.1	0.05	1
20	350	1.48	8.93	0.50	9210.7	52.6	1021.1	0.06	0
21	350	1.82	8.34	0.45	9264.0	44.2	1101.0	0.05	0
22	360	1.50	7.81	0.47	8985.2	46.6	1139.9	0.06	0
23	360	1.98	8.29	0.49	9588.7	55.5	1146.8	0.06	0
24	370	1.88	8.16	0.43	9941.0	52.6	1207.6	0.05	0
25	390	1.47	8.54	0.44	10576.4	57.9	1228.3	0.05	0
26	450	1.00	15.34	0.62	19343.6	85.6	1250.7	0.04	0
27	600	1.00	19.93	0.70	26552.5	91.8	1322.3	0.04	0
28	900	1.00	6.80	0.44	9733.8	59.2	1422.3	0.06	0
29	900	1.00	0.00	0.00	5.4	19.6	Inf	NaN	0

Figure S77

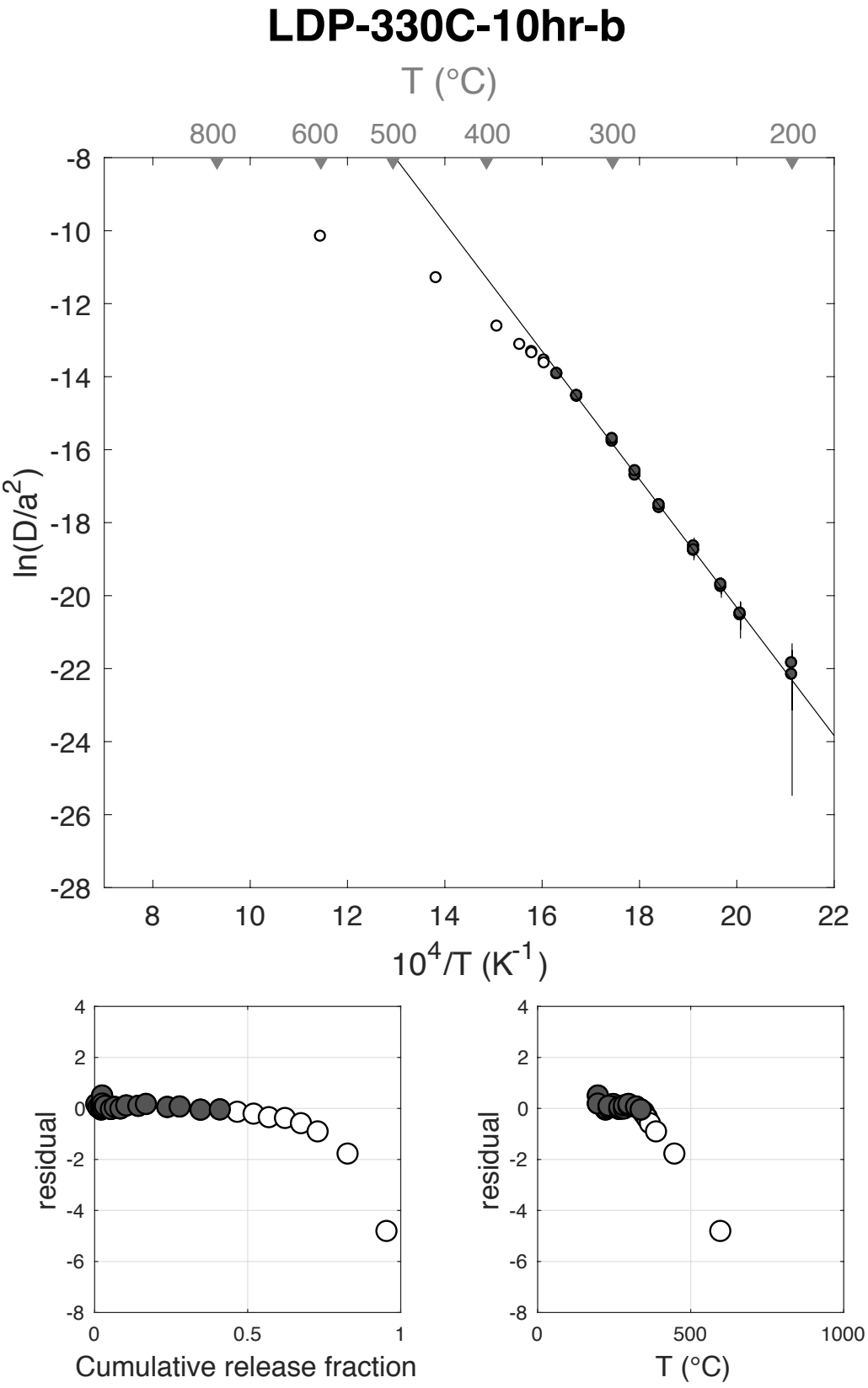
LDP-330C-10hr-b
T (°C)
800
600
500
400
300
200
ln(D/a²)
10⁴/T (K⁻¹)
residual
Cumulative release fraction
residual
T (°C)

LDP-345C-10hr-a

E_a	+/-	D_0	+/-	T_c	-	+	Total ^{3}He	Incl.	Misfit	Norm. Misfit
128.46	28.54	12.05	5.77	57.07	29.29	37.34	7.60	0.675	0.662	0.044

Step #	°C	t (hrs)	^{3}He	Error	^{4}He	Error	^{4}He/^{3}He	Err	In ^{3}He Reg.
1	250	0.25	0.14	0.09	20.2	48.7	136.8	2.49	1
2	250	0.50	0.05	0.09	10.2	41.4	176.0	4.35	0
3	250	1.00	0.15	0.09	11.2	41.8	63.2	3.78	1
4	225	1.50	0.02	0.08	5.0	49.3	226.4	10.50	0
5	200	2.50	0.03	0.09	7.1	95.6	260.3	13.94	0
6	235	2.50	0.04	0.09	1.4	96.3	29.8	67.45	0
7	270	1.16	0.20	0.10	5.5	41.5	17.6	7.61	1
8	290	1.17	0.31	0.10	11.8	41.5	28.4	3.54	1
9	300	1.30	0.45	0.12	16.9	45.7	27.4	2.73	1
10	300	1.91	0.47	0.13	19.8	69.2	32.4	3.51	1
11	310	1.57	0.42	0.12	7.8	57.7	8.5	7.41	1
12	310	1.25	0.33	0.10	9.8	46.6	19.9	4.77	1
13	320	1.56	0.44	0.14	29.6	50.0	57.1	1.72	1
14	320	1.91	0.46	0.12	34.1	65.1	64.3	1.93	1
15	330	1.45	0.44	0.12	26.7	48.1	51.2	1.82	1
16	330	1.74	0.42	0.10	34.6	59.3	72.5	1.73	1
17	340	1.32	0.31	0.12	32.5	43.2	93.5	1.38	1
18	340	1.58	0.37	0.12	35.5	54.0	85.7	1.55	1
19	340	1.89	0.23	0.11	48.4	64.4	202.1	1.41	1
20	350	1.48	0.26	0.11	44.7	48.1	159.3	1.15	0
21	350	1.82	0.26	0.09	43.4	69.6	155.7	1.64	0
22	360	1.50	0.25	0.10	54.6	48.3	204.9	0.97	0
23	360	1.98	0.30	0.11	66.6	70.2	212.1	1.12	0
24	370	1.88	0.23	0.10	75.2	66.8	315.8	0.99	0
25	390	1.47	0.29	0.10	102.9	47.5	346.3	0.58	0
26	450	1.00	0.53	0.15	267.1	42.3	492.2	0.32	0
27	600	1.00	0.00	0.00	33.7	24.3	Inf	NaN	0
28	900	1.00	0.20	0.10	195.9	39.7	979.7	0.53	0
29	900	1.00	0.00	0.00	0.0	0.0	NaN	NaN	0

Figure S78

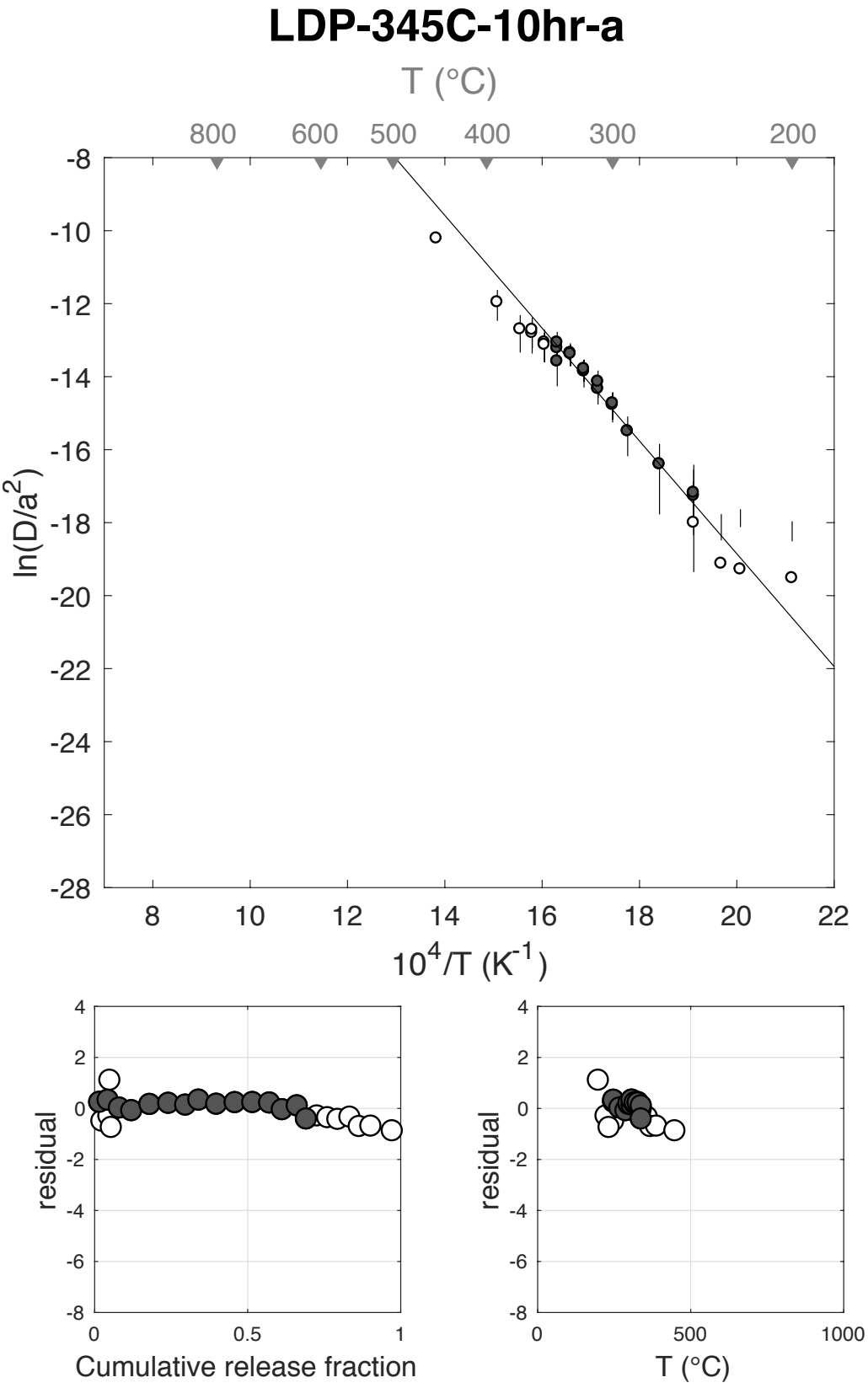
LDP-345C-10hr-a
T (°C)
800
600
500
400
300
200
-8
-10
-12
-14
-16
-18
-20
-22
-24
-26
-28
ln(D/a2)
8
10
12
14
16
18
20
22
10^4/T (K^-1)
4
2
0
-2
-4
-6
-8
residual
0
0.5
1
Cumulative release fraction
500
1000
T (°C)

E_a	+/-	D_0	+/-	T_c	-	+	Total ^{3}He	Incl.	Misfit	Norm. Misfit
133.27	5.79	12.80	1.17	63.95	6.25	6.56	78.42	0.627	0.129	0.008

Step #	°C	t (hrs)	^{3}He	Error	^{4}He	Error	^{4}He/^{3}He	Err	In ^{3}He Reg.
1	250	0.25	1.21	0.16	4019.8	2023.2	3299.8	0.52	1
2	250	0.50	0.77	0.16	2448.1	1097.3	3176.3	0.49	1
3	250	1.00	0.83	0.16	5818.7	788.7	6960.6	0.24	1
4	225	1.50	0.24	0.11	9550.2	2652.4	39942.8	0.55	0
5	200	2.50	0.02	0.11	17788.2	6387.8	725458.9	4.61	0
6	235	2.50	0.53	0.16	17397.9	6388.1	32748.3	0.48	0
7	270	1.16	1.60	0.19	4900.8	1392.7	3053.5	0.31	1
8	290	1.17	3.06	0.28	3746.2	1419.6	1212.9	0.39	1
9	300	1.30	3.66	0.31	4207.9	1905.1	1140.5	0.46	1
10	300	1.91	3.78	0.31	7106.7	4185.4	1868.3	0.59	1
11	310	1.57	4.00	0.33	5260.9	2913.6	1306.1	0.56	1
12	310	1.25	2.63	0.28	4406.1	1718.2	1663.6	0.40	1
13	320	1.56	4.25	0.32	7801.5	2882.7	1825.6	0.38	1
14	320	1.91	4.05	0.36	7760.4	4183.3	1904.5	0.55	1
15	330	1.45	3.91	0.37	3103.8	2465.4	784.5	0.80	1
16	330	1.74	3.84	0.34	3985.1	3549.9	1027.9	0.90	1
17	340	1.32	3.98	0.35	0.0	0.0	NaN	NaN	1
18	340	1.58	3.86	0.31	3749.5	2950.4	962.5	0.79	1
19	340	1.89	3.71	0.31	3989.4	4108.8	1066.0	1.03	1
20	350	1.48	3.51	0.28	1015.4	2583.3	279.0	2.55	0
21	350	1.82	3.32	0.29	3406.6	3848.8	1016.9	1.13	0
22	360	1.50	3.26	0.26	2109.0	2656.2	636.8	1.26	0
23	360	1.98	3.12	0.32	4165.3	4449.3	1324.9	1.07	0
24	370	1.88	2.98	0.27	3428.0	4078.4	1141.2	1.19	0
25	390	1.47	3.04	0.29	1989.7	2562.2	643.7	1.29	0
26	450	1.00	4.89	0.31	399.9	800.2	71.8	2.00	0
27	599	1.00	4.17	0.40	2020.6	793.2	474.7	0.40	0
28	899	1.00	0.18	0.09	10270.9	800.7	56191.9	0.50	0
29	900	0.50	0.01	0.08	5137.3	1093.4	599029.5	9.15	0

Figure S79

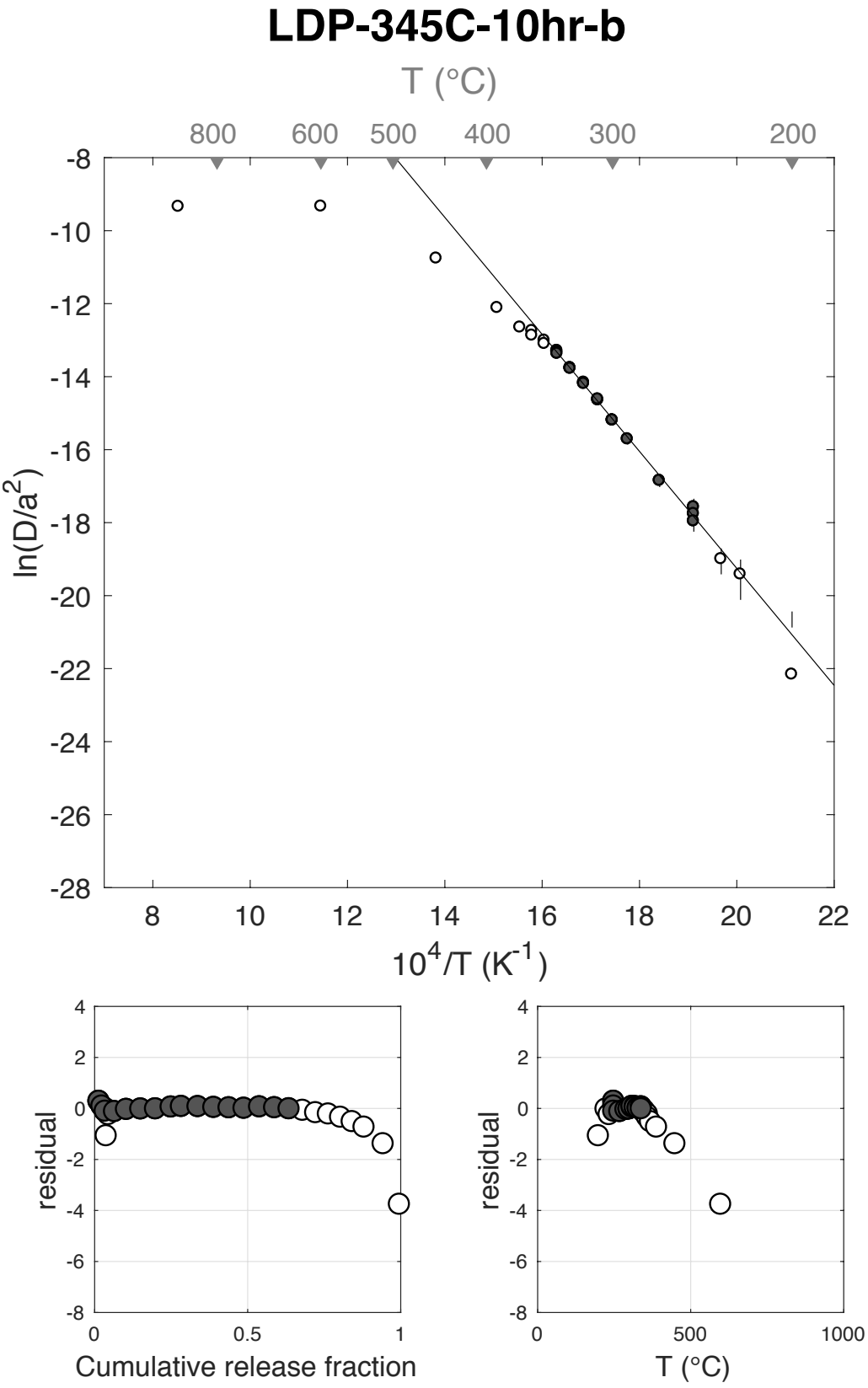
LDP-345C-10hr-b
T (°C)
800
600
500
400
300
200
-8
-10
-12
-14
-16
-18
-20
-22
-24
-26
-28
ln(D/a2)
8
10
12
14
16
18
20
22
10^4/T (K^-1)
4
2
0
-2
-4
-6
-8
residual
0
0.5
1
Cumulative release fraction
0
500
1000
T (°C)

LDP-400C-10hr-a

E_a	+/-	D_0	+/-	T_c	-	+	Total ^{3}He	Incl.	Misfit	Norm. Misfit
137.93	10.04	12.93	2.10	74.65	9.70	10.57	76.61	0.386	0.331	0.017

Step #	°C	t (hrs)	^{3}He	Error	^{4}He	Error	^{4}He/^{3}He	Err	In ^{3}He Reg.
1	250	0.25	0.68	0.14	20.9	22.9	20.8	1.11	1
2	250	0.50	0.47	0.12	9.4	14.9	9.9	1.59	1
3	250	1.00	0.50	0.13	0.0	0.0	NaN	NaN	1
4	225	1.50	0.13	0.09	0.0	0.0	NaN	NaN	1
5	225	2.50	0.21	0.12	0.0	0.0	NaN	NaN	1
6	200	3.00	0.07	0.11	0.0	0.0	NaN	NaN	1
7	200	4.00	0.06	0.15	0.0	0.0	NaN	NaN	1
8	235	2.00	0.28	0.11	0.0	0.0	NaN	NaN	1
9	235	3.00	0.37	0.14	0.0	0.0	NaN	NaN	1
10	270	1.91	1.34	0.20	48.2	32.6	25.9	0.69	1
11	270	1.57	0.88	0.17	44.9	28.5	41.3	0.66	1
12	285	1.25	1.28	0.19	87.3	27.1	58.5	0.35	1
13	285	1.57	1.34	0.19	84.1	27.7	52.9	0.36	1
14	300	1.91	2.81	0.26	209.1	36.8	64.4	0.20	1
15	300	1.45	1.76	0.20	155.4	21.9	78.3	0.18	1
16	325	1.74	4.99	0.36	552.0	32.4	100.7	0.09	1
17	325	1.32	2.87	0.27	419.3	22.8	136.0	0.11	1
18	340	1.58	5.14	0.29	886.0	34.6	162.4	0.07	1
19	340	1.89	4.42	0.34	962.4	35.6	207.5	0.08	1
20	350	1.48	4.15	0.30	1050.7	32.0	243.3	0.08	0
21	350	1.82	4.21	0.31	1241.9	34.5	284.7	0.08	0
22	360	1.50	4.09	0.33	1309.6	31.4	309.9	0.08	0
23	360	1.98	4.18	0.30	1540.1	44.0	358.3	0.08	0
24	370	1.88	4.45	0.35	1821.7	41.0	398.9	0.08	0
25	390	1.47	4.70	0.32	2299.3	41.9	479.5	0.07	0
26	450	1.00	8.25	0.42	5814.5	38.0	694.5	0.05	0
27	600	1.00	12.39	0.52	17621.7	66.4	1412.7	0.04	0
28	900	1.00	0.55	0.13	978.6	18.1	1763.2	0.23	0
29	900	1.00	0.03	0.07	0.0	0.0	NaN	NaN	0

Figure S80

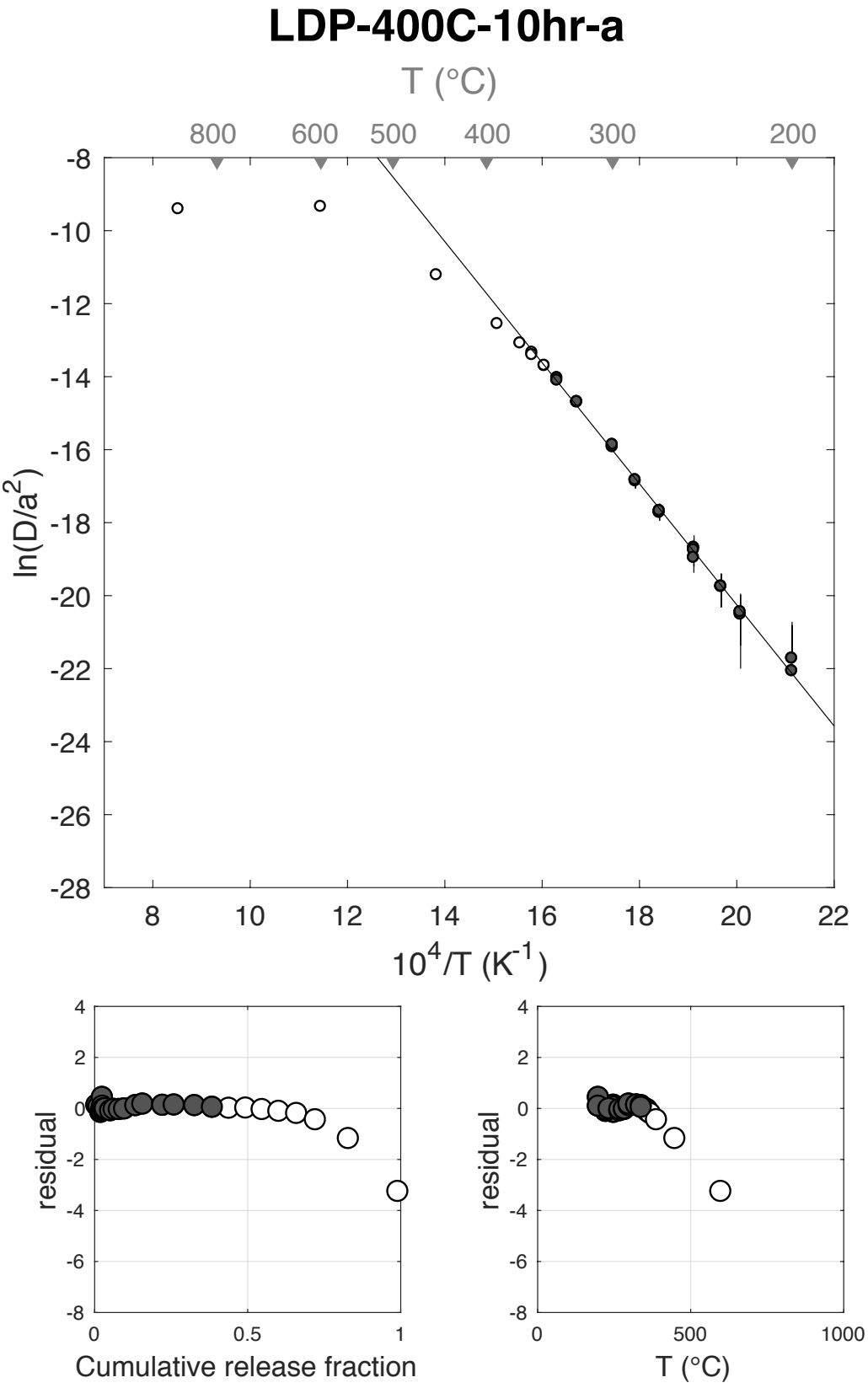
LDP-400C-10hr-a
T (°C)
800
600
500
400
300
200
-8
-10
-12
-14
-16
-18
-20
-22
-24
-26
-28
ln(D/a2)
8
10
12
14
16
18
20
22
10^4/T (K^-1)
4
2
0
-2
-4
-6
-8
residual
0
0.5
1
Cumulative release fraction
500
1000
T (°C)

LDP-400C-10hr-b

E_a	+/-	D_0	+/-	T_c	-	+	Total ^{3}He	Incl.	Misfit	Norm. Misfit
136.74	23.18	11.73	4.70	80.18	22.27	27.16	25.71	0.252	1.561	0.142

Step #	°C	t (hrs)	^{3}He	Error	^{4}He	Error	^{4}He/^{3}He	Err	In ^{3}He Reg.
1	250	0.25	0.21	0.09	3.4	17.2	6.7	5.05	1
2	250	0.50	0.13	0.07	6.7	11.4	41.5	1.79	1
3	250	1.00	0.13	0.08	0.0	0.0	NaN	NaN	0
4	225	1.50	0.02	0.06	11.6	19.8	682.5	3.86	0
5	225	2.50	0.00	0.00	0.0	0.0	NaN	NaN	0
6	200	3.00	0.00	0.00	0.0	0.0	NaN	NaN	0
7	200	4.00	0.00	0.00	8.7	77.7	Inf	NaN	0
8	235	2.00	0.05	0.07	0.0	0.0	NaN	NaN	0
9	235	3.00	0.01	0.10	0.0	0.0	NaN	NaN	0
10	270	1.91	0.27	0.11	3.9	28.6	4.3	7.40	1
11	270	1.57	0.16	0.09	0.0	0.0	NaN	NaN	0
12	285	1.25	0.22	0.09	0.0	0.0	NaN	NaN	1
13	285	1.56	0.24	0.10	0.0	0.0	NaN	NaN	1
14	300	1.91	0.54	0.14	3.6	28.4	NaN	NaN	1
15	300	1.45	0.40	0.12	0.0	0.0	NaN	NaN	1
16	325	1.74	1.08	0.18	45.0	24.6	31.8	0.57	1
17	325	1.32	0.71	0.16	33.8	15.0	37.6	0.50	1
18	340	1.58	1.31	0.20	72.1	22.2	45.0	0.34	1
19	340	1.89	1.37	0.19	75.4	29.1	45.1	0.41	1
20	350	1.48	1.29	0.20	114.1	19.8	78.5	0.24	0
21	350	1.82	1.31	0.19	128.7	26.8	87.9	0.25	0
22	360	1.50	1.21	0.18	184.1	18.9	141.5	0.18	0
23	360	1.98	1.37	0.21	220.8	30.4	151.3	0.21	0
24	370	1.88	1.62	0.23	292.0	29.8	170.7	0.17	0
25	390	1.47	1.70	0.23	417.7	22.0	235.8	0.15	0
26	450	1.00	4.39	0.36	1335.4	23.7	294.5	0.08	0
27	600	1.00	5.66	0.44	3295.0	21.3	572.5	0.08	0
28	900	1.00	0.15	0.08	138.7	10.1	913.4	0.56	0
29	900	1.00	0.05	0.06	0.0	0.0	NaN	NaN	0
30	899	1.00	0.13	0.06	116.7	9.9	864.3	0.48	0

Figure S81

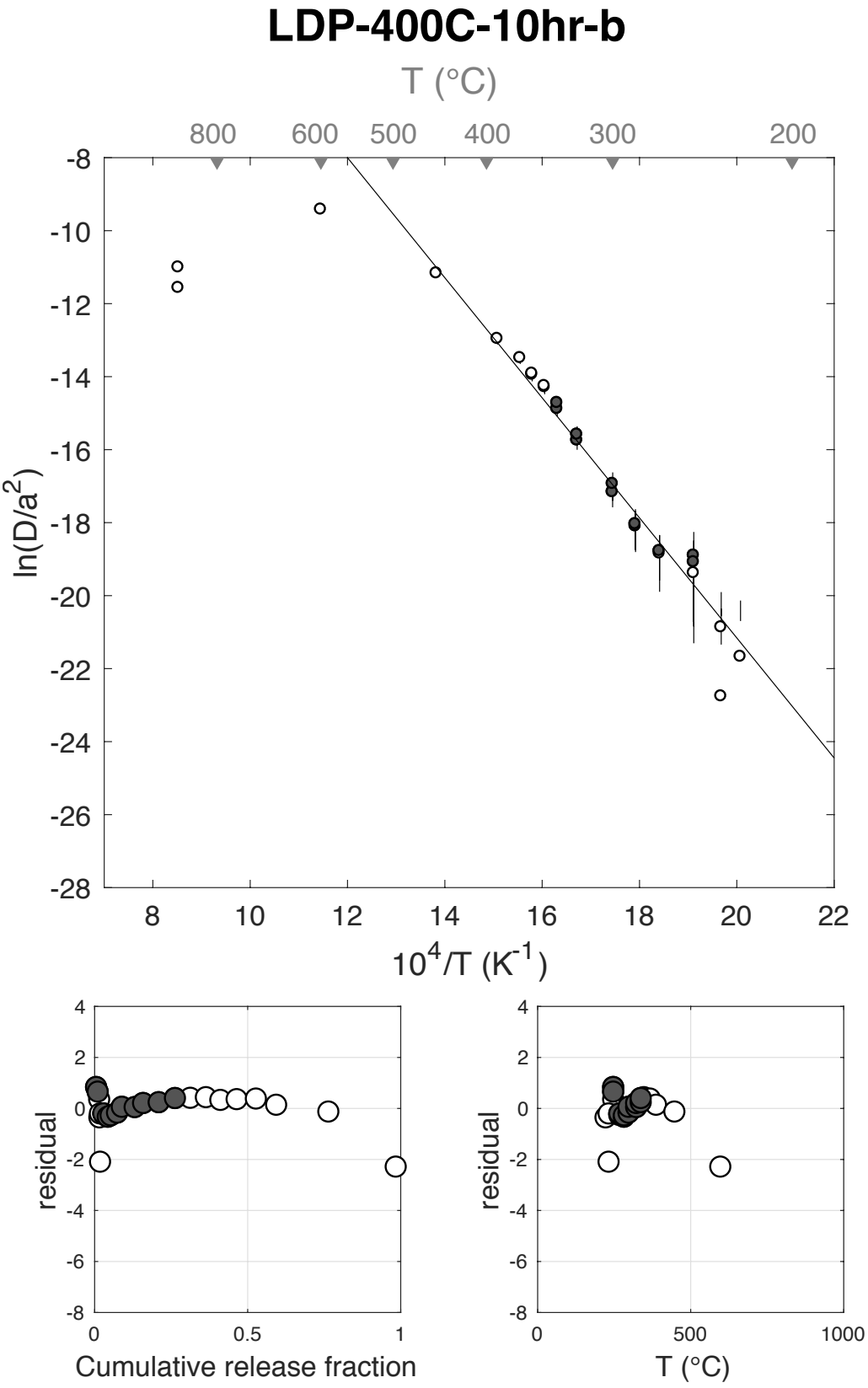
LDP-400C-10hr-b
T (°C)
800
600
500
400
300
200
-8
-10
-12
-14
-16
-18
-20
-22
-24
-26
-28
ln(D/a2)
8
10
12
14
16
18
20
22
10^4/T (K^-1)
4
2
0
-2
-4
-6
-8
residual
0
0.5
1
Cumulative release fraction
0
500
1000
T (°C)

E_a	+/-	D_0	+/-	T_c	-	+	Total ^{3}He	Incl.	Misfit	Norm. Misfit
120.97	2.63	11.07	0.55	44.55	3.04	3.12	250.05	0.651	0.877	0.046

Step #	°C	t (hrs)	^{3}He	Error	^{4}He	Error	^{4}He/^{3}He	Err	In ^{3}He Reg.
1	250	0.25	6.87	0.46	116.5	18.6	7.0	0.17	1
2	250	0.50	4.73	0.32	56.2	18.0	1.9	0.33	1
3	250	1.00	5.82	0.38	65.1	14.4	1.2	0.23	1
4	225	1.50	1.39	0.22	107.1	21.7	67.0	0.26	1
5	225	2.50	1.94	0.23	1.3	23.2	NaN	NaN	1
6	200	3.00	0.46	0.13	0.0	0.0	NaN	NaN	1
7	200	4.00	0.46	0.13	0.0	0.0	NaN	NaN	1
8	235	2.00	2.30	0.25	14.6	20.8	NaN	NaN	1
9	235	3.00	3.53	0.30	26.1	29.2	NaN	NaN	1
10	270	1.91	12.80	0.47	244.4	24.9	9.1	0.11	1
11	270	1.57	7.23	0.45	134.1	19.7	8.5	0.16	1
12	285	1.25	9.63	0.44	208.0	17.6	11.6	0.10	1
13	285	1.57	9.23	0.48	257.8	19.5	17.9	0.09	1
14	300	1.91	16.74	0.64	521.0	23.8	21.1	0.06	1
15	300	1.45	9.77	0.51	369.4	23.0	27.8	0.08	1
16	325	1.74	22.26	0.71	1044.5	26.6	36.9	0.04	1
17	325	1.32	13.51	0.58	7967.8	42.8	579.7	0.04	1
18	340	1.58	18.37	0.57	1417.4	22.4	67.2	0.03	1
19	340	1.89	15.80	0.61	1548.3	28.9	88.0	0.04	1
20	350	1.48	11.54	0.58	1377.9	28.4	109.4	0.05	0
21	350	1.82	10.48	0.52	1488.9	26.6	132.1	0.05	0
22	360	1.50	8.36	0.47	1451.4	23.3	163.7	0.06	0
23	360	1.98	8.51	0.38	1650.4	28.9	184.0	0.05	0
24	370	1.88	7.65	0.52	1619.1	36.4	201.6	0.07	0
25	390	1.47	7.61	0.44	2035.6	24.9	257.3	0.06	0
26	450	1.00	13.32	0.51	6757.3	61.5	497.4	0.04	0
27	600	1.00	14.09	0.58	10721.7	58.8	751.0	0.04	0
28	900	1.00	5.62	0.36	3717.7	38.7	651.5	0.07	0
29	900	1.00	0.04	0.07	0.0	0.0	NaN	NaN	0

Figure S82

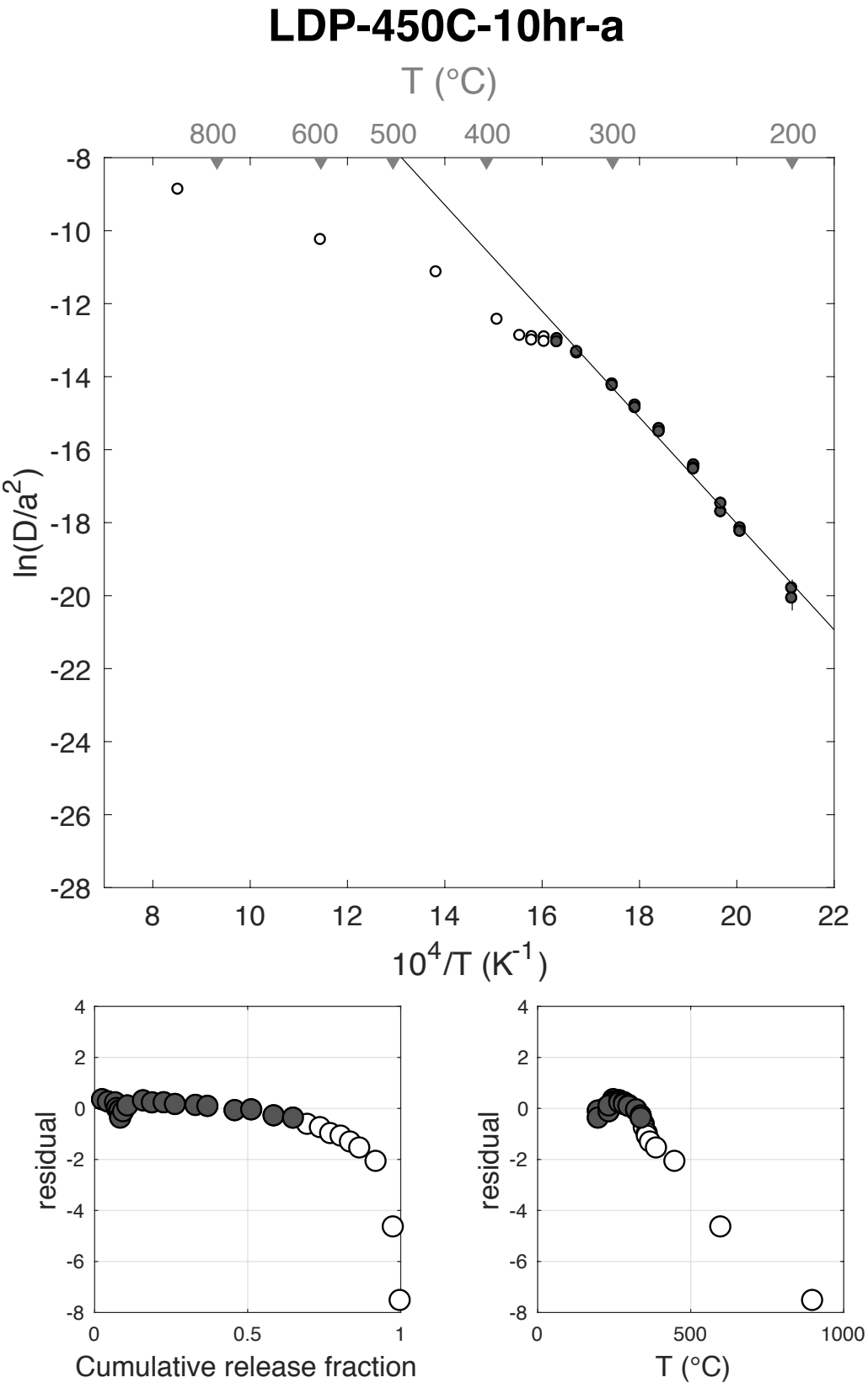
LDP-450C-10hr-a
T (°C)
800
600
500
400
300
200
-8
-10
-12
-14
-16
-18
-20
-22
-24
-26
-28
ln(D/a2)
8
10
12
14
16
18
20
22
10^4/T (K^-1)
4
2
0
-2
-4
-6
-8
residual
0
0.5
1
Cumulative release fraction
0
500
1000
T (°C)

LDP-250C-100hr-a

E_a	+/-	D_0	+/-	T_c	-	+	Total ^{3}He	Incl.	Misfit	Norm. Misfit
150.89	10.84	16.89	2.22	78.58	9.84	10.71	50.42	0.616	0.267	0.019

Step #	°C	t (hrs)	^{3}He	Error	^{4}He	Error	^{4}He/^{3}He	Err	In ^{3}He Reg.
1	250	0.25	0.72	0.17	103.7	42.9	134.8	0.48	1
2	250	0.50	0.46	0.14	96.2	28.7	199.7	0.43	1
3	250	1.00	0.59	0.14	141.1	19.0	229.0	0.27	1
4	225	1.50	0.16	0.11	59.0	48.1	365.5	1.08	0
5	225	2.50	0.25	0.19	79.7	116.2	306.4	1.65	0
6	200	3.00	0.07	0.23	44.6	150.3	649.5	4.77	0
7	200	4.00	0.10	0.32	50.9	219.3	511.6	5.42	0
8	235	2.00	0.28	0.16	104.7	81.5	365.3	0.97	0
9	235	3.00	0.43	0.25	145.3	150.4	324.8	1.18	1
10	270	1.91	1.73	0.24	618.4	75.9	347.2	0.19	1
11	270	1.57	1.13	0.20	534.1	55.0	461.5	0.21	1
12	285	1.25	1.71	0.21	870.0	36.2	500.1	0.13	1
13	285	1.57	1.65	0.22	1006.6	53.6	599.4	0.14	1
14	300	1.91	3.35	0.29	2189.5	79.6	643.5	0.09	1
15	300	1.45	1.96	0.24	1436.7	49.8	723.1	0.13	1
16	325	1.74	5.35	0.40	4362.3	85.0	805.0	0.08	1
17	325	1.32	2.99	0.27	2609.1	57.0	862.6	0.09	1
18	340	1.58	4.82	0.39	4627.0	77.3	950.5	0.08	1
19	340	1.89	4.17	0.33	4061.0	83.2	964.2	0.08	1
20	350	1.48	3.65	0.34	3635.0	55.7	985.0	0.09	0
21	350	1.82	3.31	0.31	3330.5	74.6	996.8	0.10	0
22	360	1.50	2.67	0.27	2865.8	57.9	1061.5	0.10	0
23	360	1.98	2.58	0.28	2702.5	83.8	1036.9	0.11	0
24	370	1.88	1.81	0.24	1949.6	76.9	1067.0	0.14	0
25	390	1.47	1.53	0.22	1514.2	47.4	976.7	0.14	0
26	450	1.00	2.02	0.25	2244.5	34.8	1101.4	0.12	0
27	600	1.00	0.93	0.16	1193.3	26.0	1278.8	0.17	0

Figure S83

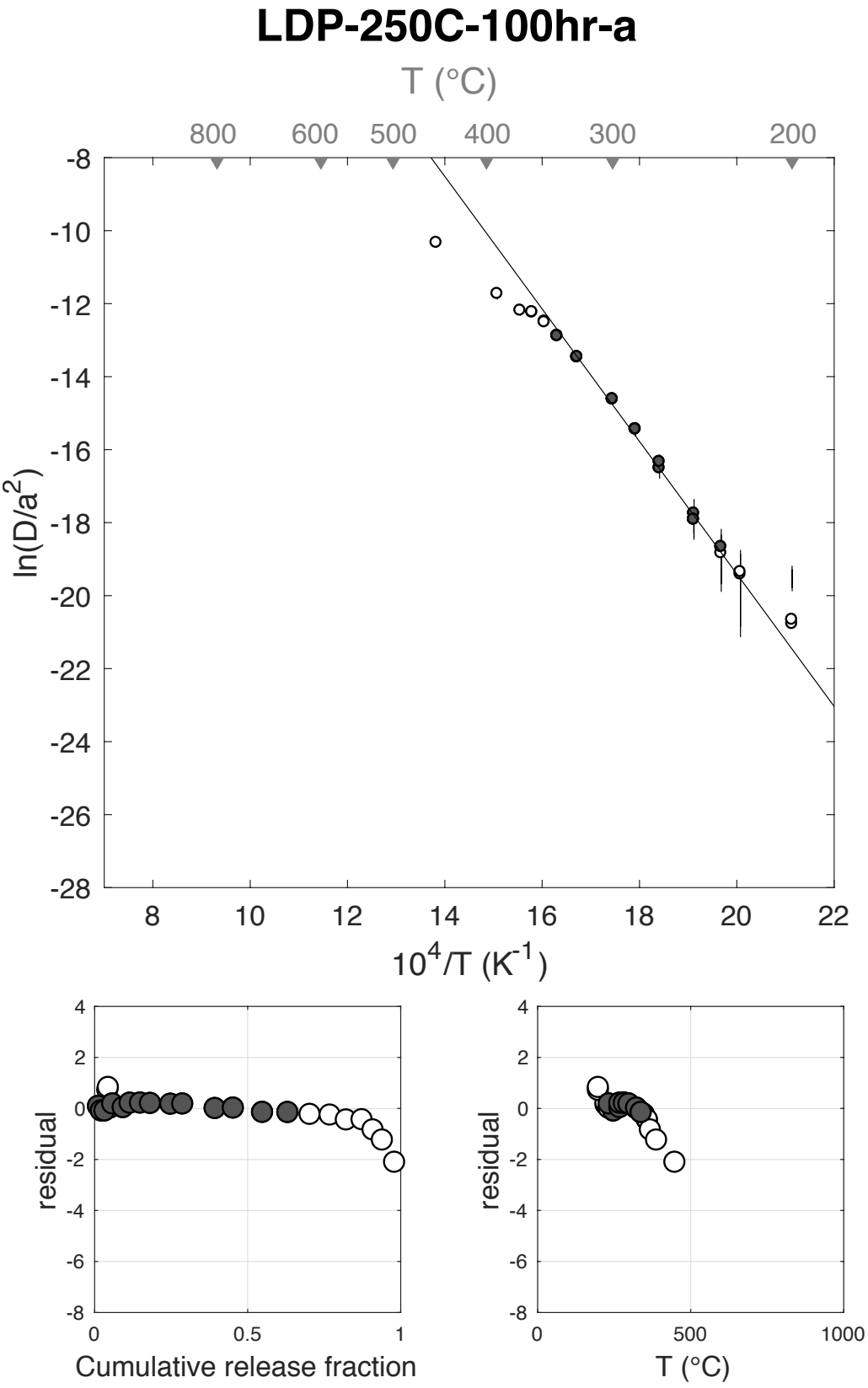
LDP-250C-100hr-a
T (°C)
800
600
500
400
300
200
-8
-10
-12
-14
-16
-18
-20
-22
-24
-26
-28
ln(D/a2)
8
10
12
14
16
18
20
22
10^4/T (K^-1)
4
2
0
-2
-4
-6
-8
residual
0
0.5
1
Cumulative release fraction
0
500
1000
T (°C)

LDP-275C-100hr-a

E_a	+/-	D_0	+/-	T_c	-	+	Total ^{3}He	Incl.	Misfit	Norm. Misfit
138.20	7.05	12.72	1.44	76.79	7.12	7.56	110.77	0.319	0.043	0.003

Step #	°C	t (hrs)	^{3}He	Error	^{4}He	Error	^{4}He/^{3}He	Err	In ^{3}He Reg.
1	250	0.25	0.86	0.16	110.0	69.8	117.8	0.66	1
2	250	0.50	0.61	0.14	83.1	41.7	125.6	0.55	1
3	250	1.00	0.69	0.15	125.4	32.2	171.3	0.34	1
4	225	1.50	0.21	0.10	161.3	91.1	745.0	0.73	0
5	225	2.50	0.29	0.13	199.4	215.2	688.5	1.17	0
6	200	3.00	0.07	0.11	201.5	278.0	3079.1	2.19	0
7	200	4.00	0.05	0.14	203.6	403.6	4289.9	3.56	0
8	235	2.00	0.35	0.12	52.5	152.8	139.6	2.93	0
9	235	3.00	0.42	0.15	96.4	277.9	217.2	2.90	0
10	270	1.91	1.84	0.22	35.4	141.7	9.3	4.00	1
11	270	1.57	1.08	0.21	13.1	99.2	2.1	7.56	1
12	285	1.25	1.72	0.24	3.3	59.3	NaN	NaN	1
13	285	1.57	1.69	0.24	13.6	99.3	NaN	NaN	1
14	300	1.91	3.55	0.31	33.4	141.8	NaN	NaN	1
15	300	1.45	2.02	0.24	2.4	83.8	NaN	NaN	1
16	325	1.74	6.06	0.37	41.2	120.3	NaN	NaN	1
17	325	1.32	3.41	0.30	5.3	69.3	NaN	NaN	1
18	340	1.58	6.03	0.37	38.4	99.9	NaN	NaN	1
19	340	1.89	5.78	0.39	61.6	138.6	0.7	2.25	1
20	350	1.48	5.48	0.37	36.8	87.8	NaN	NaN	0
21	350	1.82	5.29	0.38	59.9	130.3	1.3	2.18	0
22	360	1.50	5.23	0.35	55.7	89.9	0.6	1.62	0
23	360	1.98	5.19	0.35	70.5	150.3	3.6	2.13	0
24	370	1.88	6.06	0.35	81.5	137.7	3.5	1.69	0
25	390	1.47	6.95	0.42	119.7	87.1	7.2	0.73	0
26	450	1.00	15.06	0.63	528.8	31.4	25.1	0.07	0
27	600	1.00	22.07	0.75	4632.5	64.3	199.9	0.04	0
28	900	1.00	2.72	0.24	2217.5	49.5	806.7	0.09	0
29	899	0.50	0.00	0.00	0.0	0.0	NaN	NaN	0

Figure S84

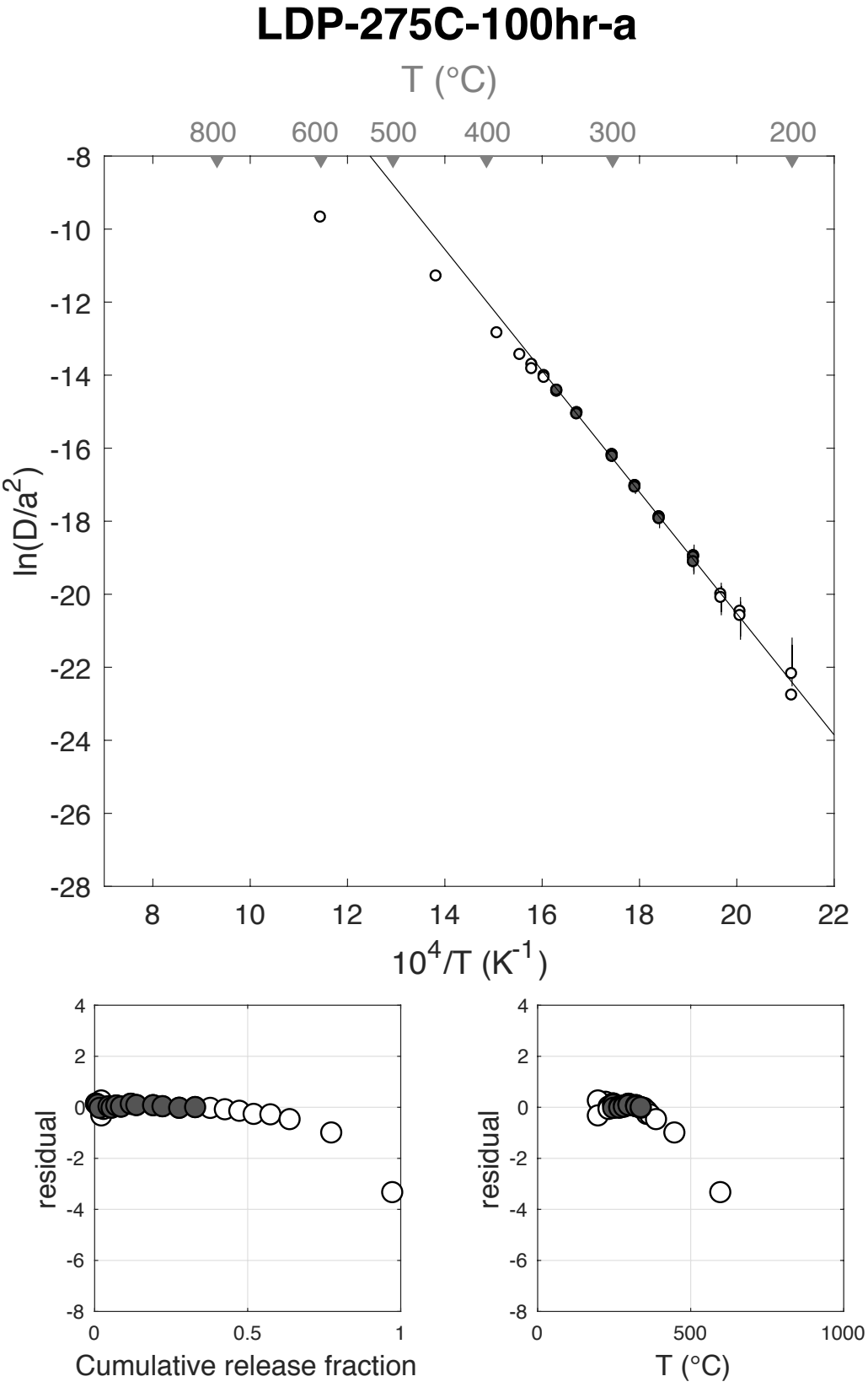
LDP-275C-100hr-a
T (°C)
800
600
500
400
300
200
ln(D/a²)
10⁴/T (K⁻¹)
residual
Cumulative release fraction
residual
T (°C)

LDP-300C-100hr-a

E_a	+/-	D_0	+/-	T_c	-	+	Total ^{3}He	Incl.	Misfit	Norm. Misfit
141.79	7.88	13.90	1.61	77.29	7.73	8.25	89.83	0.391	0.038	0.003

Step #	°C	t (hrs)	^{3}He	Error	^{4}He	Error	^{4}He/^{3}He	Err	In ^{3}He Reg.
1	250	0.25	0.83	0.18	0.0	0.0	NaN	NaN	1
2	250	0.50	0.57	0.14	0.0	0.0	NaN	NaN	1
3	250	1.00	0.70	0.16	4517.5	912.2	6428.4	0.30	1
4	225	1.50	0.18	0.08	9186.8	3100.4	49668.9	0.57	0
5	225	2.50	0.31	0.13	21113.3	7410.6	68565.3	0.55	0
6	200	3.00	0.07	0.12	24597.0	9575.2	350490.0	1.75	0
7	200	4.00	0.10	0.15	33123.3	13912.4	348440.3	1.58	0
8	235	2.00	0.36	0.13	11421.8	5246.9	32099.2	0.58	0
9	235	3.00	0.44	0.16	21547.2	9579.1	49282.8	0.58	0
10	270	1.91	1.80	0.23	10112.6	4851.6	5619.8	0.50	1
11	270	1.57	1.13	0.19	6248.6	3380.1	5506.5	0.57	1
12	285	1.25	1.56	0.22	2808.8	1998.7	1789.2	0.73	1
13	285	1.57	1.76	0.23	5793.6	3378.9	3287.6	0.60	1
14	300	1.91	3.40	0.29	8861.6	4853.2	2593.3	0.55	1
15	300	1.45	2.06	0.25	4482.5	2859.1	2161.1	0.65	1
16	325	1.74	6.03	0.42	7076.0	4116.7	1164.4	0.59	1
17	325	1.32	3.46	0.30	3067.5	2295.6	875.3	0.75	1
18	340	1.58	6.11	0.42	5309.6	3423.8	858.9	0.65	1
19	340	1.89	5.73	0.39	6750.1	4764.4	1167.5	0.71	1
20	350	1.48	5.21	0.35	2693.4	2988.1	506.6	1.11	0
21	350	1.82	5.22	0.34	6920.0	4464.0	1315.0	0.65	0
22	360	1.50	5.11	0.36	4030.6	3075.7	778.7	0.77	0
23	360	1.98	5.26	0.38	8317.8	5155.3	1572.3	0.62	0
24	370	1.88	5.51	0.39	7110.1	4723.2	1280.4	0.67	0
25	390	1.47	6.16	0.35	3837.0	2946.3	612.9	0.77	0
26	450	1.00	11.20	0.52	0.0	0.0	NaN	NaN	0
27	600	1.00	8.45	0.55	1139.6	911.1	124.9	0.80	0
28	900	1.00	1.08	0.18	8646.1	916.7	7985.2	0.20	0
29	900	0.50	0.02	0.07	7223.8	1271.2	337880.2	3.40	0

Figure S85

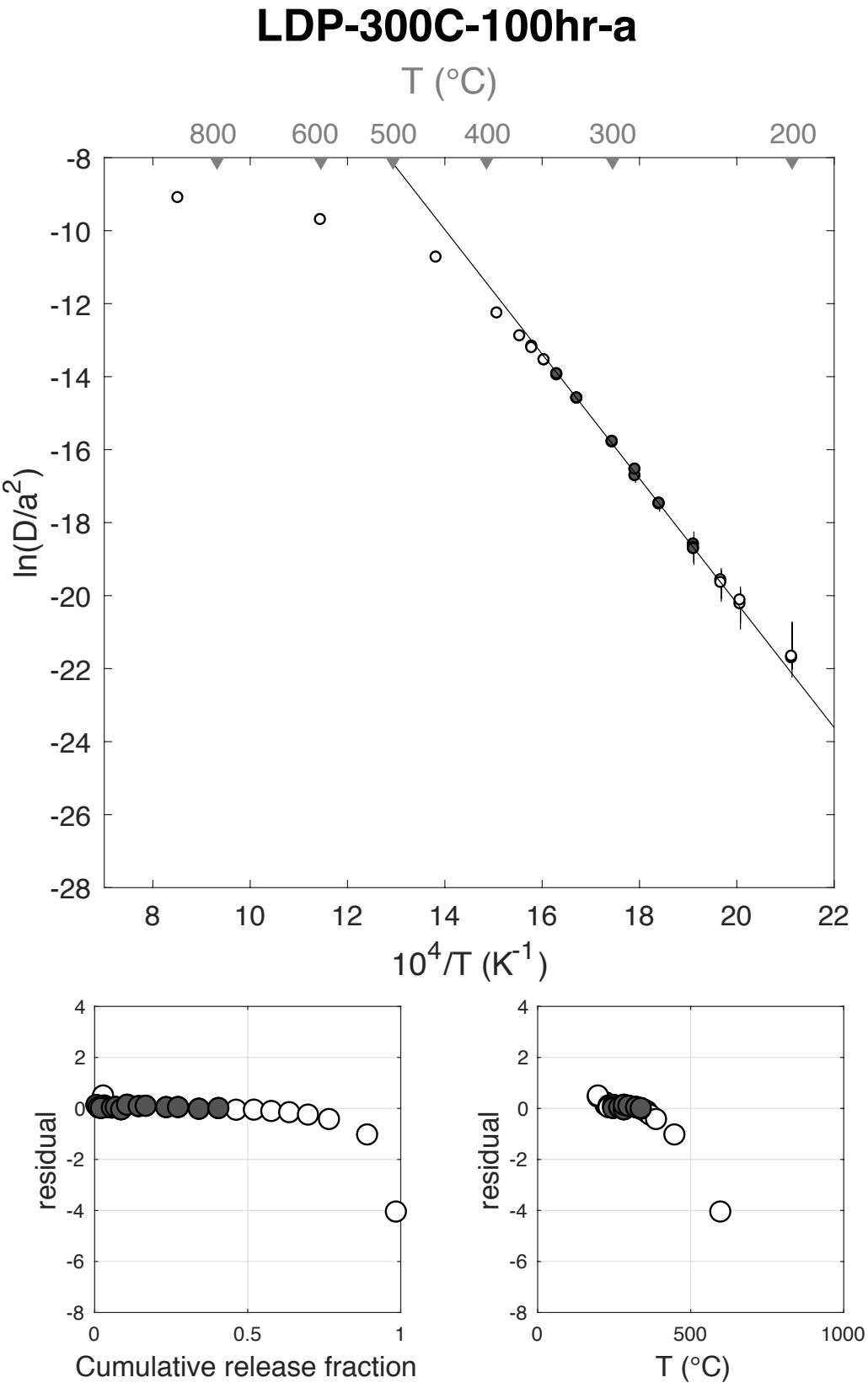
LDP-300C-100hr-a
T (°C)
800
600
500
400
300
200
-8
-10
-12
-14
-16
-18
-20
-22
-24
-26
-28
ln(D/a2)
8
10
12
14
16
18
20
22
10^4/T (K^-1)
4
2
0
-2
-4
-6
-8
residual
0
0.5
1
Cumulative release fraction
500
1000
T (°C)

LDP-325C-100hr-a

E_a	+/-	D_0	+/-	T_c	-	+	Total ^{3}He	Incl.	Misfit	Norm. Misfit
144.50	6.89	13.48	1.42	86.89	6.48	6.86	179.97	0.266	0.346	0.020

Step #	°C	t (hrs)	^{3}He	Error	^{4}He	Error	^{4}He/^{3}He	Err	In ^{3}He Reg.
1	250	0.25	1.22	0.18	34.0	22.8	17.9	0.69	1
2	250	0.50	0.66	0.14	22.1	16.7	23.4	0.78	1
3	250	1.00	0.78	0.15	31.4	14.5	30.1	0.50	1
4	225	1.50	0.20	0.10	13.8	17.4	57.7	1.34	1
5	225	2.50	0.30	0.12	28.8	30.2	87.6	1.12	1
6	200	3.00	0.05	0.11	4.8	37.0	84.8	7.94	0
7	200	4.00	0.05	0.14	17.0	52.5	335.4	4.14	0
8	235	2.00	0.38	0.13	28.9	21.5	65.6	0.82	1
9	235	3.00	0.46	0.14	37.0	35.9	70.1	1.02	1
10	270	1.91	2.09	0.25	149.2	23.2	61.5	0.20	1
11	270	1.57	1.37	0.18	113.2	21.1	72.4	0.23	1
12	285	1.25	1.99	0.21	194.2	21.1	87.8	0.15	1
13	285	1.57	1.98	0.20	216.9	22.1	99.3	0.14	1
14	300	1.91	4.20	0.36	514.4	27.1	112.4	0.10	1
15	300	1.45	2.64	0.26	385.7	17.6	136.1	0.11	1
16	325	1.74	7.82	0.47	1298.1	31.2	155.9	0.06	1
17	325	1.32	4.82	0.37	927.2	24.0	182.2	0.08	1
18	340	1.58	8.62	0.44	1947.8	28.7	216.0	0.05	1
19	340	1.89	8.34	0.45	2194.2	40.8	253.2	0.06	1
20	350	1.48	7.78	0.47	2381.9	35.7	296.0	0.06	0
21	350	1.82	7.53	0.42	2679.1	33.8	345.7	0.06	0
22	360	1.50	7.52	0.43	2967.7	34.0	384.5	0.06	0
23	360	1.98	8.10	0.46	3567.3	42.0	430.3	0.06	0
24	370	1.88	9.12	0.46	4461.8	38.5	479.1	0.05	0
25	390	1.47	10.46	0.53	6017.9	49.9	565.2	0.05	0
26	450	1.00	23.86	0.81	17352.0	80.5	717.3	0.03	0
27	600	1.00	52.35	1.07	51531.5	162.8	974.4	0.02	0
28	900	1.00	5.24	0.37	6957.8	49.7	1318.4	0.07	0
29	900	1.00	0.01	0.06	11.5	20.1	814.7	4.55	0

Figure S86

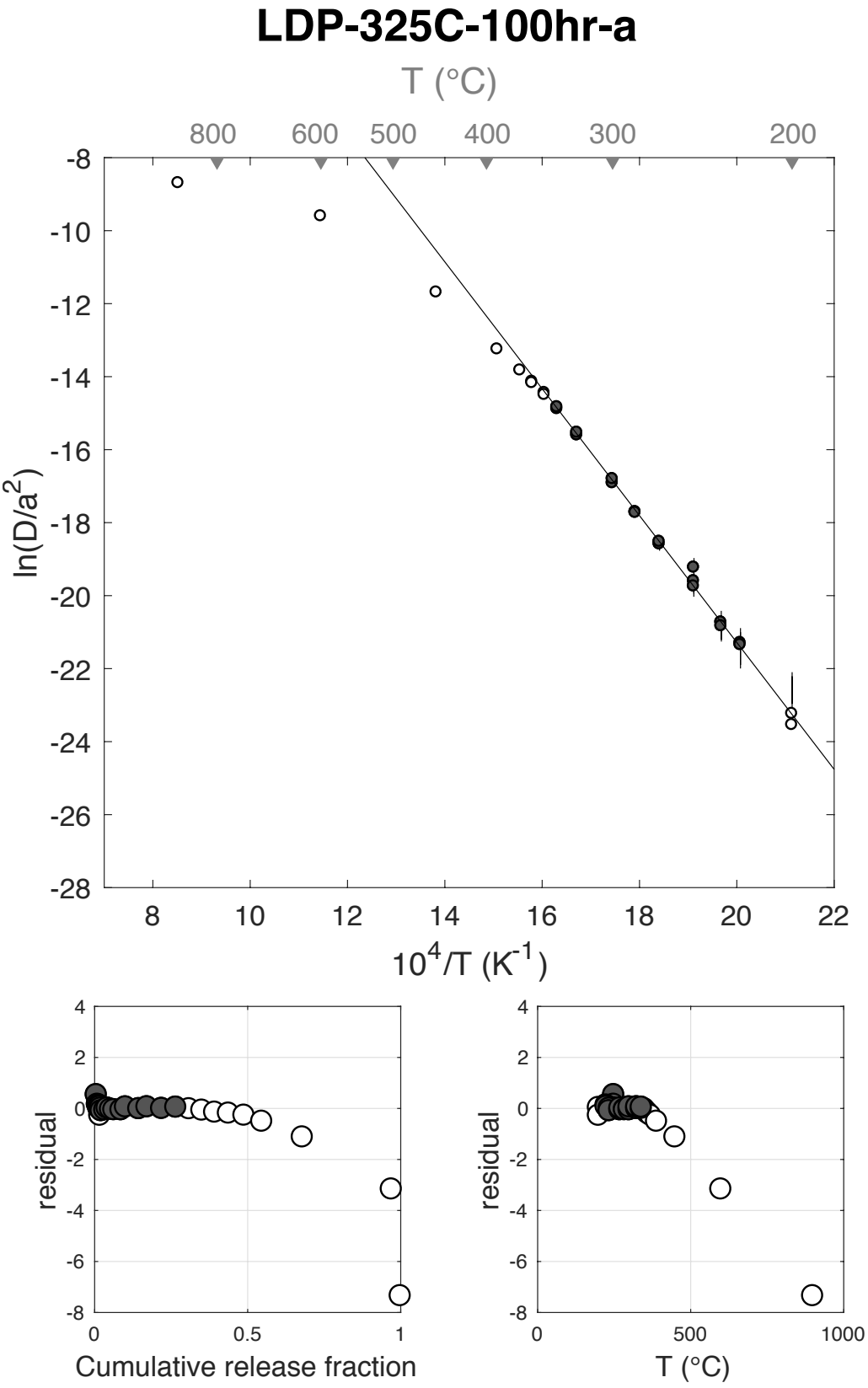
LDP-325C-100hr-a
T (°C)
800
600
500
400
300
200
ln(D/a²)
10⁴/T (K⁻¹)
residual
Cumulative release fraction
residual
T (°C)

LDP-350C-100hr-a

E_a	+/-	D_0	+/-	T_c	-	+	Total ^{3}He	Incl.	Misfit	Norm. Misfit
128.95	7.82	11.39	1.66	62.81	8.11	8.71	172.50	0.393	0.552	0.029

Step #	°C	t (hrs)	^{3}He	Error	^{4}He	Error	^{4}He/^{3}He	Err	In ^{3}He Reg.
1	250	0.25	2.36	0.20	25.5	13.9	0.8	0.55	1
2	250	0.50	1.51	0.21	14.9	13.5	NaN	NaN	1
3	250	1.00	1.74	0.23	17.7	16.4	0.2	0.93	1
4	225	1.50	0.44	0.13	3.8	18.4	NaN	NaN	1
5	225	2.50	0.69	0.15	7.3	21.5	0.6	2.95	1
6	200	3.00	0.12	0.10	0.0	0.0	NaN	NaN	1
7	200	4.00	0.17	0.14	0.0	0.0	NaN	NaN	1
8	235	2.00	0.83	0.17	11.5	19.0	4.0	1.66	1
9	235	3.00	1.17	0.19	19.3	27.8	6.6	1.45	1
10	270	1.91	4.18	0.31	60.8	21.0	4.5	0.35	1
11	270	1.57	2.59	0.24	40.5	19.1	5.6	0.48	1
12	285	1.25	3.55	0.31	63.6	19.0	7.9	0.31	1
13	285	1.57	3.40	0.28	57.4	16.1	6.9	0.29	1
14	300	1.91	6.41	0.41	151.3	19.1	13.6	0.14	1
15	300	1.45	4.06	0.34	154.4	18.1	28.0	0.14	1
16	325	1.74	10.47	0.47	355.4	21.9	24.0	0.08	1
17	325	1.32	5.78	0.35	255.2	16.9	34.2	0.09	1
18	340	1.58	9.85	0.49	525.9	21.8	43.4	0.06	1
19	340	1.89	8.49	0.47	601.3	21.9	60.8	0.07	1
20	350	1.48	7.55	0.36	653.9	18.9	76.7	0.06	0
21	350	1.82	7.92	0.44	876.1	23.4	100.6	0.06	0
22	360	1.50	7.29	0.44	1042.2	21.2	133.0	0.06	0
23	360	1.98	7.49	0.42	1337.2	22.3	168.6	0.06	0
24	370	1.88	6.87	0.40	1624.5	26.7	226.3	0.06	0
25	390	1.47	7.17	0.41	2176.6	30.4	293.6	0.06	0
26	450	1.00	15.66	0.65	7775.1	45.4	486.6	0.04	0
27	600	1.00	36.60	0.95	35274.5	111.4	953.7	0.03	0
28	900	1.00	8.16	0.40	10178.6	51.5	1237.4	0.05	0
29	899	1.00	0.00	0.00	0.0	0.0	NaN	NaN	0

Figure S87

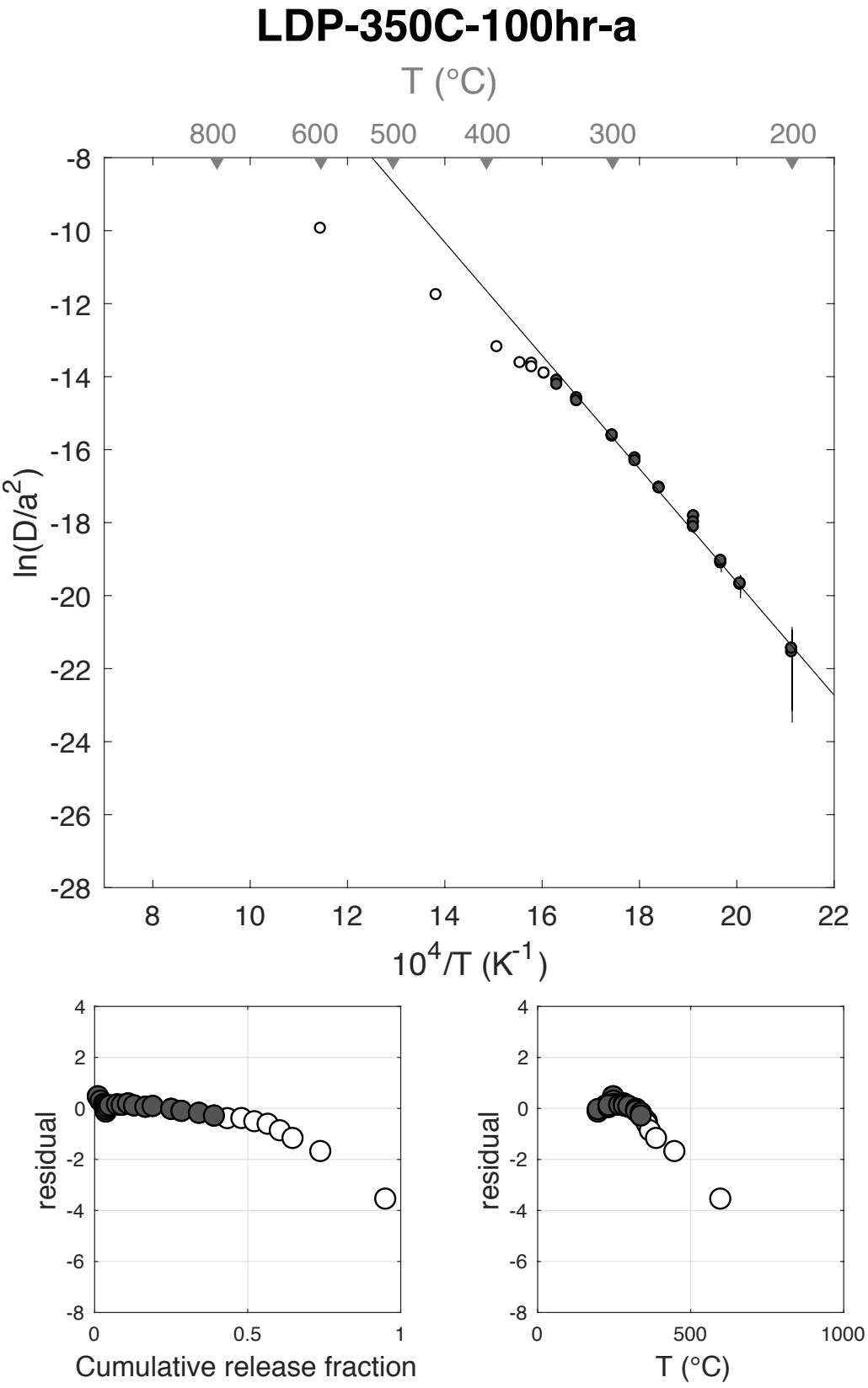
LDP-350C-100hr-a
T (°C)
800
600
500
400
300
200
ln(D/a²)
10⁴/T (K⁻¹)
residual
Cumulative release fraction
residual
T (°C)

LDP-350C-100hr-b

E_a	+/-	D_0	+/-	T_c	-	+	Total ^{3}He	Incl.	Misfit	Norm. Misfit
132.33	5.38	11.28	1.11	72.28	5.65	5.93	168.82	0.289	0.306	0.018

Step #	°C	t (hrs)	^{3}He	Error	^{4}He	Error	^{4}He/^{3}He	Err	In ^{3}He Reg.
1	250	0.25	1.46	0.21	29.0	26.3	9.9	0.92	1
2	250	0.50	0.92	0.15	27.8	19.9	20.3	0.73	1
3	250	1.00	1.10	0.16	17.9	15.0	6.2	0.85	1
4	225	1.50	0.25	0.10	39.3	24.3	145.0	0.74	1
5	225	2.50	0.35	0.11	44.0	39.6	115.0	0.95	1
6	200	3.00	0.00	0.09	19.7	49.4	5452.5	25.57	0
7	200	4.00	0.01	0.10	32.8	66.4	2196.7	6.93	0
8	235	2.00	0.46	0.12	16.3	29.1	25.3	1.80	1
9	235	3.00	0.64	0.15	33.4	47.2	41.7	1.44	1
10	270	1.91	2.58	0.23	73.8	28.1	18.6	0.39	1
11	270	1.57	1.64	0.19	51.3	24.9	21.2	0.50	1
12	285	1.25	2.31	0.21	92.1	15.7	29.9	0.19	1
13	285	1.57	2.30	0.22	103.3	22.8	34.9	0.24	1
14	300	1.91	4.55	0.29	230.2	27.0	40.6	0.13	1
15	300	1.45	2.69	0.23	168.9	21.5	52.7	0.15	1
16	325	1.74	7.75	0.42	595.0	36.9	66.8	0.08	1
17	325	1.32	4.53	0.32	422.6	25.3	83.4	0.09	1
18	340	1.58	7.93	0.47	884.4	26.0	101.5	0.07	1
19	340	1.89	7.29	0.39	1009.4	31.1	128.5	0.06	1
20	350	1.48	6.82	0.39	1111.9	26.1	153.1	0.06	0
21	350	1.82	6.91	0.40	1314.0	31.0	180.1	0.06	0
22	360	1.50	6.69	0.36	1515.3	25.3	216.7	0.06	0
23	360	1.98	7.22	0.38	1867.1	37.1	248.7	0.06	0
24	370	1.88	7.74	0.42	2324.6	37.7	290.3	0.06	0
25	390	1.47	9.00	0.48	3200.3	53.5	345.5	0.06	0
26	450	1.00	19.82	0.70	10354.0	51.8	512.3	0.04	0
27	600	1.00	46.20	1.02	49372.7	109.9	1058.7	0.02	0
28	900	1.00	9.62	0.44	16876.8	67.0	1743.4	0.05	0
29	900	1.00	0.02	0.05	18.1	20.7	1155.5	3.56	0

Figure S88

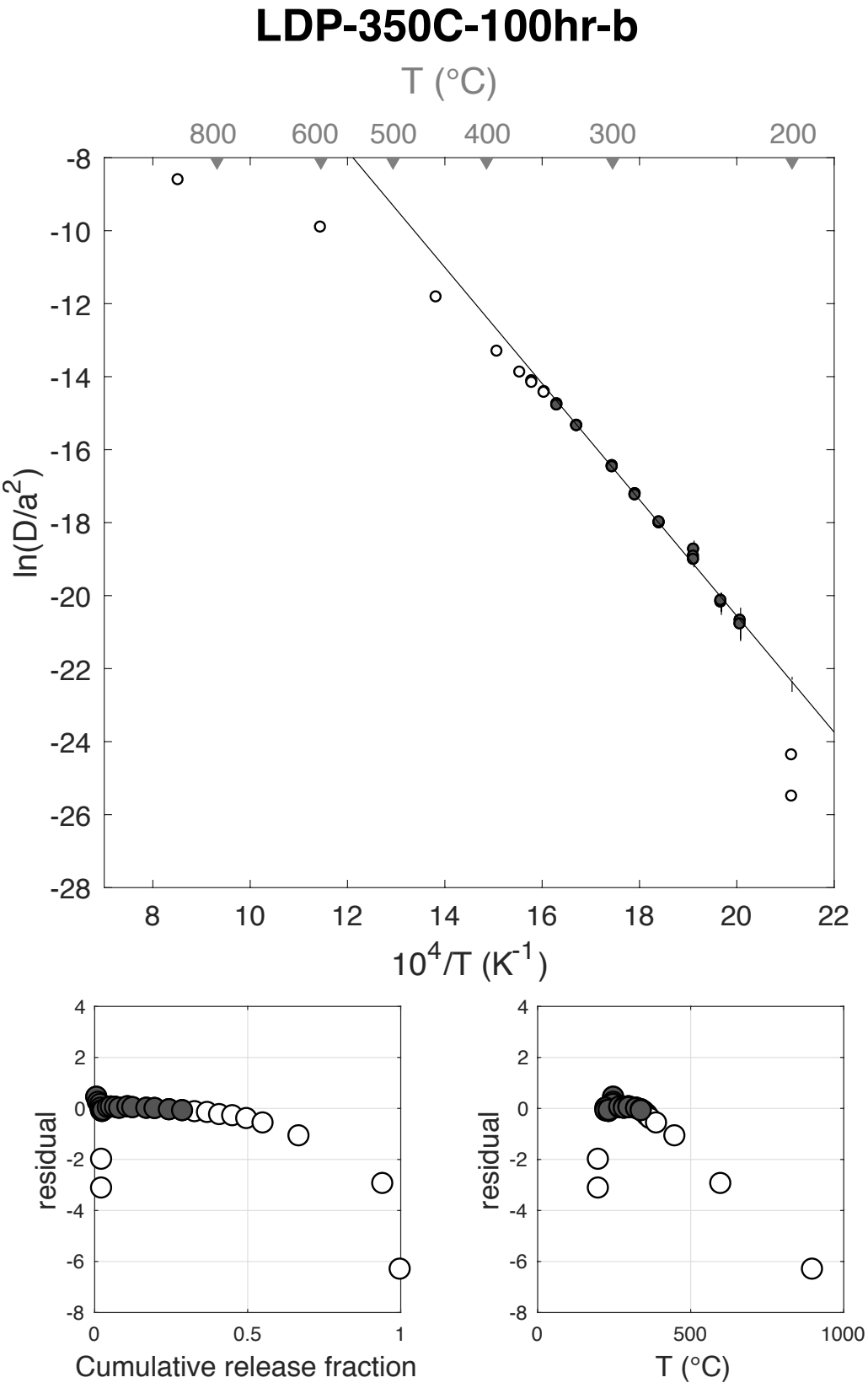
LDP-350C-100hr-b
T (°C)
800
600
500
400
300
200
-8
-10
-12
-14
-16
-18
-20
-22
-24
-26
-28
ln(D/a2)
8
10
12
14
16
18
20
22
10^4/T (K^-1)
4
2
0
-2
-4
-6
-8
residual
0
0.5
1
Cumulative release fraction
0
500
1000
T (°C)

LDP-350C-100hr-c

E_a	+/-	D_0	+/-	T_c	-	+	Total ^{3}He	Incl.	Misfit	Norm. Misfit
115.61	0.85	8.38	0.18	48.93	1.04	1.05	5349.79	0.342	1.997	0.105

Step #	°C	t (hrs)	^{3}He	Error	^{4}He	Error	^{4}He/^{3}He	Err	In Reg.
1	250	0.25	103.47	2.13	1183.6	24.8	1.4	0.03	1
2	250	0.50	43.06	2.00	598.3	18.0	3.9	0.06	1
3	250	1.00	49.41	1.40	974.2	24.9	9.7	0.04	1
4	225	1.50	14.29	0.74	14.6	13.7	NaN	NaN	1
5	225	2.50	27.86	1.24	0.0	0.0	NaN	NaN	1
6	200	3.00	3.59	0.37	0.0	0.0	NaN	NaN	1
7	200	4.00	5.16	0.43	0.0	0.0	NaN	NaN	1
8	235	2.00	21.91	1.21	0.0	0.0	NaN	NaN	1
9	235	3.00	25.16	1.33	0.0	0.0	NaN	NaN	1
10	270	1.91	112.76	2.12	1296.0	19.7	1.5	0.02	1
11	270	1.57	65.27	1.61	792.7	20.2	2.1	0.04	1
12	285	1.25	87.11	2.08	12855.7	113.0	137.6	0.03	1
13	285	1.56	96.25	2.27	6937.4	74.4	62.1	0.03	1
14	300	1.91	176.98	2.48	4396.4	38.2	14.8	0.02	1
15	300	1.45	101.29	2.07	4979.3	49.7	39.2	0.02	1
16	325	1.74	281.25	4.47	8816.7	64.3	21.3	0.02	1
17	325	1.32	150.15	2.35	36235.5	846.8	231.3	0.03	1
18	340	1.58	241.44	3.01	49504.5	492.4	195.0	0.02	1
19	340	1.89	221.62	3.87	41379.9	455.2	176.7	0.02	1
20	350	1.48	205.00	3.19	26439.0	448.2	119.0	0.02	0
21	350	1.82	208.90	4.14	38743.2	151.4	175.5	0.02	0
22	360	1.50	209.69	3.53	23109.5	106.8	100.2	0.02	0
23	360	1.98	217.16	4.14	28058.4	115.1	119.2	0.02	0
24	370	1.88	224.50	4.66	39802.4	100.1	167.3	0.02	0
25	390	1.47	235.15	3.12	0.0	0.0	NaN	NaN	0
26	450	1.00	496.09	4.51	0.0	0.0	NaN	NaN	0
27	600	1.00	1126.73	6.95	0.0	0.0	NaN	NaN	0
28	700	1.00	348.09	3.90	0.0	0.0	NaN	NaN	0
29	900	1.00	235.93	4.14	0.0	0.0	NaN	NaN	0
30	900	1.00	9.49	0.54	16317.4	41.0	1710.0	0.06	0
31	900	1.00	3.27	0.39	7067.1	61.0	2153.1	0.12	0
32	900	1.00	1.77	0.26	4562.6	46.9	2564.5	0.15	0

Figure S89

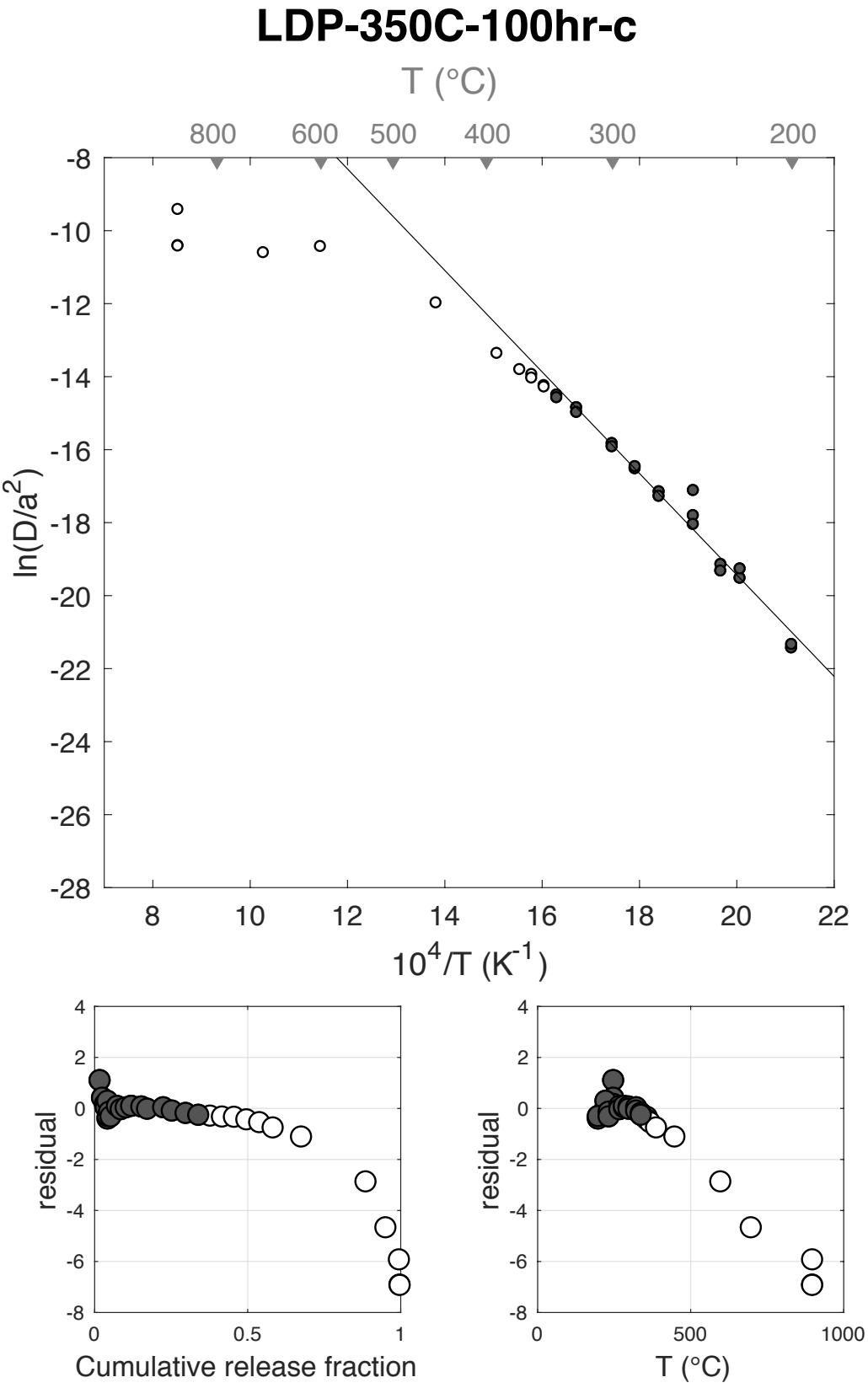
LDP-350C-100hr-c
T (°C)
800
600
500
400
300
200
-8
-10
-12
-14
-16
-18
-20
-22
-24
-26
-28
ln(D/a2)
8
10
12
14
16
18
20
22
10^4/T (K^-1)
4
2
0
-2
-4
-6
-8
residual
0
0.5
1
Cumulative release fraction
500
1000
T (°C)

LDP-375C-100hr-a

E_a	+/-	D_0	+/-	T_c	-	+	Total ^{3}He	Incl.	Misfit	Norm. Misfit
121.73	7.74	9.39	1.63	58.13	8.59	9.23	136.29	0.322	0.313	0.016

Step #	°C	t (hrs)	^{3}He	Error	^{4}He	Error	^{4}He/^{3}He	Err	In ^{3}He Reg.
1	250	0.25	1.49	0.18	18.0	17.5	2.1	0.98	1
2	250	0.50	0.96	0.19	16.1	15.0	6.8	0.95	1
3	250	1.00	1.16	0.18	19.5	17.0	6.7	0.89	1
4	225	1.50	0.32	0.11	30.6	24.1	84.4	0.86	1
5	225	2.50	0.47	0.14	19.6	25.4	32.0	1.33	1
6	200	3.00	0.14	0.10	28.8	32.5	195.7	1.34	1
7	200	4.00	0.17	0.13	18.1	43.1	94.6	2.50	1
8	235	2.00	0.52	0.13	21.8	20.9	31.9	0.99	1
9	235	3.00	0.69	0.17	22.3	32.3	22.3	1.47	1
10	270	1.91	2.66	0.28	118.5	19.9	34.6	0.20	1
11	270	1.57	1.42	0.20	51.7	22.2	26.5	0.45	1
12	285	1.25	2.14	0.24	59.2	17.0	17.7	0.31	1
13	285	1.57	2.18	0.25	60.1	17.1	17.6	0.31	1
14	300	1.91	4.20	0.36	66.0	22.8	5.7	0.36	1
15	300	1.45	2.49	0.27	37.3	13.4	5.0	0.38	1
16	325	1.74	6.82	0.41	61.9	15.9	NaN	NaN	1
17	325	1.32	3.90	0.34	48.9	16.1	2.6	0.34	1
18	340	1.58	6.49	0.42	72.5	16.4	1.2	0.24	1
19	340	1.89	5.67	0.40	58.6	22.3	0.3	0.39	1
20	350	1.48	5.20	0.33	58.4	15.8	1.2	0.28	0
21	350	1.82	5.04	0.39	63.1	20.6	2.5	0.34	0
22	360	1.50	4.91	0.38	58.6	17.1	1.9	0.30	0
23	360	1.98	5.40	0.36	71.7	20.7	3.3	0.30	0
24	370	1.88	6.01	0.40	93.5	20.9	5.6	0.23	0
25	390	1.47	7.03	0.42	105.9	17.5	5.1	0.18	0
26	450	1.00	18.07	0.66	404.0	24.8	12.4	0.07	0
27	600	1.00	35.25	0.87	4642.6	37.9	121.7	0.03	0
28	900	1.00	5.48	0.36	4470.0	30.2	806.0	0.07	0
29	900	1.00	0.01	0.07	17.2	13.7	2023.8	7.76	0

Figure S90

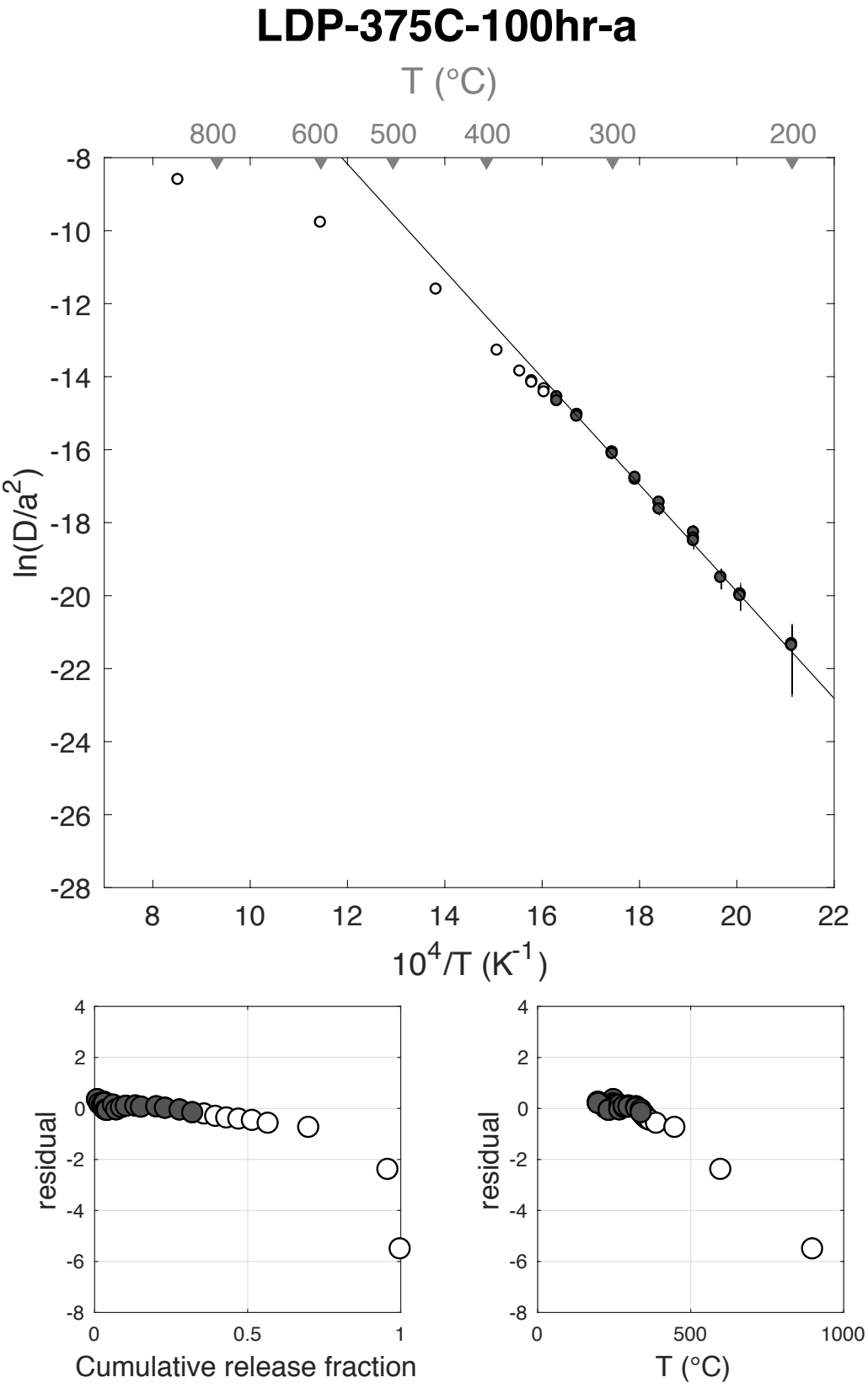
LDP-375C-100hr-a
T (°C)
800
600
500
400
300
200
-8
-10
-12
-14
-16
-18
-20
-22
-24
-26
-28
ln(D/a2)
8
10
12
14
16
18
20
22
10^4/T (K^-1)
4
2
0
-2
-4
-6
-8
residual
0
0.5
1
Cumulative release fraction
0
500
1000
T (°C)

LDP-375C-100hr-b

E_a	+/-	D_0	+/-	T_c	-	+	Total ^{3}He	Incl.	Misfit	Norm. Misfit
137.15	11.82	12.31	2.43	77.04	11.66	12.90	58.64	0.301	0.254	0.017

Step #	°C	t (hrs)	^{3}He	Error	^{4}He	Error	^{4}He/^{3}He	Err	In ^{3}He Reg.
1	250	0.25	0.48	0.12	20.2	22.1	32.5	1.12	1
2	250	0.50	0.30	0.10	7.1	24.4	13.3	3.46	1
3	250	1.00	0.34	0.12	7.9	21.8	13.3	2.79	1
4	225	1.50	0.11	0.09	3.0	29.0	17.9	9.56	1
5	225	2.50	0.10	0.09	10.3	49.5	92.9	4.87	0
6	200	3.00	0.00	0.00	21.0	59.6	Inf	NaN	0
7	200	4.00	0.00	0.00	12.8	83.4	Inf	NaN	0
8	235	2.00	0.13	0.09	2.5	36.1	9.7	14.33	0
9	235	3.00	0.24	0.11	14.6	59.7	49.9	4.12	1
10	270	1.91	0.85	0.15	10.2	34.7	2.1	3.40	1
11	270	1.57	0.54	0.14	10.9	26.8	10.2	2.47	1
12	285	1.25	0.82	0.15	6.1	24.9	NaN	NaN	1
13	285	1.57	0.84	0.14	20.3	29.0	14.3	1.44	1
14	300	1.91	1.66	0.20	25.4	35.3	5.3	1.40	1
15	300	1.45	1.00	0.16	0.0	0.0	NaN	NaN	1
16	325	1.74	2.95	0.23	16.6	30.5	NaN	NaN	1
17	325	1.32	1.72	0.23	4.4	24.4	NaN	NaN	1
18	340	1.58	3.06	0.28	33.2	25.7	0.9	0.78	1
19	340	1.89	2.76	0.26	17.3	32.4	NaN	NaN	1
20	350	1.48	2.59	0.24	28.9	23.8	1.2	0.83	0
21	350	1.82	2.57	0.27	27.0	31.3	0.5	1.17	0
22	360	1.50	2.54	0.25	17.8	21.6	NaN	NaN	0
23	360	1.98	2.64	0.26	31.1	36.3	1.8	1.17	0
24	370	1.88	2.85	0.24	34.1	40.4	2.0	1.19	0
25	390	1.47	3.47	0.29	43.6	26.5	2.6	0.61	0
26	450	1.00	7.96	0.46	89.6	14.3	1.3	0.17	0
27	600	1.00	14.37	0.56	1453.8	32.3	91.2	0.04	0
28	900	1.00	1.75	0.19	815.5	24.3	455.1	0.11	0
29	900	1.00	0.00	0.07	18.6	18.2	34918.3	130.66	0

Figure S91

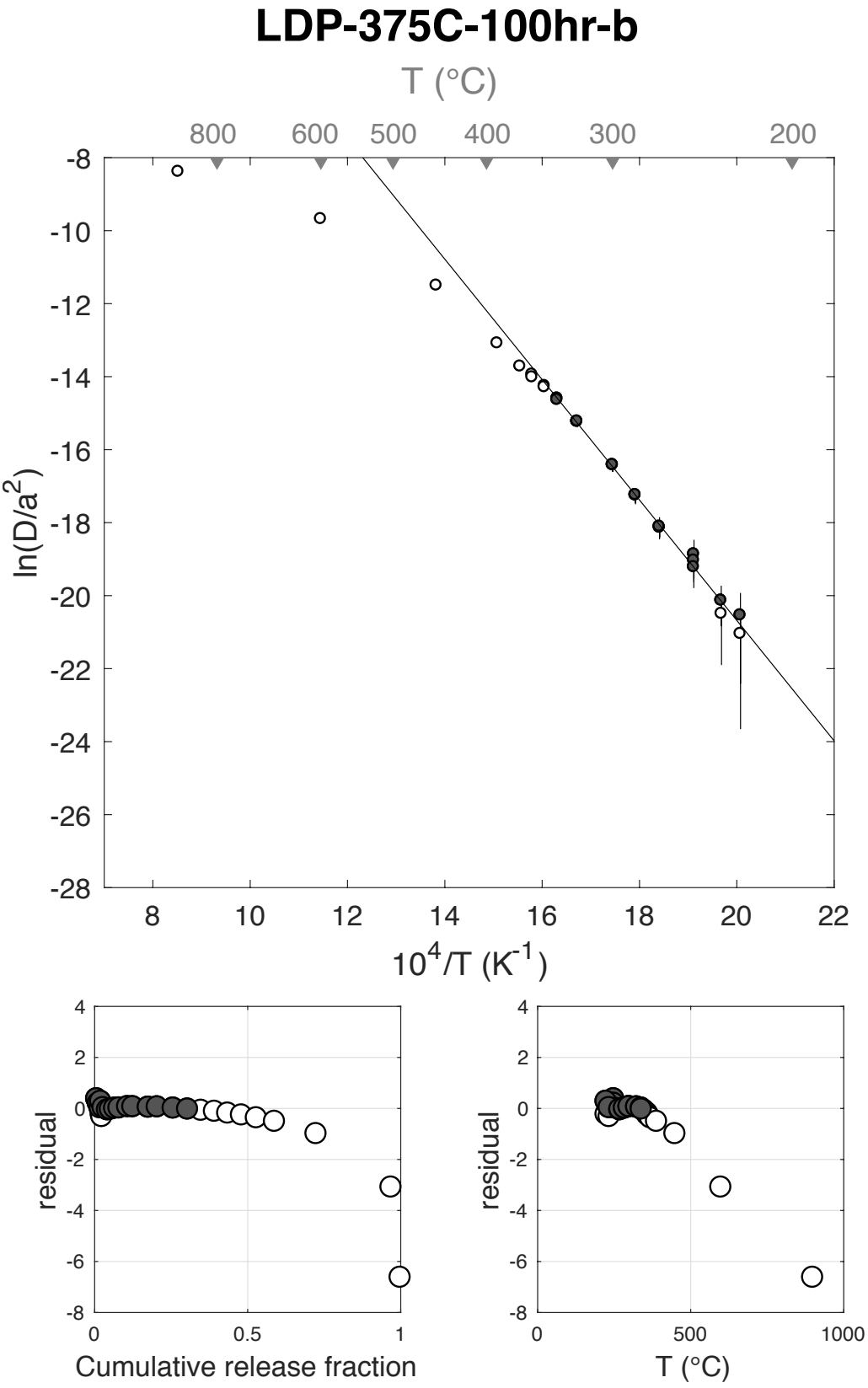
LDP-375C-100hr-b
T (°C)
800
600
500
400
300
200
-8
-10
-12
-14
-16
-18
-20
-22
-24
-26
-28
ln(D/a2)
8
10
12
14
16
18
20
22
10^4/T (K^-1)
4
2
0
-2
-4
-6
-8
residual
0
0.5
1
Cumulative release fraction
0
500
1000
T (°C)

LDP-400C-100hr-a

E_a	+/-	D_0	+/-	T_c	-	+	Total ^{3}He	Incl.	Misfit	Norm. Misfit
141.70	10.99	14.31	2.26	74.26	10.54	11.54	45.90	0.479	0.371	0.022

Step #	°C	t (hrs)	^{3}He	Error	^{4}He	Error	^{4}He/^{3}He	Err	In ^{3}He Reg.
1	250	0.25	0.60	0.13	29.3	23.6	39.1	0.83	1
2	250	0.50	0.39	0.12	22.5	18.2	48.0	0.87	1
3	250	1.00	0.47	0.12	17.6	17.3	27.6	1.02	1
4	225	1.50	0.14	0.10	103.1	27.3	722.1	0.73	1
5	225	2.50	0.14	0.13	0.0	0.0	NaN	NaN	1
6	200	3.00	0.01	0.13	4.7	74.8	319.7	18.20	0
7	200	4.00	0.02	0.17	0.0	0.0	NaN	NaN	0
8	235	2.00	0.21	0.12	10.8	43.1	42.1	4.03	1
9	235	3.00	0.30	0.14	0.0	0.0	NaN	NaN	1
10	270	1.91	1.09	0.17	15.1	40.3	3.9	2.67	1
11	270	1.57	0.73	0.15	11.8	31.4	6.1	2.67	1
12	285	1.25	1.02	0.16	8.2	20.3	NaN	NaN	1
13	285	1.57	1.08	0.17	10.3	30.3	NaN	NaN	1
14	300	1.91	2.09	0.22	16.7	38.8	NaN	NaN	1
15	300	1.45	1.28	0.19	8.7	28.2	NaN	NaN	1
16	325	1.74	3.50	0.29	32.8	36.1	NaN	NaN	1
17	325	1.32	2.17	0.24	11.9	24.7	NaN	NaN	1
18	340	1.58	3.50	0.31	29.7	30.4	NaN	NaN	1
19	340	1.89	3.30	0.32	25.7	39.5	NaN	NaN	1
20	350	1.48	2.89	0.28	28.2	27.7	NaN	NaN	0
21	350	1.82	2.79	0.24	13.3	37.4	NaN	NaN	0
22	360	1.50	2.75	0.27	23.9	28.9	NaN	NaN	0
23	360	1.98	2.74	0.27	14.2	40.6	NaN	NaN	0
24	370	1.88	2.80	0.25	18.9	40.7	NaN	NaN	0
25	390	1.47	2.94	0.26	34.8	28.7	1.8	0.83	0
26	450	1.00	4.66	0.36	69.1	18.6	4.8	0.28	0
27	600	1.00	2.16	0.23	204.1	20.7	84.5	0.15	0
28	900	1.00	0.12	0.08	117.6	15.7	949.4	0.69	0
29	900	1.00	0.00	0.00	6.1	14.6	Inf	NaN	0

Figure S92

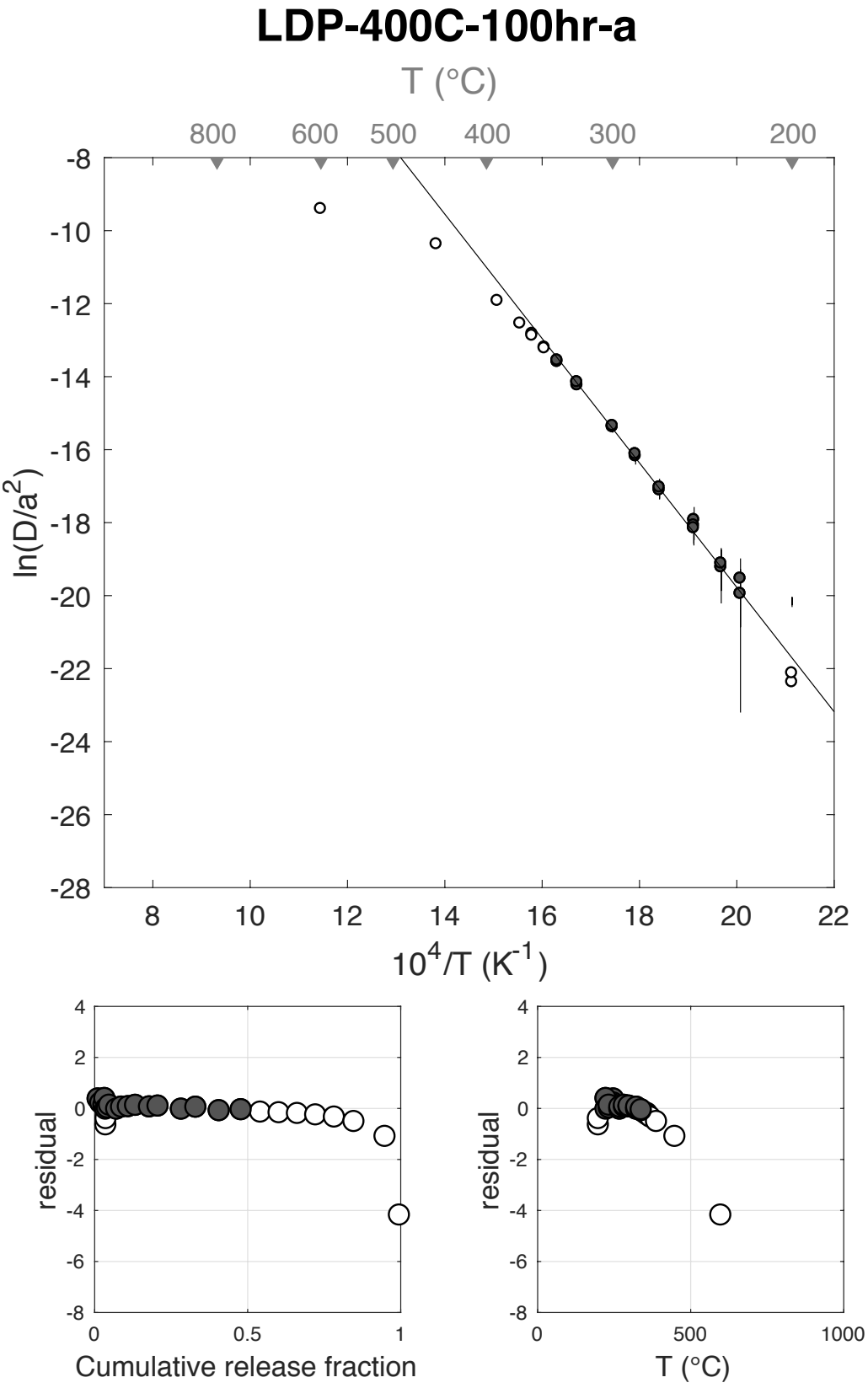
LDP-400C-100hr-a
T (°C)
800
600
500
400
300
200
-8
-10
-12
-14
-16
-18
-20
-22
-24
-26
-28
ln(D/a2)
8
10
12
14
16
18
20
22
10^4/T (K^-1)
4
2
0
-2
-4
-6
-8
residual
0
0.5
1
Cumulative release fraction
0
500
1000
T (°C)

LDP-425C-100hr-a

E_a	+/-	D_0	+/-	T_c	-	+	Total ^{3}He	Incl.	Misfit	Norm. Misfit
135.86	7.20	12.09	1.48	75.40	7.31	7.78	104.38	0.310	0.127	0.007

Step #	°C	t (hrs)	^{3}He	Error	^{4}He	Error	^{4}He/^{3}He	Err	In ^{3}He Reg.
1	250	0.25	0.82	0.14	6.0	16.8	NaN	NaN	1
2	250	0.50	0.52	0.14	13.1	16.4	15.4	1.28	1
3	250	1.00	0.73	0.15	7.6	20.0	0.4	2.65	1
4	225	1.50	0.19	0.09	15.0	26.6	69.4	1.84	1
5	225	2.50	0.26	0.10	6.2	46.5	13.5	7.49	1
6	200	3.00	0.09	0.09	1.1	60.1	2.4	55.04	0
7	200	4.00	0.11	0.10	0.0	0.0	NaN	NaN	0
8	235	2.00	0.29	0.12	1.9	35.7	NaN	NaN	1
9	235	3.00	0.43	0.12	16.1	59.2	26.9	3.70	1
10	270	1.91	1.54	0.20	13.3	33.5	NaN	NaN	1
11	270	1.57	0.97	0.16	17.2	26.7	7.8	1.56	1
12	285	1.25	1.39	0.19	13.9	20.5	0.0	1.48	1
13	285	1.57	1.39	0.18	0.0	0.0	NaN	NaN	1
14	300	1.91	2.88	0.26	34.0	33.0	1.8	0.97	1
15	300	1.45	1.80	0.21	6.5	23.7	NaN	NaN	1
16	325	1.74	5.24	0.33	45.8	31.9	NaN	NaN	1
17	325	1.32	3.15	0.28	23.5	20.4	NaN	NaN	1
18	340	1.58	5.50	0.39	51.4	26.7	NaN	NaN	1
19	340	1.89	5.22	0.33	40.2	36.9	NaN	NaN	1
20	350	1.48	4.85	0.36	46.5	27.7	NaN	NaN	0
21	350	1.82	4.79	0.36	33.9	30.3	NaN	NaN	0
22	360	1.50	4.93	0.37	49.2	25.2	NaN	NaN	0
23	360	1.98	5.16	0.35	54.4	35.4	0.5	0.65	0
24	370	1.88	5.57	0.37	50.1	33.9	NaN	NaN	0
25	390	1.47	6.37	0.42	64.8	23.0	0.2	0.36	0
26	450	1.00	14.15	0.52	159.8	17.3	1.3	0.11	0
27	600	1.00	24.53	0.72	1727.6	24.0	60.4	0.03	0
28	900	1.00	1.50	0.18	408.6	19.9	262.2	0.13	0
29	900	1.00	0.02	0.07	0.0	0.0	NaN	NaN	0

Figure S93

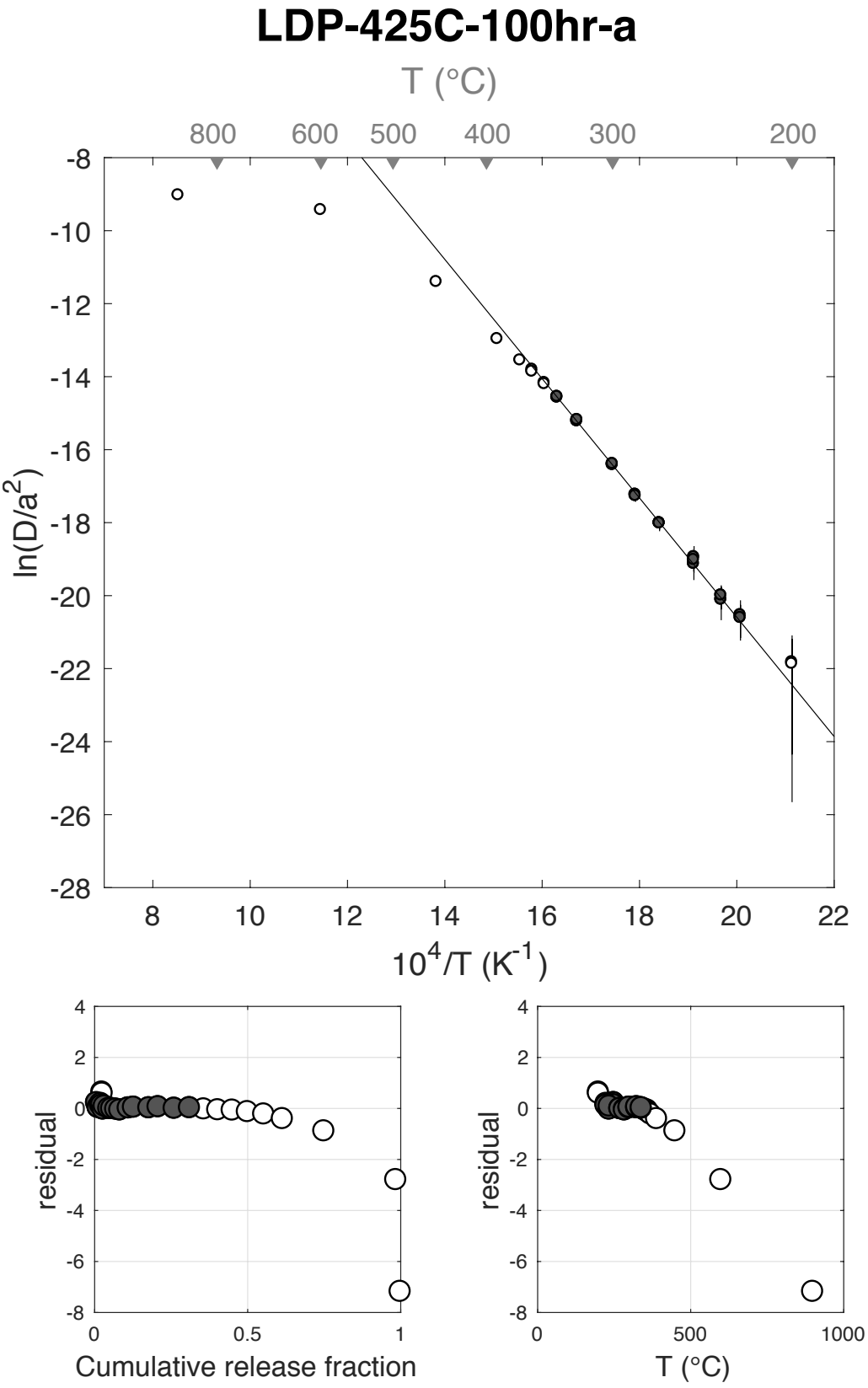
LDP-425C-100hr-a
T (°C)
800
600
500
400
300
200
-8
-10
-12
-14
-16
-18
-20
-22
-24
-26
-28
ln(D/a²)
8
10
12
14
16
18
20
22
10⁴/T (K⁻¹)
4
2
0
-2
-4
-6
-8
residual
0
0.5
1
Cumulative release fraction
500
1000
T (°C)

LDP-450C-100hr-a

E_a	+/-	D_0	+/-	T_c	-	+	Total ^{3}He	Incl.	Misfit	Norm. Misfit
134.44	9.51	11.47	1.99	76.28	9.40	10.23	122.24	0.273	0.521	0.027

Step #	°C	t (hrs)	^{3}He	Error	^{4}He	Error	^{4}He/^{3}He	Err	In ^{3}He Reg.
1	250	0.25	0.73	0.17	17.7	20.7	14.3	1.20	1
2	250	0.50	0.52	0.13	6.0	17.3	1.6	2.87	1
3	250	1.00	0.67	0.15	1.6	20.4	NaN	NaN	1
4	225	1.50	0.18	0.09	0.0	0.0	NaN	NaN	1
5	225	2.50	0.25	0.12	0.0	0.0	NaN	NaN	1
6	200	3.00	0.10	0.10	0.5	26.4	NaN	NaN	1
7	200	4.00	0.09	0.13	0.7	34.8	NaN	NaN	1
8	235	2.00	0.33	0.12	0.0	0.0	NaN	NaN	1
9	235	3.00	0.45	0.13	0.0	0.0	NaN	NaN	1
10	270	1.91	1.53	0.20	7.7	19.3	NaN	NaN	1
11	270	1.57	0.94	0.17	0.0	0.0	NaN	NaN	1
12	285	1.25	1.42	0.18	21.6	21.9	5.3	1.02	1
13	285	1.57	1.48	0.19	7.9	17.4	NaN	NaN	1
14	300	1.91	3.13	0.29	27.9	20.7	NaN	NaN	1
15	300	1.45	1.94	0.20	4.3	17.7	NaN	NaN	1
16	325	1.74	5.50	0.36	38.5	19.7	NaN	NaN	1
17	325	1.32	3.24	0.29	17.2	16.3	NaN	NaN	1
18	340	1.58	5.84	0.40	37.6	14.2	NaN	NaN	1
19	340	1.89	5.09	0.35	32.8	19.4	NaN	NaN	1
20	350	1.48	5.08	0.40	44.1	20.9	NaN	NaN	0
21	350	1.82	5.03	0.35	50.7	22.0	0.1	0.44	0
22	360	1.50	5.27	0.36	42.4	15.8	NaN	NaN	0
23	360	1.98	5.69	0.36	47.5	22.2	NaN	NaN	0
24	370	1.88	5.88	0.36	38.5	18.9	NaN	NaN	0
25	390	1.47	6.74	0.42	50.3	19.9	NaN	NaN	0
26	450	1.00	13.34	2.15	143.9	20.4	0.8	0.22	0
27	600	1.00	38.21	0.96	709.8	15.6	8.6	0.03	0
28	900	1.00	3.51	0.29	3062.9	33.5	862.5	0.08	0
29	900	1.00	0.07	0.07	60.5	17.4	911.8	1.14	0

Figure S94

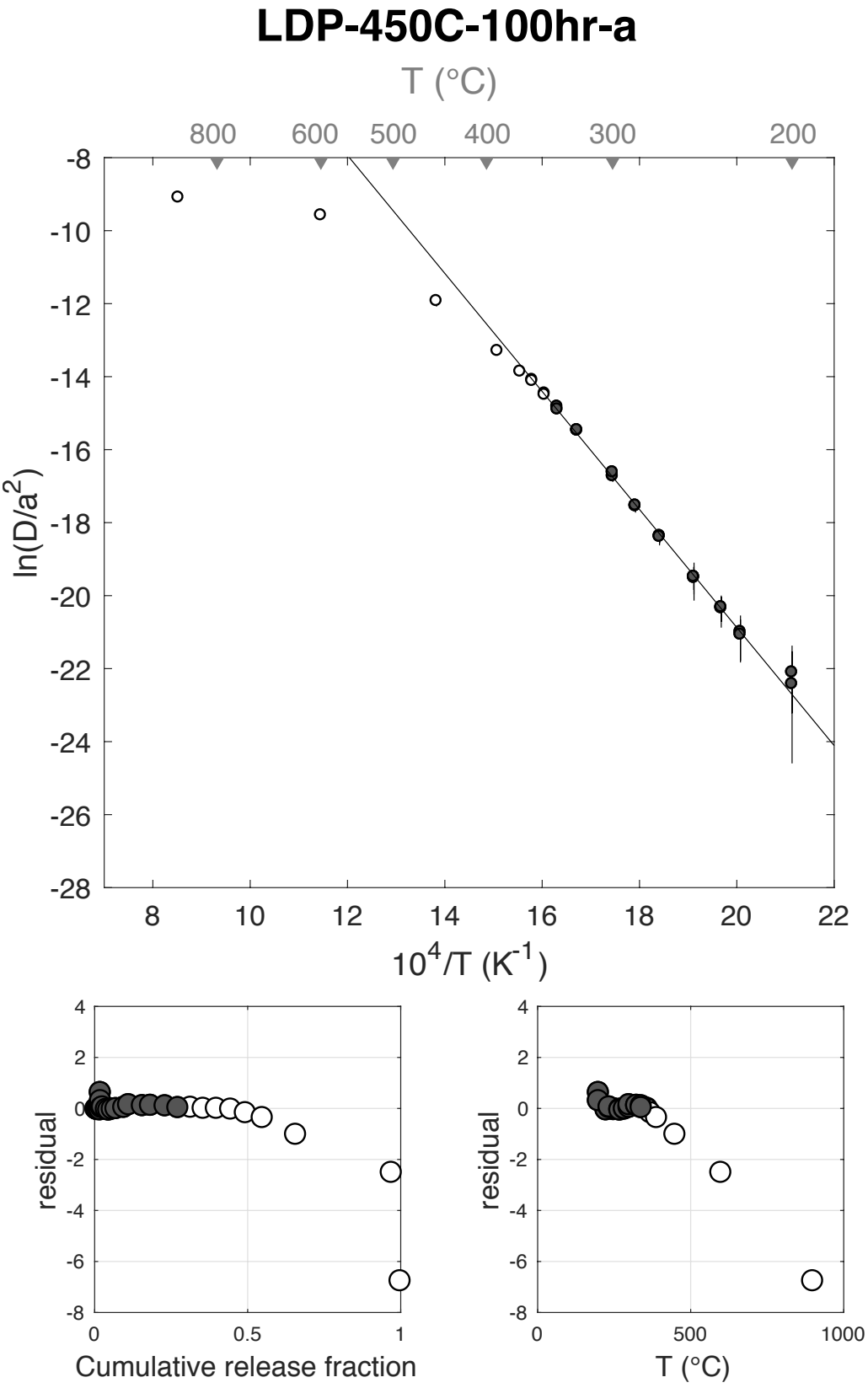
LDP-450C-100hr-a
T (°C)
800
600
500
400
300
200
-8
-10
-12
-14
-16
-18
-20
-22
-24
-26
-28
ln(D/a2)
8
10
12
14
16
18
20
22
10^4/T (K^-1)
4
2
0
-2
-4
-6
-8
residual
0
0.5
1
Cumulative release fraction
500
1000
T (°C)

LDP-450C-100hr-b

E_a	+/-	D_0	+/-	T_c	-	+	Total ^{3}He	Incl.	Misfit	Norm. Misfit
114.30	22.83	7.75	4.62	49.88	26.72	33.07	57.07	0.290	1.009	0.084

Step #	°C	t (hrs)	^{3}He	Error	^{4}He	Error	^{4}He/^{3}He	Err	In ^{3}He Reg.
1	250	0.25	0.61	0.31	56.4	96.1	83.1	1.78	1
2	250	0.50	0.60	0.25	69.3	53.6	104.7	0.88	1
3	250	1.00	0.52	0.28	36.4	44.7	60.5	1.34	0
4	225	1.50	0.14	0.37	33.4	85.9	229.1	3.68	0
5	225	2.50	0.14	0.67	0.0	0.0	NaN	NaN	0
6	200	3.00	0.01	0.83	0.0	0.0	NaN	NaN	0
7	200	4.00	0.00	1.16	0.0	0.0	NaN	NaN	0
8	235	2.00	0.26	0.50	0.0	0.0	NaN	NaN	0
9	235	3.00	0.32	0.83	0.0	0.0	NaN	NaN	0
10	270	1.91	0.94	0.50	21.9	116.5	13.3	5.34	1
11	270	1.57	0.57	0.41	0.0	0.0	NaN	NaN	1
12	285	1.25	0.94	0.35	0.0	0.0	NaN	NaN	1
13	285	1.57	0.89	0.41	0.0	0.0	NaN	NaN	1
14	300	1.91	1.64	0.50	10.9	118.0	NaN	NaN	1
15	300	1.45	1.85	0.46	3.6	94.1	NaN	NaN	1
16	325	1.74	2.42	0.53	0.0	0.0	NaN	NaN	1
17	325	1.32	1.45	0.38	0.0	0.0	NaN	NaN	1
18	340	1.58	2.40	0.52	0.0	0.0	NaN	NaN	1
19	340	1.89	2.21	0.60	0.0	0.0	NaN	NaN	1
20	350	1.48	2.02	0.46	0.0	0.0	NaN	NaN	0
21	350	1.82	1.98	0.48	0.0	0.0	NaN	NaN	0
22	360	1.50	2.02	0.46	0.0	0.0	NaN	NaN	0
23	360	1.98	2.33	0.58	8.5	129.3	NaN	NaN	0
24	370	1.88	2.26	0.55	0.0	0.0	NaN	NaN	0
25	390	1.47	2.73	0.50	0.0	0.0	NaN	NaN	0
26	450	1.00	6.73	0.53	23.6	84.5	NaN	NaN	0
27	600	1.00	15.14	0.71	1712.3	58.7	103.1	0.06	0
28	900	1.00	3.96	0.43	3168.6	71.6	789.7	0.11	0
29	900	1.00	0.00	0.00	0.0	0.0	NaN	NaN	0

Figure S95

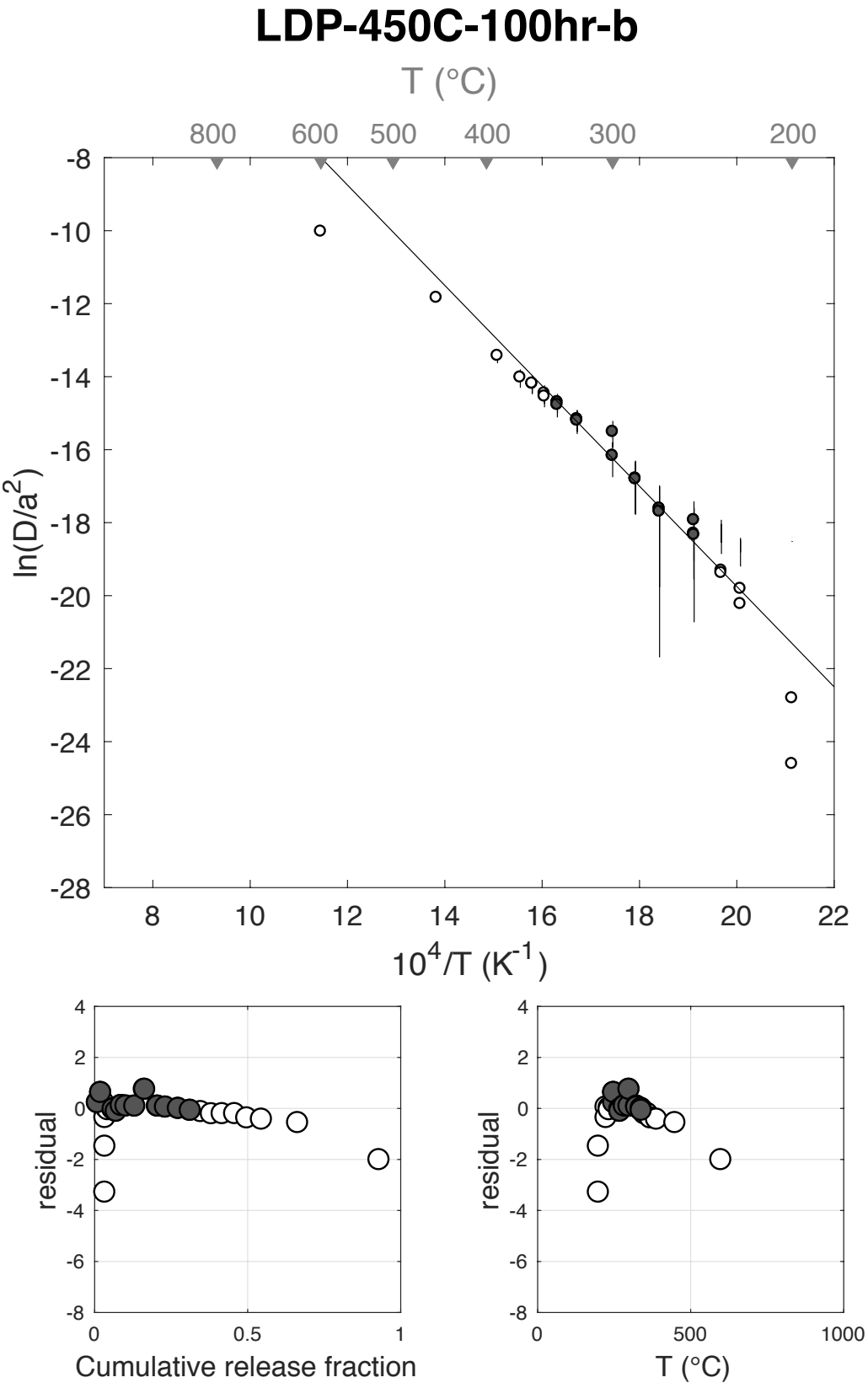
LDP-450C-100hr-b
T (°C)
800
600
500
400
300
200
ln(D/a²)
10⁴/T (K⁻¹)
residual
Cumulative release fraction
residual
T (°C)

LDP-450C-100hr-c

E_a	+/-	D_0	+/-	T_c	-	+	Total ^{3}He	Incl.	Misfit	Norm. Misfit
129.77	5.48	10.89	1.17	68.45	5.60	5.89	877.46	0.298	1.394	0.073

Step #	°C	t (hrs)	^{3}He	Error	^{4}He	Error	^{4}He/^{3}He	Err	In ^{3}He Reg.
1	250	0.25	8.74	0.59	132.2	834.5	5.1	6.31	1
2	250	0.50	5.56	0.46	2471.1	460.4	434.6	0.20	1
3	250	1.00	6.92	0.51	5328.9	351.1	759.6	0.10	1
4	225	1.50	1.83	0.26	8767.8	1083.7	4790.1	0.19	1
5	225	2.50	2.48	0.30	16178.3	2594.5	6524.5	0.20	1
6	200	3.00	0.49	0.15	20610.7	3354.4	41795.2	0.35	1
7	200	4.00	0.55	0.39	0.0	0.0	NaN	NaN	1
8	235	2.00	1.21	0.22	92492.1	1912.5	76612.4	0.19	1
9	235	3.00	3.88	0.38	12316.1	3350.3	3162.7	0.29	1
10	270	1.91	14.70	0.82	9109.9	1707.7	609.7	0.20	1
11	270	1.57	8.87	0.59	4676.4	1194.6	517.0	0.26	1
12	285	1.25	12.83	0.63	2199.7	712.3	161.5	0.33	1
13	285	1.57	12.93	0.75	5473.4	1198.1	413.3	0.23	1
14	300	1.91	25.01	0.91	6968.0	1703.3	268.6	0.25	1
15	300	1.45	15.44	0.78	3004.2	1005.3	184.6	0.34	1
16	325	1.74	43.34	1.30	5378.0	1442.6	114.1	0.27	1
17	325	1.32	24.66	0.96	2055.5	807.2	73.4	0.39	1
18	340	1.58	40.03	1.11	5073.3	1203.2	116.7	0.24	1
19	340	1.89	32.23	1.03	39921.2	1684.9	1228.7	0.05	1
20	350	1.48	32.40	1.06	2661.8	1048.0	72.2	0.40	0
21	350	1.82	31.97	1.15	5403.6	1564.6	159.0	0.29	0
22	360	1.50	30.72	1.04	2712.7	1078.9	78.3	0.40	0
23	360	1.98	32.65	1.18	5571.3	1807.3	160.6	0.33	0
24	370	1.88	33.30	1.06	5079.6	1655.5	142.6	0.33	0
25	390	1.47	39.82	1.14	2703.8	1038.7	57.9	0.39	0
26	450	1.00	127.94	24.10	1851.8	329.7	4.5	0.26	0
27	600	1.00	208.35	31.90	22400.9	423.9	97.5	0.15	0
28	900	1.00	77.77	2.27	56574.0	631.5	717.4	0.03	0
29	868	1.00	0.83	0.17	17705.2	350.6	21202.2	0.20	0

Figure S96

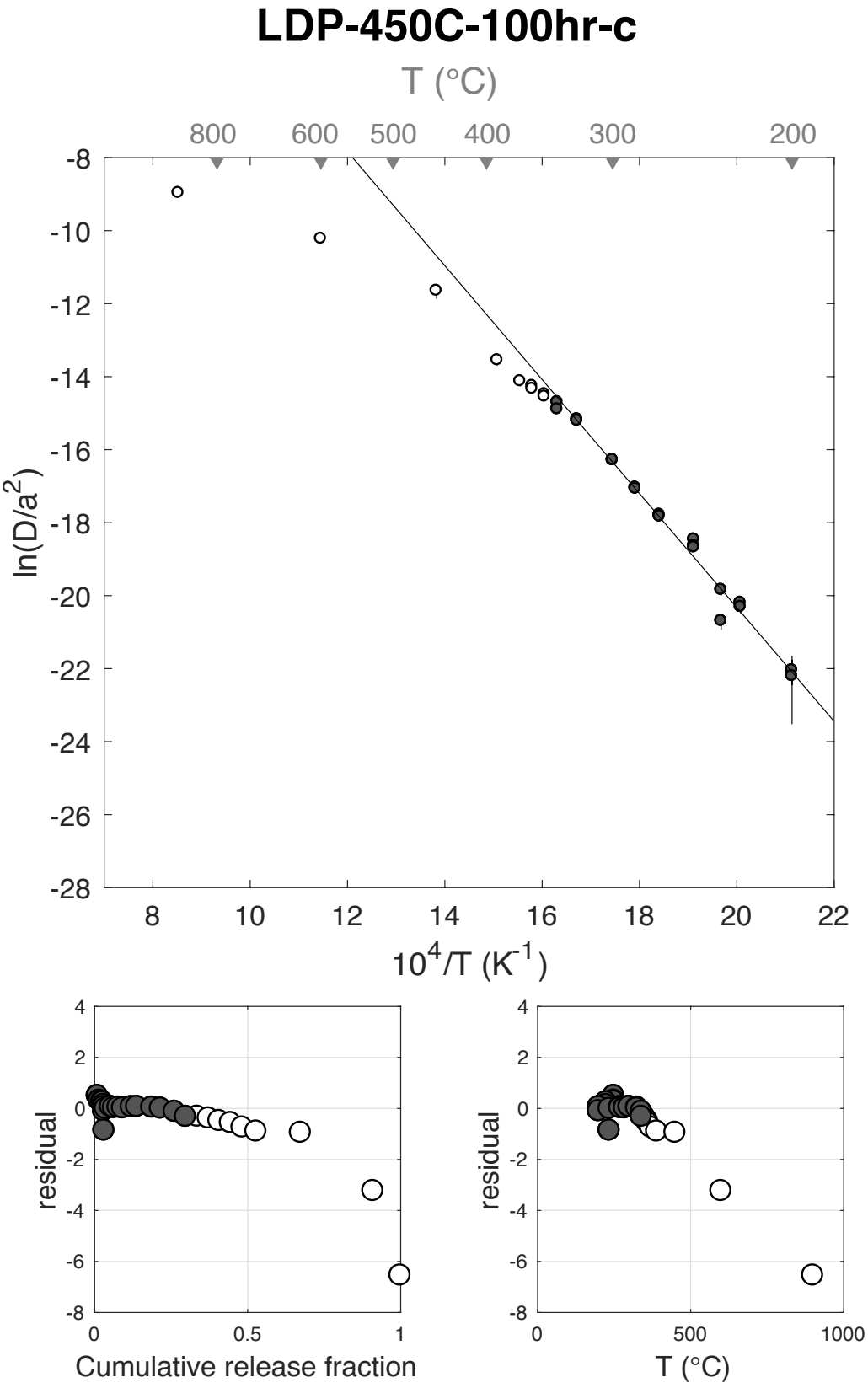
LDP-450C-100hr-c
T (°C)
800
600
500
400
300
200
ln(D/a²)
10⁴/T (K⁻¹)
residual
Cumulative release fraction
residual
T (°C)

E_a	+/-	D_0	+/-	T_c	-	+	Total ^{3}He	Incl.	Misfit	Norm. Misfit
116.15	2.80	8.90	0.59	46.66	3.37	3.46	315.35	0.458	1.312	0.047

Step #	°C	t (hrs)	^{3}He	Error	^{4}He	Error	^{4}He/^{3}He	Err	In ^{3}He Reg.
1	250	0.50	8.23	0.61	55.0	12.0	NaN	NaN	1
2	250	1.00	4.58	0.41	11.2	10.1	NaN	NaN	1
3	240	1.00	1.74	0.25	5.2	10.1	NaN	NaN	1
4	230	1.50	1.33	0.24	0.0	0.0	NaN	NaN	1
5	230	2.50	1.92	0.29	0.0	0.0	NaN	NaN	1
6	210	2.50	0.48	0.15	0.0	0.0	NaN	NaN	1
7	210	3.50	0.56	0.16	0.0	0.0	NaN	NaN	1
8	200	3.00	0.25	0.13	0.0	0.0	NaN	NaN	0
9	200	4.00	0.35	0.14	0.0	0.0	NaN	NaN	0
10	220	2.50	0.80	0.19	0.0	0.0	NaN	NaN	1
11	220	3.50	1.00	0.20	0.0	0.0	NaN	NaN	1
12	235	2.00	1.60	0.25	0.0	0.0	NaN	NaN	1
13	235	3.00	2.04	0.30	0.0	0.0	NaN	NaN	1
14	250	1.00	1.47	0.23	1.2	7.0	NaN	NaN	1
15	260	1.91	4.72	0.42	20.1	15.0	NaN	NaN	1
16	260	1.57	3.66	0.37	14.9	11.0	NaN	NaN	1
17	270	1.91	5.34	0.54	33.4	14.8	NaN	NaN	1
18	270	1.57	4.01	0.41	30.7	11.5	NaN	NaN	1
19	280	1.25	4.18	0.44	22.4	9.8	NaN	NaN	1
20	280	1.57	4.86	0.49	41.5	11.8	NaN	NaN	1
21	290	1.25	5.67	0.47	42.5	10.2	NaN	NaN	1
22	290	1.57	7.17	0.60	47.8	12.2	NaN	NaN	1
23	300	1.91	9.42	0.87	77.3	15.4	NaN	NaN	1
24	300	1.45	5.99	0.46	44.7	10.3	NaN	NaN	1
25	315	1.74	12.95	1.15	87.9	14.1	NaN	NaN	1
26	315	1.32	7.09	0.54	40.4	8.6	NaN	NaN	1
27	330	1.74	14.17	0.74	98.3	12.8	NaN	NaN	1
28	330	1.32	7.57	0.67	51.4	10.9	NaN	NaN	1
29	340	1.58	11.38	0.73	87.8	13.2	NaN	NaN	1
30	340	1.89	10.47	0.68	87.6	13.9	NaN	NaN	1
31	350	1.48	9.67	0.83	57.2	14.3	NaN	NaN	0
32	350	1.82	8.31	0.65	42.4	14.0	NaN	NaN	0
33	360	1.50	9.05	0.83	64.0	9.4	NaN	NaN	0
34	360	1.98	8.94	0.56	61.4	16.6	NaN	NaN	0
35	370	1.88	10.15	0.55	52.2	16.0	NaN	NaN	0
36	390	1.47	10.70	0.65	87.7	11.6	NaN	NaN	0
37	450	1.00	24.82	1.24	271.8	13.6	1.0	0.07	0
38	600	1.00	56.31	1.53	6278.0	47.6	101.5	0.03	0
39	900	1.00	32.28	2.90	32827.0	114.1	1006.9	0.09	0
40	900	1.00	0.13	0.10	144.7	8.7	1063.1	0.71	0
41	900	1.00	0.01	0.05	11.4	7.6	1078.5	5.21	0

Figure S97

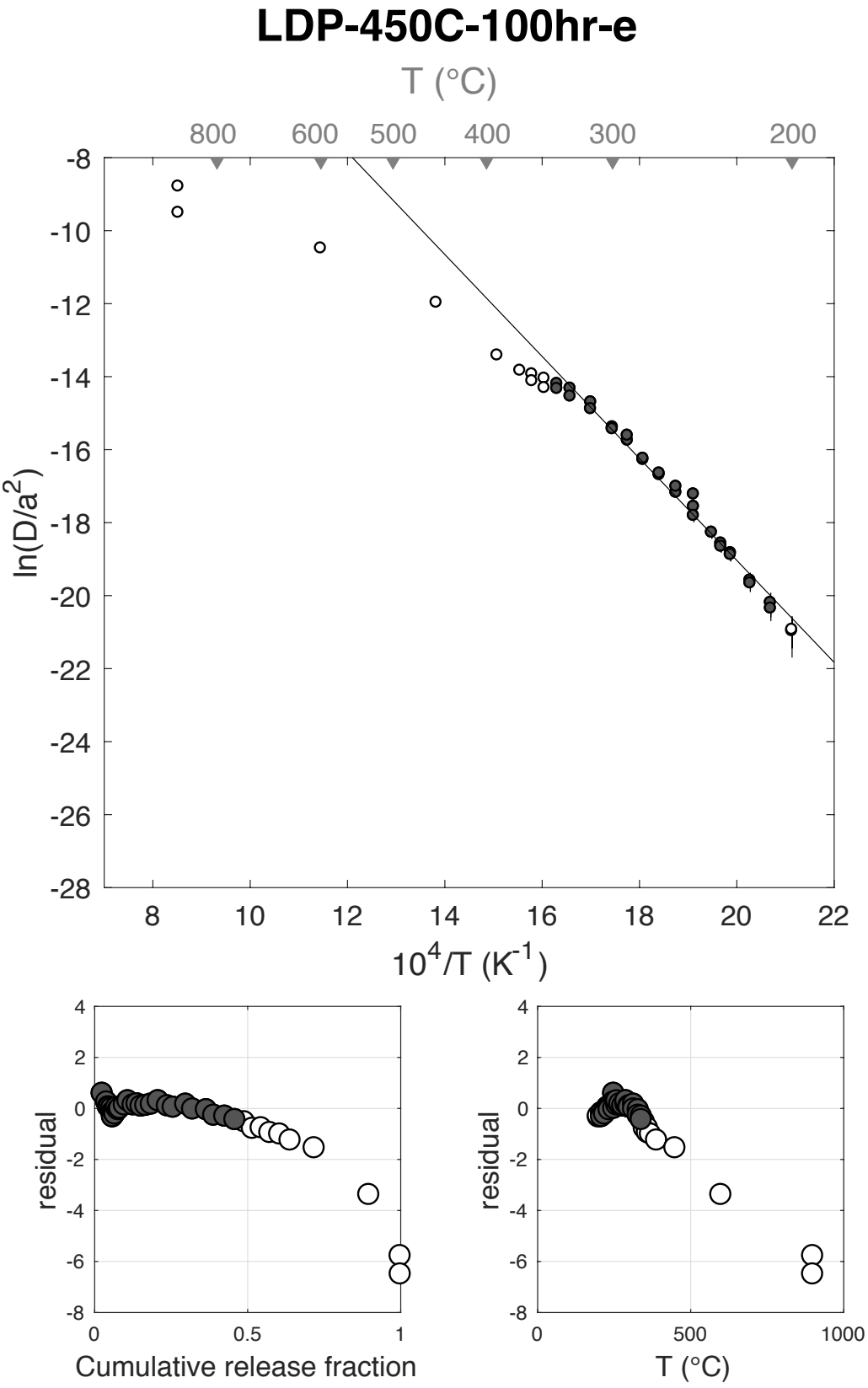
LDP-450C-100hr-e
T (°C)
800
600
500
400
300
200
-8
-10
-12
-14
-16
-18
-20
-22
-24
-26
-28
ln(D/a2)
8
10
12
14
16
18
20
22
10^4/T (K^-1)
4
2
0
-2
-4
-6
-8
residual
0
0.5
1
Cumulative release fraction
0
500
1000
T (°C)